

Synthesis, characterization and exploration of properties of some transition metal complexes with N,O Donor Ligands

**THESIS SUBMITTED FOR THE DEGREE OF
DOCTOR OF PHILOSOPHY(SCIENCE)**

OF

JADAVPUR UNIVERSITY

2022



BY

ARADHITA BHATTACHARJEE

DEPARTMENT OF CHEMISTRY

JADAVPUR UNIVERSITY

KOLKATA - 700032

WEST BENGAL, INDIA

যাদবপুর বিশ্ববিদ্যালয়
কলকাতা-৭০০০৩২, ভারত



*JADAVPUR UNIVERSITY
KOLKATA-700 032, INDIA

FACULTY OF SCIENCE: DEPARTMENT OF CHEMISTRY : INORGANIC CHEMISTRY SECTION

To whom it may concern

This is to certify that the thesis entitled “Synthesis, characterization and exploration of properties of some transition metal complexes with N,O-donor ligands” submitted by Smt. Aradhita Bhattacharjee, who got her name registered on 15th November, 2016 for the award of Ph.D. (Science) degree of Jadavpur University, is absolutely based upon her own work under the supervision of Prof. Partha Roy of Jadavpur University and that neither this thesis nor any part of it has been submitted for either any degree/diploma or any other academic award anywhere before.

Partha Roy
08.09.2022

(Signature of the Supervisor with date and official seal)

Professor Partha Roy
Department of Chemistry
Jadavpur University
Kolkata - 700032

Acknowledgement

It is a great pleasure to express my deep sense of gratitude to my supervisor, Prof Partha Roy. His dedication and keen interest in research helped me immensely during the course of my research. His timely advice, meticulous scrutiny, scholarly advice, scientific approach, have encouraged me to a great extent to accomplish this task. I wish to thank Prof S K Bhattacharya, HOD(Chemistry) and other respected faculty members of the department of chemistry, Jadavpur University. The staff members of the research section, Phd cell and department of chemistry have also been of great help during my entire journey.

I am also thankful to the fellow researchers of my lab. My special thanks lies with CSIR, New Delhi, for the fellowship granted to me. I finally acknowledge my parents who have stood by me through this entire journey and above all my daughter, Sahana, for making me the person I am today.

Date: 8/9/2022

Aradhita Bhattacharjee
Aradhita Bhattacharjee

Department of Chemistry

Jadavpur University

Kolkata 700032

Dedicated to my daughter
(Sahana)

List of abbreviations

MOF	Metal organic framework
en	Ethylenediamine
HNO ₃	Nitric acid
NH ₃	Ammonia
bipy	Bipyridine
phen	Phenanthroline
KSCN	Potassium thiocyanate
acac	acetylacetonate
ITO	Indium titanium oxide
dmg	Dimethylglyoxime
sal	Salen
CN ⁻	Cyanide
CFSE	Crystal field stabilization energy
HSAB	Hard soft acid base
EPR	Electron paramagnetic resonance
NMR	Nuclear magnetic resonance
PXRD	Powder X-ray diffraction
FID	Flame ionization detector
TGA	Thermogravimetric analysis
XPS	X-ray photoelectron spectroscopy
EDX	Energy dispersive X-ray
spectroscopy	
FESEM	Field emission scanning electron microscope
E^0	Standard reduction potential
μ	Magnetic moment
TON	Turn over number
TOF	Turn over frequency
DNA	Deoxyribonucleic acid
LMCT	Ligand to metal charge transfer
MLCT	Metal to ligand charge transfer
PET	Photo-induced electron transfer
PCT	Photo-induced charge transfer
ILCT	Intra-ligand charge transfer
RET	Resonance energy transfer

DNBA	3,5-Dinitrobenzoic acid
TNT	2,4,6-Trinitrotoluene
NB	Nitrobenzene
TNP	2,4,6-Trinitrophenol
HOMO	Highest occupied molecular orbital
LUMO orbital	Lowest unoccupied molecular
Å	Angstrom
K_{sv}	Stern-Volmer constant
I	Fluorescence intensity
FE	Fluorescence enhancement
ex	Excitation
em	Emission
UV	Ultraviolet
vis	Visible
λ	Wavelength
%T	Percentage of transmittance
h	Hours
LOD	Limit of detection
KBr	Potassium bromide
MeCN	Acetonitrile
THF	Tetrahydrofuran
CHCl ₃	Chloroform
MeOH	Methanol
NaOH	Sodium hydroxide
DCM	Dichloromethane
DMF/dmf	Dimethylformamide
^t BuOOH	Tertiary butyl hydroperoxide
H ₂ O	Water
H ₂ O ₂	Hydrogen peroxide
DMSO/dmso	Dimethyl sulfoxide
ppm	Parts per million
nm	Nanometer
mL	Milliliter
μ M	Micromolar
μ L	Microliter
epNACs	Explosive pollutant nitro aromatic

I-V	compounds
eV	Current-voltage
$\text{Cd}(\text{NO}_3)_2 \cdot 4\text{H}_2\text{O}$	Electron-volt
MS	Cadmium nitrate tetrahydrate
IR	Mass spectroscopy
Fig.	Infrared
Ref.	Figure
	Reference
<i>a</i>	Crystallographic distance along 'x' axis of a unit cell (in angstrom)
<i>b</i>	Crystallographic distance along 'y' axis of a unit cell (in angstrom)
<i>c</i>	Crystallographic distance along 'z' axis of a unit cell (in angstrom)
α	Crystallographic angle in a unit cell between <i>b</i> and <i>c</i> (in degree)
β	Crystallographic angle in a unit cell between <i>c</i> and <i>a</i> (in degree)
γ	Crystallographic angle in a unit cell between <i>a</i> and <i>b</i> (in degree)
ρ	Density (in g cm^{-3})
Mo-K α	Molybdenum K α radiation
<i>F</i> (000)	Crystallographic (000) plane
ORTEP	Oak Ridge thermal ellipsoid plot

Contents

Chapter 1

Introduction

1.1 General introduction	1
1.2 Cu Chemisty:.....	2
1.2.1 Complexes of Cu(I)	3
1.2.2 Complexes of Cu(II)	5
1.2.3 Electronic spectra and magnetic properties of copper(II) complexes	8
1.2.4 Complexes of Cu(III).....	9
1.3 Nickel chemistry.....	10
1.3.1 Complexes of Ni(II).....	11
1.3.2 Electronic spectra and magnetic properties of nickel(II) complexes	16
1.4 Copper in alcohol oxidation: A perspective of Schiff base copper complex	18
1.4.1 Model Compounds for the GO Active Site.....	25
1.5 Polymer-supported Schiff base copper and nickel complexes in oxidation reactions: ...	36
1.6 C-H activation by Schiff base complexes:	53
1.7 Schiff base metal complex in DNA/protein interaction:	67
1.8 Ascorbic acid oxidation by Schiff base complex modified electrode:	90
1.9 Objective of the Thesis	93
1.10 References :.....	94

Chapter 2

Mono-, tri- and polynuclear copper(II) complexes of Schiff-base ligands: Synthesis, characterization and catalytic activity towards alcohol oxidation

2.1 Introduction	104
2.2 Experimental Section.....	105
2.2.1 Materials and physical methods	105
2.2.2 Synthesis of [Cu(L ¹)Cl ₂] (1).....	106
2.2.3 Synthesis of [Cu ₃ (L ²) ₂ Cl ₄] (2)	106
2.2.4 Synthesis of [Cu(L ³)N ₃] _n (3)	107
2.2.5 X-ray data collection and structure determination	107
2.2.6 Alcohol oxidation	109
2.3 Results and discussion	110
2.3.1 Synthesis and characterization	110
2.3.2 UV-vis spectral studies	113
2.3.3 Crystal Structures of complexes 1, 2 and 3.....	117
2.3.4 Electrochemical studies	125
2.3.5 Alcohol oxidation studies.....	128
2.4 Conclusions	133
2.5 References	134

Chapter 3

Cu- and Ni-Grafted Functionalized Mesoporous Silica as active Catalyst for Olefin Oxidation

3.1 Introduction	138
3.2 Experimental Section.....	140
3.2.1 Materials and physical measurements	140
3.2.2 Synthesis of functionalized mesoporous silica.....	141
3.2.3 Olefin oxidation.....	142
3.3 Results and discussion	142
3.3.1 Characterization of the framework, microstructure and porosity.....	142

3.3.2 Catalytic studies.....	148
3.4 : Conclusions.....	161
3.5. References.....	163

Chapter 4

Particulate methane monooxygenase mimicking activity of dinuclear transition metal complexes

4.1 Introduction.....	169
4.2 Experimental Section.....	171
4.2.1 Materials and physical methods.....	171
4.2.3 Synthesis of $[\text{Cu}_2(\text{L})_2(\mu_2\text{-Cl})\text{Cl}] \cdot 2.5\text{H}_2\text{O}$ (1).....	172
4.2.4 Synthesis of $[\text{Ni}_2(\text{L}^1)_2(\text{N}_3)_2(\text{CH}_3\text{OH})_2] \cdot \text{CH}_3\text{OH}$ (2).....	172
4.2.5 X-ray data collection and structure determination.....	172
4.2.6 Computational details.....	174
4.2.7 Catalytic studies.....	175
4.3 Results and discussion.....	175
4.3.1 Synthesis.....	175
4.3.2 Crystal structures of 1 and 2.....	175
4.3.3 IR spectral studies.....	180
4.3.4. UV-vis spectral studies.....	180
4.3.5. Geometry optimization and computational studies.....	181
4.3.6 Thermal analysis.....	186
4.3.7. Cyclic voltametric studies.....	187
4.3.8 Catalysis studies.....	189
4.4. Conclusions.....	194
4.5. References.....	195

Chapter 5

A mononuclear copper(II)-Schiff-base complex: DNA cleavage activity, protein binding affinity and cellular imaging

5.1 Introduction	201
5.2 Experimental	204
5.2.1 Materials and methods	204
5.2.2 Synthesis of [CuL ₂] (complex 1)	205
5.2.3 X-ray data collection and structure determination	205
5.2.4 DNA binding and cleavage activities	207
5.2.5 HSA binding studies	207
5.2.6 Antibacterial study	207
5.2.7 Cell biological study	208
5.3 Results and discussion	208
5.3.1 Synthesis of complex 1 and its characterization	208
5.3.2 Crystal structure of complex 1	209
5.3.3 UV-vis spectral studies	211
5.3.4 Magnetic moment studies	212
5.3.5 Electrochemical studies	212
5.3.6 DNA binding studies	213
5.3.6.1 UV-visible spectral studies	213
5.3.6.2 Competitive binding assay	215
5.3.6.3 Fluorescence quenching spectroscopy	216
5.3.6.4 Cyclic voltametry	217
5.3.6.5 Circular Dichroism spectral studies on DNA binding	218
5.3.6.6 DNA cleavage studies	219
5.3.7 HSA binding studies	222
5.3.7.1 Absorption spectra studies	222

5.3.7.2 Fluorescence quenching studies	224
5.3.7.3 Energy transfer and binding distance between the complex 1 and HSA	226
5.3.7.5 3D fluorescence spectral studies	228
5.3.7.6 Circular Dichroism	229
5.3.7.7 Oxidative damage of HSA by complex 1	230
5.3.8 Antibacterial study by complex 1	231
5.3.9 Apoptosis evaluation by DAPI staining	232
5.4 Conclusion	233
5.5 References	234

Chapter 6

A novel Schiff-base copper(II) complex modified electrode for ascorbic acid catalytic oxidation and determination

6.1 Introduction	241
6.2 Experimental Section	242
6.2.1 Materials and physical methods	242
6.2.2 Synthesis of Synthesis of [Cu(L ¹)H ₂ O]	242
6.2.3 X-ray data collection and structure determination	243
6.2.4 Electrochemical measurements	244
6.3 Results and discussion	245
6.3.1 Synthesis	245
6.3.2 Crystal structure of 1	246
6.3.3 IR spectral data	247
6.3.4 UV- Vis spectral data	248
6.3.5 Electrochemical polymerization	249
6.3.6 Electrocatalytic oxidation of ascorbic acid	251
6.3.7 Amperometric determination of H ₂ A	253

6.4 Conclusions	255
6.5 References	256
Appendix	
List of publications	258

Preface

This work presented in this thesis entitled “**Synthesis , characterization and exploration of properties of some transition metal complexes with N,O –donor ligands**” has been carried out in the Department of Chemistry, Jadavpur University, from the period 2015 to 2022.

Different analytical and spectroscopic techniques have been used during the course of the research like ^1H , ^{13}C NMR, UV-Vis, PXRD, FTIR, and single crystal XRD. In some cases computational studies involving DFT calculations have been utilized.

The thesis contains six chapters with the following contents:

Chapter 1: This chapter is a broad introduction regarding coordination chemistry of transition metals, mainly copper and nickel. Moreover, it contains an elaborate literature survey behind the research work that has been conducted and it also contains a brief overview of the objective of the thesis.

Chapter 2: This chapter deals with the synthesis and characterization of a few Schiff base copper(II) complexes and their extensive use as catalysts in alcohol oxidation, yielding the desired products. The products have been identified and quantified by gas chromatography.

Chapter 3: This chapter elucidates the synthesis, detailed characterization and study of two heterogeneous catalysts which have been prepared by grafting Ni(II) and Cu(II) on functionalised mesoporous silica. These catalysts have been employed in olefin oxidation reactions thereafter.

Chapter 4: This chapter contains the description of Cu(II) and Ni(II) complexes, of which the Cu(II) complex resembles a natural enzyme, methane monooxygenase. These have been used to activate C-H bond in alkanes, and of the two, the copper complex was seen to carry this out successfully.

Chapter 5: This chapter is an overview of a mononuclear Cu(II) Schiff base complex, which has been effective in interacting with DNA and protein. Hence, this complex has relevant biological applications, including cell apoptosis.

Chapter 6: This chapter is a description of a novel Schiff base copper(II) complex which has been electropolymerized on a simple glassy carbon electrode. The comparison between the two electrodes show how the modified electrode carries much higher current in a voltammetric set up. It has also been used for catalyzing the oxidation of ascorbic acid.

Date : 8/9/2022

Aradhita Bhattacharjee
Aradhita Bhattacharjee

Department of Chemistry

Jadavpur University

Kolkata 700032

Chapter 1

Introduction

1.1 General introduction

Transition metals are atoms which have a partially filled d sub-shell and can produce cations with an incomplete d sub-shell. They can be described as an element in the d -block of the periodic table, which include groups 3 to 12. The f -block lanthanide and actinide series are called "inner transition metals". The properties of the d -block elements are very unique different from those of s and p block elements in which either s or p -orbitals of the valence shell gets filled. They are mostly coloured compounds and the colour is generally due to electronic transitions of two principal types. An electron may jump from a predominantly ligand based orbital to a predominantly metal based orbital, giving rise to a ligand-to-metal charge-transfer (LMCT) band. A metal-to-ligand charge transfer (MLCT) transition will be most likely just the reverse when the metal is in a low oxidation state and the ligand is easily reduced. The intense colourations of these compounds are caused by the above two transitions while the third type of transition, d - d transitions, are the ones causing weaker intensity colour when an electron jumps from one d level to another. These transitions are forbidden by selection rules and thus creates a weak colour. Transition metal compounds are paramagnetic in nature when they have one or more unpaired d electrons. Ferromagnetism occurs when individual atoms are paramagnetic and the spin vectors therein are aligned parallel to each other. Anti-ferromagnetism is another example of a magnetic property arising from a particular alignment of individual spins in the solid state in a way such that the magnetism in one direction gets cancelled off in the other.

All transition metals are metals and hence conductors of electricity. They possess high density and high melting and boiling points. These properties are attributed to metallic bonding by delocalized d electrons, causing cohesion which increases with the number of electrons shared. The transition metal complexes are also known for their homogeneous and heterogeneous catalytic property which can be ascribed to their ability to adopt multiple oxidation states.

Among the transition metal complexes, complexes of copper and nickel are of great interest as they offer several significant applications in various fields such as magnetism, sensing, catalysis, biology, separation science^[1]etc. Moreover, these are cheap as they are easily available on the earth's crust.

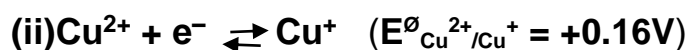
1.2 Cu Chemisty:

Copper is one of the most abundant metals in the earth's crust (68 ppm). It is an essential element for living organisms. Copper is involved in different reactions like enzymatic reactions, oxygen transportation, *etc.* within biological systems^[2] which are all vital for life. It is also important for human civilization. For thousands of years, copper has been utilized to generate objects ranging from copper bells to microelectronics. Metallic copper is used in developing electrical conductor. It is also used extensive use in the preparation of coinage alloys. Several alloys consist of copper; for example bronze (Cu plus 7-10% Sn), brass (Cu-Zn), and special alloys such as Monel (Ni-Cu). Copper plays physiological roles in bio organisms as well, it is useful in designing the way of treatment for so memetabolic disorders. A large number of copper-containing antibacterial, antiviral and antitumoragents are also common^[3].

Copper, as commonly known, exhibits a variety of compounds, mostly coloured. The two main oxidation states of copper are +1 and +2 although some +3 complexes are also known in literature. Copper(I) compounds are diamagnetic and are generally colourless, except when colour results from charge transfer or due to the anion. In solids, copper(I) is the more stable state at normal temperatures. According to the HSAB rule, Cu(I) ion is soft acid^[4]. Due to this, it is found to complex with soft donors such as unsaturated heterocyclic compounds, carbon monoxide, sulfur containing ligands,^[5] *etc.* The copper(II) ion is more stable in aqueous solutions. Compounds of the +2 state, often called cupric compounds, are usually coloured. They are affected by Jahn Teller distortions and exist as a wide range of stereoisomers with four, five, and six coordination numbers. Although researchers have been involved in evaluating the chemistry of copper complexes since a long and a number of research articles regarding this have already been published, studies on coordination complexes of Cu(II) and Cu(I) still reveals amazing coordination geometries and structural variations. Coordination number of copper in its complexes varies from two up to six and therefore these complexes exhibit different kind of geometries *e.g* linear (coordination number two), trigonal planar or T-shaped (coordination number three), tetrahedral and distorted square planar (with coordination number four), tetragonal pyramidal (coordination number five) and distorted octahedral (coordination number six).

1.2.1 Complexes of Cu(I)

It is found that Cu(I) with d^{10} configuration does not fit in any definite coordination geometry. Here the amount of steric constraints coupled with electronic effects caused by the ligands interplay in determining the stereochemistry of the complexes. The 3d shell of Cu(I) ion is fully filled and therefore, it is isoelectronic with zinc(II). As a result of this, Cu(I) exhibits no ligand field transition and it is EPR silent as well. Cu(I) is generally diamagnetic unless it is coordinated to highly polarized ligands. Contrary to Cu(II), the complexes of Cu(I) are found to be colorless as there is no electron that can be promoted to a higher energy level when the 3d sub-shell is split as and when the central metal ion interacts with the ligands. Copper(I) system is extremely unstable in aqueous phase and it tends to disproportionate and generate copper(II) along with metallic copper ($2\text{Cu(I)} = \text{Cu(II)} + \text{Cu(s)}$). Hence it spontaneously undergoes a redox change and an electrode potential value predicts this instability and therefore the observations are completely justified. The reason behind this kind of facile disproportionation may be the higher value of the heat of hydration of the corresponding divalent ion that is being formed. The system exhibits high $K (= [\text{Cu(II)}][\text{Cu(I)}]^{-2})$ value and it has been found to be $5.38 (\pm 0.37) \times 10^5 \text{ mol}^{-1}$ at 25°C . The calculated standard reduction potentials are $E^\circ(\text{Cu}^+/\text{Cu}) = +0.5072 \text{ V}$ and $E^\circ(\text{Cu}^{2+}/\text{Cu}^+) = +0.1682 \text{ V}^{[6]}$. That is,



Equation (i) represents the reduction half-cell reaction and equation (ii) with the less positive potential, will represent the oxidation change. However, stabilization of Cu(I) can be achieved through formation of complexes having extremely low solubility or by generating complexes with ligand systems that show π -accepting nature. Cu(I) ion is quite stable in its acetonitrile solution. Oxidation of metal ion following electrochemical method in acetonitrile offers a suitable preparative procedure. The common geometry of Cu(I) complexes in tetracoordinated complexes is tetrahedral as demonstrated by N.K. Szymczak *et al*^[7], e.g. $[\text{Cu}(\text{py})_4]^+$, $[\text{Cu}(\text{CN})_4]^{3-}$ and $[\text{Cu}(\text{L-L})_2]^+$ (e.g. L-L = phen, bipy) (**Fig1.1**)

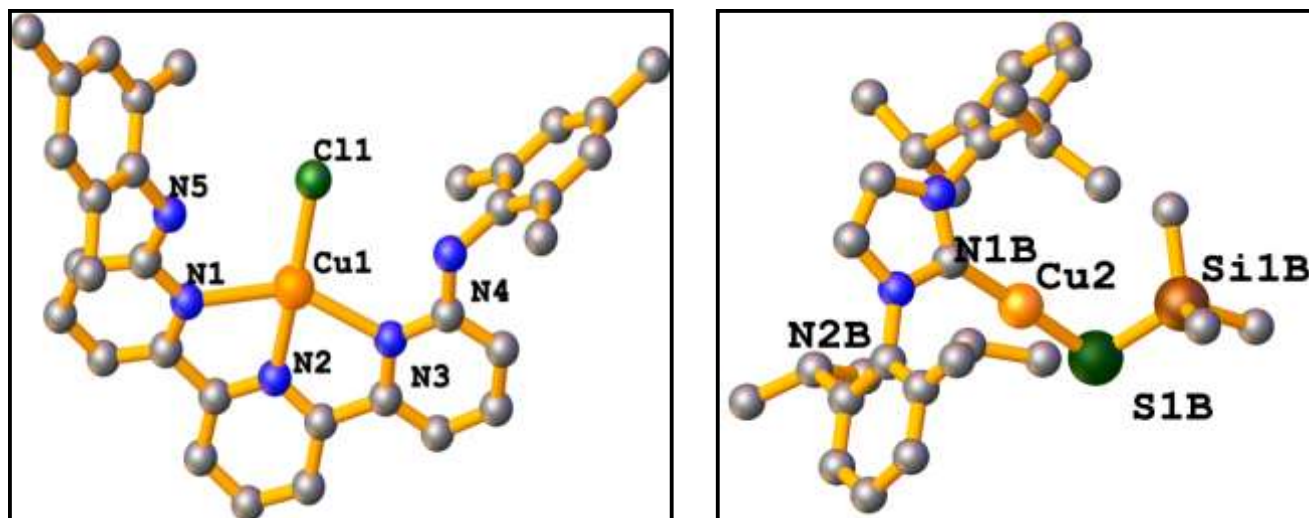


Fig 1.1 : A perspective view of Common Cu(I) complexes. H atoms are excluded for clarity^[7]

Apart from this, Cu(I) may form complexes with much lesser coordination number, as well, such as two. In linear $[\text{CuCl}_2]^-$ copper(I) exhibits coordination number two. It is formed by dissolving CuCl in HCl. Coordination number three can be found in $\text{K}[\text{Cu}(\text{CN})_2]$. In solid state it has been found to consist of almost planar, trigonal $\text{Cu}(\text{CN})_3$ units which are connected in a polymeric string (**Fig.1.2**). Whereas the distinct planar anion $[\text{Cu}(\text{CN})_3]^{2-}$ can be obtained in the case of $\text{Na}_2[\text{Cu}(\text{CN})_3] \cdot 3\text{H}_2\text{O}$. There are few examples where copper can exist with two different oxidation states. One of such complexes is $2[\text{Cu}(\text{C}_{25}\text{H}_{28}\text{N}_2\text{S}_2)\text{Cl}]^+[\text{Cu}_2\text{Cl}_4]^{2-}$. Here Cu(II) is coordinated to an N_2S_2 type macrocyclic moiety along with chloride. This ultimately ends up in the formation of a reasonably bulky cation which eventually stabilizes the anion containing Cu(I) in a strange and non-planar geometry^[8]. A large variation of polymers are found to contain Cu(I) center. Since Cu(I) is a d^{10} system, it is extremely unlikely for it to get involved in metal metal bonding. Complexes of Cu(I) also consist of an extensive variety of structures, which are often characterized by their electronic spectra containing unique charge-transfer bands^[9]. The general stoichiometries of CuXL_n (where $n = 0.5, 1, 1.5$ and 2) may show various types of geometries such as “cubane”, “ladder” and “chair”. The ultimate geometry depends on the type of ligand (L) and halide (X) used^[10].

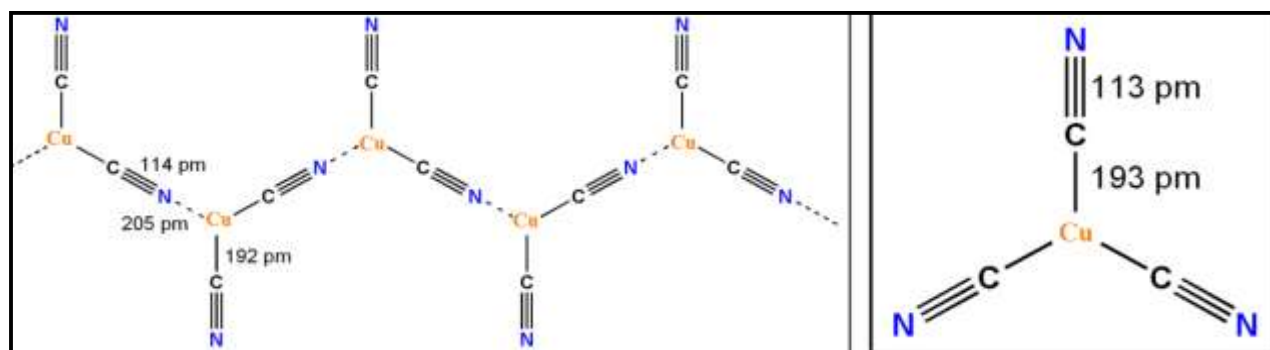


Fig 1.2 : Trigonal $\text{Cu}(\text{CN})_3$ units fused together^[11]

1.2.2 Complexes of Cu(II)

Cu(II) has a d^9 electronic configuration. It shows unique spectral and magnetic properties. In most cases, complexes of Cu(II) exhibit characteristic EPR signal. Due to its d^9 electronic configuration it is prone to Jahn-Teller distortion. Therefore, a general trend of learning the chemistry of Cu(II) complexes by studying their spectroscopic properties. The electronic spectra of coordination complexes of copper(II) consist of broad bands which provide information about the coordination geometry around the metal center. Usually the bands are due to ligand to metal charge transfer (LMCT), and are found in the ultra-violet to visible region. The electron paramagnetic resonance (EPR) spectra of copper(II) gives information about the electronic state as well as the coordination geometry. In solid state, due to interaction among the neighboring copper centers within the lattice, EPR yields broad signals. But when the samples are magnetically dilute, the EPR spectra clearly exhibits the characteristic hyperfine splitting ($I_{\text{Cu}} = 3/2$) and super hyperfine splitting ($I_{\text{N}} = 1$). In several Cu(II) complexes where two Cu(II) ions are in proximity or connected by a suitable bridging ligand, the electron spin interaction takes place if the magnetic orientations as well as the orientations of the ligand orbitals allow the overlap. These types of Cu(II) dimers are found often with a variety of bridging ligands such as hydroxide, fluoride, chloride, azide, imidazolate, thiocyanate, *etc.* Further information about this type of interactions between copper(II) centers can be obtained by studying the results of magnetic susceptibility measurements. The redox properties of the Cu(II) ion are highly

dependent on the type of atoms coordinated to it. Soft donor type ligands tend to increase the Cu(II)/Cu(I) redox potential as they are able to stabilize the corresponding lower oxidation state. Usually Cu(II) exhibits coordination numbers 4, 5 and 6 in its complexes. But the regular geometries corresponding to these coordination numbers are particularly rare. Therefore it becomes difficult often to make a difference between square-planar geometry and tetragonally distorted octahedral geometry. The cause behind this observation is attributed to the Jahn-Teller effect. Here, Jahn-Teller distortion takes place due to the uneven occupation of the **eg** orbitals (d_{z^2} and $d_{x^2-y^2}$) since the d^9 Cu(II) ion is in an overall octahedral geometry. Generally an elongation of the octahedron occurs due to the Jahn-Teller effect which may be seen as “4 + 2” coordination (4 short and 2 long bonds). This result is due to the filled d_{z^2} orbital and half-filled $d_{x^2-y^2}$ orbital. In most extreme case of the “4 + 2” coordination the axial ligands may completely vanish and consequently a square-planar complex is generated. However, a compression of the octahedron takes place in peculiar cases, *e.g.* coordination geometry in solid $KAlCuF_6$. This type of Jahn-Teller distortion can be ascribed as “2 + 4” coordination (2 short and 4 long bonds). “4 + 2” type coordination is in turn supported by the configurational mixing between higher-lying s orbital and ligand field d-orbital basis set^[12]. Veidis *et al.* reported a copper(II) complex $[Cu(bpy)(hfa)_2]$ (bpy = bipyridine, hfa = hexafluoroacetylacetonate) in which Jahn-Teller distortion was very apparent. Due to tetragonal distortion, its geometry deviated from ideal octahedral symmetry (Oh) to yield D_{4h} symmetry^[13]. **(Fig 1.3)**

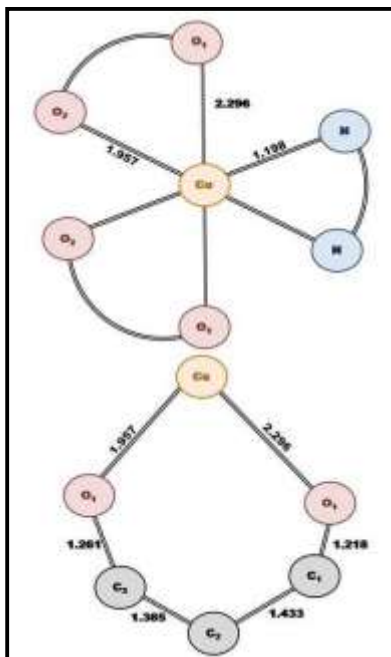


Fig 1.3 : Effects of Jahn Teller distortion^[13]

Stable complexes of copper(II) are reported with various O donor ligands for example acetylacetonate, acetate, ethyl acetoacetate, *etc.* Cu(II) also complexes with mixed N,O-donor ligands like Schiff base ligands to produce stable adducts. This type of complexes exhibit interesting stereochemistries. Examples consist square-planar coordination as well as square pyramidal geometry around the metal centre (**Fig 1.4**)^[14] whose energy level diagram has been illustrated in **Fig 1.5**. Mostly, dimerization occurs in the solid state when the metal exhibits a square pyramidal coordination.

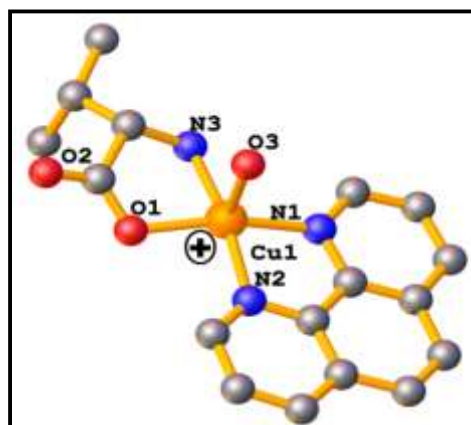
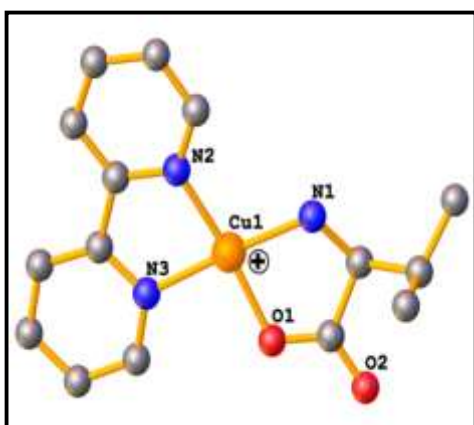


Fig 1.4 : A perspective view of square-planar and square pyramidal Cu complex. H atoms excluded^[14]

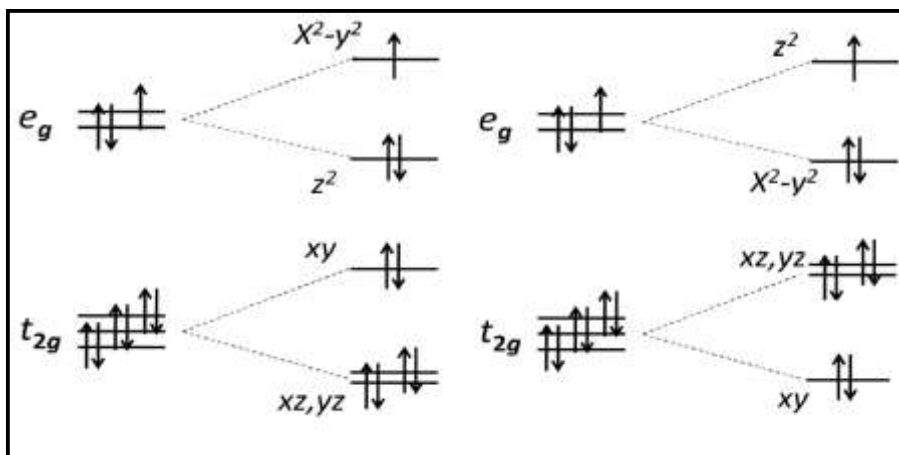


Fig 1.5 : Energy level diagram of square planar and square pyramidal geometry^[4]

1.2.3 Electronic spectra and magnetic properties of copper(II) complexes

Usually complexes in which the metal ion has d^9 electronic configuration, exhibit simpler spectra since the d^9 configuration may be treated as an inverse to d^1 electronic configuration^[11]. Cu(II) exhibits a d^9 electronic configuration. Therefore complexes containing Cu(II) are generally blue or green in color due to the existence a single broad band in the absorption spectra within the region of $11000-16000\text{ cm}^{-1}$. However, as discussed earlier, the d^9 ion is susceptible to large Jahn-Teller distortion. As a result of this distortion, its geometry deviates from ideal octahedral symmetry and therefore, the absorption band becomes unsymmetrical. Due to this reason the electronic spectra of d^9 systems consist of a number of bands whose exact assignment is extremely difficult. The ground term for a d^9 system is $2D$. The splitting of a $2D$ free ion ground term is like a $5D$ ground term that arises from d^4 electronic configuration and as a result similar electronic spectra is expected for both. The T ground term that arises due to the tetrahedral coordination of d^9 ion which has an orbital contribution towards the magnetic moment of the system. As a result, the magnitude of the magnetic moment is found to be greater than the corresponding spin-only value ($\mu_{\text{spin-only}} = 1.73\text{BM}$). The E ground term of a d^9 system with octahedral coordination can also generate a magnetic moment [$\mu_e = \mu_{\text{spin-only}} (1-2\lambda/10Dq)$] which is higher than 1.73BM . This happens due to the mixing of the excited T terms with the ground term. The sufficiently higher magnitude of λ (-850 cm^{-1}) supports this result. The magnetic moments of magnetically dilute Cu(II) complexes vary from 1.9 B.M to 2.2 BM . The

overall picture becomes clear in **Fig 1.6**. We see that the copper(II) complexes with geometries close to octahedral, show magnetic moments of lower value within the over said range and the complexes with coordination geometries close to tetrahedral exhibit magnetic moments of higher value. But this result is not very consistent and nothing can be concluded about the exact geometry without proper other practical evidences.

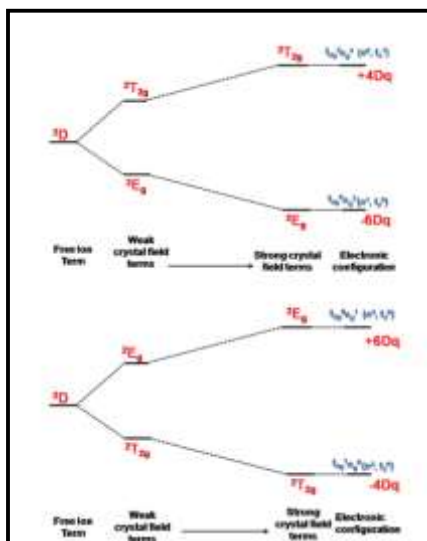


Fig 1.6 : Energy level separations of Cu(II) complexes^[4]

1.2.4 Complexes of Cu(III)

Usually the complexes containing copper(III) are rare since Cu(III) (**Fig 1.7**) is reduced to Cu(II) easily, though a few have been reported^[15]. Cu(III) ion can successfully participate in electron transfer occurring in biological systems and therefore, a range of Cu(III) containing peptides have been potentially synthesized. The pale-green colored complex K_3CuF_6 can be achieved by treating a mixture of potassium chloride and copper(I) chloride ($3KCl + CuCl$) with F_2 . This compound exhibits paramagnetism owing to the presence of two unpaired electrons and it can be reduced very easily. K_3CuF_6 , a high-spin paramagnetic Cu(III) complex, is one of its kind. Apart from this one, all the other Cu(III) complexes are low-spin and hence diamagnetic. Generally, geometries of these complexes are square planar and they are very much similar in nature to Ni(II) systems. $[CuBr_2(S_2CNBu'_2)]$ and $MCuO_2$ ($M = \text{alkali metal}$) are examples of diamagnetic

Cu(III) complexes. Violet colored $[\text{CuBr}_2(\text{S}_2\text{CNBu}'_2)]$ can be effectively synthesized by the reaction between $[\text{Cu}(\text{S}_2\text{CNBu}'_2)]$ and Br_2 in CS_2 medium, whilst blue colored MCuO_2 can be prepared by heating cupric oxide and MO_2 in the presence of oxygen. W.F. Bie et al. synthesized the following Cu(III) complex^[16]

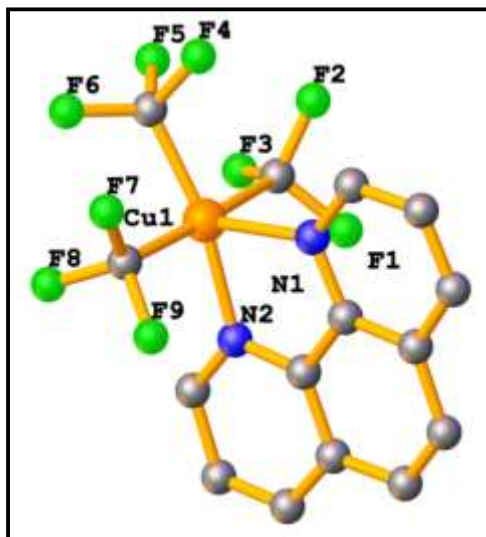


Fig 1.7 : A perspective view of Cu(III) complex. H atoms excluded^[16]

1.3 Nickel chemistry

Nickel is the twenty-second most abundant element in the earth's crust (99 ppm) and among the transition metals, its position stands in the seventh most abundant^[11]. A considerable amount of nickel is used in making of alloys. In 1889, a report published by J. Riley of Glasgow on the effect of addition of nickel to stainless steel, probed the US Navy to use nickel steels in armour plating. Amount of Ni in Stainless steels can be found up to 8%. The alloy "Alnico" is famous for its use as a permanent magnet. The non-ferrous alloy, nickel silver (or German silver) contains 55-65% Cu, 10-30% Ni and Zn, as its constituents. When this alloy is electroplated with silver, it generates the common EPNS tableware. Monel (containing 32% Cu, 68% Ni and traces of Mn and Fe) is employed in the making of apparatus for handling corrosive materials. Nichrome (60% Ni, 40% Cr), which is known for its extremely small temperature coefficient of electrical resistance, it is used in electric heaters. Another Ni alloy Invar finds its application for

its very small coefficient of expansion. Electroplated nickel can act as a perfect undercoat for electroplated chromium. Nickel plays a role in the catalytic hydrogenation of unsaturated vegetable oils and unsaturated fats. Huge quantity of nickel is also used in storage batteries. Nickel is ferromagnetic, but the extent of ferromagnetism is less than that of iron and cobalt. Its Curie point is around 375°C, which is also lower than both iron or cobalt. At normal temperature conditions, nickel is moderately resistant to atmospheric corrosion. However, when heated in air, nickel gets tarnished. Finely divided nickel is actually also pyrophoric. When heated, nickel reacts with B, Si, P, S and the halogens as well. On heating it reacts with F₂ although much more slowly than most metals otherwise do. It gets oxidized at red heat in presence of steam. Nickel metal gets dissolved in dilute mineral acids slowly but quite rapidly in dil HNO₃. On the other hand concentrated HNO₃ renders it passive. Nickel is known for its resistance aqueous alkalis and therefore it finds suitability in manufacture of apparatus for producing NaOH.

1.3.1 Complexes of Ni(II)

Undoubtedly +2 is the most common and widely existing oxidation state of Ni. Due to the absence of any other oxidation state with such good stability, compounds of Ni(II) generally do not take part in regular redox reactions. Ni(II) generates salts with several existing anions and in aqueous medium, [Ni(H₂O)₆]²⁺ ion is formed in the absence of any strongly complexing ligands. The coordination number of nickel(II) hardly exceeds six. Nickel complexes are octahedral and square planar in general, though few examples of trigonal bipyramidal, tetrahedral and square pyramidal geometries have also been found to exist. Octahedral complexes of nickel(II) can be obtained from an aqueous solution by gradually replacing coordinated water with neutral N-donor ligands (*i.e.* NH₃, en, bipy, phen*etc.*) anionic ligands (*i.e.* NCS⁻, NO₂⁻ *etc.*) and O-donor ligands such as dmsO, dmf *etc.* Some common complexes are given in **Fig 1.8**^[11].

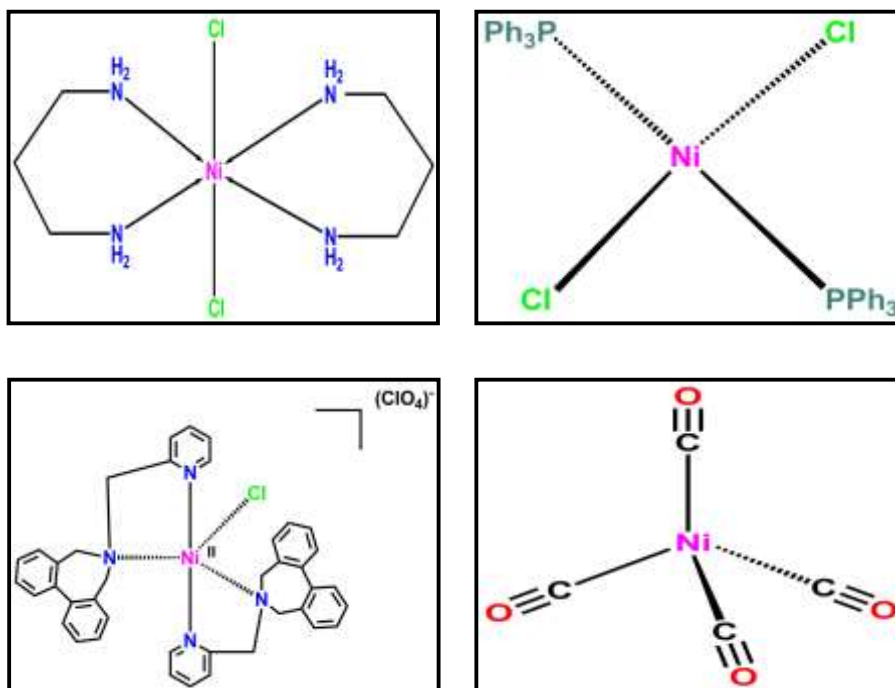


Fig 1.8 : Some nickel complexes and their geometries^[11].

The green trimeric complex, $[\text{Ni}(\text{acac})_3]$, can be prepared from the octahedral monomeric trans-dihydrate, $[\text{Ni}(\text{acac})(\text{H}_2\text{O})_2]$ by dehydrating the same. The trimer shows some really interesting magnetic properties. (Fig 1.9)^[11]

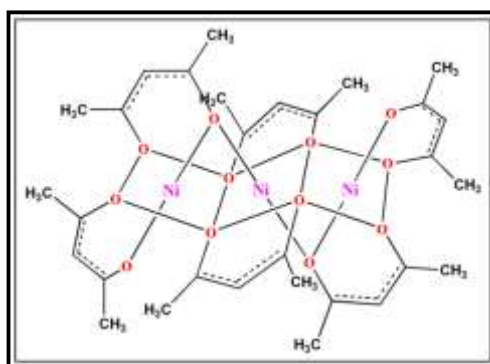


Fig 1.9 : Trimeric $[\text{Ni}(\text{acac})_3]$ complex^[11]

At low temperature of about 80 K, it behaves like a normal paramagnet but at a temperature further lower, magnetic moment is higher. At 4.3 K, magnetic moment per nickel atom increases from 3.3 to 4.1 BM. This indicates ferromagnetic coupling between the six unpaired electrons in this trimer. Trimer formation can be prevented by replacement of the methyl groups of

acetylacetonate with the bulkier groups like *tert*-butyl. This eventually paves the way for the formation of a red colored square planar monomer (**Fig 1.10**)^[11].

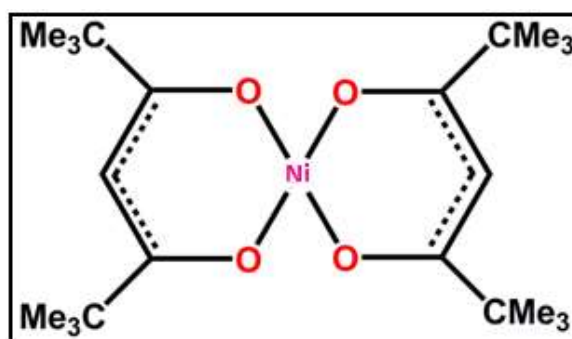


Fig 1.10 : Square planar nickel complex^[11]

Among the four coordinated Ni(II) complexes, square planar geometries are encountered the most. $[\text{Ni}(\text{CN})_4]^{2-}$, (N-methylsalicylaldiminato)nickel(II) and bis(dimethylglyoximato)nickel(II) are well-known square planar Ni(II) complexes. Its bonding and hybridization has been shown in **Fig 1.11**^[11]. The latter is highly useful to inorganic chemists as is obtained as a bright rose red precipitate during gravimetric analysis of nickel. In fact, solid bis(dimethylglyoximato)nickel(II) consists of planar molecular structures stacked on each other. Therefore Ni-Ni interactions eventually lead to a seemingly octahedrally coordinated complex. However, it dissociates into the corresponding square-planar monomer in presence of non-coordinating solvent molecules. Thus, it should be considered as square planar even in solid state.

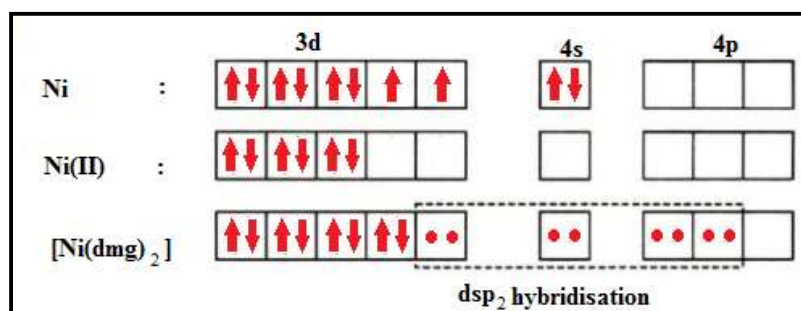


Fig 1.11 : Bonding and hybridization bis(dimethylglyoximato)nickel(II)^[11]

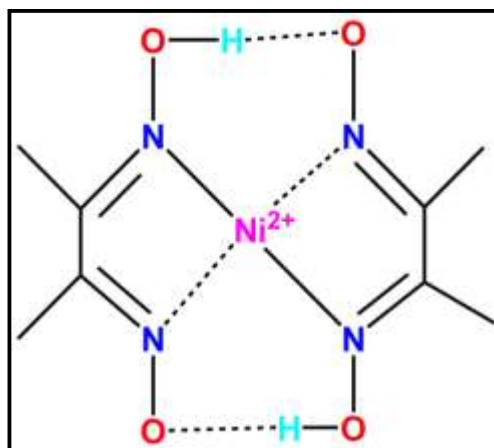


Fig 1.12 : Tetrahedral Ni complex^[11]

Tetrahedral complexes of Ni(II) with coordination number four also occur (**Fig 1.12**)^[11], although rarely. The more common geometry is square planar. The simplest among these tetrahedral Ni(II) complexes is the blue colored complex $[\text{NiX}_4]^{2-}$ ($\text{X} = \text{Cl}, \text{Br}, \text{I}$) ions, which is obtained as a precipitate from ethanolic solutions by large cations like $[\text{NR}_4]^+$, $[\text{PR}_4]^+$ and $[\text{AsR}_4]^+$ ^[17]. Others include $[\text{NiL}_2\text{X}_2]$ ($\text{L} = \text{PR}_3, \text{AsR}_3, \text{OPR}_3, \text{OAsR}_3$) type of complexes which were the earliest legitimate examples of tetrahedral Ni(II)^[18]. The justification behind the ease of formation and the relative abundances of the above mentioned stereo chemical variations among Ni(II) complexes is that the CFSEs of the d^8 configuration support an octahedral geometry and actually go against a tetrahedral stereo chemistry. The square-planar geometry on the other hand accommodates of all 8d electrons in 4 lower orbitals, rendering the uppermost (dx^2-y^2) orbital unoccupied. This kind of situation is not possible in either the octahedral or tetrahedral stereo chemical environments. When the ligand field is strong, splitting of the d orbitals occurs and the energy required for pairing-up two electrons, which is mandatory for square-planar geometry being energetically more favorable than to form tetrahedral and six coordinated octahedral geometries. Thus, nickel prefers to form square-planar $[\text{Ni}(\text{CN})_4]^{2-}$ with more strong field ligands like cyanide (CN^-) rather than the tetrahedral isomer or the octahedral $[\text{Ni}(\text{CN})_6]^{4-}$. Also, there are many complexes of the type $[\text{NiL}_2\text{X}_2]$, which are planar, where low-symmetry crystal fields are undoubtedly possible. It includes examples of tetrahedral complexes as well. Obviously several factors inter play to finally determine the exact stereochemistry of a specific complex. Proper balancing of electronic and steric factors is required. It can be demonstrated appropriately

by a series of nickel complexes $[\text{Ni}(\text{PR}_3)_2\text{X}_2]$ ($\text{X} = \text{Cl}, \text{Br}, \text{I}$). The planar diamagnetic type of complexes occur when $\text{R} = \text{alkyl}$, $\text{X} = \text{I}$, whereas tetrahedral paramagnetic type of complexes are formed when by $\text{R} = \text{aryl}$, $\text{X} = \text{Cl}$. On the contrary, when mixed alkyl aryl phosphines are used during synthesis, conformational isomerism may take place. As an example of this, the geometry and magnetic property of $[\text{NiBr}_2(\text{PEtPh}_2)_2]$ can be illustrated here. $[\text{NiBr}_2(\text{PEtPh}_2)_2]$ can be obtained as a green colored complex with $\mu = 3.20 \text{ BM}$ magnetic moment and a tetrahedral geometry as well in a brown colored form with planar geometry which on the other hand is brown coloured. These complexes with variable stereochemical configuration can be characterized by their differing magnetic moment values and spectroscopic properties. But, the conventional guidelines of color and magnetism which holds that square planar complexes are red to yellow in color and diamagnetic in nature whereas the complexes with tetrahedral orientation in space, are green to blue colored and paramagnetic, cannot be treated as the universal truth. According to the traditional guidelines, paramagnetic octahedral $[\text{Ni}(\text{NO}_2)_6]^{4-}$ should exist in green to blue color whilst diamagnetic square planar $[\text{NiI}_2(\text{quinoline})_2]$ should be red or yellow colored. But contrary to this belief, they are brownish red and greenish in color respectively. Moreover, complexes, $[\text{Bu}'_2\text{P}(\mu\text{-O}, \mu\text{-NR})\text{Ni}(\mu\text{-O}, \mu\text{-NR})\text{PBu}'_2]$ ($\text{R} = \text{Pri}$, cyclohexyl) can exist in both tetrahedral and square planar geometries and both are found to be paramagnetic^[19] though paramagnetic square planar complex is not seen in usual. Most probably the very suitably small separation between the energy levels of $d_{x^2-y^2}$ and d_{xy} orbitals permits both of these to be singly occupied with the electrons. All the electronic arrangements have been illustrated in the following figure.(Fig 1.13)^[19]

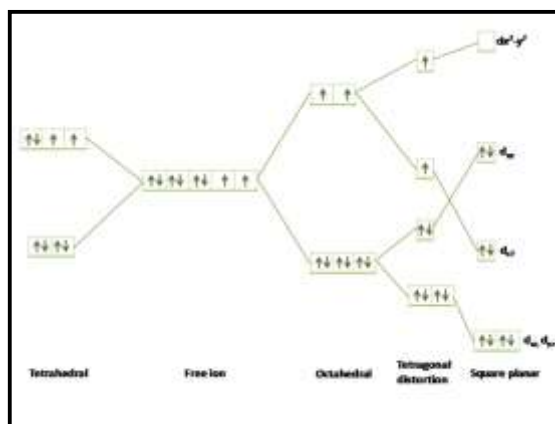
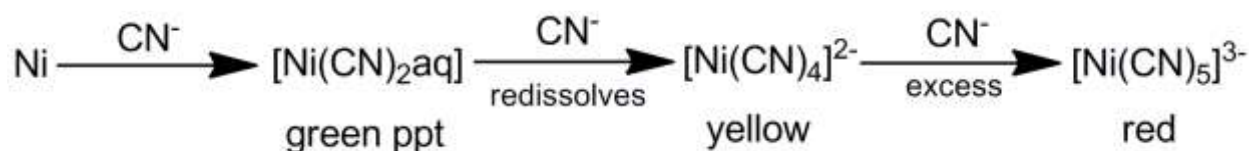


Fig 1.13 : Energy level splitting of Ni(II) complexes^[19]

The facile interconversion between two stereochemistries occurs satisfactorily. There is no evidence behind the existence of the hexacyano complex of Ni(II), rather a square pyramidal pentacyano complex is known to exist along with the well known square-planar tetracyano complex $[\text{Ni}(\text{CN})_4]^{2-}$.



The unique crystalline complex $[\text{Cr}(\text{en})_3][\text{Ni}(\text{CN})_5] \cdot 1\frac{1}{2}\text{H}_2\text{O}$ is found to comprise of both the trigonal bipyramidal and square pyramidal anions. Both are deviated from proper D_{3h} or C_{4v} symmetry. (Fig 1.14)^[11]

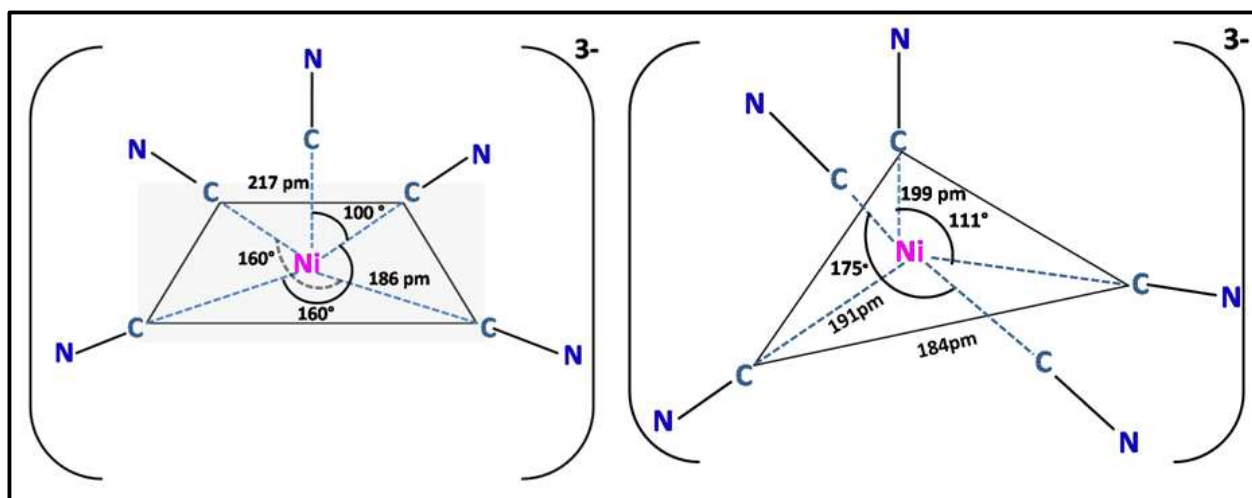


Fig 1.14 : Two geometries of $[\text{Cr}(\text{en})_3][\text{Ni}(\text{CN})_5] \cdot 1\frac{1}{2}\text{H}_2\text{O}$ ion^[11]

1.3.2 Electronic spectra and magnetic properties of nickel(II) complexes

Nickel(II) complexes have d^8 configuration. Its magnetic and spectroscopic properties are very predictable. Three spin-allowed transitions are predicted to occur as a cubic field is produced as the result of splitting of free-ion, a ground term ($3F$) and a higher $3P$ term occurs. The splitting pattern is similar to that of the d^3 ion in an identical octahedral field. The energy level diagram

helps us understand the spectra better. The electronic spectra of Ni(II) in octahedral field majorly gives three transitions which has been pictorially shown in the following fig.(Fig 1.15)^[11]

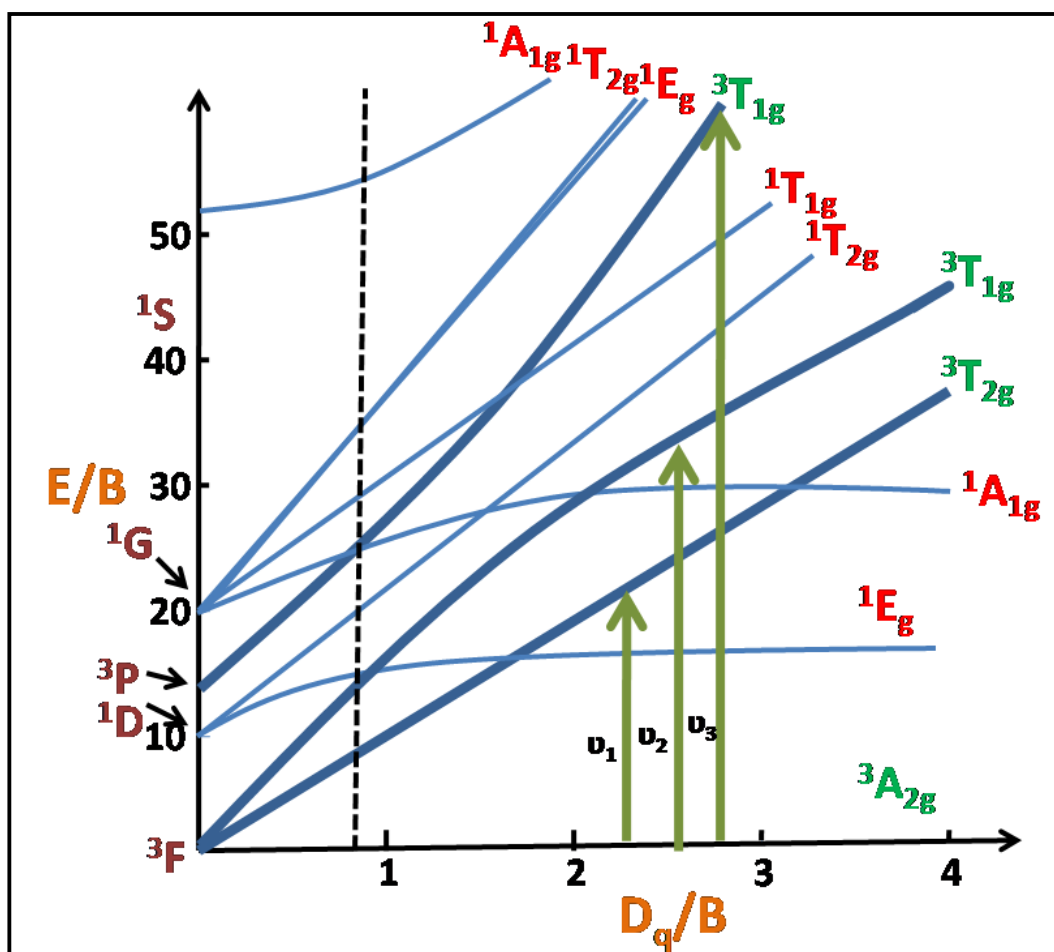


Fig 1.15 : Predicted transitions of Ni(II) system in O_h field^[11]

The magnitude of $10D_q$ can be derived from v_1 . Spin-forbidden transitions of weaker intensity are observed quite frequently these cases. For instance, the absorption spectra of complexes like $[\text{Ni}(\text{H}_2\text{O})_6]^{2+}$ and $[\text{Ni}(\text{dmsO})_6]^{2+}$ show that v_2 bands, on the other hand, has a strong shoulder along with the main absorption peak. The presence of such a shoulder is caused by the transition to the spin singlet 1E_g , which is in close proximity to the 1E_g and $^3T_{1g}(F)$ terms. The splitting of the ground term for d^8 system in tetrahedral field is exactly the reverse of the splitting observed in an octahedral field. Here $^3T_1(F)$ is lowest energy term. Here, three comparatively intense bands can be expected. These bands owe their origin to the following transitions:

$$V_1 = ^3T_2(F) \leftarrow ^3T_1(F); V_2 = ^3A_2(F) \leftarrow ^3T_1(F); V_3 = ^3T_1(P) \leftarrow ^3T_1(F)$$

The T ground term borne out of the presence of a metal ion in tetrahedral geometry generally contributes to the magnetic moment (temperature-dependent orbital contribution). No such contribution towards the magnetic moment is found from A ground term in an octahedral ligand field. But due to the mixing of the excited $3T_{2g}(F)$ with $3A_{2g}(F)$, the overall magnetic moment may be higher.

$$\mu_e = \mu_{\text{spin-only}} (1 - 4\lambda/10Dq)$$

Here $\mu_{\text{spin-only}} = 2.83$ BM and $\lambda = -315 \text{ cm}^{-1}$. It is found in most cases that the magnetic moments of tetrahedral complexes of nickel(II) generally lie between 3.2-4.1 BM. Usually the magnetic moment in tetrahedral geometry depends on temperature, and often it is reduced to its $\mu_{\text{spin-only}}$ value by delocalization of electron within the ligands or by distortions of the perfect tetrahedral geometry. Generally the magnetic moment the Ni(II) complexes with octahedral geometry are in the range of 2.9-3.3 BM.

The moderately strong band in the yellow to blue region (*i.e.* 600-450 nm) is quite helpful for the complete characterization of the spectra of square-planar d^8 complexes. This band causes the red color of the complex. Due to the prevalence of π -bonding and charge transfer transition, a simple and direct application of CFT becomes inappropriate and therefore absolutely accurate assignments may be difficult.

1.4 Copper in alcohol oxidation: A perspective of Schiff base copper complex

Oxidation of primary and secondary alcohols to the corresponding carbonyl compounds is of great importance due to its widespread utility as precursors in industrial organic chemistry majorly in drug, vitamin and fragrance industries. Old techniques used stoichiometrically measured amounts of inorganic oxidants, such as manganese dioxide, chromium(VI) etc, which are pretty toxic and produce a number of by-products. Such catalytic systems involved enormously high cost and it involved constant use of hazardous materials, harsh reaction conditions, difficulties in operation. Production of undesirable wastes along with the actual product was an issue that could not be handled well. The process has become much simpler now owing to newer methods. Many catalysts are strategically used nowadays to oxidize alcohols. Peroxide or dioxygen are nowadays used as superior oxidants and these in conjunction with transition metal based catalytic systems provide good results^[20]. The reaction involved is shown in the following figure. **(Fig 1.16)**

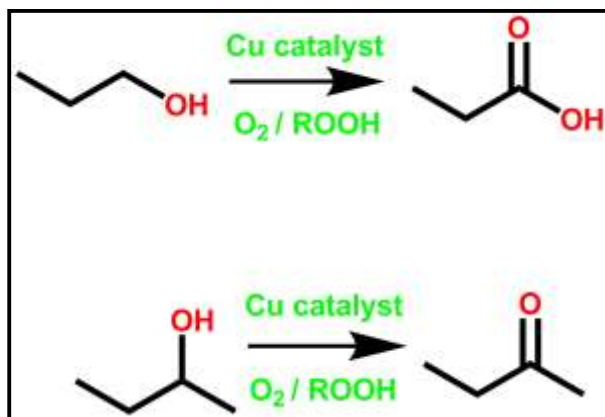


Fig 1.16 : The catalytic reaction of alcohol oxidation^[20]

Peroxidative oxidations of alcohols typically involve early transition elements in high-oxidation states and the active oxidative species is the peroxo metal intermediate. The reactions involving aerobic oxidations, on the other hand, involve an oxidative dehydrogenation and is typically catalyzed by late-transition elements. There is a high demand for producing economical and less hazardous catalysts, oxidants and solvents which can react under mild conditions. Cu-containing compounds have a high potential in this respect. In fact, copper is cheap and easily acquirable. It is present in the active sites of a large array of metalloproteins, particularly in enzymes found in nature (e.g., particulate methane monooxygenase, galactose oxidase, hemocyanin, cytochrome c, catechol oxidase, laccases or superoxide dismutase). Copper complexes, in combination with 2,2,6,6-tetramethylpiperidine-1-oxyl radical (TEMPO), is very effective in the oxidation reactions without forming a lot of undesirable side products. These catalytic systems are mostly considered the biomimetic functional model of the galactose oxidase enzyme (which we discussed a bit earlier)^[21]. Extensive research to mimic the active sites of this enzyme has been carried out, leading to a variety of Cu/TEMPO catalytic systems being repeatedly reported over the last few years. Galactose oxidase (GO) has an active site that includes a tyrosyl radical coordinated to a copper(II) and the metal center and the radical is believed to work in beautiful synergy to carry out the oxidation processes. The metal-radical unit in these systems is much more than just an association, and the advantage of such an arrangement is that hydrogen abstraction from a C–H bond by radicals is thermodynamically favored process over a hydrogen atom transfer to an inorganic metal-based oxidant (the thermodynamic affinity of a tyrosyl radical for a hydrogen atom is high). The tyrosyl radical

abstracts the hydrogen atom while the metal ion takes part in electron transfer. GO is a highly structured enzyme :its active site is unusually featured ; comprising of post-translationally modified amino acids and π -stacked residue. Its structure is particularly challenging for scientists. Chemists adopt a biomimetic approach to elucidate the morphology, which includes designing of molecules similar in structure to the active site of the enzyme and hence can mimic the functions of the enzyme^[22]. Trials for the development of mimics of GO began in 1996, and since then significant progress has been made in this respect. The structure, spectral properties, and even reactivity has been studied extensively, at least efforts have been made. Two reviews reporting the first-generation models of the active CuII-phenoxyl as well as the inactive CuII-phenolate forms of the GO active site^[23] initially appeared in the literature in 2000^[24]. Several complexes involving phenoxyl moieties coordinated to divalent metal ions other than copper, and in fact trivalent metalions, have also been synthesized successfully. Many of these have been described by Wiegardt et al., and were reviewed in 2001. These studies provided insights into the properties of coordinated phenoxyl radicals^[25]. The most important aspects of GO chemistry have being recently explored^[26]. Galactose oxidase is an extracellular type II mononuclear copper protein (68 kDa) originating from fungus. GO catalyses the two-electron oxidation of primary alcohols majorly to their corresponding aldehydes with the subsequent reduction of molecular oxygen to hydrogen peroxide. The two-electron oxidation performed by a single copper ion is suitably aided by the involvement of another active redoxc enter, i.e the tyrosyl radical from the protein, during the catalytic cycle. The physiological role of GO is not evident, probably it is involved in producing H₂O₂forfurther use as an co-oxidant for lignin- and cellulose-degrading peroxidases and could probably also provide an antibiotic defense within the rhizosphere.

X-ray crystal structure of GO was reported about ten years ago^[27]. Its active site is constituted of a copper atom in a distorted square pyramidal geometry with Tyr495 positioned at the axial position. His581, His496, Tyr272, and an exogenous ligand (H₂O or acetate, replacing the substrate) coordinate the copper effectively in the equatorial positions during the ongoing catalytic process. The most interesting feature of this complex is the cross-linking of Tyr272 to Cys228through a thio ether bond , *ortho* of the OH group, which is believed to lower the tyrosyl/tyrosine redox potential. The indole ring of Trp290 is π -stacked withTyr272 and is believed to control the general access to the active site and is also capable of shielding the Cys-

Tyr cofactor from exposure to the solvent. The enzyme structure has been elucidated in the following diagram.^[28](**Fig 1.17**)

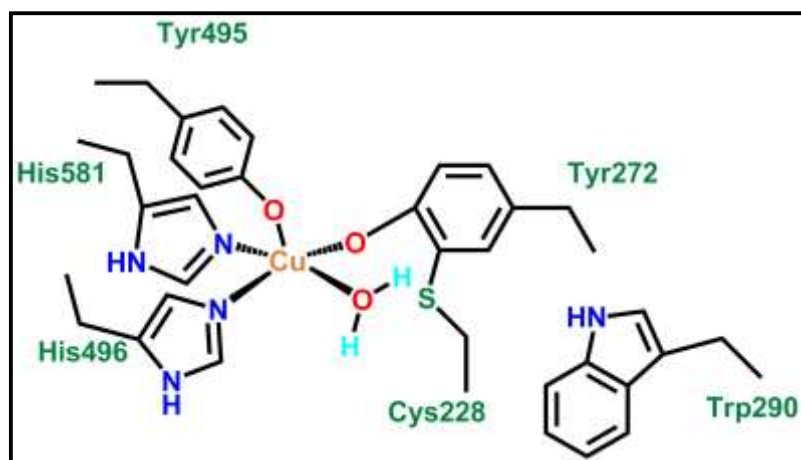


Fig 1.17 : Galactose oxidase structure^[28]

The enzyme can exist in three well-defined oxidation levels: the oxidized one, intermediate and reduced form(**Fig 1.18**)^[29]. Only the former and latter forms actively take part in catalysis. The CuII/CuI redox couple is expected to be at -0.24 V vs. Fc^+/Fc at pH 7, while the tyrosyl/tyrosinateone at 0.01 V vs. Fc^+/Fc . The CuII tyrosyl radical and the copper(I) form undergo a rapid comproportionation that renders the CuII-tyrosinate form inactive^[30].

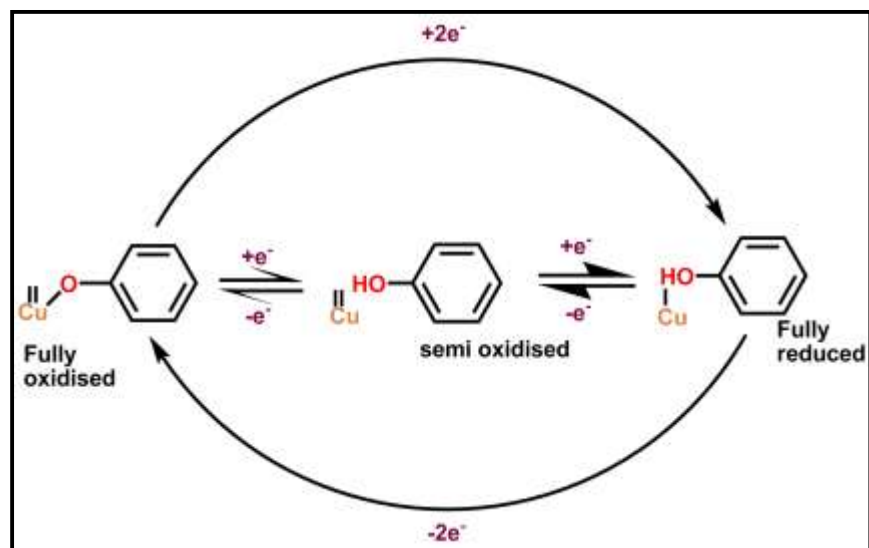


Fig 1.18 : Various forms of the GO enzyme^[29b]

Spectroscopic properties of the copper tyrosinate form are typical of a mononuclear copper(II) complexes, on the other hand, the reduced form is EPR-silent and colorless. Spectroscopic studies on the oxidized form have shown that the radical is mainly held in place by the equatorially bound Tyr272 residue. Strong antiferromagnetic coupling occurs between the tyrosyl radical and the paramagnetic copper(II) ion resulting in a diamagnetic ground state with a splitting greater than 200 cm^{-1} . GO exhibits an exceptionally intense absorption spectrum with bands at 445 and 800 nm which can be designated to $\pi\text{-}\pi^*$ transitions of the tyrosyl radical. The enzyme is more or less stable in this form, with a half life ($t_{1/2}$) of 7.2 days. Catalysis by GO follows a ping-pong turnover manner. In the first step, the alcohol substrate binds to the oxidized CuII-radical active site and reduces both the redox centers namely tyrosyl radical and copper(II) ion, and the aldehyde product is released. This aldehyde product having a low affinity for the complex, is consequently released into the medium. In the successive step, the CuI-tyrosine site binds O_2 and reduces it to H_2O_2 , and the initial CuII-tyrosyl radical is invariably regenerated. A proposed catalytic mechanism is shown^[31]. **(Fig 1.19)**

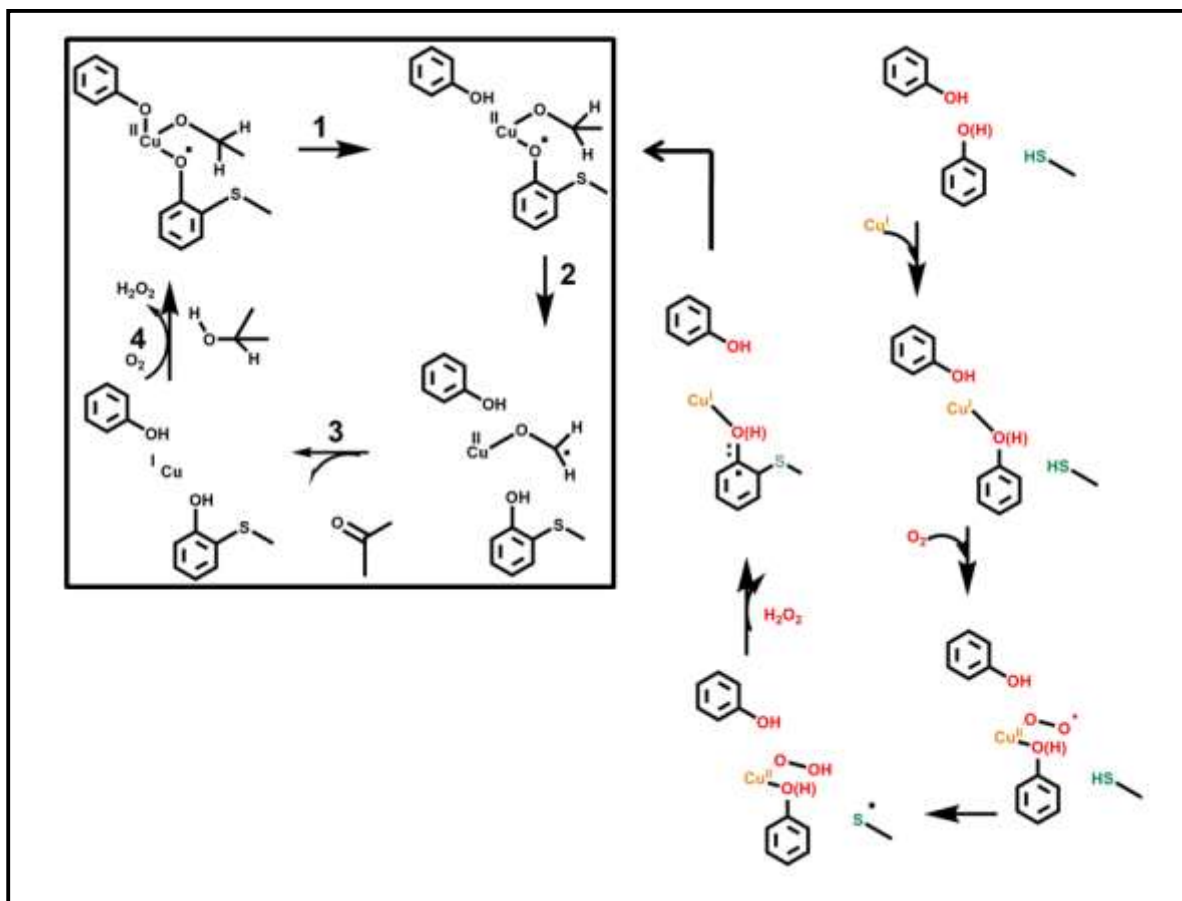


Fig 1.19 : Catalytic cyclic involved in the use of GO type enzyme^[31c]

The catalysis is initiated by a weak association with the substrate. The structure of GO comprises of a shallow channel through which the substrate remains in a bound state by Phe194, Phe464, Arg330, and Trp290 to finally reach the catalytic site. Reaction over a wide concentration range shows that the enzyme gets saturated at a point, a dissociation constant of 71 mM is observed for the initial complex with D-galactose. This denotes a fairly low affinity, which presumably results from a pretty unselective active site. In contrast, the enzyme is such that it locks the orientation of the active site in such a manner, thereby rendering a stereospecific abstraction of the pro-*S* hydrogen by the nearby tyrosyl radical. Modeling studies on galactose coordinated to the copper(II) ion of the native enzyme shows that the pro- α -*S*-hydrogen is located at a hydrogen-bonding distance from Tyr272 (ca. 2.5 Å), while the pro-*R* hydrogen is farther away. After binding of the substrate to the copper equatorial position, the first step is a proton transfer^[32]. Deprotonation of the alcohol is facilitated by copper coordination and a short H-OTyr495 bond is established^[33]. This process occurs with a very low barrier, that is almost spontaneously, due to

the favourable condition of forming a hydrogen bonded structure due to the very close values of tyrosine pK_a and pK_a of the coordinated alcohol. The first step paves the path of two processes: the CuII–substrate bond gains strength and the C–H bond energy of the deprotonated substrate is lowered. The second step is a hydrogen-atom transfer from the alkoxides substrate to the equatorial Tyr272 radical. The second step is the major rate-limiting step (at high oxygen concentrations) as indicated by the high value of kinetic isotope effect (KIE) of 7.7 for D-galactose. GO gets fully oxidized during the process. The unusually large KIE of 22 as well as the temperature dependence of the KIE point to the fact that the tunneling of a hydrogen atom in the rate-limiting step. The activation energy for hydrogen abstraction step has been calculated to be around $13.6 \text{ kcal mol}^{-1}$. Optimization of the transition state structure can be done with B3LYP calculations. It has a five membered cyclic structure in which the O–H bond length is 1.24 \AA while the C–H bond length is about 1.36 \AA . The hydrogen atom is then efficiently transferred to the phenol ring plane, rendering an overall π character to the radical. A short-lived ketyl radical anion results from the H abstraction step which in turn reduces the metal center by donating a single electron and is subsequently released to allow O₂ binding. Kinetic studies with the steady-state rate data for the oxidation of benzyl alcohol derivatives have shown that the three consecutive steps, namely proton transfer, single electron transfer, and hydrogen-atom abstraction, are asynchronous components of the entire catalytic cycle rather than being distinct kinetic intermediates. The nitro derivatives which are classically difficult to oxidize, as well as pyranosides and even physiological substrates exhibit a large KIE. C–H bond cleavage (hydrogen-atom abstraction) is essentially the rate limiting step in the case of all these substrates^[34]. On the other hand, the easier-to-oxidize methoxybenzyl alcohols exhibit a smaller KIE, thus lowering the contribution of the proton transfer step to the formation of the transition state and rather enhancing the role of the single electron transfer for the substrate oxidation. The re-oxidation step of GO (step 4) is an example of two-electron redox process catalyzed by dioxygen. Kinetic data have shown that the re-oxygenation step occurs with a rate constant of around $8 \times 10^6 \text{ M}^{-1} \text{ s}^{-1}$ at 277 K. The unstable nature of the oxygenated complex makes its formation unstable, in spite of its pivotal role. GO is a secretory protein, hence to attain maturity many steps are required: cleavage of a signal sequence that directs translocation, metal binding, and cofactor processing. The structure of a metal-free pre-form of the protein has been obtained recently. Cys-Tyr cross-link is missing in the active site, and Cys228 is oxidized into sulfenic

acid. The conversion of this pre-form into the catalytically active form occurs in a self processed manner utilising only copper and O₂. Both the +1 and +2 oxidation states of copper induce cross-linking and radical cofactor formation, but with very different time scales for the two oxidation states. The CuI-dependent path resembles the physiological conditions more. Initially copper(I) is believed to bind to the pre-form to roughly form a trigonal copper(I) complex that reacts with O₂, has been proposed recently. The species that is finally formed is a reactive CuII-O₂'- compound that abstracts hydrogen atom from Cys228 and releases a reasonable amount H₂O₂. The thiyl radical then attacks the ε-C ring carbon of Tyr272, and then again rearomatization occurs by proton and electron transfer to the metal center. Finally, the fully reduced form of GO is achieved which spontaneously undergoes oxidation by O₂ to give the catalytically potent CuII-tyrosyl radical form of the enzyme and H₂O₂ alongside.

1.4.1 Model Compounds for the GO Active Site

Chemists have tried to mimic the CuII-phenoxy radical of the active site to give GO like properties. This is strategically done by blocking the *ortho* and *para* positions of the phenol to increase steric protection as well as resonance, to make the whole system stay longer in solution. The phenoxy radicals are richly colored giving absorption bands around 400 and 450 nm and above 600 nm that has been assigned to π - π^* transitions^[35]. Such modified phenol ligands are being synthesized by coordination chemists, which can possibly behave structurally and functionally as GO. A wide number of copper(II) salen compounds have been described which serves the purpose.

Nobumasa Kitajima and coworkers developed a few copper(II) salen complexes^[36] (**Fig 1.20**) which were employed in the catalysis of EtOH.

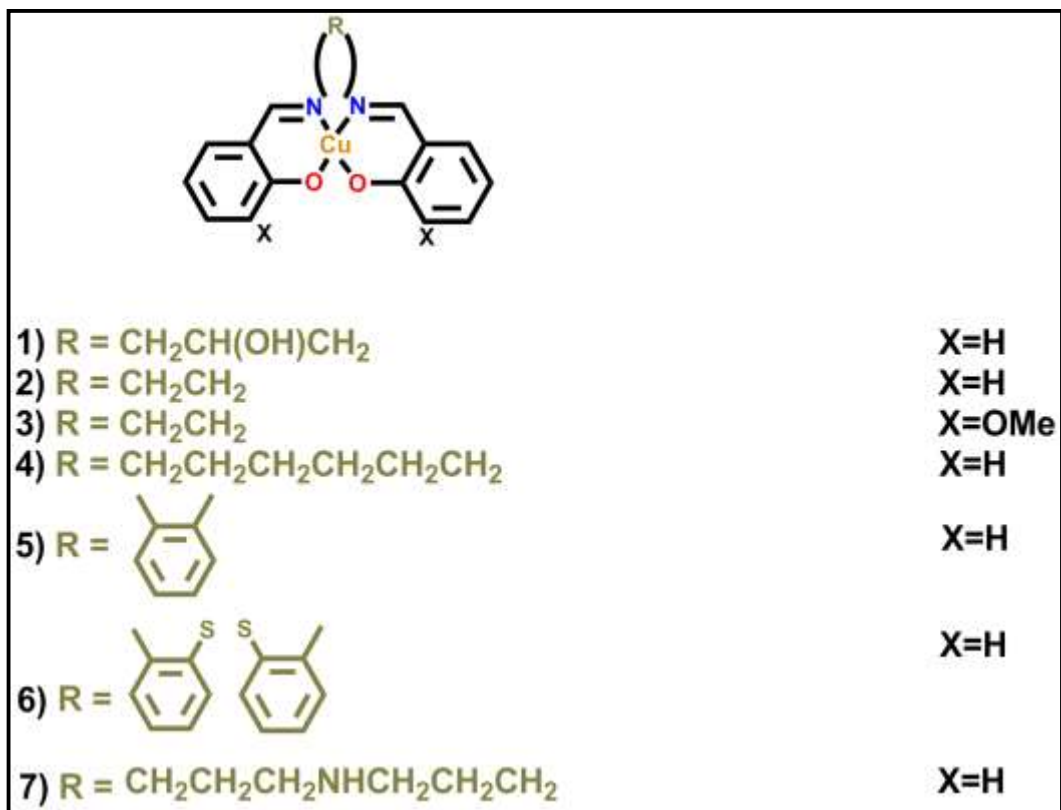


Fig 1.20 : Copper salen complexes^[36]

In the presence of additive KOH, complex 1 showed considerable catalytic activity under 1 atm O_2 for 10 h at 40°C . Acetaldehyde was formed as the major product. Propionaldehyde and pyruvic aldehyde were formed with propanol and hydroxyl acetone, respectively. Complex (1) in DMF gives an electronic spectrum with two absorption bands at 370 and 611 nm which is in close agreement with the behavior of galactose oxidase, yielding bands at 445, 630 and 775 nm. Even the ESR spectrum of both are in close similarity. The structure of the active complex is a copper complex in a distorted square planar geometry. The structure is given in the following figure. (Fig 1.21)

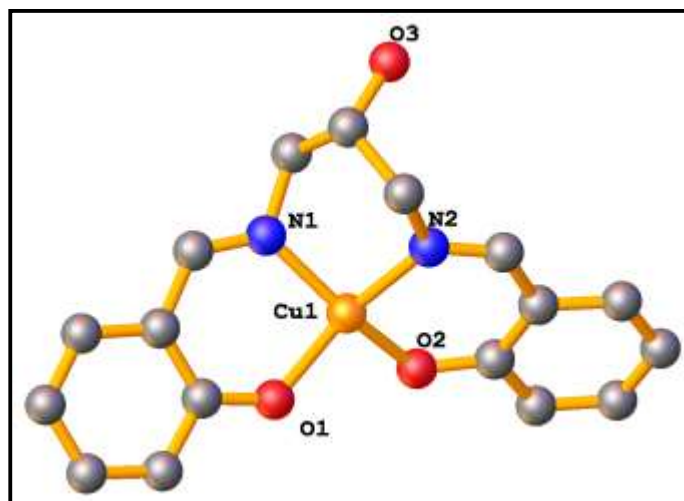


Fig 1.21 : Perspective view of complex 1^[36]

T.D.P Stack and coworkers presented galactose oxidase model complexes having most of the unique properties of GO^[37] (Fig 1.22). The species were EPR silent produced via one electron oxidation of Cu(II) and the complexes yielded aldehyde with primary alcohols which is a characteristic property of GO.

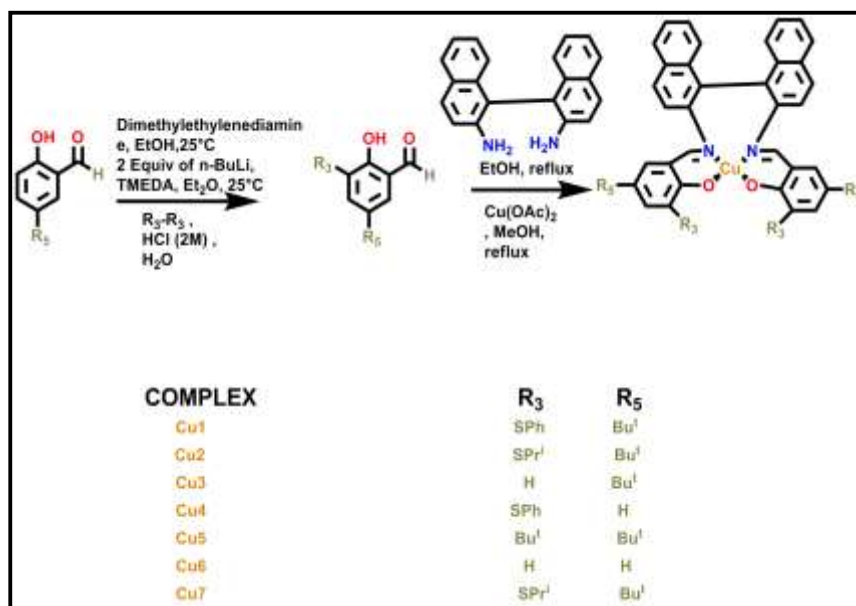


Fig 1.22 : GO mimicking Cu(II) complexes.^[37]

They found the crystal structure as well. The crystal structure of Cu(II) complex is a monomeric, four-coordinate, distorted square planar structure(Fig 1.23).

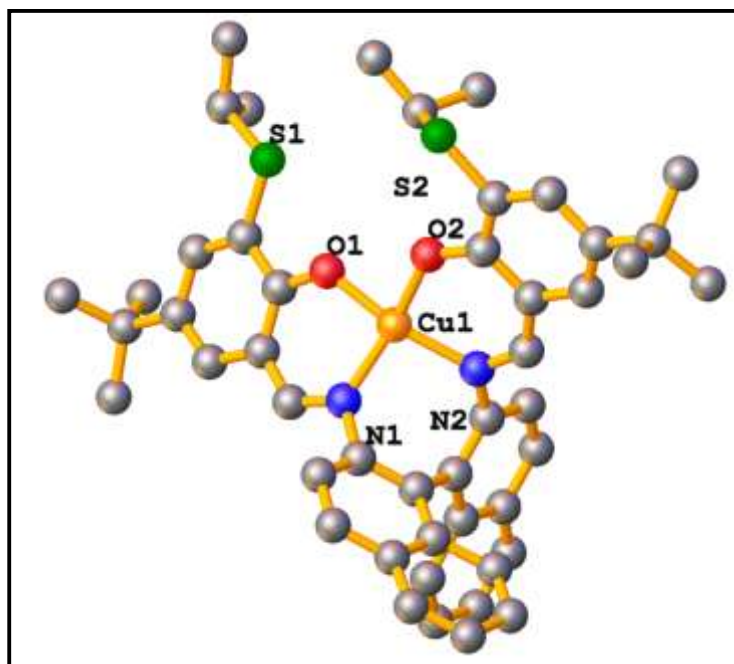


Fig 1.23 : A perspective view of Cu(II) monomeric complex^[37]

The binaphthyl backbone renders a tetragonal distortion. This distortion is not because of the steric strain between the SP^i groups, as the unsubstituted complex also gives similar distortion. The latter complex is shown in Fig 1.24.

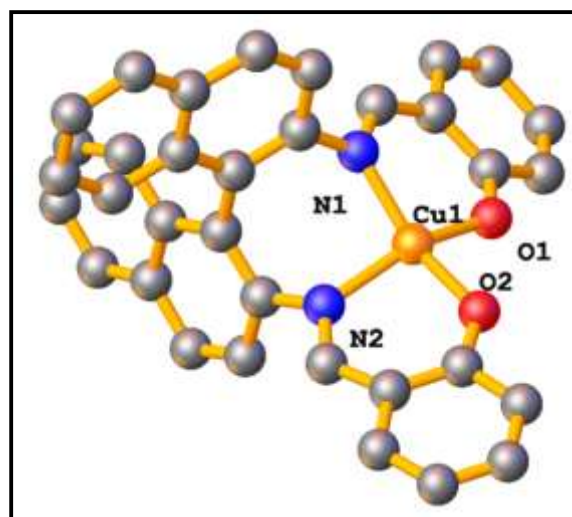


Fig 1.24 : A perspective view of unsubstituted Cu(II) complex^[37]

The EPR spectra of the complexes are similar to that of GO. The EPR data has been summarized below (**Table 1.1**):

COMPLEX	g_{parallel}	$g_{\text{perpendicular}}$	$A_{\text{parallel}}(\text{G})$	$A_{\text{perpendicular}}(\text{G})$	EPR signal quenched by oxd.
1	2.191	1.994	183.7	17.2	yes
2	2.145	1.959	192.8	12.8	yes
3	2.241	2.012	167.1	12.4	no
4	2.163	1.975	193.6	12.8	no
5	2.215	2.047	173	14	yes
7	2.354	2.042	193.0	32.1	yes

Table 1.1 : EPR data of the copper complexes^[37]

Addition of the oxidant tris(4-bromophenyl)aminium hexachloroantimonate, (TPA⁺) at -40 °C gave varied results. EPR signals of the complexes with 3,5-disubstituted salicylates are fully quenched, while for the other complexes, the signals are greatly altered. The ability to oxidatively quench the Cu(II) EPR signals at par with the oxidase activity towards benzyl alcohol. The cyclic voltammetry data are given in **Table 1.2**.

COMPLEX1	COMPLEX2	COMPLEX3	COMPLEX4	COMPLEX5	COMPLEX6
1.00	0.92	1.08	1.00	1.08	1.10

Table 1.2 : Cyclic voltammetry data of Cu(II)^[37]

Variation of structural features of the complexes reveals that certain fixed properties of the ligand are required for the GO like activity like a nonsquare planar arrangement and 3,5-substitution of the salicylate ring. These generate of a stable EPR silent species by one-electron oxidation of the Cu(II) complexes. The experiments indicate that the oxidized forms must accept two electrons to successfully oxidize an alcohol to an aldehyde which is similar to that of GOase. Thomas and coworkers described salen copper complexes (1 and 2)^[38] (**Fig 1.25-1.26**)

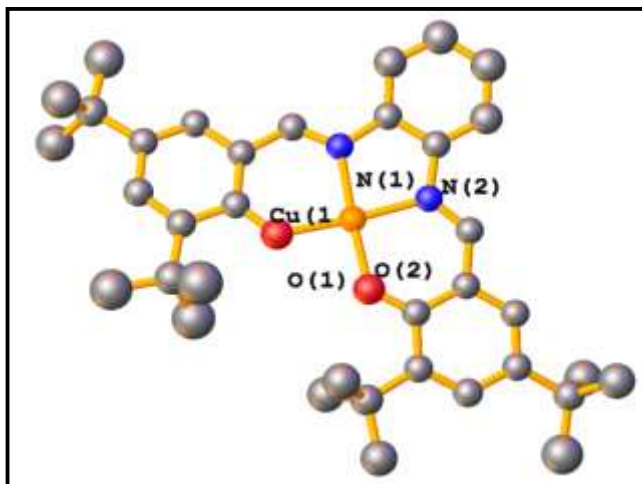


Fig 1.25 : A perspective view of Cu(II) 1 salen complex^[38]

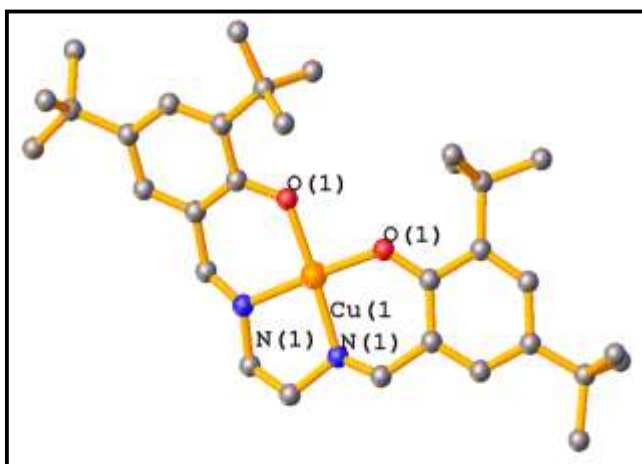


Fig 1.26 : A perspective view of Cu(II) 2 salen complex^[38]

The geometry around the copper atom in the first complex (complex 1) is a distorted square planar, the metal ion is coordinated to two imine nitrogens (N1, N2) and two phenolate oxygens (O1, O2), quite similar to the case of galactose oxidase. The bond lengths Cu–O1 and Cu–O2 are shorter than the Cu–N1 and Cu–N2 . The angles O1–Cu–O2, O1–Cu–N1, O2–Cu–N2 and N1–Cu–N2 differ only slightly from 90°, while the O1–Cu1–N2 and O2–Cu1–N1 angles are 175.6(7)° and 176.9(6)°(pretty close to 180).

In the second complex, the two halves of the complex (complex 2) [CuII(L3)] have a twofold axis of symmetry running through the middle. The coordination polyhedron N₂O₂Cu is a distorted square planar again, with a dihedral angle between the two O–Cu–N planes of similar magnitude as the first complex.

The absorbance spectrum of the complexes are similar, exhibiting intense absorption peak at around 400 to 450 nm owing to CT transitions and weaker d–d transitions at around 550 nm.

The EPR spectra of the copper(II) complexes in CH₂Cl₂ (+ 0.1 M TBAP) at 100 K show axial symmetry, with copper hyperfine structure. A superhyperfine (shf) structure occurs in the perpendicular region of the spectra, which is a consequence of the interaction of the electronic spin with two equivalent nitrogen nuclear spins. EPR spectra of the first complex also shows interaction with the distant hydrogen nuclear spins. The values suggest a nearly square planar arrangement which is in agreement with the XRD data. The EPR data has been illustrated in the following table(**Table 1.3**)

COMPLEX	1	2
$g_1=g_2$	2.043	2.044
g_3	2.194	2.200
$A_1=A_2$	3.1	3.1
A_3	20.220.2	
g_3/A_3	9595	
A_N	1.41.4	
A_H	0.7	-

Table 1.3 : EPR data of Cu complexes 1 and 2^[38]

The CV curve of the first complex in CH₂Cl₂ (0.1 M TBAP) at 298 K, produces two well separated one-electron oxidation waves at 0.646 V and 0.830 V. CV curves of both the complexes can be attributed to the successive formation of copper(II) phenoxyl and copper(II) bis(phenoxyl) radical species.

The complete characterization of the two complexes gives clear picture of their behavior and hence how they can be biologically viable like galactose oxidase.

TDP Stack and group did another work similar to the earlier one already discussed. They have reported Cu-Schiff base systems which catalyse aerobic oxidation of primary alcohols^[39]. They have described two compounds, whose reactions with benzyl alcohol are quite relevant to the oxidizing reactions characteristic of GOase. The complexes are shown in **Fig 1.27**.

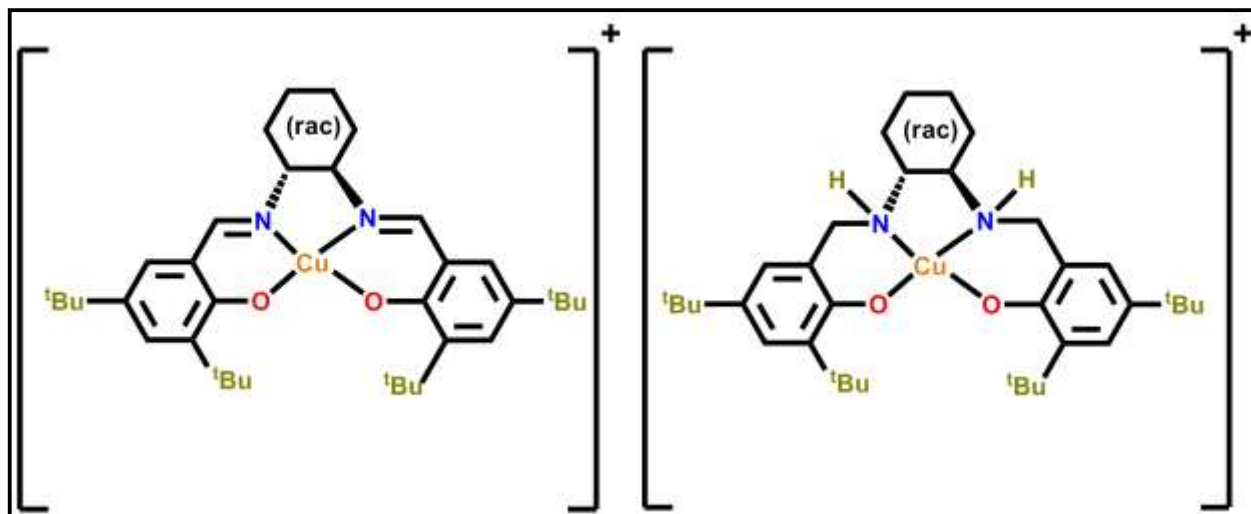


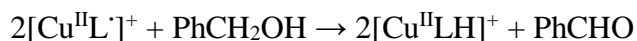
Fig 1.27 : Cu(II)-Schiff base systems^[39]

Cyclic voltammetry of the complexes show two reversible oxidations which can be attributed to the oxidation of the phenolic moieties. Treatment of the first complex with AgSbF_6 in CH_2Cl_2 gives a purple solution of SbF_6^- . Oxidation of the second complex produces a deep blue solution. Such oxidation leads attenuation of EPR signals which denotes the formation of antiferromagnetic CuII-phenoxy complexes as found in the oxidized form of GOase.

Near-infrared (NIR) spectra of both compounds were studied. The transitions are consistent with the oxidized form of GO. The stability of the complexes are strongly dependent on solvent and counterion: addition of most organic solvent leads to the decay of the first complex which is otherwise stable. The addition of anions like nitrate or chloride, reverts the complexes to their natural precursors. This group had studied that in earlier works the reactivity with benzyl alcohol used to be low under basic conditions, so they proceeded with neutral conditions.

Addition of benzyl alcohol to the complexes in CH_2Cl_2 medium induces a first-order decay process as monitored by UV-vis spectroscopy which correlates to the formation of benzaldehyde.

The following reaction stoichiometry is expected:



The first-order rate constant for the first complex does not depend on the concentration of the complex, but varies linearly with the concentration of the alcohol. But, the reaction rate depends on substrate concentration and saturates at a point as seen in the figure (**Fig 1.28**)

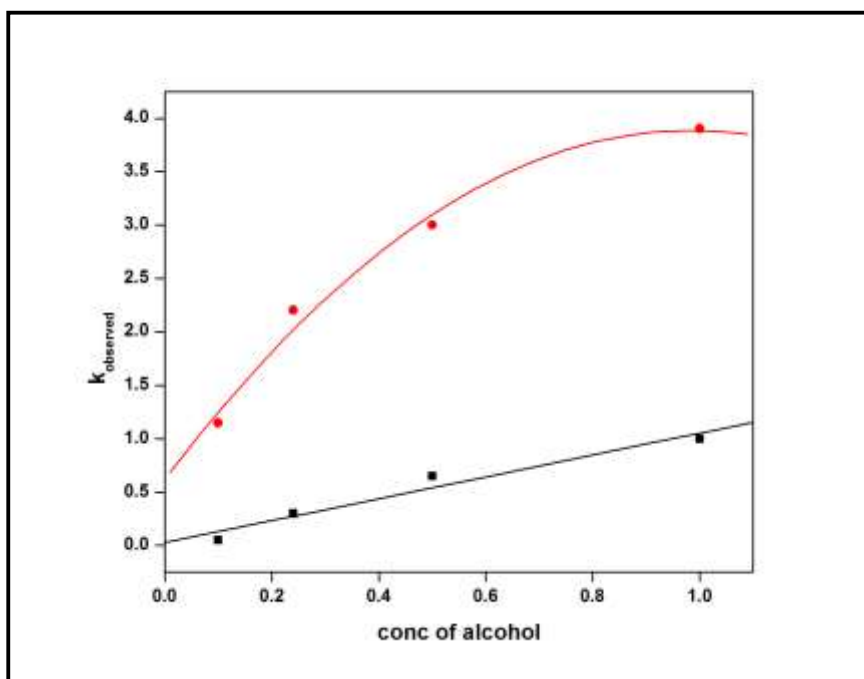


Fig 1.28 : Rate constant versus concentration plot^[39]

The second complex reacts at a much faster rate though the first one is a stronger oxidant which is probably due to the mechanistic pathway which makes the second complex more selective. The complexes were correlated well with GOase.

Thomas and group did another work which is pretty similar to the earlier work, though a bit different^[40]. They have succeeded in obtaining the radical complex $[\text{Cu}(\text{SalOMe})]^+$ as single crystals (**Fig 1.29**)

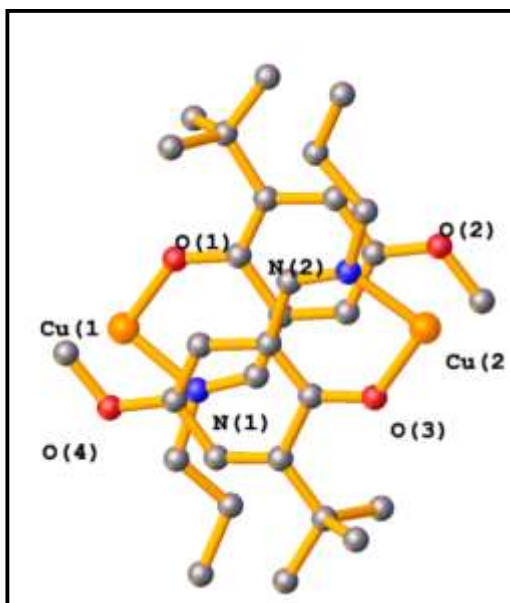
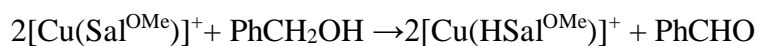


Fig 1.29 : A perspective view of $[\text{Cu}(\text{SalOMe})]^+$ radical complex^[40]

Prior to preparing the radical species, the bis(phenolate)precursor $[\text{Cu}(\text{SalOMe})]$ was structurally characterized; the copper ion has an almost square-planar geometry. Its cyclic voltammogram curve displays two which can be assigned to the formation of mono- and bis(phenoxyl) radical species. Electrochemically generated $[\text{Cu}(\text{SalOMe})]^+$ gives absorption bands about 450 nm, as well as a broad band over 1100 nm which can probably correspond to $\pi-\pi^*$ and charge-transfer transitions of phenoxyl radicals^[25]. It is X-band EPR-silent, as a consequence of magnetic coupling between the radical and metal spins. Single crystals of $[\text{Cu}(\text{SalOMe})]^+$ which studied by XRD, were obtained by oxidation of the neutral precursor with a silver salt. An interesting feature of the structure is the nonequivalence in the two Cu-O bond lengths. The C-C and C-O bond lengths within the ring which contains O1 are analogous to the phenolate moieties of $[\text{Cu}(\text{SalOMe})]$. In contrast, the bond lengths in the ring containing O2 show totally different properties. The C-C bond lengths also show variable properties throughout. These features are consistent with a quinoid structure for the ring containing the O2 atom, and hence an overall radical character of the moiety is understandable. From the structural data, the magnetic nature of the complex was speculated. DFT studies show that the ground spin state of the radical complex $[\text{Cu}(\text{SalOMe})]^+$ is presumed to be paramagnetic(S=1). The broken symmetry DFT calculations suggest a strong ferromagnetic interaction between the metal and the radical. The reactivity of the complex was studied under single-turnover conditions with the benzyl alcohol as substrate.

[Cu(SalOMe)]⁺ is generally stable at 300 K in CH₂Cl₂ but it quickly decomposes in the presence of benzyl alcohol. Reduction of the phenoxyl moiety by benzyl alcohol is proven by the disappearance of the radical band in the UV-Vis spectrum and the enhancement in the rate constant of the reaction as the alcohol concentration increases. The plot of the rate constant as a function of the benzyl alcohol concentration rendered a straight line from which the second-order rate constant was derived. No saturation is achieved at high benzyl alcohol concentrations, which indirectly shows that the affinity of the substrate for [Cu(SalOMe)]⁺ is low, as similarly observed in the case of GO. Analysis of the product by gas chromatography showed that benzaldehyde was formed as the major product.



There are several types of other complexes of particularly Cu, which catalyse the reaction of alcohols to corresponding aldehyde under homogeneous conditions. Thus, copper has drawn a lot of attention among researchers. But a lot of challenges are yet to be overcome in the field of copper-catalyzed aerobic or peroxidative alcohol oxidations with high turnover and selectivity. A lot of changes from the conventional methods can be made. This includes mild reaction conditions, low pressures of O₂, or low amounts of peroxide, lesser catalyst amount and low temperatures (more greener conditions), and the avoidance of cumbersome additives.

Peroxidative oxidations i.e. by the use of hydrogen peroxide or tert-butyl hydroperoxide oxidants, and simple methods are appreciated more. As peroxides are commercially obtained in aqueous solutions mostly, people are trying to improvise the oxidation methods in such a way that the reactions can be carried out in aqueous solvents leading to greener reaction pathways. Hydrogen peroxide is the oxidant of choice as it is easily decomposed under chemical conditions into environment friendly water and oxygen. Despite this, its decomposition renders it useless at high temperatures. Thus, tert-butyl hydroperoxide (TBHP) is used more widely. Molecular O₂ is also used as the oxidant as the end products (water and hydrogen peroxide) are environment friendly. Again, Cu centered metal complexes are favoured due to their close resemblance with a lot of natural enzymes. The low cost and the wide availability of these complexes aid the selection process. Kani and Ünver^[41] etc reported homogeneous oxidation of primary and secondary alcohols with copper complexes. Shul'pin and coworkers carried out similar oxidation with monoclear copper complex with oxidant as tert butyl hydroperoxide^[42]. Martins *et al.*^[43], Frija *et al.*^[44], did the same conversions with Cu complex in microwave assisted manner with

TBHP. Pombeiro and coworkers did aerobic TEMPO-mediated oxidation of benzyl alcohol and its derivatives^[45]. Liu *et al.* did utilize a Cu(I)/TEMPO system^[46], so did Repo and coworkers^[47]. Swarts *et al.*^[48].

1.5 Polymer-supported Schiff base copper and nickel complexes in oxidation reactions:

Polymer-supported Schiff base ligands are made with ease and loaded with different metal ions to use them conveniently. These are very useful as catalysts. A wide array of complexes could be used as homogeneous catalysts, which showed great selectivity and good turn over as well. Yet there has been a constant need for heterogeneous catalysts because of its added advantages. Difficulty in separation from the final reacted mixture has always been a difficulty which gives heterogeneous catalyst an edge because they are easily separable. To overcome these difficulties, heterogeneous catalysts are developed, either by dispersing metal ions on porous solid supports (SLPC), or by chemically binding the metal ions on functionalized polymer supports (PBC)^[49]. The second method is favoured as in that case the final catalysts can easily be separated by filtration without any hassle. Polymer supports are cross-linked resins which have a good surface area^[50], which further swelling reaction media to enhance the action of the immobilized catalysts by increasing the contact surface with the reactants^[51]. The functionalized polymer beads find application as reagents^[52], chelating agents and also as adsorbent materials^[53]. Phase transfer catalysis also uses them effectively^[54]. However, there is one major issue with these polymer supported metal catalysts. The metal ion tends to leach out of the polymer beads while the catalytic reaction is going on i.e dissociation occurs. Therefore, the leaching of metal ions from supported catalyst is a major issue and had to be addressed. This leaching could be minimalized by increasing the amount of immobilized ligand on the polymer beads or by not using coordinated solvents. Chelating ligands also reduced the dissociation process. Polystyrene is widely used to the many advantages associated with it and its cheap rate. Polymer supported catalysts are always better than silica or alumina, as the polymer chain provides a lot of flexibility for immobilization purpose. Jacobsen and co-workers had used Co(salen)^[55] (**Fig 1.30**) complexes on functionalized polystyrene for a range of chemical reactions, which proved effective in hydrolytic kinetics, resolution of racemic epoxides, and enantioselective parallel synthesis^[56].

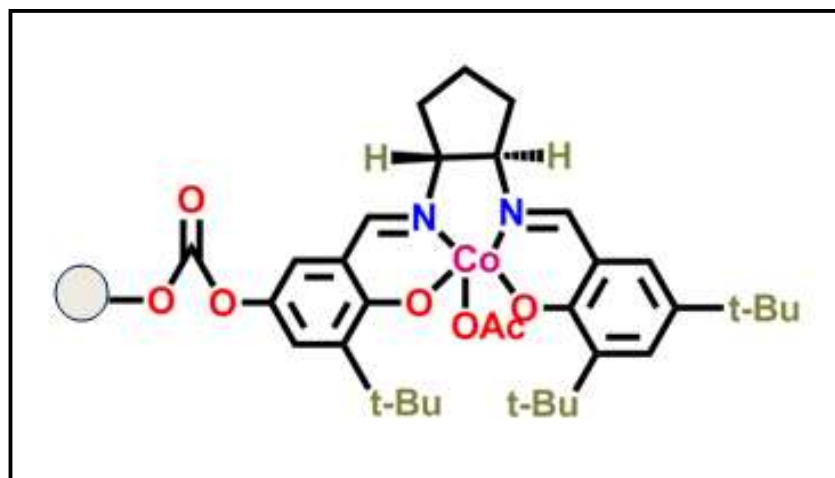


Fig 1.30 : Co salen complex^[55]

Transition metal catalysts offer miraculous results in numerous organic transformations. However, only separation remains a challenge in the case of homogeneous catalysts. The current developments in catalysis are mainly focused on immobilizing of metal complexes on functionalized solid supports as these catalysts can overcome the problems associated with homogeneous catalysts. Early transition metal compounds like Mo, Ti etc in conjunction with hydrogen peroxide or alkyl hydroperoxide prove to be very efficient in the epoxidation of alkenes. Carreiro et al. utilized boronic acid type resins as a support for Mo(VI) catalyst for epoxidation reactions^[57]. G. Grivani and group also worked on polymer-supported Mo(IV) catalysts^[58] (**Fig 1.31**)

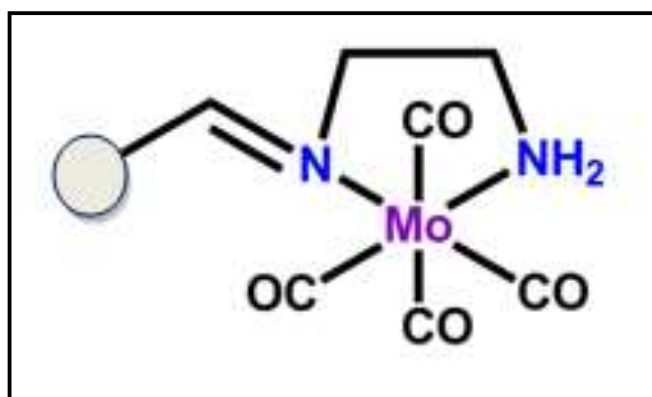


Fig 1.31 : Mo(IV) complex^[58]

Polymer-supported vanadium have also been reported. In spite of the roaring amount of research and development in this field of heterogeneous catalysts, leaching out of the metal ions from the support material still poses a trouble. Use of chelating ligand on the polymer support helps this problem. Polymer-supported ruthenium Schiff base complexes^[59] (**Fig 1.32**) showed high catalytic activities in a range of hydrogenation and oxidation reactions^[60].

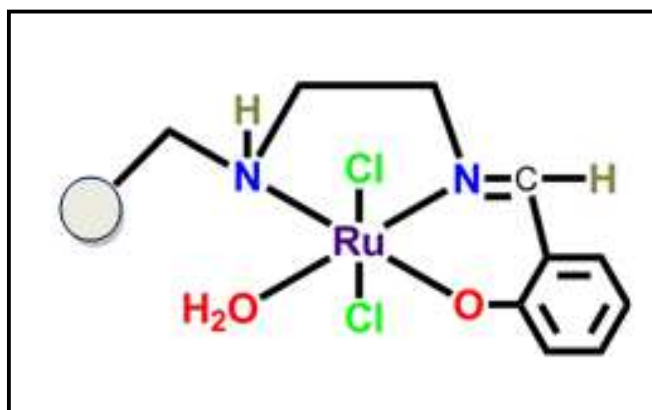
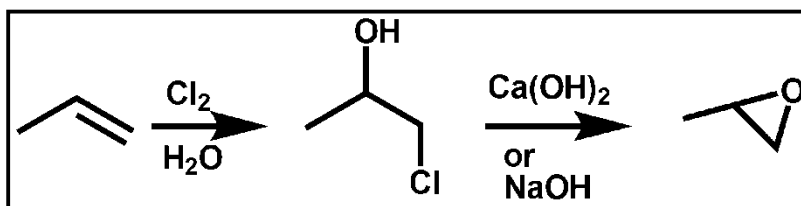


Fig 1.32 : Ru Schiff base complex^[59]

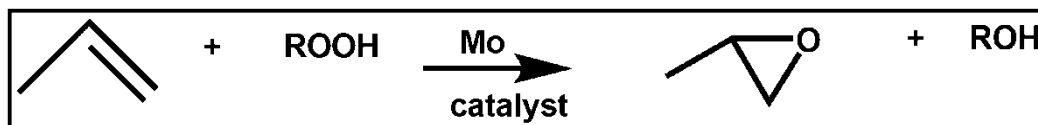
There has been reports of polymer supported vanadium chiral Schiff bases complexes which catalyze the enantioselective oxidation of sulfides to sulfoxides^[61]. The immobilization process is either through true chemical bonds or physical interactions. The polymer supported catalysts are used in various forms: (a) metal complexes anchored on polymer surfaces that coordinate with reactants during the reaction process, (b) colloidal metal ion catalysts dispersed in a polymer network which is swollen up first by imbibing the solvent, and (c) enzymes structures supported on the polymers. Environment friendly routes are always preferred. The reactivity of these supported catalysts is limited as compared to the unsupported versions, but this is increased by increasing accessibility by various means. The co-polymerization of metal containing monomers with styrene and divinyl benzene are being increasingly used. Soluble supports for the anchoring purpose have received considerable attention lately as these ensure phase homogeneity to catalyst and reactants. The recycleability of the catalyst is very important, which is being achieved by varying various reaction parameters. Oxidation is in itself an important industrial process. The transition metal catalyzed oxidation is viable in industry as well as biological systems. Polymer supported Schiff base complexes are being explored by researchers.

Epoxides, are raw materials in the synthetic pathway of chemicals such as, glycols, glycol ethers and alkanolamines and a wide range of polymers. The first commercial preparation was done by vapor-phase oxidation of ethylene with air or oxygen with the aid of an alkali metal promoted supported silver catalyst. The chlorohydrin process replaced this traditional method and was used routinely in the production of propene oxide^[62]. (Scheme 1.1)



Scheme 1.1 : Production of propene oxide^[62]

But the above process remains environmentally harmful. Therefore, epoxidation of olefins was preferred using hydrogen peroxide alone or with osmium tetroxide, manganese dioxide and tungsten and molybdenum oxides, but these process are not very viable on a large scale. Hawkins (1937) compiled the first report of metal-catalyzed epoxidation of cyclohexene using cumene hydroperoxide in conjunction with V_2O_5 , which subsequently yielded 30% of the corresponding oxide. Brill and group(1963) first reported the use of *tert*-butyl hydroperoxide (TBHP) for epoxidation. The Shell and ARCO/Halcon process is by far the most efficient in industrial scale. They utilized molybdenum catalysts for this purpose^[62] (Scheme 1.2)



Scheme 1.2 : Mo catalyst in the production of propene oxide^[62]

The most common epoxidation reagent is *meta*-chloroperoxybenzoic acid(*m*-CPBA)^[63]. As environment specialists prefer hydrogen peroxide, scientists are specially trying to utilize hydrogen peroxide on a large scale industrially though it has got its own disadvantages. Enichem gave the ideas of a synthetic pathway in which hydrogen peroxide is produced from water and methanol by utilising anthraquinone and then further epoxidation is done in the presence of titanium-substituted silicate (TS-1) as catalyst^[64]. Degussa also developed an industrial process using TS-1 catalyst and H_2O_2 as oxidant. Chirally modified lithium and magnesium *tert*-butyl

peroxide are employed in the epoxidation of electron deficient olefins, like chalcones, giving fantastic yields^[65]. Jacobsen's catalyst(**Fig 1.33**) is pretty enantioselective as well.

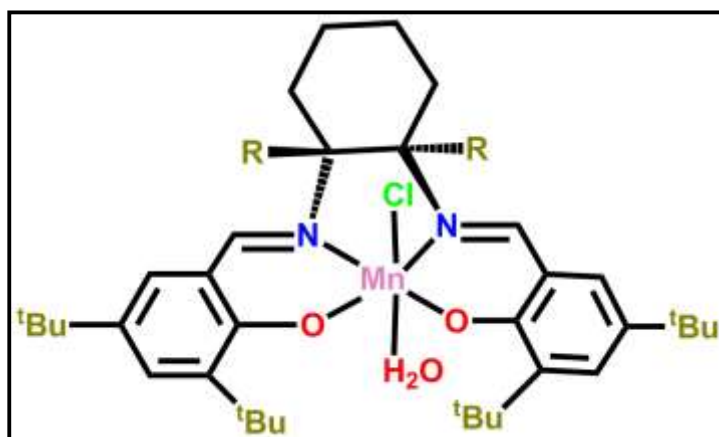
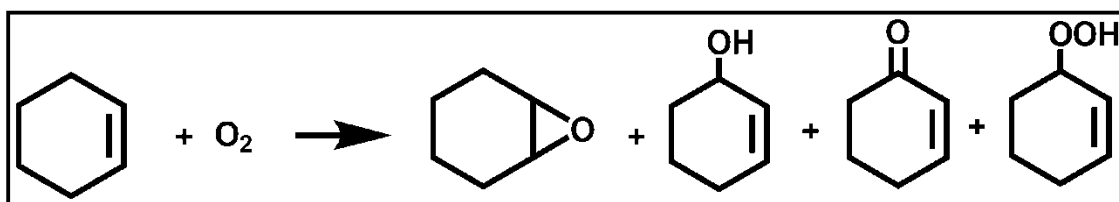


Fig 1.33 : Jacobsen catalyst^[65]

Hence we can say that in current times, polymer-supported Schiff base complexes are promising catalysts in the oxidation of alkenes.

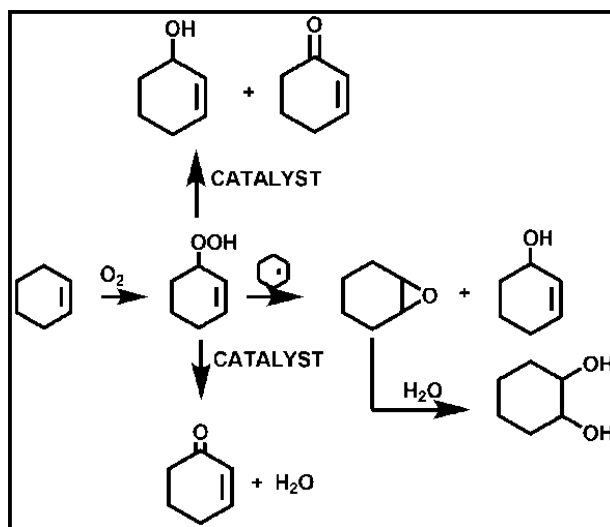
Immense effort was given in the field of science for the oxidation of cyclohexene. Conversion of cyclohexene into adipic acid with H_2O_2 as oxidant in addition with polymer-supported $\text{Na}_2\text{WO}_4 \cdot 2\text{H}_2\text{O}$ was made by Sato et al^[66]. But most of the literature gives evidence of use of harsh condition ultimately yielding poor quantity product and the selectivity also was not appreciable.

These days molecular oxygen is becoming the oxidant of choice owing to its environmental benefits. Biopolymers are being paid some attention these days. Chitosan, which is a natural amino polysaccharide is largely found in crustaceans shells and is a by-product of the fishing industry. It readily forms films or fibres. The property makes it an excellent choice as a heterogeneous catalyst. The conversion of cyclohexene into its oxidation products was efficiently carried out by chitosan base Mn catalysts. The reaction and the products have been shown in **Scheme 1.3^[67]**.



Scheme 1.3 : Conversion of cyclohexene into its oxidation products^[67]

The literature reports say that the oxidation of cyclohexene with the aid of molecular oxygen firstly forms 2-cyclohexene-1-hydroperoxide which is not stable and gradually gets converted to 2-cyclohexene-1-ol and 1,2-cyclohexenediol. But in the presence of catalyst this conversion is hastened. The mechanism is shown below^[68](**Scheme 1.4**).



Scheme 1.4 : The mechanistic pathway of cyclohexene oxidation^[68]

Sol - gel technique is effectively used to heterogenize homogeneous catalysts. This can be either done by physical doping or functional modifications. The manganese-anchored catalyst^[69] shown here has been prepared by functionalisation(**Fig 1.34**).

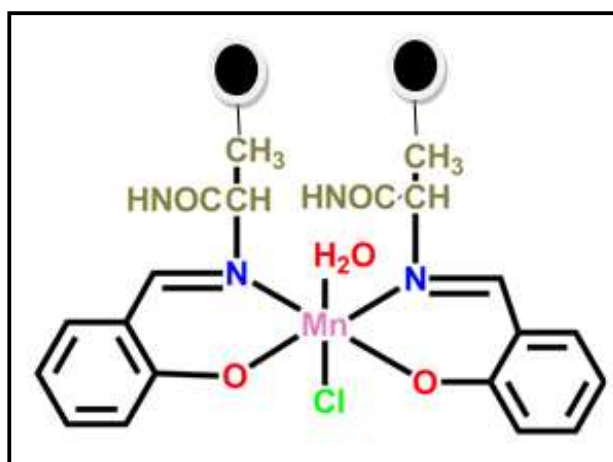
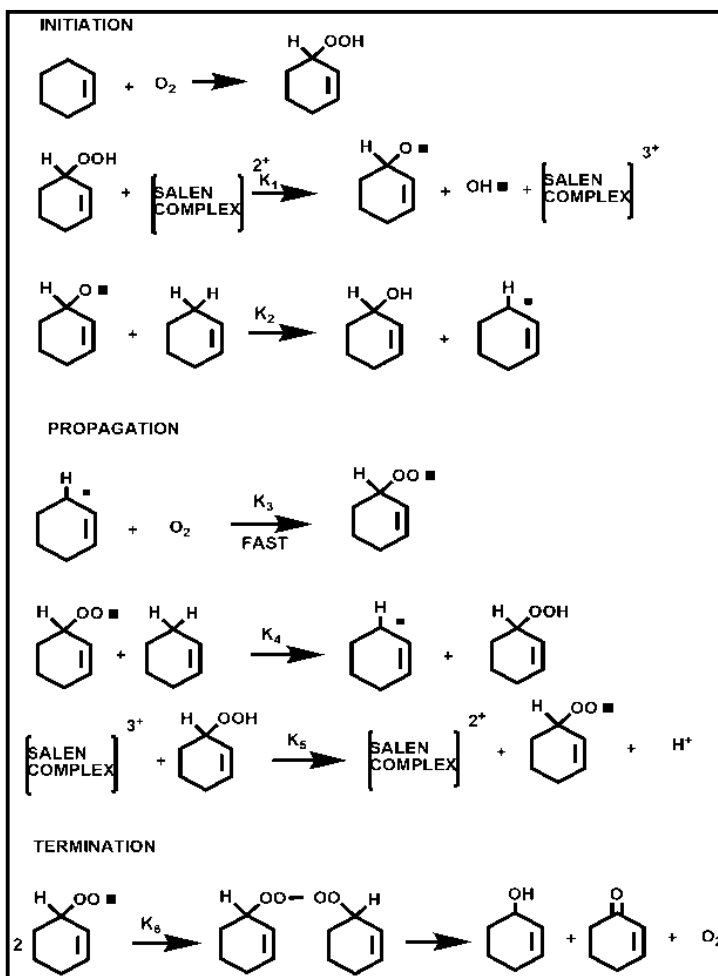


Fig 1.34 : Manganese-anchored catalyst^[69]

The amount of catalyst is proportional to the rate. Beyond a limit, even selectivity was seen to increase. Hence it could be assumed that Schiff base complexes could catalyze the aerobic oxidation of olefins to propenol derivatives. Moreover, epoxidation of cyclohexene catalyzed by salen complexes bearing electronegative substituents went through a radical-chain sequence mechanism as shown below. This process was studied by A. Bottcher *et al*^[70]. The metal aided in decomposing the hydroperoxide finally yielding the products(**Scheme 1.5**)



Scheme 1.5 : Detailed mechanistic pathway of cyclohexene oxidation^[68]

Hydrazine Schiff base supported catalyst was effective in epoxidation of cyclohexene in the presence of hydrogen peroxide^[71]. The data given below shows that the supported catalysts always gave better yield than the unsupported ones.^[72](**Table 1.4**)

Complex		Yield _{Unsupported}	Yield _{Supported}
HPHZ-Fe		92%	96.5%
HPHZ-Co		88%	94.2%
HPHZ-Ni		92%	95.9%
HPHZ-Cu		89%	88.8%
HPHZ-Zn		82%	86.1%
HPpn-Fe		93%	98.3%
HPpn-Cu		91.8%	93.0%

Table 1.4 : Comparison between yields of supported and unsupported catalysts^[72]

The epoxidation of cyclo-octene has also been widely explored. Various solvent mixtures have been tried for this epoxidation to act in a two phase system, but the 2:1 mixture of acetonitrile/ Water proved to be excellent. Aq. acetonitrile provided the best polarity required and also helped in proper swelling of the polymer support. Manganese Schiff base complexes on polystyrene-bound imidazole Schiff base ligand were quite effective^[73]. The epoxidation of cis cyclooctene in with Ru catalysts^[74] (**Fig 1.35**) gave good results at room as well as elevated temperatures.

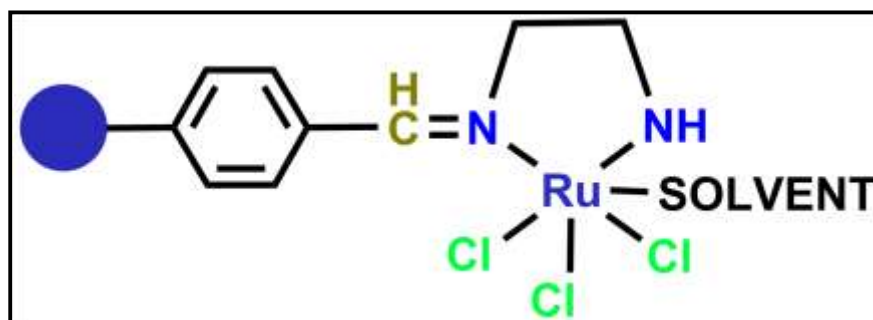


Fig 1.35 : Polymer supported Ru catalyst^[74]

Mn(II) supported complexes catalysed epoxidation of electron rich olefins such as norbornene and cis cyclooctene^[75]. The following table(**Table 1.5**) gives the details of epoxidation of this category showing that slightly elevated temperatures helped the process.

Catalyst	Solvent	Temp(deg C)	Epoxide
Mn cat	Chloroform	25	10.1
	Chloroform	40	13.9
	Acetonitrile	25	3.2
	Acetonitrile	50	4.6

Fig 1.5 : Epoxidation rates at temperature variation with Mn(II) catalysts^[75]

The iron(III) supported on functionalized polystyrene Schiff base ligands was used as well in conjunction with *tert*-butylhydroperoxide at normal and 50°. Here also elevated temperature played the same role as the above one^[76]. The polymer-supported molybdenum carbonyl Schiff base catalyst (**Fig 1.36**) exhibited high conversion of cyclo octene into corresponding oxide in carbon tetrachloride^[58].

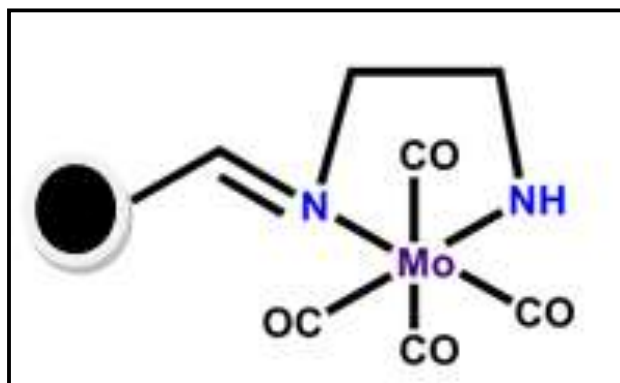
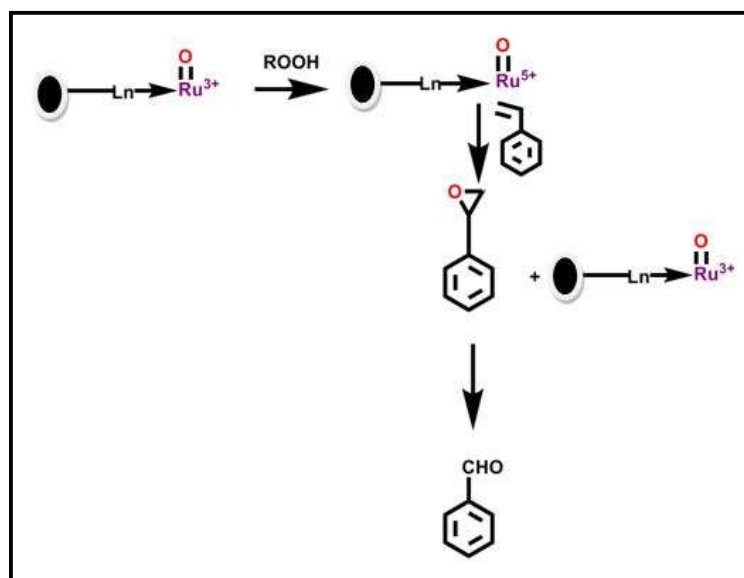


Fig 1.36 : Polymer-supported molybdenum carbonyl Schiff base catalyst^[58]

This catalyst showed excellent selectivity and reproducibility. Styrene generally is resistant to epoxidation without a catalyst. Along with styrene oxide, benzaldehyde which is a secondary product, was also formed in substantial amount. Methanol solvent gave better results than acetonitrile. The following oxo based mechanism is widely interpreted^[68] (**Scheme 1.6**).



Scheme 1.6 : Oxo based mechanism of epoxidation^[68]

Vanadium and iron supported catalysts are well known in epoxidation of styrene as well^[76]. Sometimes the activity is increased by adding nitrogen co catalyst. Polystyrene-bound imidazole complexes of manganese are useful in catalyzing stilbene^[76]. Epoxidation of trans-stilbene has occurs stereo specifically but cis stilbene epoxidation progresses with some loss in stereochemistry.

Bhaumik and co workers reported a synthesis and characterization of two complexes, one copper and the other nickel, which were eventually turned into heterogenized catalysts^[77], Cu-AMM and Ni-AMM (Fig 1.37).

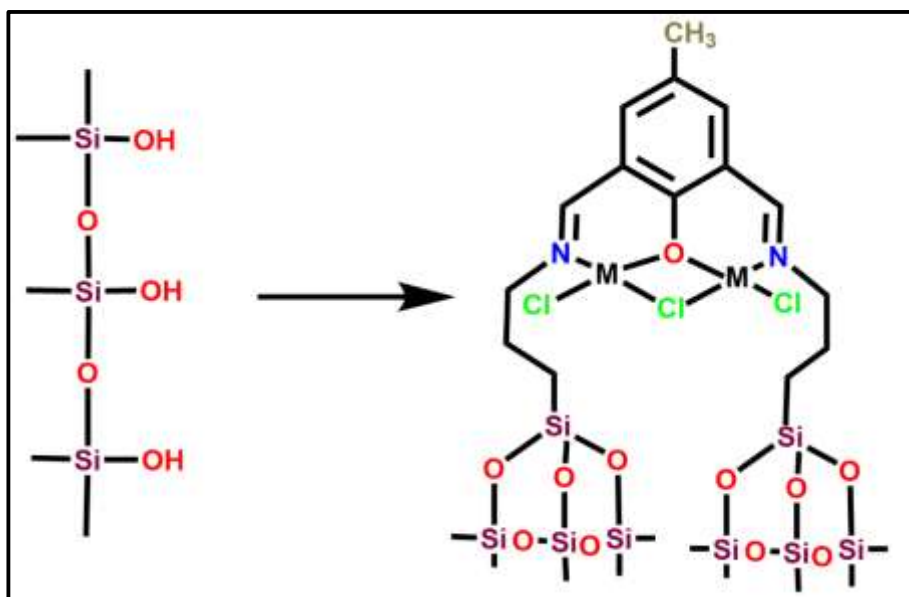


Fig 1.37 : Cu-AMM and Ni-AMM^[77]

Mesoporous silica was functionalized with 3-aminopropyltriethoxysilane (3-APTES) and gradually made to react with 4-methyl-2,6-diformylphenol (DFP). Then, Cu(II) and Ni(II) salts was made to react with the resulting complex, to produce heterogeneous Cu-AMM and Ni-AMM respectively. The resultant was successfully used as catalysts in the epoxidation of alkenes. The catalysts were synthesized by immobilizing the metal ions over the silica bed and this happened by coordination with the electron donor sites Atomic absorption spectroscopy was used to confirm the amount of metal ions embedded in the complex. The results show that Cu-AMM and Ni-AMM contained 0.34% copper and 0.42% nickel respectively. This data was further supported by the elemental analyses findings. Absorption spectroscopy showed bands

dueto $p \rightarrow p^*$ and LMCT transitions. d - bands of lower intensities were also observed at higher wavelengths. The powder X-ray diffraction patterns showed strong diffractions for (100), (110) and (200) planes and a weaker one for the (210) plane of 2D-hexagonal mesophase, pointing towards the formation of a highly ordered mesophase. Upon complexation with the metal ions, there occurs a gradual decrease in d -spacing which happened due to the contraction of unit cells upon surface functionalization. TEM images confirmed the hexagonal ordering of the mesopores. N_2 adsorption - desorption isotherms showed the volume of and the position of the pores and these are in agreement with the TEM data. ^{13}C CP MAS NMR study confirmed the presence of organic moiety and its immediate chemical surroundings.

Epoxidation of cyclohexene, *trans*-stilbene, styrene, *o*-methyl styrene, cyclooctene and norbornene was done heterogeneously with Cu-AMM and Ni-AMM as catalysts and *tert*-butyl hydroperoxide as the oxidant at 333 K. The corresponding epoxide turned out to be the major product in all the cases. The results are shown in the **Table 1.6**.


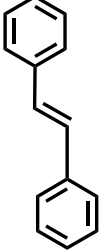
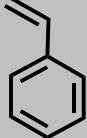
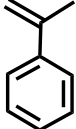


Alkene	Conversion (Cu cat)	Selectivity (Cu cat)	TOF (Cu cat)	Conversion (Ni cat)	Selectivity (Ni cat)	TOF (Ni cat)
	93.4	90.0	88.0	84.2	89.5	60.0
	89.5	91.0	38.4	75.2	88.0	24.1
	86.3	95.0	64.2	78.2	90.0	44.1
	84.0	92.1	55.0	80.1	86.4	39.2
	92.2	93.1	65.4	83.8	92.0	44.8
	90.3	94.0	74.1	82.5	93.1	51.7

Table 1.6 : Epoxidation of few alkenes and their corresponding yields^[77]

The efficiency of the catalysts after consecutive cycles was checked to understand its recyclability. After each cycle, the catalysts were filtered out, washed thoroughly and then the catalysts were reused like the earlier one. Upto five consecutive cycles, the efficiency remained unaltered. Hot filtration was carried out to make the reaction mixture catalyst free, to check whether any leached out metal ion from the surface is aiding the reaction. But nothing of that sort was observed. The reaction probably proceeded *via* formation of a copper - peroxy species together with the formation of *tert* butanol. In the case of Ni-complexes, the Ni - hydroperoxy species remained the active intermediate

P Banerjee *et al.* synthesized two new tetranuclear polymeric Ni complexes^[78], namely $[\text{Ni}_4\text{L}_41(\mu\text{-tp-}\kappa_4\text{-O})\text{-(H}_2\text{O)}_2(\mu\text{-tp-}\kappa_2\text{-O})]\cdot 2\text{C}_2\text{H}_5\text{OH}\cdot\text{CH}_3\text{OH}\cdot 3\text{H}_2\text{O}$ (**Fig 1.38**) and $[\text{Ni}_4\text{L}_42(\mu\text{-tp-}\kappa_4\text{-O})(\text{H}_2\text{O})_2(\mu\text{-tp-}\kappa_2\text{-O})]\cdot 3\text{H}_2\text{O}$ where L1 = N-(3-aminopropyl)-5-bromosalicylalimine and L2 = N-(3-aminopropyl) salicylalimine]. The complexes were bridged by phenolate moieties. Two such bridged binuclear unit are connected by a terephthalate moiety to ultimately end up in a tetranuclearnickel(II) complex (**Fig 1.39**). They synthesized and elucidated the crystal structure of the first complex and it has been elaborately discussed down below. They could not effectively crystallize the second complex but they did other characterization study with it.

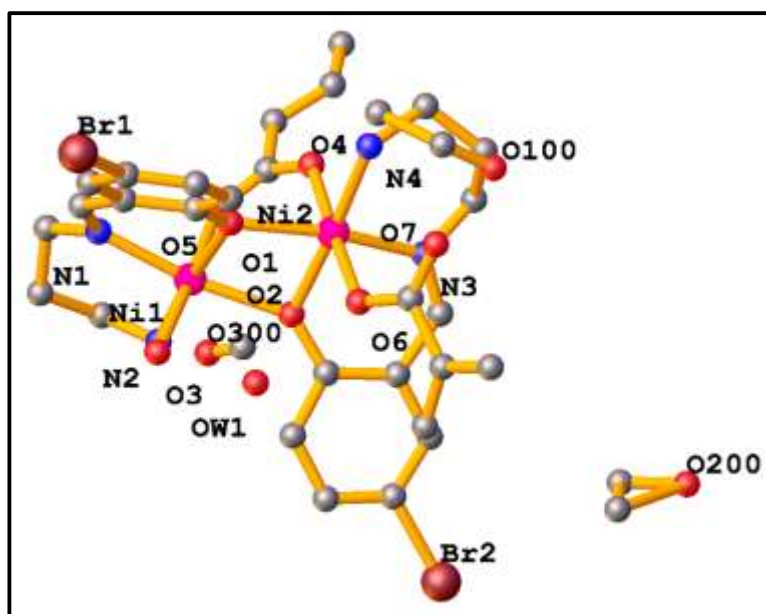


Fig 1.38 : Perspective view of $[\text{Ni}_4\text{L}_41(\mu\text{-tp-}\kappa_4\text{-O})\text{-(H}_2\text{O)}_2(\mu\text{-tp-}\kappa_2\text{-O})]\cdot 2\text{C}_2\text{H}_5\text{OH}\cdot\text{CH}_3\text{OH}\cdot 3\text{H}_2\text{O}$.
H atoms omitted for clarity^[78]

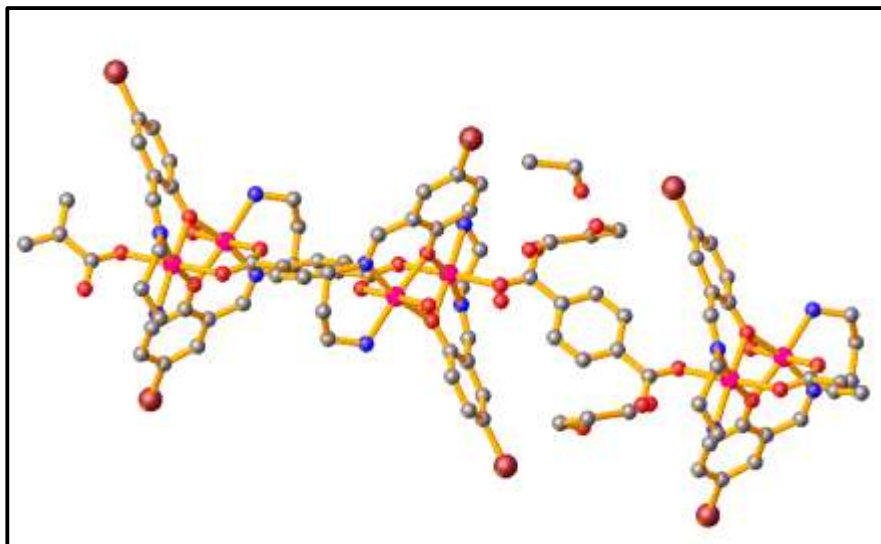


Fig 1.39 : Perspective view of tetranuclearnickel(II) complex^[78]

The above structure shows how the terephthalate moieties ultimately connect the units to form the final structure. Like terephthalate, cyanometalate anions play a similar role in supramolecular coordination polymers. This group has to examined the ability of the linear dicyano argentate ion $[\text{Ag}(\text{CN})_2]^-$ to form supramolecular frameworks (Fig 1.40-1.41). The syntheses and structures of two such complexes have been largely described by them (complexes 1&2). This group then went onto the study of epoxidation of alkenes such as styrene, α -methylstyrene and cyclohexene in the presence of *tert*-butyl hydroperoxide heterogeneously.

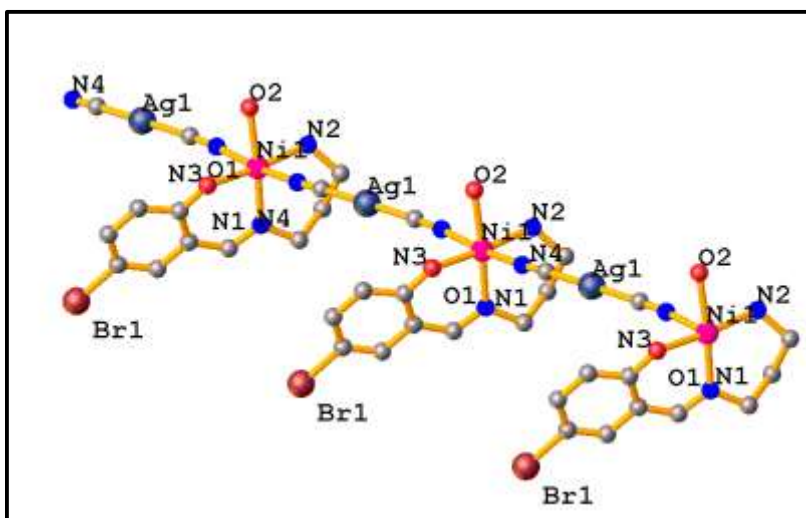


Fig 1.40 : Perspective view of dicyano argentite linked Ni(II) complex(1)^[78]

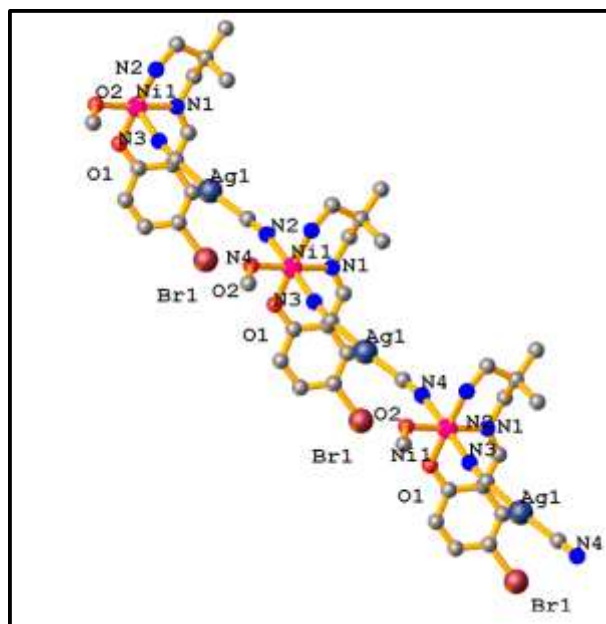
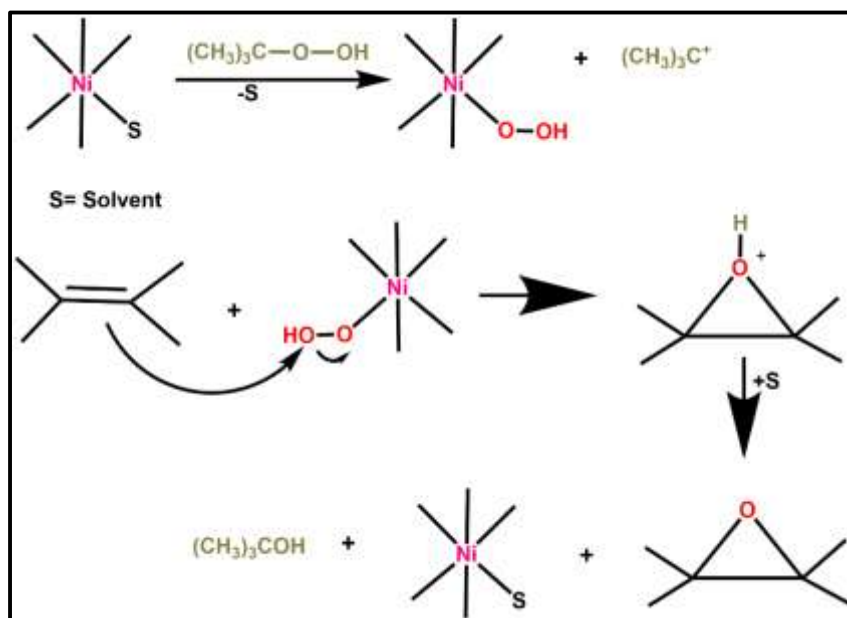


Fig 1.41 : Perspective view of dicyano argentite linked Ni(II) complex(2)^[78]

The heterogeneous oxidation reactions with 1.0 g of substrate and 0.200 g of catalyst in acetonitrile at 333 K using *tert*-Butyl hydroperoxide. The end products were analyzed by gaschromatography. The predicted mechanism is shown in **Scheme 1.7**.



Scheme 1.7 : Proposed mechanism of epoxidation^[78]

The alkene conversion ratios as shown in the bar graphs (Fig 1.42-1.44)

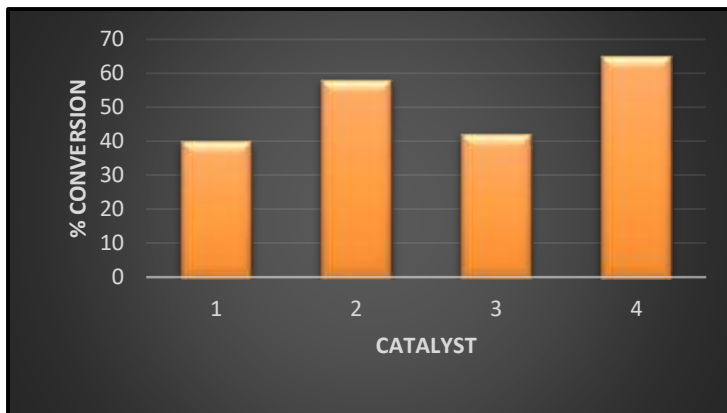


Fig 1.42 : Yield percentage of styrene oxidation with the catalysts^[78]

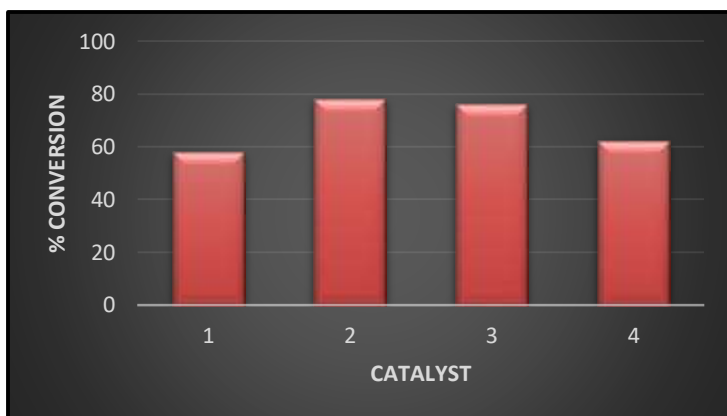


Fig 1.43 : Yield percentage of α -methyl styrene oxidation with the catalysts^[78]

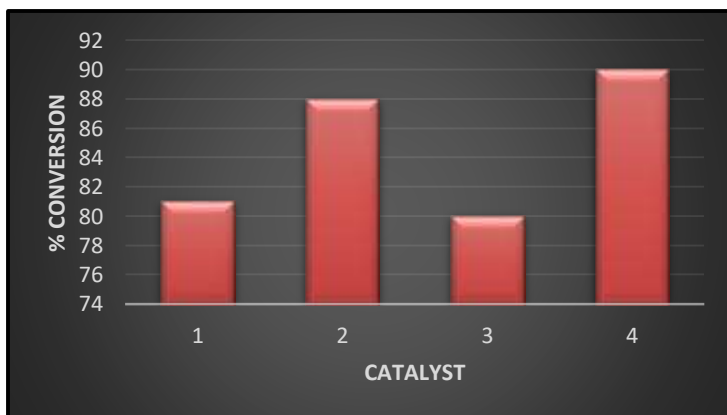


Fig 1.44 : Yield percentage of cyclohexene oxidation with the catalysts^[78]

P Banerjee and coworkers reported the synthesis of a copper(II) complex $[\text{Cu}_2\text{L}-(\mu_{1,1}\text{-N}_3)(\mu_{1,3}\text{-N}_3)(\mu_{1,1,1}\text{-N}_3)]$ where $\text{HL} = 4\text{-methyl-2,6-bis(phenylmethyliminomethyl)pheno}$ ^[79]. X-ray crystallography data shows the azide bindings clearly (**Fig 1.45**)

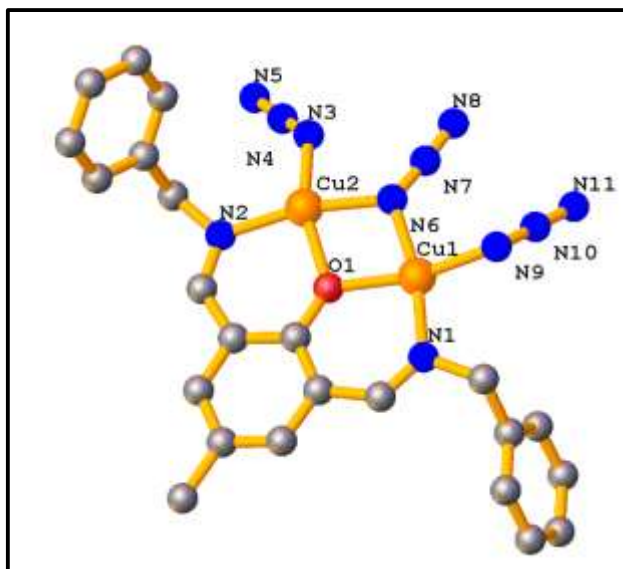


Fig 1.45 : Perspective view of $[\text{Cu}_2\text{L}-(\mu_{1,1}\text{-N}_3)(\mu_{1,3}\text{-N}_3)(\mu_{1,1,1}\text{-N}_3)]$ ^[79]

The catalyst for the oxidation of olefin was complex 1, immobilized on mesoporous silica and it was used for the epoxidation of alkenes like the previous case. Conversion versus time plot for the epoxidation of olefin is shown in **Fig 1.46**.

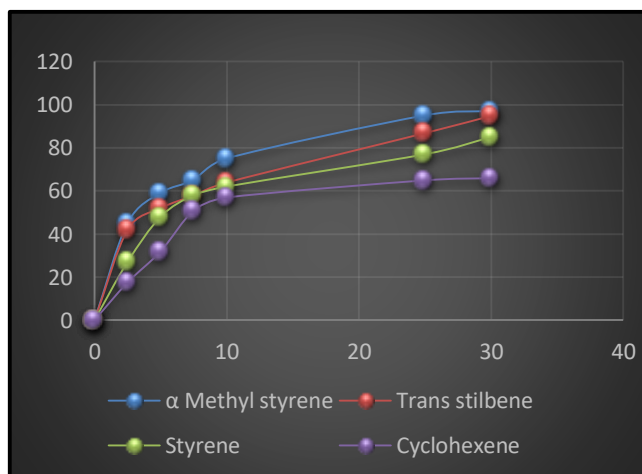


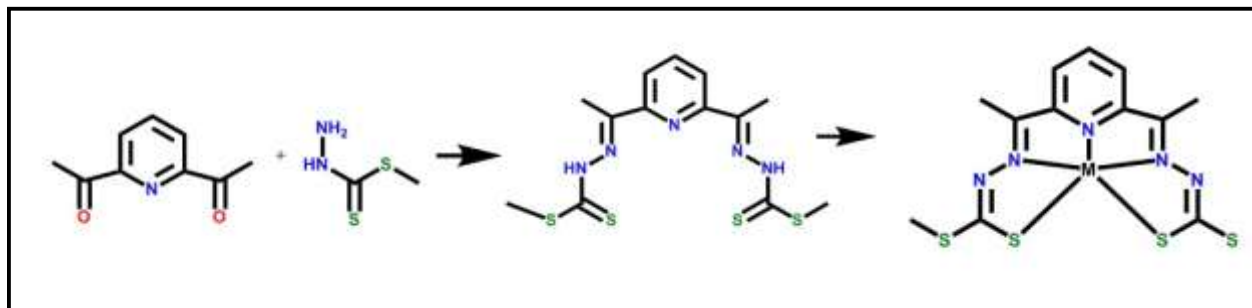
Fig 1.46 : Conversion versus time plot for the epoxidation of olefin^[79]

1.6 C-H activation by Schiff base complexes:

The oxidation of saturated hydrocarbons is very challenging as C–H bond is extremely inert and at the same time this is of utmost importance in industries. Cyclohexane oxidation is of special interest, because cyclohexanol and cyclohexanone which are used for the production of adipic acid and caprolactam, are obtained as major products. Cyclohexanol and cyclohexanone are together known as KA oil^[80]. Conventionally, on a large scale, the oxidation of cyclohexane is executed by a homogeneous cobalt catalyst at a temperature of around 150°C^[81]. Then it is further oxidised to adipic acid which along with the main reaction, gives undesirable decarboxylated by products also. So, the conversion is carried out in such a way that the percentage conversion is compromised so as to keep the selectivity high. The main challenge remains as to how to increase the percent of products by not reducing the selectivity as well as keeping it as environment friendly as possible. In present times, several catalysts (homogeneous and heterogeneous) such as metal nanoparticles, Gd(60)-AlPO-5, zeolite Y, N-hydroxyphthalimide (NHPI), and metalloporphyrins^[82] are being continually developed^[83].

Metal-organic frameworks are of special interest because of their structural diversity as well as catalytic capabilities. Great progress is being made in the usage of metal complexes for the oxidation of cyclohexane, including Schiff-base complexes. Schiff-base ligands are very versatile and can bond a lot of metals and hence are very diverse. They can effectively catalyse the oxidation of cyclohexane^[84].

Tawfik A. Saleh *et al* prepared a Schiff base SMdiAP complex^[85] in the following manner that is elucidated in **Scheme 1.8**.



Scheme 1.8 : Schiff base SMdiAP complex^[85]

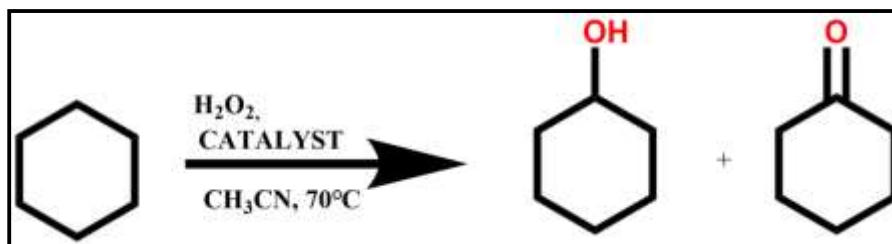
These were characterized by different analytical techniques. They prepared Co(II), Cu(II), Fe(II), Mn(II), Ni(II) and Zn(II) complexes of the Schiff base.

These were employed for cyclohexane oxidation to give cyclohexanone and cyclohexanol. The reaction did not proceed well without the catalyst. The conversion rates and the selectivities are clearly mentioned in the table below (**Table 1.7**).

CATALYST	%CONV.	%CONC _{CYCLOHEXANONE}	%CONC _{CYCLOHEXANOL}	TOT. YIELD	%SELECTIVITY _{CYCLOHEXANONE}	%SELECTIVITY _{CYCLOHEXANOL}	TOTAL
Fe(SMdiAP)	16.72	13.89	2.58	16.47	83	16	99
Cu(SMdiAP)	28.29	22.96	4.72	27.68	81	18	98
Ni(SMdiAP)	8.34	5.18	2.12	7.30	62	25	87
Co(SMdiAP)	10.57	8.21	1.15	9.36	78	11	89
Mn(SMdiAP)	9.71	7.72	1.78	9.50	80	18	98
Zn(SMdiAP)	4.23	2.95	0.98	3.93	70	23	93

Table 1.7 : % conversion and the concentrations of the oxidation products and their respective selectivities^[85]

The reaction proceeds in the following fashion (**Scheme 1.9**):



Scheme 1.9 : Oxidation of cyclohexane^[85]

The reaction yield was directly proportional to the time and temperature. The reaction yield was also seen to increase with increased catalyst amount as well as peroxide concentration.

M. Manassero *et al*^[86] synthesized the following Schiff base Cu complex (Fig 1.47).

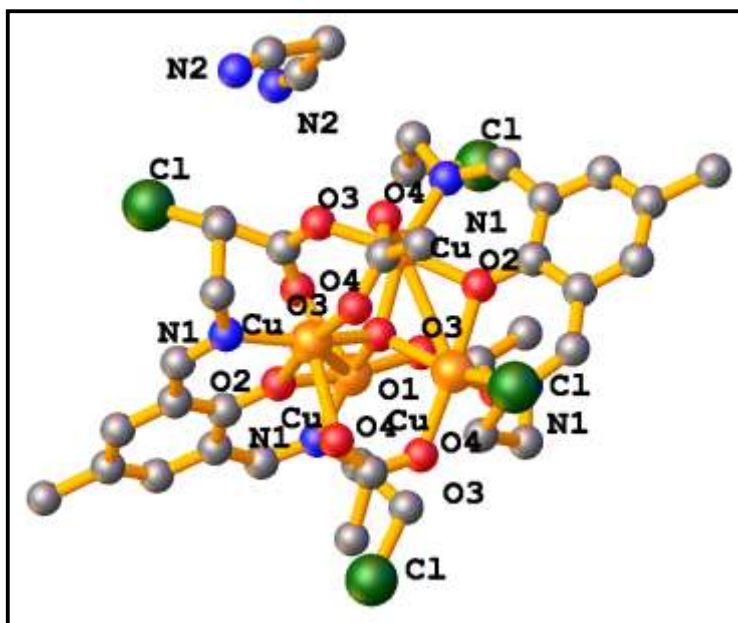


Fig 1.47 : Perspective view of Cu(II) Schiff base complex^[86]

Basically they synthesized three complex but could elucidate the crystal structure of only one.

To an acetonitrile solution of 4-methyl-2,6-diformyl, measured amounts of 2-fluoroethylamine hydrochloride, 2-chloroethylamine hydrochloride and 2-bromoethylamine hydrobromide were added for the first, second and third complex respectively. Triethylamine and copper acetate monohydrate were also added. Single crystals of the second complex was found. These were employed for peroxidative oxidation of cyclohexane and toluene by hydrogen peroxide oxidant. The products of cyclohexane oxidation are cyclohexanol and cyclohexanone, whilst for toluene it is benzyl alcohol and benzaldehyde. The reaction proceeded well in acidic medium, i.e. nitric acid. The reaction could be fine tuned by altering the amounts of nitric acid or the oxidant or the reaction time. Nitric acid has a definitive role^[87], i.e. increasing the unsaturation at the metal center by suitably protonating the ligand of the catalyst and thereby increasing the oxidative properties of the catalyst as well as to increase the stability of the peroxo intermediate. The exact structure of the complex in solution is unfathomable. ESI mass spectra of the complexes in nitric acid medium showed that one acetato group was lost from the complex every time. Ratio of $n(\text{HNO}_3)/n(\text{catalyst}) = 10$ has been optimized and maintained. It has also been verified that normal inorganic salts are not effective in catalyzing the reaction. The results for cyclohexane

oxidation have been indicated in **Table 1.8** and for toluene oxidation in **Table 1.9** and the proposed scheme has been shown in **Fig 1.48**.

Catalysts	n(H ₂ O ₂)/n(catalyst)	Time/h	Yield (%)			Selectivity of Cyclohexanol in (%)	TON
			Cyclohexanol	Cyclohexane	Total		
1	125	6	13.2	9.1	22.3	59.2	11.2
		48	15.0	13.4	28.4	52.8	14.2
	250	6	15.6	11.8	27.4	56.9	13.7
		48	19.4	14.7	34.1	56.9	17.1
	500	6	15.5	9.7	25.2	61.5	12.6
		48	21.1	14.3	35.4	59.6	17.7
2	125	6	15.0	12.2	27.2	55.1	13.6
		48	19.3	15.4	34.7	55.6	17.4
	250	6	17.3	11.0	28.3	61.1	14.2
		48	22.0	15.0	37.0	59.5	18.5
	500	6	14.9	10.3	25.2	59.1	12.6
		48	17.9	13.6	31.5	56.8	15.8
3	35.7	6	14.4	10.3	24.8	58.0	12.4
		48	17.3	12.8	30.1	57.5	15.1
	250	6	18.9	11.5	30.4	62.2	15.2
		48	19.4	15.0	34.4	56.4	17.2
	500	6	21.3	14.4	35.7	59.7	17.9
		48	24.0	14.2	38.2	62.8	19.1

Table 1.8 : Oxidation products of cyclohexane, their yield % and their selectivities ^[86]

Catalyst s	n(H ₂ O ₂)/n(catalyst)	Time/h	Yield (%)			Selectivity of Cyclohexanol in (%)	TON
			Cyclohexanol	Cyclohexane	Total		
1	125	6	9.2	17.3	26.5	65.3	13.3
		48	11.0	23.5	34.5	68.1	17.3
	250	6	12.4	23.6	36.0	65.6	18.0
		48	15.6	24.0	39.6	60.6	19.8
	500	6	14.0	19.2	33.2	57.8	16.6
		48	17.5	20.4	37.9	53.8	19.0
2	125	6	8.2	17.1	25.3	67.6	12.7
		48	10.6	23.5	34.1	68.9	17.1

	250	6	12.4	25.4	35.8	70.9	17.9
		48	16.6	26.4	41.3	63.9	20.7
	500	6	14.2	18.0	32.2	55.9	16.1
		48	16.5	21.2	37.7	56.2	18.9
3	125	6	10.2	18.5	28.7	64.5	14.4
		48	11.8	24.3	36.1	67.3	18.1
	250	6	12.8	25.1	35.9	69.9	18.0
		48	16.0	26.4	42.4	62.3	21.2
	500	6	15.1	19.1	34.2	55.9	17.1
		48	14.0	23.7	37.7	62.9	18.9

Table 1.9 : Oxidation products of toluene , their yield % and their selectivities ^[86]

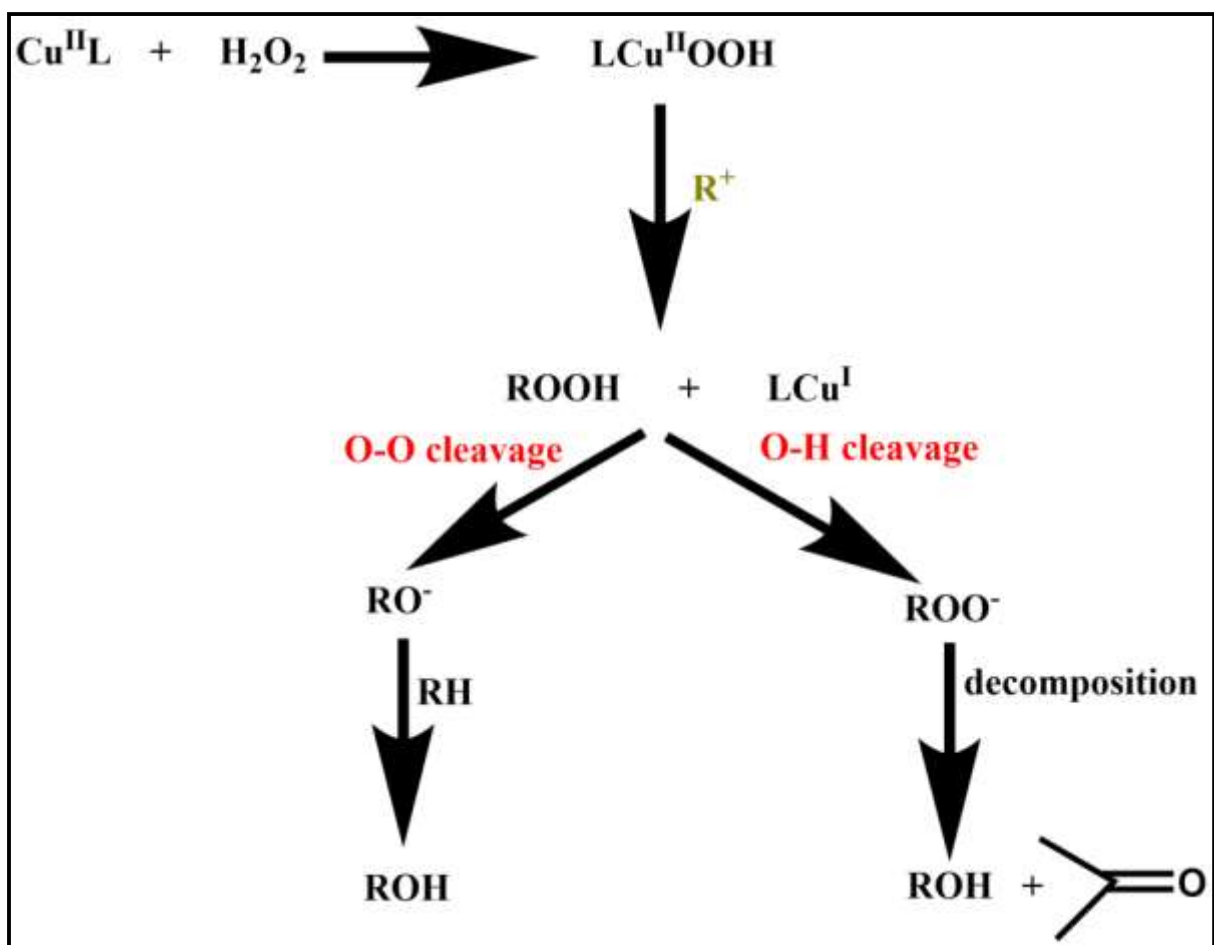


Fig 1.48 : Proposed scheme of catalysis ^[86]

A.J.L Pombeiro and co workers synthesized an Fe(III) Schiff base complex **1** (Fig 1.49) and then employed it for mild oxidation of cyclohexane^[88].

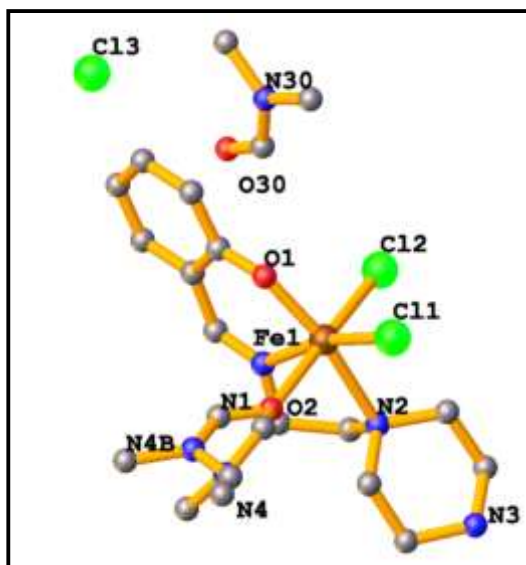


Fig 1.49 : Perspective view of an Fe(III) Schiff base complex **1**^[88]

The complex **1** was treated as a catalyst for the oxidation of cyclohexane to cyclohexanol and cyclohexanone by hydrogen peroxide as the oxidant. The product yield % of the products after 5h of reaction has been depicted in the graph(Fig 1.50)

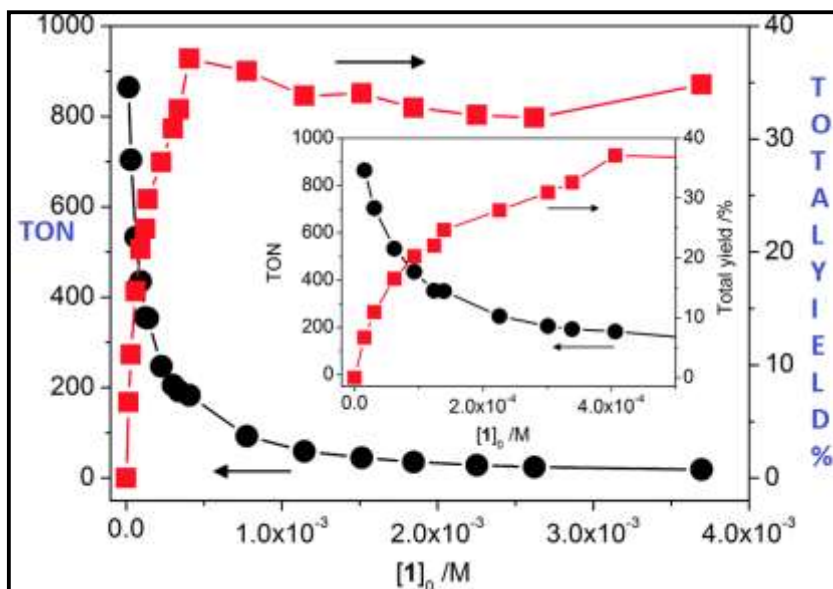


Fig 1.50 : Yield % of products after 5h of reaction^[88]

The highest total yield was 37% at catalyst concentration of 4.1×10^{-4} M whilst highest TON of 0.9×10^3 was achieved at concentration 1.6×10^{-5} M. The selectivity towards cyclohexanol and cyclohexanone products is high. A number of by products like diols, hydroxycyclohexanones, ring cleavage products, 6-hydroxyhexanoic and adipic acids, and others. Increasing the initial concentration of cyclohexane, could improve the TON significantly. This has been clearly shown in the graph below(**Fig 1.51**). In this work also, nitric acid promoter has a major role.

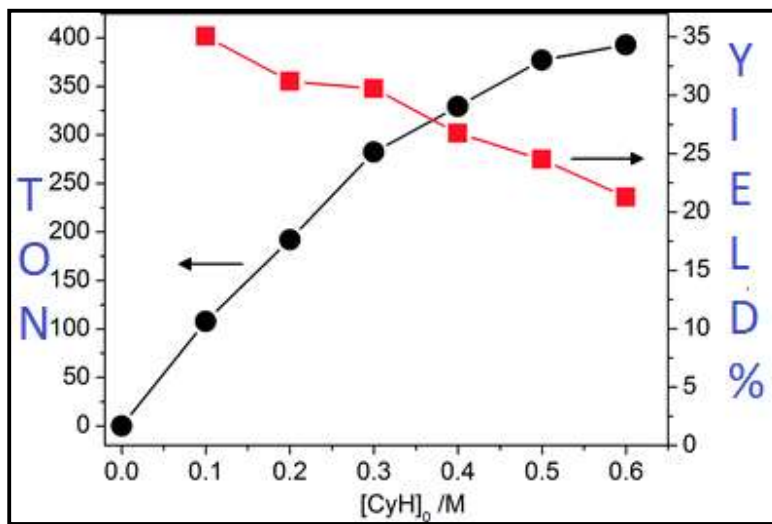


Fig 1.51 : Yield % of products on increasing the initial concentration of cyclohexane^[88]

W. Grunert and group synthesized^[89] the following cobalt complex(**Fig 1.52**).

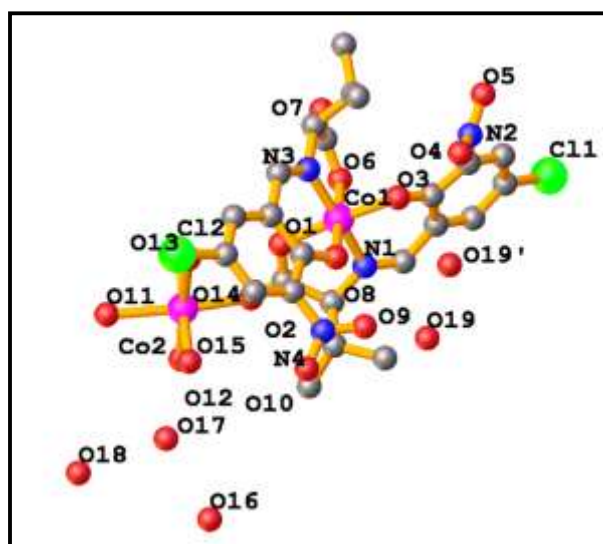


Fig 1.52 : Perspective view of Co(III) complex^[89]

They further studies the structure by various means like IR spectroscopy, X Ray photoelectron spectroscopy (to throw light on the oxidation state of the central metal atom). They did cyclic voltammetry as well. The complex was tried as a catalyst in the oxidation of cyclohexane in the presence of air to result in a mixture of cyclohexanol and the ketone as well. The hydroperoxide was also formed as a result of the radical chain mechanism. The process is initiated by reaction of Co^{3+} with alkane yielding free radicals and Co^{2+} . This gradually leads to the accumulation of a large amount of cyclohexyl hydroperoxide, which gives the corresponding alcohol and ketone on decomposition. In the absence of catalyst, a large amount unreacted hydroperoxide was left behind but with the aid of the catalyst, it was seen to undergo decomposition. The conversion % with and without the catalyst has been depicted in **Fig 1.53**.The product selectivities with freshly prepared catalyst has been shown in **Fig 1.54**. Even the re used catalyst was almost as good as the original one, though the major products differed a bit.

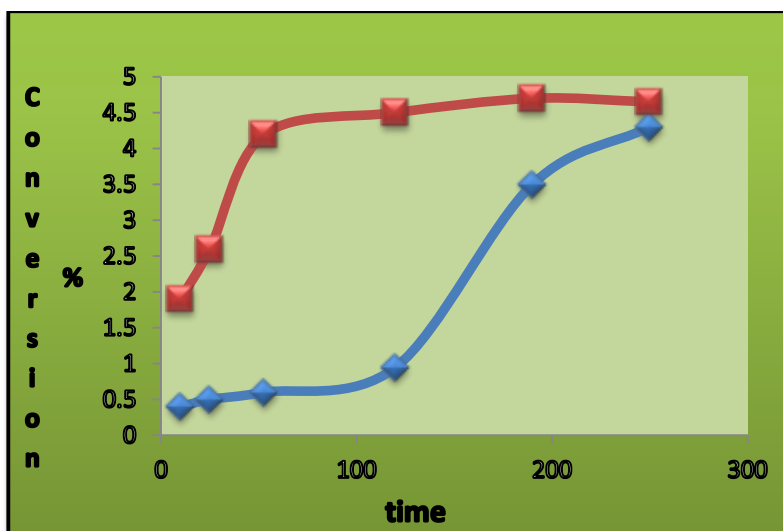


Fig 1..53 : Conversion % vs time plot fr the oxiadation reaction (i)red- with catalyst (ii)blue – without catalyst^[89]

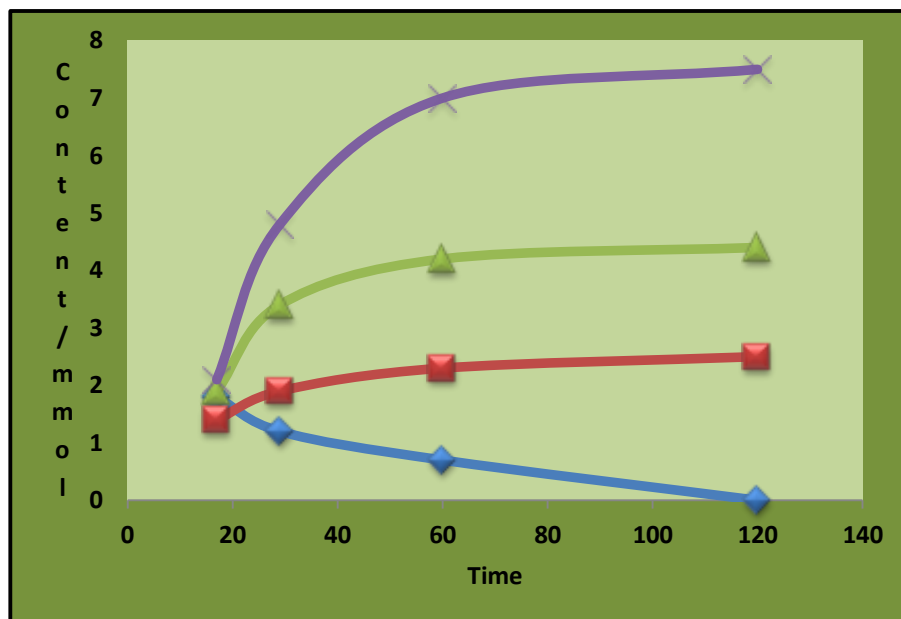


Fig 1.54 : Product selectivities for oxidation of cyclohexane with the catalyst (i)purple: cyclohexyl hydroperoxide (ii)green- adipic acid (iii)red- cyclohexanone(iv)blue- cyclohexanol^[89]

Pombeiro *et al* synthesized the following Cu(II) and Mn(III) complexes^[90] (Complexes 1-5)(**Fig 1.55-1.58**).

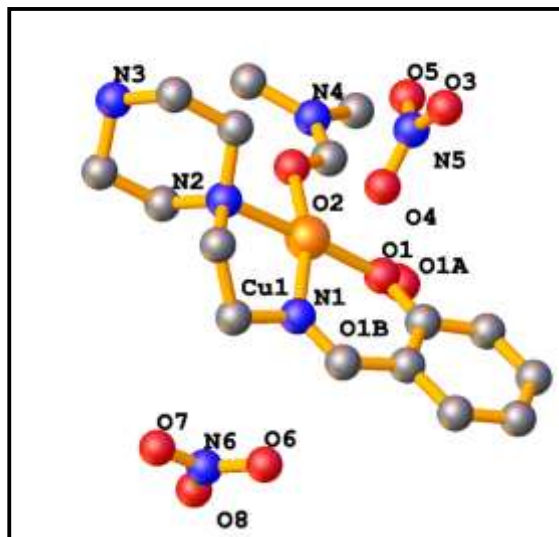


Fig 1.55 : Perspective view of Cu(II) complex(Complex 1)^[90]

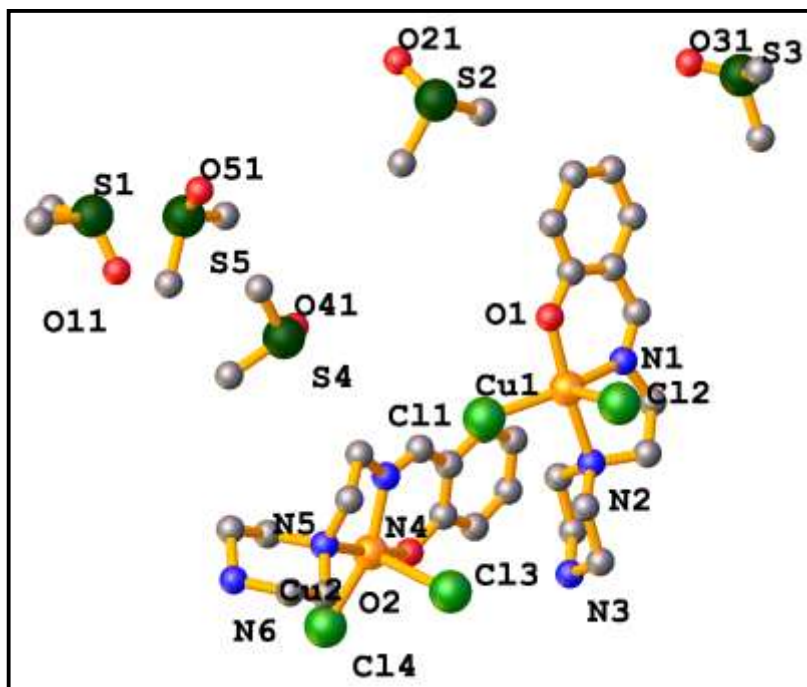


Fig 1.56 : Perspective view of Cu(II) complex (Complex 2)^[90]

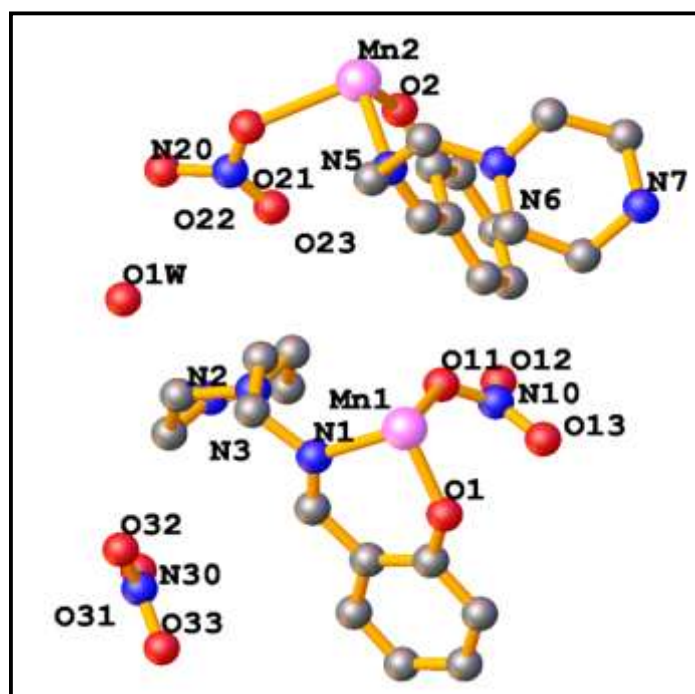


Fig 1.57 : Perspective view of Mn(III) complex (Complex 3)^[90]

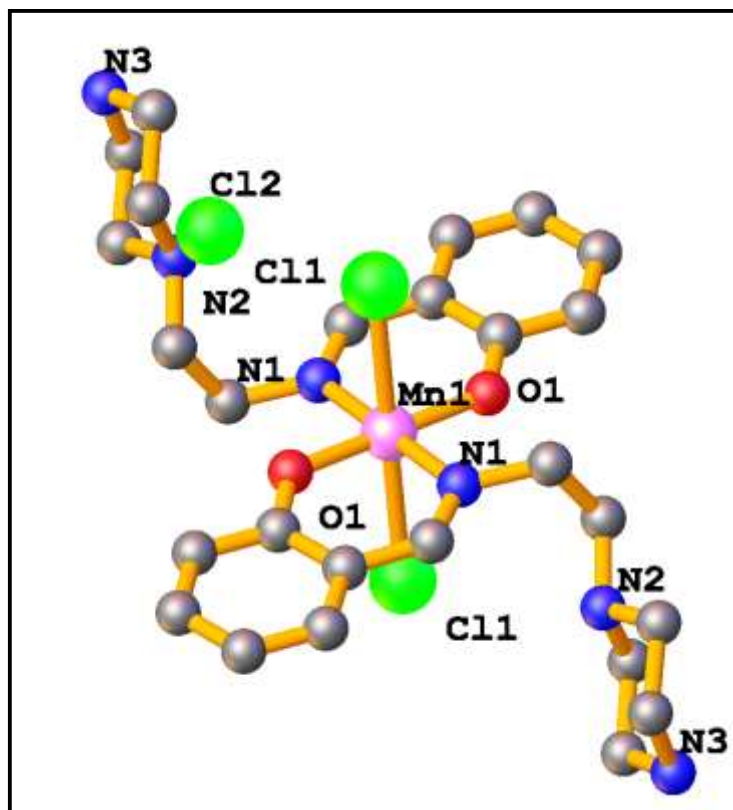


Fig 1.58 : Perspective view of Mn(III) complex (Complex 4)^[90]

Complexes 1–4 were employed as catalysts in the oxidation of cyclohexane with oxidant H_2O_2 in acetonitrile medium, with the aid of several co-catalysts (promoters). The products, cyclohexanol and cyclohexanone could be quantified well. Promoting agents also contribute well. Strong protic acids help creating an unsaturated coordination environment around the metal center and also stops the undesired decomposition of hydrogen peroxide. Carboxylic acids help as stabilizers. Basic promoters like triethylamine, pyridine interact with the catalysts converting them into active species. Catalysts 1 and 2, i.e. the copper complexes, show enhanced activity in cyclohexane oxidation in the presence of protic acid promoters whilst the manganese compounds, i.e. 3 and 4, is aided in the presence of carboxylic acids. This group studied the effect of acid promoters, as well as of a basic one, pyridine, for proper comparison of their effect on the catalytic process. The yields of products have been shown in **Table 1.10**.

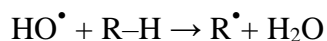
Promoter	Yield of products (%)			
	1	2	3	4
HNO ₃	4.6	14.8	0.1	0.1
HCl	12.4	11.2	<0.1	<0.1
H ₂ O _x	<0.1	<0.1	<0.1	<0.1
Py	21.6	15.3	0.3	0.2

Table 1.10: Yield of oxidation products^[90]

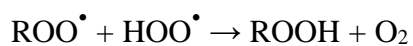
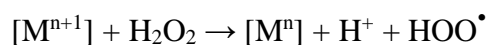
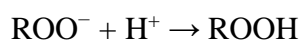
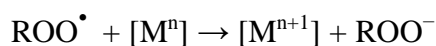
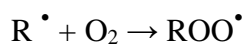
The copper complexes are good enough as catalysts in all cases, except of oxalic acid. Despite similar structure, their catalytic exhibitions are different, in the presence of same promoter.

The manganese complexes **3** and **4** were pretty inactive. Pyridine was the best promoting agent, though even in that case the yield was as low as 0.3%.

Reduction of H₂O₂ by a [Mⁿ] goes about in the following way:

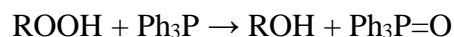


The alkyl radical alongwith dioxygen to form alkyl peroxide radical which transforms into alkyl hydroperoxide,



The main product is alkyl hydroperoxide (ROOH). Cyclohexyl hydroperoxide decomposes into its products. As the hydroperoxide may decompose into other unwanted products in the hot GC column, direct GC analysis could not be done.

The reaction mixture was quenched with reducing agent (Ph₃P) before GC analysis, the following reaction takes place:



In this study, pyridine probably i)coordinates the metal centre, (ii) facilitates proton-transfer (iii) favors the oxidation of Cu(I) to Cu(II). For hydrochloric acid promoter, both copper complexes **1** and **2** showed similar activity. The complete absence of any activity in the presence of oxalic acid is probably due to its irreversible coordination to metal centre leaving no vacant position for substrate attachment.

Complexes **1–4** were also tested as catalysts for the oxidation of 1-phenylethanol to acetophenone using *tert*-butylhydroperoxide (TBHP) as oxidizing agent under solvent free conditions. It has been summarized in the table below(**Table 1.11**)

Entry	Catalyst	Catalyst amount (mol% vs substrate)	Temperature (°C)	Additive	Yield	TON
1	1	0.05	80	-	12.3	246
2		0.05	80	TEMPO	14.4	288
3		0.05	80	K ₂ CO ₃	26.1	522
4		0.05	80	HNO ₃	Trace	0
5		0.05	80	NHPI	17.4	348
6		0.1	80	K ₂ CO ₃	46.0	460
7		0.1	50	K ₂ CO ₃	18.2	182
8		0.1	100	K ₂ CO ₃	62.0	620
9	2	0.05	80	-	23.4	468
10		0.05	80	TEMPO	22.0	440
11		0.05	80	K ₂ CO ₃	30.0	600
12		0.05	80	HNO ₃	12.2	244
13		0.05	80	NHPI	24.2	484
14		0.1	80	K ₂ CO ₃	30.5	305
15		0.1	50	K ₂ CO ₃	13.5	135
16		0.1	100	K ₂ CO ₃	53.0	530
17		0.05	80	-	10.5	210
18	0.05	80	TEMPO	17.9	358	
19	0.05	80	K ₂ CO ₃	18.0	360	

20	3	0.05	80	HNO ₃	Trace	0
21		0.05	80	NHPI	13.7	274
22		0.1	80	K ₂ CO ₃	18.0	180
23		0.1	50	K ₂ CO ₃	10.8	108
24		0.1	100	K ₂ CO ₃	13.4	134
25	4	0.05	80	-	18.4	368
26		0.05	80	TEMPO	17.7	354
27		0.05	80	K ₂ CO ₃	19.7	394
28		0.05	80	HNO ₃	Trace	0
29		0.05	80	NHPI	16.4	328
30		0.1	80	K ₂ CO ₃	20.0	200
31		0.1	50	K ₂ CO ₃	14.6	146
32		0.1	100	K ₂ CO ₃	16.4	164
33	-	-	80	-	5.0	-
34	-	-	80	TEMPO	7.0	-
35	-	-	80	K ₂ CO ₃	8.0	-

Table 1.11 : Oxidation products yield of 1-phenylethanol^[90]

In all experiments, a high selectivity towards the formation of the ketone was found since no traces of by-products were detected by GC and GC–MS analyses of the final reaction mixtures (only the unreacted alcohol and the ketone product were found).

G.B. Shul'pin *et al* synthesized the following complex^[91](Fig 1.59)

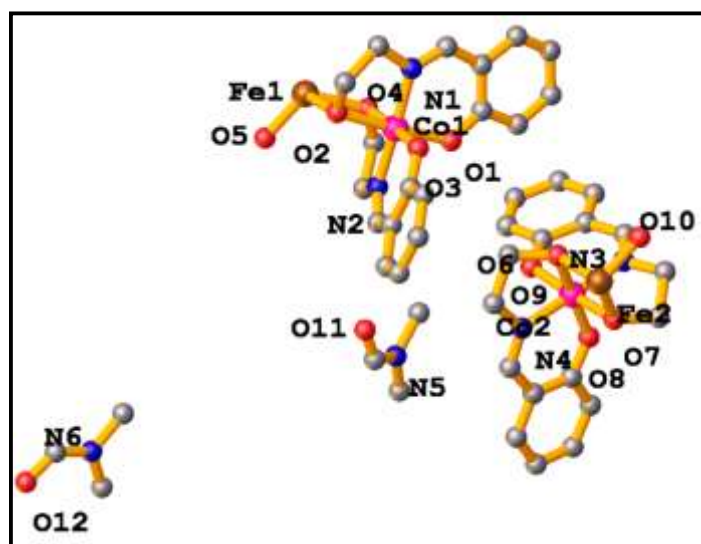


Fig 1.59 : Perspective view of heterometallic Fe(II) & Co (II)^[91]

It is a very unique heterometallic compound whose structure has been revalidated by a lot of physical measurements like magnetic studies, Mössbauer Spectroscopy, (HF-EPR) Spectroscopy etc. They have shown the “Direct Synthesis” method and also using a polydentate Schiff base ligand, such as salicylidene-2-ethanolamine. An extensive literature survey revealed that this type of coordination is very a rare example of the $M_6(\mu-X)_9$ MST, where two trinuclear $M_3(\mu-X)_4$ species are linked by a $M(\mu-X)M$ bonding together into the hexanuclear assembly. Antiferromagnetic coupling was also indicated between the Fe(III)–Fe(III) centers in magnetic studies. The HF-EPR spectra revealed uncommon parameters for an iron dimer. These methods, along with the Mössbauer spectroscopy and charge balance equations, support the finding of Co(III) and Fe(III) together in the complex.

This group investigated the use of the compound in alkane oxidation. Acetonitrile is the media of choice and nitric acid promoter is used as in earlier case. Again the alkyl hydroperoxide path was followed. Pretty high turnover numbers were achieved. Reported yield was also high and along with the high TON, its an excellent combination offered by the catalyst. Both linear and branched alkane systems have been utilized in the reactions to understand the proper efficacy of the catalytic system. The ESI-MS studies revealed two entities, $[Co(HSae)_2]^+$ and $[Co_2Fe(Sae)_4]^+$ in solution. It was thus concluded that trinuclear species Co_2Fe results for the intensive growth of the initial reaction rate. The advantages of this system lie in the great TOF values, which is as high as $1.12 \times 10^4 \text{ h}^{-1}$ (3.1 s^{-1}). It has been believed that the $[Co_2Fe(Sae)_4]^+$ particles actively generate hydroxyl radicals. The proposed catalytic path is a unique example of heterometallic coordination compound in homogeneous catalysis. The enhanced activity of the $[Co_2Fe(Sae)_4]^+$ was probably due to the specific coordination environment of a tetracoordinated iron center and also the hydrogen-bonded assistance along with Co–Fe Ox-Red interactions.

1.7 Schiff base metal complex in DNA/protein interaction:

Antibiotic-resistance is a major issue these days. It's important to develop new therapies which is away from this. Schiff bases metal complexes are effective as anti-inflammatory, antifungal, antibacterial, antiproliferative, antimalarial, antipyretic, antiviral agents. They are useful pharmacophore for developing bioactive compounds^[92]. The biological activities are explained in a crux in **Fig 1.60**.

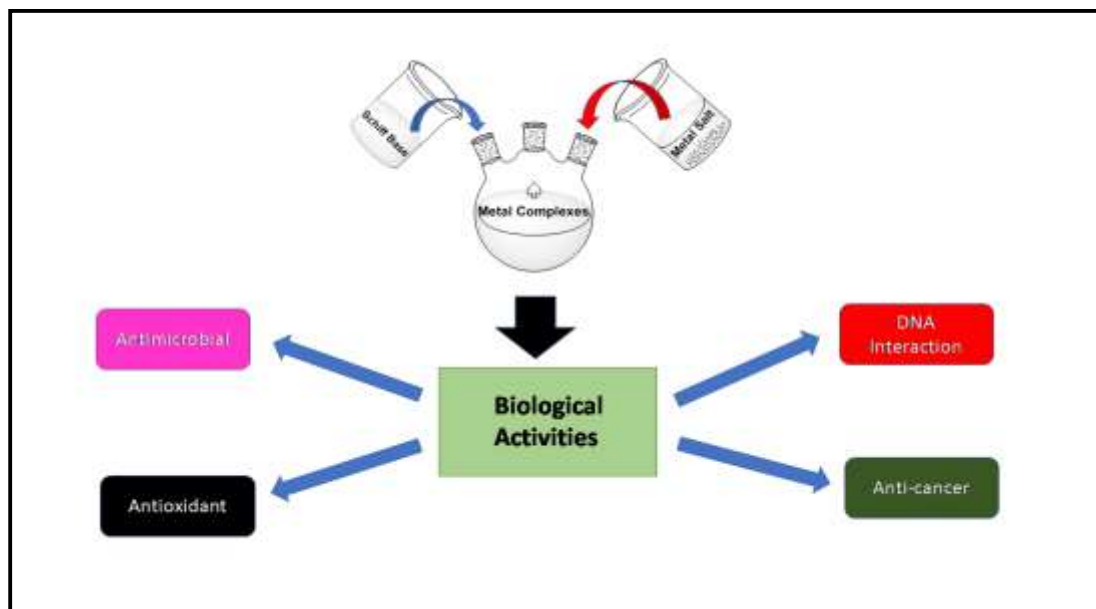


Fig 1.60 : Biological activities of metal complexes.^[92]

Abid *et al.* reported ZrO^{2+} , VO^{2+} , Pd^{2+} , V^{3+} , Cd^{2+} , and Rh^{3+} Schiff base complexes^[93] with the following ligand (**Fig 1.61**) that showed biological activity. Azomethine metal complexes act as antimicrobials for Gram-positive and Gram negative bacteria.

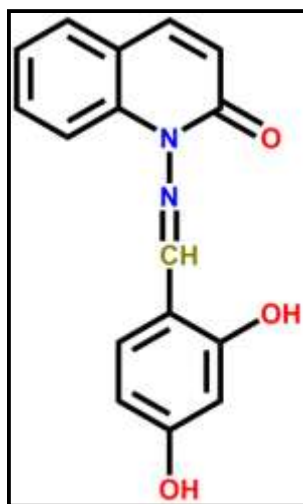


Fig 1.61 : Schiff base ligand^[93]

Abdulghani *et al.* designed complexes of Co^{2+} , Cd^{2+} , Pd^{4+} , Pt^{2+} , Ni^{2+} , and Cu^{2+} [94] with azomethines of cefotaxime antibiotic (**Fig 1.62**) and was thoroughly studied.

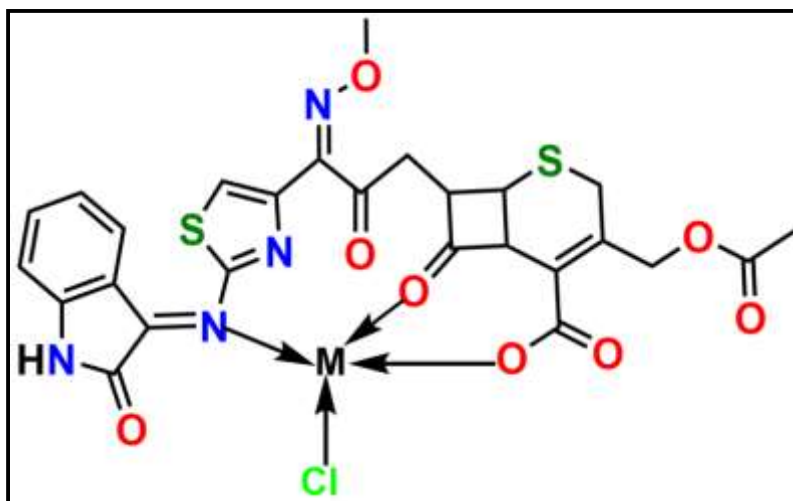


Fig 1.62 : Azomethine metal complex^[94]

Most of these showed octahedral geometry. It displayed antibacterial property towards *E. coli*, *P. aeruginosa*, *S. aureus*, and *S. pneumonia* etc. Some divalent metals have been prepared the above ligand.

Koz *et al.* studied divalent transition metals like cobalt, nickel, and copper along with azomethine^[95]. The ligands are shown in the following figure(**Fig 1.63**).

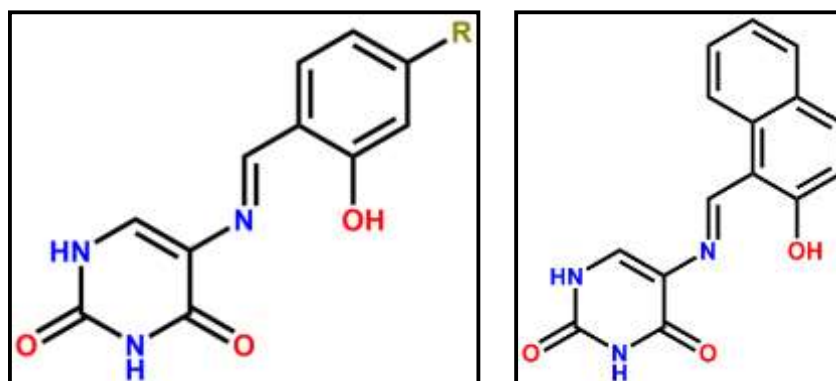


Fig 1.63 : Ligands that complex transition metal ions^[95]

The synthesized complexes were trialed against pathogenic bacteria and fungal species. Cu^{2+} , Co^{2+} , and Ni^{2+} complexes of Schiff bases having $-\text{SiOCH}_3$ ^[96] groups were obtained. (**Fig 1.64**). The complexes were tested as a growth inhibiting agent towards fungus.

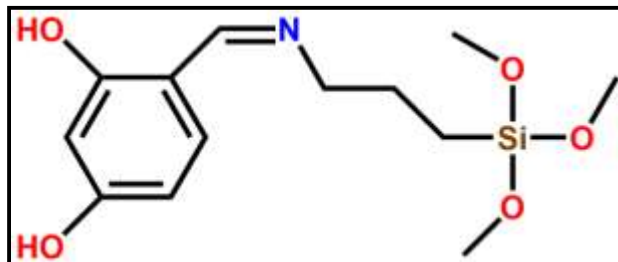


Fig 1.64 : Schiff bases having $-\text{SiOCH}_3$ groups^[96]

Gaballa *et al.* synthesized Pt^{2+} Schiff base complexes^[97]. They showed antibacterial activity towards *P. aeruginosa*, *S. aureus*, *E. coli*, and *B. subtilis*.

El-Sherif *et al.* synthesized metal complexes of Cu^{2+} , Zn^{2+} , and Ni^{2+} (**Fig 1.65**). They were good antibacterial agents^[98].

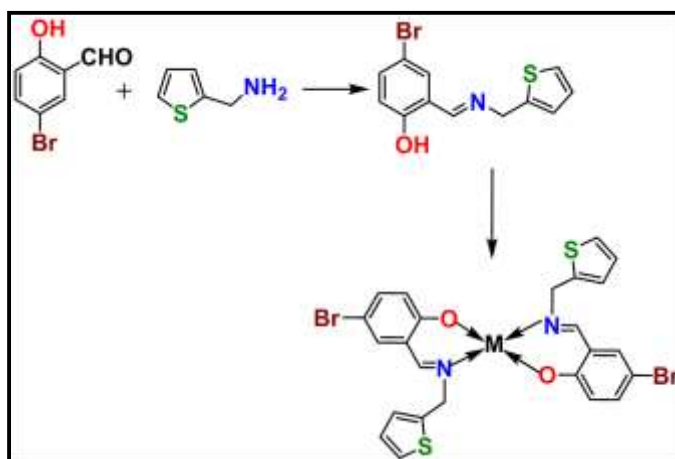


Fig 1.65 : Schiff base metal complexes to act as antibacterials^[98]

Abdel-Rahman *et al.* made Schiff base Fe^{2+} complexes^[99] (**Fig 1.66**) all of which displayed antibacterial activity.

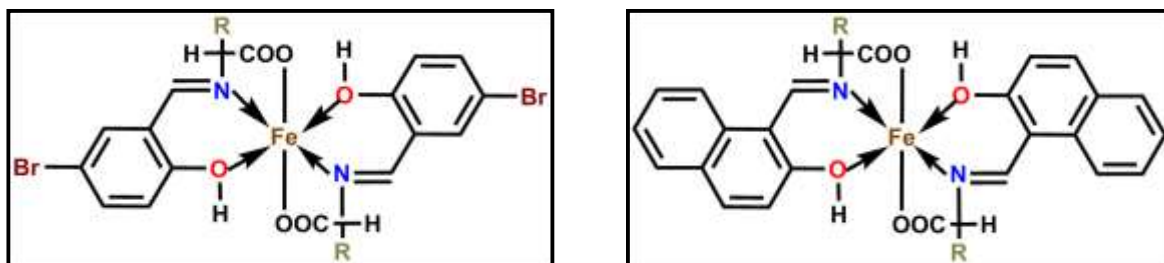


Fig 1.66 : Schiff base Fe^{2+} complexes^[99]

Shaker *et al.* synthesized octahedral iron complexes with ligands from sodium 3-formyl-4-hydroxybenzenesulfonate and amino acid (**Fig 1.67**) which again showed antibacterial action towards various kinds of pathogenic bacterial strains^[100].

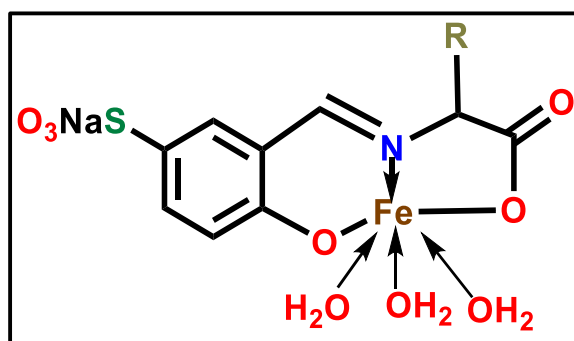


Fig 1.67 : Octahedral iron complexes^[100]

Abu-Dief *et al.* designed amino acid azomethine Cu^{2+} complexes showing antibacterial activity towards *P. aeruginosa*, and *B. cereus*^[101].

Neelakantan *et al.* got azomethine from amino acids and o-phthalaldehyde, which was eventually used to prepare Ni^{2+} , Co^{2+} , Mn^{2+} , VO^{2+} , and Cu^{2+} complexes. These were antifungal in nature^[102].

Rajasekar *et al.* reported Ni^{2+} and Cu^{2+} complexes with azomethine(**Fig 1.68**). These were antibacterial in nature. As compared to the free ligand, complexes were better in antimicrobial properties^[103].

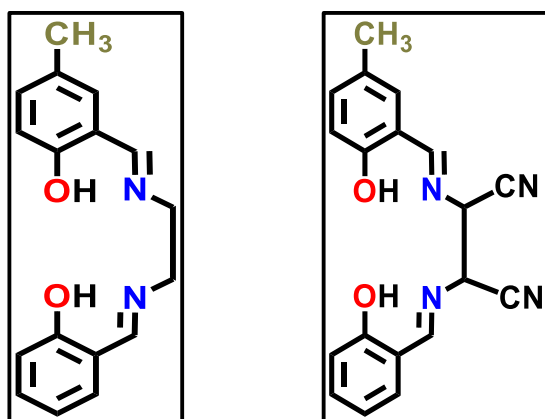


Fig 1.68 : Schiff base ligands with azomethine^[103]

Abdel-Rahman *et al.* synthesized nano-sized Cu^{2+} and Fe^{2+} complexes of the following ligands (Fig 1.69). They were antimicrobial towards *M. luteus*, *E. coli*, *B. subtilis*, *A. niger*, *S. cerevisiae*, and *C. glabrata*^[104].

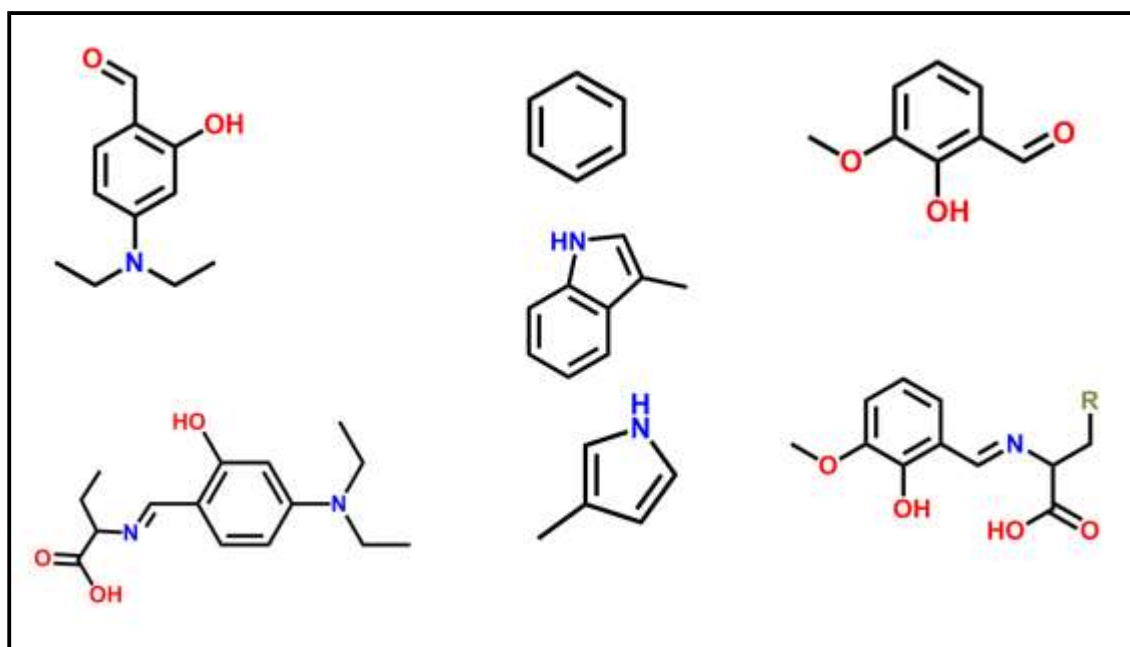


Fig 1.69 : Schiff base ligands designed to bind Cu^{2+} and Fe^{2+} in nano complexes^[104]

Miloud *et al.* synthesized and characterized metal complexes of the following (Fig 1.70) and they showed excellent antifungal activity^[105].

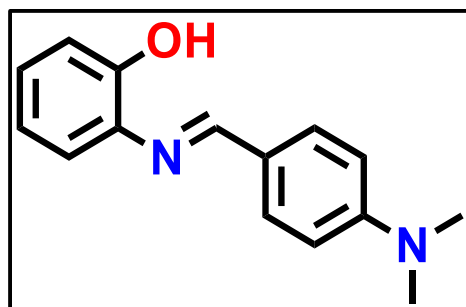


Fig 1.70 : Ligands to bind metal complexes^[105]

El-zweay *et al.* synthesized the following with mixed ligand (catechol being primary and salicylaldehyde co ligand)^[106](**Fig 1.71**). By magnetic moment measurements and electronic spectra, it was seen that the Mn^{2+} , Fe^{3+} , Co^{2+} complexes exhibited octahedral geometry, Zn^{2+} remained tetrahedral and Cu^{2+} and Ni^{2+} in square planer geometry. These were proven to be antifungal towards strains responsible for eye infections (BCEI), such as *K. pneumoniae*, *E. coli*, and *S. aureus*. The catechol moiety is more effective than salicylaldehyde.

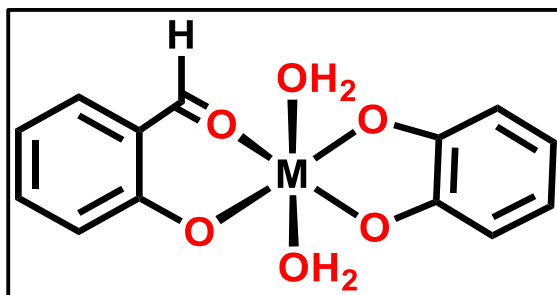


Fig 1.71 : Schiff base mixed ligand^[106]

El-Sonbati *et al.* synthesized the following^[107](**Fig 1.72**).

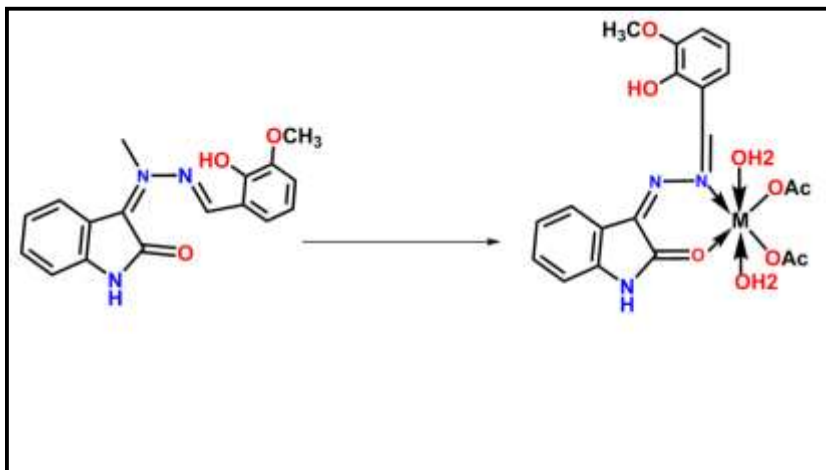


Fig 1.72 : Octahedral metal Schiff base complex^[107]

These were fully characterized and the result showed that octahedral configuration of metal complexes and the Schiff base together behaves as a neutral bidentate forming a six-membered chelate ring to the metal ion through azomethine ketonic oxygen atoms and nitrogen. Further these compounds were antimicrobial towards *C. albicans*, *E. coli*, and *S. aureus*.

Several azomethine thiohydantoin derivatives^[108] and their homonuclear Th^{4+} , ZrO^{2+} , and UO_2^{4+} complexes have been studied by Dash *et al*(**Fig 1.73**). Spectroscopy was used to characterize them and were screened for antifungal property.

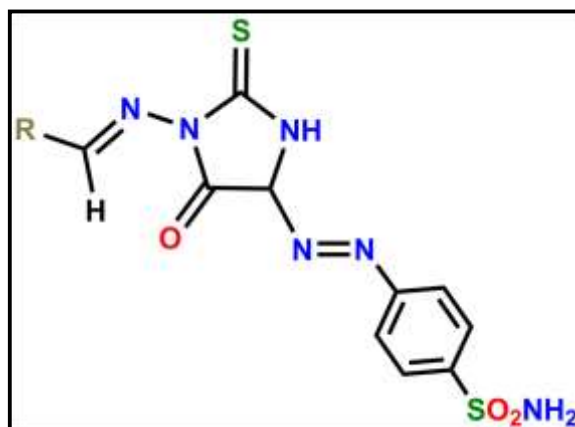


Fig 1.73 : Azomethine thiohydantoin derivatives^[108]

Vadde *et al.*^[109] describe tetradentate N₂O₂ donor ligands or azomethine and their mononuclear Pd²⁺, Ni²⁺, Co²⁺, and Cu²⁺ complexes. These were characterized by NMR, IR, mass, ESR, thermal and elemental analysis and conductivity measurements, finally revealing an octahedral geometry of Ni and Co complexes and square planar geometry of Pd and Cu complexes. They displayed *in vitro* antibacterial activity against *K. pneumonia*, *S. aureus*, *B. subtilis*, and *E. coli* and were found to be more active than the standard drugs ampicillin and streptomycin.

Body cells suffer damage by biomolecular oxidation. Free radicals cause oxidative chain reactions. To decelerate the process, antioxidants come handy by scavenging the free radicals stopping the detrimental effects to the cell walls. Recently metal-based antioxidants are wisely chosen for their effectiveness against oxidative stress. Research has been carried out on Schiff base metal complexes for their proven free radical scavenging properties. A study was performed i.e. DPPH free radical scavenging study, to assess the antioxidant characteristics of synthetically prepared compounds on the principles of their radical scavenging capacities. DPPH attains an odd electron that is being used in favor of scavenging activity.

Reddy *et al.* reported antioxidant activity of bi-metallic Zn²⁺, Co²⁺, Cu²⁺, Ni²⁺, and U⁴⁺ as illustrated in **Fig 1.74**. These were characterized and examined through NO DPPH, reducing power, and hydroxyl radical scavenging^[110].

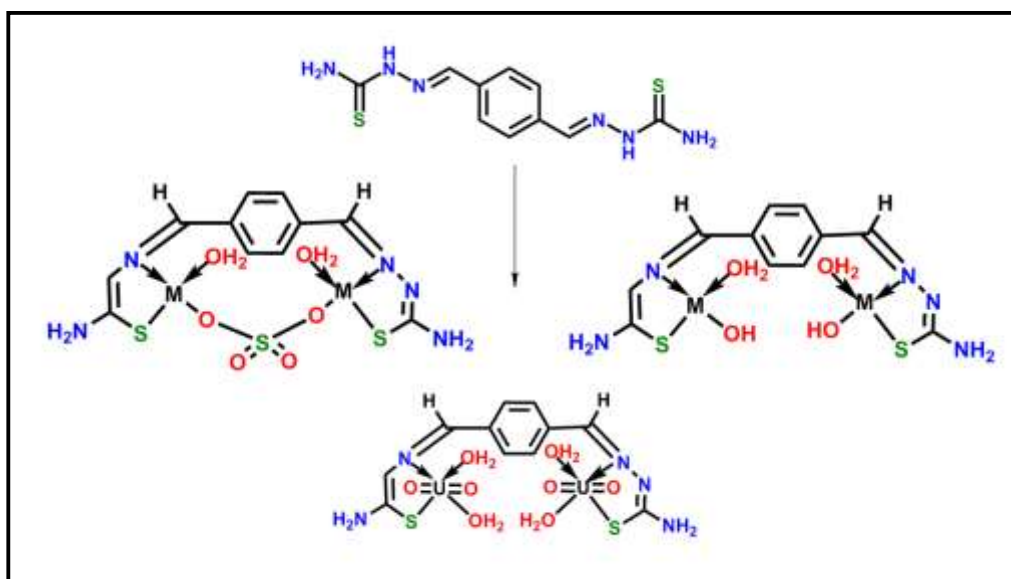


Fig 1.74 : Bi-metallic Zn²⁺, Co²⁺, Cu²⁺, Ni²⁺, U⁴⁺^[110]

Akila *et al.*^[111] synthesized VO^{2+} , Cu^{2+} , and Ni^{2+} complexes along with azomethine(**Fig 1.75**). They were evaluated for DPPH activity which yielded good results. They are all neutral and with a square pyramidal geometry for $[\text{VO}_2\text{L}]$ and square planar geometry for $[\text{Ni}_2\text{L}]$ and $[\text{Cu}_2\text{L}]$ complexes. DNA cleavage study shows that Cu^{2+} complex cleaves the DNA molecule completely. They were highly effective in arresting the formation of the DPPH radicals and lowering IC_{50} values as displayed in antioxidant assays.

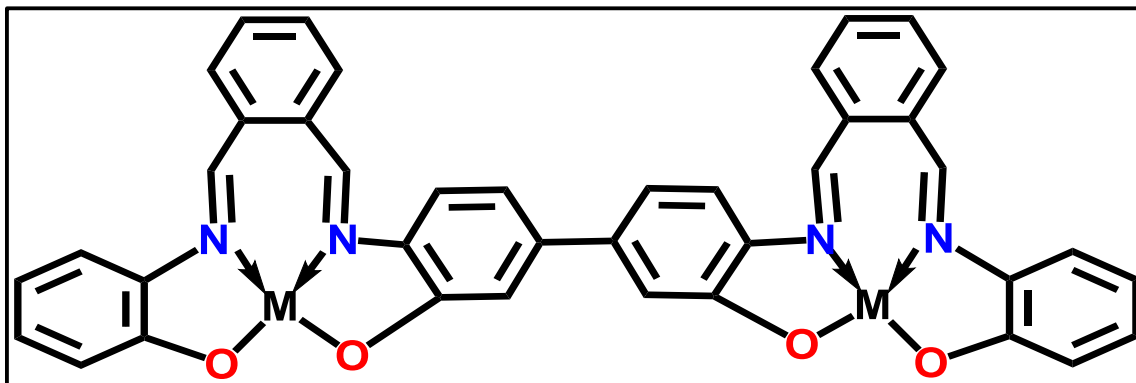


Fig 1.75 : VO^{2+} , Cu^{2+} , and Ni^{2+} complexes of azomethine^[111]

Prathima *et al.*^[112] made Ni^{2+} and Cu^{2+} complexes of benzyloxybenzaldehyde-4-phenyl3-thiosemicarbazone ligand(**Fig 1.76**).

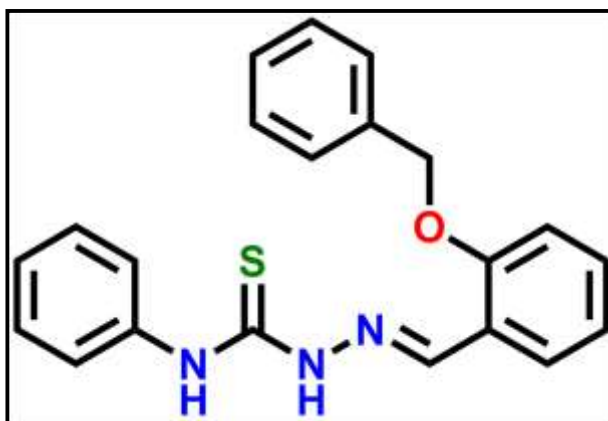


Fig 1.76 : Ni^{2+} and Cu^{2+} complexes of benzyloxybenzaldehyde-4-phenyl3-thiosemicarbazone ligand^[112]

These have shown reasonable activity in ferric ion-induced lipid peroxidation (60%) in DPPH scavenging as compared to standard antioxidant α -tocopherol.

Tadavi *et al.*^[113] synthesized the metal complexes with the following ligand(**Fig 1.77**). These were characterized by SEM–EDX, cyclic voltammetry, and single-crystal XRD etc. The nickel complex was in dimeric form with asymmetrical square planar geometry around each nickel centre. They were treated as an antioxidant against ascorbic acid.

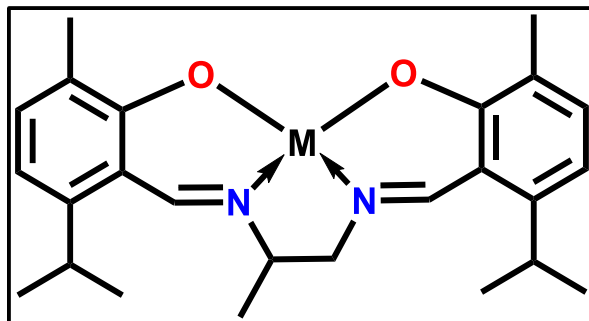


Fig 1.77 : Schiff base ligand for complexation^[113]

The analysis of the DNA binding effects of metal complexes is useful to understand whether they can be utilized as chemotherapeutic agents. This can inhibit the growth and reproduction of cancer cells over transcription inhibition.

Ni^{2+} , Co^{2+} , Zn^{2+} , and Cu^{2+} complexes of diaminothane and 5-nitro-o-vanillin (**Fig 1.78**) were studied by Raman *et al.*^[114].

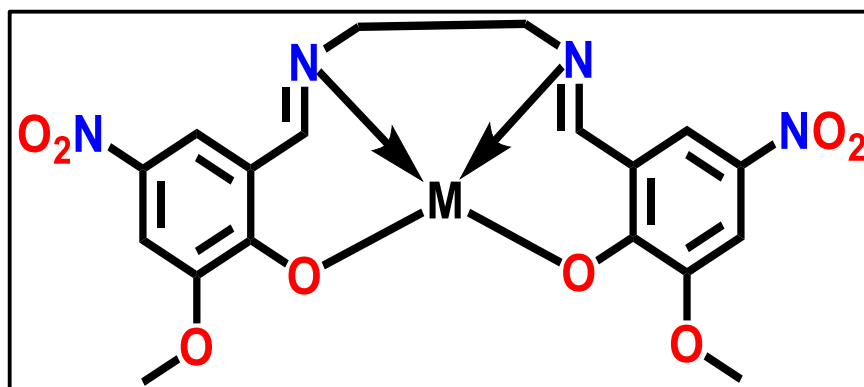


Fig 1.78 : Ni^{2+} , Co^{2+} , Zn^{2+} , and Cu^{2+} complexes of diaminothane and 5-nitro-o-vanillin^[114]

They displayed DNA binding properties. DNA-binding showed intrinsic binding constant of complexes from 1.58×10^4 to 2.71×10^4 (mol L^{-1}) $^{-1}$ which is similar to those of some DNA intercalative complexes. They bind DNA by classical intercalation. It is oxidative cleavage. Raman *et al.*^[115] studied Schiff base complexes. Supercoiled pBR322 DNA interactions were evident in gel electrophoresis. Cu^{2+} complexes showed highest nuclease activity.

Co^{2+} , Ni^{2+} , Cu^{2+} , Cd^{2+} , and Zn^{2+} complexes of the following were studied by Begum *et al.*^[116]. Structural features were elucidated by spectral and analytical techniques like ^1H NMR, IR, UV-vis, molar electric conductivity, elemental analysis, magnetic susceptibility and thermal studies. These complexes were soluble in DMSO and DMF. Binding with calf thymus DNA was analysed. They showed tight binding with DNA as they successfully slide between two piled base pairs and exhibit their fluorescent properties.

Reddy *et al.*^[117] synthesized ternary Cu^{2+} complexes with 1,10-phenanthroline/2,20-bipyridine and salicylidene tyrosine. The complex was square planar. The complexes showed binding with CT DNA ($K_b = 3.47 \times 10^4 \text{ M}^{-1}$ and $3.01 \times 10^4 \text{ M}^{-1}$ respectively).

Kalaivani *et al.*^[118] made Pd-complexes with the following (**Fig 1.79**).

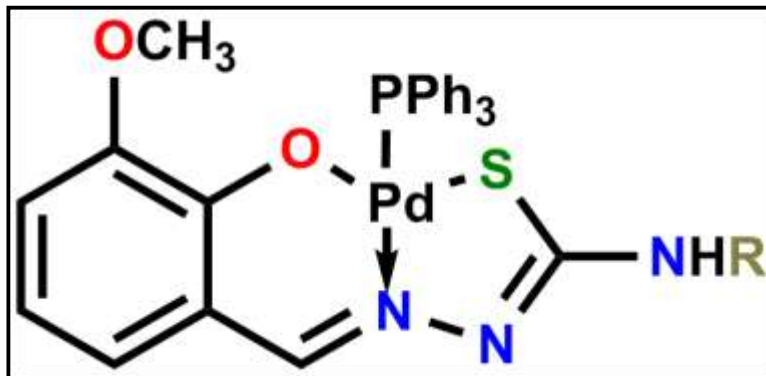


Fig 1.79 : Pd complexes^[118]

They were characterized with various spectroscopic techniques (mass, ^1H NMR, absorption, IR). They were all studied by single crystal X-ray diffraction. The two ligands are coordinated as ONS donor ligands, making six and five member rings. These were studied for CT DNA binding properties using emission titration and absorption techniques. Protein binding was also observed by quenching tryptophan and tyrosine residues.

Schiff base metal complexes were found to have anticancer properties as well. Schiff base Cu complexes of the following were studied by Amer *et al.*^[119]. These complexes display antitumor

activity in vitro studies against the colon carcinoma (HCT116), HepG2 cell lines and MCF-7, cell lines.

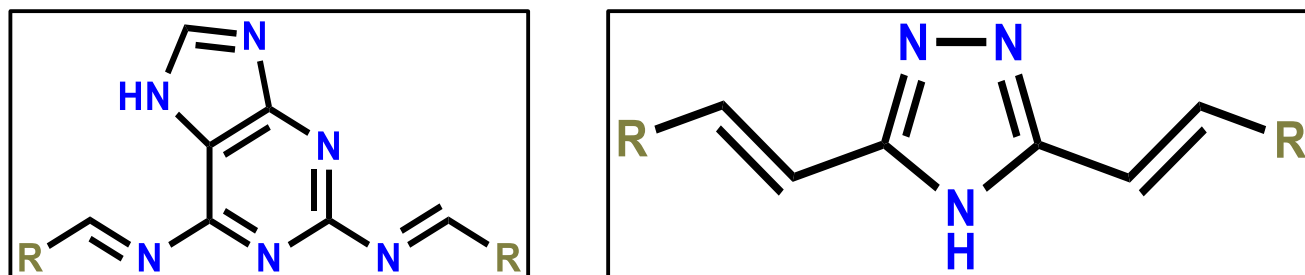


Fig 1.80 : Anticancer Schiff base Cu complexes^[119]

The Cu complexes of the following ligand(**Fig 1.81**) was reported by Creaven *et al*^[120]. They were screened for their anticancer action by using MTT process by the human Hep-G2, hepatic carcinoma cell line, and they showed better efficacy than cis platin.

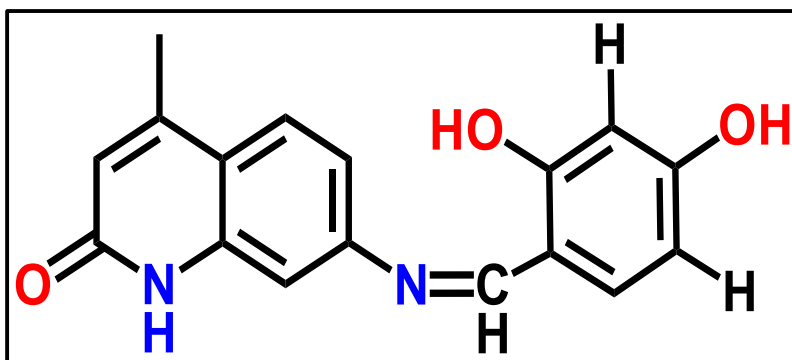


Fig 1.81 : Schiff base ligand for Cu complex^[120]

Patterson *et al.*^[121] prepared 12 salicylaldiminato Pt^{2+} complexes. They were checked for cytotoxicity towards three human glioma cell lines Hs683, LN405, and LN18. The correlation was drawn between aromatic rings in the complexes and the aliphatic group length with cytotoxicity.

T. Maity *et al*^[122] designed the following complexes(Fig 1.82-1.83).

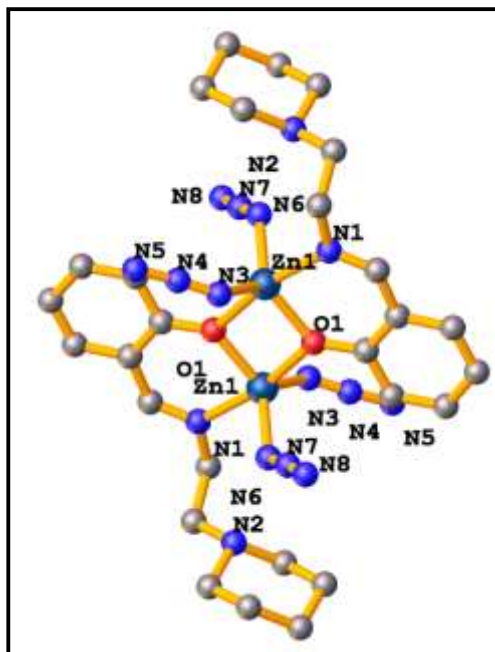


Fig 1.82 : Perspective view of Zn²⁺ Schiff base complex^[122]

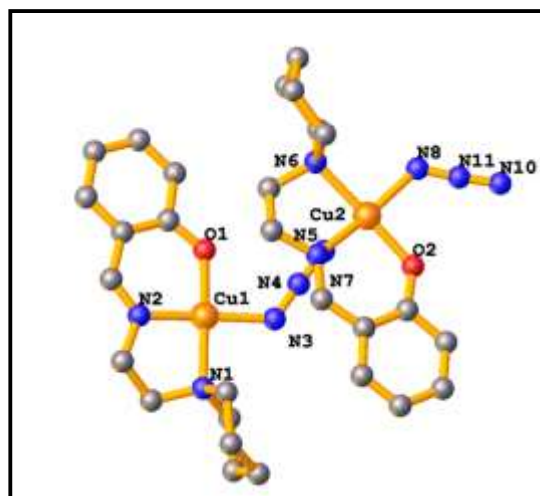


Fig 1.83 : Perspective view of Cu²⁺ Schiff base complex^[122]

Interaction of these complexes with DNA was checked. Non-covalent interaction with DNA involves intercalative or minor groove binding. Absorption spectroscopy was employed to study the association constant. The binding affinity of the complexes was assessed by gradually adding CT-DNA. The absorption maxima for both the complexes was seen to decrease upon addition of CT-DNA along with a little blue shift. The binding constant was found to be 1.04×10^5 and

1.903×10^5 for the complexes which indicates strong binding. Ethidium bromide, which is a strong intercalator, displacement studies was also carried out. When DNA-EtBr adduct is exposed to the complexes, the emission intensity of the adduct is observed to diminish. This is due to the displacement of EtBr from the DNA-EtBr adduct. CD spectroscopic studies was also done. The CD spectrum of CT DNA shows a canonical B-conformation with a large positive band around 270–280 nm and a negative band around 248 nm. Molar ellipticity of the positive bands decreased upon addition of the complexes. The relative viscosity of DNA increases gradually upon incubation with the sample. Hence, it could be said that the complexes interact with DNA in a strong intercalative mode.

To understand the binding of the complexes with HSA, UV-absorption titration was carried out. A decrease in the absorbance was seen for complexes 1 and 2 at 325 nm and 268 nm respectively. The association constant was calculated to be $5.3 \times 10^5 \text{ M}^{-1}$ and $3.95 \times 10^5 \text{ M}^{-1}$ for respectively. Fluorescence quenching studies show an intrinsic due to the presence of two chromophores, tryptophan (Trp) and tyrosine (Tyr). If tyrosine gets ionized, the emission intensity of HSA diminishes. A distinct decrease in the emission maxima of HAS at 340 nm was observed upon gradual addition of complex. The quenching constants for complexes 1 and 2 were found to be $1.58 \times 10^5 \text{ M}^{-1}$ and $8.8 \times 10^4 \text{ M}^{-1}$ from the Stern volmer equation which demonstrates effective binding. Molecular docking reveals that the complexes interact with the nearest adenine residue of the CT-DNA helix via a suitable π - π stacking interaction involving the phenyl ring of the ligand backbone. Calculations prove that the distance between the phenyl ring and the aromatic core of the adenine residue is 2.97 Å and 1.92 Å, for the two complexes paving the path for efficient interaction. The docking of the complexes with HSA also proves good interaction. MTT assay showed the cytotoxicity of both the complexes towards cell lines. Complexes 1 and 2 also showed apoptosis of cell lines.

A.H. Kianfer *et al.*^[123] synthesized the following(Fig 1.84):

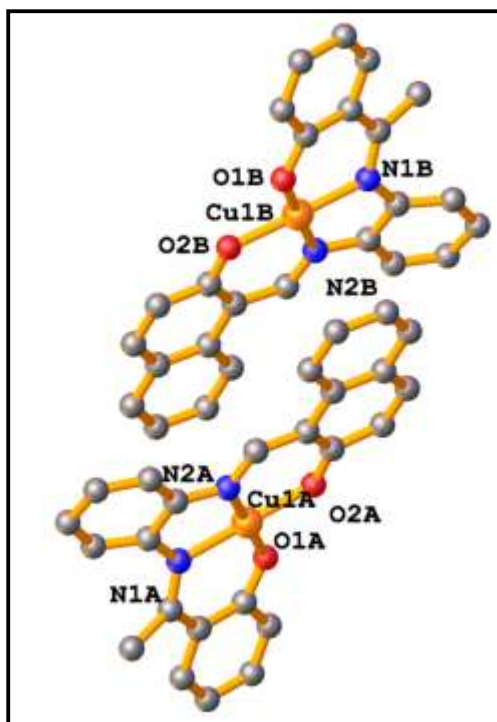


Fig 1.84 : Perspective view of Cu^{2+} Schiff base complex^[123]

The addition of increasing amounts of DNA to the complex solution significantly changes the electronic spectra. Hypochromism and bathochromism of was observed for both the complexes which indicates interaction of some sort. K_b , the binding constant was calculated by monitoring the decay of the absorbance at k_{max} with increased DNA concentration. These values were found to be similar to classical intercalators such as ethylene blue and ethidium bromide. Further, competitive binding between methylene blue and complexes for CT-DNA was studied. The complexes generally showed no emission. Methylene Blue is an intercalator for DNA. Increasing concentrations of the complexes were added to the CT-DNA which had been previously treated with MB. The addition of CT-DNA quenched the MB emission intensity. Again, the emission spectra of MB-DNA solutions increased significantly on addition of the complex. This suggests intercalative binding. Addition of complexes also alters the CD spectra. Protein binding was also analysed. Absorption intensity of BSA around 220–240 nm decreases on the addition of complexes because of alteration in the secondary structure of the protein. The fluorescence

spectra is altered as well. Quenching studies point towards static quenching. Overall, it can be said that the complex has considerable interaction with BSA as well.

Z. Li *et al* ^[124] synthesized the following (Fig 1.85-1.89):

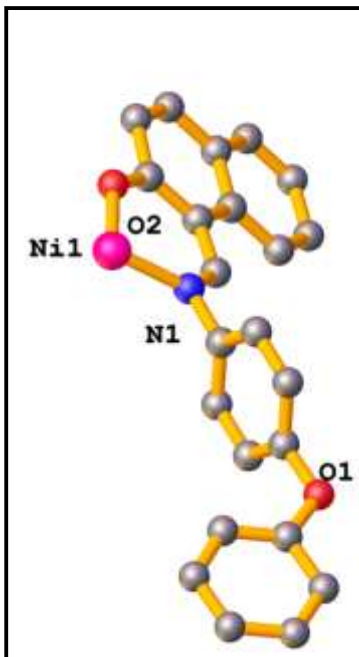


Fig 1.85 :Perspective view of Ni²⁺ Schiff base complex^[124]

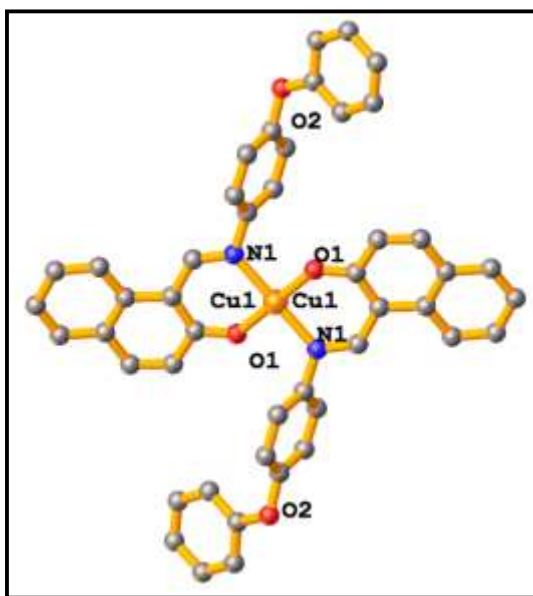


Fig 1.86 : Perspective view of Cu²⁺ complex^[124]

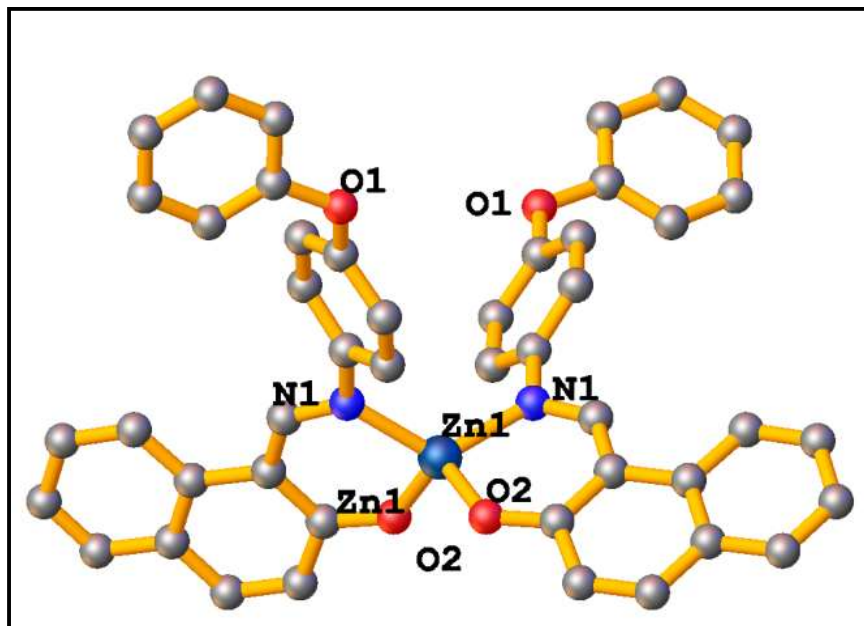


Fig 1.87 : Perspective view of Zn²⁺ complex^[124]

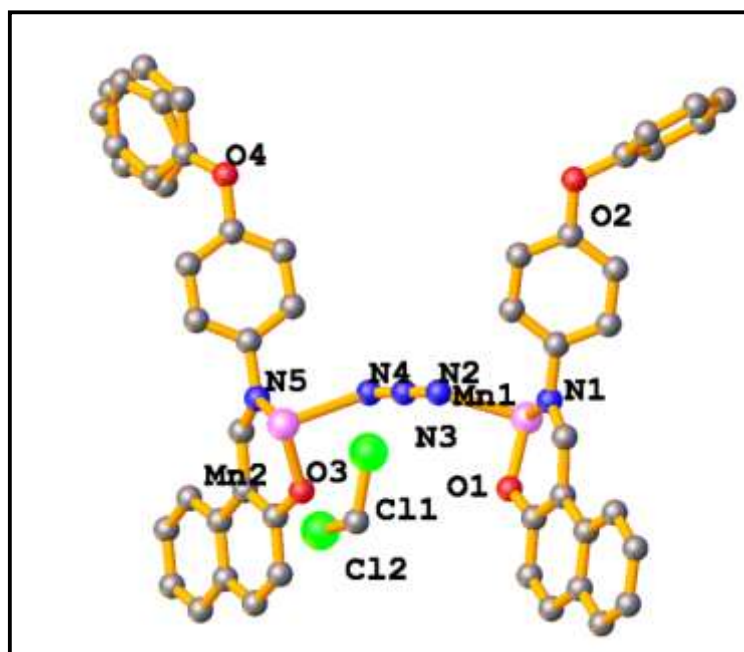


Fig 1.88 : Perspective view of Mn²⁺ complex^[124]

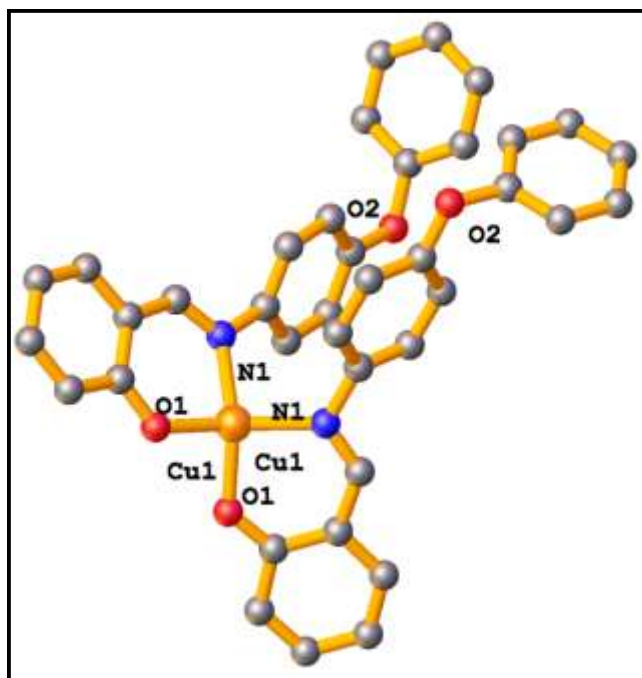


Fig 1.89 : Perspective view of Cu²⁺ complex^[124]

The absorption spectra of the complexes exhibited two bands in the range of 300 to 430 nm. With the addition of CT-DNA, the absorption spectra of the complexes show hypochromicity and a strong bathochromic shift is also seen proving intercalative DNA binding. The binding constant was the ratio of the slope to the intercept, from the plot of $- [DNA] / (\epsilon_a - \epsilon_f)$ versus $[DNA]$. The binding constant of the complexes were in the range 10^3 and 10^4 M⁻¹. The zinc(II) complex interacted more powerfully with CT-DNA and the magnitude order is (Zn²⁺) > (Cu²⁺) > (Ni²⁺) > (Mn³⁺). Planarity was an important criterion. Copper complex with a more planar naphthanyl ring shows higher K_b value than the other copper complex. Competitive binding between EB and complexes for CT DNA was studied. The fluorescence spectra of EB-DNA complex revealed that these complexes can quench the fluorescence of EB-DNA system through an intercalative mode. In the presence of every complex, both the positive (278 nm) and negative (246 nm) peaks of CD spectra increased in intensity which clearly signifies binding between the complexes and DNA. Interaction with BSA was also confirmed by absorbance and fluorescence studies.

M. Niu *et al* synthesized the following^[125](Fig 1.90-1.92),

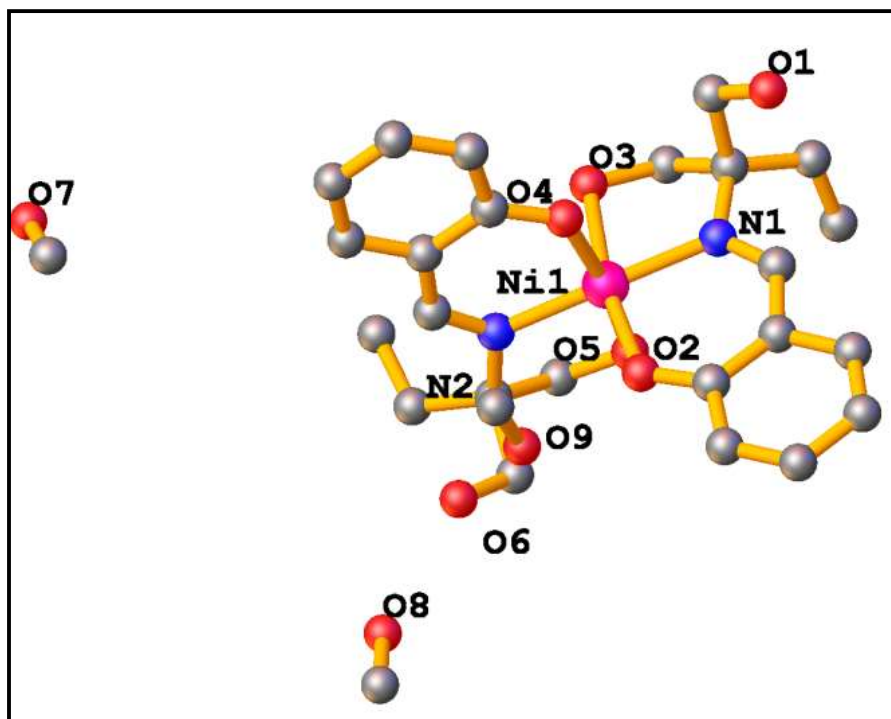


Fig 1.90 : Perspective view of Ni²⁺ complex^[125]

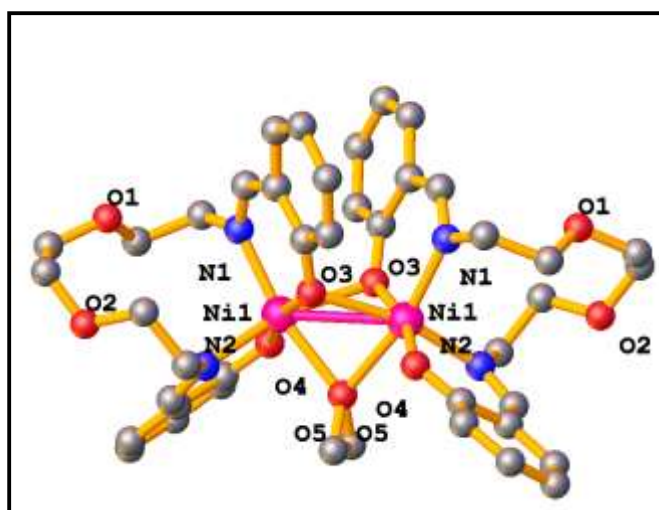


Fig 1.91 : Perspective view of Ni²⁺ complex^[125]

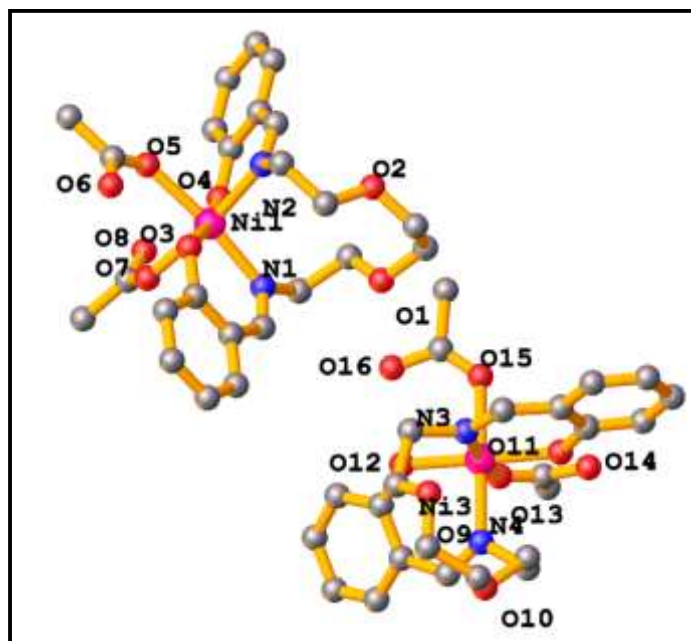


Fig 1.92 : : Perspective view of Ni²⁺ complex^[125]

The interactions of complexes with DNA were studied by the EB–DNA complex. The fluorescence spectra of EB–DNA system was quenched by the first complex and with increasing concentrations of the complexes 1–3, the intensity of the fluorescence band at 590 nm of the EB–DNA system decreased visibly. It could hence be concluded that the complexes showed intercalative binding with DNA. From the electronic spectra data, gradual addition of DNA to the solutions of the complexes, hypochromism and bathochromic shifts were clearly seen.

The CD-spectra also indicated binding of the complexes to CT-DNA. Addition of the complexes to BSA solution resulted in the quenching of fluorescence emission intensity. The complexes suppressed cell growth and promoted apoptosis

J.Y. Xu^[126] synthesized the following copper complexes(Fig 1.93-1.96):

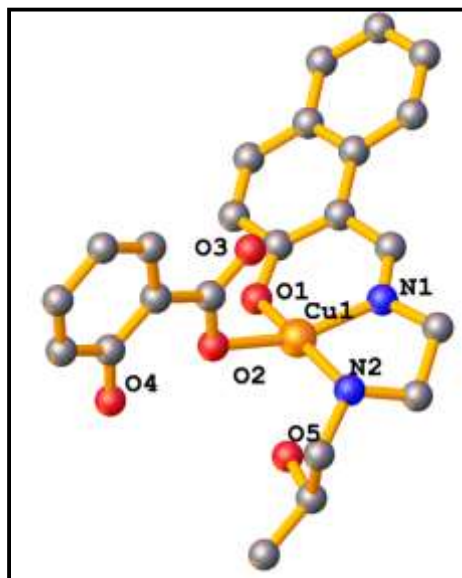


Fig 1.93 : Perspective view of Cu²⁺ complex1^[126]

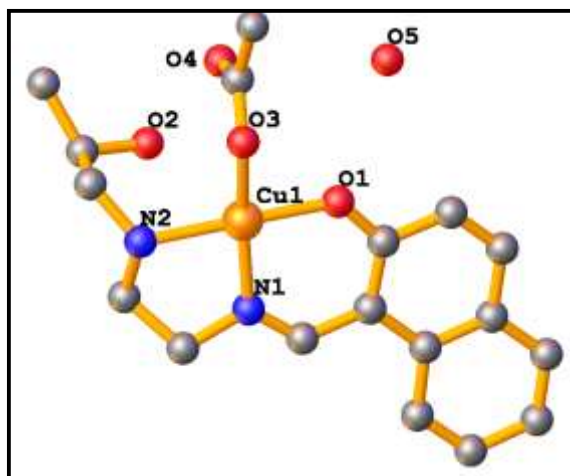


Fig 1.94 : Perspective view of Cu²⁺ complex2^[126]

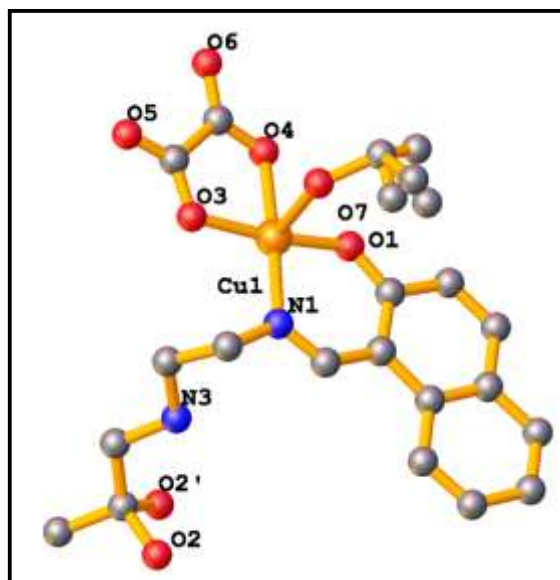


Fig 1.95 : Perspective view of Cu²⁺ complex3^[126]

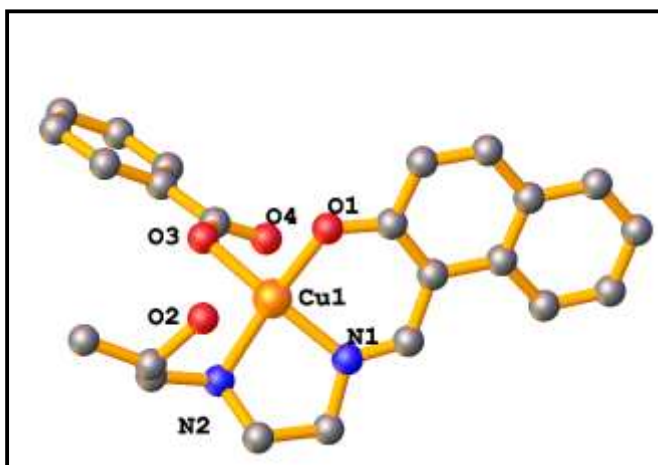


Fig 1.96 : Perspective view of Cu²⁺ complex4^[126]

In this study, four novel mononuclear Cu(II) complexes were synthesized and characterized. The complexes display efficient DNA binding activity by the intercalative mode, and are capable of causing double strand breaks in pUC19 plasmid DNA in the presence of H₂O₂ through an oxidative pathway. They also showed a high quenching ability of HSA fluorescence. All four complexes demonstrated high cytotoxic activity against two human cancer cell lines. Cotreating the complexes with salicylic acid disrupts the anticancer activity, indicating that mixed-ligand structures are crucial for the cytotoxicity. Especially, introducing the nonsteroidal

antiinflammatory drug salicylic acid to the Schiff base copper complex moiety induces additional antiproliferative effects. Adding acetic auxiliary ligands could manipulate the biological effects of Schiff base copper complexes, significantly increasing the cytotoxicity. Thus, it can be said that mixed-ligand copper(II) Schiff base complexes could function as great alternatives to platinum-based treatment in cancer chemotherapy.

1.8 Ascorbic acid oxidation by Schiff base complex modified electrode:

Ascorbic acid exists in biological bodies. Measuring amount of a chemical marker helps assessing food quality etc; ascorbic acid such an indicator. Various techniques have been utilised, such as spectrometry^[127], titrimetry^[128], HPLC^[129] and electrochemical methods^[130] as well. Recently, a growing interest is being observed in measuring ascorbic acid by chemically modified electrodes (CME-s) on the basis of their electrocatalytic effect. The electrode modified appropriately by an electro-active species, generally possesses one or more redox peaks. While scanning the potential in a supporting electrolyte solution, the corresponding redox peak current increases or decreases with the amount of ascorbic acid. The difference of currents is proportional to the concentration of ascorbic acid. Oxidation occurs at potentials above +500mV (vs SCE) at bare platinum or glassy carbon electrodes, while for modified electrode, it is much lower. Wring and Kang^[131] investigated the catalytic oxidation of ascorbic acid on an phthalocyanine derivative modified electrode estimated that the oxidation potential was lowered by 100-200mV. Janda *et al.*^[132] utilised a potentiometric method to detect ascorbic acid by a carbon fiber microelectrode coated with cobalt tetramethylpyridophyrazine where potential changed greatly. Kulys *et al.*^[133] used electrochemical sensor modified by 7,7,8,8,-tetrathianoquinodimethane (TCNQ) to detect ascorbic acid.

R.Q. Yu^[134] reported the electro-catalysis of ascorbic acid on a modified electrode of polymerized cobalt complex of N, N'-bis (salicylidene)- ethane -1,2 -diamine.

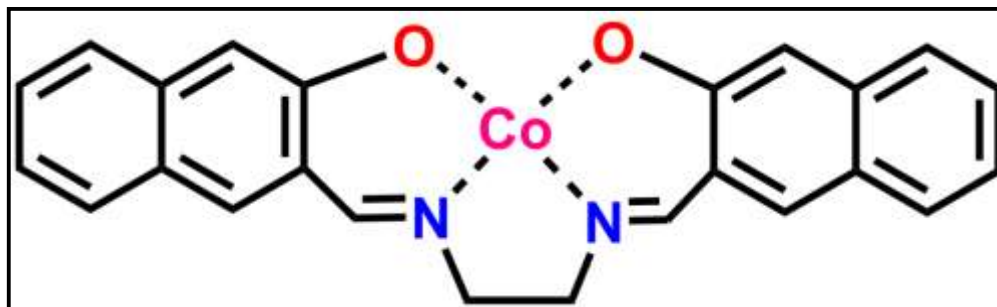


Fig 1.97 : Co²⁺ complex^[134]

The over-potential of ascorbic acid is reduced greatly in this work. In the past, preparation of electrodes modified by salen complexes of Ni and Cu was carried out in MeCN medium and added TBAP. The electrochemical nature is differs in different media. In the experiments done by this group, several supporting electrolytes, including dimethylformamide (DMF)/TBAP, ethanol/TBAP, acetonitrile/TBAP, acetonitrile/NaOH and ethanol/NaOH couples were applied. It was found that with the complex modified electrode, the anodic peak does not appear in the case of the salen ligand, whilst the redox peak currents decrease a bit , the peak potential remains unshifted and the peak potential separation increased. This indicates that the Co-salen film has an electrocatalytic effect on ascorbic acid. The effect of scan rate was in the range of 20-300mV/s. The oxidation peak current is seen to be proportional to the square root of scan rate below 200mV/s. The whole oxidation process of ascorbic acid on an unmodified electrode consisted of two steps: 1. ascorbic acid loses one electron 2. hydrolysis of the oxidized species. In this work, the anodic reaction couple [Co (III)/Co (II)] occurred at +0.3V, which is pretty close to the oxidation potential of ascorbic acid on an unmodified electrode. On the other hand, the oxidation potential of ascorbic acid on a modified electrode is reduced to +0.15V. It could thus be concluded that Co (III)/Co (II) pair has an electro-catalytic effect on the oxidation process. For different metal-salen complex modified electrode, the oxidation current shows the following trend : Co-salen> Ni -salen> Cu -salen > salen, whilst the oxidation potential has the reverse order: salen > Cu-salen>Nisalen>Co-salen. The metals have variable number of unpaired electrons with the order Co > Ni > Cu. Hence, Co complex provides the highest anodic current and the most negative potential.

X. Li *et al*^[135] synthesized the following copper complex(**Fig 1.98**)

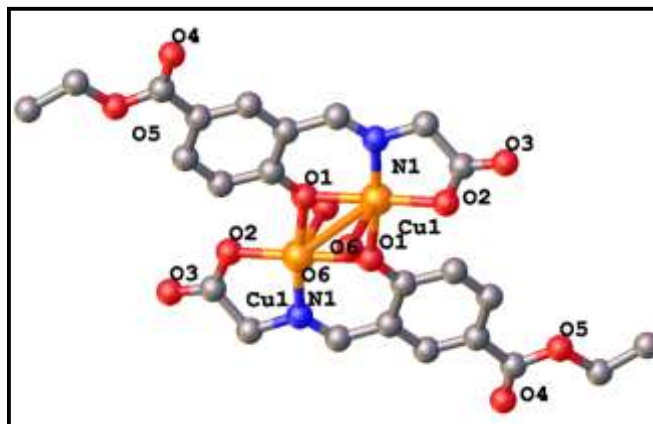


Fig 1.98 : Perspective view of Cu²⁺ Schiff base complex^[135]

Cyclic voltammetry for electropolymerization of the complex in DMSO at the potential of -0.3 to 1.4 V was done. Three anodic peaks were observed at 0.22 , 0.53 and 0.91 V. Peaks I and II are due to oxidation of Cu(I) to Cu(II) and Cu(II) to Cu(III), respectively. The third peak is due to the electron transfer from ligand-centered orbitals. The redox peaks increase with every subsequent scan for 40 cycles, indicating the deposition of copper complex on the electrode. A scan rate dependent study was also conducted alongside. The results again indicate a strongly adsorbed electroactive material. Electrochemistry impedance spectrum (EIS) was also used to elucidate the properties of the surface modified electrodes. The electrocatalytic property of the modified electrode towards the oxidation of ascorbic acid in pH 6.8 PBS buffer is remarkable. At bare GC electrode, an irreversible oxidation peak occurs at 0.28 V while with the modified one, the oxidation peak shifted to 0.16 V and the subsequent current also increased. This clearly indicates the catalytic effect. The oxidation of ascorbic acid is considered to undergo two one-electron transfers involving the involvement of a radical anion intermediate. This species then undergoes hydration reaction. Amperometric determination of ascorbic acid was carried out using the modified GC in PBS (pH 6.8) with KCl as supporting electrolyte. The oxidation peak currents were measured at 0.2 V and plotted against concentration of the acid. The modified electrode has high sensitivity and specificity for ascorbic acid whilst it exhibits no response to citric acid.

1.9 Objective of the Thesis

Study of transition metal complexes attracts immense interest of the scientists because of not only for their structural diversity but also for their application in many fields. Their structure and nuclearity can be controlled by the use of suitable metal center, Schiff base ligands, bridging ligands and reaction conditions. Appropriate tuning of mononuclear complexes can lead to the formation of multinuclear complexes. Accordingly, properties of the complexes change to a significant level when multinuclear complexes are under consideration. Interaction of metal centers in a multinuclear complex plays a crucial role in exhibition of their important properties and applications. Characterization of the complexes are possible by elemental analysis, different spectroscopic techniques including FT-IR, UV-visible, mass, fluorescence etc. The structure of metal complexes can be confirmed by single crystal X-ray diffraction studies when single crystals are obtained. Transition metal complexes can be used in many areas of science e.g magnetism, biology, catalysis, sensor, etc. Transition metal complexes of Cu(II), Ni(II), Co(II), etc. are being efficiently use as catalyst in different reactions e.g. epoxidation, alkane oxidation, alcohol oxidation, sulfoxidation, catechol oxidation. Despite of the fact that the research has advanced in this field, catalysis with high efficiency and selectivity are still being sought after. Our focus was to prepare some transition metal complexes of Cu(II), Ni(II), Co(II), etc. with the N,O – donor ligands and to design multinuclear complexes we used bridging ligands like pseudohalides, carboxylates, etc. The complexes will be characterized and employed as catalyst. Other properties were also explored like magnetic, electrical, biological, etc.

1.10 References :

- [1] a) M. Sarkar, R. Clérac, C. Mathonière, N. G. R. Hearn, V. Bertolasi, D. Ray, *Inorganic Chemistry* **2010**, *49*, 6575-6585; b) M. Sarkar, R. Clérac, C. Mathonière, N. G. R. Hearn, V. Bertolasi, D. Ray, *Inorganic Chemistry* **2011**, *50*, 3922-3933; c) S. Saha, A. Sasmal, C. Roy Choudhury, C. J. Gómez-García, E. Garrriba, S. Mitra, *Polyhedron* **2014**, *69*, 262-269.
- [2] a) D. R. Smith, *Coordination Chemistry Reviews* **1998**, *172*, 457-573; b) D. Rabinovich, *Journal of Chemical Education* **2000**, *77*, 311.
- [3] J. R. Prohaska, *Physiological Reviews* **1987**, *67*, 858-901.
- [4] J. E. Huheey, *Inorganic Chemistry: Principles of Structure and Reactivity*, Harper & Row, **1983**.
- [5] D. H. Brown, W. E. Smith, in *Enzyme Chemistry: Impact and applications* (Ed.: C. J. Suckling), Springer Netherlands, Dordrecht, **1984**, pp. 162-195.
- [6] D. Burnat, R. Kontic, L. Holzer, P. Steiger, D. Ferri, A. Heel, *Journal of Materials Chemistry A* **2016**, *4*, 11939-11948.
- [7] E. W. Dahl, N. K. Szymczak, *Angewandte Chemie International Edition* **2016**, *55*, 3101-3105.
- [8] L. Escriche, M.-P. Almajano, J. Casabó, F. Teixidor, J. C. Lockhart, G. A. Forsyth, R. Kivekäs, M. Sundberg, *Polyhedron* **1996**, *15*, 4203-4209.
- [9] M. Melnik, C. E. Holloway, *Coordination Chemistry Reviews* **2006**, *250*, 2261-2270.
- [10] G. B. Deacon, T. Feng, S. Nickel, B. W. Skelton, A. H. White, *Journal of the Chemical Society, Chemical Communications* **1993**, 1328-1329.
- [11] N. N. Greenwood, A. Earnshaw, *Chemistry of the Elements 2nd Edition*, **1997**.
- [12] M. Gerloch, *Inorganic Chemistry* **1981**, *20*, 638-640.
- [13] M. V. Veidis, G. H. Schreiber, T. E. Gough, G. J. Palenik, *Journal of the American Chemical Society* **1969**, *91*, 1859-1860.
- [14] S. Y. Shaban, A. E.-M. M. Ramadan, M. M. Ibrahim, F. I. Elshami, R. van Eldik, *Inorganica Chimica Acta* **2019**, *486*, 608-616.
- [15] S. M. Abu-El-Wafa, R. M. Issa, C. A. McAuliffe, *Inorganica Chimica Acta* **1985**, *99*, 103-106.

- [16] S.-L. Zhang, W.-F. Bie, *RSC Advances* **2016**, 6, 70902-70906.
- [17] N. S. Gill, R. S. Nyholm, *Journal of the Chemical Society (Resumed)* **1959**, 3997-4007.
- [18] L. M. Venanzi, *Journal of the Chemical Society (Resumed)* **1958**, 719-724.
- [19] J. W. Goodby, I. M. Saez, S. J. Cowling, V. Görtz, M. Draper, A. W. Hall, S. Sia, G. Cosquer, S.-E. Lee, E. P. Raynes, *Angewandte Chemie International Edition* **2008**, 47, 2754-2787.
- [20] T. F. S. Silva, L. M. D. R. S. Martins, *Molecules* **2020**, 25.
- [21] R. A. Sheldon, *Catalysis Today* **2015**, 247, 4-13.
- [22] Z. Ma, L. Wei, E. C. B. A. Alegria, L. M. D. R. S. Martins, M. F. C. Guedes da Silva, A. J. L. Pombeiro, *Dalton Transactions* **2014**, 43, 4048-4058.
- [23] B. A. Jazdzewski, W. B. Tolman, *Coordination Chemistry Reviews* **2000**, 200, 633-685.
- [24] S. Itoh, M. Taki, H. Kumei, S. Takayama, S. Nagatomo, T. Kitagawa, N. Sakurada, R. Arakawa, S. Fukuzumi, *Inorganic Chemistry* **2000**, 39, 3708-3711.
- [25] P. Chaudhuri, K. Wieghardt.
- [26] a) A. Messerschmidt, R. Huber, K. Wieghardt, T. Poulos, (Eds.: A. Messerschmidt, R. Huber, K. Wieghardt, T. Poulos), Wiley, Chichester, UK, **2001**; b) J. W. Whittaker, *Chemical Reviews* **2003**, 103, 2347-2364.
- [27] N. Ito, S. E. V. Phillips, C. Stevens, Z. B. Ogel, M. J. McPherson, J. N. Keen, K. D. S. Yadav, P. F. Knowles, *Nature* **1991**, 350, 87-90.
- [28] N. Ito, S. E. Phillips, K. D. Yadav, P. F. Knowles, *Journal of molecular biology* **1994**, 238, 794-814.
- [29] a) N. G. Connelly, W. E. Geiger, *Chemical Reviews* **1996**, 96, 877-910; b) V. V. Pavlishchuk, A. W. Addison, *Inorganica Chimica Acta* **2000**, 298, 97-102.
- [30] C. Wright, A. G. Sykes, *Journal of inorganic biochemistry* **2001**, 85, 237-243.
- [31] a) M. M. Whittaker, J. W. Whittaker, *Journal of Biological Chemistry* **1988**, 263, 6074-6080; b) M. M. Whittaker, D. P. Ballou, J. W. Whittaker, *Biochemistry* **1998**, 37, 8426-8436; c) B. P. Branchaud, M. P. Montague-Smith, D. J. Kosman, F. R. McLaren, *Journal of the American Chemical Society* **1993**, 115, 798-800.
- [32] M. M. Whittaker, J. W. Whittaker, *Biophysical Journal* **1993**, 64, 762-772.
- [33] F. Himo, L. A. Eriksson, F. Maseras, P. E. M. Siegbahn, *Journal of the American Chemical Society* **2000**, 122, 8031-8036.

- [34] B. E. Turner, B. P. Branchaud, *Bioorganic & Medicinal Chemistry Letters* **1999**, *9*, 3341-3346.
- [35] J. G. Radziszewski, M. Gil, A. Gorski, J. Spanget-Larsen, J. Waluk, B. a. J. Mróz, *The Journal of Chemical Physics* **2001**, *115*, 9733-9738.
- [36] N. Kitajima, K. Whang, Y. Moro-oka, A. Uchida, Y. Sasada, *Journal of the Chemical Society, Chemical Communications* **1986**, 1504-1505.
- [37] Y. Wang, T. D. P. Stack, *Journal of the American Chemical Society* **1996**, *118*, 13097-13098.
- [38] F. Thomas, O. Jarjaves, C. Duboc, C. Philouze, E. Saint-Aman, J.-L. Pierre, *Dalton Transactions* **2004**, 2662-2669.
- [39] R. C. Pratt, T. D. P. Stack, *Journal of the American Chemical Society* **2003**, *125*, 8716-8717.
- [40] M. Orio, O. Jarjaves, H. Kanso, C. Philouze, F. Neese, F. Thomas, *Angewandte Chemie International Edition* **2010**, *49*, 4989-4992.
- [41] H. Ünver, I. Kani, *Polyhedron* **2017**, *134*, 257-262.
- [42] A. N. Kulakova, A. N. Bilyachenko, M. M. Levitsky, V. N. Khrustalev, A. A. Korlyukov, Y. V. Zubavichus, P. V. Dorovatovskii, F. Lamaty, X. Bantreil, B. VILLEMEJEANNE, J. Martinez, L. S. Shul'pina, E. S. Shubina, E. I. Gutsul, I. A. Mikhailov, N. S. Ikonnikov, U. y. S. Tsareva, G. B. Shul'pin, *Inorganic Chemistry* **2017**, *56*, 15026-15040.
- [43] S. Hazra, L. M. D. R. S. Martins, M. F. C. Guedes da Silva, A. J. L. Pombeiro, *RSC Advances* **2015**, *5*, 90079-90088.
- [44] L. M. T. Frija, E. C. B. A. Alegria, M. Sutradhar, M. L. S. Cristiano, A. Ismael, M. N. Kopylovich, A. J. L. Pombeiro, *Journal of Molecular Catalysis A: Chemical* **2016**, *425*, 283-290.
- [45] A. G. Mahmoud, M. F. C. Guedes da Silva, E. I. Śliwa, P. Smoleński, M. L. Kuznetsov, A. J. L. Pombeiro, *Chemistry – An Asian Journal* **2018**, *13*, 2868-2880.
- [46] Z. Liu, Z. Shen, N. Zhang, W. Zhong, X. Liu, *Catalysis Letters* **2018**, *148*, 2709-2718.
- [47] E. Lagerspets, K. Lagerblom, E. Heliövaara, O.-M. Hiltunen, K. Moslova, M. Nieger, T. Repo, *Molecular Catalysis* **2019**, *468*, 75-79.
- [48] L. Marais, J. Burés, J. H. L. Jordaan, S. Mapolie, A. J. Swarts, *Organic & Biomolecular Chemistry* **2017**, *15*, 6926-6933.

- [49] S. Kulkarni, M. Alurkar, A. Kumar, *Applied Catalysis A: General* **1996**, *142*, 243-254.
- [50] C. H. Bamford, K. G. Al-Lamee, *Polymer* **1996**, *37*, 4885-4889.
- [51] T. Balakrishnan, V. Rajendran, *Journal of Applied Polymer Science* **2000**, *78*, 2075-2080.
- [52] T. Malmström, C. Andersson, J. Hjortkjaer, *Journal of Molecular Catalysis A: Chemical* **1999**, *139*, 139-147.
- [53] M. Chanda, A. Sarkar, J. M. Modak, *Journal of Applied Polymer Science* **2004**, *93*, 883-893.
- [54] S.-s. Jew, H.-g. Park, *Chemical Communications* **2009**, 7090-7103.
- [55] D. A. Annis, E. N. Jacobsen, *Journal of the American Chemical Society* **1999**, *121*, 4147-4154.
- [56] V. Mirkhani, M. Moghadam, S. Tangestaninejad, B. Bahramian, *Applied Catalysis A: General* **2006**, *311*, 43-50.
- [57] E. da Palma Carreiro, A. J. Burke, *Journal of Molecular Catalysis A: Chemical* **2006**, *249*, 123-128.
- [58] G. Grivani, S. Tangestaninejad, A. Halili, *Inorganic Chemistry Communications* **2007**, *10*, 914-917.
- [59] M. K. Dalal, M. J. Upadhyay, R. N. Ram, *Journal of Molecular Catalysis A: Chemical* **1999**, *142*, 325-332.
- [60] D. R. Patel, M. K. Dalal, R. N. Ram, *Journal of Molecular Catalysis A: Chemical* **1996**, *109*, 141-148.
- [61] A. Barbarini, R. Maggi, M. Muratori, G. Sartori, R. Sartorio, *Tetrahedron: Asymmetry* **2004**, *15*, 2467-2473.
- [62] B. K. Hodnett, **2000**.
- [63] W. Lautsch, W. Broser, W. Rothkegel, W. Biedermann, U. Doering, H. Zoschke, *Journal of Polymer Science* **1952**, *8*, 191-213.
- [64] T. Berndt, O. Böge, J. Heintzenberg, P. Claus, *Industrial & Engineering Chemistry Research* **2003**, *42*, 2870-2873.
- [65] C. L. Elston, R. F. W. Jackson, S. J. F. MacDonald, P. J. Murray, *Angewandte Chemie International Edition in English* **1997**, *36*, 410-412.
- [66] K. Sato, M. Aoki, R. Noyori, *Science* **1998**, *281*, 1646-1647.

- [67] Z.-w. Yang, Q.-x. Kang, H.-c. Ma, C.-l. Li, Z.-q. Lei, *Journal of Molecular Catalysis A: Chemical* **2004**, *213*, 169-176.
- [68] K. C. Gupta, A. Kumar Sutar, C.-C. Lin, *Coordination Chemistry Reviews* **2009**, *253*, 1926-1946.
- [69] J. Zhao, J. Han, Y. Zhang, *Journal of Molecular Catalysis A: Chemical* **2005**, *231*, 129-135.
- [70] A. Böttcher, M. W. Grinstaff, J. A. Labinger, H. B. Gray, *Journal of Molecular Catalysis A: Chemical* **1996**, *113*, 191-200.
- [71] K. C. Gupta, A. K. Sutar, *Journal of Macromolecular Science, Part A* **2007**, *44*, 1171-1185.
- [72] K. C. Gupta, A. K. Sutar, *Journal of Molecular Catalysis A: Chemical* **2008**, *280*, 173-185.
- [73] J. P. Collman, L. Zeng, J. I. Brauman, *Inorganic Chemistry* **2004**, *43*, 2672-2679.
- [74] R. Antony, G. L. Tembe, M. Ravindranathan, R. N. Ram, *Polymer* **1998**, *39*, 4327-4333.
- [75] S. A. Patel, S. Sinha, A. N. Mishra, B. V. Kamath, R. N. Ram, *Journal of Molecular Catalysis A: Chemical* **2003**, *192*, 53-61.
- [76] R. Antony, G. L. Tembe, M. Ravindranathan, R. N. Ram, *Journal of Molecular Catalysis A: Chemical* **2001**, *171*, 159-168.
- [77] M. Nandi, P. Roy, H. Uyama, A. Bhaumik, *Dalton Transactions* **2011**, *40*, 12510-12518.
- [78] J. Chakraborty, M. Nandi, H. Mayer-Figge, W. S. Sheldrick, L. Sorace, A. Bhaumik, P. Banerjee, *European Journal of Inorganic Chemistry* **2007**, *2007*, 5033-5044.
- [79] P. Roy, K. Dhara, M. Manassero, P. Banerjee, *Inorganic Chemistry Communications* **2008**, *11*, 265-269.
- [80] U. Schuchardt, W. A. Carvalho, E. V. Spinacé, *Synlett* **1993**, *1993*, 713-718.
- [81] S. Hanessian, *ChemInform* **1989**, *20*, no-no.
- [82] R.-M. Wang, C.-J. Hao, Y.-P. Wang, S.-B. Li, *Journal of Molecular Catalysis A: Chemical* **1999**, *147*, 173-178.
- [83] W. J. Geary, *Coordination Chemistry Reviews* **1971**, *7*, 81-122.
- [84] D. Yang, L. Gao, W. Zhao, *Catalysis Letters* **2008**, *126*, 84.
- [85] A. A. Alshaheri, M. I. M. Tahir, M. B. A. Rahman, T. B. S. A. Ravoof, T. A. Saleh, *Chemical Engineering Journal* **2017**, *327*, 423-430.

- [86] P. Roy, M. Manassero, *Dalton Transactions* **2010**, 39, 1539-1545.
- [87] C. Di Nicola, Y. Y. Karabach, A. M. Kirillov, M. Monari, L. Pandolfo, C. Pettinari, A. J. L. Pombeiro, *Inorganic Chemistry* **2007**, 46, 221-230.
- [88] D. S. Nesterov, O. V. Nesterova, M. F. C. Guedes da Silva, A. J. L. Pombeiro, *Catalysis Science & Technology* **2015**, 5, 1801-1812.
- [89] L. I. Rodionova, A. V. Smirnov, N. E. Borisova, V. N. Khrustalev, A. A. Moiseeva, W. Grünert, *Inorganica Chimica Acta* **2012**, 392, 221-228.
- [90] O. V. Nesterova, D. S. Nesterov, A. Krogul-Sobczak, M. F. C. Guedes da Silva, A. J. L. Pombeiro, *Journal of Molecular Catalysis A: Chemical* **2017**, 426, 506-515.
- [91] D. S. Nesterov, E. N. Chygorin, V. N. Kokozay, V. V. Bon, R. Boča, Y. N. Kozlov, L. S. Shul'pina, J. Jezierska, A. Ozarowski, A. J. L. Pombeiro, G. B. Shul'pin, *Inorganic Chemistry* **2012**, 51, 9110-9122.
- [92] M. S. More, P. G. Joshi, Y. K. Mishra, P. K. Khanna, *Materials Today. Chemistry* **2019**, 14, 100195 - 100195.
- [93] K. Abid, S. Al-Bayati, A. Rasheed, *American Journal of Chemistry* **2016**, 6, 1-7.
- [94] A. J. Abdulghani, R. K. Hussain, *Open Journal of Inorganic Chemistry* **2015**, Vol.05No.04, 19.
- [95] K. Gamze, K. Hale, D. Astley, Y. İhsan, S. ASTLEY, *Gazi University Journal of Science* **2011**, 24, 407-413.
- [96] E. İspir, M. Kurtoğlu, F. Purtaş, S. Serin, *Transition Metal Chemistry* **2005**, 30, 1042-1047.
- [97] A. S. Gaballa, M. S. Asker, A. S. Barakat, S. M. Teleb, *Spectrochimica Acta Part A: Molecular and Biomolecular Spectroscopy* **2007**, 67, 114-121.
- [98] A. A. El-Sherif, T. M. A. Eldebss, *Spectrochimica Acta Part A: Molecular and Biomolecular Spectroscopy* **2011**, 79, 1803-1814.
- [99] L. H. Abdel-Rahman, R. M. El-Khatib, L. A. E. Nassr, A. M. Abu-Dief, M. Ismael, A. A. Seleem, *Spectrochimica Acta Part A: Molecular and Biomolecular Spectroscopy* **2014**, 117, 366-378.
- [100] A. M. Shaker, L. A.-M. E. Nassr, M. S. S. Adam, I. M. A. Mohamed, *Journal of The Korean Chemical Society* **2013**, 57, 560-567.

- [101] A. M. Abu-Dief, L. A. E. Nassr, *Journal of the Iranian Chemical Society* **2015**, *12*, 943-955.
- [102] M. A. Neelakantan, F. Rusalraj, J. Dharmaraja, S. Johnsonraja, T. Jeyakumar, M. Sankaranarayana Pillai, *Spectrochimica Acta Part A: Molecular and Biomolecular Spectroscopy* **2008**, *71*, 1599-1609.
- [103] M. Rajasekar, S. Sreedaran, R. Prabu, V. Narayanan, R. Jegadeesh, N. Raaman, A. Kalilur Rahiman, *Journal of Coordination Chemistry* **2010**, *63*, 136-146.
- [104] L. H. A. Rahman, A. M. Abu-Dief, N. A. Hashem, A. A. Seleem, *Int. J. Nano. Chem* **2015**, *1*, 79-95.
- [105] M. M. Miloud, F. S. Alassbaly, M. M. El-ajaily, T. Al-Noor, *J Biol Chem Chron* **2016**, *2*, 42-46.
- [106] R. El-zweay, M. El-ajaily, O. Salem, A. Maihub, **2017**.
- [107] A. Z. El-Sonbati, M. A. Diab, A. A. El-Bindary, M. I. Abou-Dobara, H. A. Seyam, *Journal of Molecular Liquids* **2016**, *218*, 434-456.
- [108] R. Mohapatra, A. Mahapatra, P. Naik, S. Naik, D. Dash, *Journal of the Korean Chemical Society* **2011**, *55*, 412-417.
- [109] G. Budige, M. R. Puchakayala, S. R. Kongara, A. Hu, R. Vadde, *Chemical and Pharmaceutical Bulletin* **2011**, *59*, 166-171.
- [110] D. H. Reddy, S.-M. Lee, K. Seshaiyah, R. Kasetti, *Journal of the Serbian Chemical Society* **2013**, *78*, 229-240.
- [111] E. Akila, M. Usharani, R. Rajavel, *International Journal of Pharmacy and Pharmaceutical Sciences* **2013**, *5*, 573-581.
- [112] B. Prathima, Y. Subba Rao, S. Adinarayana Reddy, Y. P. Reddy, A. Varada Reddy, *Spectrochimica Acta Part A: Molecular and Biomolecular Spectroscopy* **2010**, *77*, 248-252.
- [113] S. K. Tadavi, A. A. Yadav, R. S. Bendre, *Journal of Molecular Structure* **2018**, *1152*, 223-231.
- [114] N. Raman, K. Pothiraj, T. Baskaran, *Journal of Coordination Chemistry* **2011**, *64*, 4286-4300.
- [115] N. Raman, K. Pothiraj, T. Baskaran, *Journal of Coordination Chemistry* **2011**, *64*, 3900-3917.

- [116] A. Bushra Begum, N. D. Rekha, B. C. Vasantha Kumar, V. Lakshmi Ranganatha, S. A. Khanum, *Bioorganic & Medicinal Chemistry Letters* **2014**, *24*, 3559-3564.
- [117] P. R. Reddy, A. Shilpa, *Polyhedron* **2011**, *30*, 565-572.
- [118] P. Kalaivani, R. Prabhakaran, E. Ramachandran, F. Dallemer, G. Paramaguru, R. Renganathan, P. Poornima, V. Vijaya Padma, K. Natarajan, *Dalton Transactions* **2012**, *41*, 2486-2499.
- [119] S. Amer, N. El-Wakiel, H. El-Ghamry, *Journal of Molecular Structure* **2013**, *1049*, 326-335.
- [120] B. S. Creaven, B. Duff, D. A. Egan, K. Kavanagh, G. Rosair, V. R. Thangella, M. Walsh, *Inorganica Chimica Acta* **2010**, *363*, 4048-4058.
- [121] A. E. Patterson, J. J. Miller, B. A. Miles, E. L. Stewart, J.-M. E. Melanson, C. M. Vogels, A. M. Cockshutt, A. Decken, P. Morin Jr, S. A. Westcott, *Inorganica Chimica Acta* **2014**, *415*, 88-94.
- [122] M. Das, S. Mukherjee, B. Koley, I. Choudhuri, N. Bhattacharyya, P. Roy, B. C. Samanta, M. Barai, T. Maity, *New Journal of Chemistry* **2020**, *44*, 18347-18361.
- [123] M. Sedighipoor, A. H. Kianfar, W. A. Kamil Mahmood, M. H. Azarian, *Polyhedron* **2017**, *129*, 1-8.
- [124] M. Niu, M. Hong, G. Chang, X. Li, Z. Li, *Journal of Photochemistry and Photobiology B: Biology* **2015**, *148*, 232-241.
- [125] P. li, M. Niu, M. Hong, S. Cheng, J. Dou, *Journal of Inorganic Biochemistry* **2014**, *137*, 101-108.
- [126] W.-J. Lian, X.-T. Wang, C.-Z. Xie, H. Tian, X.-Q. Song, H.-T. Pan, X. Qiao, J.-Y. Xu, *Dalton Transactions* **2016**, *45*, 9073-9087.
- [127] E. Y. Backheet, K. M. Emara, H. F. Askal, G. A. Saleh, *Analyst* **1991**, *116*, 861-865.
- [128] G. Moody, J. Thomas, *International Journal of Food Science & Technology* **1979**, *14*, 535-538.
- [129] L. A. Pachla, D. L. Reynolds, P. T. Kissinger, *Journal of Association of Official Analytical Chemists* **1985**, *68*, 1-12.
- [130] M. B. Gelbert, D. J. Curran, *Analytical chemistry* **1986**, *58*, 1028-1032.
- [131] S. A. Wring, J. P. Hart, B. J. Birch, *Analytica Chimica Acta* **1990**, *229*, 63-70.
- [132] P. Janda, J. Weber, L. Dunsch, A. Lever, *Analytical Chemistry* **1996**, *68*, 960-965.

- [133] J. Kulys, E. J. D'Costa, *Analytica chimica acta* **1991**, *243*, 173-178.
- [134] G.-d. Liu, Z.-q. Li, S.-s. Huan, G.-L. Shen, R.-Q. Yu, **2000**.
- [135] Z. Zhang, X. Li, C. Wang, C. Zhang, P. Liu, T. Fang, Y. Xiong, W. Xu, *Dalton Transactions* **2012**, *41*, 1252-1258.

Chapter 2

**Mono-, tri- and polynuclear
copper(II) complexes of
Schiff-base ligands:
Synthesis, characterization
and catalytic activity
towards alcohol oxidation**

2.1 Introduction

Development and applications of transition metal complexes with N,O-donor ligands draw appreciable interest of the researchers over the last few decades. Preparation of N,O donor ligands by Schiff-base condensation is popular among scientists as this type of ligands can be synthesized by one step condensation between a keto/aldehyde group and a primary amine group with very high yield.^[1] The appropriate selection of the aldehyde/ketones and primary amine with extra hetero atoms could produce ligands with desired number of donor atoms. Softness or hardness of the donor group could be incorporated by judicial choice of the reactants and requirement for coordination of the metal center. Moreover, Schiff-base ligands can stabilize various oxidation states of the metal center. Transition metal complexes with Schiff-base ligands have utilized in a number of important fields of application e.g. magnetism,^[2] catalysis,^[3] biological sciences,^[4] optoelectronics,^[5] sensing,^[6] etc.^[7] Copper(II) complexes have been used as catalyst in different organic reactions such as oxidation of alkane, epoxidation of alkene, catechol oxidation, benzylic oxidation, aromatic C–H oxidation, Glaser–Hay acetylenic coupling reactions, alcohol oxidation, Baeyer–Villiger oxidation, sulfoxidation, etc.^[3f-3i] Till date research is being conducted on the catalytic aspects of newly synthesized metal complexes to find better catalyst with remarkable yield and selectivity over the desired product(s).

The oxidation of alcohols is one of the most important functional transformations in synthetic organic chemistry. This can be done by following several methods and using different reagents.^[8] However, these reactions are often done with the stoichiometric amounts of the reactants. The generation of inorganic salt(s) mixed with the target molecules demands time and labor for the work-up procedure. To avoid these problems, suitable catalysts may be used. Copper(II)-phenoxyl radical complexes as the model of the reaction of Galactose Oxidase can oxidize primary alcohols into aldehydes.^[9] Galactose oxidase is a fungal enzyme with one copper atom at the active site, it is square pyramidal geometry and it catalyzes the oxidation of a number of primary alcohols to aldehydes.^[10]

A number of Schiff-base complexes of copper(II) ion have been developed where different aldehydes, e.g. salicylaldehyde or its derivative, were used for the formation of Schiff-bases.^[11] Copper(II) complexes have been synthesized with these ligands where 1, 2, 3 or more copper atom(s) are present in the asymmetric unit. These complexes find applications in many fields, in particular N,N donor and N,O donor ligands have been used for the preparation copper

complexes with different nuclearity as catalyst for oxidation of alcohols.^[12] However, in spite of the excellent results obtained, there is still scope for the improvement of the activity of the catalyst with respect to yield and time.

In this context, synthesis, characterization and catalytic properties of mono-, tri- and polynuclear copper(II) complexes, $[\text{Cu}(\text{L}^1)\text{Cl}_2]$ (**1**), $[\text{Cu}_3(\text{L}^2)_2\text{Cl}_4]$ (**2**) and $[\text{Cu}(\text{L}^3)\text{N}_3]_n$ (**3**) respectively, where $\text{L}^1 = 2\text{-morpholino-}N\text{-(pyridin-2-ylmethylene)ethanamine}$, $\text{HL}^2 = 4\text{-bromo-}2\text{-}((2\text{-morpholinoethylimino)methyl)phenol}$ and $\text{HL}^3 = 4\text{-chloro-}2\text{-}((2\text{-dimethylamino)ethylimino)methyl)phenol}$ are being reported. These complexes have been synthesized and characterized by standard methods including single crystal X-ray diffraction analysis. These complexes have been used as catalyst for the oxidation benzyl alcohols with *tert.*-butylhydroperoxide (TBHP) as the oxidant under ambient conditions. These ligands have been chosen to create coordination environment nearly similar to galactose oxidase and make variation in nuclearity of the complexes to compare catalytic results obtained under identical conditions.

2.2 Experimental Section

2.2.1 Materials and physical methods

Pyridine-2-carboxaldehyde, 5-chloro-2-hydroxybenzaldehyde, *N*-methyl-1,3-diaminopropane, 5-bromo-2-hydroxybenzaldehyde, 4-(2-aminoethyl)morpholine, copper(II) perchlorate hexahydrate, copper(II) chloride dihydrate and sodium azide were purchased from Sigma Aldrich and used without further purification. Other reagents were obtained from commercial sources and used as received. Solvents were purchased from commercial sources and were used for synthesis without further purification while purified and dried solvents¹³ were used for spectroscopic measurements. Elemental analyses (carbon, hydrogen and nitrogen) were performed using a Perkin–Elmer 2400C elemental analyzer. FT-IR spectra were obtained on a Perkin Elmer spectrometer (Spectrum Two) with the samples by using the attenuated total reflectance (ATR) technique. The UV-visible spectral measurements were done in Agilent 8453 diode array spectrophotometer. Analysis of reaction mixture of catalytic reactions was performed with a Shimadzu made next generation high speed gas chromatography system (model: GC-2025 AF) equipped with a fused silica capillary column and a FID detector. Cyclic voltammetric measurements were performed on a CHI Electrochemical workstation. A platinum wire working

electrode, a platinum wire auxiliary electrode and Ag/AgCl reference electrode were employed in a standard three-electrode configuration. Bu_4NPF_6 was used as the supporting electrolyte in CH_3CN and the scan rate was 50 mV s^{-1} under nitrogen atmosphere. All experiments were carried out at room temperature in air unless reported otherwise.

2.2.2 Synthesis of $[\text{Cu}(\text{L}^1)\text{Cl}_2]$ (1)

4-(2-Aminoethyl)morpholine (0.5 mmol, 0.065 mL) was added to a methanolic solution (10 mL) of 2-pyridinecarboxaldehyde (0.5 mmol, 0.053 mL) under stirring condition. The mixture was stirred for 30 min. Then the resulting solution was refluxed for 5 h. The color of the mixture turned orange. The mixture was then cooled and it was used as 'ligand (L^1)' without any characterization and further purification. The solution of L^1 in methanol was allowed to cool to room temperature. Then, a methanolic solution (10 mL) of copper(II) chloride dihydrate (0.5 mmol, 0.067 g) was added to the ligand solution. The mixture was stirred till it turned greenish. It was then refluxed for 1 h. Color of the solution became dark green. The mixture was finally cooled to room temperature and filtered to remove any precipitate or suspended materials. The filtrate was kept at ambient temperature. Green crystals suitable for X-ray diffraction study were produced after few days.

Data for **1**: yield (65%); C, H, N analysis: anal. calc. for $\text{C}_{12}\text{H}_{17}\text{Cl}_2\text{CuN}_3\text{O}$: C, 40.74; H, 4.84; N, 11.88; found: C, 40.54; H, 4.57; N, 11.98%.

2.2.3 Synthesis of $[\text{Cu}_3(\text{L}^2)_2\text{Cl}_4]$ (2)

4-(2-Aminoethyl)morpholine (0.5 mmol, 0.065 mL) was added to a methanolic solution (10 mL) of 5-bromo-2-hydroxybenzaldehyde (0.5 mmol, 0.100 g) and stirred. The mixture was refluxed for 2 h forming an orange solution of Schiff base ligand. The mixture was then cooled and it was used as 'ligand (HL^2)' without any characterization and purification. A methanolic solution of copper(II) chloride dihydrate (0.5 mmol, 0.067g) was added to the solution of HL^2 and the mixture was stirred for 30 min when it turned as greenish. It was then refluxed for 1 h. Color of the solution turned dark green. The mixture was cooled and filtered to remove any undissolved or precipitate materials. The filtrate was kept at ambient temperature. Black single crystals suitable for X-ray diffraction analysis were obtained within few days.

Data for **2**: yield (58%); C, H, N analysis: anal. calc. for $C_{26}H_{32}Br_2Cl_4Cu_3N_4O_4$: C, 32.64; H, 3.37; N, 5.86; found: C, 32.54; H, 3.22; N, 5.68%.

2.2.4 Synthesis of $[Cu(L^3)N_3]_n$ (**3**)

N-methyl-1,3-diaminopropane (0.6 mmol, 0.0528 g) was added to a methanolic solution (10 mL) of 5-chloro-2-hydroxybenzaldehyde (0.6 mmol, 0.093 g) under stirring condition. The mixture was stirred for 30 min and then it was refluxed for 2 h. The resulting solution was orange in color. The mixture was then cooled and it was used as ‘ligand (HL³)’ without any characterization and purification. A methanolic solution (10 mL) of copper(II) perchlorate hexahydrate (0.6 mmol, 0.222 g) was added slowly to the ligand solution of HL³ under stirring condition. The stirring continued for 30 min. The mixture turned greenish. Sodium azide (0.6 mmol, 0.039 g) in methanol/water mixed solvent (methanol:water (v/v) ratio 1:2) (2 mL) of was added dropwise with constant stirring. The color of solution became dark. The resultant mixture was refluxed for 1 h when the mixture became dark green. The mixture was then cooled to room temperature and filtered to remove any undissolved or suspended materials. The filtrate was kept at ambient temperature. Green single crystals suitable for X-ray diffraction analysis were produced within few days.

Data for **3**: yield (55%); C, H, N analysis: anal. calc. for $C_{11}H_{14}ClCuN_5O$: C, 39.88; H, 4.26; N, 21.14; found: C, 39.79; H, 4.22; N, 20.97%.

2.2.5 X-ray data collection and structure determination

Details of the data collection and refinement parameters for complexes **1**, **2** and **3** are summarized in Table 1. The diffraction experiments were carried out on a Bruker SMART 1000

Complex	1	2	3
Formula	C ₁₂ H ₁₇ Cl ₂ CuN ₃ O	C ₂₆ H ₃₂ Br ₂ Cl ₄ Cu ₃ N ₄ O ₄	C ₁₁ H ₁₄ ClCuN ₅ O
Formula weight	353.72	956.79	331.26
<i>T</i> (K)	294(2)	294(2)	294(2)
Crystal color	dark green	black	green
Crystal system	orthorhombic	orthorhombic	monoclinic
Space group	<i>Pca</i> 2 ₁	<i>Pbca</i>	<i>Cc</i>
<i>a</i> (Å)	24.123(6)	9.1230(9)	13.5037(6)
<i>b</i> (Å)	6.7026(16)	16.1575(15)	16.8086(6)
<i>c</i> (Å)	17.890(4)	21.934(2)	6.7657(3)
<i>α</i> (°)	90.00	90.00	90.00
<i>β</i> (°)	90.00	90.00	119.501(4)
<i>γ</i> (°)	90.00	90.00	90.00
<i>V</i> (Å ³)	2892.6(12)	3233.2(5)	1336.56(11)
<i>Z</i>	8	4	4
Crystal dimensions (mm)	0.10 × 0.16 × 0.23	0.11 × 0.23 × 0.32	0.06 × 0.09 × 0.16
<i>F</i> (0 0 0)	1448	1892	676
<i>D_c</i> (g cm ⁻³)	1.625	1.966	1.646
<i>λ</i> (Mo Kα) (Å)	0.71073	0.71073	0.71073
<i>θ</i> Range (°)	1.7- 25.2	1.9- 25.2	2.1- 25.5
Reflection collected/ unique/observed	29647, 5223, 4611	30022, 2926, 2501	9687, 2448, 2252
Absorption correction	multi-scan	multi-scan	multi-scan
<i>R</i> _{int}	0.067	0.045	0.034
Final <i>R</i> ₁ index [<i>I</i> > 2σ(<i>I</i>)]	0.053	0.026	0.029

Complex	1	2	3
Final wR_2 index (all reflections)	0.134	0.071	0.063
Goodness-of-fit	1.05	1.04	1.04

Table 2.1: Crystal data of complexes 1, 2 and 3

CCD diffractometer for **1** and on a Bruker APEX-II CCD diffractometer for **2** and **3** using graphite monochromated Mo $K\alpha$ radiation at 294(2) K. Data were processed using the Bruker *APEX2* and *SAINT* packages.^[14] Absorption corrections based on multi-scans using the *SADABS* software^[14] were applied to the intensity data. The structures were solved by direct methods using *SHELXT*^[15] and refined with full-matrix least-squares on F^2 on all unique reflections using *SHELXL-2014/7*.^[16] All the non-hydrogen atoms of the complexes were refined anisotropically. The crystal selected for the X-ray diffraction experiment of **1** and **3** was refined as a merohedral twin with a fractional contribution of the minor component of 0.18(3) and 0.03(2), respectively. In **1**, the poor quality of the crystal and the presence of twinning may account for the limited overall precision of the structure, the presence of high residual peaks and the relatively high R and wR_2 values.

CCDC 1535655, 1535654, 1535653 contain the supplementary crystallographic data for **1**, **2** and **3** respectively.

2.2.6 Alcohol oxidation

Primary alcohol oxidation was achieved by using *tert*.-butyl hydroperoxide as oxidant in the presence of copper(II) complexes as catalyst. Typically, 0.5 mmol of the substrate (alcohol) in 5.0 ml of acetonitrile was taken in a two necked round-bottomed flask connected with a condenser, followed by the addition of 0.025 mmol of copper(II) complex. The temperature of the mixture was maintained by a thermostat. 0.5 mmol of *tert*.-butyl hydroperoxide was added to the mixture to initiate the catalytic reaction under stirring condition. Aliquots from the mixture were collected at regular time interval. The reaction mixture was analyzed by gas

chromatography. The substrate and product(s) were identified by the comparison with known standards.

Blank experiments, namely oxidation of the alcohols, were performed in absence of any catalyst under the same experimental conditions.

2.3 Results and discussion

2.3.1 Synthesis and characterization

L^1 , HL^2 and HL^3 have been synthesized by one step Schiff-base condensation between aldehyde and respective amine in 1:1 molar ratio in methanol. The ligands were not characterized and used for complex formation without further purification. Complex **1** was obtained by the reaction between L^1 and $CuCl_2$ in 1:1 molar ratio. Reaction between HL^2 and $CuCl_2$ led to the formation of **2**. However, reaction of copper(II) perchlorate, HL^3 and sodium azide in 1:1:1 molar ratio produced **3**. Both, HL^2 and HL^3 underwent deprotonation in the reaction medium without any external deprotonating base.

FT-IR spectra of all of the complexes were obtained with powder sample by ATR technique (**Fig. 2.1-2.3**). Peaks at 1651, 1633 and 1628 cm^{-1} in the spectra of complexes **1**, **2** and **3**, respectively indicates the presence of azomethine bond in the complexes. A strong peak at 2047 cm^{-1} in **3** confirms the presence of azido moiety.

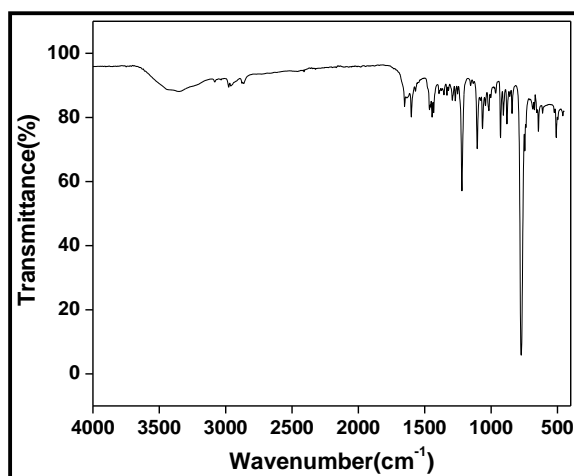


Fig. 2.1: FT-IR of complex 1

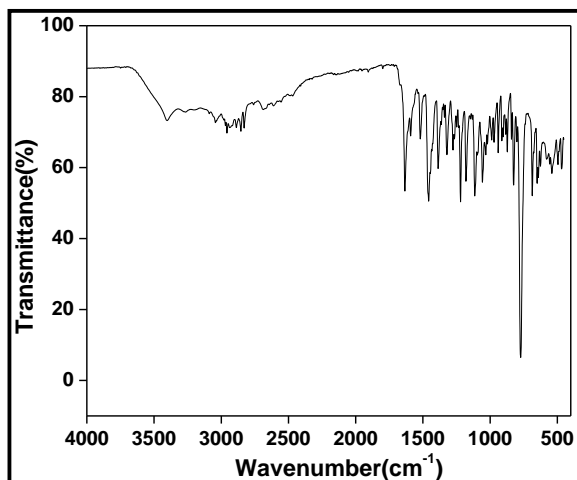


Fig. 2.2 : FT-IR of complex 2

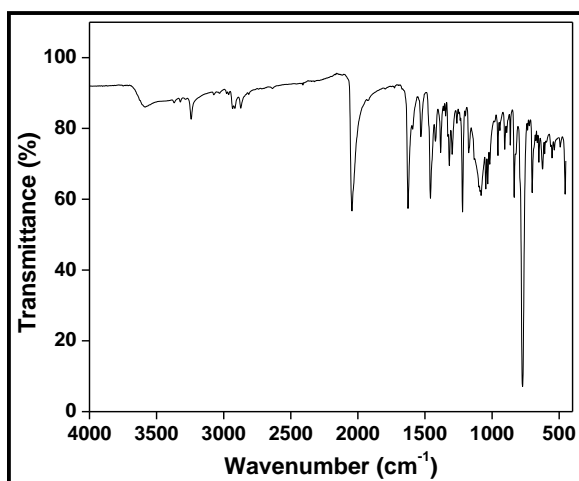


Fig. 2.3 : FT-IR of complex 3

ESI-mass spectrometry measurements were performed with methanolic solutions of the complexes (**Fig. 2.4-2.6**). Mass spectrum of **1** shows an m/z peak at 316.96. This peak may be attributed to the $[\text{Cu}(\text{L}^1)\text{Cl}]^+$ fragment. ESI-mass spectrum of **2** exhibits an m/z peak at 507.27 which is due to the presence of $[\text{Cu}_2(\text{L}^2)\text{Cl}_2]^+$ fragment. Complex **3** shows an m/z peak at 347.97 and this peak may arise due to the presence of $[\text{Cu}(\text{L}^3)(\text{N}_3)\text{CH}_3\text{O}]^+$ fragment.

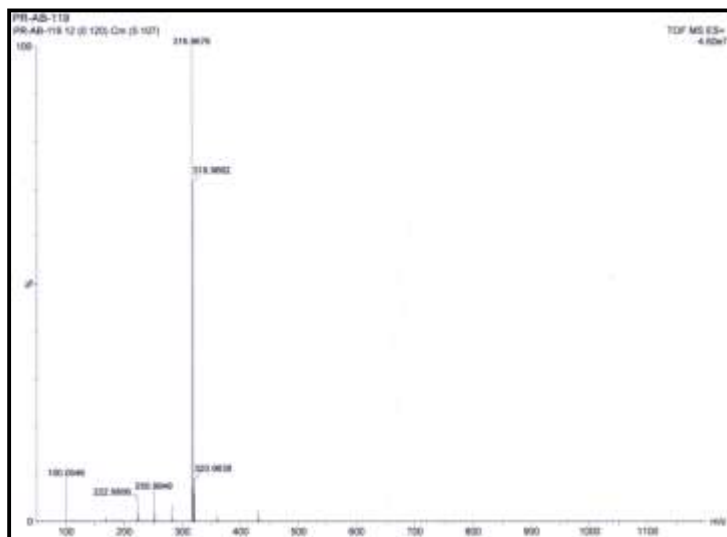


Fig. 2.4: ESI-mass spectrum of complex 1 in methanol

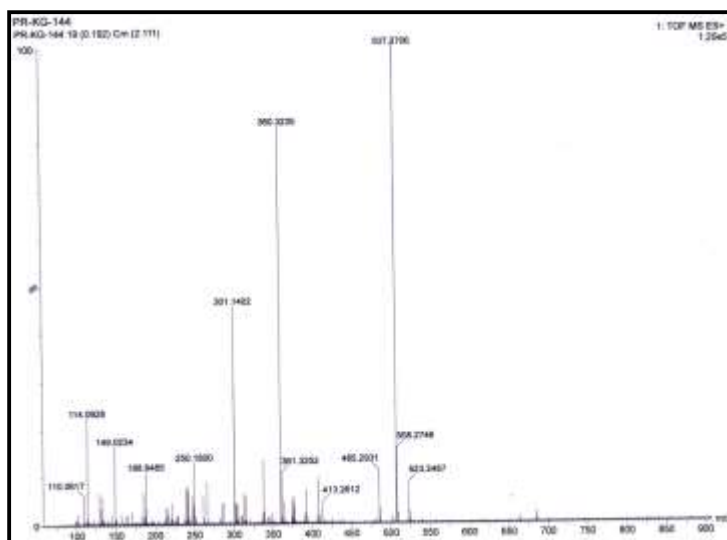


Fig. 2.5: ESI-mass spectrum of complex 2 in methanol

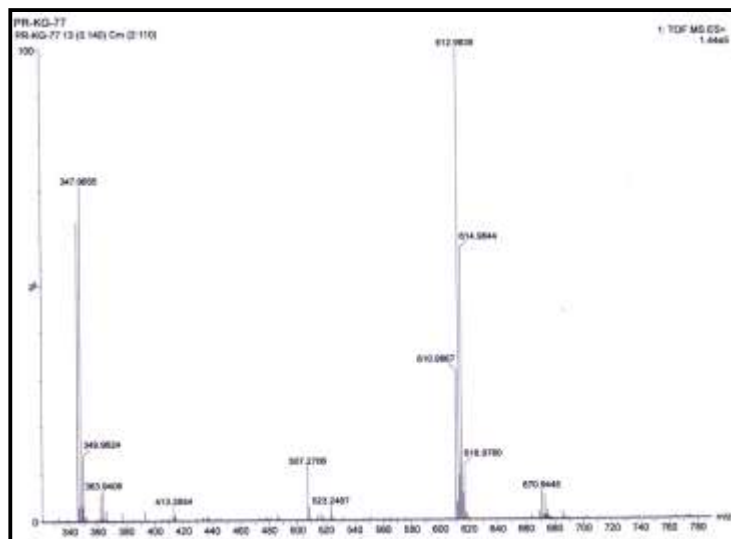


Fig. 2.6: ESI-mass spectrum of complex 3 in methanol

Room temperature magnetic susceptibilities of all of the complexes were measured with powder samples using the Guoy balance method. Complexes **1**, **2** and **3** are expected to exhibit different magnetic moment values as the number of unpaired electron(s) and geometry of the complexes are different. The magnetic moments of complexes **1**, **2** and **3** have been determined to be 1.64, 2.90 and 1.53 BM, respectively. The asymmetric units of complexes **1** and **3** contain only one copper(II) center. Complex **3** shows slightly lower magnetic moment value than the calculated values indicating the presence of weak antiferromagnetic interaction in the complex at room temperature. The calculated magnetic moment of complex **2** at room temperature is 3.87 BM as there are three copper(II) centers.^[17] However, measured magnetic moment of the complex signifies the presence of moderately strong antiferromagnetic interaction between the metal centers.

2.3.2 UV-vis spectral studies

The electronic spectra of complexes **1**, **2** and **3** were recorded in methanol at room temperature (**Fig. 2.7-2.9**).

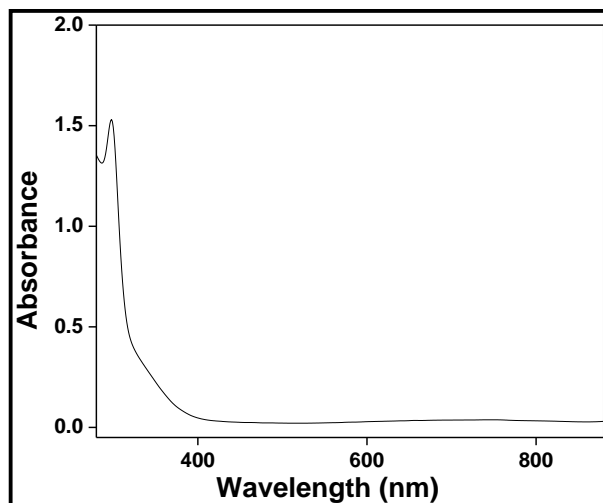


Fig. 2.7: UV-vis spectrum of complex 1 in methanol at room temperature

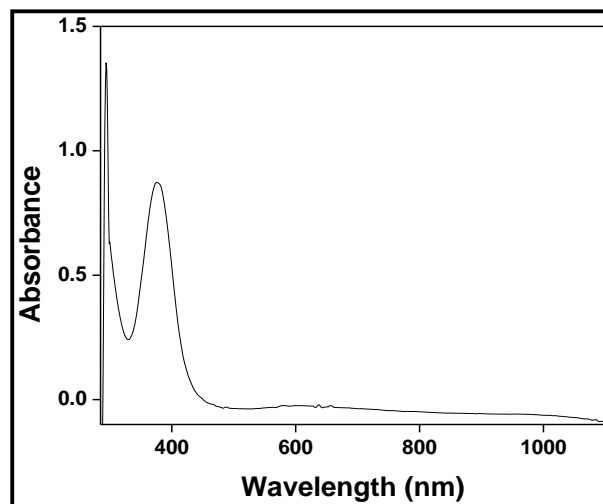


Fig. 2.8: UV-vis spectrum of complex 2 in methanol at room temperature

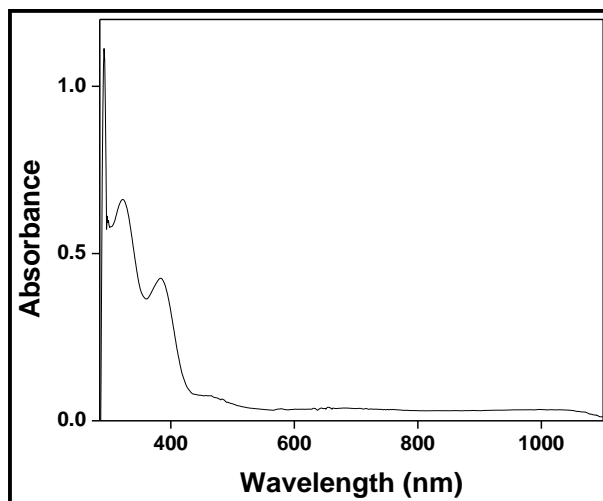


Fig. 2.9: UV-vis spectrum of complex 3 in methanol at room temperature

UV-vis spectra of complexes 2 and 3 were obtained in solid state at room temperature (**Fig. 2.10 and 2.11**).

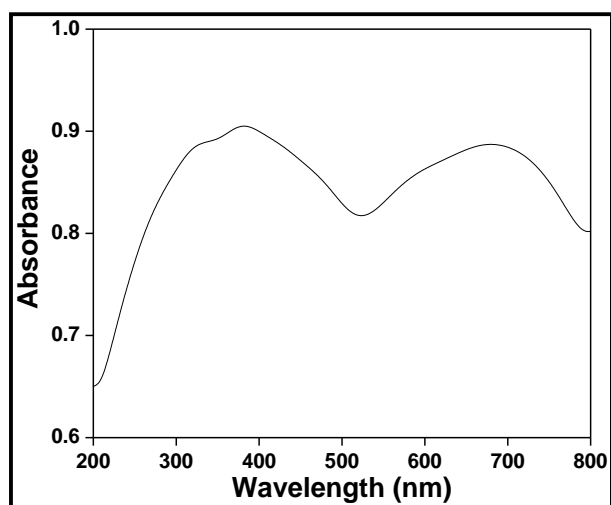


Fig. 2.10: UV-vis spectrum of complex 2 in solid state at room temperature

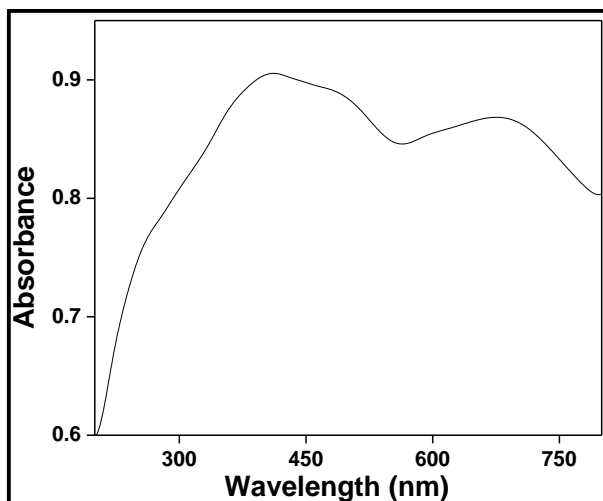


Fig. 2.11: UV-vis spectrum of complex 3 in solid state at room temperature

For complex **2**, high intensity bands appear at 374 and 295 nm (molar extinction coefficient: $9,000 \text{ M}^{-1}\text{s}^{-1}$ and $13,000 \text{ M}^{-1}\text{s}^{-1}$, respectively) which may be attributed to the ligand to metal charge transfer ($\text{PhO}^- \rightarrow \text{Cu(II)}$, $\text{N(amino)} \rightarrow \text{Cu(II)}$) and intraligand charge transfer. UV-vis spectrum of complex **3** exhibits high intensity bands at 382 nm and 321 nm with molar extinction coefficient of $44,000 \text{ M}^{-1}\text{s}^{-1}$ and $7,000 \text{ M}^{-1}\text{s}^{-1}$ respectively. These bands are probably due to $\text{PhO}^- \rightarrow \text{Cu(II)}$, $\text{N(amino)} \rightarrow \text{Cu(II)}$ LMCT. Another band at 291 nm with molar extinction coefficient of $11,000 \text{ M}^{-1} \text{ s}^{-1}$ is probably due to intraligand charge transfer transition.

Complexes **1**, **2** and **3** show broad bands centered at 700, 640 and 680 nm respectively with low intensity in methanol. These spectral characteristics are in consistence with copper(II) complexes of distorted square pyramidal (SP) geometry. The observed bands originate $d_{xz}, d_{yz} \rightarrow d_{x^2-y^2}$ transitions ^[18] and they may or may not be accompanied by a low-energy shoulder (> 800 nm). A low energy single d–d band at > 800 nm ($d_{xy}, d_{x^2-y^2} \rightarrow d_{z^2}$) with a high energy shoulder (spin forbidden, $d_{xz}, d_{yz} \rightarrow d_{z^2}$) is typically observed in trigonal bipyramidal (TBP) geometry. Thus, copper atoms in complexes **2** and **3** are in distorted SP environment which is further evident from their solid state electronic spectra. Solid state spectra (**Fig. 2.10 and 2.11**) show bands with maxima at 680 and 683 nm for **2** and **3** respectively along with other peaks indicating the presence of distorted SP geometry in the solid state.

2.3.3 Crystal Structures of complexes 1, 2 and 3

ORTEP of the asymmetric unit of complex 1 is provided in Fig. 2.12. Selected bond lengths and angles for complexes 1, 2 and 3 are given in Table 2.2.

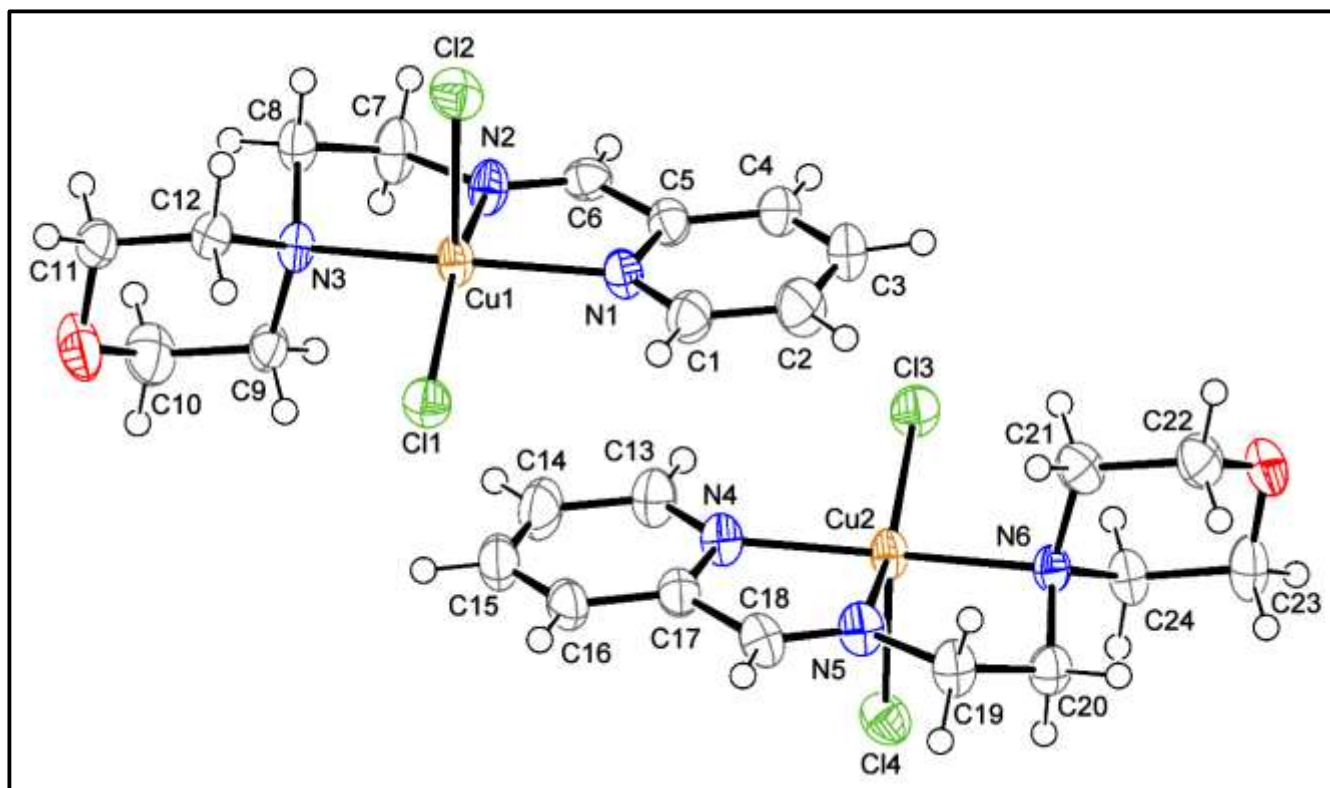


Fig 2.12 : A perspective view of the asymmetric unit of complex 1 with displacement ellipsoids drawn at the 50% probability level

Complex 1

Cu1–N1	2.058(6)	Cu2–N4	2.052(6)
Cu1–N2	1.985(7)	Cu2–N5	1.975(7)
Cu1–N3	2.082(6)	Cu2–N6	2.099(6)
Cu1–Cl1	2.258(2)	Cu2–Cl3	2.256(2)
Cu1–Cl2	2.480(3)	Cu2–Cl4	2.475(3)

N2–Cu1–N1	79.4(3)	N5–Cu2–N4	79.5(3)
N2–Cu1–N3	81.5(3)	N5–Cu2–N6	81.7(3)
N1–Cu1–N3	158.5(2)	N4–Cu2–N6	158.7(3)
N2–Cu1–Cl1	156.8(2)	N5–Cu2–Cl3	157.1(2)
N1–Cu1–Cl1	96.1(2)	N4–Cu2–Cl3	96.2(2)
N3–Cu1–Cl1	97.79(19)	N6–Cu2–Cl3	97.25(19)
N2–Cu1–Cl2	97.1(2)	N5–Cu2–Cl4	97.2(2)
N1–Cu1–Cl2	94.0(2)	N4–Cu2–Cl4	94.7(2)
N3–Cu1–Cl2	97.85(19)	N6–Cu2–Cl4	97.5(2)
Cl1–Cu1–Cl2	105.88(9)	Cl3–Cu2–Cl4	105.64(9)

Complex 2

Cu1–O1	1.9546(19)	Cu2–N2	2.048(2)
Cu1–Cl1	2.8787(8)	Cu2–O1	1.980(2)
Cu1–Cl2	2.3327(8)	Cu2–Cl1	2.2713(9)
Cu1...Cu2	2.9512(4)	Cu2–Cl2	2.6982(9)
Cu2–N1	1.944(2)		

O1–Cu1–O1 ⁱ	180	N1–Cu2–N2	85.53(10)
O1–Cu1–Cl2	85.39(6)	O1–Cu2–N2	171.69(9)
O1–Cu1–Cl2 ⁱ	94.61(6)	N1–Cu2–Cl1	157.08(8)
O1–Cu1–Cl1	74.03(6)	O1–Cu2–Cl1	89.55(6)
O1–Cu1–Cl1 ⁱ	105.97(7)	N2–Cu2–Cl1	97.05(7)
Cl1–Cu1–Cl1 ⁱ	180	N1–Cu2–Cl2 ⁱ	109.15(8)
Cl1–Cu1–Cl2	87.24(6)	O1–Cu2–Cl2 ⁱ	75.51(7)
Cl1–Cu1–Cl2 ⁱ	92.76(6)	N2–Cu2–Cl2 ⁱ	99.01(7)
Cl2–Cu1–Cl2 ⁱ	180	Cl1–Cu2–Cl2 ⁱ	93.00(3)
N1–Cu2–O1	90.35(9)		

Complex 3

Cu1–O1	1.916(4)	Cu1–N1	1.987(5)
--------	----------	--------	----------

Cu1–N2	2.045(5)	Cu1–N3	2.028(5)
Cu1–N3 ⁱⁱ	2.427(5)		
O1–Cu1–N1	90.65(19)	O1–Cu1–N3	88.11(19)
N1–Cu1–N3	155.11(19)	O1–Cu1–N2	173.4(2)
N1–Cu1–N2	95.70(17)	N3–Cu1–N2	86.8(2)
O1–Cu1–N3 ⁱⁱ	85.35(17)	N1–Cu1–N ⁱⁱ	96.77(18)
N3–Cu1–N3 ⁱⁱ	107.9(2)	N2–Cu1–N3 ⁱⁱ	92.24(19)

Symmetry codes: (i) -x, 1-y, 1-z; (ii) x, 1-y, -1/2+z.

Table 2.2 : Selected bond lengths (Å) and bond angles (°) of complexes 1, 2 and 3

The mononuclear complex **1** crystallizes from methanol in the orthogonal system, space group *Pca2₁*, with two complex molecules of similar geometry in the asymmetric unit. In each molecule the copper atom is coordinated by the N donor atoms of the neutral ligand L¹ and by two chloride anions in a distorted square pyramidal geometry as indicated by the value of the trigonal index τ . The trigonal index is calculated as the difference between the two largest donor–metal–donor angles divided by 60. Its value is 1 for the ideal trigonal bipyramid and 0 for the square pyramid.^[19] The values of τ are 0.028 and 0.027 for atoms Cu1 and Cu2, respectively, indicating that the coordination environments are nearly ideal square pyramidal. The Cu1 and Cu2 metals are displaced by 0.3380(9) and 0.3383(9) Å with respect to the corresponding basal plane formed by atoms N1/N2/N3/C11 and N4/N5/N6/C13, respectively. In the crystal, C–H...O hydrogen bonds (**Table 2.3**) between aromatic H atoms and the oxygen atoms of the morpholino moieties lead to the formation molecular chains parallel to the *a* axis. In addition, adjacent chains are connected into a two-dimensional double layers parallel to the *ab* plane by C–H...Cl hydrogen bonds (**Fig. 2.13**).

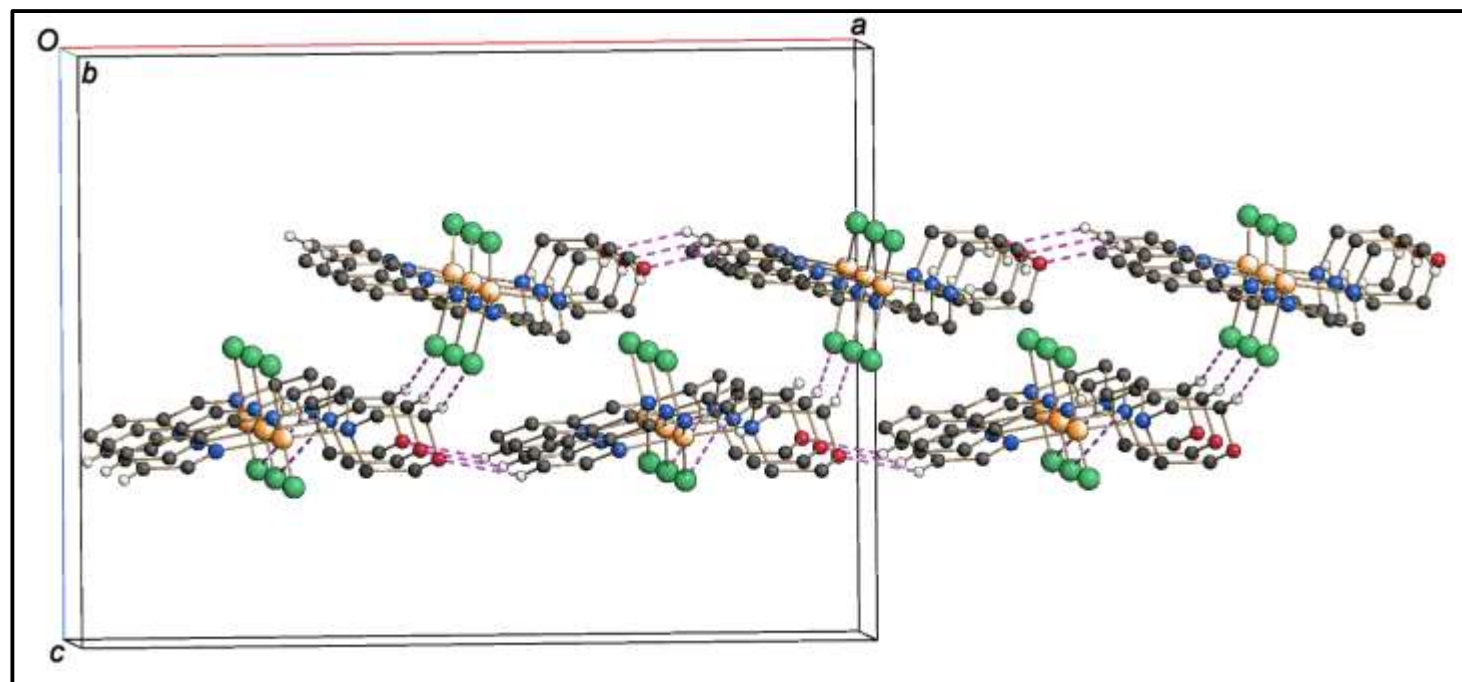


Fig. 2.13 : Partial crystal packing of complex 1 approximately viewed down the *b* axis, showing the formation molecular double layers parallel to the *ab* plane by C–H...O and C–H...Cl hydrogen bonds (dashed lines). H atoms not involved in intermolecular hydrogen bonds are omitted for clarity

D–H... A	D–H	H...A	D...A	∠ D–H...A
C24–H24A...Cl3	0.97	2.77	3.430(9)	126.1
C2–H2...O1 ⁱ	0.93	2.55	3.257(12)	132.8
C7–H7A...Cl1 ⁱⁱ	0.97	2.79	3.490(12)	130.0
C11–H11A...Cl4 ⁱⁱⁱ	0.97	2.83	3.768(10)	163.8
C14–H14...O2 ^{iv}	0.93	2.54	3.268(11)	135.3

Symmetry codes: (i) $1/2+x, 1-y, z$; (ii) $x, -1+y, z$; (iii) $1/2-x, 1+y, -1/2+z$; (iv) $-0.5+x, -y, z$.

Table 2.3 : . Hydrogen bonding geometry (Å, °) for complex 1.

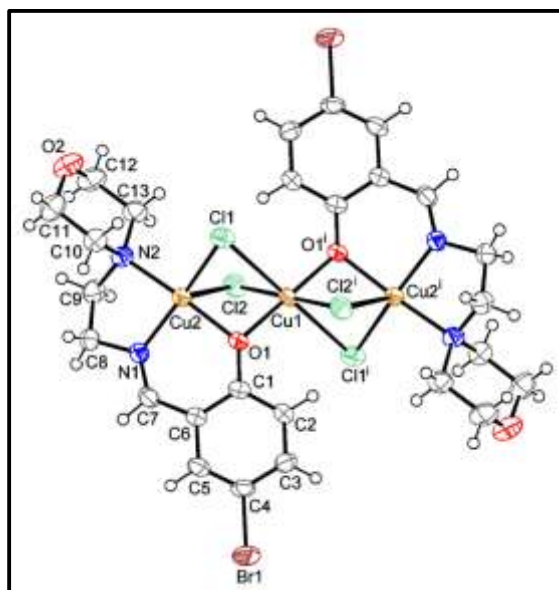
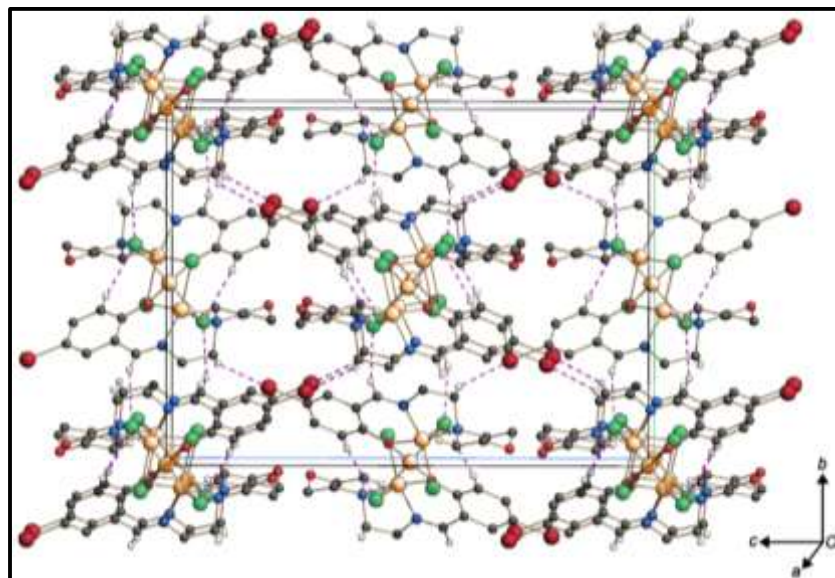


Fig. 2.14 : The molecular structure of complex **2** with displacement ellipsoids drawn at the 50% probability level. Symmetry code: (i) $-x, 1-y, 1-z$.

ORTEP plot of the asymmetric unit of complex **2** is shown in **Fig. 2.14**. The discrete molecule of complex **2** consists of three copper atoms, two 2-((2-morpholinoethylimino)methyl)-4-bromophenol Schiff-base ligands deprotonated at the O atoms (L^2), and four μ -bridging chlorine atoms. The trinuclear complex has crystallographically imposed inversion symmetry, the Cu1 metal lying on the Wyckoff special position 4a of the space group *Pbca*. Cu1 is coordinated to four μ_2 -Cl atoms and two μ_2 -phenoxido oxygen atoms in a remarkably distorted octahedral geometry elongated along the Cu1–Cl1 bonds. Atom Cu2 coordinates to the O1 bridging phenoxido oxygen, the N1 and N2 atoms from the HL^2 ligand, and two μ_2 -Cl atoms in distorted square pyramidal geometry as indicated by the τ value of 0.243. Atoms O1, N1, N2 and Cl1 constitute the basal plane whereas Cl2 occupies the apical position. Cu2 is out of the mean basal plane towards Cl2 by 0.1751(4) Å. In the crystal, there exists both C–H...Cl and C–H...Br hydrogen bonds (**Table 2.4**) linking molecules into a three-dimensional network (**Fig. 2.15**).



**Fig. 2.15 : Packing diagram of 2 showing the H...Cl and H...Br hydrogen bonds (dashed lines).
Hydrogen atoms not involved in hydrogen bonding are omitted**

D-H...A	D-H	H...A	D...A	\angle D-H...A
C2-H2...Cl2 ⁱ	0.93	2.69	3.396(3)	133.0
C7-H7...Cl2 ⁱⁱ	0.93	2.72	3.574(3)	152.9
C9-H9A...Br1 ⁱⁱⁱ	0.93	2.92	3.696(3)	138.2
C10-H10B...Cl1 ^{iv}	0.97	2.80	3.724(3)	158.5

Symmetry codes: (i) -x, 1-y, 1-z; (ii) 1/2+x, 0.5-y, 1-z; (iii) x, 1/2-y, 1/2+z; (iv) 1-x, 1-y, 1-z.

Table 2.4 : Hydrogen bonding geometry (\AA , $^\circ$) for complex 2.

Asymmetric unit of complex **3** is given in **Fig. 2.16**. The asymmetric unit of complex **3** consists of one CuL^3 moiety including one 2-((3-(methylamino)propylimino)methyl)-4-chlorophenol ligand deprotonated at the O atoms (L^3), and one azido anion.

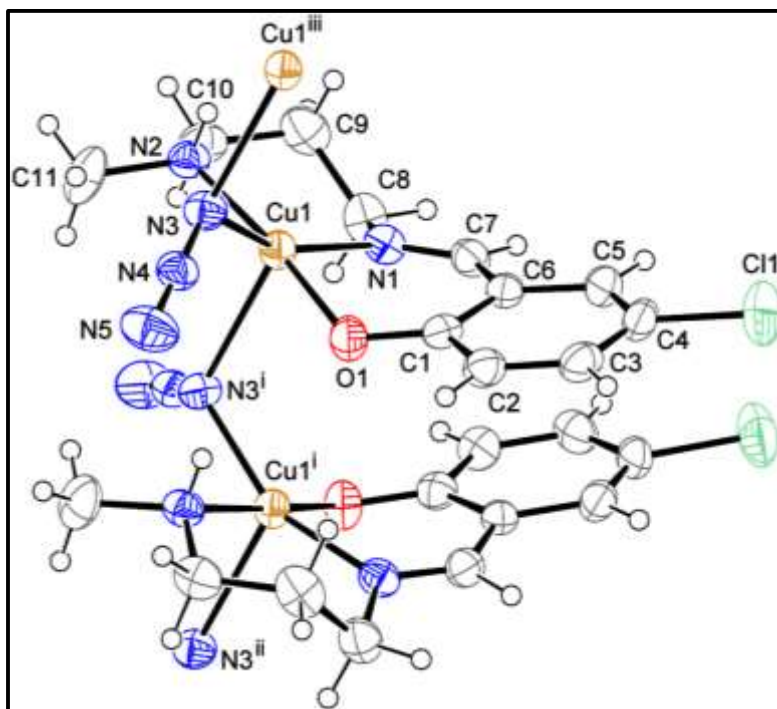


Fig. 2.16 : The molecular structure of complex 3 with displacement ellipsoids drawn at the 40% probability level. Symmetry codes: (i) $x, 1-y, -1/2+z$; (ii) $x, y, -1+z$; (iii) $x, 1-y, 1/2+z$.

The Cu metal exhibits a distorted square pyramidal coordination geometry provided by the O- and N-donor atoms of the Schiff base, and by the N atoms of two μ -azido anions, with atoms O1, N1, N2 and N3 at the basal plane and atom N3ⁱⁱ occupying the apical position (ii = $x, 1-y, -1/2+z$). The Cu metal protrudes by 0.1500(8) Å from the mean basal plane, which shows a remarkable tetrahedral distortion (r.m.s. = 0.2501 Å; maximum displacement 0.340(7) Å for atom N3). The amplitude of the distortion from the ideal square pyramidal geometry may be inferred also from the value of 0.306 of the trigonal index τ . The azido anion acts as an end-on bridging group (μ -1,1) linking the CuL³ moieties into polymeric chains running parallel to the *c* axis (**Fig. 2.17**). Within the chains N–H...N hydrogen bonds involving the terminal N5 azido nitrogen atoms are observed (**Table 2.5**). In the crystal, adjacent chains interact through C–H...N hydrogen bonds to form a three-dimensional network.

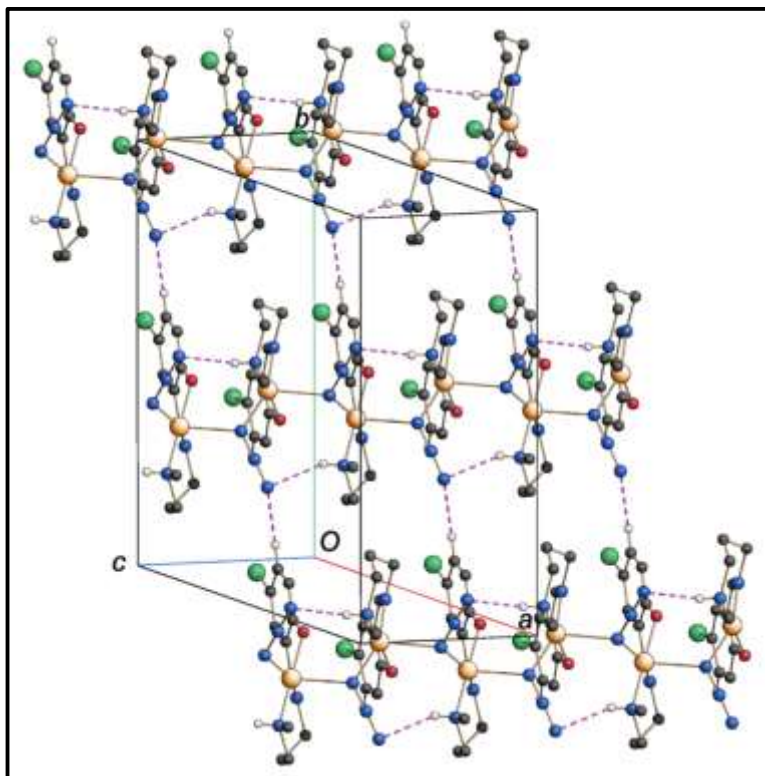


Fig. 2.17 : Crystal packing of complex 3 displaying the formation of one-dimensional chains parallel to the *c* axis linked into layers parallel to (110) by C–H...N hydrogen bonds (dashed lines). Hydrogen atoms not involved in hydrogen bonding are omitted for clarity.

D–H... A	D–H	H...A	D...A	∠ D–H...A
N2–H1...N52 ⁱ	0.79(7)	2.47(6)	3.117(9)	139(5)
C3–H3...N5 ⁱⁱ	0.93	2.53	3.331(7)	145.0

Symmetry codes: (i) $x, 1-y, 1/2+z$; (ii) $-1/2+x, 3/2-y, -1/2+z$.

Table 2.5: Hydrogen bonding geometry (Å°) for complex 3.

2.3.4 Electrochemical studies

Electrochemical studies of all of the copper(II) complexes were carried out in acetonitrile using TBAP as supporting electrolyte. A typical cyclic voltammogram (CV) was obtained by using a Pt working electrode and an Ag/AgCl reference electrode.

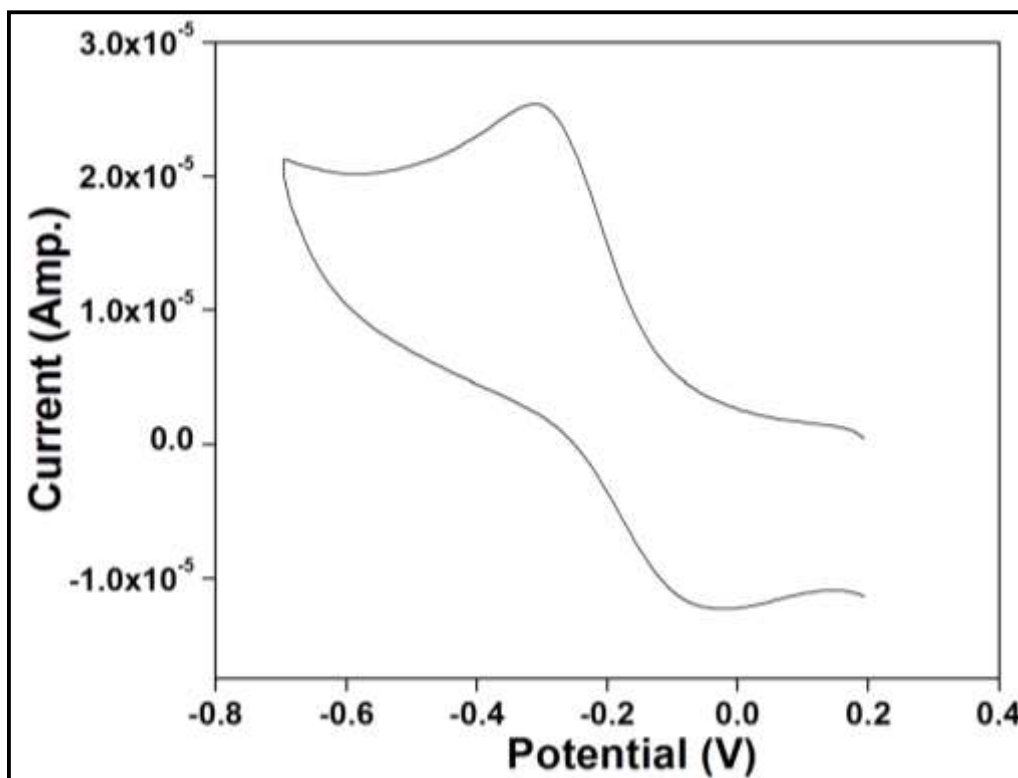


Fig. 2.18 : Cyclic Voltammogram showing reduction at Cu center of complex 1.

The CV of **1** (Fig. 2.18) shows a quasi-reversible reduction in the negative potential region indicating conversion of Cu(II) species to Cu(I). The plot in this region shows a peak at a potential of -0.05 V with a corresponding i_{pc} value of -1.21×10^{-5} A. Cu(I) is getting oxidized back to Cu(II) as indicated by a peak at -0.31 V with the corresponding i_{pa} of 2.54×10^{-5} A. $E_{1/2}$ was determined as -0.18 V. The copper center's interaction with the ligand system may be the probable cause of quasi-reversibility.

Coming to any probability of any further oxidation of the Cu(II) center, a scan was done in the positive potential region (Fig. 2.19). The plot shows a possible oxidation of Cu(II) \rightarrow Cu(III) with a peak at potential of 0.22 V and I_{pa} of 5.31×10^{-6} A which completes a quasi-

reversible cycle as it get reduced back to Cu(II), yielding a peak at 0.36 V and I_{pc} of -7.48×10^{-6} A. $E_{1/2}$ was determined as 0.29 V.

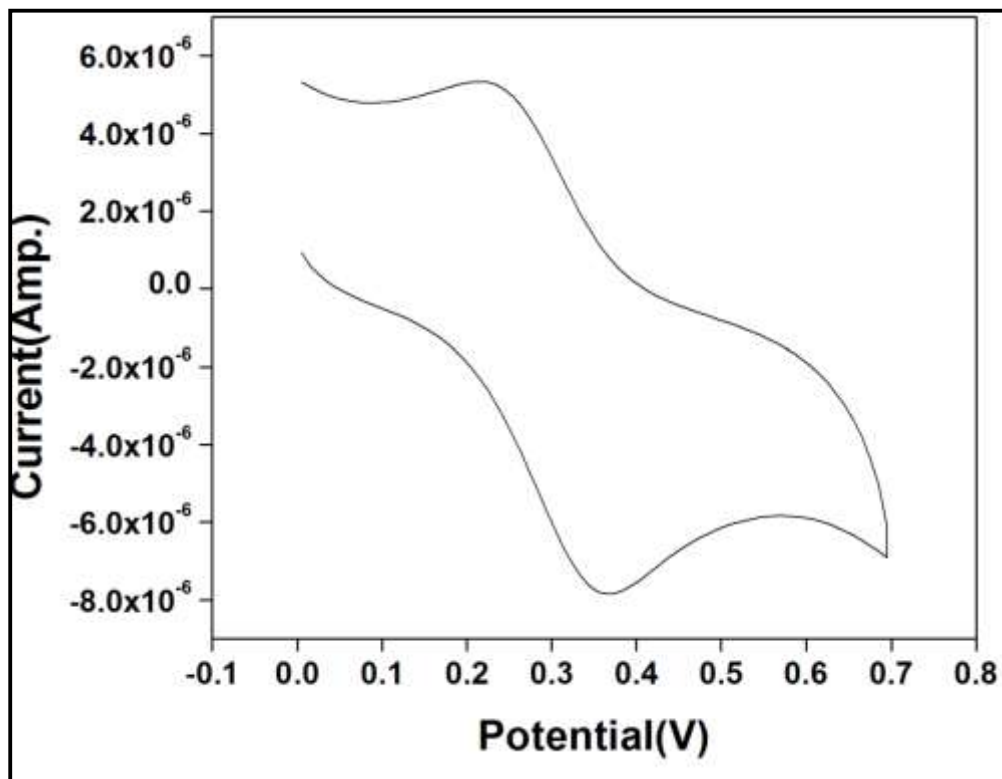


Fig. 2.19 : Cyclic Voltammogram showing oxidation at Cu center of complex 1

The CV of the trinuclear copper complex, **2**, shows a quasi-reversible reduction of Cu(II) to Cu(I) (**Fig. 2.20a**). The reduction from Cu(II) to Cu(I) occurs in the forward sweep as shown in the peak value of -0.88 V with an I_{pc} of -0.317×10^{-7} A. The trinuclear complex, as shown in the crystal structure, has two Cu atoms in identical positions while the other one, which links both the other Cu atoms, has a different electronic environment. It is possible that when the potential is applied in the forward sweep, the three Cu atoms end up experiencing an overall similar electronic environment due to some electronic delocalization. This might have caused the three Cu centers to behave identically and give one reduction peak while getting reduced to Cu(I) species. In the reverse sweep, while getting oxidized it shows two major peaks i.e. at -0.77 V with an I_{pa} of $9.94 \mu\text{A}$ and another at -0.50 V with corresponding I_{pa} of $9.41 \mu\text{A}$. The presence of two peaks here can be explained by the fact that probably after getting reduced to Cu(I) species, the electronic environment changes in such a manner that the two Cu atoms start behaving

differently due to the probable lack of the electronic delocalization which had earlier caused them to behave similarly. Hence we get two peaks for oxidation of two Cu centers from Cu(I) to Cu(II).

A scan in the positive potential region of the trimeric complex shows an oxidation of Cu(II) species to Cu(III) species (**Fig. 2.20b**). The forward sweep is an oxidation forming Cu(III) with a peak potential of 0.308 V and corresponding I_{pa} of 1.96 μA . This tripositive species gets reduced back in the backward sweep with a potential of 0.418 V and I_{pc} of $-1.52 \mu\text{A}$.

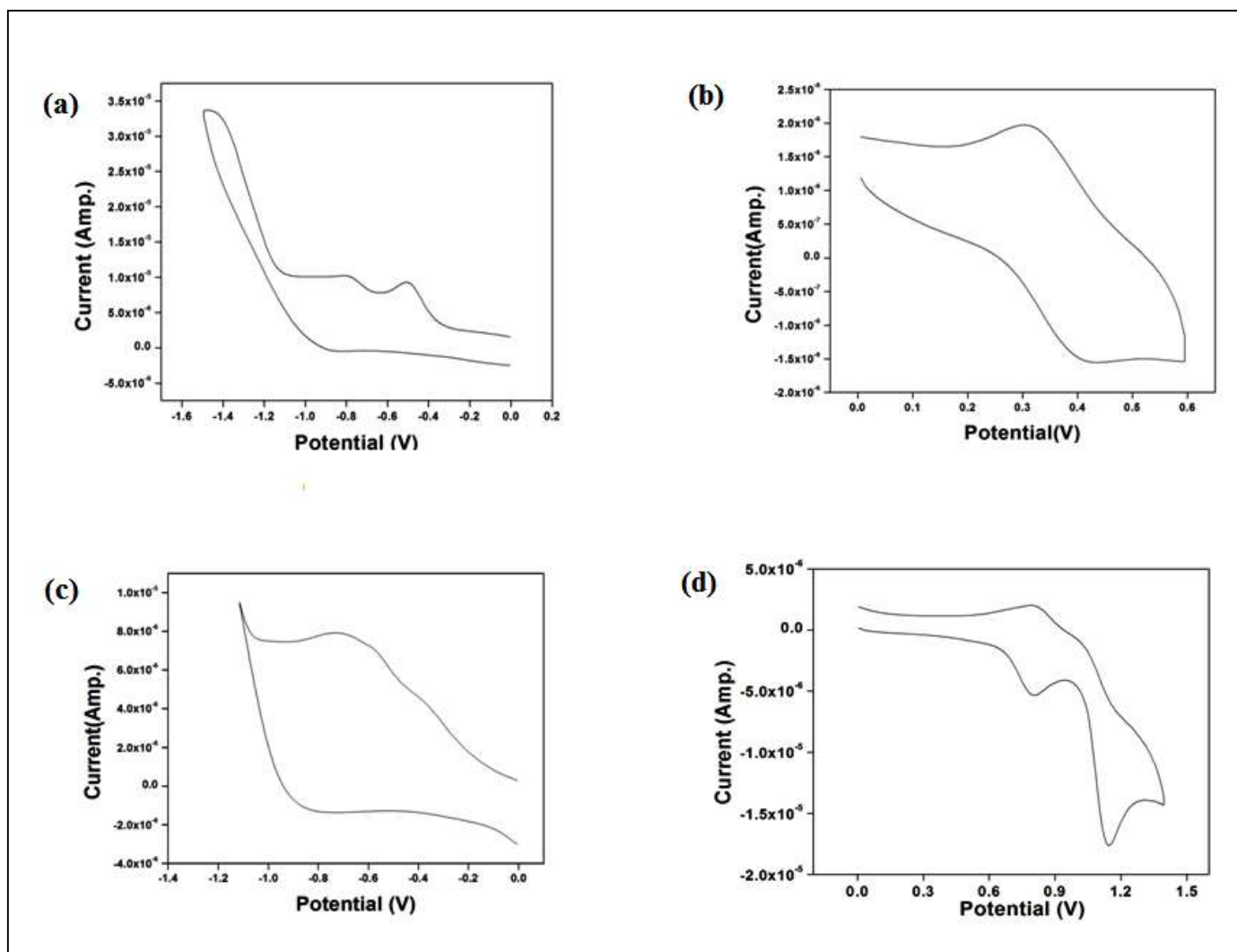


Fig. 2.20 : Cyclic voltammogram showing reduction at Cu center of complex 2 (a) and 3 (c); CV showing oxidation at Cu center of complex 2 (b) and 3 (d).

The CV of the polynuclear complex, **3**, (**Fig. 2.20c**) shows an almost reversible reduction at Cu center as Cu(II) gets reduced to Cu(I) at -0.92 V with I_{pc} of -7.10×10^{-7} A which again gets oxidized back to Cu(II) at -0.70 V with I_{pa} of $7.90 \mu\text{A}$. The positive potential region shows a quasi-reversible oxidation process wherein the Cu(II) is oxidized to Cu(III). In the forward sweep, the Cu(II) gets oxidized to Cu(III) with potential of 0.79 V and I_{pa} of $1.96 \mu\text{A}$ and gets reduced back to Cu (II) with potential of 0.80 V and I_{pc} of $-5.31 \mu\text{A}$. One irreversible peak is observed at 1.15 V which may be attributed to the irreversible reduction of the ligand.

2.3.5 Alcohol oxidation studies

The ability of complexes **1**, **2** and **3** to catalyze organic transformation reaction was checked. These complexes showed galactose oxidase mimicking activity i.e. they act as catalyst for the oxidation of benzyl alcohol, 4-methyl benzyl alcohol, 4-methoxy benzyl alcohol, 4-nitro benzyl alcohol and 4-bromo benzyl alcohol in the presence of *tert*-butylhydroperoxide (TBHP) as the oxidant. The corresponding aldehyde has been obtained as the sole product (**Fig 2.21**). The results of the oxidation reactions are given in **Table 2.6**.

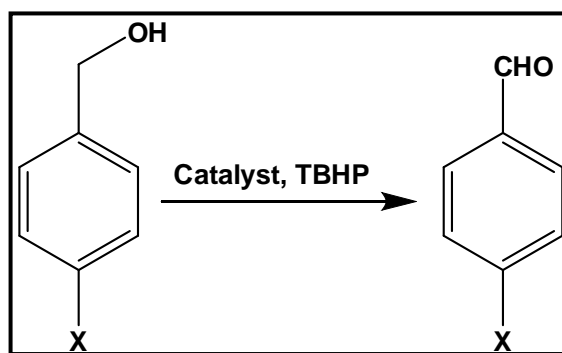


Fig 2.21 : Alcohol oxidation

Entry	Catalyst	Yield ^b % for benzyl alcohol (TON ^c)	Yield % for 4-methyl benzyl alcohol (TON ^c)	Yield % for 4-methoxy benzyl alcohol (TON ^c)	Yield % for 4-bromo benzyl alcohol (TON ^c)	Yield % for 4-nitro benzyl alcohol (TON ^c)
1	1	90 (18)	90 (18)	92 (18.4)	78 (15.6)	74 (14.8)
2	2	70 (14)	72 (14.4)	74 (14.8)	65 (13)	63 (12.6)
3	3	50 (10)	51 (10.2)	53 (10.6)	48 (9.6)	44 (8.8)
4	Blank ^d	9	10	9	7	10

Table 2.6 : Oxidation^a of primary alcohol with complexes 1, 2 and 3

^a Oxidant: TBHP; temperature: 298 K; solvent: acetonitrile;

^b Yield calculated after 14 h

^c TON: turnover number = number of moles of product/number of moles of catalyst

^d Catalytic reaction without any catalyst under identical conditions

It may be inferred from the table that complex **1** performs better in comparison to the other two complexes as catalyst for the alcohol oxidation for all the substrates. Conversion of benzyl alcohol is 90% with **1** whereas with complexes **2** and **3**, the yields are 70 and 50%, respectively, indicating a much lower activity of the latter two catalysts. When varying the substrates by introducing an electron pushing and electron withdrawing group in the aromatic ring of benzyl alcohol the trends of conversion are the same, i.e. the highest conversion is achieved with **1**, then with **2** and least with complex **3**. In the case of 4-methoxy benzyl alcohol, the yield is increased slightly with each of the catalysts. However, the presence of a bromo or nitro group in the aromatic ring decreases the yield to 78 and 74% respectively in the presence complex **1**. Only 44% of yield is achieved for 4-nitro benzyl alcohol with complex **3** as catalyst. Aliquots from the reactions mixture were collected at regular time intervals and analyzed to check the progress of the reaction. Plots of time vs. yield for complexes **1**, **2** and **3** are given in **Fig. 2.22, 2.23 and 2.24** respectively. It is evident that yield of the reaction increases with passage of time for all the catalyst, the maximum being observed after 14 h of reaction.

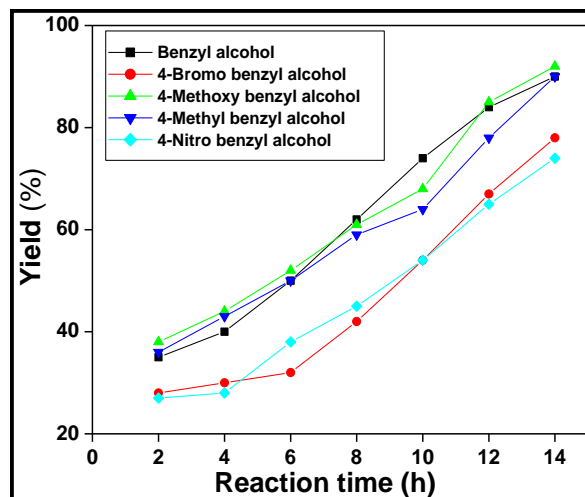


Fig. 2.22 : Plot of yield vs reaction time for complex 1.

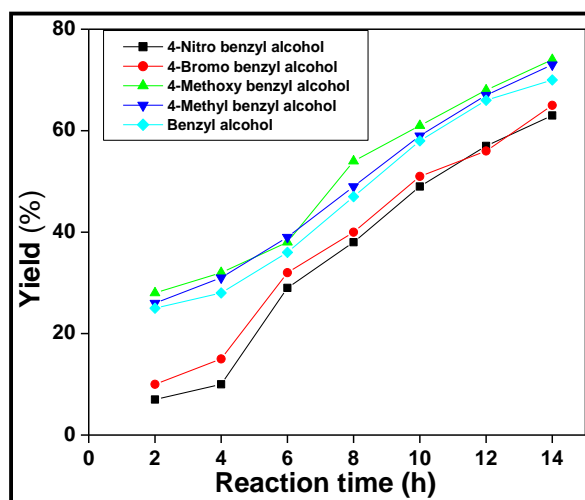


Fig. 2.23 : Plot of yield vs reaction time for complex 2

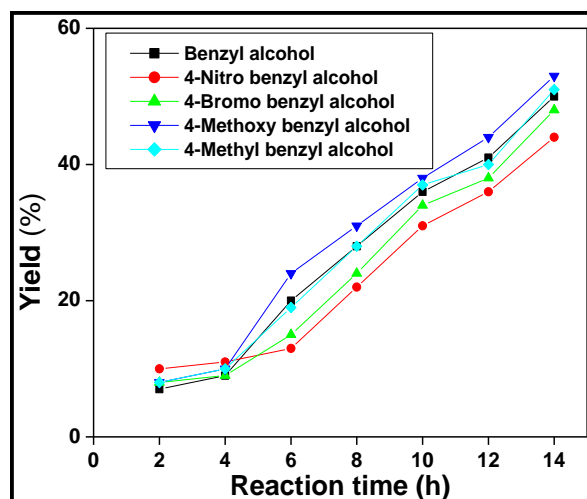


Fig. 2.24 : Plot of yield vs reaction time for complex 3.

Blank reactions with all the substrates were carried out under same experimental conditions but without any catalyst. It is to be noted that in case of blank reaction, the reaction proceeds very slowly and very poor conversion (Table 2.6 , entry 4). It takes much longer time for the conversion of the alcohol into the aldehyde. In other words, when we compare yield of a particular reaction in the same duration of time, e.g. 2 h, with and without catalyst, there is almost no conversion of alcohol to corresponding aldehyde in the initial time frame while the presence of copper complex as catalyst increases the yield of aldehyde manifold. These facts signify the importance of the copper(II) complexes as catalysts.

The effect of elevated temperature on the reaction rate and yield was also examined. At higher temperature, the reaction proceeds slowly and produces lower yield. Moreover, the solution turned a little brownish after being subjected to the reaction condition of 338 K. This probably indicates that the structure of the catalyst got altered, hence rendering it ineffective in catalytic reactions at temperatures higher than 298K.

In order to investigate the role of the solvent and define whether the catalyst could actively participate in the oxidation process under homogeneous condition, the oxidation of benzyl alcohol was performed in different solvents and the yields obtained are listed in **Table 2.7**.

Catalyst	Yield (%) in hexane	Yield (%) in DCM	Yield (%) in acetonitrile
Complex 1	21	77	90
Complex 2	13	47	60
Complex 3	10	33	40

Table 2.7 : Oxidation of benzyl alcohol in various solvent

Solubility of complex **1** increases in the following order: acetonitrile>dichloromethane>hexane. Reaction in hexane showed almost no conversions probably because of the low solubility of the catalysts in this solvent, hence the conversion yields were comparable to that obtained in the blank reactions. When dichloromethane was used, the reactions produced lower yields in comparison to acetonitrile, later was therefore selected as solvent of choice. Another possible explanation for the better yield achieved with acetonitrile may be found in the propensity of this solvent to stabilize Cu(I) species through coordination.

Catalytic reactions of benzyl alcohol as representative substrate with complexes **1**, **2** and **3** were also performed in the presence of TBHP under anaerobic condition in order to check the role of oxygen, if any, in the oxidation. The results of catalytic reactions under anaerobic condition are given in **Table 2.8**, showing the yield of benzaldehyde with each catalyst decreases to some extent. This fact indicates that oxidation of alcohol is mainly due to the oxidant, TBHP, not the oxygen of air which, at most, may influence the catalysis slightly.

Catalyst	Yield (%)
Complex 1	75
Complex 2	50
Complex 3	35

Table 2.8 : Oxidation of benzyl alcohol with complexes 1, 2 and 3 under anaerobic condition

Catalytic reactions were also carried out with varied amount of catalyst. The results, however, indicated that the effects in term of reaction yield were not significant, thus for all complexes a 1:20 catalyst/substrate ratio was used. Finally, unsuccessful attempts to recover and reuse the

complexes after reaction were carried out in anticipation of recycling the catalyst. In fact, the IR spectra of the compounds collected and dried after the catalytic reactions suggested a substantial decomposition of the complexes, thus preventing their reuse as catalysts.

A possible mechanistic pathway for the oxidation of benzyl alcohol may be proposed based on the present work and results that were obtained from earlier studies. It is known that reactions between TBHP and Cu(II) may lead to the formation of tBuO[•] radical and Cu(I) species.^[20] This radical is known as hydrogen atom abstractors from the alcohol.^[21] Thus, mechanism for this type of oxidation may be occurred via radical generation as proposed by Pombeiro and others.^[22]

It is clear from the electrochemical studies that reduction of Cu(II) to Cu(I) in complex **1** occurs at the potential of -0.05 V; for complexes **2** and **3**, values, at which reduction of Cu(II) to Cu(I) occurs, are -0.88 and -0.92 V respectively. These values indicate that reduction of metal center is most easy for **1** then in **2** and most difficult in **3**. Formation of Cu(I) is necessary in the catalytic reaction as discussed in possible mechanism. The system, where formation of Cu(I) is most feasible, should be most active in the oxidation reaction. Thus, results obtained in electrochemical and catalytic studies corroborate perfectly establishing complexes **1** is most active catalyst among all.

2.4 Conclusions

In the present paper, the synthesis and characterization by elemental analysis, spectral analysis and single crystal X-ray diffraction of three novel mono-, tri- and polynuclear copper(II) complexes is reported.

These complexes show galactose oxidase mimicking activity making them able to catalyze the oxidation of primary alcohols to the corresponding aldehydes. Among the three complexes, the mononuclear complex showed a far superior catalytic activity compared to the tri- and polynuclear complexes.

2.5 References

- [1] a) L. Mandal, S. Mandal and S. Mohanta, *New Journal of Chemistry.*, **2017**. b) A. Panja, N. C. Jana, S. Adak, P. Brandão, L. Dlhán, J. Titiš and R. Boča, *New Journal of Chemistry* **2017**, *41*, 3143; c) K. Hu, F. Li, Z. Zhang and F. Liang, *New Journal of Chemistry*, **2017** *41*, 2062; d) S. Dey, A. Roy, G. P. Maiti, S. K. Mandal, P. Banerjee and P. Roy, *New Journal of Chemistry* **2016**, *40*, 1365; e) F. A. Mautner, R. C. Fischer, M. Spell, A. R. Acevedo, D. H. Tran and S. S. Massoud, *Crystals* **2016**, *6*, 91; f) S. Adhikari, S. Lohar, B. Kumari, A. Banerjee, R. Bandopadhyay, J. S. Matalobos and D. Das, *New Journal of Chemistry* **2016**, *40*, 10094; g) J. L. Segura, M. J. Mancheño and F. Zamora, *Chemical Society Review*, 2016, **45**, 5635; h) T. T. Tidwell, *Angewandte Chemie International Edition* **2008**, *47*, 1016.
- [2] a) S. Karasawa, K. Nakano, D. Yoshihara, N. Yamamoto, J.-i. Tanokashira, T. Yoshizaki, Y. Inagaki and N. Koga, *Inorganic Chemistry* **2014**, *53*, 5447; b) A. M. Abu-Dief, I. M.A. Mohamed, *Beni-Suef University Journal Basic Applied Science* **2015**, *4*, 119; c) R. E. P. Winpenny, *Chemical Society Reviews* **1998**, *27*, 447; d) P. Roy, M. Nandi, M. Manassero, M. Riccò, M. Mazzani, A. Bhaumik and P. Banerjee, *Dalton Transactions* **2009**, 9543.
- [3] a) S. Halder, A. Mukherjee, K. Ghosh, S. Dey, M. Nandi and P. Roy, *Journal of Molecular Structure* **2015**, *1101*, 1; b) S. Halder, S. Dey, C. Rizzoli and P. Roy, *Polyhedron* **2014**, *60*, 85; c) M. Nandi and P. Roy, *Indian Journal of Chemistry* **2013**, *52A*, 1263-1268; d) P Roy and M. Manassero, *Dalton Transactions* **2010**, *39*, 1539; e) P. Roy, K. Dhara, M. Manassero and P. Banerjee, *Inorganic Chemical Communications* **2008**, *11*, 265; f) T. Punniyamurthy and L. Rout, *Coordination Chemistry Reviews* **2008**, *252*, 134; g) K.C. Gupta and A.K. Sutar, *Coordination Chemistry Reviews* 2008, **252**, 1420; h) K.C. Gupta, A.K. Sutar and C.-C. Lin, *Coordination Chemistry Reviews* **2009** *253*, 1926; i) L. Canali and D.C. Sherrington, *Coordination Chemistry Reviews* **1999**, *28*, 85.
- [4] a) W.-J. Lian, X.-T. Wang, C.-Z. Xie, H. Tian, X.-Q. Song, H.-T. Pan, X. Qiao and J.-Y. Xu, *Dalton Transactions* **2016**, *45*, 9073; b) R. Vafazadeh, F. Jafari, M. M. Heidari and A. C. Willis, *J. Coordination Chemistry Reviews* **2016**, *69*, 1313; c) B. K. Seth, A. Saha, S.

- Haldar, P. P. Chakraborty, P. Saha and S. Basu, *Journal of Photochemistry Photobiology B* **2016**, *162*, 463.
- [5] a) S. Halder, A. Layek, K. Ghosh, C. Rizzoli, P. P. Ray and P. Roy, *Dalton Transactions* **2015**, *44*, 16149; b) S. Roy, A. Dey, P. P. Ray, J. Ortega-Castro, A. Frontera and S. Chattopadhyay, *Chemical Communications* **2015**, *51*, 12974; c) V. Stavila, A. A. Talin and M. D. Allendorf, *Chemical Society Reviews* **2014**, *43*, 5994.
- [6] S. Halder, J. Mondal, J. Ortega-Castro, A. Frontera and P. Roy, *Dalton Transactions* **2017**, *46*, 1943.
- [7] P. G. Lacroix, *European Journal of Inorganic Chemistry* **2001**, 339.
- [8] T. Mallat, A. Baiker, *Chemical Reviews* **2004**, *104*, 3037.
- [9] a) P. Chaudhuri, M. Hess, T. Weyhermüller and K. Wieghardt, *Angewandte Chemie International Edition* **1999**, *38*, 1095; b) S. Itoh, M. Taki, S. Takayama, S. Nagatomo, T. Kitagawa, N. Sakurada, R. Arakawa and S. Fukuzumi, *Angewandte Chemie International Edition* **1999**, *38*, 2774.
- [10] a) J. P. Klinman, *Chemical Reviews* **1996**, *96*, 2541; b) J. Stubbe and W. A. van der Donk, *Chemical Reviews* **1998**, *98*, 705.
- [11] a) P. A. Vigato and S. Tamburini, *Coordination Chemistry Reviews* **2004**, *248*, 1717; b) P.A. Vigato, S. Tamburini, L. Bertolo, *Coordination Chemistry Reviews* **2007**, *251*, 1311; c) P.A. Vigato, S. Tamburini, *Coordination Chemistry Reviews* **2008**, *252*, 1871; d) P.A. Vigato, V. Peruzzo, S. Tamburini, *Coordination Chemistry Reviews* **2012**, *256*, 953.
- [12] a) J.M. Hoover, B.L. Ryland and S.S. Stahl, *ACS Catalysis* **2013**, *3*, 2599; b) J.M. Hoover, B.L. Ryland and S.S. Stahl, *Journal of American Chemical Society* **2013**, *135*, 2357; c) G. Zhang, L. Li, C. Yang, E. Liu, J. A. Golen and A. L. Rheingold, *Inorganic Chemical Communications* **2015**, *51*, 13; d) S. Hazra, L.M.D.R.S. Martins, M. F. C. G. da Silva and A.J.L. Pombeiro, *Inorganica Chimica Acta* **2017**, *455*, 549; e) G. Zhang, Y. Z. Zhang, W.-F. Lo, J. Jiang, J. A. Golen and A. L. Rheingold, *Polyhedron* **2016**, *103*, 227; f) E. Safaei, L. Hajikhanmirzaei, B. Karimi, A. Wojtczak, P. Cotič and Y.-I. Lee, *Polyhedron* **2016**, *106*, 153.
- [13] D. D. Perrin, W. L. F. Armarego and D. R. Perrin, *Purification of Laboratory Chemicals*, Pergamon Press, Oxford, U.K., **1980**.
- [14] Bruker, APEX2, SAINT and SADABS, Bruker AXS Inc., Madison, Wisconsin, USA,

2008.

- [15] G. M. Sheldrick, *Acta Crystallographica* **2015**, A71, 3.
- [16] G. M. Sheldrick, *Acta Crystallographica*. **2015**, C71, 3.
- [17] J. E. Huheey, E. A. Keiter and R. L. Keiter, *Inorganic Chemistry: Principles of Structure and Reactivity*, 4th Edition, Pearson, **1993**.
- [18] a) B.J. Hathaway, G. Wilkinson, R.D. Gillard, J.A. McCleverty (Eds.), *Comprehensive Coordination Chemistry*, vol. 5, Pergamon Press, Oxford, England, **1987**; b) F. A. Mautner, C. N. Landry, A. A. Gallo and S. S. Massoud, *Journal of Molecular Structure* **2007**, 837, 72;
c) F. A. Mautner, J. H. Albering, R. Vicente, F. R. Louka, A. Gallo and S. S. Massoud, *Inorganica Chimica Acta* **2011**, 365, 290; d) S. S. Massoud, L. L. Quan, K. Gatterer, J. H. Albering, R. C. Fischer and F. A. Mautner, *Polyhedron* **2012**, 31, 601.
- [19] A. W. Addison, T. N. Rao, J. Reedijk, J. Vanriijn and G. C. Verschoor, *Journal of Chemical Society, Dalton Transactions* **1984**, 1349.
- [20] a) J. K. Kochi, *Tetrahedron*, **1962**, 18, 483; b) J. K. Kochi, *Journal of American Chemical Society* **1962**, 84, 1572; c) G. Rothenberg, L. Feldberg, H. Wiener and Y. Sasson, *J. Chem. Soc., Perkin Transactions* **1998**, 2, 2429.
- [21] a) M. S. Dronova, A. N. Bilyachenko, A. I. Yalymov, Y. N. Kozlov, L. S. Shul'pina, A. A. Korlyukov, D. E. Arkhipov, M. M. Levitsky, E. S. Shubina and G. B. Shul'pin, *Dalton Transactions* **2014**, 43, 872; b) V. Mahdavi and M. Mardani, *Journal of Chemical Sciences* **2012**, 124, 1107; c) R. R. Fernandes, J. Lasri, A. M. Kirillov, M. F. C. Guedes da Silva, J. A. L. da Silva, J. J. R. Fraústo da Silva and A. J. L. Pombeiro, *European Journal of Inorganic Chemistry* **2011**, 3781
- [22] a) I. Timokhin, C. Pettinari, F. Marchetti, R. Pettinari, F. Condello, S. Galli, E. C. B. A. Alegria, L. M. D. R. S. Martins and A. J. L. Pombeiro, *Crystal Growth and Design* **2015**, 15, 2303; b) A. Sabbatini, L. M. D. R. S. Martins, K. T. Mahmudov, M. N. Kopylovich, M. G. B. Drew, C. Pettinari and A. J. L. Pombeiro, *Catalysis Communications* **2014**, 48, 4048; c) M. N. Kopylovich, Y. Y. Karabach, M. F. C. G. da Silva, P. J. Figiel, J. Lasri and A. J. L. Pombeiro, *Chemical European Journal*, **2012** 18, 899; d) R. R. Fernandes, J. Lasri, M. F. C. G. da Silva, J. A. L. Silva, J. J. R. F. da Silva and A. J. L. Pombeiro, *Journal of Molecular Catalysis A* **2011**, 351, 100.

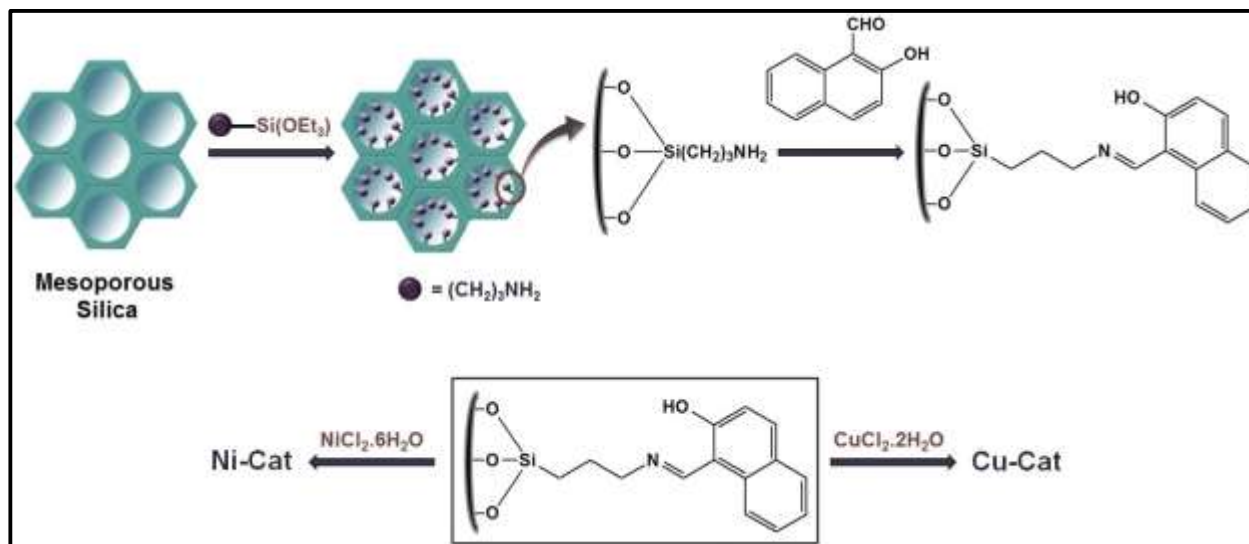
Chapter 3

Cu- and Ni-Grafted Functionalized Mesoporous Silica as active Catalyst for Olefin Oxidation

3.1 Introduction

Transition metal catalyzed organic transformations are of great importance because they can not only help to achieve valuable products but also new functional groups are introduced in comparatively inert starting materials. Oxidation of olefins and alkanes is important because a large quantity of these materials is available in nature in the form of fuel and gas. Desired products/fine chemicals are obtained from these materials. Transition metal compounds play a pivotal role in their transformation. Transition metal compounds with copper(II) and nickel(II) are widely used as catalyst in different reactions e. g. oxidation of alkane^[1-5] CS coupling,^[6] epoxidation of olefins,^[7,8] sulfoxidation,^[9,10] alcohol oxidation^[11] CC bond formation^[12,13,14] hydrogenolysis,^[15,16] etc.^[17,18] Cu(II) or Ni(II) compounds are used because they are relatively cheap and effective as catalyst. Oxidation of alkane in the presence of copper(II) catalysts often produces corresponding alcohol and aldehyde while alkene oxidation is generally done with hydrogen peroxide, tert-butyl hydroperoxide, iodosyl benzene, molecular oxygen, etc. as terminal oxidant in the presence of a suitable catalyst to get corresponding epoxide as the major product.^[19] Conversion of olefins into the corresponding epoxide is studied because epoxides are important building blocks for the synthesis of several organic fine chemicals and molecules with biological importance. Epoxidation of olefins is also vital as it may induce two chiral carbon centers.^[20,21] However, oxidation of alkenes may lead to the formation of several other products. Catalytic reactions are performed either in homogeneous medium or in heterogeneous medium. Catalysis in heterogeneous medium has some advantages over that in homogeneous medium. Main problem associated with homogeneous catalysis is separation of product(s) from the catalyst because the substrate, oxidant, product and catalyst all remain in a single phase. Simple filtration in heterogeneous catalysis is employed to separate product and catalyst as catalyst in heterogeneous medium is generally insoluble in liquid phase. Heterogeneous catalyst can be reused for several times in same organic transformation without deteriorating its efficiency and character. A drawback in heterogeneous catalysis is leaching of metal ion in solution which is not at all desirable. Under catalytic condition, a small amount of metal ion that can leak in solution will disturb the heterogeneous nature of the reaction. Thus, heterogenized catalyst should be prepared in a manner so that leaching does not occur. Strong binding of metal ion in the solid matrix can prevent metal leaching.

For heterogenized catalyst, there should be a solid support to which metal atoms are bonded strongly. There are different types of solid support e. g. polymer,^[22,23] zeolite,^[24] alumina,^[25] silica^[26–28] graphene,^[29] mesoporous carbon,^[30] carbon nanotube,^[31] metal-organic framework,^[32,33] metal oxide nanoparticles,^[34] etc.^[35,36] Use of mesoporous silica as solid support adds few advantages. Mesoporous silica has large surface area^[37] which allows greater interaction between the metal center and the substrate thus increasing the efficiency of the catalyst. In addition to that, the pore size of the silica support can be tuned according to requirement. Suitable selection of template, in the presence of which the mesoporous silica is synthesized, can allow achieving the desired pore size. Silica framework is thermally and chemically stable. Functionalization of silica matrix can be done to introduce appropriate number/nature of heteroatom (e. g. O, N or S) in the framework which can act as strong binding sites for metal center. Covalent bonds are formed when interaction between the functionalized material and the metal ion takes place. Heteroatoms in the silica framework are selected on the basis of possible hard-soft interactions. Mo,^[38] Ru,^[39,40] Pd,^[41] Fe,^[42] Mn,^[43] Cu,^[44] Ni,^[45] etc.^[46] incorporated materials have been used as catalysts in CH activation of alkenes. We have effectively used copper(II) complexes of Schiff-base ligands as catalyst in the epoxidation of olefins in homogeneous medium.^[47,48] Impregnated copper(II) or nickel(II) complexes with Schiff-base ligands on mesoporous silica can turn homogeneous catalysts into heterogeneous ones and these heterogenized catalysts have been effective in olefin epoxidation in liquid phase.^[49–51] In these cases, transition metal complexes have been synthesized and characterized by standard techniques. These complexes were then immobilized on to mesoporous silica to be used as the catalyst. However, immobilized Cu-catalyst showed metal leaching in catalytic solution. In this respect, covalently grafted metal incorporated silica can be effective to stop metal leaching in solution under catalytic conditions. 4-Methyl-2,6-diformylphenol functionalized mesoporous silica supported copper(II) and nickel(II) catalysts have been found to be active in liquid phase oxidation of olefins.^[52] But there is scope to improve catalytic efficiency in terms of conversion, reaction time, product selectivity, recyclability, etc. So, thrust is to develop new and better catalyst for important transformations. Here syntheses, characterization and heterogeneous catalytic properties of copper(II) (Cu-Cat) and nickel(II) (Ni-Cat) incorporated mesoporous silica materials,(**Scheme 3.1**) has been reported.



Scheme 3.1 : Syntheses of Cu-Cat and Ni-Cat.

2-Hydroxy-naphthyl functionalized mesoporous silica^[53] has been used to anchor copper and nickel ions strongly by covalent bond formation. Cu-Cat and Ni-Cat have been used as catalyst in oxidation of styrene, α -methyl styrene, cyclohexene, trans stilbene and cyclooctene in the presence of tert.-butyl hydroperoxide (TBHP) as the terminal oxidant under mild conditions.

3.2 Experimental Section

3.2.1 Materials and physical measurements

The reagents used in the syntheses are all procured from commercial sources and used without further purification. The Powder X-ray diffraction patterns of the samples are recorded on a Bruker D-8 Advance instrument using Ni-filtered $\text{Cu-K}\alpha$ radiation ($\lambda = 1.5406 \text{ \AA}$) operated at 40 kV and 40 mA. Nitrogen adsorption-desorption isotherms of the samples are measured at 77 K using a NOVA 2200e, Quantachrome Instruments, Surface Area and Pore Size Analyzer. The transmission electron microscopic (TEM) images are recorded in a JEOL JEM-1400 transmission electron microscope. FT-IR spectra of the samples are recorded on a Perkin Elmer spectrometer (Spectrum Two) using attenuated total reflectance (ATR) technique. UV-visible diffuse reflectance spectra of the solid samples are measured using BaSO_4 as the background standard in a Shimadzu UV-2450 spectrophotometer. Solid state MAS NMR analyses are carried out in a CHEMAGNETICS 300 MHz CMX 300 spectrometer. Thermal analyses of the samples

are carried out under nitrogen atmosphere (flow rate: 50 cc/min) from ambient to 1200°C (heating rate of 2°C/min) using a Mettler Toledo TGA 850 instrument. Copper and nickel contents of the samples are estimated by inductively coupled plasma atomic emission spectroscopy (ICP-AES) using a Shimadzu ICPS-7510 Sequential Plasma Spectrometer. The solutions for analyses are prepared by digesting 30 mg of the catalysts in 1 mL of hydrofluoric acid and then by adding 1 mL of nitric acid to dissolve the samples completely. The volumes are then made up to 25 mL using Milli-Q water, the solutions are membrane filtered and fed into the auto-sampler of the spectrometer. The products formed in the catalytic reactions are analyzed by using a next generation high speed gas chromatography system, Shimadzu GC-2025 AF, equipped with a fused silica capillary column and a FID detector. Substrate and products have been identified by PerkinElmer Clarus 680/600 T Gas Chromatography/Mass Spectrometer (GC-MS).

3.2.2 Synthesis of functionalized mesoporous silica

Mesoporous silica used as the solid support has been synthesized following a published procedure.^[1] In a general protocol, 4.0 g of cetyltrimethylammonium bromide and 2.0 g of Brij-35 ($C_{12}H_{25}(OC_2H_4)_{23}OH$), are dissolved in 90 mL of water containing 1.0 g of tartaric acid. To it 4.8 g of tetraethylorthosilane is added slowly under continuous stirring and the pH of the gel is adjusted to 11 by adding NaOH solution. The reaction mixture is stirred overnight, transferred into a polypropylene bottle and kept under hydrothermal treatment at 75 °C for 3 days. The white precipitate is filtered off, washed thoroughly with distilled water and dried under vacuum. The product is calcined in air at 450 °C for 8 h to remove the organic surfactants and obtain the mesoporous silica (**Scheme 3.1**). 1.0 g of this calcined silica is then stirred with 1.0 g of 3-aminopropyl triethoxy silane (3-APTES) in chloroform under inert 2 atmosphere for 12 h. The resultant material is collected through filtration, washed with chloroform followed by dichloromethane and dried. Finally, 1.0 g of the 3-APTES grafted silica is refluxed with 0.75 g of 2-hydroxy-1-naphthaldehyde in methanol for 4 h to obtain the functionalized mesoporous silica with well-positioned N and O-donor sites capable of metal-binding.^[2] The product is filtered, washed with hot methanol to remove the unreacted aldehyde and dried prior to use for metal loading. Synthesis of the catalysts: Cu-Cat and Ni-Cat For the synthesis of Cu-Cat, 0.08 g of cupric chloride dihydrate ($CuCl_2 \cdot 2H_2O$) is dissolved in 20 mL of methanol, to it 1.0 g of 2-

hydroxy-1-naphthaldehyde functionalized silica is added and the mixture is stirred at 333 K for 2 h. The suspension is filtered to recover the metal bound catalyst, washed with methanol to remove any unreacted salt and dried under vacuum. Ni-Cat is also prepared using an identical technique where 0.11 g of nickel chloride hexahydrate ($\text{NiCl}_2 \cdot 6\text{H}_2\text{O}$) is used in place of the copper salt and the rest of the process remains the same.

3.2.3 Olefin oxidation

The oxidation reactions of styrene, α -methyl styrene, cyclohexene, trans-stilbene and cyclooctene have been carried out heterogeneously using Cu-Cat and Ni-Cat. Similar procedure has been followed for all the substrates in presence of both of the catalysts. Typically, Cu-Cat or Ni-Cat (0.020 g) and 0.5 g of substrate (styrene: 4.80 mmol; α -methyl styrene: 4.23 mmol; cyclohexene: 6.09 mmol; trans-stilbene: 2.77 mmol and cyclooctene: 4.54 mmol) are taken in 10 mL of acetonitrile in a two-necked round bottom flask fitted with a reflux condenser. The mixture is preheated to 65 °C. To the mixture, tert-butylhydroperoxide (equimolar with respect to substrate) is added to initiate the catalytic reactions. Aliquots from the catalytic reaction mixtures are collected at regular intervals of time and analyzed by gas chromatography. Product(s) and substrate, if any, are identified either by GC-MS or comparison with known standards. One blank reaction is also carried out without any catalyst keeping other reaction conditions unaltered. To reuse the catalyst, the materials are recovered by filtration, washed thoroughly with acetonitrile and then treated with 0.1 M HCl solution in ethanol for 8 h at 70 °C and finally dried at 100 °C for 2 h. The catalytic reactions with the recovered catalysts are performed following the same experimental procedure.

3.3 Results and discussion

3.3.1 Characterization of the framework, microstructure and porosity

Powder X-ray diffraction study of all the samples from the starting mesoporous silica to the catalysts has been carried to elucidate their microstructure. The patterns for calcined mesoporous silica catalysts, Cu-Cat and Ni-Cat are shown in **Figure 3.1**

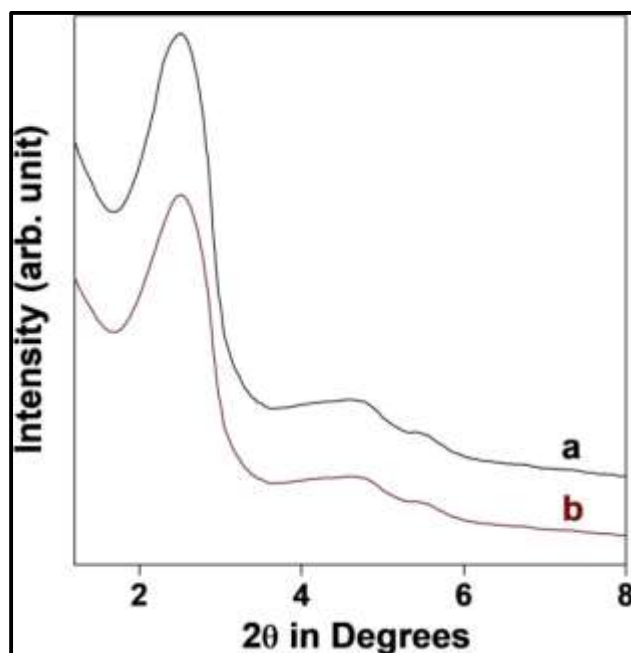


Fig 3.1 : Powder X-ray diffraction patterns of (a) Cu-Cat and (b) Ni-Ca

All the samples exhibit ordered 2D-hexagonal mesophase, evident from the three distinct diffraction peaks that can be assigned to the 100, 110 and 200 planes and a weak one for 210 plane.^[54-56] Nevertheless, the mesopore ordering in the samples decreases to some extent in each step of modification as reflected from the decrease in intensity of the peaks in the diffraction patterns.

The nitrogen adsorption/desorption isotherms of the calcined mesoporous silica and the catalysts are given in **Figure 3.2**. The BET (Brunauer-Emmett-Teller) surface area and pore volume of the calcined mesoporous silica (**Figure 3.2a**) which is taken as the starting material are 992 m²/g and 1.207 cc/g, respectively. On gradual functionalization the surface area decreases as well as the pore volume. For 3-APTES functionalized and 2-hydroxy naphthaldehyde loaded silica the surface areas are 462 and 305 m²/g, respectively whereas the corresponding pore volumes are 0.72 and 0.53 cc/g. The materials show a typical type IV isotherm with steep rise due to capillary condensation at higher pressure indicating that the samples are mesoporous.^[57,58] The desorption hysteresis in the P/P₀ range of 0.6-1.0 that is observed for the samples originate due to intercrystallite adsorption.^[59] The pore volume of the Schiff base functionalized sample (0.53 cc/g) containing N and O-donor sites suggests that there is reasonable space to accommodate the metal ions inside its pores. The nitrogen adsorption-desorption isotherms for the catalysts, Cu-

Cat and Ni-Cat (**Figure 3.2b and c**) also show similar type IV isotherms suggesting their mesoporous structure (Y-axis values are offset by 100 cc/g for plot b). The specific surface area and pore volume of Cu-Cat and Ni-Cat are 209 and 213 m² g⁻¹, and 0.428 and 0.436 cc/g, respectively. The pore diameter of the starting mesoporous silica as obtained from the NL-DFT (Non-local density functional theory) model is around ca. 4.0 nm and on functionalization and metal loading the size of the pores decreases to ca. 2.5 nm (Inset of Figure 1.2).

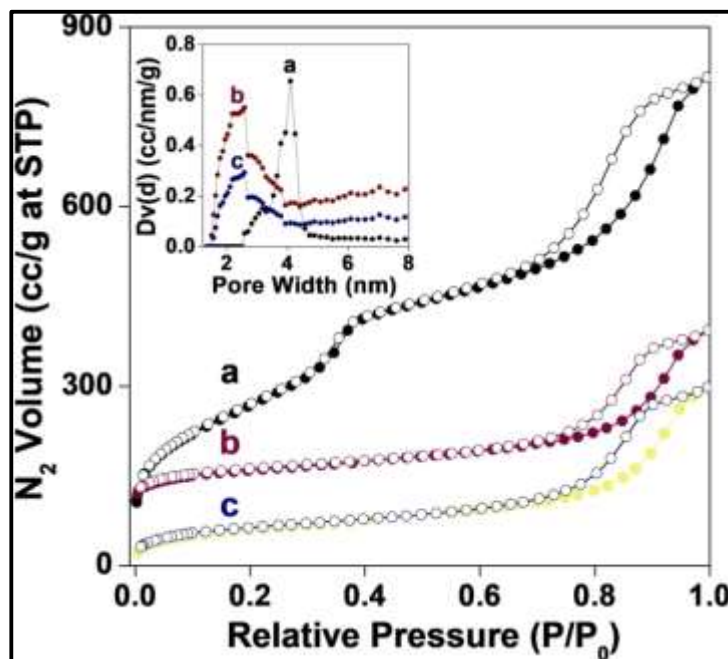


Fig 3.2 : Nitrogen adsorption desorption isotherms of (a) calcined mesoporous silica, (b) Cu-Cat and (c) Ni-Cat (For clarity, the Y-axis values are offset by 100 cc/g for plot b); Inset: Pore size distribution using NL-DFT model for the respective samples (For clarity, the Y-axis values are multiplied by 20 and 10 for plots b and c, respectively).

The pore volume and pore size of the heterogeneous solid catalysts are well-suited to carry out organic transformations inside them. The TEM images of the catalysts have been illustrated in **Figure 3.3**.

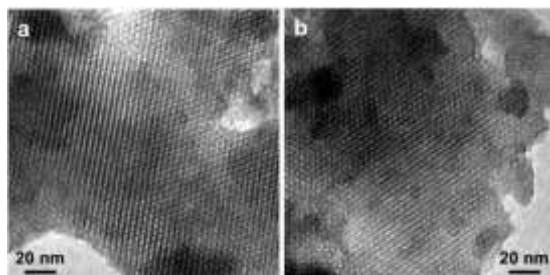


Figure 3.3 : TEM images of (a) Cu-Cat and (b) Ni-Cat.

TEM images of calcined mesoporous silica, 3-APTES functionalized and 2-hydroxy naphthaldehyde loaded silica are taken. In all the materials, hexagonal arrangement of the pores with a different contrast than the pore walls can be seen. With gradual functionalization the ordering of the pores are affected, which is not unusual. The pore sizes of the samples estimated from the TEM images are in close agreement with the pore size obtained from nitrogen adsorption isotherms. Thus, the results of small angle powder XRD patterns, gas adsorption and TEM studies confirmed the existence of mesoporosity in the samples.

The FT-IR spectra of the samples have been studied by ATR technique. The 3-APTES functionalized mesoporous silica shows a broad band in the region of $3625\text{--}2924\text{ cm}^{-1}$ that can be ascribed to the presence of amino and methylene groups. For the Schiff-base modified sample an additional band centered around 1635 cm^{-1} originates due to the presence of azomethine group. After the Schiff base interacts with the copper and nickel salts, these bands shift to somewhat lower wavenumber region in case of the catalysts which indicates the retention of the azomethine group as well as confirms complex formation.

Mesoporous silica, functionalized mesoporous silica and metal incorporated mesoporous silica have been further characterized by solid state MASNMR spectroscopy. ^{13}C CP MASNMR spectra of all but the mesoporous silica are given in **Figure 3.4**.

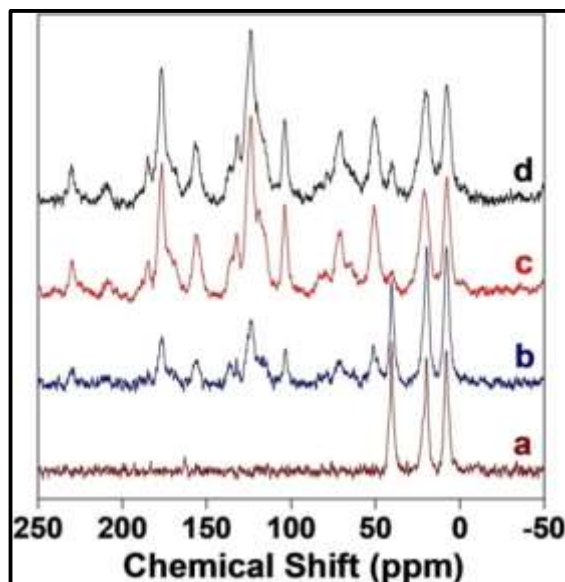


Fig 3.4 : Solid state ^{13}C CP-MAS NMR spectra of (a) APTES-loaded mesoporous silica, (b) 2-hydroxy naphthaldehyde loaded silica, (c) Cu-Cat and (d) Ni-Cat.

Signals for the presence of aliphatic carbons in 3- APTES functionalized material appear at 8.3, 19.7 and 40.6 ppm (**Figure 3.4a**). After Schiff-base condensation with 2-hydroxy-1-naphthaldehyde, the material shows retention of these aliphatic peaks along with the appearance of signals for aromatic carbons at (**Figure 3.4b**) 7.8, 19.3, 40.2, 51.8, 71.7, 104.3, 124.2, 133.0, 137.0, 156.2, 176.8, 184.8, 210.8 and 229.5 ppm confirming the Schiff-base condensation between amine functionalized silica and 2-hydroxynaphthaldehyde. ^{13}C CP MAS NMR spectra of Cu-Cat and Ni-Cat are shown in **Figure 3.4c and 3.4d**. It is clear from the figures that organic moieties in these materials retain their framework and slight shifting of peak positions in Cu-Cat and Ni-Cat indicate formation of bonds between metal center and donor atoms of the functionalized silica.

^{29}Si MAS NMR studies give idea about the chemical environment around Si atom in all the mesoporous silica materials. The results of the analyses are shown in **Figure 3.5**.

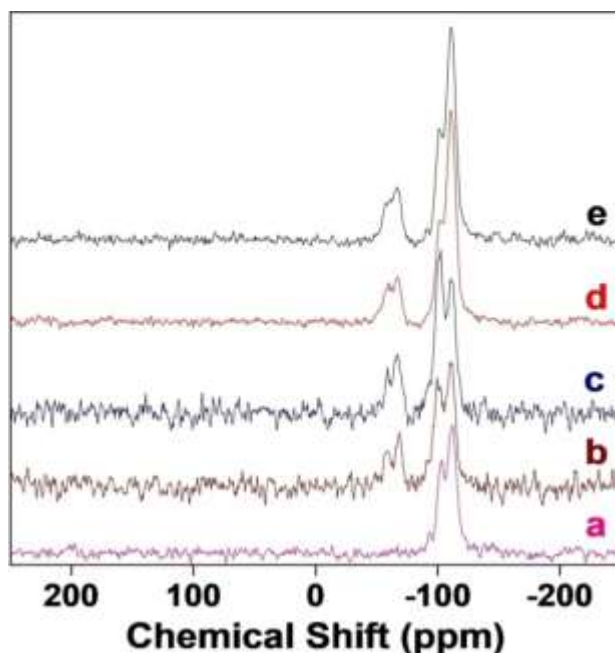


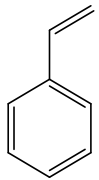
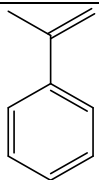
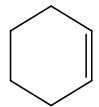
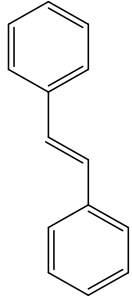
Fig 3.5 : Solid state ^{29}Si MASNMR spectra of (a) calcined mesoporous silica, (b) APTES-loaded mesoporous silica, (c) 2-hydroxy naphthaldehyde loaded silica, (d) Cu-Cat and (e) Ni-Cat.

Before any functionalization, mesoporous silica gives peak at 111.4 and 103.5 ppm (**Figure 3.5a**). These peaks may be assigned to the presence of Q4 and Q3 silica species of the $\text{Si}(\text{OSi})_n(\text{OH})_{4-n}$ units. In 3-APTES functionalized material, peak positions slightly shift and new signals appear at 67.8 and 57.7 ppm (**Figure 3.5b**) confirming the incorporation of 3-APTES in mesoporous silica. Inagaki et al. previously showed that peaks at around 67 and 58 ppm appear for similar organic-inorganic mesoporous silica material. These peaks can be attributed to the presence of T3 ($(\text{SiO})_3\text{Si-R-Si}(\text{OSi})_3$) and T2 ($(\text{HO})_2(\text{OSi})\text{Si-R-Si}(\text{OSi})_2(\text{OH})$) species, respectively.^[60,61] However, materials with further functionalization with 2-hydroxy-1-naphthaldehyde followed by Cu or Ni grafting show similar peaks for silicon with different environment. These facts confirm Schiff-base condensation leading to the imine bond formation and retention of similar frameworks in Cu-Cat and Ni-Cat after complexation of the metal ions. Thermogravimetric analyses (TGA) on various silica materials have been performed to examine thermal stability of the frameworks and also to find out the amount of organic functionalization on the mesoporous silica. TGA analyses have been carried out in the range of 30 to 1200°C. The amount of Schiff-base functionalized moiety on silica framework has been determined from the

figure and it has been found to be around 6.42% i. e. ~ 0.30 mmol of Schiff-base functionality per gram of silica framework. Presence of Cu or Ni metal in Cu-Cat and Ni-Cat has been confirmed by ICP-AES measurements. The amounts of the metal content in Cu-Cat and Ni-Cat have been determined to be 17.4 mg/g (0.274 mmol/g) and 7.8 mg/g (0.133 mmol/g), respectively. Cu(II) and Ni(II) centers in the catalysts may have tetracoordinate environment.^[52] Here O,N donor atoms come from heterogenized Schiff-base ligand; one chloride species and another solvent molecule may provide all the coordinations. Some square planar Ni(II) complexes are known to display yellow color.^[62] Color of Cu-Cat and Ni-Cat are yellowish green. UV-vis diffuse reflectance spectra of Cu-Cat and Ni-Cat are done. Peaks at ~ 230 nm and 310 nm are present for both the compounds. These peaks may be attributed to the intraligand charge transfer. The most important peaks appear are at 398 nm and in the range of 400–420 nm for Cu-Cat and Ni-Cat, respectively. These peaks are due to the presence of ligand to metal charge transfer (LMCT).

3.3.2 Catalytic studies

Cu-Cat and Ni-Cat has been used as catalyst in oxidation of some olefins e. g. styrene, α -methyl styrene, cyclohexene, trans stilbene and cyclooctene in the presence of tert.-butyl hydroperoxide as the terminal oxidant in acetonitrile medium under mild conditions. The results of the catalytic reactions are given in **Table 3.1**. It is clearly evident from the results that both the catalysts are quite effective in the oxidation of different substrates. Oxidation of styrene is of special attention to the researchers. Cu-Cat and Ni-Cat are active as catalyst in styrene oxidation as the yield of reaction is 90 and 70%, respectively. Benzaldehyde has been identified as the major product in both cases with 91 and 98% selectivity, respectively. In case of Cu catalyzed oxidation, minor amount of phenylacetaldehyde and benzoic acid are produced while in case of Ni-catalyzed reaction only benzoic acid has been obtained as the minor product. There is no production of phenylacetaldehyde with the nickel catalyst.

Substrate	Catalyst	Products (% Yield)			Total Yield (%)	Major product and Selectivity (%)	TON
		Benzaldehyde	Benzoic acid	Phenylacetaldehyde		Benzaldehyde	
	Cu-Cat	82	3	5	90	91	
	Ni-Cat	68	2	--	70	98	
	Blank				5		
		α -Methyl styrene oxide		Acetophenone		α -Methyl styrene oxide	
	Cu-Cat	51		41	92	55	
	Ni-Cat	51		25	76	67	
	Blank				7		
		2-Cyclohexen-1-one	2-Cyclohexen-1-ol	Cyclohexene oxide		2-Cyclohexen-1-one	
	Cu-Cat	65	5	2	72	90	
	Ni-Cat	60	10	3	73	82	
	Blank				4		
		<i>Trans</i> stilbene oxide	Benzil	Benzaldehyde		<i>Trans</i> stilbene oxide	
	Cu-Cat	65	9	10	84	77	
	Ni-Cat	41	10	35	86	48	
	Blank				7		

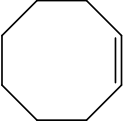
		Cyclooctene oxide		Cyclooctene oxide	
	Cu-Cat	81	81	100	
	Ni-Cat	71	71	100	
	Blank		6		

Table 3.1 : A Solvent: acetonitrile; temperature: 658C; catalyst: Cu–Cat and Ni-Cat (0.020 g each); amount of substrate: 0.5 g and oxidant: TBHP (equimolar with respect to substrate) bYields are measured after 12 h of the reaction, c TOF: turnover frequency = moles of substrate converted per mole of metal center per hour.

Oxidation of α -methyl styrene gives α -methyl styrene oxide and acetophenone as the products in the presence of both the catalysts. Yield is high but selectivity is poor for both the catalysts. Yields of 92 and 76% have been obtained with Cu–Cat and Ni-Cat, respectively, with methyl styrene oxide as the major product. Selectivity for methyl styrene oxide is only 55 and 67% in the presence Cu–Cat and Ni-Cat, respectively. Oxidation of cyclohexene gives 72 and 73% yield for the Cu- and Ni-catalyst, respectively, and three products, namely 2- cyclohexen-1-one, 2-cyclohexen-1-ol and cyclohexene oxide are formed in the presence of both the catalysts. 2-Cyclohexen-1- one has been identified as the major product with excellent selectivity for both the catalysts. Oxidation of trans stilbene has been achieved with high conversion value. Similar activity has been recorded for Cu–Cat and Ni-Cat with 84 and 86% yield, respectively. Trans stilbene oxide has been identified as the major product with high selectivity (77%) for the copper catalyst. But selectivity for nickel catalyst is poor. Benzil and benzaldehyde are produced as minor product in case of the copper compound. However, selectivity for benzaldehyde with Ni-Cat is quite comparable with that of the trans stilbene oxide. For nickel catalyst, stilbene oxide and benzaldehyde are produced with 41 and 35% yield, respectively. Both the catalysts show excellent catalytic activity towards oxidation of cyclooctene. Although yields are obtained as 81 and 71% for Cu–Cat and Ni-Cat, respectively, in both the cases cyclooctene oxide has been identified as the sole product which implies 100% selectivity. Both the catalysts have been found to be very active in these oxidation reactions as evident from their high TOF values. However, Ni-Cat shows higher TOF value than that of Cu–Cat in each reaction. Ni-Cat has highest TOF

value of 105 for styrene oxidation and lowest TOF of 35 has been marked for Cu-Cat in trans-stilbene oxidation reaction. A blank reaction has been carried out with all the substrates without any catalyst under similar reaction conditions. Very small amount of conversion has been observed in each case. Low conversion in blank reactions signifies the pivotal role played by these catalysts. Aliquots from catalytic reaction mixtures have been collected at regular time intervals and analyzed by gas chromatography to monitor progress of the reactions. The results are given in **Figure 3.6-3.10**.

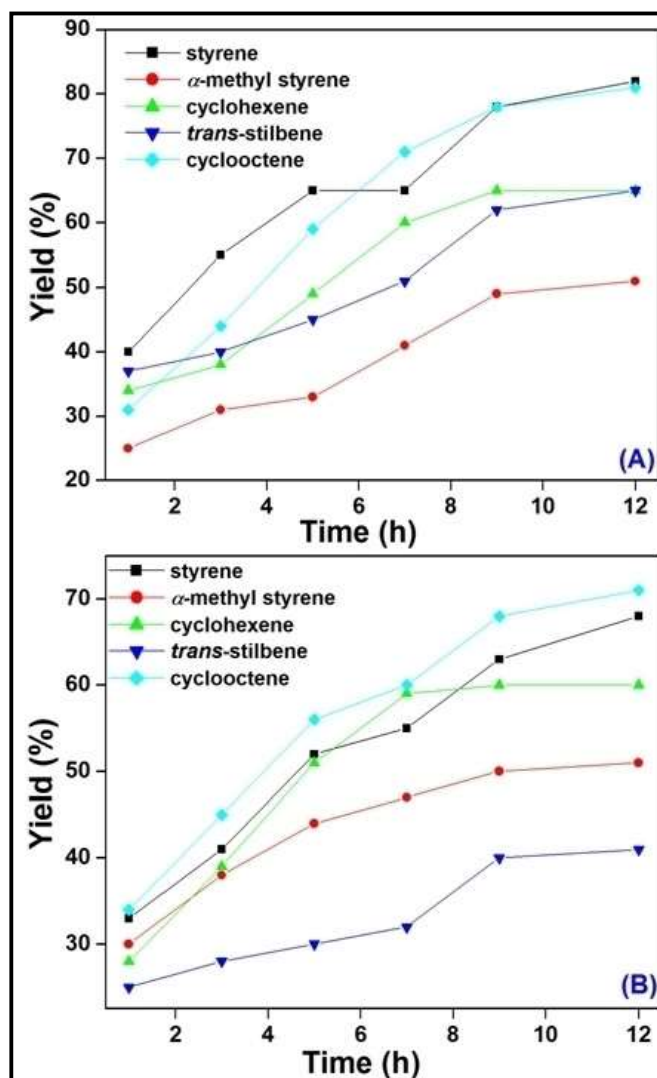


Fig 3.6 : Oxidation of different substrates in the presence of (A) Cu–Cat and(B) Ni-Cat. Yield of major product from oxidation reaction has been plotted against time.

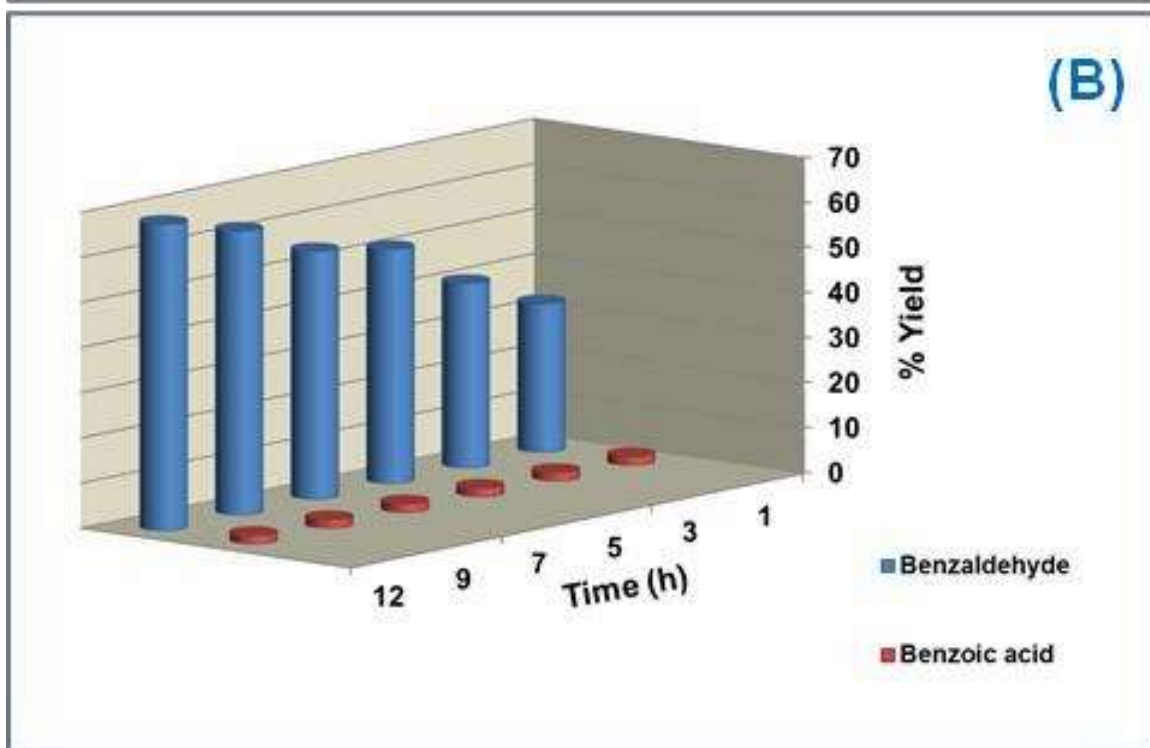
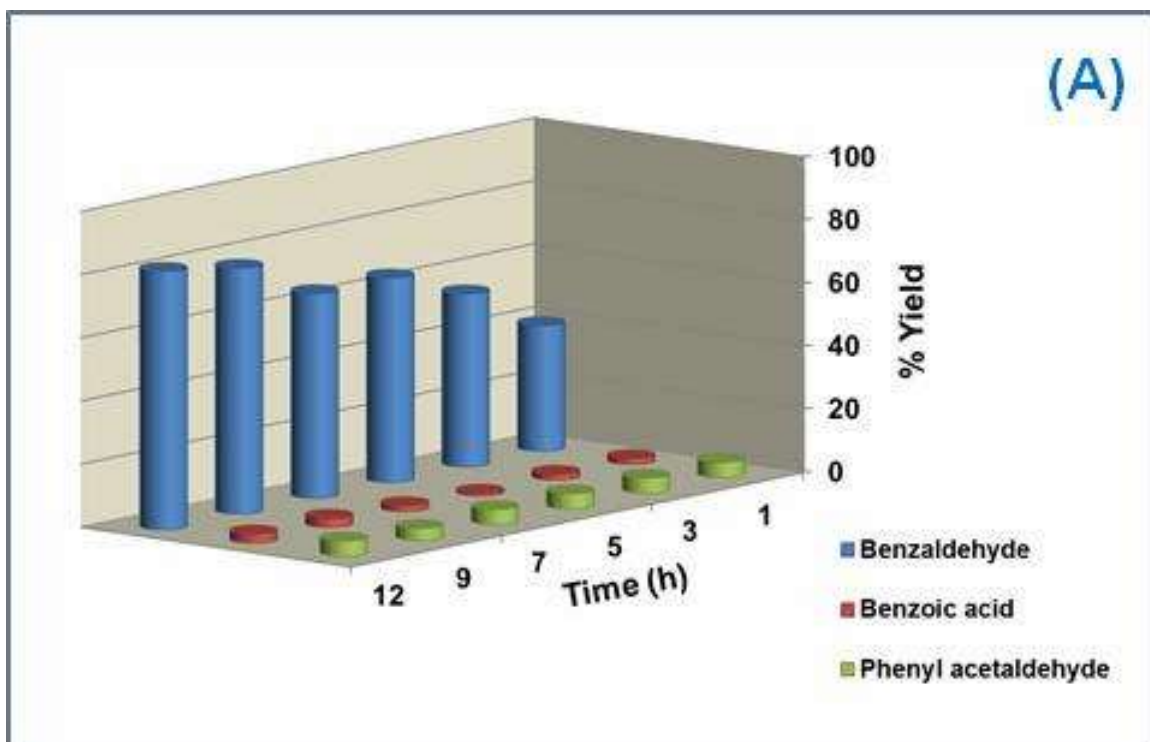


Fig 3.7 : Oxidation of styrene in the presence of Cu-Cat (A) and Ni-Cat (B)

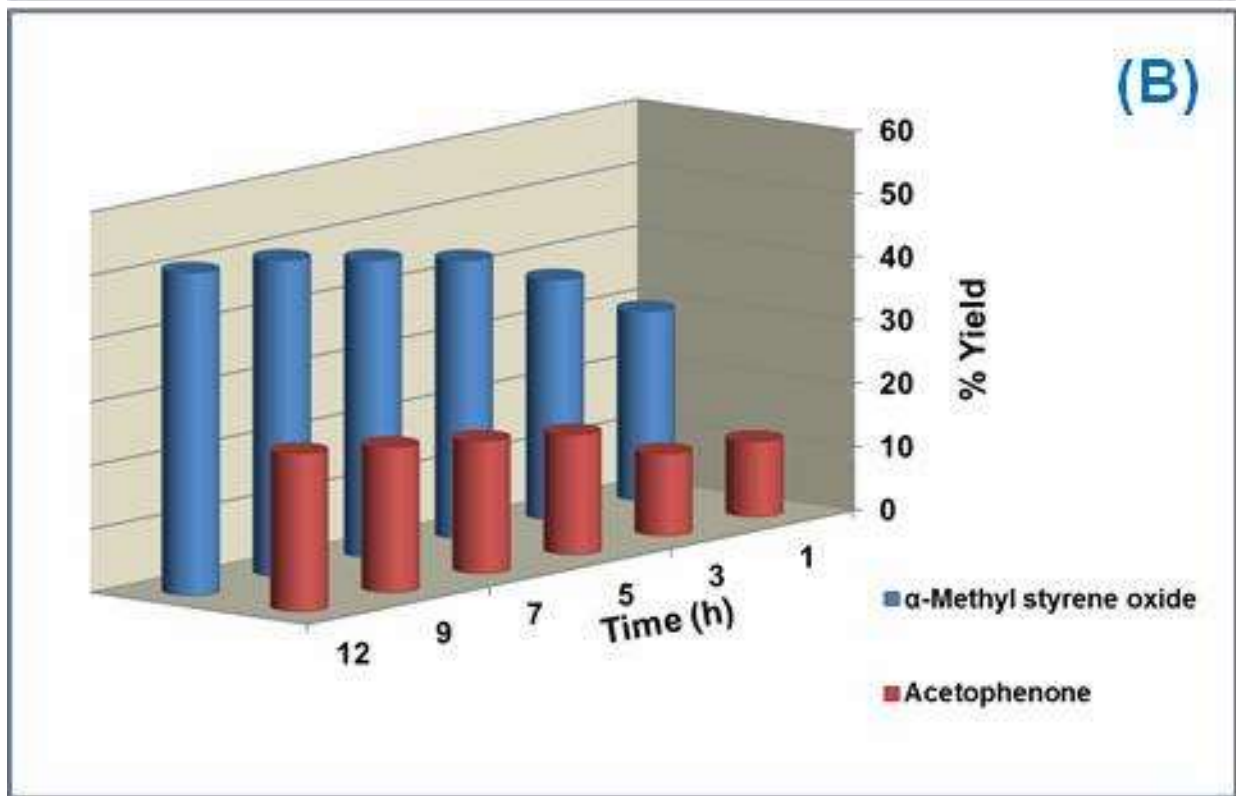
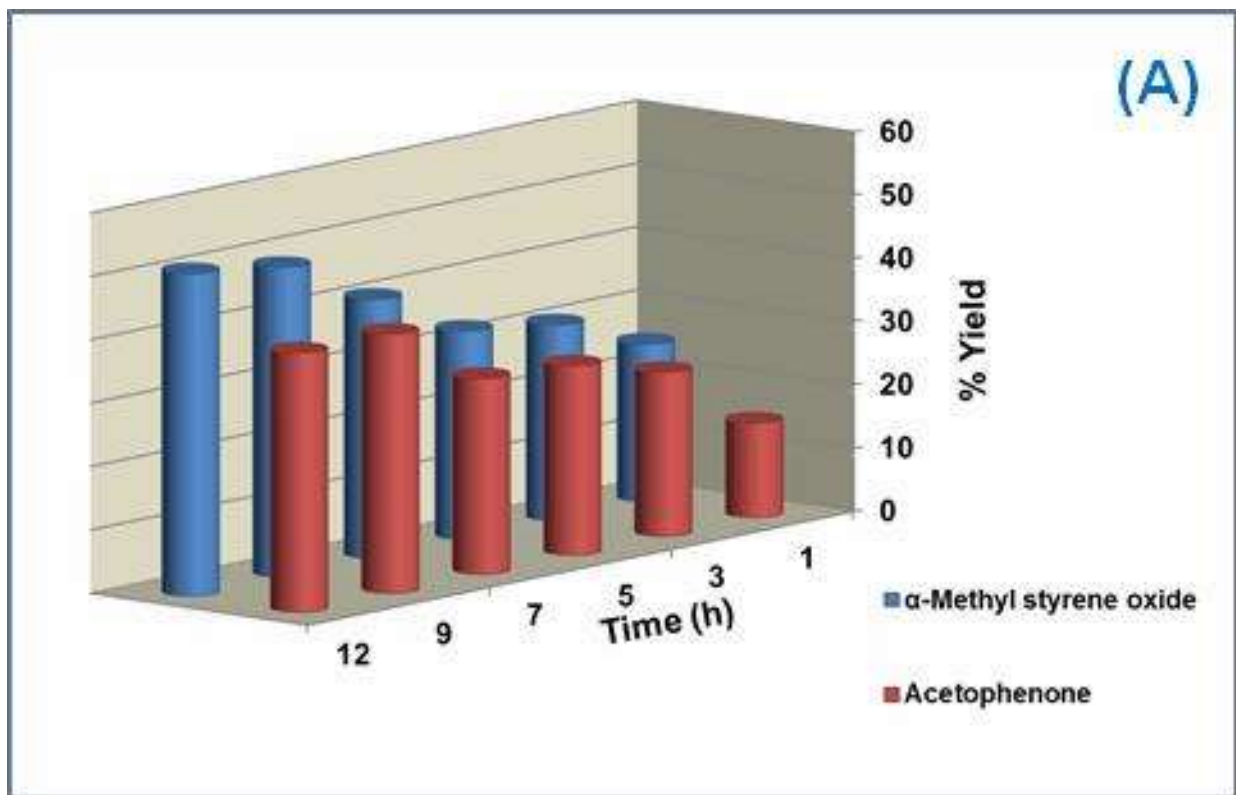


Fig 3.8 : Oxidation of α -methyl styrene in the presence of Cu-Cat (A) and Ni-Cat (B)

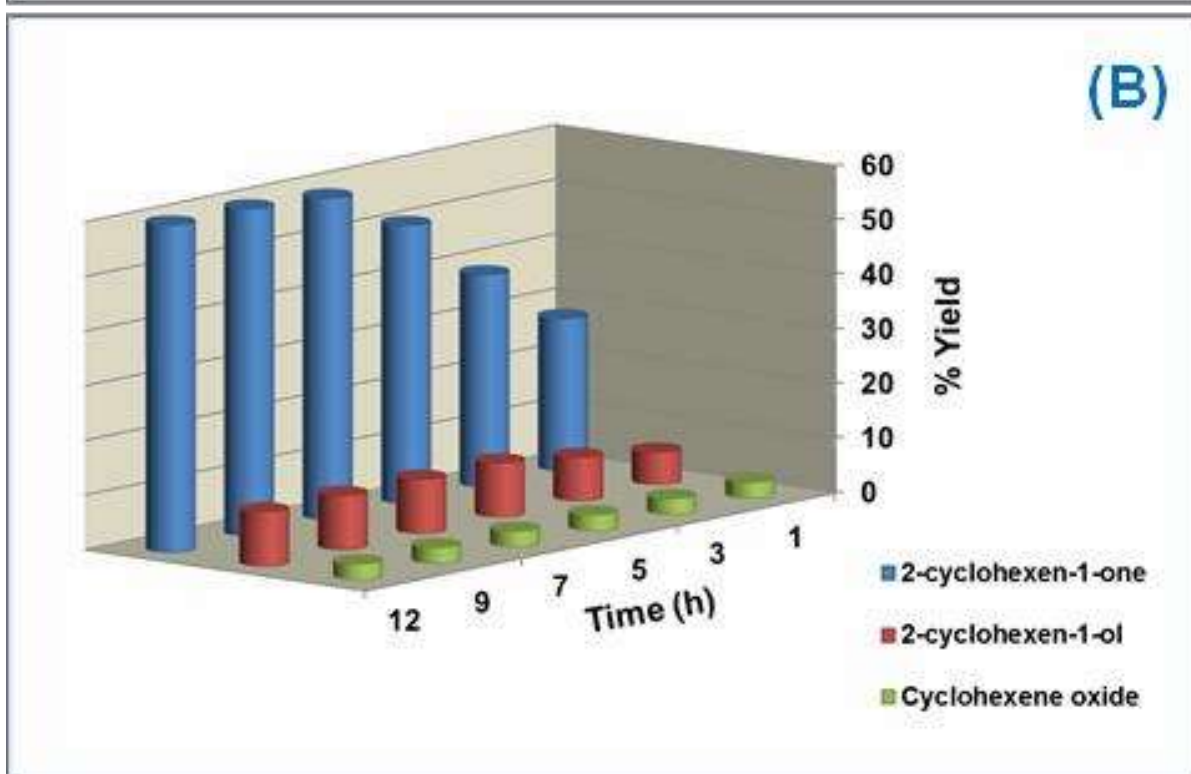
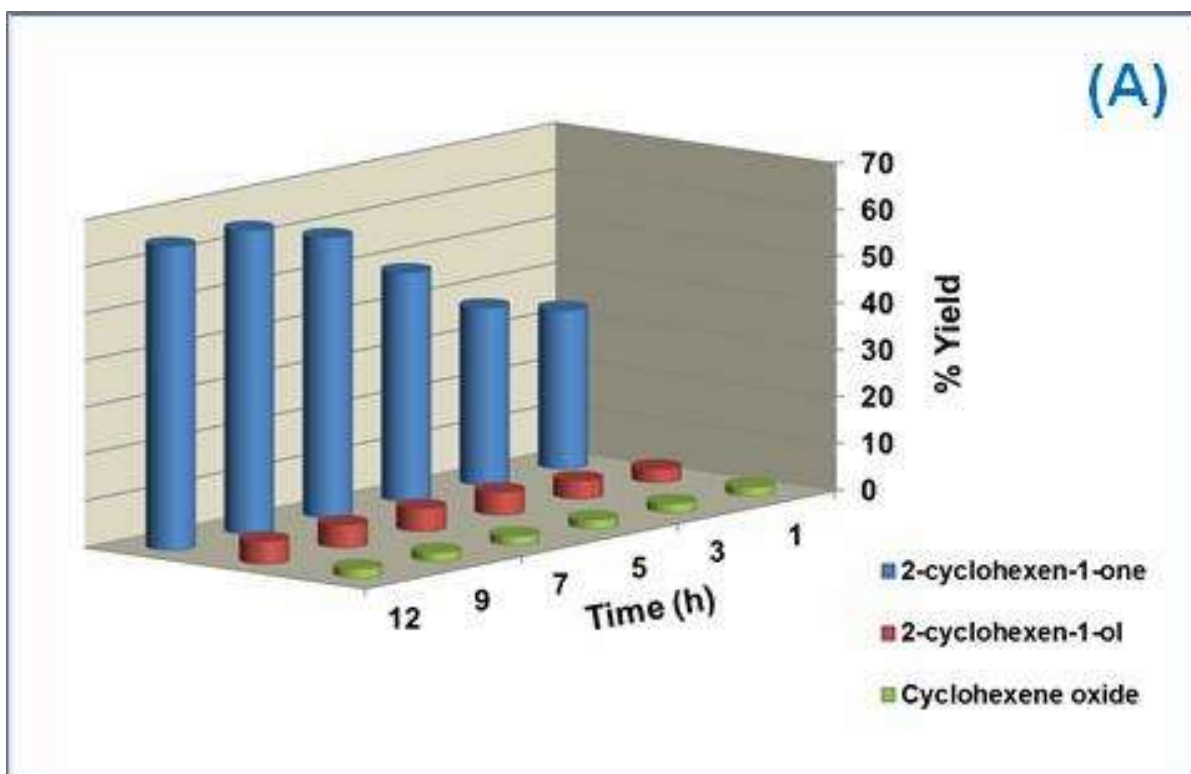


Fig 3.9 : Oxidation of cyclohexene in the presence of Cu-Cat (A) and Ni-Cat (B)

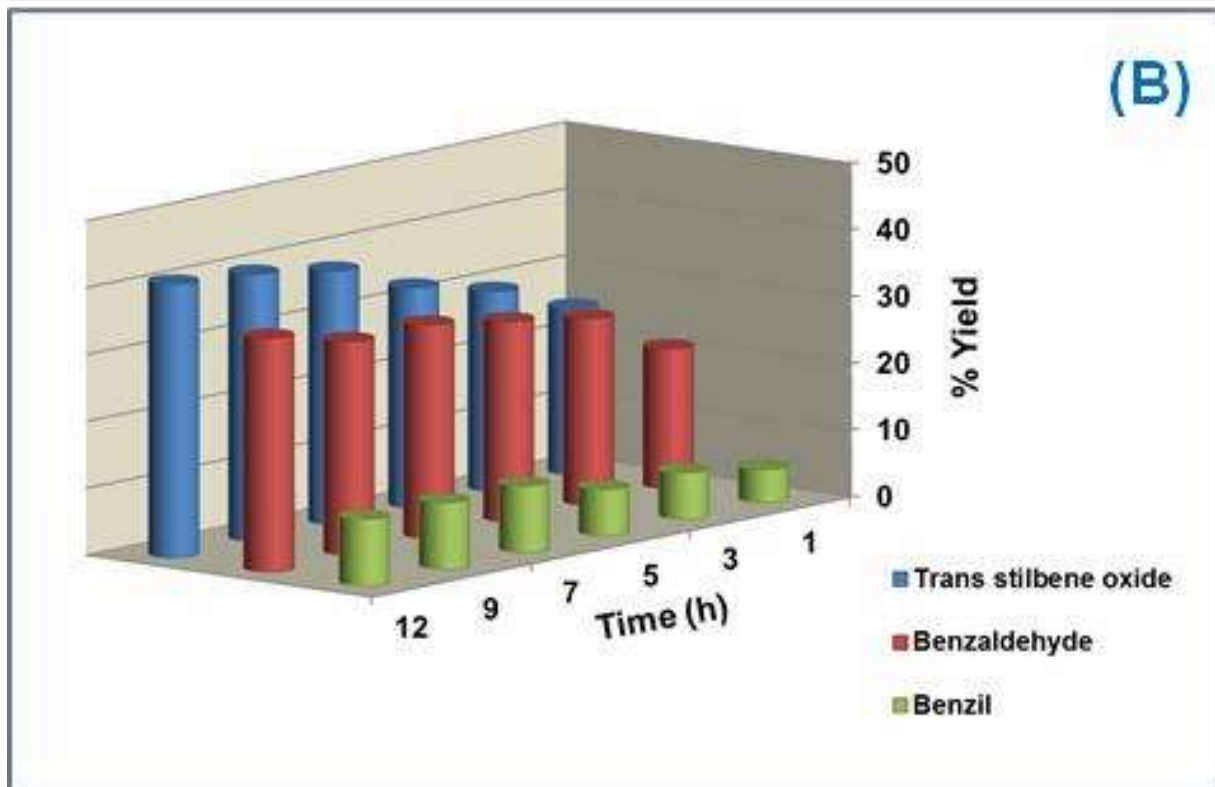
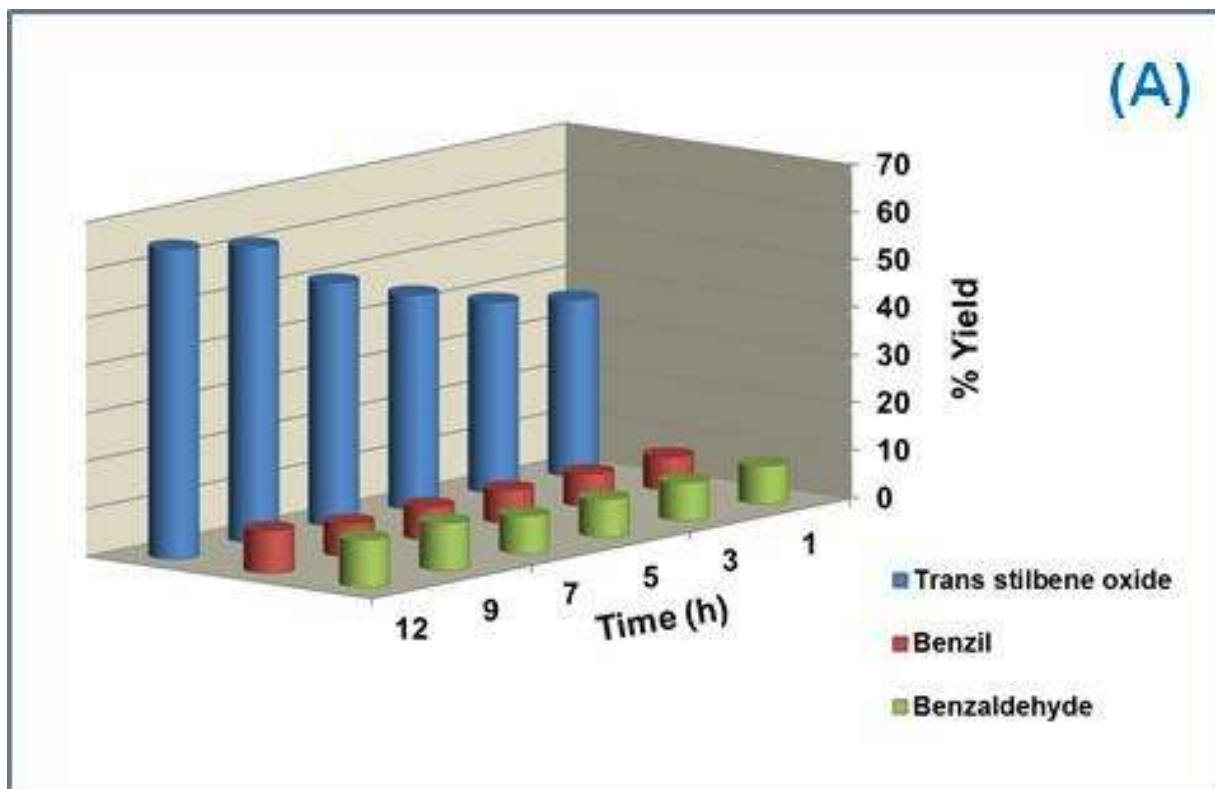


Fig 3.10 : Oxidation of *trans* stilbene in the presence of Cu-Cat (A) and Ni-Cat (B)

It has been found that after 12 h of the reaction, yields do not increase noticeably for all the products. In case of styrene oxidation, benzaldehyde has been identified as the major product. With the gradual increase in reaction time, yield of benzaldehyde has also increased. After 1 h, yields of benzaldehyde are 40 and 33% (**Figure 3.7**) which increased to 82 and 68% after 12 h in the presence of Cu–Cat and Ni-Cat, respectively. Formation of minor products after 1 h does increase significantly for both the catalysts. In case of *o*-methyl styrene oxidation, corresponding oxide and acetophenone are obtained as the products. 25 and 30%

of methyl styrene oxide is formed for Cu–Cat and Ni-Cat, respectively, after the first 1 h of reaction (**Figure 3.8**). However, yields reach to 51% for both the catalysts at the end of 12 h. Acetophenone is identified as another product with 15 and 12% yield after 1 h for Cu–Cat and Ni-Cat, respectively. It reaches up to 41 and 25% after 12 h. 2-Cyclohexen-1-one is the major product in cyclohexene oxidation with the formation of 34 and 28% after 1 h, and 65 and 60% after 12 h in the presence of Cu–Cat and Ni-Cat, respectively (**Figure 3.9**). The increase in the amount of minor products, namely, 2-cyclohexen-1-ol and cyclohexene oxide, is not visible on going from the first hour to twelfth hour of the reaction i. e. most of the amount of minor products are formed within 1 h in case of cyclohexene oxidation. Yield of trans stilbene oxide increases from 40 to 65% in the presence of Cu–Cat within 1 h to 12 h in case of trans stilbene oxidation reaction (**Figure 3.10**). The increase for the corresponding Ni-Cat is 25 to 41% during the same time period of the reaction. The other product that is formed in the nickel catalyzed reaction is benzaldehyde. Its yield increases from 21 to 35% within the same time interval. In case of the copper catalyst benzaldehyde is formed in much less amount and the yield is 10% after 12 h. Finally, in the case of cyclooctene oxidation, there is gradual increase in yield of cyclooctene oxide as the sole product with time and it is the sole product of the oxidation reaction for both the catalysts. The yield increases from 31 to 81% for the copper catalyst while that for the nickel catalyst it goes from 34 to 71% within 1 h to 12 h of the reaction (**Figure 1.6**). Hot filtration test and tests for recycling ability of the catalysts have been performed to further investigate the efficiency of the catalysts. It is known that if unbound metal is present in solution in any catalytic reaction mixture, it can catalyze the olefin oxidation reaction. Thus, it becomes extremely important to detect metal leaching or metal containing any species in solution in order to comment on the heterogeneous nature of a catalyst. For this purpose, hot filtration tests have been performed on styrene oxidation reaction in the presence of Cu–Cat and Ni-Cat. The

catalysts have been separated from the reaction mixtures by filtration under hot condition after completion of initial 1 h. Formation of benzaldehyde is 40 and 33% (**Figure 3.11**) for Cu–Cat and Ni-Cat, respectively, at this time. After separation, the reaction is continued in absence of catalysts and it is observed that yield of benzaldehyde increases only marginally. For the uninterrupted reactions in the presence of catalysts, catalytic process proceeds in normal course with further formation of benzaldehyde. In absence of Cu–Cat and Ni-Cat, slight increase in yield of benzaldehyde may be because of the presence of the oxidant, tert-butyl hydroperoxide. Blank reactions show that tert-butyl hydroperoxide can oxidize styrene in little yield. To further ensure about metal leaching in to the reaction mixtures ICP-AES measurement have been performed with the filtrates after catalyst separation to determine the amount of metal ion, if any. However, there is no detectable amount of copper or nickel ion in reaction mixture which confirms that no metal leaching takes place. Recycling ability of the catalysts has been studied to check whether these catalysts can be used for several catalytic cycles without significant loss in their efficiency. For this, styrene has been chosen as the substrate. After completion of each catalytic reaction, the catalyst has been recovered and regenerated, and then used for next cycle of the same reaction. All the catalytic reactions are carried out following the original protocol. Results of styrene oxidation in three cycles in the presence of Cu–Cat and Ni-Cat are given in **Figure 3.12** and it is evident from it that catalytic efficiency of the samples reduces slightly in consecutive runs. However, it is observed that selectivity for benzaldehyde always remains high. This indicates significant reusability of both the catalysts.

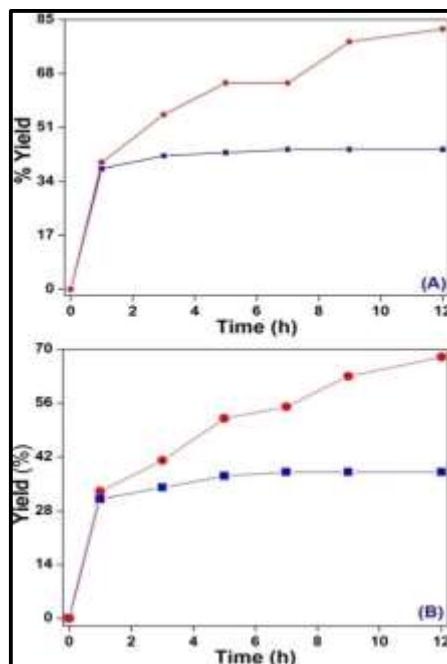


Fig 3.11 : Hot filtration test for oxidation of styrene in the presence of (A)Cu–Cat and (B) Ni-Cat. Red line with circle indicates normal route of benzaldehyde formation whereas blue line with square box shows growth of benzaldehyde after removal of Cu–Cat and Ni-Cat after 1 h of the reaction

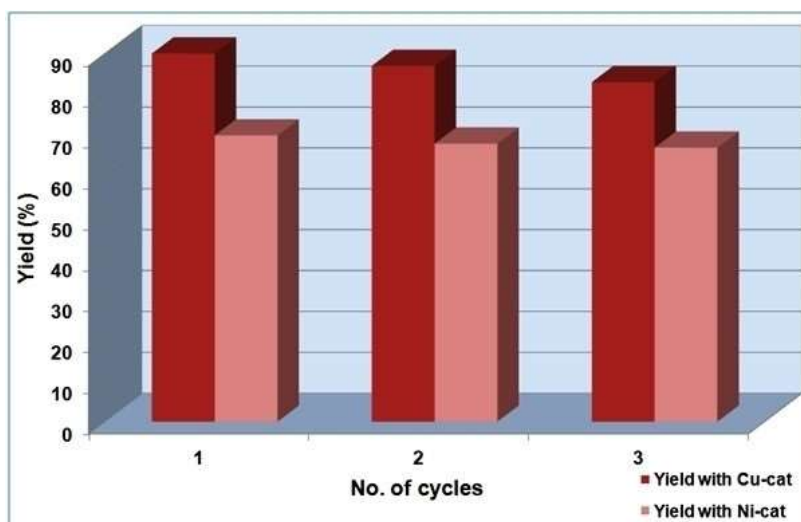


Fig 3.12 : Oxidation of styrene in the presence of Cu–Cat and Ni-Cat in subsequent cycles.

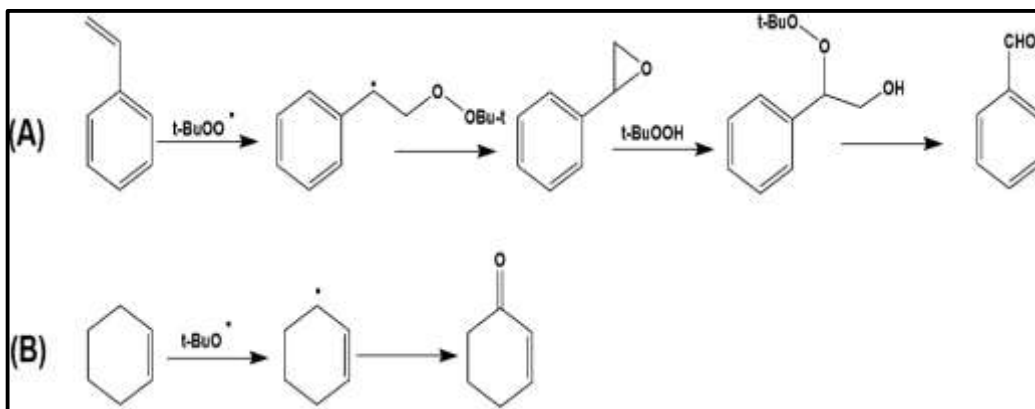
To study solvent dependence and select suitable medium for the catalysis with TBHP as the oxidant, styrene oxidation reaction has been carried out in different solvents, e. g. water, methanol, dichloromethane, toluene and acetonitrile. The results of the study are given in

Table 3.2.

Reaction medium	Yield (%)	
	Cu-Cat	Ni-Cat
Water	20	25
Methanol	32	30
Dichloromethane	35	13
Toluene	53	40
Acetonitrile	90	70

Table 3.2 : Oxidation of styrene in the presence of Cu-Cat and Ni-Cat in different solvents under similar conditions

It is clear from the table that highest yield is obtained in acetonitrile and that is the reason for using it as a solvent in all other catalytic reactions. In addition to that, acetonitrile is known to stabilize Cu(I) species, which is produced during catalysis, in solution by coordinating with the metal center.^[63] This can be a possible reason for higher activity of Cu-Cat in this medium. Experiments have also been carried out to check for the efficiency of different oxidizing agents in the catalysis. Firstly, H₂O₂ has been employed for carrying out the reaction (with styrene as a representative case), which results in poor yield. The Cu-catalyst still shows about 35% conversion but the Nicatalyst responded very poorly (only about 15% conversion). Hence, TBHP is chosen to carry out all the oxidation reactions which is found to be very efficient. Based on previous results on catalytic oxidation of olefins by Cu(II) compounds, a plausible mechanism has been proposed to explain the formation of the products. It is well understood that tBuOO* and tBuO* radicals could be formed from the reaction between TBHP and Cu(II) with the subsequent reduction of the metal center to Cu(I).^[64-67] Oxidation of styrene under similar conditions has been reported to follow radical mechanism.^[68-70] Different possible steps for styrene and cyclohexene oxidation are depicted in **Scheme 3.2**.



Scheme 3.2 : Possible mechanistic route for oxidation of olefins.

Other olefins also follow similar steps. One of the reasons behind various product formation in such reactions is the competition between oxidation of C=C bond and the allylic position. Styrene may first give corresponding epoxide on oxidation of double bond as there is no allylic hydrogen present in it. Benzaldehyde is then obtained from the ring opening of the styrene epoxide. In case of cyclohexene, allylic oxidation may occur resulting in the formation of 2-cyclohexen-1-one as the major product. However, cyclooctene undergoes epoxidation to give cyclooctene oxide as the sole product. Cyclohexene has half chair conformation and its double bond and allylic hydrogen remains in the same plane^[71] whereas double bond of cyclooctene lies in a different plane from other carbon atoms of its chair conformation.^[72] Therefore, oxidation of allylic hydrogen is more observed in cyclohexene than in cyclooctene. Other substrates where corresponding oxide is obtained as major product either follow similar route as depicted for styrene or their catalysis proceeds through cyclohexene route. Oxidation of olefins catalyzed by Ni-Cat may proceed via formation of nickel-peroxo species^[51] similar to the titanium silicates where corresponding peroxo species are generated.^[73] Examples of Cu or Ni anchored functionalized mesoporous silica materials are known; some of these materials have been used as catalysts in different organic transformations.^[74,75] Few of them have been used for epoxidation of olefins. Schiff-base condensation of salicylaldehyde with amine functionalized MCM-41 affords bidentate binding sites for Cu(II) to give a heterogenized catalyst for epoxidation of styrene and results show high conversion (97%) as well as high epoxide selectivity (89%).^[76] Use of unsubstituted and tert-butyl substituted salicylaldehyde Cu(II) compounds supported on mesoporous and amorphous silica as catalysts for the oxidation cyclohexene exhibits

comparatively inferior conversion and selectivity of the products.^[77] SBA-15 material bound with salicylaldehyde has been used to prepare Cu containing heterogeneous catalyst which has been found to be highly active catalyst for the epoxidation of cyclooctene, cyclohexene and styrene (conversion over 95%) with high selectivity towards corresponding epoxide.^[78] Cu(II)-diamine complex has been incorporated into 3-APTES functionalized MCM-41 where amine N forms bond with the metal center and this material has been used as catalyst for the epoxidation of styrene (conversion 94%).^[79] 4-Methyl-2,6-diformylphenol functionalized modified mesoporous silica has been used to prepare two heterogeneous catalysts with Cu and Ni metals. These compounds show their catalytic ability for the epoxidation of cyclohexene, trans stilbene, styrene, *o*-methyl styrene and cyclooctene. Results are more or less comparable with the present studies although TOF values in the present study are significantly higher.^[52] Nickel(II) Schiff-base complex onto salicylaldehyde functionalized mesoporous silica is active catalyst for the epoxidation of several olefins with high conversion and TOF values, but time taken for the catalytic reaction is quite long (24 h).^[80] MCM-41-Ni, which has been synthesized by anchoring the metal center on 2-pyridinecarboxaldehyde functionalized MCM-41, shows excellent conversion of styrene (~95%) but selectivity towards epoxide is reasonably low (~67%).^[81] Cu(II)-Schiff complex immobilized onto three dimensional mesoporous silica KIT-6 is active on styrene epoxidation with high conversion and high selectivity towards epoxide (both ~97%).^[82] Modified SBA-15 supported Ni(II)-oxime-imine catalysts are comparable with the present study in conversion of styrene or cyclohexene, but only 26% conversion is achieved with cyclooctene.^[83] There are several factors which control conversion and selectivity of the products. Thus, in comparison to other reported heterogenized silica catalyst, our catalysts are better in few aspects whereas Cu-Cat and/or Ni-Cat are lacking in some features.

3.4 : Conclusions

In summary, Cu(II) and Ni(II) anchored functionalized mesoporous materials have been synthesized and characterized. These metal grafted silica materials have been found to be effective as catalysts for the oxidation of various olefins. Epoxidation and oxidation at allylic site occurs to give different products within a reasonable reaction period and at relatively low temperature. The catalysts have been recycled for a few times without seriously compromising their activities. Although the catalytic reactions show good conversion, yet similar product

selectivity could not be observed i. e. the corresponding oxides are not obtained for each substrate as the major product. Thus, despite their excellent conversion and recycling ability, there is scope for improvement of product selectivity. The results obtained for cyclooctene epoxidation is significant as it yields cyclooctene oxide as the sole product.

3.5. References

- [1] A. M. Kirillov, M. N. Kopylovich, M. V. Kirillova, M. Haukka, M. F. C. G. da Silva, A. J. L. Pombeiro, *Angewandte Chemie, International Edition* **2005**, *44*, 4345–4349.
- [2] T. Punniyamurthy, L. Rout, *Coordination Chemistry Reviews* **2008**, *252*, 134–154.
- [3] M. Nandi, P. Roy, *Indian Journal of Chemistry* **2013**, *52 A*, 1263–1268.
- [4] R. Antony, S. T. D. Manickam, S. Balakumar, *Journal of Inorganic Organometallic Polymer Materials* **2017**, *27*, 418–426.
- [5] D. S. Nesterov, O. V. Nesterova, A. J. L. Pombeiro, *Coordination Chemistry Reviews* **2017**.
- [6] J. Mondal, A. Modak, A. Dutta, A. Bhaumik, *Dalton Transactions* **2011**, *40*, 5228–5235.
- [7] S. Banerjee, C. Adhikary, C. Rizzoli, R. Pal, *Inorganica Chimica Acta* **2014**, *409*, 202–207.
- [8] C. Adhikary, S. Banerjee, J. Chakraborty, S. Ianelli, *Polyhedron* **2013**, *65*, 48–53.
- [9] H. Mahdavi, M. Nikoorazm, A. Ghorbani-Choghamarani, S. Arshadi, *Journal of Porous Materials* **2016**, *23*, 75–82.
- [10] Z. -H. Zhang, X. -S. Yang, Q. -Q. Zhang, L. Wang, M. -Y. He, Q. Chen, X. -F. Huang, *RSC Advances* **2016**, *6*, 104036–104040.
- [11] A. Bhattacharjee, S. Halder, K. Ghosh, C. Rizzoli, P. Roy, *New Journal of Chemistry* **2017**, *41*, 5696–5706.
- [12] M. Tobisu, N. Chatani, *Accounts of Chemical Research* **2015**, *48*, 1717–1726.
- [13] S. L. Zultanski, G. C. Fu, *Journal of American Chemical Society* **2013**, *135*, 624–627.
- [14] P. Drabina, J. Svoboda, M. Sedl_k, *Molecules* **2017**, *22*, 865 (1-18).
- [15] V. Molinari, C. Giordano, M. Antonietti, D. Esposito, *Journal of American Chemical Society* **2014**, *136*, 1758_1761.
- [16] F. Gao, J. D. Webb, J. F. Hartwig, *Angewandte Chemie* **2016**, *128*, 1496–1500.
- [17] S. Z. Tasker, E. A. Standley, T. F. Jamison, *Nature* **2014**, *509*, 299–309.
- [18] K. C. Gupta, A. K. Sutar, *Coordination Chemistry Reviews* **2008**, *252*, 1420–1450
- [19] R. Noyori, M. Aoki, K. Sato, *Chemical Communications* **2003**, 1977–1986.
- [20] K. A. Jorgensen, *Chemical Reviews* **1989**, *89*, 431–458.
- [21] T. Mukaiyama, T. Yamada, *Bull. Chemical Society of Japan* **1995**, *68*, 17–35.

- [22] K. C. Gupta, A. K. Sutar, C. -C. Lin, *Coordination Chemistry Reviews* **2009**, 253, 1926–1946.
- [23] A. Maria P. Salvo, F. Giacalone, M. Gruttadauria, *Molecules* **2016**, 21, 1288 (1-60).
- [24] D. R. Godhani, H. D. Nakum, D. K. Parmar, J. P. Mehta, N. C. Desai, *Journal of Molecular Catalysis. A* **2017**, 426, 223–237.
- [25] A. Finiels, F. Fajula, V. Hulea, *Catalysis. Science and. Technology.* **2014**, 4, 2412–2426.
- [26] H. Albuquerque, L. Carneiro, A. P. Carvalho, J. Pires, A. R. Silva, *Polyhedron* **2014**, 79, 315–323.
- [27] L. Ma, F. Su, X. Zhang, D. Song, Y. Guo, J. Hu, *Microporous Mesoporous Materials.* **2014**, 184, 37–46.
- [28] R. K. Sharma, S. Sharma, G. Gaba, S. Dutta, *Journal of Material Science* **2016**, 51, 2 2121–2133.
- [29] A. Zarnegaryan, M. Moghadam, S. Tangestaninejad, V. Mirkhani, I. Mohammdpour-Baltork, *New Journal of Chemistry* **2016**, 40, 2280–2286.
- [30] X. Wang, S. Wu, Z. Li, X. Yang, H. Su, J. Hu, Q. Huo, J. Guan, Q. Kan, *Microporous Mesoporous Materials* **2016**, 221, 58–66.
- [31] M. Bazarganipoura, M. Salavati-Niasari, *Applied Catalysis A* **2015**, 502, 57–64.
- [32] T. Toyao, K. Miyahara, M. Fujiwaki, T. -H. Kim, S. Dohshi, Y. Horiuchi, M. Matsuoka, *Journal of Physical Chemistry C* **2015**, 119, 8131–8137.
- [33] H. Noh, Y. Cui, A. W. Peters, D. R. Pahls, M. A. OrtuÇ, N. A. Vermeulen, C. J. Cramer, L. Gagliardi, J. T. Hupp, O. K. Farha, *Journal of American Chemical Society*, **2016**, 138, 14720–14726.
- [34] D. Dehe, L. Wang, M. K. Müller, G. Dçrr, Z. Zhou, R. N. Klupp-Taylor, Y. Sun, S. Ernst, M. Hartmann, M. Bauer, W. R. Thiel, *ChemCatChem* **2015**, 7, 127–136.
- [35] C. M. A. Parlett, K. Wilson, A. F. Lee, *Chemical Society Review* **2013**, 42, 3876–3893.
- [36] A. E. Fernandes, A. M. Jonas, O. Riant, *Tetrahedron* **2014**, 70, 1709–1731.
- [37] C. T. Kresge, M. E. Leonowicz, W. J. Roth, J. C. Vartuli, J. S. Beck, *Nature* **1992**, 359, 710–712.
- [38] M. Zare, Z. Moradi-Shoeili, *Applied Organometallic Chemistry* **2017**, 31, 3611.

- [39] P. B. Arockiam, C. Bruneau, P. H. Dixneuf, *Chemical Reviews* **2012**, *112*, 5879–5918.
- [40] H. Kotz, S. Mapolie, *Applied Organometallic Chemistry* **2016**, *31*, 3643.
- [41] W. -J. Kong, Y. -J. Liu, H. Xu, Y. -Q. Chen, H. -X. Dai, J. -Q. Yu, *Journal of American Chemical Society* **2016**, *138*, 2146–2149.
- [42] R. Shang, L. Ilies, E. Nakamura, *Chemical Reviews* **2017**, *117*, 9086–9139.
- [43] K. K. Krishnan, A. M. Thomas, K. S. Sindhu, G. Anilkumar, *Tetrahedron* **2016**, *72*, 1–16.
- [44] G. Yang, H. Du, J. Liu, Z. Zhou, X. Hu, Z. Zhang, *Green Chemistry* **2017**, *19*, 675–681.
- [45] A. R. Jeong, J. W. Shin, J. H. Jeong, K. H. Bok, C. Kim, D. Jeong, J. Cho, S. Hayami, K. S. Min, *Chemistry- A European Journal* **2017**, *23*, 3023–3033.
- [46] A. E. Kerenkan, F. Bland, T. -O. Do, *Catalysis Science and Technology* **2016**, *6*, 971–987.
- [47] S. Halder, A. Mukherjee, K. Ghosh, S. Dey, M. Nandi, P. Roy, *Journal of Molecular Structure* **2015**, *1101*, 1–7.
- [48] S. Halder, S. Dey, C. Rizzoli, P. Roy, *Polyhedron* **2014**, *78*, 85–93.
- [49] P. Roy, M. Nandi, M. Manassero, M. Ricci, M. Mazzani, A. Bhaumik, P. Banerjee, *Dalton Transactions* **2009**, 9543–9554.
- [50] P. Roy, K. Dhara, M. Manassero, P. Banerjee, *Inorganic Chemistry Communications* **2008**, *11*, 265–269.
- [51] J. Chakraborty, M. Nandi, H. Mayer-Figge, W. S. Sheldrick, L. Sorace, A. Bhaumik, P. Banerjee, *European Journal of Inorganic Chemistry* **2007**, 5033–5044.
- [52] M. Nandi, P. Roy, H. Uyama, A. Bhaumik, *Dalton Transactions* **2011**, *40*, 12510–2518.
- [53] T. Das, A. Roy, H. Uyama, P. Roy, M. Nandi, *Dalton Transactions* **2017**, *46*, 7317–7326.
- [54] A. P. Wight, M. E. Davis, *Chemical Reviews* **2002**, *102*, 3589–3614.
- [55] A. Stein, *Advanced Materials*, **2003**, *15*, 763–775.
- [56] O. Olkhoviyk, M. Jaroniec, *Journal of American Chemical Society* **2005**, *127*, 60–61.
- [57] S. Inagaki, Y. Fukushima, K. J. Kuroda, J. Chem. Soc., *Chemical Communications*

- 1993**, 680–682.
- [58] P. T. Tanev, M. Chibwe, T. J. Pinnavaia, *Nature* **1994**, *368*, 321–323.
- [59] P. T. Tanev, T. J. Pinnavaia, *Science* **1996**, *271*, 1267–1269.
- [60] S. Inagaki, S. Guan, Y. Fukushima, T. Ohsuna, O. Terasaki, *Journal of American Chemical Society* **1999**, *121*, 9611–9614.
- [61] S. Inagaki, S. Guan, T. Ohsuna, O. Terasaki, *Nature* **2002**, *416*, 304–307.
- [62] N. N. Greenwood, A. Earnshaw, *Chemistry of the Elements, 2nd Ed., Elsevier Butterworth Heinemann, Woodburn, 2005.*
- [63] C. L. Gatlin, F. Tureček, T. Valsar, *Analytical Chemistry* **1994**, *66*, 3950–3958.
- [64] J. K. Kochi, *Tetrahedron* **1962**, *18*, 483–497.
- [65] J. K. Kochi, *Journal of American Chemical Society* **1962**, *84*, 1572–1579.
- [66] G. Rothenberg, L. Feldberg, H. Wiener, Y. Sasson, *J. Chem. Soc., Perkin Transactions* **1998**, *2*, 2429–2434.
- [67] U. Junghans, C. Suttkus, J. Lincke, D. Lössig, H. Krauyscheid, R. Glaser, *Microporous Mesoporous Materials*, **2015**, *216*, 151–160.
- [68] L. M. Slaughter, J. P. Collman, T. A. Eberspacher, J. I. Brauman, *Inorganic Chemistry* **2004**, *43*, 5198–5204.
- [69] F. Farzaneh, J. Taghavi, R. Malakooti, M. Ghandi, *Journal of Molecular Catalysis A* **2006**, *244*, 252–257.
- [70] M. Sarkheil, M. Lashanizadegan, *Applied Organometallic Chemistry* **2017**.
- [71] E. L. Eliel, S. H. Wilen, *Stereochemistry of Organic Compounds*, John Wiley, New York, **1994**.
- [72] U. Neuenschwander, I. Hermans, *Journal of Organic Chemistry* **2011**, *76*, 10236–10240.
- [73] A. Bhaumik, T. Tatsumi, *Journal of Catalysis* **2000**, *189*, 31–39.
- [74] N. Pal, A. Bhaumik, *RSC Advances* **2015**, *5*, 24363–24391.
- [75] M. Ozdemir, *Inorganica Chimica Acta* **2014**, *421*, 1–9.
- [76] S. Jana, B. Dutta, R. Bera, S. Koner, *Langmuir* **2007**, *23*, 2492–2496.
- [77] N. Malumbazo, S. F. Mapolie, *Journal of Molecular Catalysis A* **2009**, *312*, 70–77.
- [78] M. Selvaraj, V. Narayanan, S. Kawi, *Microporous Mesoporous Materials* **2010**, *132*, 494–500.

- [79] S. Jana, S. Bhunia, B. Dutta, S. Koner, *Applied Catalysis A* **2011**, 392,225–232.
- [80] S. Bhunia, S. Koner, *Polyhedron* **2011**, 30, 1857–1864.
- [81] Y. Gang, C. Xing, W. Xiaoli, X. Weihong, X. Nanping, *Chinese Journal of Catalysis* **2013**, 34,1326–1332.
- [82] J. Sun, Q. Kan, Z. Li, G. Yu, H. Liu, X. Yang, Q. Huo, J. Guan, *RSC Advances* **2014**, 4, 2310–2317.

Chapter 4

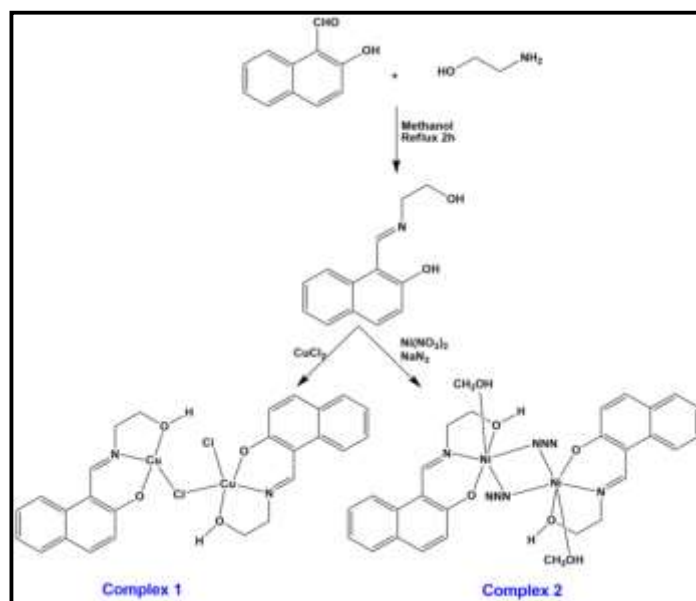
**Particulate methane
monooxygenase mimicking
activity of dinuclear
transition metal complexes**

4.1 Introduction

Activation of C_{sp³}-H bond is one of the most difficult tasks in chemistry. Natural gas and fuel are mainly saturated hydrocarbons. As C_{sp³}-H bond is very strong and inert, oxidation of alkanes requires high temperature and pressure and/or acidic reaction media in addition to the presence of metal as catalyst.^[1] Transformation of these compounds may give different valuable organic fine chemicals which are of great industrial importance. For example, methane can be converted to methanol proving one functional group which could be converted to other compounds easily.^[2] Modeling of metalloenzymes with particular catalytic activity is of great interest for the design and development of bio-inspired catalysts. In connection with C_{sp³}-H bond oxidation, we could recall the enzyme, methane monooxygenase.^[3] It exists in two forms; (a) particulate methane monooxygenase (pMMO) and (b) soluble methane monooxygenase (sMMO). Both of these forms are able to convert methane to methanol. sMMO contains two iron(III) centers in active site. Active site of pMMO is not identified unambiguously by structural characterization of the enzyme. However, existence of two Cu(II) centers in the active site of pMMO is of most acceptable belief.^[4] Therefore, there are several copper(II) including dinuclear copper(II) compounds have been prepared and used as catalyst for activation of C_{sp³}-H bond.^[5] Substrates used are methane, cyclohexane and others. Oxidation of cyclohexane is useful because its oxidized products, mainly cyclohexanol and cyclohexanone, are of great industrial importance.^[5] Cyclohexanol is mainly used as the raw material for the manufacture of adipic acid. Adipic acid is used for the preparation of nylon-6,6', soaps and detergents, pesticides, etc. Cyclohexanone is mainly utilized as a solvent in industries and activator in oxidation reactions. Pombeiro et al. have been working for long time on the development of different copper(II) complexes as active catalyst for such oxidation reactions.^[6] Few other groups also reported C-H activation by Cu(II) complexes.^[7] But, conversion of substrate to product is of comparatively low percentage because high C-H bond energy. Although there is significant importance of copper(II) complexes as catalysts in various catalytic transformations,^[7i-7n] field of alkane oxidation by copper complexes is less explored. It is to be noted that in addition to the original metal present in the metalloenzyme, some functional models with other transition metals have been designed and reported. For example, phenoxazinone synthase mimicking activity has been reported by complexes with Mn(II), Co(III), etc.^[8] So other transition metal complexes can be designed for pMMO activity to enable C_{sp³}-H bond activation. Thus, search for active catalyst for high

conversion and better selectivity of a particular product continues. Effort should be given to design the catalyst which can mimic activity of naturally abundant enzymes.

In this respect, synthesis, characterization and catalytic properties of dinuclear Cu(II) and Ni(II) complexes, $[\text{Cu}_2(\text{L}^1)_2(\mu_2\text{-Cl})\text{Cl}] \cdot 2.5\text{H}_2\text{O}$ (**1**) and $[\text{Ni}_2(\text{L}^1)_2(\mu_2\text{-N}_3)_2(\text{CH}_3\text{OH})_2] \cdot \text{CH}_3\text{OH}$ (**2**) where HL^1 is 1-((2-hydroxyethylimino)methyl)naphthalen-2-ol. (**Scheme 4.1**) has been reported. Cu(II) complex has been prepared by reaction between copper(II) chloride and HL^1 under mild conditions. It has been used as catalyst for oxidation of cyclohexane, toluene and cyclopentane using hydrogen peroxide as terminal oxidant. It has been checked if replacement of copper by other metal, say nickel, in similar environment has any effect on catalytic activity. In other words, we use Ni for pMMO mimicking activity. Although Ni(II) complexes have been used as catalyst for different reactions including olefin epoxidation, C-C bond formation, etc.,^[9] attempt to use of nickel compounds in alkane oxidation is rare. Dinuclear Ni(II) complex has been synthesized with same ligand to provide similar chemical environment around the metal center. Some theoretical calculations have been performed to investigate spectral transitions of these complexes.



Scheme 4.1: Synthesis of complexes 1 and 2

4.2 Experimental Section

4.2.1 Materials and physical methods

2-Hydroxy-1-naphthaldehyde, 2-aminoethanol, copper(II) chloride dihydrate, nickel(II) nitrate hexahydrate, sodium azide and tetrabutylammonium perchlorate (TBAP) were purchased from Sigma Aldrich and used without further purification. Other reagents and solvents were obtained from commercial sources and used as received. Elemental analyses (carbon, hydrogen and nitrogen) were performed using a Perkin–Elmer 2400C elemental analyzer. FT-IR spectra were recorded on a Perkin Elmer spectrometer (Spectrum Two) with the samples by the use of attenuated total reflectance (ATR) technique. The UV-visible spectral measurements were recorded in Agilent 8453 diode array spectrophotometer. Analysis of reaction mixture of catalytic reactions was performed with a Shimadzu next generation high speed gas chromatography system (model: GC-2025 AF) equipped with a fused silica capillary column and FID detector. Cyclic voltammetric measurements were performed on Metrohm Autolab potentiostat galvanostat AOT72915. A platinum wire working electrode, a platinum wire auxiliary electrode and Ag/AgCl reference electrode were employed in a standard three-electrode configuration. TBAP was used as supporting electrolyte in MeCN and the scan rate was 50 mV s⁻¹ under nitrogen atmosphere. TG-DTA analysis was carried out on Perkin-Elmer Pyris Diamond TG/DTA unit. All experiments were carried out at room temperature in air unless reported otherwise.

4.2.2 Synthesis of 1-((2-hydroxyethylimino)methyl)naphthalen-2-ol (HL¹)

2-Aminoethanol (0.5 mmol, 0.030 mL) was added to a methanolic solution (5 mL) of 2-hydroxy-1-naphthaldehyde (0.5 mmol, 0.086 g) under stirring condition. The mixture was stirred for 30 min. Then the resulting solution was refluxed for 2 h. The color of the mixture turned yellow. It was then cooled to room temperature and it was used as ‘ligand (HL¹)’ without any characterization and further purification.

4.2.3 Synthesis of $[\text{Cu}_2(\text{L})_2(\mu_2\text{-Cl})\text{Cl}]\cdot 2.5\text{H}_2\text{O}$ (1)

A methanolic solution (10 mL) of copper(II) chloride dihydrate (0.5 mmol, 0.067 g) was added to the ligand solution. The mixture was stirred till it turned greenish. It was then refluxed for 1 h. Color of the solution became dark green. The mixture was finally cooled to room temperature and filtered to remove any precipitate or suspended materials. The filtrate was kept at ambient temperature. Green crystals suitable for X-ray diffraction study were produced within few days. Yield 65%, 0.218 g; C, H, N analysis: anal. calc. for $\text{C}_{26}\text{H}_{29}\text{Cl}_2\text{Cu}_2\text{N}_2\text{O}_{6.5}$: C, 46.50; H, 4.35; N, 4.17; found: C, 46.44; H, 4.23; N, 4.32%.

4.2.4 Synthesis of $[\text{Ni}_2(\text{L}^1)_2(\text{N}_3)_2(\text{CH}_3\text{OH})_2]\cdot \text{CH}_3\text{OH}$ (2)

The 'ligand (HL^1)' was prepared in the same procedure as described above. A methanolic solution (10 mL) of nickel(II) nitrate hexahydrate (0.5mmol, 0.091 g) was added to it while constantly stirring the mixture. It was stirred for 30 min. Then, sodium azide (0.5mmol, 0.034 g) in 2 mL of methanol/water was added dropwise to the resulting green solution. After addition of azide, the solution turned dark green. The solution was stirred for another 30 min before it was refluxed for 1 h. The mixture was finally cooled to room temperature and filtered to remove any precipitate or suspended materials. The filtrate was kept at ambient temperature. Green crystals suitable for X-ray diffraction study were produced within few days. Yield 70%, 0.253 g; C, H, N analysis: anal. calc. for $\text{C}_{29}\text{H}_{36}\text{N}_8\text{Ni}_2\text{O}_7$: C, 47.97; H, 5.00; N, 15.43; found: C, 47.84; H, 4.92; N, 15.36%.

4.2.5 X-ray data collection and structure determination

Details of the data collection and refinement parameters for complexes **1** and **2** are summarized in **Table 4.1**. The diffraction experiments were carried out on a Bruker APEX-II CCD diffractometer using graphite monochromated Mo $K\alpha$ radiation at 298 K for both the complexes **1** and **2**. Data were processed using the Bruker APEX2 and SAINT packages.^[10] Absorption corrections based on multi-scans using the SADABS software^[10] were applied to the intensity data. The structures were solved by direct methods using SHELXT^[11] and refined with full-

matrix least-squares on F^2 on all unique reflections using SHELXL-2014/7.^[12] All the non-hydrogen atoms of the complexes were refined anisotropically. A few hydrogen atoms, which are highly acidic, are disordered due to thermal disturbances. These have been assigned to their best possible positions by chemical speculation.

CCDC 1848336 and 1848337 contain the supplementary crystallographic data for **1** and **2** respectively.

Complex	1	2
Formula	C ₅₂ H ₅₂ Cl ₄ Cu ₄ N ₄ O ₁₃	C ₂₉ H ₃₆ N ₈ Ni ₂ O ₇
Formula weight	1336.93	726.08
<i>T</i> (K)	298 K	298 K
Crystal color	Dark green	Green
Crystal system	orthorhombic	Monoclinic
Space group	P212121	P 21/n
<i>a</i> (Å)	13.5722(7)	16.7002(5)
<i>b</i> (Å)	11.8931(6)	7.4796(2)
<i>c</i> (Å)	17.3627(8)	25.7434(7)
α (°)	90.00	90.00
β (°)	90.000(3)	100.802(2)
γ (°)	90.00	90.00
<i>V</i> (Å ³)	2802.6(2)	3158.65(15)
<i>Z</i>	2	4
Crystal dimensions (mm)	0.5 × 0.2 × 0.15	0.4 × 0.2 × 0.1
<i>F</i> (0 0 0)	1360	1512
<i>D</i> _c (g cm ⁻³)	1.584	1.527

λ (Mo K α) (Å)	0.71073	0.71073
θ Range (°)	1.90- 27.5	1.601 – 27.220
Reflection collected/ unique/observed	39364, 6438 , 4699	51406, 7017, 5070
Absorption correction	multi-scan	multi-scan
R_{int}	0.079	0.0342
Final R_1 index [$I > 2\sigma(I)$]	0.0488	0.0513
Final wR_2 index (all reflections)	0.1328	0.1450
Goodness-of-fit	1.09	1.033

Table 4.1 : Crystal data of complex 1 and 2

4.2.6 Computational details

The singlet ground state (S_0) geometry of ligand, HL¹ and its copper and nickel complexes i.e. complexes **1** and **2** have been fully optimized by DFT method with B3LYP (Becke's three-parameter hybrid functional and Lee–Yang–Parr's gradient corrected correlation functional) exchange correlation functional approach using the Gaussian 09 program.^[13] The B3LYP functional has been adopted along with the 6-31G basis set for H, C, N, O atoms whereas the 6-311G (d,p) basis set was utilized for Cl atoms and LANL2DZ was adopted as the basis set for Cu and Ni atoms.^[14] The nature of all the stationary points was confirmed by carrying out a normal mode analysis, where all vibrational frequencies were found to be positive. On the basis of the optimized ground state (S_0) geometrical structures, the UV–vis absorption transition properties of the corresponding ligand and complexes **1** and **2** in methanol were computed by a time-dependent density functional theory (TDDFT)^[15] approach associated with the conductor-like polarizable continuum model (CPCM)^[16] using the same B3LYP level and the previous basis sets. Frontier Molecular Orbital (FMO) analysis has been done with gauss view software.^[17]

4.2.7 Catalytic studies

Oxidation of cyclohexane, toluene and cyclopentane has been performed in similar procedure in the presence of both the metal complexes as catalysts. Typically, 3-10 mmol of hydrogen peroxide (30% in H₂O) was added to the metal complex (0.03 mmol) in 5 mL of acetonitrile taken in a two-neck round bottom flask which was fitted with a condenser. To this, varying amount of HNO₃ was added. Catalytic reaction started as soon as 1.5 mmol of substrate was mixed. The mixture was continuously stirred for 48 h at ambient temperature under atmospheric pressure. Aliquots were collected after regular time intervals. The substrate and products from the reaction mixture were extracted with 2 mL diethyl ether and then treated with triphenylphosphine (PPh₃). Mixture was analyzed in gas chromatograph. The identification was done by the comparison with known standards.

4.3 Results and discussion

4.3.1 Synthesis

Synthesis of complexes **1** and **2** has been performed following route given in **Scheme 4.1**. First, HL¹ has been synthesized by one step Schiff-base condensation between 2-hydroxy-1-naphthaldehyde and 2-aminoethanol in 1:1 molar ratio in methanol. The ligand has not been characterized and it has been used directly for complex formation without further purification. Reaction between HL¹ and copper(II) chloride dihydrate gives **1**. Complex **2** has been synthesized by the reaction between the as-synthesized ligand, nickel (II) nitrate hexahydrate and sodium azide where azide acts as a bridging ligand. HL¹ undergoes deprotonation in the reaction medium without any external deprotonating base.

4.3.2 Crystal structures of **1** and **2**

The dinuclear copper complex i.e. complex **1** crystallizes from methanol in orthorhombic system with P212121 space group. A perspective view of the complex is given in **Fig. 4.1**. Selected bond lengths and bond angles are given in **Table 4.2**. In the molecule, coordination environment around a copper center is different from that of other copper center. Cu1 is tetracoordinated

whereas Cu2 is in pentacoordination geometry. The two chloride ions from the copper(II) salt used for the complex formation, bind the Cu atoms differently as confirmed by the crystal structure. One chlorido is bridging while the other is terminal. Cu1 is in a distorted square planar environment bonded to O1, O2, N1 and Cl1. Two oxygen atoms and one nitrogen atom come from the ligand where O1 is from the deprotonated phenoxide ion, O2 is from the protonated alcohol and N1 is the imine nitrogen of the Schiff base ligand. Cl1 is the bridging chlorine atom which links Cu1 and Cu2. There is deviation of donor-metal-donor bond angle from 90°. The O2-Cu1-N1 bond angle is 83°, O1-Cu1-N1 angle is 92°, Cl1-Cu1-O2 angle is 93° and Cl1-Cu1-O1 angle is around 94°. The Cu1-Cl1 bond is slightly out of plane. This confirms the approximate square planar geometry around the Cu1 center. Cu2, on the other hand, is bonded to O3, O4, N2, Cl1, Cl2. Oxygen and nitrogen atoms are from the ligand and Cl2 is the terminal chlorine atom bonded to Cu2 center. It is in distorted square pyramidal geometry as indicated by the value of the trigonal index, τ . The trigonal index is calculated as the difference between the two largest donor-metal-donor angles divided by 60.^[18] Its value is 1 for the ideal trigonal bipyramid and 0 for the square pyramid. Here the τ value is calculated to be 0.25 which indicates its significantly distorted square pyramidal environment. O3, O4, N2 and Cl2 atoms form the basal plane of the square pyramid and Cl1 occupies the apical position. However, Cu center is out of the mean plane by 0.150 Å towards Cl1. There are 2.5 water molecules in the crystal structure. The solvent water molecules are disordered due to molecular vibrations. The H atoms in the alcoholic moiety and the water molecule have been assigned their best possible positions in spite of being disordered. The crystal has been refined as a merohedral twin. In packing structure, there are π - π and CH- π interactions. The metal-metal distance is 3.485 Å. Metal-chlorine bond distances are long compared to other metal-donor distances as expected. However, all of these bond distances are in agreement with the reported values.^[8c,d]

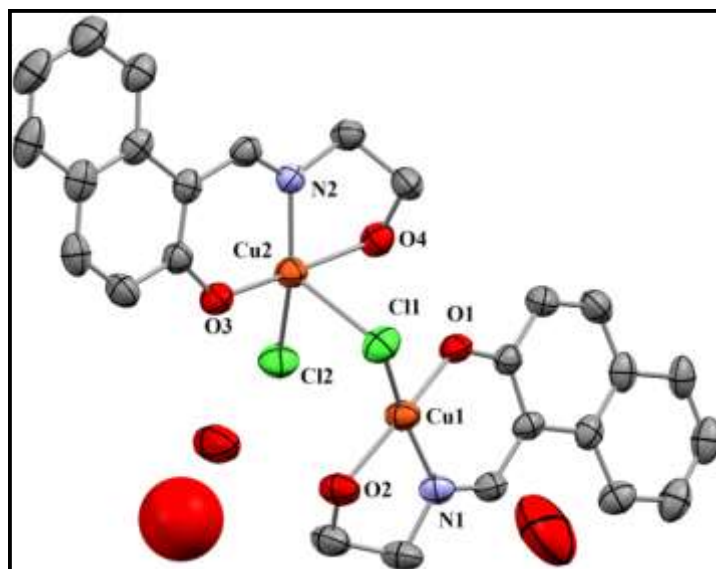


Fig. 4.1 : A perspective view of complex 1 with partial atom numbering scheme. Hydrogen atoms are omitted for the clarity.

Complex 2 crystallizes from methanol into a monoclinic system with P 21/n space group. A perspective view of the complex is given in **Fig. 4.2**. Selected bond lengths and bond angles are given in **Table 4.2**. The molecule consists of two nickel atoms, two deprotonated ligands, 1-((2-hydroxyethylimino)methyl)naphthalen-2-ol (HL^1), two azido ligands and two coordinated methanol molecules. One methanol is present as solvent of crystallization. Two Ni atoms are bridged by two azido moieties to form a dinuclear complex. Each Ni atom is in similar coordination geometry i.e. in octahedron geometry. Ni1 is bonded with O4, N8 and O6 from the ligand, N1 and N4 from two different azido moieties and O5 from a methanol molecule. Bond angles and bond lengths involving Ni1 indicate distorted octahedron geometry around this metal center. On the other hand, Ni2 is coordinated to O2, N7 and O3 atoms from the ligand, Ni and N4 from two different azido species and O1 from a methanol molecule. It is also in distorted octahedral geometry. Two intramolecular hydrogen bonds are present in this molecule involving non-coordinated methanol. Coordinated O3 atom is present in H-bonding with H-O moiety of methanol molecule and second hydrogen bond is found involving O atom of the methanol molecule and H-O6 moiety of alcoholic group. All of the donor-Ni bond distances are in agreement with the reported values.^[20]

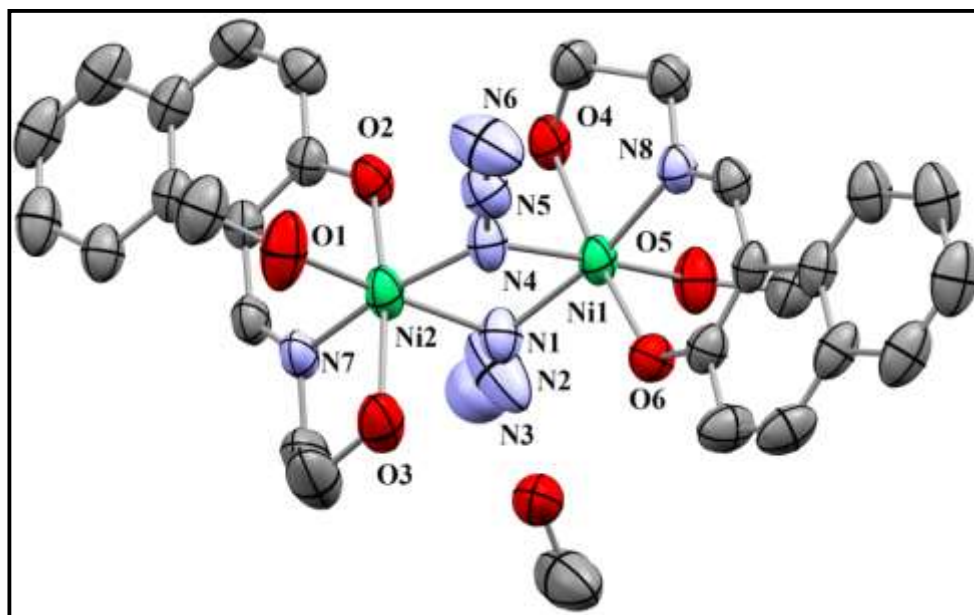


Fig. 4.2 : A perspective view of complex 2 with partial atom numbering scheme. Hydrogen atoms are omitted for the clarity.

Complex 1			
Cu1–O2	1.906(4)	Cu2–O3	1.888(4)
Cu1–N1	1.908(5)	Cu2–N2	1.918(5)
Cu1–O1	2.005(4)	Cu2–O4	2.028(4)
Cu1–Cl1	2.2503(17)	Cu2–Cl2	2.2797(18)
		Cu2–Cl1	2.7209(18)
O2–Cu1–N1	91.91(19)	N2–Cu2–O4	82.66(18)
O2–Cu1–O1	170.39(19)	O3–Cu2–Cl2	96.56(13)
N1–Cu1–O1	83.38(19)	N2–Cu2–Cl2	157.02(15)
O2–Cu1–Cl1	94.42(13)	O4–Cu2–Cl2	89.73(13)
N1–Cu1–Cl1	163.09(16)	O3–Cu2–Cl1	89.67(14)
O1–Cu1–Cl1	92.42(14)	N2–Cu2–Cl1	106.92(14)
O3–Cu2–N2	92.97(18)	O4–Cu2–Cl1	85.81(12)
O3–Cu2–N2	172.50(18)	Cl2–Cu2–Cl1	94.04(6)

Complex 2

Ni1- N7	1.970(3)	Ni2- N8	1.962(4)
Ni1- O1	1.975(3)	Ni2- O3	1.995(3)
Ni1- N1	2.049(4)	Ni2- N4	2.032(4)
Ni1- N4	2.134(4)	Ni2- N1	2.147(4)
Ni1- O2	2.160(3)	Ni2- O6	2.165(4)
Ni1- O5	2.173(3)	Ni2- O4	2.166(3)
N7- Ni1- O1	91.21(13)	N8- Ni2- O3	89.33(13)
N7- Ni1- N1	170.05(15)	N8- Ni2- N4	171.06(16)
O1- Ni1- N1	97.73(14)	O3- Ni2- N4	94.42(14)
N7- Ni1-N4	95.78(14)	N8- Ni2- N1	92.20(15)
O1- Ni1- N4	92.55(14)	O3- Ni2- N1	91.47(14)
N1- Ni1-N4	79.55(16)	N4- Ni2-N1	79.61(15)
N7- Ni1- O2	82.19(12)	N8- Ni2- O6	96.22(15)
O1- Ni1- O2	173.40(11)	O3- Ni2- O6	93.79(14)
N1- Ni1- O2	88.81(13)	N4- Ni2- O6	91.64(15)
N4- Ni1- O2	87.76(13)	N1- Ni2- O6	170.12(14)
N7- Ni1- O5	91.11(13)	N8- Ni2- O4	81.98(14)
O1- Ni1- O5	92.78(13)	O3- Ni2- O4	171.17(12)
N1- Ni1- O5	92.79(14)	N4- Ni2- O4	94.41(14)
N4- Ni1- O5	171.20(13)	N1- Ni2- O4	90.46(15)
O2- Ni1- O5	87.75(13)	O6- Ni2- O4	85.61(15)

Table 4.2 : Selected bond lengths (Å) and bond angles (°) of complexes 1 and 2

4.3.3 IR spectral studies

FT-IR spectra of all of the complexes have been obtained with powder samples by ATR technique. Peaks at 1622 and 1617 cm^{-1} in the IR spectra of Cu and Ni complex respectively, confirm the presence of azomethine bond in both the complexes (**Fig. 4.3**). A sharp peak at 2054 cm^{-1} indicates the presence of azido moiety in complex **2**. Both the complexes show broad band in the range of 3500-3400 cm^{-1} . Broad peak of complex **1** is the result of water molecule which is present as solvent of crystallization in Cu complex and that for complex **2** is may be due to the presence of methanol present in Ni complex as solvent of crystallization.

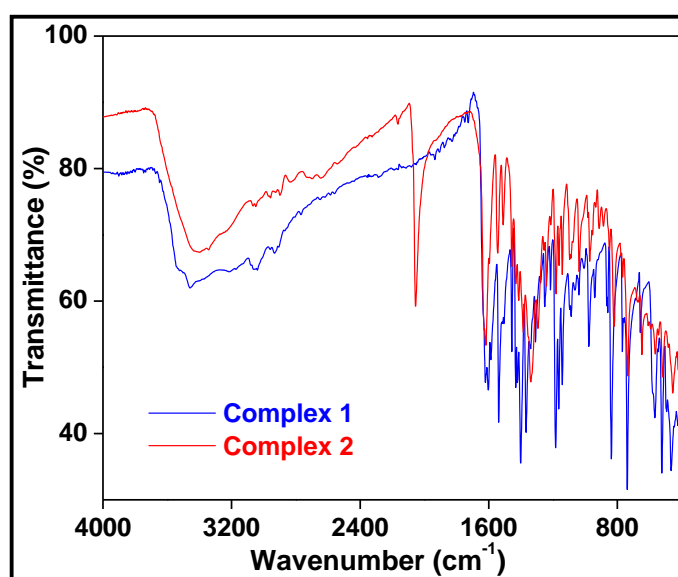


Fig 4.3 : FT-IR spectra of complexes 1 and 2.

4.3.4. UV-vis spectral studies

The electronic spectra of complexes **1** and **2** have been recorded in methanol at room temperature(**Fig 4.4**). For complex **1**, high intensity bands appear at 383 and 316 nm (molar extinction coefficient of 12100 and 13500 $\text{Lmol}^{-1}\text{cm}^{-1}$ respectively) which may occur due to ligand to metal charge transfer ($\text{PhO}^- \rightarrow \text{Cu(II)}$ and $\text{N(imino)} \rightarrow \text{Cu(II)}$) and intraligand charge transfer respectively. The Cu complex shows broad bands at 646, 673 and 720 nm with low intensity. These spectral characteristics are in consistence with copper(II) complexes of distorted square pyramidal (SP) geometry. The observed bands originate from $d_{xz}, d_{yz} \rightarrow d_{x^2-y^2}$ transitions.^[21] They are accompanied by a low energy shoulder at around 844 nm due to d_{xy} ,

$d_{x^2-y^2} \rightarrow d_{z^2}$ transitions. As the structure moves more towards TBP structure the low energy band along with high energy spin forbidden band becomes more pronounced. The characteristic bands observed here are results of distorted square pyramidal geometry.

UV spectrum of complex **2** shows high intensity bands at 312 and 395 nm with molar extinction coefficient 9335 and 8261 $\text{Lmol}^{-1}\text{cm}^{-1}$ respectively. These bands are probably due to the intraligand charge transfer, and LMCT ($\text{PhO}^- \rightarrow \text{Ni(II)}$ and $\text{N(imino)} \rightarrow \text{Ni(II)}$), respectively. Complex **2** also shows d-d transitions. The broad bands are obtained at 750 and 860 nm which probably indicate $d_{xz}, d_{yz} \rightarrow d_{z^2}$ and $d_{xy}, d_{x^2-y^2} \rightarrow d_{z^2}$ transitions.^[21]

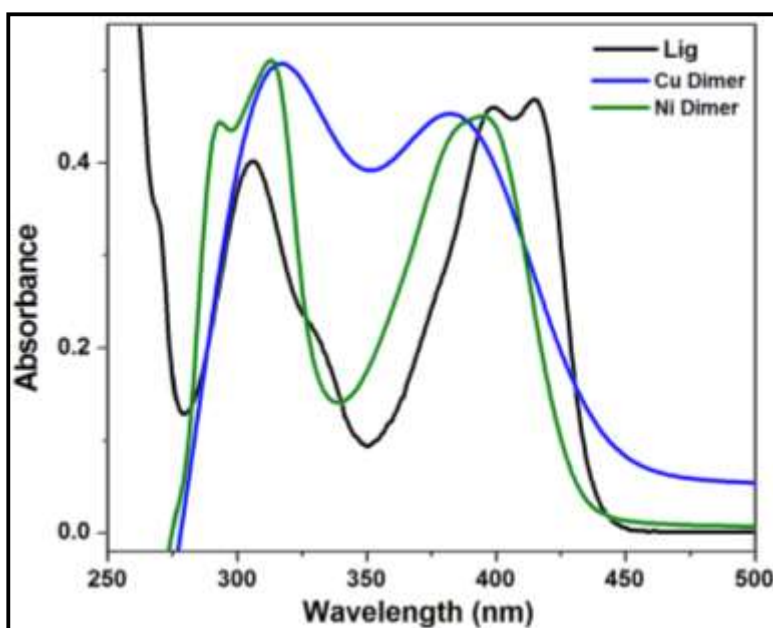


Fig 4.4 : Absorption spectra of ligand (black), complexes 1 (blue) and 2 (green) in methanol at room temperature

4.3.5. Geometry optimization and computational studies

Molecular structures of HL^1 and its Cu, Ni complex have been optimized at their electronic ground state (S_0) by means of DFT at B3LYP/(6-31G) level. For better understanding of the electronic transitions involved in absorption process, TD-DFT calculations have been carried out by the B3LYP/CPCM method in methanol by utilizing the ground state optimized geometries.

The lowest 40 singlet–singlet transitions have been evaluated and results of the TD calculations are qualitatively very similar with the experimental results. The computed absorption energies along with their oscillator strengths, the main configurations, are summarized in **Table 4.3**. **Fig.4.5** displays the energy levels of different Frontier Molecular Orbital's of the ligand and complexes **1** and **2** associated with their HOMO-LUMO energy gap. Due to the presence of electronic correlation in the TD-DFT (B3LYP) method, it can yield more accurate electronic excitation energies. The UV spectra computed by TD-DFT calculations in methanol show the important peaks in the range 200–500 nm.

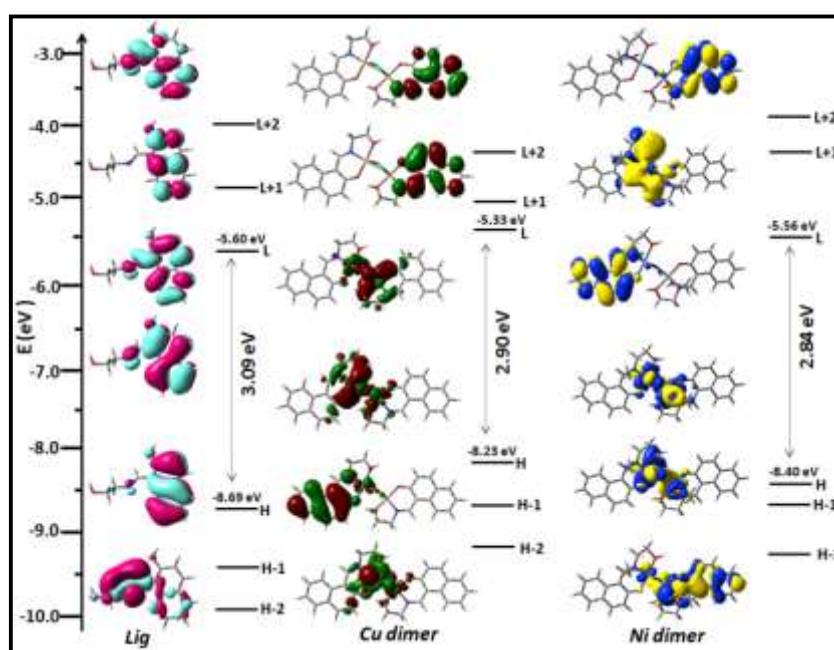


Fig. 4.5 : Frontier MOs along with their HOMO-LUMO energy gap of HL^1 , complexes **1** and **2**.

HL^1 shows lowest lying distinguishable singlet \rightarrow singlet absorption band at 418.14 nm (experimentally 415 nm) which is due to the contribution of HOMO-1 \rightarrow LUMO+1, HOMO \rightarrow LUMO, HOMO \rightarrow LUMO+1 transitions, also a moderately intense peak at 400.12 nm (experimentally 400 nm) that corresponds to HOMO-1 \rightarrow LUMO, HOMO \rightarrow LUMO, HOMO \rightarrow LUMO + 1 transitions along with a shoulder at 311.24 nm (experimentally 306 nm) corresponding to HOMO-3 \rightarrow LUMO+1, HOMO \rightarrow LUMO+1, HOMO-1 \rightarrow LUMO+2 and HOMO-1 \rightarrow LUMO transitions.

Complex **1** shows an intense absorption peak at 384.21 nm (experimentally 383 nm) corresponding to HOMO-1→LUMO+1, HOMO-3→LUMO, HOMO→LUMO transitions along with moderately intense absorption band at 317.88 nm (experimentally 316 nm) corresponding to HOMO-2→LUMO+4, HOMO→LUMO+6 transitions (**Fig. 4.6A**). Besides the nickel dimer shows absorption peaks at 396.12 nm (experimentally 395 nm) due to the contribution of HOMO-3→LUMO, HOMO-2→LUMO, HOMO-1→LUMO+1 transitions and peak at 314.40 nm (experimentally 312 nm) corresponding to HOMO-1→LUMO+4, and HOMO→LUMO+1 transitions (**Fig. 4.6B**).

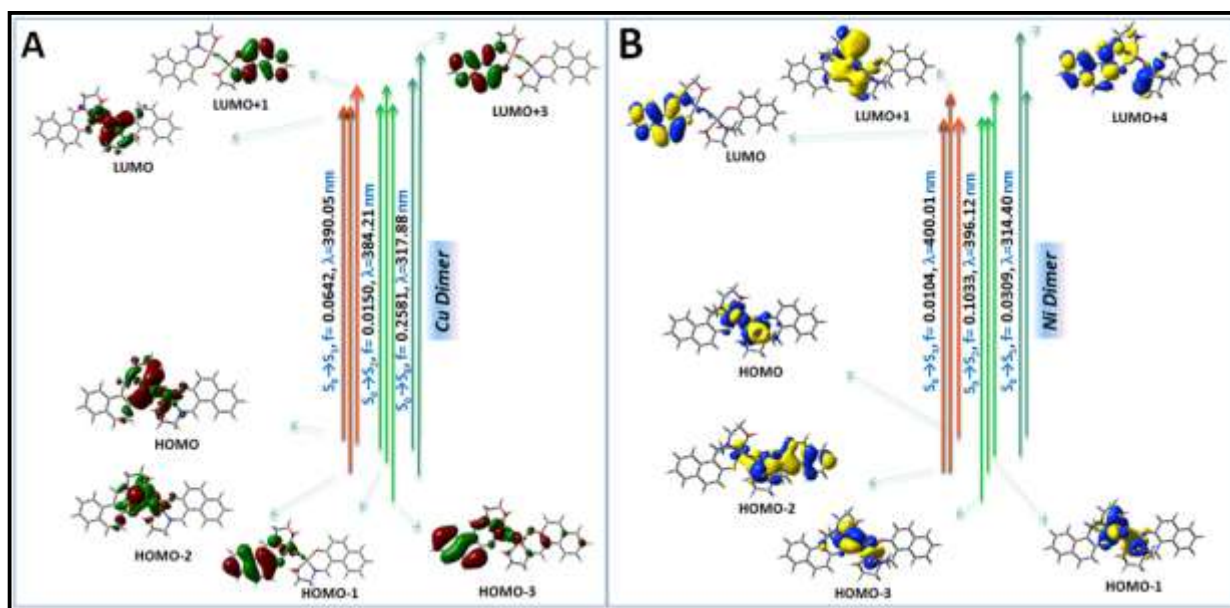


Fig. 4.6 : Frontier molecular orbitals involved in the UV-vis absorption of complexes 1 (A) and 2 (B).

Compound	Excitation (eV)	Electronic transition State	excitation (nm)	Osc. strength (f)	CI	Key transitions
	2.904	S ₀ -S ₁	418.14	0.0423	0.1965	(08%)HOMO-1 →LUMO+1
					0.6204	(77%)HOMO→LUMO
					0.1274	(03%)HOMO

HL ¹						→LUMO+1
	2.991	S ₀ -S ₂	400.12	0.0252	0.5570	(62%)HOMO-1→LUMO
					0.1192	(02%)HOMO-1→LUMO+1
					0.2872	(16%)HOMO→LUMO+1
	3.983	S ₀ -S ₅	311.24	0.6564	0.1188	(03%)HOMO-3→LUMO+1
					0.4700	(44%)HOMO-1→LUMO
					0.1195	(43%)HOMO-1→LUMO+2
					0.4220	(35%)HOMO→LUMO+1
Complex 1	3.070	S ₀ -S ₁	390.05	0.0642	0.6714	(89%)HOMO→LUMO
					0.2031	(08%)HOMO-2→LUMO
					0.1180	(02%)HOMO→LUMO+1
	3.227	S ₀ -S ₂	384.21	0.1501	0.6418	(82%)HOMO-1→LUMO+1
					0.1114	(02%)HOMO-3→LUMO
					0.1834	(06%)HOMO→LUMO
	3.254	S ₀ -S ₄	380.93	0.0402	0.2215	(10%)HOMO-2→LUMO
					0.1046	(02%)HOMO-9→LUMO
					0.5468	(60%)HOMO→LUMO+1
	3.900	S ₀ -S ₈	317.88	0.2581	0.1483	(04%)HOMO-2→LUMO+3
					0.6705	(90%)HOMO→LUMO+1

	3.956	S ₀ -S ₉	313.40	0.0304	0.6101	(74%)HOMO-4→LUMO+3
					0.2635	(14%)HOMO-4→LUMO+5
					0.1190	(03%)HOMO-4→LUMO+8
Complex 2	3.083	S ₀ -S ₁	400.01	0.0104	0.2156	(10%)HOMO-2→LUMO
					0.1169	(02%)HOMO-2→LUMO+1
					0.6153	(74%)HOMO→LUMO
	3.120	S ₀ -S ₂	396.12	0.1033	0.1788	(06%)HOMO-2→LUMO
					0.3422	(23%)HOMO-3→LUMO
					0.4418	(39%)HOMO-1→LUMO+1
	3.961	S ₀ -S ₅	314.40	0.0309	0.2967	(17%)HOMO-1→LUMO+4
					0.5512	(61%)HOMO→LUMO+1
	3.986	S ₀ -S ₆	311.21	0.0571	0.2806	(15%)HOMO-3→LUMO+2
					0.1165	(02%)HOMO-3→LUMO+1

Table 4.3 : Main calculated UV-Vis transition for HL¹, complexes 1 and 2 with vertical excitation energies (E_{cal}), oscillator strengths (f_{cal}) of the lowest few excited singlets obtained from TDDFT/B3LYP/CPCM method in methanol.

4.3.6 Thermal analysis

Thermogravimetric analysis (TGA) and differential thermal analysis (DTA) have been performed on powdered samples of complexes **1** and **2** from 35 to 800 °C (for complex **1**) and 35 to 750 °C (for complex **2**) to examine thermal stability of the complexes and fate of solvent of crystallization molecules.

In the TGA DTA plot of complex **1**(**Fig 4.7**), an initial loss of 2.6% is seen at temperature 50 °C which corresponds to an endothermic DTA peak depicts the loss of surface water probably . The next visible loss at 190 °C is a weight loss of around 6% which probably indicates the loss of the 2.5 water molecules of crystallization (calculated loss 6.7%) also depicted by an endothermic peak. A loss of almost 32% occurs at around 280 °C which probably shows loss of one ligand moiety (calculated loss 32.2%). The next decomposition around 370 °C probably indicates loss of two Cl (observed ~10% vs calculated 10.6%).The final loss of 33% is attributed to the loss of another ligand moiety after which a stable residue of CuO is obtained. All of the last three losses accompany a corresponding exothermic peak in the DTA curve.

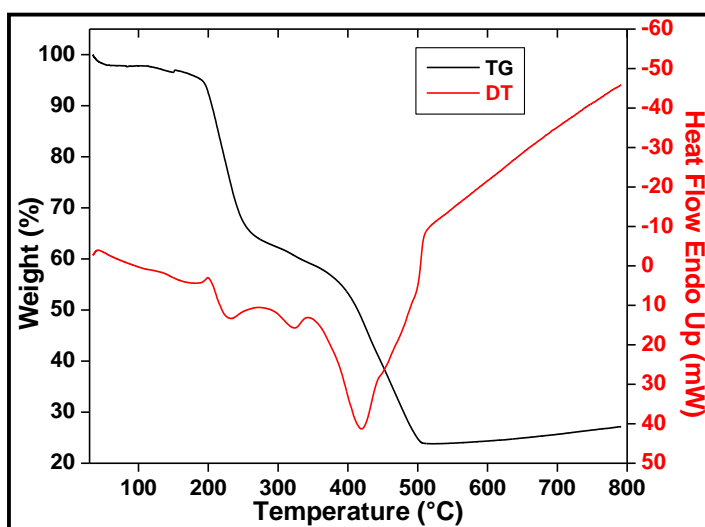


Fig. 4.7 : Thermal analysis of complex 1.

In the TGA DTA plot of complex **2**, the initial loss of 13% at 86 °C can be attributed to the loss of 3 methanol molecules (bound and unbound (calculated loss 13.2%)) as confirmed by endothermic DT peak (**Fig.4.8**). There are next two consecutive losses, each of 4% which can be the loss of N₂ twice from the azide bridges. This loss occurs between 132 and 180 °C of

temperature. The next loss of another 4% is the final decomposition of the nitrogens of the azide bridge and its evolution as another molecule of N_2 at and the process completes at 270 °C. The next loss of around 40% probably confirms the loss of one part of the dinuclear complex which continues upto 400 °C. The residue is the stable NiO left behind. All show exothermic DT peaks other than the loss of solvent molecules at the starting temperatures.

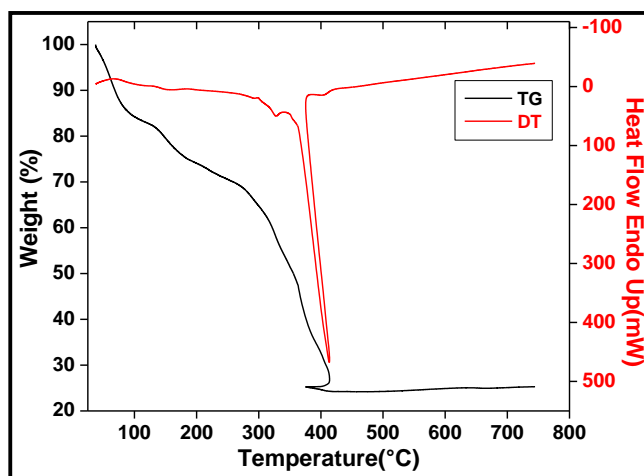


Fig. 4.8 : Thermal analysis of complex 2.

4.3.7. Cyclic voltametric studies

Electrochemical studies of complexes **1** and **2** have been carried out in acetonitrile using TBAP as supporting electrolyte. A typical cyclic voltammogram (CV) has been obtained by using a Pt working electrode and an Ag/AgCl reference electrode. The scan rate has been maintained at 50 mV s^{-1} . CV plots of the complexes are shown in **Fig. 4.9**.

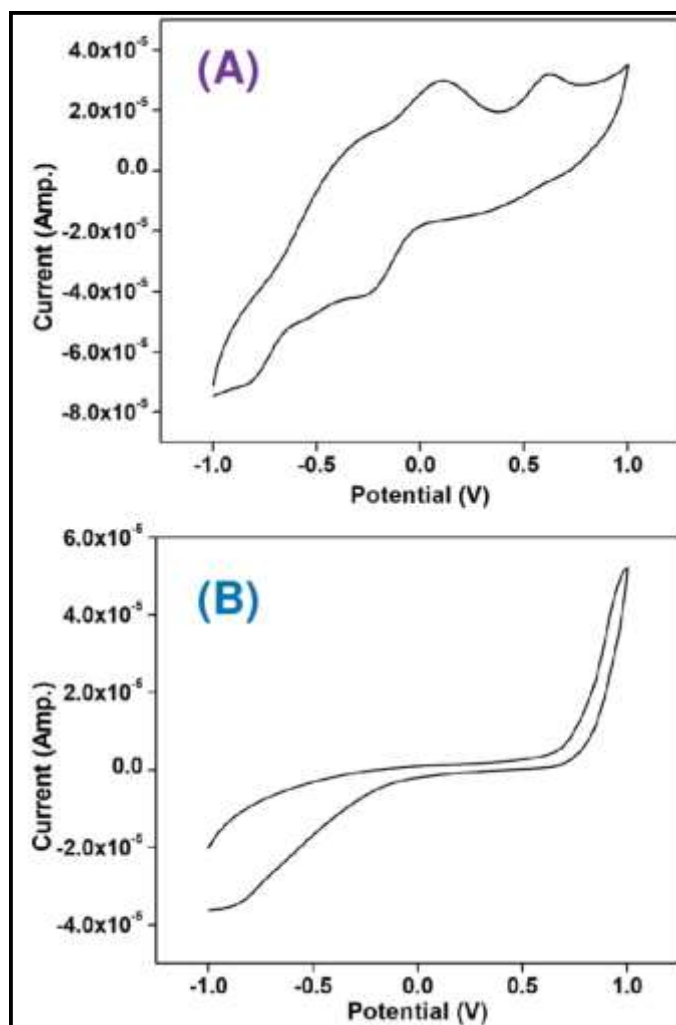
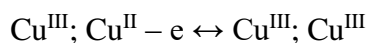
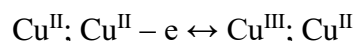


Fig. 4.9 : Cyclic voltammograms of complexes 1 (A) and 2 (B).

The CV plot of the dinuclear complex, **1** has been obtained in the range of -1.0 V to $+1.0$ V. In the range, $+1.0$ to 0.0 , oxidation processes in copper center are observed. In the range 0.0 to -1.0 V, reduction processes involving metal and ligand are monitored.^[22] Cyclic voltammogram between 1.0 and 0.0 V gives two anodic peaks at around E_{pa} 0.10 V with I_{pa} 9.9×10^{-5} A and around E_{pa} 0.62 V with I_{pa} 1.2×10^{-5} A. As HL^1 is electrochemically inert in the said potential range, this oxidation may be attributed to be metal centered. This process is involved one electron in each step.^[23] The electrochemical responses of the complex may be assigned as:



Since the two copper atoms are not in the same coordination environment, their oxidation potentials are seen to be different as observed. In the reverse scan, the cathodic peak at $E_{\text{pc}} 0.40$ V with $I_{\text{pc}} 4.5 \times 10^{-5}$ A corresponds to the two above oxidations forming a quasireversible couple $\text{Cu}^{3+}/\text{Cu}^{2+}$. The two different copper centers with different coordination geometry give rise to two such distinguished redox couples.

In the scan of range 0.0 to -1.0 V, the other anodic peak at $E_{\text{pa}} -0.88$ V with $I_{\text{pa}} 1.84 \times 10^{-5}$ A is associated with a small cathodic peak at $E_{\text{pc}} -0.80$ V with I_{pc} around 10×10^{-5} A which signifies the quasireversible redox system $\text{Cu}^{2+}/\text{Cu}^{1+}$. Another quasireversible redox couple for $\text{Cu}^{2+}/\text{Cu}^{1+}$ process is indicated by the peaks with values $E_{\text{pa}} -0.40$ V and $I_{\text{pa}} 7.15 \times 10^{-5}$ A and $E_{\text{pc}} -0.23$ V and I_{pc} around 7.0×10^{-5} A. The varied environment around Cu center causes these two redox couples.

For the Ni complex, no significant redox peaks have been obtained in the said range of voltage in the cyclic voltammogram. Only in the reverse sweep, a peak at around -0.86 V is observed which may be attributed to an irreversible reduction of ligand.^[24]

4.3.8 Catalysis studies

The catalytic activity of both the complexes for oxidation of cyclohexane, toluene and cyclopentane have been analyzed. The oxidation of the substrates has been performed by H_2O_2 as the oxidant in a slightly acidic medium under ambient conditions. To set optimum conditions, variation in the amount of hydrogen peroxide (30% in H_2O) and HNO_3 , has been made, keeping fixed amount of the metal complex (0.03 mmol) in 5 mL of acetonitrile. The ratio $n(\text{HNO}_3)/n(\text{catalyst})$ has been varied from 5-25. The $n(\text{H}_2\text{O}_2)/n(\text{catalyst})$ has been varied from 100–500 with the best yield obtained at 500.

Results of oxidation are summarized in **Table 4.4**. The products of the oxidation of cyclohexane are cyclohexanol and cyclohexanone as major product; toluene is oxidized mainly to benzyl alcohol and benzaldehyde, whereas cyclopentane gives cyclopentanol and cyclopentanone as the major products. Cyclohexane oxidation also gives a small amount of adipic acid (around 9%) when the ratio $n(\text{H}_2\text{O}_2)/n(\text{catalyst})$ is around 250-300. At lesser ratio

$n(\text{H}_2\text{O}_2)/n(\text{catalyst})$, say around 100, no adipic acid has been detected and at still higher ratio of around 500 (which is the most optimized condition) the amount of adipic acid formed remains the same i.e. 9%. Benzoic acid has been obtained as a minor product from oxidation of toluene. Benzoic acid is generally obtained by aerial oxidation of benzaldehyde, hence this benzoic acid could have come from the benzaldehyde formed during the oxidation of toluene. Oxidation of cyclopentane gives some high boiling combustion products along with the major cyclopentanol and cyclopentanone.

The yield has been optimized by varying the relative proportions of nitric acid and hydrogen peroxide with respect to the catalysts, temperature and varying the reaction time. It has been obvious from previous studies^[6,7,25] that the presence of nitric acid has positive role in these catalytic reactions. Nitric acid has, mainly, two important roles: (i) it could increase the vacant coordination site at the metal center by the protonation of the ligand of these complexes and hence enhances oxidative properties of the catalyst; and (ii) decomposition of peroxide is retarded in the presence of nitric acid, the stability of peroxy intermediate is increased. However, it is difficult to determine the exact structure of the complex in solution. Copper center in dinuclear complex is in both tetra and penta-coordination. Thus, these metal centers would need nitric acid to increase the unsaturation at the metal center. The highest conversion has been ascertained at $n(\text{HNO}_3)/n(\text{catalyst})$ ratio 20, while the yield decreases on further increasing the ratio. Hence, this ratio is maintained throughout for all the reaction sets. The reaction mixture has been stirred for 48 h at room temperature (35 °C) under atmospheric pressure. Different temperatures conditions have been applied to optimize the highest yield. Reaction has been carried out at 40, 50, 60 and 70 °C. The best yield was obtained at 40 °C. Up to 50 °C, the reaction proceeds showing slight decrease in yield at around 50 °C which gradually declines up to 60 °C. After 60 °C, there is a drastic decrease in the yield of products as it has been confirmed by gas chromatographic analysis.

The catalysis has also been done at high pressure conditions which fail to yield the products. This indicates that normal pressure conditions are most desired condition for the reaction. The reaction has also been performed with TBHP as the oxidant but it shows lower yield, around 5% in total. This can, probably, be due to its bulky structure which destabilizes the intermediate. Then, the same catalytic reaction was carried out under inert (argon) atmosphere to examine effect of presence of oxygen. However, it has been found that this reaction shows

almost equal yield when same catalytic reaction is carried out under normal experimental conditions. There is only a small decrease in amount of products formed which indicates only little participation of atmospheric oxygen in the oxidation process. Instead of nitric acid, organic acid such as acetic acid has been employed in the reaction. The yield of product remains the same showing that organic acid is as effective in the role played by nitric acid. In order to find out the probable mechanisms, the catalytic reaction of cyclohexane with the complex have been carried out maintaining $n(\text{HNO}_3)/n(\text{catalyst})$ ratio of 20 and $n(\text{H}_2\text{O}_2)/n(\text{catalyst})$ ratio of 500 in the presence of TEMPO (2,2,6,6-tetramethylpiperidin-1-oxyl). The yield of the reaction is greatly suppressed in its presence. TEMPO is well known as a radical trap. This indirectly indicates that oxidation reactions occur mainly by mechanisms involving the formation radicals as elucidated in the catalytic scheme (**Scheme 4.2**).

Cyclohexane

$n(\text{H}_2\text{O}_2)/n(\text{catalyst})$	Time (h)	Yield (%)		Total	Selectivity of cyclohexanol (%)	TON
		Cyclohexanone	Cyclohexanol			
100	8	3.2	5.8	9	64.4	4.5
	48	6.4	9.1	15.5	58.7	7.75
250	8	7.6	14.1	21.7	65	10.8
	48	9.3	21.4	30.7	69.7	15.3
500	8	11.1	19.3	30.4	63.4	15.2
	48	18.4	29.8	48.2	62	24.1

Toluene

$n(\text{H}_2\text{O}_2)/n(\text{catalyst})$	Time (h)	Yield (%)		Total	Selectivity of benzyl alcohol (%)	TON
		Benzyl alcohol	Benzaldehyde			
100	8	7.4	4.8	12.2	60.6	6
	48	11.1	7.2	18.3	60.6	9
250	8	11.8	9.3	21.1	56	10.55
	48	19.4	14.4	33.8	57.4	16.9

500	8	19.1	13.8	32.9	58	16.45
	48	23.8	15.9	39.7	60	19.8
<u>Cyclopentane</u>						
$n(\text{H}_2\text{O}_2)/n(\text{catalyst})$	Time (h)	Yield (%)		Total	Selectivity of	TON
		Cyclopentane	Cyclopentanol		Cyclopentanol (%)	
100	8	5.2	5.8	11	52.7	5.5
	48	9.2	11.4	20.6	55.3	10.3
250	8	8.5	10.9	19.4	56.1	9.8
	48	13.6	14.9	28.5	52.2	14.25
500	8	14.5	17.2	31.7	54.2	15.85
	48	16.7	19.1	35.8	53.3	17.9

Table 4.4 : Yields and selectivities of the catalysis reactions

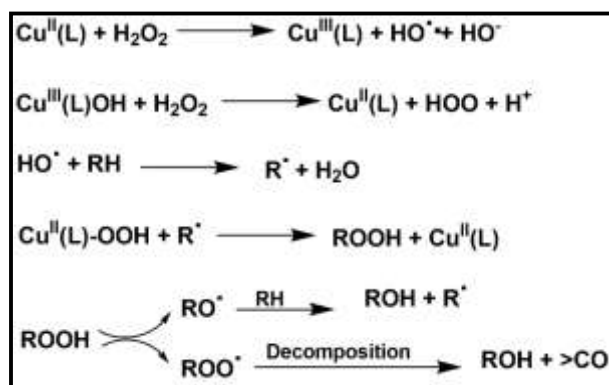
Copper salts like $\text{Cu}(\text{NO}_3)_2$, under the same reaction conditions exhibit at much lower activity towards oxidation of all substrates under same experimental condition. It showed only about 2% conversion. So it is evident that the presence of N and O donor ligands is quite relevant.

The reaction is believed to proceed through alkyl hydroperoxide (ROOH) (cyclohexyl peroxide or benzyl peroxide) formation. The carbonyl compounds i.e. cyclohexanone, benzaldehyde or cyclopentanone are formed probably through decomposition of the radical. The formation of alkyl hydroperoxide has been confirmed by following the method introduced by G. B. Shul'pin.^[26] The reaction mixture has been analyzed by GC before and after treating with excess PPh_3 . Treatment of the reaction mixture (alkyl hydroperoxide) by PPh_3 leads to the formation alcohol with subsequent formation of phosphane oxide (OPPh_3). After the reduction, the alcohol peak in the GC rises markedly while the intensity of the $>\text{C}=\text{O}$ compound's peak reduces.

The hydroxyl radical HO^\bullet could be formed as a result of metal-assisted decomposition of hydrogen peroxide. The hydroxyl radical abstracts H from the substrate (RH) to form R^\bullet .^[25a] The formation of ROOH may be occurred by the reaction between a metal-peroxo intermediate, e.g. bearing a $\text{Cu}(\text{II})\text{-OOH}$ type moiety and the organoradical R^\bullet , to form ROOH.^[27] The formation

of Cu–peroxo species has been determined by UV-vis spectra. The metal-assisted homolytic cleavage of alkyl hydroperoxide generates alkoxy (RO^\cdot , upon O–O bond rupture) and alkylperoxy (ROO^\cdot , upon O–H bond breakage) radicals which can form an alcohol (ROH) upon H-abstraction from the alkane (RH) by RO^\cdot or both ROH and the $>\text{C}=\text{O}$ upon decomposition of ROO^\cdot .^[28]

UV-vis spectra for the complexes have been recorded in methanol at room temperature as discussed earlier. To further observe the effect of hydrogen peroxide, the UV-vis spectra of the complexes in the presence of hydrogen peroxide, have been recorded. It has been observed that an intense peak at around 400 nm, with a shoulder in the range of 410–420 nm, appears for complex **1**. This may be attributed to the existence of Cu–hydroperoxo or Cu–peroxo species.^[29] However, there is no observable change in the UV-vis spectrum of complex **2** when it is recorded in the presence of hydrogen peroxide.



Scheme 4.2 : Probable mechanism of catalytic reactions.

Complex **2** has also been checked for its catalytic property in oxidizing the substrates. But the Ni catalyst shows very poor conversion i.e. about 7% total yield for cyclohexane, 5% for toluene and 4 % for cyclopentane. This could be attributed to the coordinatively saturated nature of the each Ni center in complex **2** with coordination number 6. The UV vis data of the complex in the presence of H_2O_2 could not confirm the presence of Ni-hydroperoxo or peroxo species like Cu–hydroperoxo or Cu–peroxo in case of complex **1**. Also electrochemical studies of the complex indicate no formation of higher oxidation state species in the said voltage range whereas

Cu(III) species has been detected in the said voltage range indicating more vulnerability character of complex **1**.

4.4. Conclusions

We have been able to synthesize and characterize two dinuclear transition metal complexes with a Schiff-base ligand. One of them is copper containing complex, complex **1** and another with nickel, complex **2**. Complex **1** has been found to be active catalyst for the oxidation of cyclohexane, toluene and cyclopentane in the presence of hydrogen peroxide as the terminal oxidant. Corresponding alcohol and aldehyde have been produced as major products. Conversion of the substrates is high. However, complex **2** is not able to convert these substrates under similar conditions. UV-vis spectral analysis shows that complex **1** could generate Cu-peroxo or Cu-hydroperoxo species in the presence of hydrogen peroxide whereas formation of such type of species with nickel complex is not evident from the UV-vis spectral studies. CV of complex **1** shows that two Cu(II) centers could be converted to Cu(III) center with transfer of one electron in each of two steps. Formation of higher oxidation state species of Ni is not indicated from its electrochemical studies. These analyses support that formation of Cu-peroxo as active species for the catalytic conversions. Possible mechanism indicates the involvement of Cu(III) species. Probably other metals also need higher oxidation states for this catalysis. As generation of Cu(III) center is feasible, not the Ni(III) center evident from electrochemical studies under normal condition, the dinuclear copper complex can mimic activity of particulate methane monooxygenase while dinuclear nickel complex cannot.

4.5. References

- [1] a) A.E. Shilov and G.B. Shul'pin, *Chemical Reviews*, **1997**, 97, 2879; b) A.A. Fokin and P.R. Schreiner, *Chemical Reviews* **2002**, 102, 1551; c) A. Sen, *Accounts of Chemical Research* **1998**, 31, 550; d) R.A. Periana, O. Mironov, D. Taube, G. Bhalla and C.J. Jones, *Science* **2003**, 301, 814.
- [2] a) L. Que Jr and W. B. Tolman, *Nature* **2008**, 455, 333; b) J. C. Nesheim and J. D. Lipscomb, *Biochemistry* **1996**, 35, 10240; c) T. Punniyamurthy, S. Velusamy and J. Iqbal, *Chemical Reviews* **2005**, 105, 2329.
- [3] a) A. S. Hakemian and A. C. Rosenzweig, *Annual Reviews of Biochemistry* **2007**, 76, 223; b) M. O. Ross and A. C. Rosenzweig, *Journal of Biological Inorganic Chemistry* **2017**, 22, 307; c) S. Sirajuddin and A. C. Rosenzweig, *Biochemistry* **2015**, 54, 2283; d) C. E. Tinberg and S. J. Lippard, *Accounts of Chemical Research* **2011**, 44, 280.
- [4] a) A. M. Kirillov, M.V. Kirillova and A.J.L. Pombeiro, *Coordination Chemistry Reviews* **2012**, 256, 2741; b) M. M. Vinogradov, Y. N. Kozlov, A. N. Bilyachenko, D. S. Nesterov, L. S. Shul'pina, Y. V. Zubavichus, A. J. L. Pombeiro, M. M. Levitsky, A. I. Yalymov and G. B. Shul'pin, *New Journal of Chemistry* **2015**, 39, 187; c) C.-C. Liu, D. Janmanchi, D.-R. Wen, J.-N. Oung, C.-Y. Mou, S. S.-F. Yu and S. I. Chan, *ACS Sustainable Chemical Engineering* **2018**, 6, 5431.
- [5] A. E. Shilov and G. B. Shul'pin, *Activation and Catalytic Reactions of Saturated Hydrocarbons in the Presence of Metal Complexes* Kluwer Academic Publishers, Dordrecht, The Netherlands, **2000**.
- [6] a) A. M. Kirillov, M. N. Kopylovich, M. V. Kirillova, M. Haukka, M. F. C. G. da Silva and A. J. L. Pombeiro, *Angewandte Chemie* **2005**, 117, 4419; b) Y. Y. Karabach, A. M. Kirillov, M. Haukka, M. N. Kopylovich and A.J.L. Pombeiro, *Journal of Inorganic Biochemistry* **2008**, 102, 1190; c) M. V. Kirillova, Y. N. Kozlov, L. S. Shul'pina, O. Y. Lyakin, A. M. Kirillov, E. P. Talsi, A. J.L. Pombeiro and G. B. Shul'pin, *Journal of Catalysis* **2009**, 268, 26; d) K. R. Gruenwald, A. M. Kirillov, M. Haukka, J. Sanchiz and A.J. L. Pombeiro, *Dalton Transactions* **2009**, 2109; e) M. Sutradhar, E. C.B.A. Alegria, T. R. Barman, F. Scorcelletti, M. F. C. G. da Silva and A. J.L. Pombeiro, *Molecular Catalysis* **2017**, 439, 224; f) E. A. Buvaylo, V. N. Kokozay, O. Yu. Vassilyeva, B. W.

- Skelton, O. V. Nesterova and A. J.L. Pombeiro, *Inorganic Chemical Communications* **2017**, 78, 85.
- [7] a) A. A. Alshaheri, M. I. M. Tahir, M. B. A. Rahman, T. B.S.A. Ravoof, T. A. Saleh, *Chemical Engineering Journal* **2017**, 327, 423; b) I. Garcia-Bosch and M. A. Siegler, *Angewandte Chemie* **2016**, 128, 13065; c) A. N. Bilyachenko, A. N. Kulakova, M. M. Levitsky, A. A. Petrov, A. A. Korlyukov, L. S. Shul'pina, V. N. Khrustalev, P. V. Dorovatovskii, A. V. Vologzhanina, U. S. Tsareva, I. E. Golub, E. S. Gulyaeva, E. S. Shubina and G. B. Shul'pin, *Inorganic Chemistry* **2017**, 56, 4093; d) A. N. Bilyachenko, V.V. Zubavichus, L.S. Shul'pin, N. KhrustalevY., A.N. Kulakova, X. Bantreil, F. Lamaty, M. M. Levitsky, E. I. Gutsul, E. S. Shubina, and G. B. Shul'pin, *Inorganic Chemistry* **2018**, 57, 528; e) A. N. Bilyachenko, M. M. Levitsky, A. A. Korlyukov, V. N. Khrustalev, Y. V. Zubavichus, L. S. Shul'pina, E. S. Shubina, A. V. Vologzhanina and G. B. Shul'pin, *European Journal of Inorganic Chemistry* **2018**, 2505; f) P. Roy, K. Dhara, M. Manassero and P. Banerjee, *European Journal of Inorganic Chemistry*, **2008**, 4404; g) S. Thakurta, P. Roy, R. J. Butcher, M. S. E. Fallah, J. Tercero, E. Garribba and S. Mitra, *European Journal of Inorganic Chemistry* **2009**, 4385; h) S. Thakurta, P. Roy, G. Rosair, C. J. Gómez-García, E. Garribba and S. Mitra, *Polyhedron* **2009**, 28, 695; i) K. C. Gupta and A. K. Sutar, *Coord. Chem. Rev.*, **2008**, 252, 1420; j) K. C. Gupta, A. K. Sutar and C.-C. Lin, *Coordination Chemistry Reviews* **2009**, 253, 1926; k) A. Bhattacharjee, S. Halder, K. Ghosh, C. Rizzoli and P. Roy, *New Journal of Chemistry* **2017**, 41, 5696; l) S. Halder, S. Dey, C. Rizzoli and P. Roy, *Polyhedron*, 2014, **60**, 85; m) M. Nandi, P. Roy, H. Uyama and A. Bhaumik, *Dalton Transactions* 2011, **40**, 12510; n) P. Roy, M. Nandi, M. Manassero, M. Riccò, M. Mazzani, A. Bhaumik and P. Banerjee, *Dalton Transactions* **2009**, 9543.
- [8] a) A. Panja, *Polyhedron* **2014**, 79, 258; b) A. Panja, M. Shyamal, A. Saha and T. Kanti Mandal, *Dalton Transactions* 2014, **43**, 5443; c) A. Panja, *Dalton Transactions* **2014**, 43, 7760; d) K. Ghosh, K. Harms and S. Chattopadhyay, *Polyhedron* **2017**, 123, 162; e) S. K. Dey and A. Mukherjee, *Coordination Chemistry Reviews* **2016**, 310, 80.
- [9] a) C. Kordulis, K. Bourikas, M. Gousi, E. Kordouli, A. Lycourghiotis, *Applied Catalysis B* **2016**, 181, 156; b) S. Chakraborty, P. Bhattacharya, H. Dai and H. Guan, *Accounts of Chemical Research* **2015**, 48, 1995; c) X. Lu, B. Xiao, Z. Zhang, T. Gong, W. Su, J. Yi,

- Y. Fu and L. Liu, *Nature Communications* **2016**, 7, 11129; d) J. Chakraborty, M. Nandi, H. Mayer-Figge, W. S. Sheldrick, L. Sorace, A. Bhaumik and P. Banerjee, *European Journal of Inorganic Chemistry* **2007**, 5005;
- [10] Bruker, APEX2, SAINT and SADABS, Bruker AXS Inc., Madison, Wisconsin, USA, **2008**.
- [11] G. M. Sheldrick, *Acta Crystallographica* **2015**, A71, 3.
- [12] G. M. Sheldrick, *Acta Crystallographica* **2015**, C71, 3.
- [13] M. J. Frisch, G. W. Trucks, H. B. Schlegel, G. E. Scuseria, M. A. Robb, J. R. Cheeseman, G. Scalmani, V. Barone, B. Mennucci, G. A. Petersson, H. Nakatsuji, M. Caricato, X. Li, H. P. Hratchian, A. F. Izmaylov, J. Bloino, G. Zheng, J. L. Sonnenberg, M. Hada, M. Ehara, K. Toyota, R. Fukuda, J. Hasegawa, M. Ishida, T. Nakajima, Y. Honda, O. Kitao, H. Nakai, T. Vreven, J. A. Montgomery Jr., J. E. Peralta, F. Ogliaro, M. Bearpark, J. J. Heyd, E. Brothers, K. N. Kudin, V. N. Staroverov, R. Kobayashi, J. Normand, K. Raghavachari, A. Rendell, J. C. Burant, S. S. Iyengar, J. Tomasi, M. Cossi, N. Rega, J. M. Millam, M. Klene, J. E. Knox, J. B. Cross, V. Bakken, C. Adamo, J. Jaramillo, R. Gomperts, R. E. Stratmann, O. Yazyev, A. J. Austin, R. Cammi, C. Pomelli, J. W. Ochterski, R. L. Martin, K. Morokuma, V. G. Zakrzewski, G. A. Voth, P. Salvador, J. J. Dannenberg, S. Dapprich, A. D. Daniels, Ö. Farkas, J. B. Foresman, J. V. Ortiz, J. Cioslowski and D. J. Fox, GAUSSIAN 09, Revision D.01, Gaussian Inc., Wallingford, CT, **2009**.
- [14] A. D. Becke, *Journal of Chemical Physics* **1993**, 98, 5648.
- [15] P. J. Hay and W. R. Wadt, *Journal of Chemical Physics* **1985**, 82, 299.
- [16] S. Miertus, E. Scrocco and J. Tomasi, *Chemical Physics* **1981**, 55, 117.
- [17] V. Barone, M. Cossi and J. Tomasi, *Journal of Computational Chemistry* **1998**, 19, 404.
- [18] A. W. Addison, T. N. Rao, J. Reedijk, J. Vanriijn and G. C. Verschoor, *Journal of Chemical Society, Dalton Transactions* **1984**, 1349.
- [19] a) S. Banerjee, P. Ghorai, P. Brandão, D. Ghosh, S. Bhuiya, D. Chattopadhyay, S. Das and A. Saha, *New Journal of Chemistry* **2018**, 42, 246; b) P. Ghorai, R. Saha, S. Bhuiya,

- S. Das, P. Brandão, D. Ghosh, T. Bhaumik, P. Bandyopadhyay, D. Chattopadhyay and A. Saha, *Polyhedron* **2018**, *141*, 153; c) S. Dey, K. Ghosh, S. Halder, C. Rizzoli and P. Roy, *Indian Journal of Chemistry* **2015**, *54A*, 1451.
- [20] a) S. Halder, J. Mondal, J. Ortega-Castro, A. Frontera and P. Roy, *Dalton Transactions* **2017**, *46*, 1943; b) P. Ghorai, A. Chakraborty, A. Panja, T. K. Mondal and A. Saha, *RSC Advances* **2016**, *6*, 36020; c) S. Roy, A. Bhattacharyya, S. Purkait, A. Bauzá, A. Frontera and S. Chattopadhyay, *Dalton Transactions* **2016**, *45*, 15048.
- [21] a) Comprehensive Coordination Chemistry, ed. B. J. Hathaway, G. Wilkinson, R. D. Gillard and J. A. McCleverty, Pergamon Press, Oxford, England, **1987**, vol. 5; b) F. A. Mautner, C. N. Landry, A. A. Gallo and S. S. Massoud, *Journal of Molecular Structure* **2007**, *837*, 72; c) F. A. Mautner, J. H. Albering, R. Vicente, F. R. Louka, A. Gallo and S. S. Massoud, *Inorganica Chimica Acta* **2011**, *365*, 290; d) S. S. Massoud, L. L. Quan, K. Gatterer, J. H. Albering, R. C. Fischer and F. A. Mautner, *Polyhedron*, **2012**, *31*, 601.
- [22] D. X. West, A. E. Liberta, S. B. Padhye, R. C. Chikate, P. B. Sonawane, A. S. Kumbhar and R. G. Yerande, *Coordination Chemistry Review* **1993**, *123*, 49.
- [23] a) E. Franco, E. López-Torres, M. A. Mendiola and M. T. Sevilla, *Polyhedron*, **2000**, *19*, 441; b) J. P. Naskar, B. Guhathakurta, L. Lu and M. Zhu, *Polyhedron* **2012**, *43*, 89.
- [24] S. Rayati, E. Khodaei, M. Jafarian, A. Bahrami, A. Wojtczak and A. Kozakiewicz, *Journal of Coordination Chemistry* **2017**, *70*, 1424.
- [24]
- [25] a) T. F. S. Silva, G. S. Mishra, M. F. G. da Silva, R. Wanke, L. M. D. R. S. Martins and A. J. L. Pombeiro, *Dalton Transactions* **2009**, 9207; b) M. Nandi and P. Roy, *Indian Journal of Chemistry* **2013**, *52A*, 1263.
- [26] G. B. Shul'pin, *J. Molecular Catalysis A: Chemistry*, **2002**, *189*, 39.
- [27] a) T. F. S. Silva, E. C. B. Alegria, L. R. Martins and A. J. L. Pombeiro, *Advanced Synthetic Catalysis* **2008**, *350*, 706; b) M. Costas, M. P. Mehn, M. P. Jensen and L. Que Jr., *Chemical Reviews* **2004**, *104*, 939; c) M. Costas, K. Chen and L. Que Jr., *Coordination Chemistry Reviews* **2000**, *200–202*, 517; d) T. Hogan and A. Sen, *Journal of American Chemical Society* **1997**, *119*, 2642.
- [28] a) G. B. Shul'pin in *Transition Metals for Organic Synthesis* (ed.: M. Beller, C. Bolm), 2nd edn, vol. 2, Wiley-VCH, New York, **2004**, p. 215; b) G. B. Shul'pin, H. Stoeckli-

Evans, D. Mandelli, Y. N. Kozlov, A. T. Vallina, C. B. Woitiski, R. S. Jimenez and W. A. Carvalho, *Journal of Molecular Catalysis A* **2004**, *219*, 255.

- [29] a) J. Reim, R. Werner, W. Haase, B. Krebs, *Chemistry-A European Journal* **1998**, *4*, 289;
b) P. Roy, K. Dhara, M. Manassero and P. Banerjee, *Inorganic Chemical Communications* **2008**, *11*, 265; c) S. Halder, S. Dey, C. Rizzoli and P. Roy, *Polyhedron* **2014**, *78*, 85.

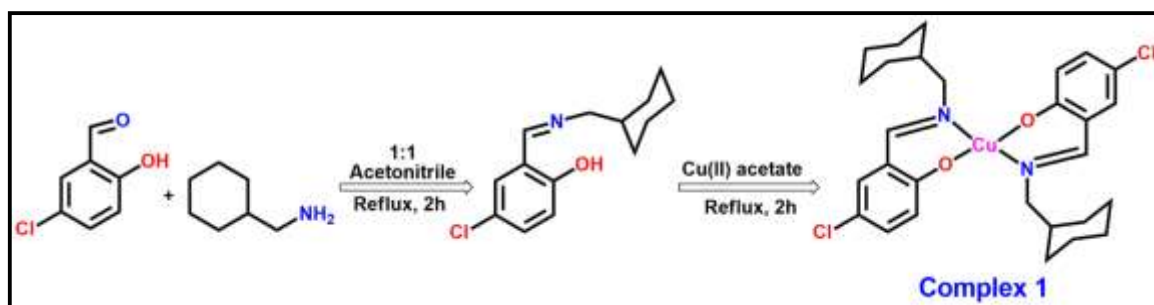
Chapter 5

**A mononuclear
copper(II)-Schiff-base
complex: DNA cleavage
activity, protein binding
affinity and cellular
imaging**

5.1 Introduction

After first report of antitumor activity of some platinum compounds such as cisplatin by Rosenber et al.^[1], a significant amount of attention has been paid to develop and understand metal-based anticancer drugs. Cisplatin and analogous platinum-based drugs suffer from severe associated toxic effects such as emetogenesis, neurotoxicity, myelotoxicity and nephrotoxicity.^[2] Thus, there is a need for new compounds having antiproliferative properties and therapeutic solutions. Non-platinum complexes have then been emerged as potential anticancer agents as their alternatives.^[3] Different metal complexes may become potential candidate as therapeutic agents in medicinal research as these compounds are able to interact with proteins and DNA under physiological conditions very efficiently. During last few decades, tremendous effort has been provided to grow a number of different transition metal complexes including that of copper(II) as possible anticancer drugs.^[4] A number of copper(II) complexes have been used as tools for mediation of strand scission of duplex DNA^[5] and as probes of DNA structure in solution phase.^[6] Chelates of 3,4,7,8-tetramethyl-1,10-phenanthroline with divalent copper and ruthenium showed inhibition to the growth of Landschiitz ascites tumour cells.^[7] Sigman et al. have shown that copper complexes of 1,10-phenanthroline act as effective chemical nuclease for double-stranded DNA, with the aid of molecular oxygen and a reducing agent.^[8] A number of metal complexes are shown to hydrolyze phosphate ester^[9] as well as RNA with varying efficiencies.^[10] Burstyn and co-workers have reviewed metal-promoted phosphodiester hydrolysis by copper complexes and synthetic nucleases and peptidases.^[11] Cu(II/I) complexes of synthetic and naturally occurring ligands act as nuclease mimics and a few copper(II) complexes are shown to be capable of mediating non-random double-strand cleavage of plasmid DNA.^[12] Schiff base complexes with transition metal ions are one such important class of compounds in medicinal and pharmaceutical field. They show biological applications including antibacterial,^[13,14] antifungal^[14] and antitumor activity.^[15] Diamino tetradentate Schiff-bases and their complexes have been used as models for understanding the structures of biomolecules and biological processes.^[16] The interaction of metal complexes containing N₂O₂ Schiff-base ligands has been studied amply.^[17] DNA binding is the critical step for DNA activity. To design effective chemotherapeutic agents and better anticancer drugs, it

is needed to explore the interactions of metal complexes with DNA. Recently, there has been growing interest in studies related to the interaction of transition metal ions with nucleic acid as mentioned earlier because of their relevance in the development of tools for biotechnology and medicine.^[18] These studies are important to understand the toxicity of drugs containing metal ions.^[19] Moreover, molecular design of synthetic metalloproteases that cleave protein at a specific site and act as multifunctional biochemical agents is suitable for understanding the structure–activity correlations of proteins.^[20] Protein degradation plays an important role in many cellular functions such as (i) removal of misfolded and damaged proteins from the cells to avoid toxicity and, (ii) to maintain the cellular concentration of regulatory proteins at optimal levels.^[21]



Scheme 5.1 : Synthesis of complex 1

Synthetic proteases are also vital in the emerging chemistry of anti-metastasis agents to control tumor malignancy.^[22] The specific delivery of a drug to target cells may be done by the use of targeting groups or by tuning the chemical and physical characteristics of the drug or drug carrier such as hydrophobicity and molecular size.^[23] Different types of macromolecules such as liposomes, dendrimers, poly(ethylene glycol)-polymers, nanoparticles, and protein biomolecules are used as carrier molecules.^[24] HSA is the most versatile carrier protein, which is known to accumulate in tumors and has been considered as the carrier conjugate of various organic anticancer drugs.^[25] The main role of HSA is to maintain the osmotic blood pressure and to scavenge free radicals as an antioxidant. It is a macromolecular carrier, the lack of toxicity and immunogenicity make it ideal for drug delivery. HSA is the most multifunctional transport protein and plays role in the transport and deposition of a variety of endogenous and exogenous substances in blood.^[26] The interactions of drugs with protein result in the formation of a stable drug–

protein complex, which can exert an important effect on the distribution, free concentration and metabolism of the drug in the blood stream. Drug distribution is controlled by HSA, because most drugs circulate in plasma and reaches the target tissues by binding to HSA.^[27] Therefore, drug binding to proteins such as HSA has become an important determinant of pharmacokinetics.

These complexes often show distinct antibacterial properties probably by binding to bacterial DNA and killing them in the process. Apoptosis, or programmed cell death, is a crucial process, closely related to a variety of diseases, and apoptosis induced by copper complexes has been studied extensively. Often, due to their redox property, reactive oxygen species (ROS) is formed, which might cause oxidative modification of the cellular components or hamper redox processes of the cell. All these along with ROS related other intracellular cascade reactions can cause apoptosis. A clear understanding of this can help in the designing of copper based antitumor drugs.^[28]

In this respect, the synthesis of a Schiff-base Cu(II) complex in N₂O₂ binding environment, has been reported. The complex [CuL₂] (**1**) has been synthesized under mild conditions by reaction between HL and copper(II) acetate in acetonitrile (Scheme 1.1) (where HL = 4-chloro-2-((cyclohexylmethylimino)methyl)phenol). Although some antimicrobial properties of HL and related compounds have been reported ^[29] but a very few number of metal complexes have been prepared.^[30] It has been characterized by different standard methods including single crystal X-ray diffraction analysis. Complex **1** has been successfully applied in cleaving DNA as well as binding to HSA. It is predicted that the complex first binds to HSA and then gradually released to DNA for binding with it. This is probably the same path which is followed inside living cells as HSA is an excellent carrier molecule which helps the complex to reach the target cells with the diseased DNA. The DNA binding has been ascertained through various biophysical experiments like UV-Vis spectroscopy, fluorescence, cyclic voltametry and circular dichroism studies. The cleavage of DNA has been confirmed on agarose gel electrophoresis. Similarly, protein binding has been confirmed by various spectroscopic methods.

5.2 Experimental

5.2.1 Materials and methods

5-Chloro-2-hydroxybenzaldehyde, 1-cyclohexylmethanamine and copper(II) acetate monohydrate were purchased from Sigma Aldrich and used without further purification. Other chemicals were purchased from commercial sources and used as received. Solvents were purchased from commercial sources and for synthesis purpose they were used without further purification while a purified and dried version was used for spectroscopic measurements.^[31] Elemental analysis was carried out on a 2400 Series-II CHN analyzer, Perkin Elmer, USA. FT-IR spectra were recorded on a Perkin Elmer spectrometer (Spectrum Two) with the samples using the attenuated total reflectance (ATR) technique. The UV-vis spectral analysis was done in Agilent 8453 diode array spectrophotometer. The ESI-MS spectra were recorded on Qtof Micro YA263 mass spectrometer. Single crystal X ray diffraction was done on a Bruker: D8 VENTURE. Emission spectra were recorded using a Horiba Fluoromax-4C spectrofluorometer. The cyclic voltametry instrument used was METROHM AUTOLAB PGSTAT101. A glassy carbon working electrode and a platinum wire auxiliary electrode and saturated Ag/AgCl reference electrode were employed in a standard three-electrode configuration. KCl was used as supporting electrolyte in the DMSO/buffer system as the system was mostly aqueous in the form of Tris/NaCl buffer and the scan rate was 50 mV s^{-1} under argon atmosphere. CD spectra were recorded by using a quartz cuvette of 10 mm pathlength in a JASCO J-815 CD spectropolarimeter. The DNA cleavage studies were done by resolving the DNA on 1% agarose gel electrophoresis in Tris Acetyl EDTA buffer at 80V. The HSA protein was run on 10 % SDS polyacrylamide page gel. Cell lines used for the experiment were HeLa (human cervical cancer cell line). Cells were grown in 10% fetal bovine serum (FBS; Gibco, Grand Island, NY, USA)/Dulbecco's modified Eagle's medium (DMEM; Himedia, Mumbai, India) media at 37°C and 5% CO_2 . 4-chloro-2-((cyclohexylmethylimino)methyl)phenol (HL) was synthesized following a published procedure.^[29]

5.2.2 Synthesis of [CuL₂] (complex 1)

A solution of copper(II) acetate monohydrate (0.5 mmol, 0.100 g) in acetonitrile (5 mL) was added dropwise to an acetonitrile solution (5 mL) of HL (1.0 mmol, 0.252 g) under stirring condition. The mixture turned to yellowish green in color. The mixture was stirred for another 30 min. The color of the solution changed to greenish. The resulting solution was then refluxed for 2 h and the solution became green. The mixture was finally cooled to room temperature and filtered to remove any undissolved or suspended materials. The filtrate was kept at ambient temperature. Green single crystals suitable for X-ray diffraction study were produced within few days. (Scheme 5.1)

Data for **1**: yield (78%); C, H, N analysis: anal. calc. for C₂₈H₃₄Cl₂CuN₂O₂: C, 59.52; H, 6.07; N, 4.96; found: C, 59.54; H, 5.92; N, 4.78%.

5.2.3 X-ray data collection and structure determination

Details of the data collection and refinement parameters for complex **1** are summarized in Table 5.1. Single crystal data collections were performed with an automated Bruker D8 VENTURE diffractometer using graphite monochromatized Mo K α radiation. The spots were measured using 10 s counting time. Unit cell parameters were determined from least-squares refinement of setting angles with θ in the range $2.79 \leq \theta \leq 27.39^\circ$. Data were processed using the Bruker SAINT package.^[32] Absorption corrections based on multi scans using the SADABS software were applied to all intensity data. The structures were solved and refined by full-matrix least-squares techniques on F^2 using the SHELXS-2016/6 program.^[33,34] The absorption corrections were done by the multi-scan technique. All data were corrected for Lorentz and polarization effects, and the non-hydrogen atoms were refined anisotropically. Hydrogen atoms were generated using SHELXL-2016/6 and their positions calculated based on the riding mode with thermal parameters equal to 1.2 times that of the associated C atoms, and participated in the calculation of the final R-indices.

Compound	Complex 1
Formula	C ₂₈ H ₃₄ Cl ₂ CuN ₂ O ₂
Formula weight	565.01
<i>T</i> (K)	293
Color	clear light brown
Crystal system	triclinic
Space group	P-1
<i>a</i> (Å)	6.3371(2)
<i>b</i> (Å)	10.0817(4)
<i>c</i> (Å)	10.9103(4)
<i>α</i> (°)	85.6440(10)
<i>β</i> (°)	79.9620(10)
<i>γ</i> (°)	78.1860(10)
<i>V</i> (Å ³)	671.25(4)
<i>Z</i>	1
Crystal dimensions (mm)	0.3 × 0.21 × 0.11
Minimum and maximum transmission factors	0.769 - 0.892
<i>F</i> (0 0 0)	295
<i>D_c</i> (g cm ⁻³)	1.398
<i>λ</i> (Mo Kα) (Å)	1.040
<i>θ</i> Range (°)	2.79 - 27.39
Reflection collected/unique/observed	12185, 2945, 2775
Absorption correction	multi-scan

R_{int}	0.0538
Final R_1 index [$I > 2\sigma(I)$]	0.0578
Final wR_2 index (all reflections)	0.1188
Goodness-of-fit	1.261

Table 5.1 : Crystal data, data collection and structure refinement of complexes

5.2.4 DNA binding and cleavage activities

Calf thymus (CT)-DNA was purchased from Sigma Aldrich and the supercoiled FAM134BGFP plasmid DNA was obtained from a biotechnology lab. The stock solution of CT-DNA was prepared in 5 mM Tris–HCl/50 mM NaCl buffer at pH 7.2, which gave a ratio of UV absorbance at 260 nm and 280 nm (A_{260}/A_{280}) of ca. 1.8–1.9, indicating that the DNA was sufficiently free of protein^[35] and the concentration was determined by UV absorbance at 260 nm ($\epsilon = 6600 \text{ M}^{-1}\text{cm}^{-1}$) and the plasmid DNA was used as it is in the wet lab cleavage studies.

5.2.5 HSA binding studies

Human serum albumin (HSA) was purchased from Sigma Aldrich. Human serum albumin of $1.0 \times 10^{-4} \text{ M}$ was prepared by dissolving protein in Tris–HCl buffer solution at pH 7.2.^[36] The protein concentration was determined spectrophotometrically using an extinction coefficient of $35,219 \text{ M}^{-1} \text{ cm}^{-1}$ at 280 nm.

5.2.6 Antibacterial study

Overnight grown cultures of *E. coli* and *S. aureus* were incubated in Luria Bertani broth. Approximately, 1×10^8 cells of each bacterial strain were incubated in test tubes containing 2.0 mL of LB media and to it different concentrations of the complex was added. The tubes were incubated at 37 °C for 16-18 h. The growth observed were cells which was plated on LB media following which the plates were incubated at 37 °C again for 16-18 h and the next day colonies were counted.

5.2.7 Cell biological study

Cell lines used for the experiment were HeLa (human cervical cancer cell line). Cells were grown in 10% fetal bovine serum (FBS; Gibco, Grand Island, NY, USA)/Dulbecco's modified Eagle's medium (DMEM; Himedia, Mumbai, India) media at 37°C and 5% CO₂. The HeLa cells were seeded in 35 mm plates. The cells were treated with different concentrations of the complex and incubated for different time intervals. The cells were fixed with 4% formalin in PBS buffer. They were then blocked with 0.1% Triton X in PBS. Then, they were stained with DAPI and mounted on the slides.

5.3 Results and discussion

5.3.1 Synthesis of complex 1 and its characterization

Complex 1 has been synthesized following route given in Scheme 1. First, HL has been prepared by the condensation between cyclohexylmethylamine and 5-chlorosalicylaldehyde 1:1 molar ratio in acetonitrile. This has not been isolated. The reaction between HL and copper(II) acetate monohydrate yields the complex, [CuL₂]. HL deprotonates to bind to the Cu(II) center without any external agent. Probably anion of copper salt helps in deprotonation process.

ESI-MS spectrum of complex 1 confirms the formation of the complex (**Fig. 5.1**). The *m/z* peak at 565.05 may be attributed to the presence of [ML₂] species. Another peak at 313.96 may be assigned to [ML]⁺ species which could be fragmented from the original molecule by losing a ligand. FT-IR spectrum of complex 1 has been recorded with samples by ATR technique (**Fig. 5.2**). The strong peaks at 2848 cm⁻¹ confirms the presence of methylene moieties. The sharp peak at 1633 cm⁻¹ shows the presence of C=N bond which justifies formation of the Schiff base ligand and retention of it in the complex.^[37] A band at 1170 cm⁻¹ indicates the presence of C-O bond i.e. carbon being attached to hydroxyl group. Almost strong band at 718 cm⁻¹ signifies C-Cl bond in the ligand. Medium intensity at 560–570 cm⁻¹ indicates that the ligand is coordinated to the metal center.

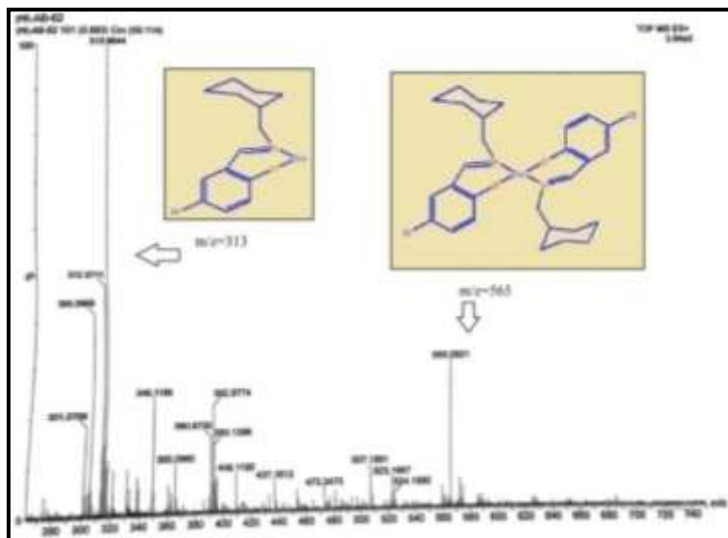


Fig 5.1 : ESI-mass spectrum of complex 1 in methanol.

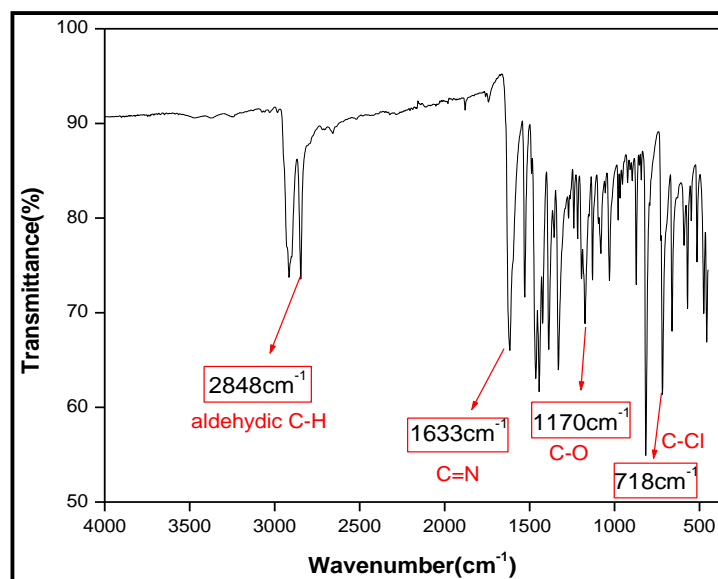


Fig 5.2 : FT-IR spectrum of complex 1.

5.3.2 Crystal structure of complex 1

The complex 1 crystallizes in the P-1 space group from acetonitrile. A perspective view of the complex is given in **Fig. 5.3**. Selected bond angles and bond lengths are listed in **Table 5.2**. The complex 1 consists of two deprotonated ligands (4-chloro-2-((cyclohexylmethylimino)methyl)phenoxide) and one copper atom. Copper atom is in a

tetracoordinated environment. Cu1 is coordinated to two phenolic oxygen atom (O1), two nitrogen atoms (N1) from each of the ligand. It is almost a perfect square planar molecule. Both the *trans* angles O1–Cu1–O1 and N1–Cu–N1 are 180° and the O1–Cu1–N1 angle is 88° which is very close to the ideal 90°. The Cu–O and Cu–N bond lengths are in good agreement with the literature values.^[38]

Cu1 – O1	1.890(2)
Cu1 – N1	2.011(2)
Cu1 – O1_a	1.890(2)
Cu1 – N1_a	2.011(2)
O1 – Cu1 – N1	91.67(9)
O1 – Cu1 – O1_a	180.00
O1 – Cu1 – N1_a	88.33(9)
O1_a – Cu1 – N1	88.33(9)
N1 – Cu1 – N1_a	180.00
O1_a – Cu1 – N1_a	91.67(9)

Table 5.2 : Selected bond lengths (Å) and bond angles (°) of complex 1

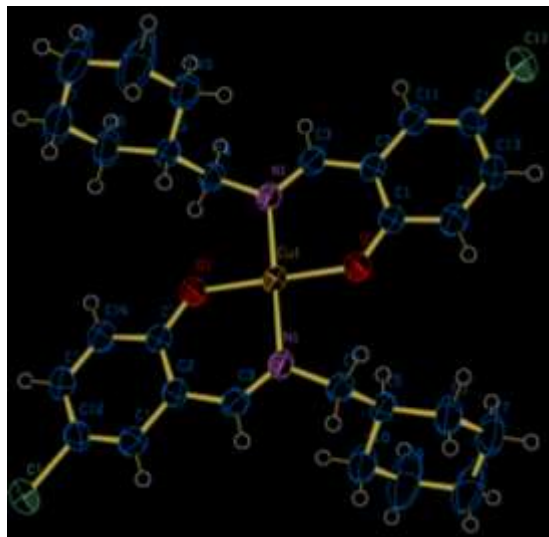


Fig. 5.3 : A perspective view of complex **1** with partial atom numbering scheme.

5.3.3 UV-vis spectral studies

The electronic spectrum of complex **1** has been recorded in acetonitrile at room temperature. UV-vis spectrum of complex **1** is given in **Fig. 5.4**. It could be seen from the figure that it exhibits a broad band at 615 nm (molar extinction coefficient: $3010 \text{ Lmol}^{-1}\text{cm}^{-1}$), which may be assigned to $d-d$ transition. Two strong peaks are observed at 372 and 300 nm, with molar extinction coefficients of $9800 \text{ Lmol}^{-1}\text{cm}^{-1}$ and $9500 \text{ Lmol}^{-1}\text{cm}^{-1}$, respectively. These peaks may be attributed to $\text{PhO}^- \rightarrow \text{Cu(II)}$, $\text{N(amino)} \rightarrow \text{Cu(II)}$ (LMCT) transfer.^[38]

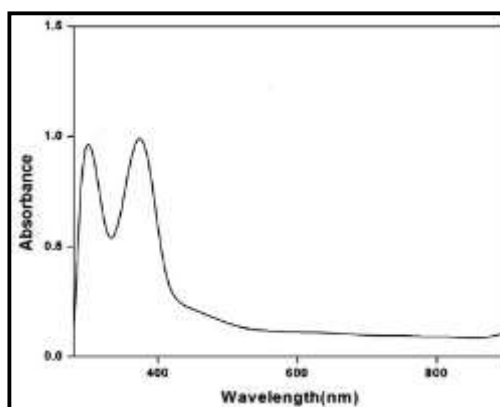


Fig 5.4 : UV-vis spectrum of complex **1** in acetonitrile

5.3.4 Magnetic moment studies

Magnetic properties of complex 1 have been analyzed with powdered samples at 297 K. The expected value of magnetic moment for Cu(II) system is 1.73 BM. The experimental value of χ_M has been determined to be 1.58 BM. This value is almost close to the theoretical value of 1.73 BM indicating the presence of one copper atom in the complex.

5.3.5 Electrochemical studies

The electrochemical behavior of the complex has been investigated using voltammetry. Electrochemical studies were carried out in DMF solution by cyclic voltammetry at room temperature with TBAB (tetrabutylammonium bromide) as supporting electrolyte under argon atmosphere. The negative scan shows that the Cu(II) center gets reduced to a Cu(I) species (**Fig. 5.5**).^[39] The graph shows a I_{cathodic} peak indicating a reduction of Cu(II) \rightarrow Cu(I) which is getting oxidized back Cu(I) \leftarrow Cu(II) as indicated by I_{anodic} value. Thus, $I_{\text{anodic}}/I_{\text{cathodic}}$ ratio is nearly 1 which signifies a quasireversible reduction at a mononuclear copper center. ΔE_p is approximately 0.07 V indicating a one electron change i.e. Cu(II) \rightarrow Cu(I).^[40] The scan in the positive potential region shows an irreversible oxidation of the ligand at high potentials (~ 1.2 V) showing that the ligand is oxidatively robust (**Fig. 5.5**).^[41]

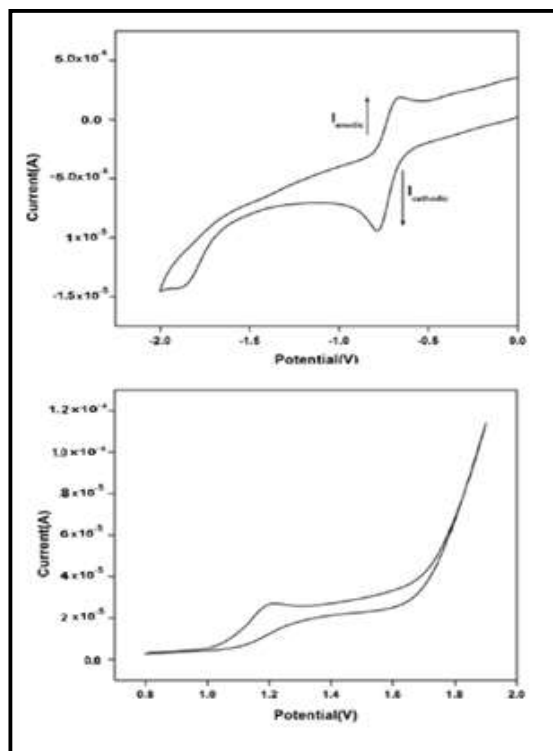


Fig. 5.5 : Cyclic voltametric plot of complex 1

5.3.6 DNA binding studies

5.3.6.1 UV–visible spectral studies

The study of the interaction of small molecules with DNA has been the subject of intensive investigation for decades. It provides insight into the screening design of new and more efficient multifarious drugs targeting to DNA for the development of anticancer drugs. However, most drugs bind to DNA through non-covalent interaction such as groove binding, intercalation and non-specific electrostatic surface binding.^[36,42] Hence, absorption titration can be used to observe the nature of interaction of molecules with DNA. The absorption spectra of complex **1** in absence and in the presence of CT-DNA (at constant concentration of the complex) are given in **Fig. 5.6**. The absorption spectra of the complex in DMSO – buffer mixture (4×10^{-5} M) displays an intense interligand $\pi \rightarrow \pi^*$ absorption that is characteristic for this complex at 380 nm and the higher energy band at 305 nm may be due to some other charge transfer band. In the presence of fixed metal

complex concentration and increasing concentrations of CT-DNA, $(3.3-22.5) \times 10^{-5}$, ratio $[\text{DNA}]/[\text{Complex 1}] = (0.0, 0.80, 1.6, 2.4, 3.2, 4.0, 4.8)$, a marked hyperchromism is observed with a strong red shift of 18 nm,^[43] suggesting covalent binding. Presence of red shift indicates coordination of complex with DNA through N7 position of guanine. Hyperchromism results from breakage of secondary structure of DNA due to the fact that phosphate group can provide the suitable anchors for coordination with the complex. The intrinsic binding constant, K_b , of the complex to CT DNA has been determined from Wolfe–Shimer Equation, through a plot of $[\text{DNA}]/\epsilon_a - \epsilon_f$ vs. $[\text{DNA}]$, where $[\text{DNA}]$ represents the concentration of DNA, and ϵ_a , ϵ_f and ϵ_b the apparent extinction coefficient ($A_{\text{obs}}/[\text{M}]$), the extinction coefficient for free metal complex (M), and the extinction coefficient for the metal complex (M) in the fully bound form, respectively. In plots of $[\text{DNA}]/\epsilon_a - \epsilon_f$ vs. $[\text{DNA}]$, K_b is given by the ratio of slope to intercept^[44]. K_b has been found to be $1.68 \times 10^5 \text{ M}^{-1}$ which suggests a modest DNA intercalative binding affinity for the complex.

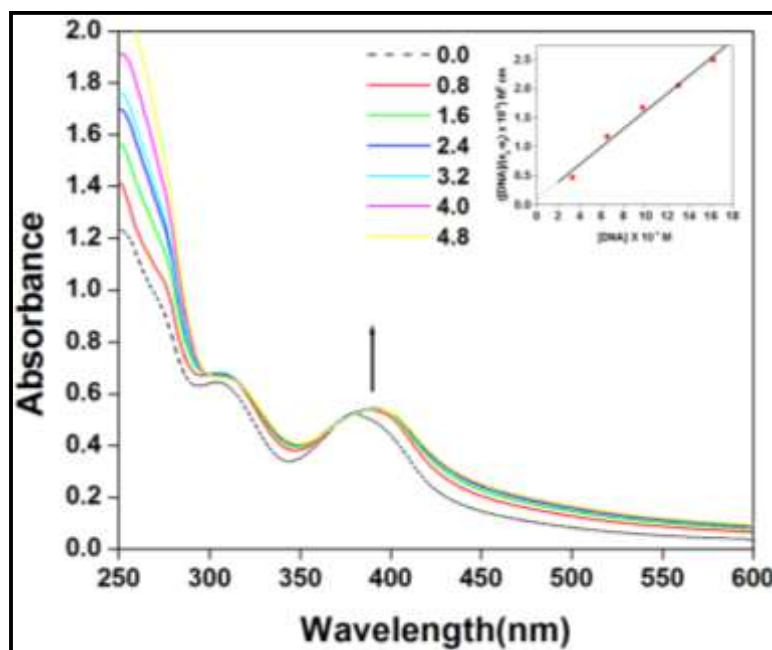


Fig. 5.6 : Absorption spectra of complex 1 in absence (---) and in the presence (—) of increasing concentration of CT-DNA. $[\text{Complex 1}] = 4 \times 10^{-5} \text{ M}$. The upside arrow shows the absorbance changes upon increasing the DNA concentration. Inset: linear plot for the calculation of the intrinsic DNA binding constant (K_b).

5.3.6.2 Competitive binding assay

To further verify an intercalative binding of the Cu(II) complex to DNA, competitive binding experiment involving the addition of the complex to DNA pretreated with ethidium bromide (EB), a typical indicator of inter-calation, and subsequent measurement of the absorption intensity has been performed by UV-vis spectroscopy (**Fig. 5.7**). Initially, the absorbance of free ethidium bromide is measured and then DNA is added to it. The concentration of ethidium bromide and DNA both have been kept at 13.3×10^{-5} M. As seen in the figure, the maximum absorption peak of EB at 479 nm decreases and shifts to 484 nm after addition of DNA, which is characteristic of intercalation of EB into the DNA base pairs. Upon addition of the complex at increasing concentration ($0 - 10 \times 10^{-6}$) to the EB-DNA system, a continuous increase in the maximum absorption and blue shift toward its original position have been observed, indicating that there exists a competitive intercalation between the complex and EB with DNA, thus releasing some free EB from the DNA-EB system.^[45]

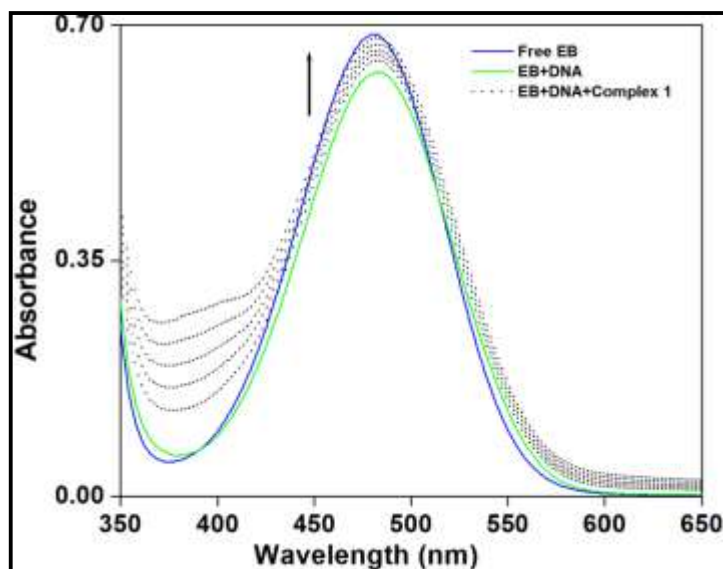


Fig. 5.7 : Absorption spectra of free EB and EB bound to CT-DNA in the absence and presence of increasing amount of the complex 1. [EB] = [DNA] = 13.3×10^{-5} M, [Complex 1] = $0 - 10 \times 10^{-6}$ M. The upside arrow shows the absorbance changes upon increasing the complex concentration

5.3.6.3 Fluorescence quenching spectroscopy

EB is a classical intercalator that gives significant fluorescence emission intensity when it intercalates into the base pairs of DNA. When it is replaced or excluded from the internal hydrophobic circumstance of the DNA double helix by other small molecules, its fluorescence emission is effectively quenched by external polar solvent molecules like H₂O.^[46] The fluorescence quenching curves of EB bound to DNA in absence and in the presence of the complex are shown in **Fig. 5.8**. A remarkable reduction in emission intensity has been observed as the complex is added to the EB-DNA system, indicating that some EB molecules have been replaced by the complex and released into solution from EB-DNA adduct, characteristic for the intercalative binding of the complex to DNA. Initially, the fluorescence intensity of free EB is remarkably increased on the addition of DNA. Concentrations of both EB and DNA have been kept equal at 6.7×10^{-5} M and titrated with gradually varying concentrations of complex **1** in [complex **1**]/[DNA] ratio of 0.28 to 2.26. The fluorescence intensities have been measured with the excitation wavelength set at 525 nm (λ_{max} for EB) and the fluorescence emission at 592 nm has been recorded. The fluorescence quenching results are in good agreement with the obtained results by UV spectroscopic studies. The quenching efficiency for each complex has been evaluated by the Stern–Volmer constant K_{sq} , which varies with the experimental conditions.^[47]

$$I_0 / I = 1 + K_{\text{sq}}r$$

where I_0 and I are the fluorescence intensities in absence and in the presence of complex **1**, respectively, and r is the ratio of total concentration of complex to that of DNA. K_{sq} is a linear Stern–Volmer quenching constant. The quenching plots illustrate that the fluorescence quenching of the EB-DNA system by the complex is in good agreement with the linear Stern–Volmer equation, with the K_{sq} value obtained as the ratio of the slope to intercept 0.135.

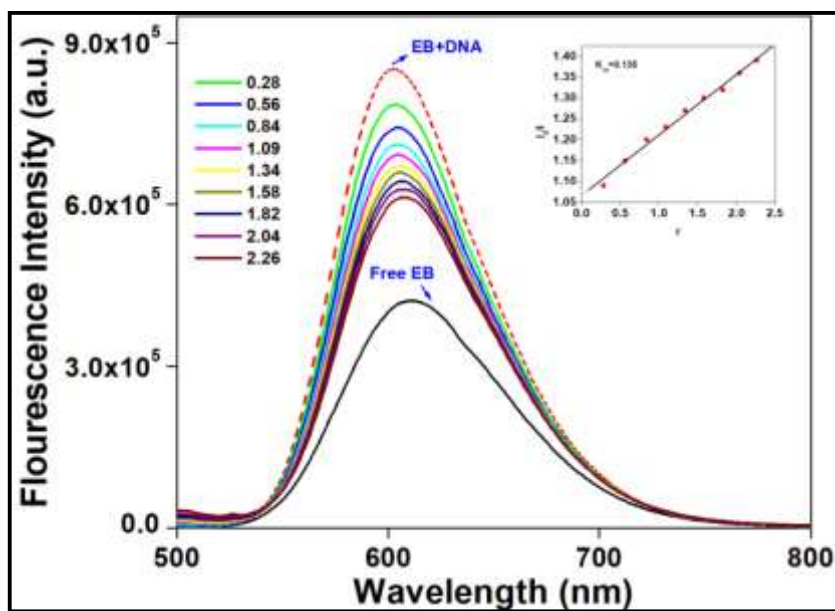


Fig. 5.8 : Emission spectra of EB bound to CT-DNA in absence (---) and in the presence (—) of complex 1. [Complex 1]/[DNA] = 0, 0.28, 0.56, 0.84, 1.09, 1.34, 1.58, 1.82, 2.04, 2.26; $\lambda_{\text{ex}}= 525 \text{ nm}$. Inset: Stern–Volmer quenching curve

5.3.6.4 Cyclic voltametry

Electrochemical techniques are complementary to other related biophysical techniques that are applied to study the interaction between the redox active molecules and biomolecules. The cyclic voltammogram of the complex has been recorded in absence and in the presence of CT-DNA in aqueous solution (buffer 50 mM NaCl/5 mM Tris–HCl pH 7.2) (**Fig. 5.9**). The supporting electrolyte has been chosen to be KCl. A significant reduction in their respective peak potentials, cathodic and anodic peak currents can be attributed to slow diffusion of the equilibrium mixtures of these complexes (free and DNA bound) at the electrode surface. The negative shift in the E_{PC} or E_{PA} value reveals the involvement of electrostatic interactions in the binding process of DNA and complex.^[48]

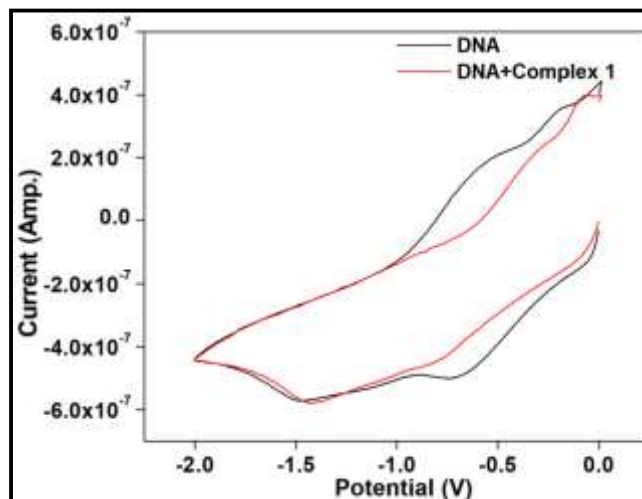


Fig. 5.9 : Cyclic voltammogram of DNA in absence and in the presence of complex 1

5.3.6.5 Circular Dichroism spectral studies on DNA binding

CD spectroscopy is a useful technique in diagnosing changes in DNA morphology during drug-DNA interactions. The CD spectrum of CT-DNA exhibits a positive band at 274 nm due to base stacking and a negative band at 242 nm due to the right-handed helicity of the B-DNA form,^[49] which are quite sensitive to the modes of inter-action between small molecules and DNA. Simple electrostatic or groove binding interaction of complexes with DNA shows less or no perturbation of the base stacking and helicity bands,^[50] while an inter-calative interaction enhances the intensities of both bands. The interaction of complex 1 with DNA induces a change in the CD spectrum of B-DNA as shown in **Fig. 5.10**. The intensities of both the negative and positive bands decreased significantly (shifting to zero levels) with the increasing concentration of the complex, accompanied with a small red shift (242 → 244 nm and 274 → 284 nm for negative and positive bands, respectively), suggesting that the complex intercalates to the DNA double helix and disturbs the base stacking involving a stacking interaction between the aromatic heterocyclic plane of the Cu(II) complex and the adjacent base pairs of DNA. This binding interaction induces certain conformational changes within DNA, such as the conversion from a more B-like to a more C-like structure.^[51] Furthermore, the formation of the hydrogen bonds between the Cu(II) complex and DNA bases may also make some differences.

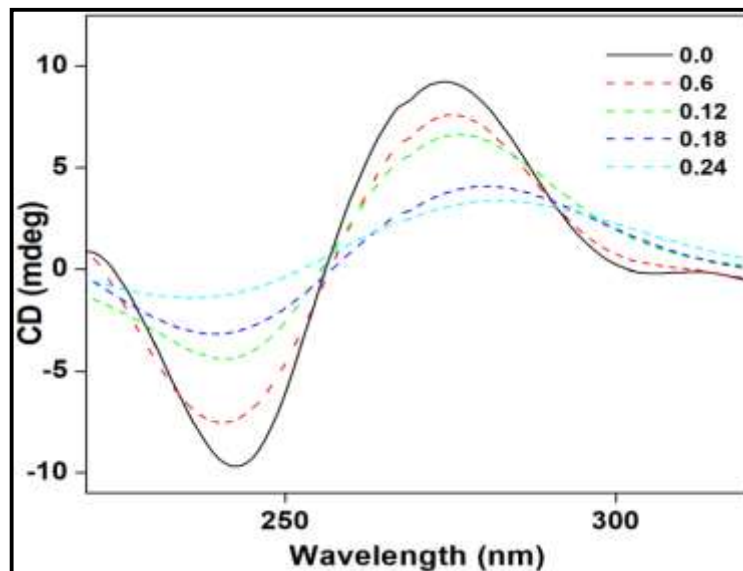


Fig. 5.10 : CD spectra of DNA (1.2×10^{-4} M) in absence (—) and in the presence (---) of complex 1 in the $[\text{Complex 1}]/[\text{DNA}] = 0.6, 0.12, 0.18$ and 0.24 .

5.3.6.6 DNA cleavage studies

The DNA cleavage activities of complex **1** have been studied by supercoiled FAM134BGFP plasmid DNA as a substrate in a medium of 100 mM Tris–HCl/NaCl buffer (pH = 7.5) under physiological conditions. The DNA is seen to be chopped when treated with the complex and the intact DNA is seen as a smear in the agarose gel electrophoresis. We have performed a concentration dependant study. The concentration of the metal complex has been increased from 20 to 40 μM gradually in 100 mM Tris–HCl/NaCl buffer (pH = 7.2) and 0.5 $\mu\text{g}/\mu\text{L}$ (6.53 nM) DNA is added to the mixture in the presence H_2O_2 (2 μM) and incubated for 30 min at 36 °C. Te results are shown in **Fig. 5.11**. The chopping off of DNA is clearly seen. We have initially standardized the time of 30 min by trying various time intervals starting from 2 min. The nuclease activity of the complex is really very high as no further breakage into other forms of the DNA has been seen but vigorous chopping off is evident from the very start. The results clearly show that as the concentration of metal complex is increased gradually, the cleavage is more pronounced and at 40 μM concentration the DNA is completely chopped off. This shows the complex is actually binding to DNA and chopping it off. The

control tests have been done with all reagents except the complex. It shows no cleavage as shown in Fig. 8. The role of H_2O_2 is very crucial in this process because without the presence of H_2O_2 the cleavage is not very effective as seen from experimental results. It can be claimed that cleavage of this type of complex most likely occurs through an oxidative mechanism. In the presence of the reducing agent H_2O_2 , the Cu(II) complexes could be reduced to the CuI complexes.^[52] The CuI complex then reacted with endogenous oxygen to produce hydrogen peroxide, which could again react with another equivalent of CuI complex to generate copper-oxido species with DNA damaging properties. The efficient DNA cleavage activity of these complexes in the presence of external H_2O_2 is probably due to the generation of a higher concentration of CuI ions. Most cancer cells have an elevated intracellular concentration of H_2O_2 , which may facilitate the intracellular generation of highly active copper-oxido species and ROS, causing oxidative DNA damage in cells.^[53] So, H_2O_2 enhances the cleavage process started by the metal complex.

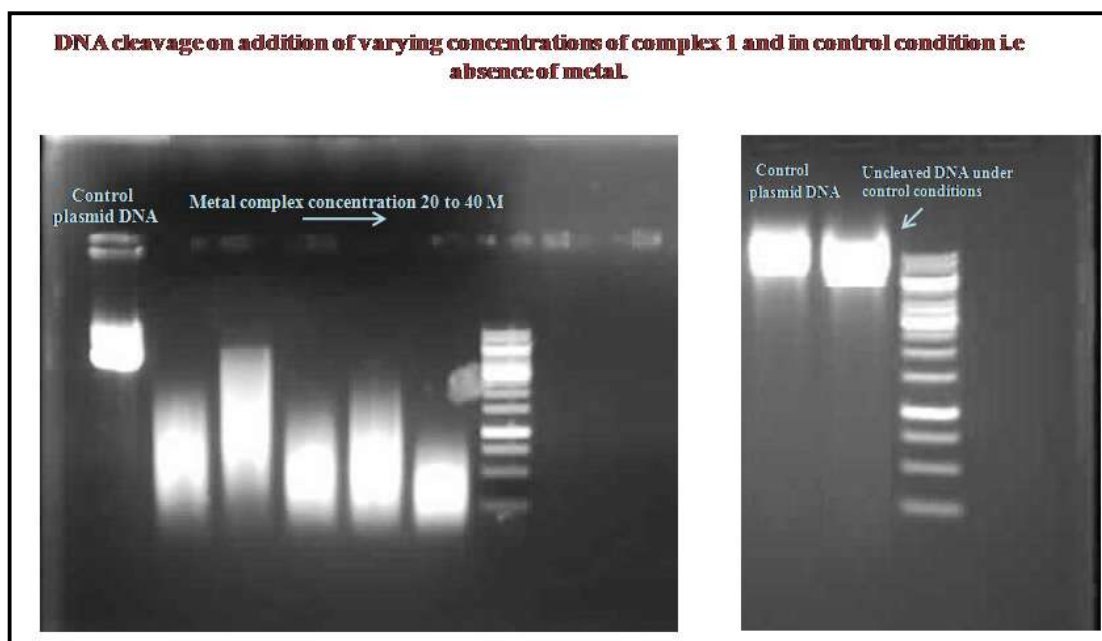


Fig. 5.11 : DNA cleavage by adding varying amounts of complex 1.

In order to obtain a good knowledge of the active chemical species that is responsible for the DNA damage activities for the complex, we have further investigated the influence of different potentially inhibiting agents including hydroxyl radical scavenger (DMSO, EtOH, *tert.*-butyl alcohol), reducing agent (GSH), singlet oxygen quenchers (NaN₃), hydrogen peroxide scavenger (KI), redox reagent (DTT), chelating agent (EDTA) and DNA minor groove binding agent (DAPI) (**Fig. 5.12**). The DNA has been taken at 500 ng and the various additives at 0.4 mM concentration. The rest of the reagents like Tris/NaCl, H₂O₂ and the metal complex have been taken at the concentrations optimized in the previous set of experiment. Addition of DMSO shows no inhibition in cleavage process as we can see from lane 2 that the plasmid has been entirely chopped. But EtOH shows a marked decrease in the cleavage as seen in lane 3 of the gel electrophoresis data, and so does *tert.*-butyl alcohol as seen in lane 6, which demonstrates that the hydroxyl radical participates in the oxidative DNA cleavage, with an inhibitory activity observed from the addition of EtOH and *tert.*-butyl alcohol. The addition of reducing agent GSH significantly reduces the cleavage action of the complex as seen in lane 4. Sodium azide does not have any significant effect on the DNA cleavage (lane 5). This fact rules out the involvement of ¹O₂ or singlet oxygen-like entities. When hydrogen peroxide scavenger potassium iodide (lane 7) is added to the reaction mixture, the DNA cleavage mediated by the complex has been inhibited to some extent, confirming that freely diffusible hydroxyl radical is one of the intermediates involved in the DNA scission process. Reducing agent like DTT also reduces the cleavage action of the complex (lane 8). The chelating agent EDTA totally inhibited DNA cleavage (lane 9), indicating Cu(II) complex plays the key role in the DNA breakage. The cleavage is unaffected by the addition of minor groove binder (DAPI) which shows the non-affinity of the complex towards DNA groove (lane 10).^[36,52] From these results we can conclude that complex **1** is capable of promoting DNA cleavage through an oxidative DNA damage pathway, and hydroxyl radical and hydrogen peroxide are the active species involved in the cleavage reaction.

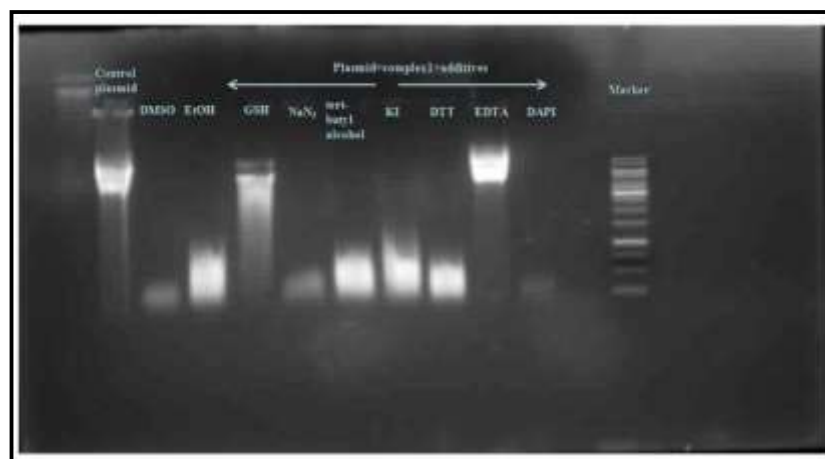


Fig.5.12 : DNA cleavage studies in the presence of various additives.

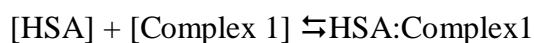
5.3.7 HSA binding studies

5.3.7.1 Absorption spectra studies

UV-vis absorption spectra have been used to monitor the changes in the secondary structure of protein (HSA) induced by complex 1 (**Fig. 1.13**). The strong absorption peak at 208 nm originates from the $n \rightarrow \pi^*$ transition for the peptide bond of α helix in HSA; the comparatively weaker absorption peak at 280 nm arises from the phenyl rings in aromatic acid residues (Trp, Tyr and Phe).^[54] Upon incremental addition of the complex ($0.76\text{-}5.8 \times 10^{-5}$ M) to HSA of constant concentration (4.0×10^{-6} M), a dramatic decrease in the 208 nm absorbance peak has been observed which can be put down to the induced perturbation of α -helix of HSA by a specific interaction with the complex. Besides, an obvious red shift (from 208 to 226 nm) in the position of the absorbance peak indicates that the microenvironment of Trp-214 residue in HSA is altered and the tertiary structure of the HSA has been destroyed. Simultaneously, the intensity of the absorption peak at 280 nm is increased by addition of the complex, suggesting that aromatic acid residues originally buried in a hydrophobic cavity in HSA are exposed to an aqueous milieu to a certain degree. Moreover, the π - π stacking interaction between aromatic rings of complex 1 and phenyl rings of aromatic acid residues also makes some differences.

In order to evaluate the binding propensity quantitatively with HSA, the intrinsic binding constant (K) of complex 1 with HSA has been determined. By assuming that there is only

one type of interaction between complex 1 and HSA in aqueous solution,^[54]



$$K = [\text{HSA : Complex 1}] / [\text{HSA}][\text{Complex 1}]$$

where K is the binding constant for complex, assuming $[\text{HSA: Complex}] = C_B$

$$K = C_B / [C_{\text{HSA}} - C_B] [C_{\text{Complex 1}} - C_B]$$

where C_{HSA} and $C_{\text{complex 1}}$ are analytical concentration of HSA and complex in the solution, respectively. According to the Beer–Lambert law

$$C_{\text{HSA}} = A_0 / \epsilon_{\text{HSA}} \cdot l$$

$$C_B = (A - A_0) / \epsilon_B \cdot l$$

where A_0 and A are the absorbance of HSA at 280 nm, in absence and in the presence of complex 1, respectively.^[36] ϵ_{HSA} and ϵ_B are the molar extinction coefficient of HSA and the bound complex, respectively, and l is the light path of the cuvette (1 cm).

By substituting ϵ_{HSA} and ϵ_B in Equations.

$$A_0 / (A - A_0) = \epsilon_{\text{HSA}} / \epsilon_B + \epsilon_{\text{HSA}} \cdot l / \epsilon_B K C_{\text{Complex 1}} \cdot l$$

Thus, the double reciprocal plot of $1/A - A_0$ vs. $1/\text{Complex}$ is linear and the binding constant can be estimated from the ratio of the intercept to the slope. The K_B has been found to be $1.91 \times 10^4 \text{ M}^{-1}$.

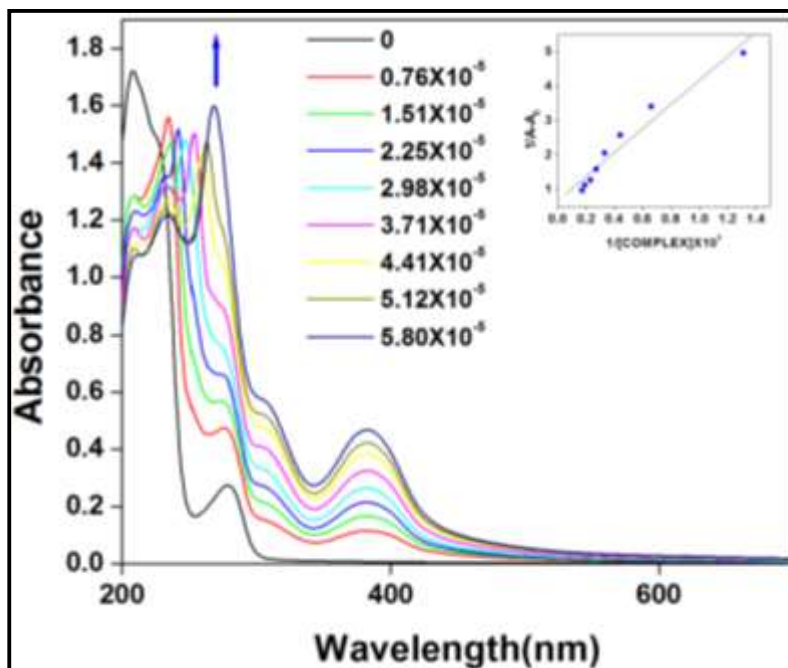


Fig. 5.13 : UV absorption spectra of the complex 1 in presence of HSA obtained in 5 mM Tris–HCl buffer, pH 7.2, at room temperature: [HSA]= 4×10^{-6} M; [complex 1] = 0, 0.76, 1.51, 2.25, 2.98, 3.71, 4.41, 5.12, 5.80×10^{-5} M, respectively. Arrow shows the intensity changes upon increasing concentration of complex 1. Inset: Plot of $1/A-A_0$ vs. $1/[\text{Complex}]$.

5.3.7.2 Fluorescence quenching studies

Fluorescence spectroscopy is an effective method used to explore the interaction between small molecules and bio macromolecules. The fluorescence emission spectra of Human serum albumin (HSA) have been recorded in the range of 300–500 nm by exciting the HSA at 280 nm in the presence of various concentration of the Cu(II) complex (**Fig. 5.14**). HSA is the most abundant plasma protein and displays extraordinary drug binding capacity, providing a depot and carrier for many endogenous and exogenous behaviors towards the complex. The intrinsic fluorescence of HSA mainly comes from tryptophan residue when excited at 295 nm. Phenylalanine has a very low quantum yield and the fluorescence of tyrosine is almost totally quenched if it is ionized or present near to an amino group, a carboxyl group or a tryptophan since tyrosine and phenylalanine does not absorb in this region. The HSA shows a strong fluorescence emission with a peak at 344 nm, while complex 1 has no intrinsic fluorescence under the present experiment conditions. The fluorescence intensity of the HSA (fixed concentration, 4×10^{-6} M) decreases continually with increasing concentration of the complex (0.76×10^{-5} to $5.81 \times$

10⁻⁵ M) indicating that the binding of the complex to HSA changes the local micro environment around the Trp-214 residue in HSA, and concomitantly the tertiary structure of the HSA.

Commonly, fluorescence quenching can be described by the Stern–Volmer equation:^[47]

$$F_0/F = 1 + K_q\tau_o [Q] = 1 + K_{sv} [Q]$$

where F_0 and F are the fluorescence intensities in absence and in the presence of quencher, respectively, K_q , K_{sv} , τ_o and $[Q]$ are the quenching rate constant of the biomolecules, the Stern–Volmer quenching constant, the average life time of the molecule without quencher ($\tau_o = 10^{-8}$ s) and the concentration of the quencher, respectively. The Stern–Volmer plots of F_0/F versus $[Q]$ for the quenching of HSA fluorescence by complex **1** is depicted and the calculated K_{sv} and K_q values have been found to be $4 \times 10^5 \text{ M}^{-1}$ and $4 \times 10^{13} \text{ M}^{-1} \text{ s}^{-1}$, respectively. The observed K_q value is larger than the limiting diffusion constant K_{dif} of the biomolecules ($K_{dif} = 2.0 \times 10^{10} \text{ M}^{-1} \text{ s}^{-1}$), indicating that the fluorescence quenching is happened due to the specific interaction of complex **1** with HSA, consistent with the static quenching mechanism.^[55,56] For static quenching, the Scatchard equation is employed to calculate the binding constant and number of binding sites,^[57] $\log [F_0 - F / F] = \log K + n \log [Q]$ where, F_0 and F are the fluorescence intensities of HSA in absence and in the presence of quencher, K and n are the binding constant and the number of binding sites, respectively. Thus, a plot of $\log[(F_0 - F)/F]$ versus $\log[Q]$ is used to determine K (binding constant) from the intercept on Y-axis and n (binding sites) from the slope of the inset graph. From the corresponding Scatchard plot, the K and n values are found to be $1 \times 10^7 \text{ M}^{-1}$ and 1.54, respectively, which is comparable to those observed for previously reported binding constant.

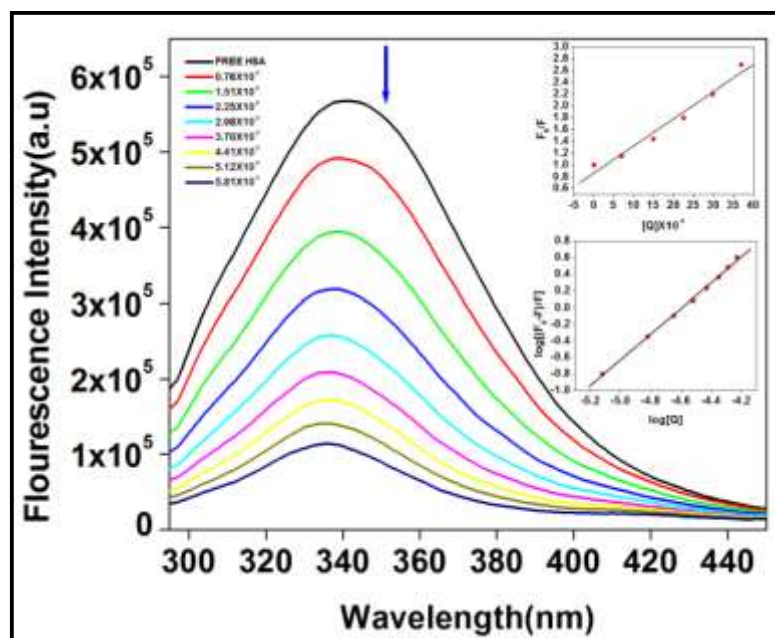


Fig. 5.14 : The fluorescence quenching spectra of HSA by different concentrations of complex 1 with the excitation wavelength at 295 nm in 5 mM Tris–HCl buffer, pH 7.2, at room temperature: [HSA], 4.0×10^{-6} M; the concentration of complex 1 = 0, 0.76, 1.51, 2.25, 2.98, 3.70, 4.41, 5.12, 5.81 $\times 10^{-5}$ M, respectively. Arrow shows the intensity changes upon increasing concentration of the quencher.

5.3.7.3 Energy transfer and binding distance between the complex 1 and HSA

Fluorescence energy transfer occurs via overlapping of the spectrum of a fluorophore (donor) with the absorption spectrum of a molecule (acceptor). The overlap of the absorption spectrum of complex 1 with the fluorescence emission spectrum of HSA is observed (**Fig. 5.15**). Here the donor and acceptor are HSA and the complex, respectively.

A Forster resonance energy transfer (FRET) mechanism is involved in the quenching of Trp fluorescence by complexes, the efficiency of energy transfer (E) can be given by^[58]

$$E = 1 - F/F_0 = R_0^6 / R_0^6 + r^6$$

where F and F_0 are the fluorescence intensities of HSA in the presence and in absence of quencher, respectively, r is the distance between acceptor and donor, and R_0 is the critical distance when the transfer efficiency is 50%. The value of R_0

can be calculated using the equation:^[59]

$$R_0^6 = 8.78 \times 10^{-25} K^2 n^{-4} \phi J$$

where K^2 is the spatial orientation factor between the emission dipole of the donor and the absorption dipole of the acceptor, n is the refractive index of the medium, ϕ is the fluorescence quantum yield of the donor, and J is the overlap integral of the fluorescence emission spectrum of the donor and the absorption spectrum of the acceptor and can be given by:^[53]

$$J = \frac{\int_0^\infty F(\lambda) \epsilon(\lambda) \lambda^4 d\lambda}{\int_0^\infty F(\lambda) d\lambda}$$

where $F(\lambda)$ is the corrected fluorescence intensity of the donor at wavelength λ , and $\epsilon(\lambda)$ is the molar absorption coefficient of the acceptor at wavelength λ . Under the experimental conditions, for a solution with random orientation as in this case, $K^2 = 2/3$, $n = 1.36$, $\phi = 0.15$, J was calculated to be 6.54×10^{-14} (from the graph), R_0 found to be 3.44 nm, $E = 0.3$ and $r = 3.96$ nm. The distance between HSA and complex 1 is less than 7 nm, indicating that a static quenching interaction has occurred.

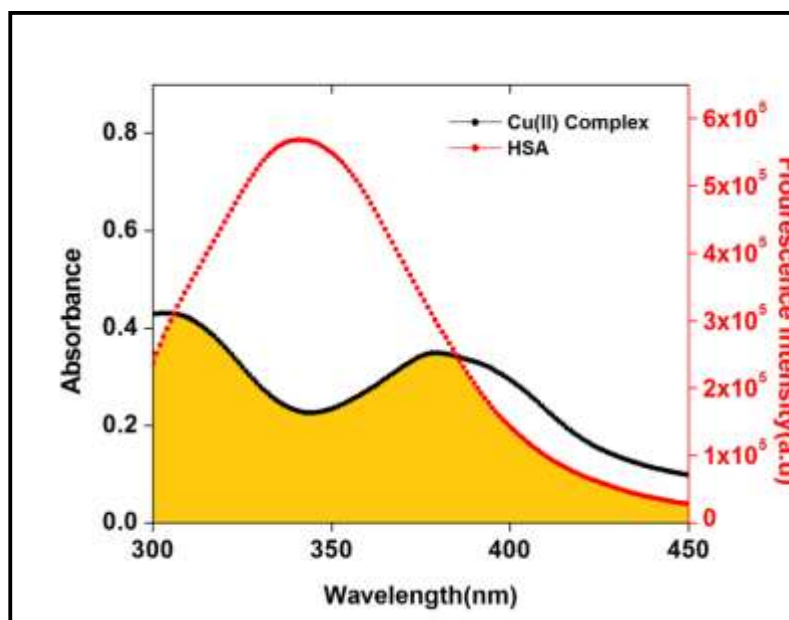


Fig. 5.15 : Overlap of the fluorescence spectra of HSA and the absorbance spectra of the Cu(II) complex, $[HSA] = [Cu(II) \text{ complex}] = 4.0 \times 10^{-6} M$.

5.3.7.4 IR spectral studies

IR spectrum of proteins is typically used to determine conformational changes in the structure of proteins. Infrared spectra of proteins show a number of amide bands that represent different vibrations of peptide moiety (**Fig. 5.16**). The spectrum has been obtained by subtracting the absorption of Tris buffer from the spectrum of HSA solution. The protein amide bands have a relationship with the secondary structure of protein, and amide I band is more sensitive to the change of protein secondary structure than amide II and amide III. The evident peak shift of amide I band from 1649.4 to 1657 cm^{-1} , amide II band from 1547.03 to 1553.65 cm^{-1} reveals the interaction between complex 1 and HSA.^[52] These changes in these peak positions demonstrate that the secondary structure of HSA has been changed upon the interaction resulting in the perturbation of amide vibrational frequencies.^[60]

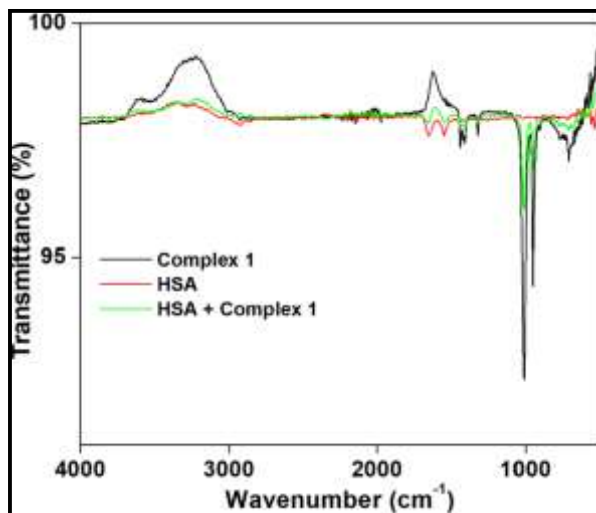


Fig. 5.16 : FTIR spectra of complex 1, HSA and complex 1 + HSA.

5.3.7.5 3D fluorescence spectral studies

The 3D fluorescence of HSA has been studied initially and after binding with complex 1. The first peak, Peak A is a Rayleigh scattering peak ($\lambda_{\text{ex}} = \lambda_{\text{em}}$), Peak B ($\lambda_{\text{ex}} = 280 \text{ nm}$, $\lambda_{\text{em}} = 350 \text{ nm}$), mainly reflects the spectral behavior of the Trp residue, and the maximum emission wavelength and fluorescence intensity of the residue associated with its micro environment's polarity (**Fig. 5.17**). Peak C is the second-ordered scattering peak ($\lambda_{\text{em}} \approx 2$

λ_{ex}).^[59] It could be seen that after interaction with complex, intensity of peak A significantly increases while that of peak B decreases remarkably. Peak C shows huge increase in the intensity.^[52] All of these facts prove that the interaction of the complex with HSA induces some conformational and micro environmental changes in HSA, corroborated well our spectroscopic results obtained from UV–vis, fluorescence and CD measurements.

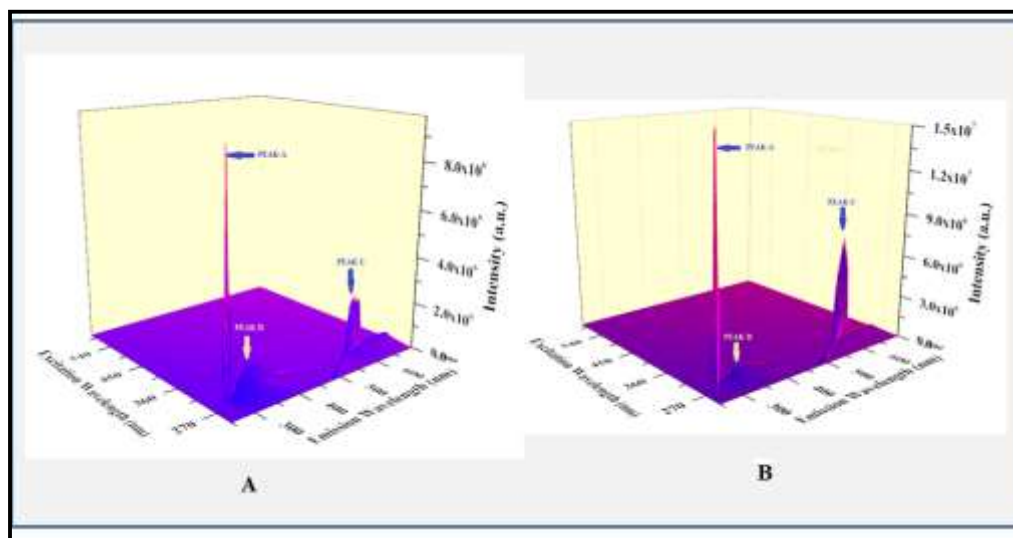


Fig. 5.17 : 3D fluorescence spectrum of HSA (A), and Cu(II) complex–HSA conjugate system (B). [HSA] = [Cu(II) complex] = 1.0×10^{-5} M pH 7.2, at room temperature.

5.3.7.6 Circular Dichroism

CD measurement has been performed in the presence of the Cu(II) complex at different concentrations to ascertain the possible influence of the complex binding on the secondary structure of HSA. As the figure (**Fig. 5.18**) shows, the CD spectra of HSA (line a) exhibit two negative bands in the ultraviolet region at 206 and 220 nm assignable to $\pi \rightarrow \pi^*$ and $n \rightarrow \pi^*$ transfers for the peptide bond, respectively, which are characteristic of α -helix structure of the protein. With the addition of complex **1**, the CD signal of HSA increases, indicating that the binding of the complex induces a significant conformational change in HSA. Moreover, the CD spectra of HSA change a lot in shape also after

addition of the complex which proves that a lot of α -helical part has been destroyed on binding.^[59]

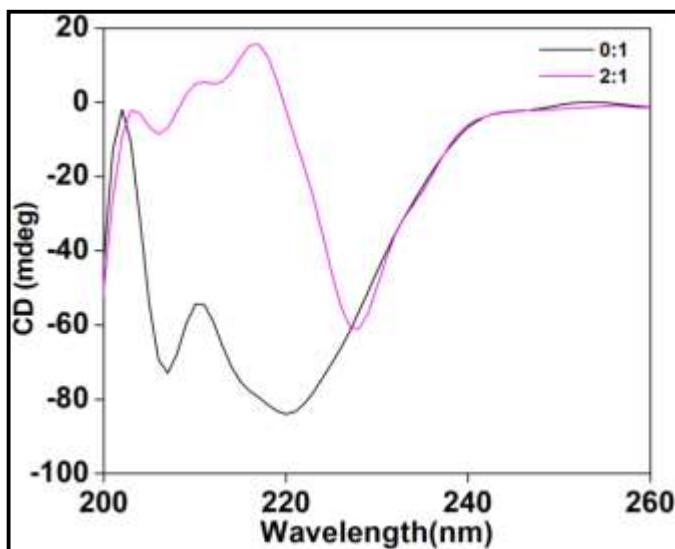


Fig. 5.18 : CD spectra of HSA in the absence and presence of the complex 1 : (a) 1.5×10^{-6} M HSA;(b) 1.5×10^{-6} M HSA + 3.0×10^{-6} M complex 1.

5.3.7.7 Oxidative damage of HSA by complex 1

After being incubated with complex 1, for 30 min, at 37 °C, in the presence of hydrogen peroxide, HSA exhibits remarkable degradation as indicated by a continuum of protein fragments at SDS–PAGE in 12% acrylamide gel while for the control condition, which does not include the complex, there is no degradation at all. We see the clear and thick protein band at the expected molecular weight range. Different concentrations of the protein and the metal complex have been incubated with H_2O_2 .^[60] Blank sets have been also kept for comparison. The results have been indicated in **Fig. 5.19**

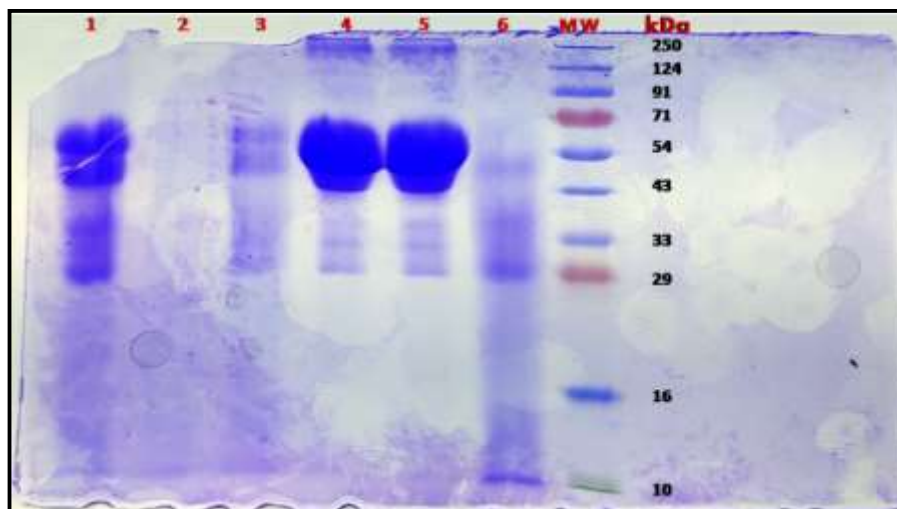


Fig. 5.19 : SDS–PAGE electrophoresis in 12% polyacrylamide gel of HSA fragmentation, in the presence of complex 1, treated with H₂O₂, for 30 min at 37 °C, in Tris buffer 100 mM, pH 7.2, MW: Molecular weight marker, Lane 1:75 μM HSA , 75 μM complex and 750 μM H₂O₂ , Lane 2: 25 μM HSA, 50 μM complex and 750 μM H₂O₂ , Lane 3: 50 μM HAS, 100 μM complex and 750 μM H₂O₂, Lane 4: Blank (75 μM HSA and 750 μM H₂O₂), Lane 5: Blank (75 μM HSA), Lane 6: 75 μM HSA , 200 μM complex and 750 μM H₂O₂.

5.3.8 Antibacterial study by complex 1

Different concentrations (400 μg/mL, 350 μg/mL, 250 μg/mL, 100 μg/mL, 25 μg/mL, 10 μg/mL) of complex 1 have been added to the bacterial cells in 2.0 mL LB broth and followed by incubation in a 37 °C incubator. The next day, growth has been observed in the test tubes (**Fig. 5.20**). From the tubes, fixed amount of cell mixture has been plated on LB media again followed by incubation at 37 °C. After overnight incubation, the cell colonies have been counted on the LB plates. A stark decrease in the number of colonies were observed for both gram positive *S. aureus* and gram negative *E. coli* with increasing concentration of complex 1 which clearly indicates a strong antibacterial property of the complex.

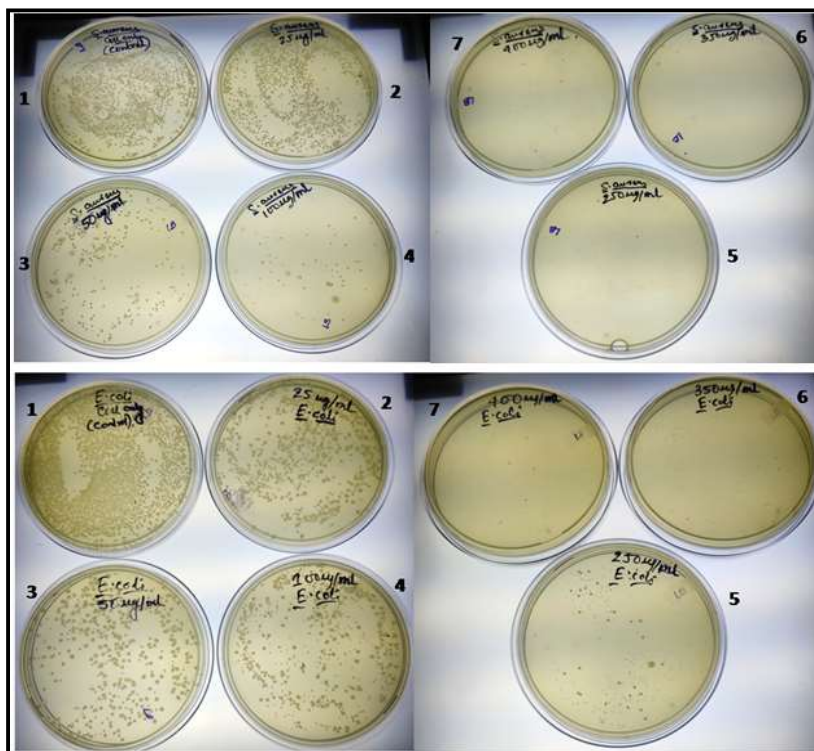


Fig. 5.20 : *S. aureus* and *E. coli* colonies with gradually increasing concentrations of complex 1 , 1: control (without complex 1), 2: 25 µg/ml complex 1, 3: 50 µg/ml complex 1, 4: 100 µg/ml complex 1, 5: 250 µg/ml complex 1, 6: 350 µg/ml complex 1, 7: 400 µg/ml complex 1.

5.3.9 Apoptosis evaluation by DAPI staining

To visualize nuclear changes, HeLa cells have been treated with complex 1 at different concentrations (5 µM, 10 µM, 20 µM) for three time intervals (12 h, 24 h, 48 h). After treatment, the cells have been fixed and stained with DAPI and visualized on a fluorescence microscope. The cells have been observed to undergo a stark change with increasing concentration and time of treatment (**Fig. 5.21**). It is clear from the figure that as time of treatment and the concentration of complex 1 have been increased, the more number of nucleuses show structure deterioration. The white arrows indicate more number of bilobed nuclei. Such bilobed structure and nuclear shrinkage can be seen with increasing complex concentration and time of treatment. Moreover, as seen from the bright field images, that the HeLa cells show clear rounding and shrinkage which is a clear indication of apoptosis.

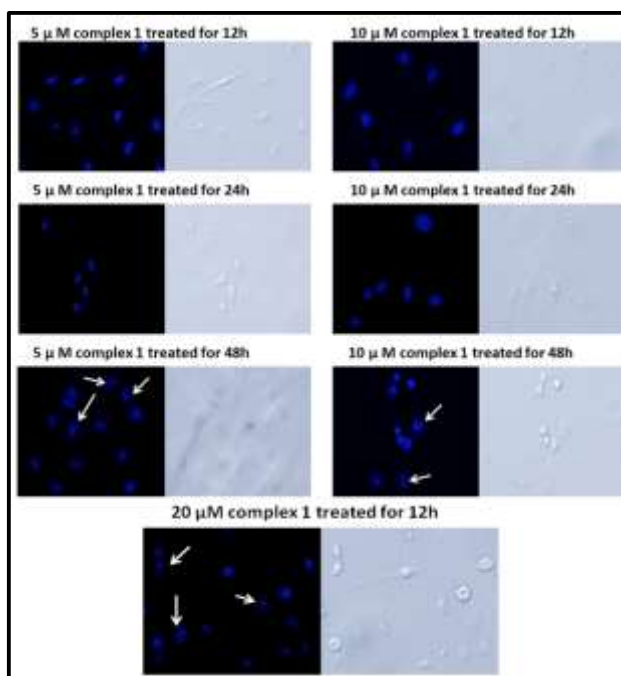


Fig. 5.21 : Confocal microscopy images of HeLa cells treated with different concentrations of complex 1 and different durations.

5.4 Conclusion

In summary, a mononuclear copper(II) complex (Complex 1) with an N,O-donor ligand has been prepared. This has been prepared under mild conditions and characterized by different techniques including single crystal X-ray diffraction analysis. From different studies, it has been observed that complex 1 shows the intercalative binding with DNA. Moreover, it exhibits protein (here HSA) binding properties with appreciable changes in protein structure. This indicates that the complex could be transported by human serum albumin into the blood. Antibacterial activity of the complex has been observed for both gram positive *S. aureus* and gram negative *E. coli*. When HeLa cells have been treated with complex 1, a clear indication of apoptosis has been noticed. All of these facts indicate the complex could be a potential candidate for chemotherapeutic applications.

5.5 References

- [1] a) B. Rosenberg, L. Vancamp, J. E. Trosko and V. H. Mansour, *Nature*, **1969**, 222, 385.
- [2] R. Oun, Y. E. Moussa and N. J. Wheate, *Dalton Transactions*, **2018**, 47, 6645.
- [3] a) C. Santini, M. Pelli, V. Gandin, M. Porchia, F. Tisato and C. Marzano, *Chemical Reviews* **2014**, 114, 815; b) W. Liu and R. Gust, *Coordination Chemistry Reviews*, **2016**, 329, 191; c) U. Ndagi, N. Mhlongo and M. E. Soliman, *Drug Design Development and Therapy* **2017**, 11, 599; d) T.J.P. McGivern, S. Afsharpour and C.J. Marmion, *Inorganica Chimica Acta* **2018**, 472, 12; e) D. Denoyer, S. Masaldan, S. L. Fontaine and M. A. Cater, *Metallomics*, **2015**, 7, 1459; f) R. Tabti, N. Tounsi, C. Gaidon, E. Bentouhami and L. Désaubry, *Medicinal Chemistry*, **2017**, 7, 875.
- [4] a) C. R. Munteanu and K. Suntharalingam, *Dalton Transactions*, **2015**, 44, 13796; b) A. Bergamo and G. Sava, *Dalton Transactions* **2011**, 40, 7817; c) C. J. Dhanaraj, I. U. Hassan, J. Johnson, J. Joseph and R. S. Joseyphus, *Journal of Photochemistry and Photobiology B*, **2016**, 162, 115; d) M. A. Malik, O. A. Dar, P. Gull, M. Y. Wani and A. A. Hashmi, *Medicinal Chemistry Communications* **2018**, 9, 409; e) T. Zou, C.-N. Lok, P.-K. Wan, Z.-F. Zhang, S.-K. Fung and C.-M. Che, *Current Opinions in Chemical Biology* **2018**, 43, 30.
- [5] a) R. F. Brissos, A. Caubet and P. Gamez, *European Journal of Inorganic Chemistry* **2015**, 2633; b) S. Khan, A. M. Malla, A. Zafar and I. Naseem, *PLoS ONE*, **2017**, 12, 181783; c) P.B. Dervan, *Science*, **1986**, 232, 464; d) P.G. Schultz and P.B. Dervan, *J. Biomolecular Structural Dynamics* **1984**, 1, 1133.
- [6] a) J.K. Barton, *Journal of Biomolecular Structural Dynamics* **1983**, 1, 621; b) J.K. Barton, *Science*, **1986**, 223, 727; c) S. Neidle, Z. Abraham, *CRC Critical Reviews in Biochemistry* **1984**, 17, 73; d) B.P. Hudson, J.K. Barton, *Journal of American Chemical Society* **1998**, 120, 6877; e) B. S. Rajebhosale, S. N. Dongre, S. S. Deshpande, A. N. Kate and A. A. Kumbhar, *Journal of Inorganic Biochemistry* **2017**, 175, 129.
- [7] F. P. Dwyer, E. Mayhew, E. M. Roe and A. Shulman, *British Journal of Cancer* **1965**, 19, 195.
- [8] A. Spassky and D.S. Sigman, *Biochemistry*, **1985**, 24, 8050.
- [9] a) E. Y. Tirel, Z. Bellamy, H. Adams, V. Lebrun, F. Duarte and N. H. Williams,

Angewandte Chemie **2014**, *53*, 8246; b) A. A. Muxel, A. Neves, M. A. Camargo, A. J. Bortoluzzi, B. Szpoganicz, E. E. Castellano, N. Castilho, T. Bortolotto and H. Terenzi, *Inorganic Chemistry* **2014**, *53*, 2943; c) P. Hendry and A.M. Sargeson, *Progress in Inorganic Chemistry* **1990**, *38*, 201.

[10] a) D. Bím, E. Svobodová, V. Eigner, L. Rulíšek and J. Hodačová, *Chemistry A European Journal* **2016**, *22*, 10426; b) S. S. Massoud, C. C. Ledet, T. Junk, S. Bosch, P. Comba, R. Herchel, J. Hošek, Z. Trávníček, R. C. Fischerd and F. A. Mautner, *Dalton Transactions* **2016**, *45*, 12933; c) A.N. Modak, J.K. Gard, M.C. Merriman, K.A. Winkler, J.K. Bashkin and M.K. Stern, *Journal of American Chemical Society* **1991**, *113*, 283.

[11] E.L. Hegg and J.N. Burstyn, *Coordination Chemistry Reviews* **1998**, *171*, 133.

[12] a) C. Mari, V. Pierroz, S. Ferrari and G. Gasser, *Chemical Sciences* **2015**, *6*, 2660; b) C. Sissi, F. Mancin, M. Gatos, M. Palumbo, P. Tecilla and U. Tonellato, *Inorganic Chemistry* **2005**, *44*, 2310; c) A. Bencini, E. Berni, A. Bianchi, C. Giorgi, B. Valtancoli, D.K. Chand and H.J. Schneider, *Dalton Transactions* **2003**, *5*, 793; d) D.K. Chand, H.J. Schneider, A. Bencini, A. Bianchi, C. Georgi, S. Ciattini and B. Valtancoli, *Chemistry A European Journal* **2000**, *6*, 4001; e) A. Sitlani, E.C. Long, A.M. Pyle and J.K. Barton, *Journal of American Chemical Society* **1992**, *114*, 2303.

[13] a) A.A.A. Abu-Hussen, *Journal of Coordination Chemistry* **2006**, *59*, 157; b) M.S. Karthikeyan, D.J. Prasal, B. Poojary, K.S. Bhat, B.S. Holla and N.S. Kumari, *Bioorganic Medicinal Chemistry* **2006**, *14*, 7482; c) K. Singh, M.S. Barwa and P. Tyagi, *European Journal of Medicinal Chemistry* **2006**, *41*, 147; d) P. Panneerselvam, R.B. Nair, G. Vijayalakshmi, E.H. Subramanian, S.K. Sridhar, *European Journal of Medicinal Chemistry* **2005**, *40*, 225.

[14] a) S.K. Sridhar, M. Saravanan and A. Ramesh, *European Journal of Medicinal Chemistry* **2001**, *36*, 615; b) S.N. Pandeya, D. Sriram, G. Nath and E. DeClercq, *European Journal of Pharmaceutical Sciences* **1999**, *9*, 25.

[15] a) A. C. Hangan, G. Borodi, R. L. Stan, E. Páll, M. Cenariu, L. S. Oprean and B. Sevestre, *Inorganica Chimica Acta* **2018**, *482*, 884; b) Z. Bao, D. Lai, P. Shen, M. Yu, R. Kumar, Y. Liu, Z. Chen and H. Liang, *Z. Anorg. Allg. Chem.*, **2019**, *645*, 570; c) R. Mladenova, M. Ignatova, N. Manolova, T. Petrova and I. Rashkov, *European Polymer Journal* **2002**, *38*, 989; d) O.M. Walsh, M.J. Meegan, R.M. Prendergast and T.A. Nakib,

European Journal of Medicinal Chemistry **1996**, *31*, 989.

[16] a) J.E. Kovacic, *Spectrochimica Acta* **1967**, *23A*, 183; b) R. Atkins, G. Brewer, E. Kokot, G.M. Mockler and E. Sinn, *Inorganic Chemistry* **1985**, *24*, 127.

[17] a) K.E. Erkkila, D.T. Odom and J.K. Barton, *Chemical Reviews* **1999**, *99*, 2777; b) C. Metcalfe and J.A. Thomas, *Chemical Society Reviews* **2003**, *32*, 215.

[18] a) B. J. Pages, D. L. Ang, E. P. Wright and J. R. Aldrich-Wright, *Dalton Transactions*, **2015**, *44*, 3505; b) V. Uma, V.G. Vaidyanathan and B.U. Nair, *Bulletin of the Chemical Society of Japan* **2005**, *78*, 845.

[19] a) Y. Yan, J. Zhang, L. Rend and C. Tang, *Chemical Society Reviews* **2016**, *45*, 5232; b) C. S. Allardyce and P. J. Dyson, *Dalton Transactions* **2016**, *45*, 3201; c) W. Szczepanik, J. Ciesiolka, J. Wrzesinski, J. Skala and M. Jezowska-Bojczuk, *Dalton Transactions* **2003**, 1488.

[20] a) T. M. Rana and C. F. Meares, *Journal of the American Chemical Society* **1991**, *113*, 1859; b) R. Miyake, J. T. Owens, D. Xu, W. M. Jackson and C. F. Meares, *Journal of the American Chemical Society* **1999**, *121*, 7453.

[21] K. Tsumura, A. Suzuki, T. Tsuzuki, S. Tanimoto, H. Kaneko, S. Mastumara, M. Imoto, K. Umezawa, D. Takahashi and K. Toshima, *Dalton Transactions* **2011**, *40*, 6357.

[22] a) A. Bergamo and G. Sava, *Dalton Transactions* **2007**, 1267; b) H.-K. Liu, S. J. Berners-Price, F. J. Wang, A. Parkinson, J. Xu, J. Bella and P. J. Sadler, *Angewandte Chemie* **2006**, *45*, 8153; c) G. Sava, I. Capozzi, K. Clerici, R. Gagliardi, E. Alessio and G. C. Mestroni, *Clinical Experiment Metastasis* **1998**, *16*, 371.

[23] M. Yokoyama, *Journal of Artificial Organs* 2005, *8*, 77.

[24] a) R. Haag and F. Kratz, *Angewandte Chemie* **2006**, *45*, 1198; b) J. Shi, P. W. Kantoff, R. Wooster and O. C. Farokhzad, *Nature Reviews Cancer* **2017**, *17*, 20; c) S. Vandghanoonia, M. Eskandania, J. Barara and Y. Omid, *European Journal of Pharmaceutical Science* **2018**, *117*, 301; d) D. Mehta, N. Leong, V. M. McLeod, B. D. Kelly, R. Pathak, D. J. Owen, C.J.H. Porter and L. M. Kaminskas, *Mol. Pharmaceutics*, **2018**, *15*, 4568.

[25] a) Z. Liu and X. Chen, *Chemical Society Reviews* **2016**, *45*, 1432; b) V. T. G. Chuang, U. Kragh-Hansen and M. Otagiri, *Pharmaceutical Research* **2002**, *19*, 569; c) R.

- K. Jain, *Cancer Research* **1990**, *50*, 814.
- [26] a) W. H. Ang, E. Daldini, L. Juillerat-Jeanneret and P. J. Dyson, *Inorganic Chemistry* **2007**, *46*, 9048; b) T. Kosta, T. Maryama and M. Otagiri, *Pharmaceutical Research* **1997**, *14*, 1607.
- [27] N. Shahabadi and M. Maghsudi, *Journal of Molecular Structure* **2009**, *929*, 193.
- [28] a) C. Trejo-Solis, G. Palencia, S. Zuniga, A. Rodriguez-Ropon, L. Osorio-Rico, S.T. Luvia, I. Gracia-Mora, L. Marquez-Rosado, A. Sanchez, M.E. Moreno-Garcia, A. Cruz, M.E. Bravo-Gomez, L. Ruiz-Ramirez, S. Rodriguez-Enriquez, J. Sotelo, *Neoplasia*, **2005**, *7*, 563; b) F. Carvallo-Chaigneau, C. Trejo-Solis, C. Gomez-Ruiz, E. Rodriguez-Aguilera, L. Macias-Rosales, E. Cortes-Barberena, C. Cedillo-Pelaez, I. Gracia-Mora, L. RuizAzua, V. Madrid-Marina and F. Constantino-Casas, *Biometals*, **2008**, *21*, 17; c) A. De Vizcaya-Ruiz, A. Rivero-Muller, L. Ruiz-Ramirez, G.E. Kass, L.R. Kelland, R.M. Orr and M. Dobrota, *Toxicology In Vitro*, **2000**, *14*, 1; d) L. Hernandez-Esquivel, A. Marin-Hernandez, N. Pavon, K. Carvajal and R. MorenoSanchez, *Toxicology Applied Pharmacology* **2006**, *212*, 79.
- [29] L. Shi, H.-M. Ge, S.-H. Tan, H.-Q. Li, Y.-C. Song, H.-L. Zhu and R.-X. Tan, *European Journal of Medicinal Chemistry* **2007**, *42*, 558.
- [30] R.-Q. Fang, H.-K. Yuan, X.-L. Wang and H.-L. Zhu, *Inorganic Nano-Materials Chemistry* **2017**, *47*, 756.
- [31] D.D. Perrin, W.L.F. Armarego, D.R. Perrin, Purification of Laboratory Chemicals, Pergamon Press, Oxford, U.K, **1980**.
- [32] Bruker, APEX2, SAINT and SADABS, Bruker AXS Inc., Madison, Wisconsin, USA, **2008**.
- [33] G. M. Sheldrick, *Acta Crystallographica* **2015**, *A71*, 3.
- [34] G. M. Sheldrick, *Acta Crystallographica* **2015**, *C71*, 3.
- [35] B. Selvakumar, V. Rajendiran, P.U. Maheswari, H. Stoeckli-Evans and M. Palaniandavar, *Journal of Inorganic Biochemistry* **2006**, *100*, 316.
- [36] M. Zaki, M. Afzal, M. Ahmad and S. Tabassuma, *Journal of Photochemistry and Photobiology B*, **2016**, *161*, 318.
- [37] S. Dey, K. Ghosh, S. Halder, C. Rizzoli and P. Roy, *Indian Journal of Chemistry* **2015**, *54A*, 1451.

- [38] a) A. Bhattacharjee, S. Halder, K. Ghosh, C. Rizzoli and P. Roy, *New Journal of Chemistry* **2017**, *41*, 5696; b) A. Bhattacharjee, S. Dey and P. Roy, *Inorganica Chimica Acta*, **2019**, *490*, 93; c) P. Roy, K. Dhara, M. Manassero and P. Banerjee, *European Journal of Inorganic Chemistry* **2008**, 4404.
- [39] S. Zolezzi, E. Spodine and A. Decinti, *Polyhedron*, **2002**, *21*, 55.
- [40] Shaju K. S., Joby Thomas K., V. P. Raphael, N. Kuriakose, *Journal of Applied Chemistry* **2014**, *10*, 2278.
- [41] D. M. Boghaei and S. Mohebi, *Journal of Molecular Catalysis A*, **2002**, *179*, 41.
- [42] A. Kurutos, I. Orehovec, A. T. Paic, I. Crnolatac, L. Horvat, N. Gadjev, I. Piantanida and T. Deligeorgiev, *Dyes Pigments* **2018**, *148*, 452.
- [43] N. Shahabadi, S. Kashanian and F. Darabi, *European Journal of Medicinal Chemistry* **2010**, *45*, 4239.
- [44] A. Wolfe, G.H. Shimer and T. Meehan, *Biochemistry*, **1987**, *26*, 6392.
- [45] B.D. Wang, Z.Y. Yang, D.D. Qin and Z.N. Chen, *Journal of Photochemistry and Photobiology A* **2008**, *194*, 49.
- [46] C.V. Kumar, J.K. Barton and N.J. Turro, *Journal of the American Chemical Society* **1985**, *107*, 5518.
- [47] J.R. Lakowicz and G. Weber, *Biochemistry*, **1973**, *12*, 4161.
- [48] L. Z. Li, C. Zhao, T. Xu, H. W. Ji, Y. H. Yu, G. Q. Guo and H. Chao, *Journal of Inorganic Biochemistry* **2005**, *99*, 1076.
- [49] P. Lincoln, E. Tuite and B. Norden, *Journal of the American Chemical Society* **1997**, *119*, 1454.
- [50] B. Norden and F. Tjerneld, *Nature New Biology* **1982**, *236*, 67.
- [51] S. Mahadevan and M. Palaniandavar, *Bioconjugation Chemistry* **1996**, *7*, 138.
- [52] S. Tabassum, M. Zaki, M. Ahmad, M. Afzal, S. Srivastav, S. Srikrishna and F. Arjmand, *European Journal of Medicinal Chemistry* **2014**, *83*, 141.
- [53] Y.Q. Wang, X.Y. Wang, J. Wang, Y.M. Zhao, W.J. He and Z.J. Guo, *Inorganic Chemistry* **2011**, *50*, 12661.
- [54] J.J. Stephanos, *Journal of Inorganic Biochemistry* **1996**, *62*, 155.
- [55] C.-Y. Gao, X. Qiao, Z.-Y. Ma, Z.-G. Wang, J. Lu, J.-L. Tian, J.-Y. Xu and S.-P. Yan, *Dalton Transactions* **2012**, *41*, 12220.

- [56] G. Zhang, N. Zhao and L. Wang, *Journal of Luminescence* **2011**, *131*, 880.
- [57] S. Naveenraj and S. Anandan, *Journal of Photochemistry and Photobiology C*, **2013**, *14*, 53.
- [58] T. Forster, in *Modern Quantum Chemistry: O. Sinanoglu (Ed.)*, Modern Quantum Chemistry, vol. 3, Academic, New York, **1996**, pp. 93–137.
- [59] X.-B. Fu, G.-T. Weng, D.-D. Liu and X.-Y. Le, *Journal of Photochemistry and Photobiology A*, **2014**, *276*, 83.
- [60] S. Tabassum, W.M. Al-Asbahy, M. Afzal, F. Arjmand and R.H. Khan, *Molecular Biosystems* **2012**, *8*, 2424.
- [61] S. Kumar, R. P. Sharma, P. Venugopalan, V. Ferretti, S. Perontsis and G. Psomasc, *Journal of Inorganic Biochemistry* **2018**, *187*, 97.
- [62] B. Deka, T. Sarkar, S. Banerjee, A. Kumar, S. Mukherjee, S. Deka, K. K. Saikia and A. Hussain, *Dalton Transactions* **2017**, *46*, 396.
- [63] M. K. Koley, S. U. Parsekar, N. Duraipandy, M. S. Kiran, B. Varghese, P. T. Manoharan and A. P. Koley, *Inorganica Chimica Acta* **2018**, *478*, 211.
- [64] K.N. Aneesrahman, K. Ramaiah, G. Rohini, G.P. Stefy, N.S.P. Bhuvanesh and A. Sreekanth, *Inorganica Chimica Acta* **2019**, *492*, 131.
- [65] S. Banerjee, P. Ghorai, P. Brandão, D. Ghosh, S. Bhuiya, D. Chattopadhyay, S. Das and A. Saha, *New Journal of Chemistry* **2018**, *42*, 246.

Chapter 6

**A novel Schiff-base
copper(II) complex
modified electrode for
ascorbic acid catalytic
oxidation and
determination**

6.1 Introduction

Ascorbic acid (H_2A) i.e. vitamin C, is an essential nutrient mainly in fruits and vegetables and is an important antioxidant. The body requires it. Whilst it is necessary for vital body functions, excess of it causes kidney stones. H_2A has is a neuromodulator for dopamine and glutamate in the human body. It is a water soluble small-molecular-weight compound. It is used in food industry as antioxidant and free-radical scavenger. Hence, fast and accurate estimation of H_2A becomes important. Various methods are utilized for the same starting from titration to HPLC^[1] and spectrophotometry^[2]. Electroanalytical techniques are also used for H_2A determination^[3]. But accuracy could not be achieved. This is because it adsorbs on the electrode surface and causes electrode fouling^[4]. Therefore transition-metal complex modified electrodes, are utilized as electron mediators for ascorbic acid catalytic oxidation and subsequent determination^[5]. The modification lowers the overpotential and gives a better response current to yield better sensitivity.

The electrocatalytic oxidation of ascorbic acid by the modified metal complexes in aqueous solution is believed to occur by an electron-transfer mechanism. The reactive species is the ascorbate ion, HA^- , which gets oxidized by electron transfer, followed by deprotonation to yield ascorbyl radical. This rapidly converts to dehydroascorbic acid^[6]. Transition-metal salicylaldehyde Schiff-base complexes are broadly studied by scientists, and they are incorporated in various fields, including biology, catalysis, and also as catalyst for H_2A oxidation. This class of compounds show markedly good electropolymerization properties on electrode surfaces to form a conductive film^[7]. Thus they are potential candidates to modify electrodes for electrocatalytic oxidation and detection of H_2A .

In this work, a mononuclear copper(II)-Schiff-base complex has been synthesized and characterized by different standard method (**Scheme 6.1**). Its electropolymerization on a glassy carbon electrode (GC) and the consequent electrocatalytic activity of the modified GC to the oxidation of H_2A has been extensively studied. The determination of H_2A with modified GC by amperometric method has also been done. Analysis of vitamin C tablets has been performed.

6.2 Experimental Section

6.2.1 Materials and physical methods

1,2-Diaminopropane, 5-bromo-2-hydroxybenzaldehyde, copper(II) nitrate were purchased from Sigma Aldrich and used without further purification. Other reagents were obtained from commercial sources and used as received. Solvents were purchased from commercial sources and were used for synthesis without further purification while purified and dried solvents¹³ were used for spectroscopic measurements. Elemental analyses (carbon, hydrogen and nitrogen) were performed using a Perkin–Elmer 2400C elemental analyzer. FT-IR spectra were obtained on a Perkin Elmer spectrometer (Spectrum Two) with the samples by using the attenuated total reflectance (ATR) technique. The UV-visible spectral measurements were done in Agilent 8453 diode array spectrophotometer. Cyclic voltammetric measurements were performed on a CHI Electrochemical workstation. A glassy carbon working electrode, a platinum wire auxiliary electrode and Ag/AgCl reference electrode were employed in a standard three-electrode configuration. KCl was used as the supporting electrolyte in buffer systems under nitrogen atmosphere. All experiments were carried out at room temperature in air unless reported otherwise.

6.2.2 Synthesis of Synthesis of [Cu(L¹)H₂O]

Ethanol solution of 1,2- diamopropane (0.25 mmol, 0.018 g) was added dropwise to an ethanolic solution (10 mL) of 5-bromo-2-hydroxybenzaldehyde (0.5 mmol, 0.100 g) and stirred. The mixture was refluxed for 2 h forming an orange solution of Schiff base ligand. The mixture was then cooled and it was used as ‘ligand (HL¹)’ without any characterization and purification. An ethanolic solution of copper(II) nitrate (0.25 mmol, 0.047 g) was added to the solution of HL¹ and the mixture was stirred for 30 min when it turned as greenish. It was then refluxed for 1 h. Color of the solution turned dark green. The mixture was cooled and filtered to remove any undissolved or precipitate materials. The filtrate was kept at ambient temperature. Brownish green single crystals suitable for X-ray diffraction analysis were obtained within few days.

6.2.3 X-ray data collection and structure determination

Details of the data collection and refinement parameters for complex **1** are summarized in **Table 6.1**. The diffraction experiments were carried out on a Bruker APEX-II CCD diffractometer using graphite monochromated Mo $K\alpha$ radiation at 298 K. Data was processed by the use of Bruker APEX2 and SAINT packages^[8]. Absorption corrections based on multi-scans using the SADABS software were applied to the intensity data. The structures were solved by direct methods using SHELXT^[9] and refined with full-matrix least-squares on F^2 on all unique reflections using SHELXL-2014/7^[10]. All the non-hydrogen atoms of the complexes were refined anisotropically.

Complex	1
Formula	2(C ₁₇ H ₁₄ Br ₂ Cu N ₂ O ₂), C ₂ O
Formula weight	1043.32
<i>T</i> (K)	298 K
Crystal color	Dark green
Crystal system	Monoclinic
Space group	C2/c
<i>a</i> (Å)	26.4369(12)
<i>b</i> (Å)	7.2231(3)
<i>c</i> (Å)	20.9363(10)
α (°)	90.00
β (°)	113.410(2)
γ (°)	90.00
<i>V</i> (Å ³)	3668.8(3)
<i>Z</i>	4

Crystal dimensions (mm)	0.5 × 0.2 × 0.15
<i>F</i> (0 0 0)	2040
<i>D</i> _c (g cm ⁻³)	1.889
λ (Mo Kα) (Å)	0.71073
θ Range (°)	2.3- 27.1
Reflection collected/ unique/observed	59280, 4065 , 2416
Absorption correction	multi-scan
<i>R</i> _{int}	0.094
Final <i>R</i> ₁ index [<i>I</i> > 2σ(<i>I</i>)]	0.0541
Final <i>wR</i> ₂ index (all reflections)	0.1356
Goodness-of-fit	1.07

Table 6.1 : Crystallographic data for complex 1

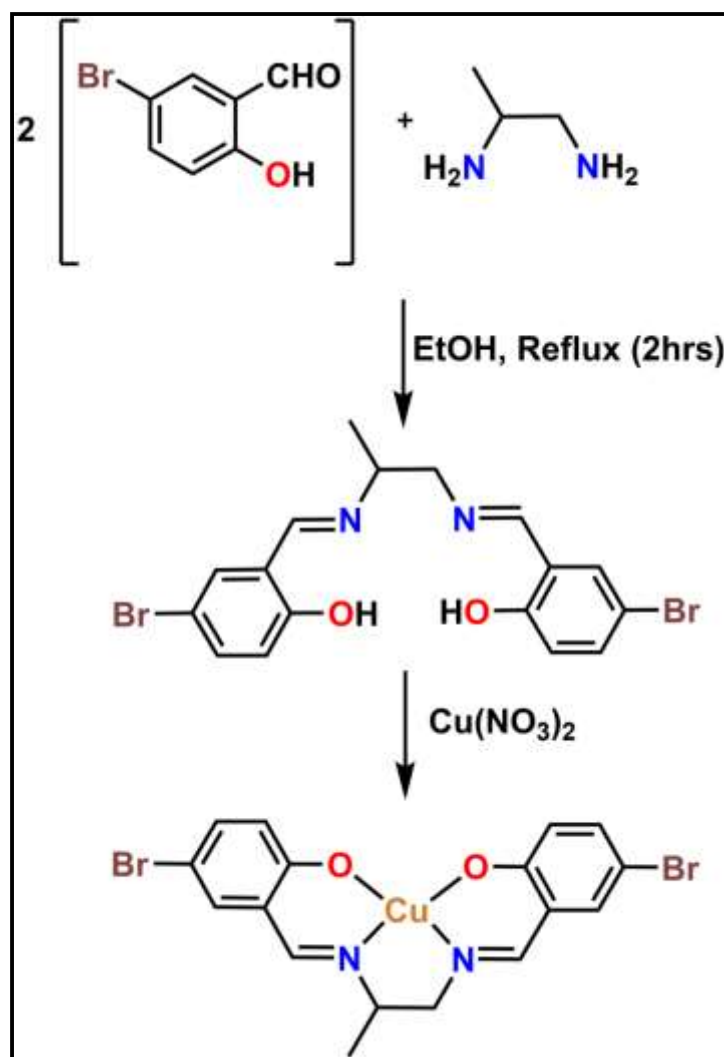
6.2.4 Electrochemical measurements

Electropolymerization was done in DMSO solution under N₂ atmosphere containing 5×10⁻⁴ M copper complex and 0.1 M NaNO₃ as supporting electrolyte. The modified electrode was then utilized to perform the scan-rate dependent study under same conditions. Electrocatalytic oxidation of ascorbic acid and its amperometric determination were carried out in pH 6.8 PBS with 0.1 M KCl. Amperometric studies were performed at 0.2 V vs. SCE and different concentrations of H₂A were injected into the electrolytic setup whilst stirring. Ground vitamin tablets of vitamin C were dissolved in double distilled water. A known amount was injected to the five times and then equivalent amount of H₂A solution was also added.

6.3 Results and discussion

6.3.1 Synthesis

Synthesis of the complex has been performed following route given in **Scheme 6.1**. First, the ligand has been synthesized by one step Schiff-base condensation between 5-bromo-2-hydroxybenzaldehyde and 1,2-diaminopropane in 1:1 molar ratio in ethanol. The ligand has not been characterized and it has been used directly for complex formation without further purification. Reaction between HL¹ and copper(II) nitrate gives **1**.



Scheme 6.1 : Synthesis scheme

6.3.2 Crystal structure of 1

The copper complex crystallizes from ethanol in a monoclinic system with $C2/c$ space group. A perspective view of the complex is given in **Fig 6.1**. The selected bond lengths and angles are given in **Table 6.2**. The copper is tetra coordinated with two two nitrogen and two oxygen atoms. There appears to be two formula units of the complex in one unit cell. One solvent molecule (ethanol) is crystallized along with the main crystalline unit. The solvent molecule is highly disordered as the crystal data have been collected at room temperature and not low temperature. The solvent molecule has been omitted from the pictorial representation for clarity.

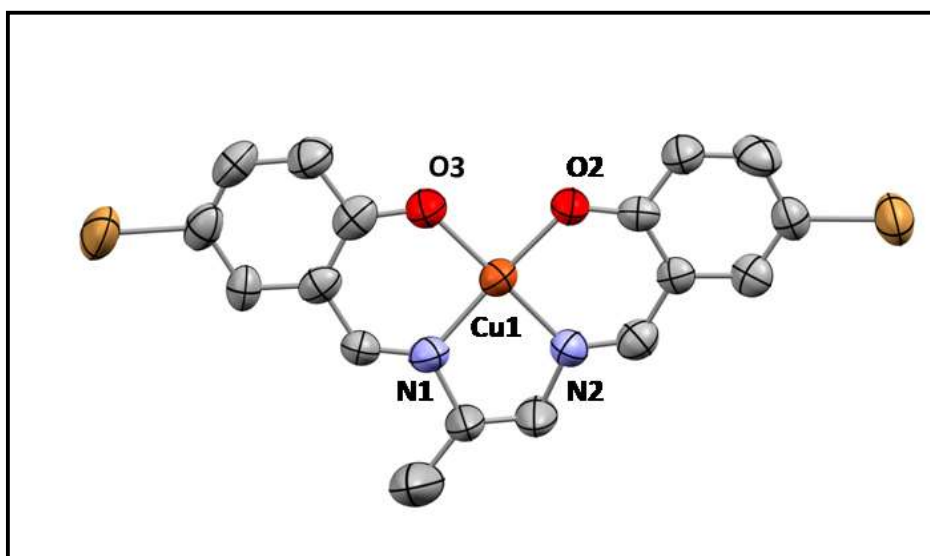


Fig 6.1 : A perspective view of complex 1 with partial atom numbering scheme.

Cu1-O2	1.897(6)	O2-Cu1-O3	88.5(3)
Cu1-O3	1.894(6)	O2-Cu1-N1	176.6(3)
Cu1-N1	1.940(8)	O2-Cu1-N2	93.4(3)
Cu1-N2	1.943(6)	O3-Cu1-N1	94.2(3)
N1-Cu1-N2	84.0(3)	O3-Cu1-N2	175.3(3)

Table 6.2: Selected bond lengths (\AA) and bond angles ($^\circ$) of complex 1

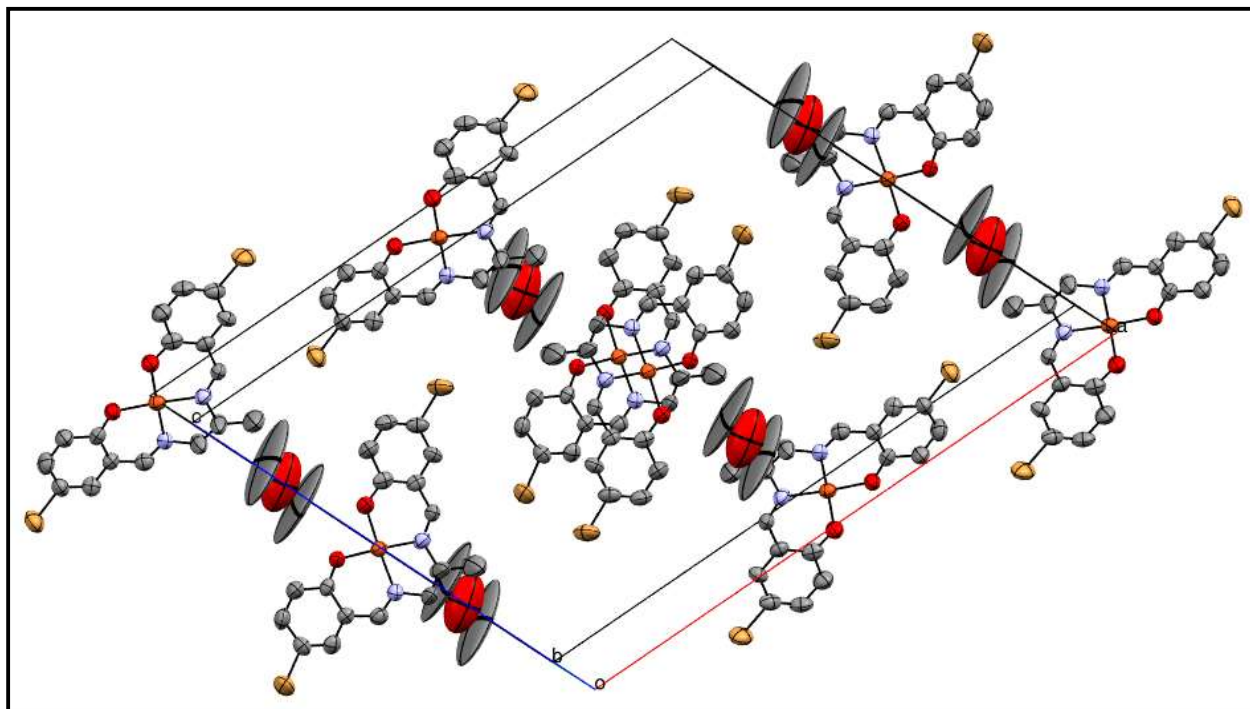


Fig 6.2 : Packing diagram along b axis

The packing diagram (**Fig 6.2**) gives a clear idea of the arrangement of the asymmetric units in space along the b axis. No significant C-H- π or π - π interaction has been observed within the rings. The packing diagram clearly shows the highly disordered ethanol molecule in the crystal structure.

6.3.3 IR spectral data

FT-IR spectrum of the complex has been recorded by ATR technique (**Fig. 6.3**). The strong peaks at 2848 cm^{-1} confirms the presence of methylene moieties. The sharp peak at around 1630 cm^{-1} shows the presence of C=N bond which absolutely justifies formation of the Schiff base complex. A band at 1170 cm^{-1} indicates the presence of C-O bond i.e. carbon being attached to hydroxyl group. Medium intensity bands around $560\text{--}570\text{ cm}^{-1}$ indicates that the ligand is coordinated to the metal center.

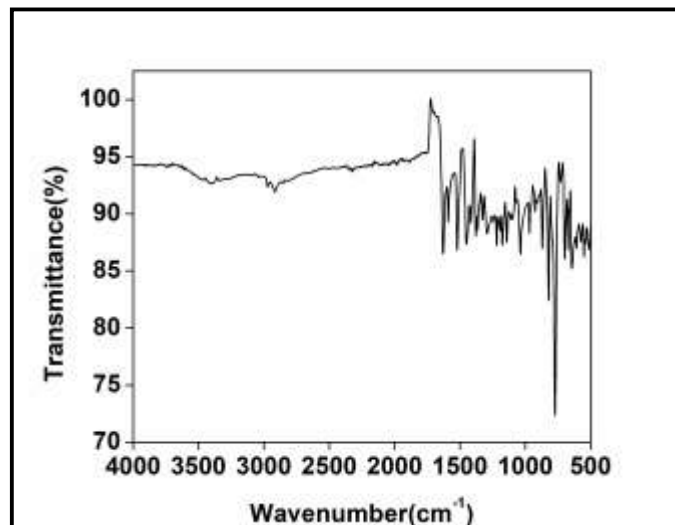


Fig 6.3 : IR spectral data of complex 1

6.3.4 UV- Vis spectral data

The electronic spectrum of complex **1** has been recorded in DMF at room temperature. UV-vis spectrum of complex **1** is given in **Fig. 6.4**. It could be seen from the figure that it exhibits a broad band at 575 nm (molar extinction coefficient: $5780 \text{ Lmol}^{-1}\text{cm}^{-1}$), which may be assigned to $d-d$ transition. Another strong peak is observed at 372 nm, with molar extinction coefficient value of $164400 \text{ Lmol}^{-1}\text{cm}^{-1}$ [11]. These peaks may be attributed to $\text{N}(\text{amino}) \rightarrow \text{Cu}(\text{II})$ (LMCT) transfer.

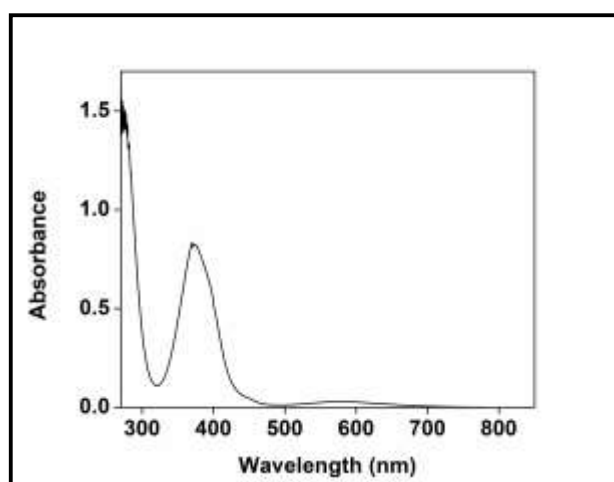


Fig 6.4 : Absorption spectra of complex 1

6.3.5 Electrochemical polymerization

Cyclic voltammetry (CV) curves for electropolymerization of complex 1 in DMSO at a potential range of -0.5 to 1.4 V are illustrated in **Fig 6.5**. The cyclic voltammogram exhibits two anodic peaks at 0.25V and 0.48V which can be assigned to oxidation of Cu(I) to Cu(II) and Cu(II) to Cu(III) respectively, of the salen complex on the surface of the glassy carbon electrode. The CuII/CuI reductive peak has been observed at about -0.18 V(I'). The magnitude of redox peaks in the voltammogram increases with subsequent scans for over 40 cycles, demonstrating that the copper salen films are continually being deposited on the electrode surface. The electropolymerization did not occur at low scan potentials as indicated in the graph (**Fig 6.6**). This clearly portrays that the electropolymerization of the oversaid Cu salen complex on the electrode surface requires a higher potential range. Plots of the selected peak I' vs. the cycle number are shown in the inset of graph 1. The growth rate of peak I' decreases with increasing number of scans indicating that the conductivity of the solution of the copper salen complex decreases with successive deposition^[12].

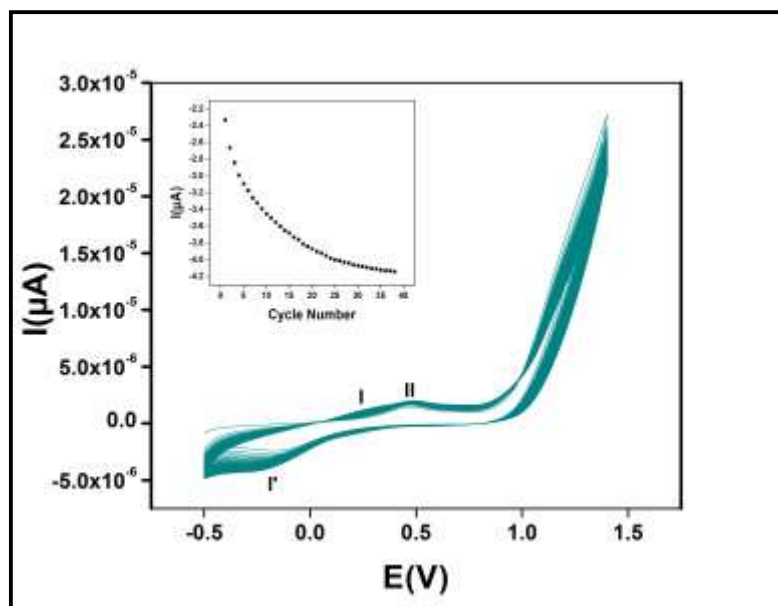


Fig 6.5 : Cyclic voltammetry for electropolymerization of 1 mM of complex 1 in DMSO, 0.1 M NaNO_3 (supporting electrolyte) on GC, 50 mV s^{-1} (Electropolymerization cycles from 1, 5, ... , 40 at -0.3 to 1.4 V)

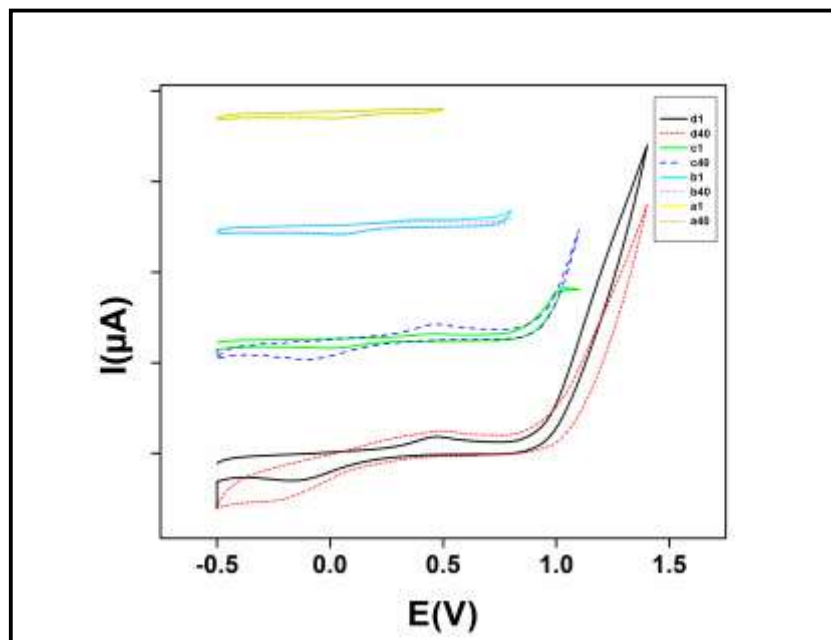


Fig 6.6 : Electropolymerization at different potential ranges: (a) -0.3 to 0.5 V, (b) -0.3 to 0.8 V, (c) -0.3 to 1.1 V, (d) -0.3 to 1.4 V; dashed line is the first cycle, solid line is the 40th cycle.

A scan rate dependent study has been conducted on poly(L)CuII in a monomer-free DMSO solution containing 0.1 M NaNO₃ and is shown in **Fig. 6.7**. As shown in the inset of Fig. 3, the peak currents increases linearly with sweep rate up to 200 mV/s, which is commonly seen in the case of voltammetric response for a surface confined film. The change in the anodic and cathodic peak currents has been shown in the inset graph. The result shows a strongly adsorbed electroactive material that is not limited by the ionic flux of counter ions and also implies conductivity of the polymer film^[13].

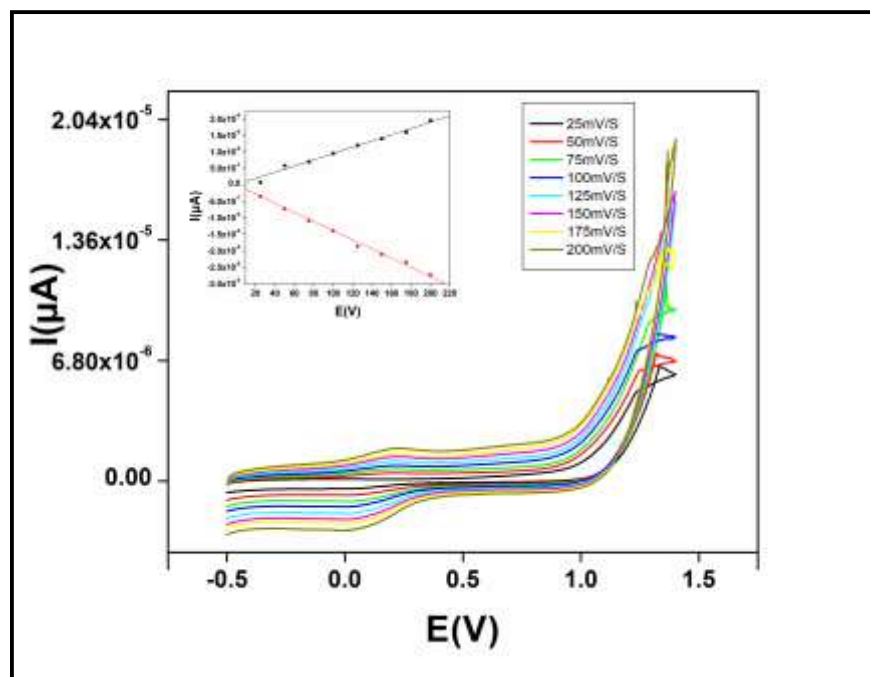


Fig 6.7 : Scan-rate dependent study. Inset: plot of linear current increase vs. scan rate

6.3.6 Electrocatalytic oxidation of ascorbic acid

The electrocatalytic property of the modified electrode towards the oxidation of ascorbic acid is pretty remarkable. It has been demonstrated in pH 6.8 PBS (0.1 M KCl) (**Fig 6.8**). With bare GC, an irreversible oxidation peak has been observed at 0.3 V with a corresponding current of 1.8 mA (**Fig. 6.8 red line**). At the modified GC, the oxidation peak shifted to 0.61 V and the current increases to 4.4 mA (**Fig. 6.8 green line**). The remarkable enhancement in the peak current clearly shows the catalytic effect of P(L)CuII toward H_2A ^[14].

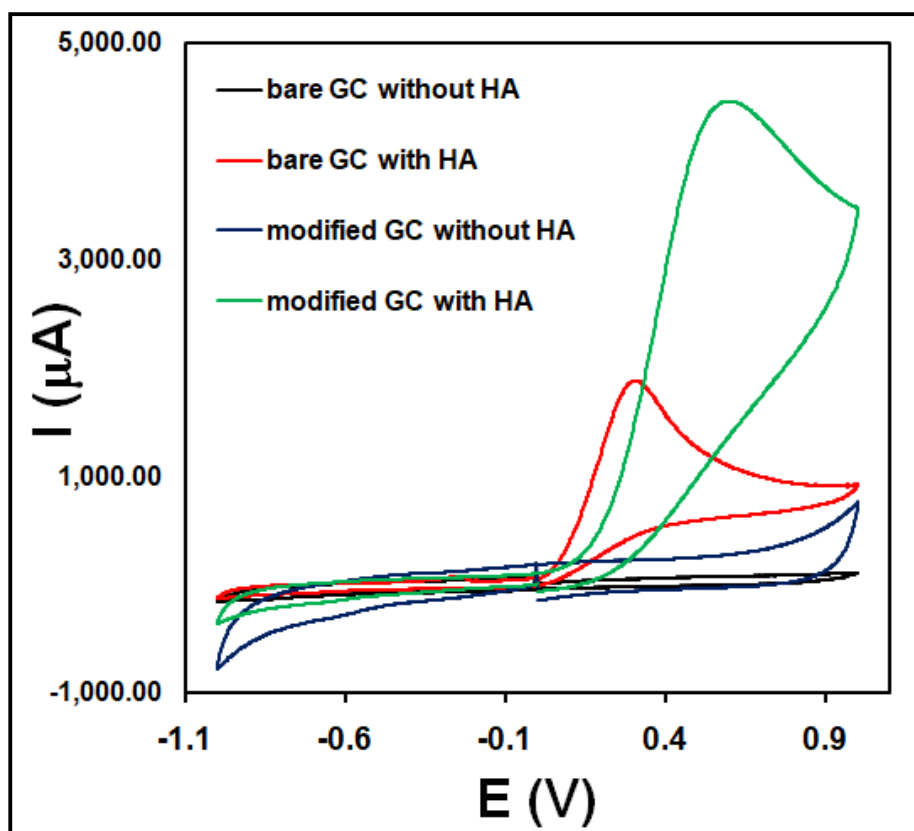
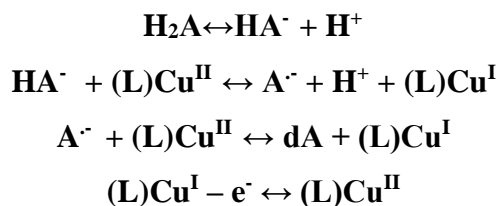
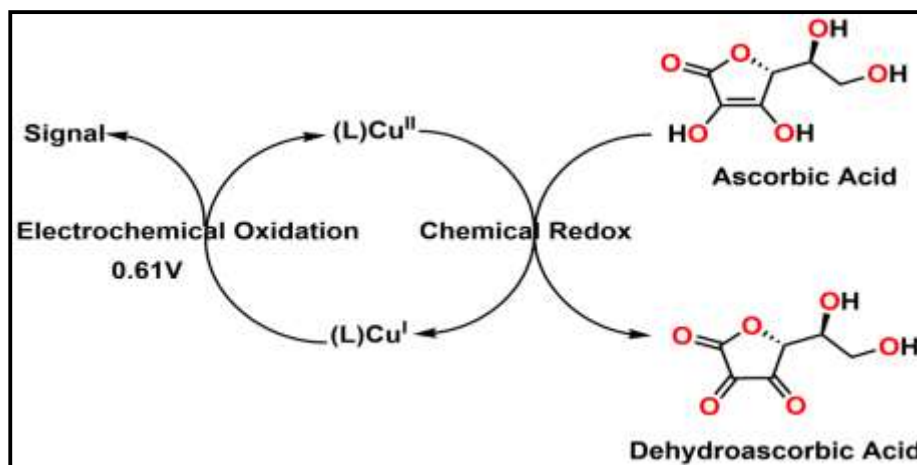


Fig 6.8 : CVs of bare (black, red) and modified GC (blue, green) electrodes in pH6.8 PBS (0.1 M KCl) solution: $H_2A = 0$ mM (black, red), 3 mM (blue, green); scan rate 100 mV s^{-1}

The electrochemical oxidation of H_2A is believed to undergo two consecutive one-electron transfer processes involving the participation of a radical anion intermediate to form dehydroascorbic acid(dA)^[15]. This species hydration is characteristic of carbonyl groups to form an electro inactive product. The electrocatalytic oxidation of ascorbic acid at the modified electrode can be described by the following equations and **Scheme 6.2**.





Scheme 6.2 : Reaction mechanism of ascorbic acid at the modified electrode

pK_{a1} for ascorbic acid is about 4.5^[15], so the predominant reactive species is the ascorbate ion HA^- which is initially oxidized by (L)Cu^{II} to produce the ascorbate radical anion ($A^{\Sigma-}$) and (L)Cu^I, which is again oxidized by (L)Cu^{II} to produce dehydroascorbic acid (dA) and (L)Cu^I. (L)Cu^I is electrochemically oxidized to give a strong anodic peak shown in Fig. 6.7 (green), which indicates that the Cu(I) center in the complex undergoes oxidation at 0.61 V.

6.3.7 Amperometric determination of H₂A

Amperometric experiments of H₂A have been carried out using P(L)Cu^{II} modified GC in PBS (pH 6.8) solution with 0.1 M KCl as supporting electrolyte. The oxidation peak currents have been measured at 0.2 V and plotted against the bulk concentration of H₂A. The modified GC electrode is highly sensitive to ascorbic acid. It has been seen that injected citric acid, glucose and H₂O₂ exhibit no response on the system, but injected ascorbic acid shows a major jump in current. The plot of I vs t, shows the amperometric response of H₂A (over the range 2–500 μ M concentration), addition of measured amounts of H₂A occurring with increasing times. A similar increase in current has also been observed as seen from **Fig 6.9**. The only drop of current at times 500s on addition of 100 μ M of the acid, may be attributed to a voltage drop artifact of the amperometric set up. The standard addition plot (**Fig 6.10**), shows a more or less good fit indicating that the P(L)Cu^{II} modified electrode has a good response to addition of ascorbic acid with substantial reproducibility.

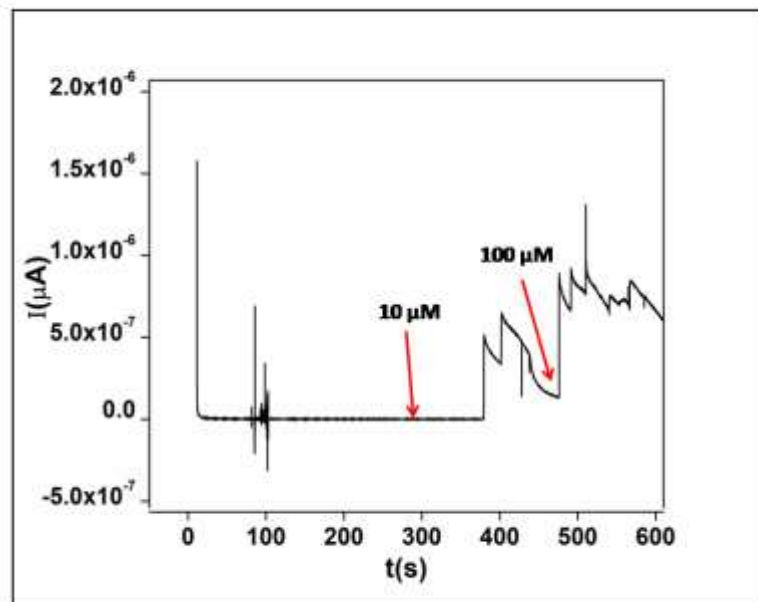


Fig 6.9 : Typical amperometric curve obtained with a modified GC in pH 6.8 PBS (0.1 M KCl) at an applied potential of 0.2 V vs. SCE showing response with successive injection of H2A in the range 2–500 μM

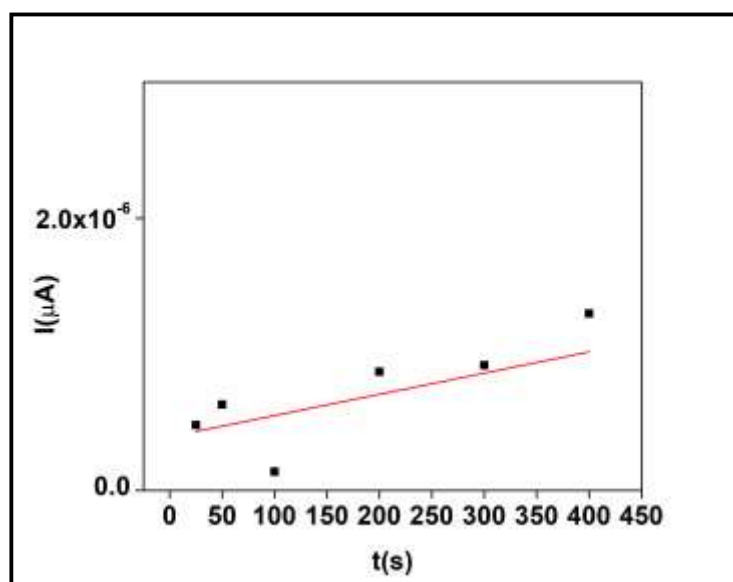


Fig 6.10 : Standard addition plot

The method has also been applied to analyze vitamin C tablets(Limcee brand purchased from market). The recovery has been studied by the corresponding addition of ground tablets with a certain fixed value of standard solution of H₂A. The determination results are shown in **Table 6.3**. The RSD and recovery are in the acceptable range^[3], showing that the proposed method can be used for sample determination and presented a good stable model.

Sample	Specified (mg)	Detected (mg) (n=5)	Added (mM)	Detected (mM)	Recovery (%)
Limcee	500	445	50	46.25	98.25

Table 6.3 : Detection of H₂A in vitamin C tablets

6.4 Conclusions

The new copper Schiff-base complex can be electropolymerized on a glassy carbon electrode when the high scan potential of around +1.4 V is reached, but at low scan potential no polymerization occurred. The complex modified electrode shows good electrocatalytic oxidation properties towards ascorbic acid. This modified electrode can show amperometric determination of H₂A with a good sensitivity

6.5 References

- [1] E. S. Wagner, B. Lindley, R. D. Coffin, *Journal of Chromatography B: Biomedical Sciences and Applications* **1979**, *163*, 225-229.
- [2] W. Zeng, F. Martinuzzi, A. MacGregor, *Journal of pharmaceutical and biomedical analysis* **2005**, *36*, 1107-1111.
- [3] S. A. Kumar, P.-H. Lo, S.-M. Chen, *Biosensors and Bioelectronics* **2008**, *24*, 518-523.
- [4] R. N. Adams, *Analytical Chemistry* **1976**, *48*, 1126A-1138A.
- [5] R. S. Freire, L. T. Kubota, *Analyst* **2002**, *127*, 1502-1506.
- [6] Y.-N. Wang, K.-C. Lau, W. W. Y. Lam, W.-L. Man, C.-F. Leung, T.-C. Lau, *Inorganic Chemistry* **2009**, *48*, 400-406.
- [7] P. H. Aubert, P. Audebert, M. Roche, P. Capdevielle, M. Maumy, G. Ricart, *Chemistry of Materials* **2001**, *13*, 2223-2230.
- [8] Bruker, APEX2, SAINT and SADABS, Bruker AXS Inc., Madison, Wisconsin, USA, **2008**.
- [9] G. M. Sheldrick, *Acta Crystallographica* **2015**, *A71*, 3.
- [10] G. M. Sheldrick, *Acta Crystallographica* **2015**, *C71*, 3.
- [11] F. A. Mautner, C. N. Landry, A. A. Gallo and S. S. Massoud, *Journal of Molecular Structure* **2007**, *837*, 72
- [12] C. Demetgül, D. Deletioğlu, F. Karaca, S. Yalçinkaya, M. Timur, S. Serin, *Journal of Coordination Chemistry* 2010, *63*, 2181-2191.
- [13] X. J. Zhu, B. J. Holliday, *Macromolecular rapid communications* 2010, *31*, 904-909.
- [14] J. Fei, L. Luo, S. Hu, Z. Gao, *Electroanalysis: An International Journal Devoted to Fundamental and Practical Aspects of Electroanalysis* 2004, *16*, 319-323.
- [15] M. Rueda, A. Aldaz, F. Sanchez-Burgos, *Electrochimica Acta* 1978, *23*, 419-424.

Appendix

List of publications


- 1) A Bhattacharjee, S Das, B Das, P Roy “**Intercalative DNA binding, protein binding, antibacterial activities and cytotoxicity studies of a mononuclear copper(II) complex**” *Inorganica Chimica Acta*, 2021,514,119961.**
- 2) A Barma, A Bhattacharjee, P Roy “**Dinuclear Copper(II) Complexes with N,O Donor Ligands: Partial Ligand Hydrolysis and Alcohol Oxidation Catalysis**” *Eur. J. Chem*, 2021, 23, 2284-2292.
- 3) A Hazra, A Roy, A Bhattacharjee, A Barma, P Roy “**Quinoline based chromogenic and fluorescence chemosensor for pH: Effect of isomer**” *Journal of Molecular Structure*, 2020, 1201, 127173.
- 4) A.Bhattacharjee, S.Dey, P.Roy “**Particulate methane monooxygenase mimicking activity of dinuclear transition metal complexes**” *Inorganica Chimica Acta*, 2019,490,93-103. **
- 5) A.Bhattacharjee, T. Das, H. Uyama, P.Roy, M.Nandi “**Cu- and Ni-Grafted Functionalized Mesoporous Silica as active Catalyst for Olefin Oxidation**” *Chem. Select* , 2017, 2, 10157 –10166**
- 6) A. Bhattacharjee, S. Halder, K. Ghosh, C. Rizzoli, P. Roy “**Mono-, tri- and polynuclear copper(II) complexes of Schiff-base ligands: synthesis, characterization and catalytic activity towards alcohol oxidation**” *New J. Chem.*, 2017, 41, 5696-5706. **
- 7) K. Ghosh, S. Dey, S. Halder, A. Bhattacharjee, C. Rizzoli, P. Roy “**A turn-on fluorescent chemosensor for Zn²⁺ ion: X-ray structure and application in cell imaging study**” *Journal of Molecular Structure* , 2016 , 1118 ,325-334
- 8) S. Halder, A. Bhattacharjee, A. Roy , S. Chatterjee ,P. Roy “**Chromogenic and fluorescence sensing of pH with a Schiff-base molecule**” *RSC Adv.*, 2016,6, 39118-39124
- 9) S. Halder , A. Dey , A. Bhattacharjee , J. Castro, A. Fontera, P .P. Ray, P. Roy “**Cd(II)-based MOF as a photosensitive Schottky diode: experimental and theoretical studies**” *Dalton Trans.*, 2017, 46, 11239-11249 .

**** Publications included in thesis**



Cite this: *New J. Chem.*, 2017, 41, 5696

Mono-, tri- and polynuclear copper(II) complexes of Schiff-base ligands: synthesis, characterization and catalytic activity towards alcohol oxidation†

Aradhita Bhattacharjee,^a Shibashis Halder,^a Koushik Ghosh,^a Corrado Rizzoli^b and Partha Roy *^a

Three new copper(II) complexes with different Schiff-base ligands, namely, [Cu(L¹)Cl₂] (**1**), [Cu₃(L²)₂Cl₄] (**2**) and [Cu(L³)N₃]_n (**3**) where L¹ = 2-morpholino-*N*-(pyridin-2-ylmethylene)ethanamine, HL² = 4-bromo-2-((2-morpholinoethylimino)methyl)phenol and HL³ = 4-chloro-2-((2-(dimethylamino)ethylimino)methyl)phenol, have been synthesized and characterized by elemental analysis, standard spectroscopic methods, cyclic voltammetry and single crystal X-ray diffraction analysis. The X-ray diffraction analysis confirms the formation of mononuclear (**1**), trinuclear (**2**) and polynuclear (**3**) complexes. These complexes have been applied as catalysts for alcohol oxidation reactions using *tert*-butyl hydroperoxide (TBHP) as the terminal oxidant under mild conditions. The catalytic reaction mixture has been analyzed by gas chromatography and it shows that the mononuclear complex has the highest conversion while the other two complexes exhibit moderate catalytic activities. The corresponding aldehyde has been obtained as the sole product. The obtained catalysis results have been corroborated with electrochemical studies.

Received 14th March 2017,
Accepted 19th May 2017

DOI: 10.1039/c7nj00846e

rsc.li/njc

Introduction

The development and application of transition metal complexes with N,O-donor ligands have drawn appreciable interest from researchers over the last few decades. Preparation of N,O donor ligands by Schiff-base condensation is popular among scientists as these types of ligands can be synthesized by one step condensation between a keto/aldehyde group and a primary amine group with a very high yield.¹ The appropriate selection of the aldehyde/ketones and primary amine with extra hetero atoms could produce ligands with a desired number of donor atoms. Softness or hardness of the donor group could be incorporated by judicious choice of the reactants and the requirement for the coordination of the metal center. Moreover, the Schiff-base ligands can stabilize various oxidation states of the metal center. Transition metal complexes with Schiff-base ligands have been used in a number of important fields of application *e.g.* magnetism,² catalysis,³ biological sciences,⁴ optoelectronics,⁵ sensing,⁶ *etc.*⁷ Copper(II) complexes have been used as catalysts in different organic reactions such as oxidation of alkanes, epoxidation of alkenes, catechol oxidation,

benzylic oxidation, aromatic C–H oxidation, Glaser–Hay acetylenic coupling reactions, alcohol oxidation, Baeyer–Villiger oxidation, sulfoxidation, *etc.*^{3*f–i*} Till date, research has been conducted on the catalytic aspects of the newly synthesized metal complexes to find a better catalyst with remarkable yield and selectivity over the desired product(s).

The oxidation of alcohols is one of the most important functional transformations in synthetic organic chemistry. This can be done by following several methods and using different reagents.⁸ However, these reactions are often done with stoichiometric amounts of the reactants. The generation of inorganic salt(s) mixed with the target molecules demands time and labor for the work-up procedure. To avoid these problems, suitable catalysts may be used. Copper(II)-phenoxyl radical complexes as the model of the reaction of galactose oxidase can oxidize primary alcohols into aldehydes.⁹ Galactose oxidase is a fungal enzyme with one copper atom at the active site; it has a square pyramidal geometry and it catalyzes the oxidation of a number of primary alcohols to aldehydes.¹⁰

A number of Schiff-base complexes of copper(II) ions have been developed where different aldehydes, *e.g.* salicylaldehyde or its derivatives, were used for the formation of Schiff-bases.¹¹ Copper(II) complexes have been synthesized with these ligands where 1, 2, 3 or more copper atom(s) are present in the asymmetric unit. These complexes find applications in many fields; in particular N,N donor and N,O donor ligands have been used for the preparation of copper complexes with different nuclearities

^a Department of Chemistry, Jadavpur University, Jadavpur, Kolkata-700 032, India.
E-mail: proy@chemistry.jdvu.ac.in

^b Università degli Studi di Parma, Dipartimento S.C.V.S.A.,
Parco Area delle Scienze 17/A, I-43124 Parma, Italy

† Electronic supplementary information (ESI) available. CCDC 1535653–1535655.
For ESI and crystallographic data in CIF or other electronic format see DOI: 10.1039/c7nj00846e

as a catalyst for the oxidation of alcohols.¹² However, in spite of the excellent results obtained, there is still scope for the improvement of the activity of the catalysts with respect to yield and time.

In this context, we report here the synthesis, characterization and catalytic properties of mono-, tri- and polynuclear copper(II) complexes, [Cu(L¹)Cl₂] (1), [Cu₃(L²)₂Cl₄] (2) and [Cu(L³)N₃]_n (3) respectively, where L¹ = 2-morpholino-*N*-(pyridin-2-ylmethylene)ethanamine, HL² = 4-bromo-2-((2-morpholinoethylimino)methyl)phenol and HL³ = 4-chloro-2-((2-(dimethylamino)ethylimino)methyl)phenol. These complexes have been synthesized and characterized by standard methods including single crystal X-ray diffraction analysis. These complexes have been used as catalysts for the oxidation of benzyl alcohols with *tert*-butylhydroperoxide (TBHP) as the oxidant under ambient conditions. We have chosen these ligands to create a coordination environment similar to that in galactose oxidase and create variation in the nuclearity of the complexes to compare the catalytic results obtained under identical conditions.

Experimental section

Materials and physical methods

Pyridine-2-carboxaldehyde, 5-chloro-2-hydroxybenzaldehyde, *N*-methyl-1,3-diaminopropane, 5-bromo-2-hydroxybenzaldehyde, 4-(2-aminoethyl)morpholine, copper(II) perchlorate hexahydrate, copper(II) chloride dihydrate and sodium azide were purchased from Sigma Aldrich and used without further purification. Other reagents were obtained from commercial sources and used as received. Solvents were purchased from commercial sources and were used for synthesis without further purification, while purified and dried solvents¹³ were used for spectroscopic measurements. Elemental analyses (carbon, hydrogen and nitrogen) were performed using a Perkin-Elmer 2400C elemental analyzer. The FT-IR spectra of the samples were obtained on a Perkin Elmer spectrometer (Spectrum Two) by using the attenuated total reflectance (ATR) technique. The UV-visible spectral measurements were done in an Agilent 8453 diode array spectrophotometer. The analysis of the reaction mixture of catalytic reactions was performed with a Shimadzu made next generation high speed gas chromatography system (model: GC-2025 AF) equipped with a fused silica capillary column and a FID detector. The cyclic voltammetric measurements were performed on a CHI Electrochemical workstation. A platinum wire working electrode, a platinum wire auxiliary electrode and a Ag/AgCl reference electrode were employed in a standard three-electrode configuration. Bu₄NPF₆ was used as the supporting electrolyte in CH₃CN and the scan rate was 50 mV s⁻¹ under nitrogen atmosphere. All the experiments were carried out at room temperature in air unless reported otherwise.

Synthesis of [Cu(L¹)Cl₂] (1)

4-(2-Aminoethyl)morpholine (0.5 mmol, 0.065 mL) was added to a methanolic solution (10 mL) of 2-pyridinecarboxaldehyde (0.5 mmol, 0.053 mL) under stirring condition. The mixture was stirred for 30 min. Then the resulting solution was refluxed for 5 h.

The color of the mixture turned orange. The mixture was then cooled and it was used as 'ligand (L¹)' without any characterization and further purification. The solution of L¹ in methanol was allowed to cool to room temperature. Then, a methanolic solution (10 mL) of copper(II) chloride dihydrate (0.5 mmol, 0.067 g) was added to the ligand solution. The mixture was stirred until it turned greenish. It was then refluxed for 1 h. The color of the solution became dark green. The mixture was finally cooled to room temperature and filtered to remove any precipitate or suspended materials. The filtrate was kept at ambient temperature. Green crystals suitable for X-ray diffraction studies were produced after a few days.

Data for 1: yield (65%); C, H, N analysis: anal. calc. for C₁₂H₁₇Cl₂CuN₃O: C, 40.74; H, 4.84; N, 11.88; found: C, 40.54; H, 4.57; N, 11.98%.

Synthesis of [Cu₃(L²)₂Cl₄] (2)

4-(2-Aminoethyl)morpholine (0.5 mmol, 0.065 mL) was added to a methanolic solution (10 mL) of 5-bromo-2-hydroxybenzaldehyde (0.5 mmol, 0.100 g) and stirred. The mixture was refluxed for 2 h forming an orange solution of Schiff base ligand. The mixture was then cooled and it was used as 'ligand (HL²)' without any characterization and purification. A methanolic solution of copper(II) chloride dihydrate (0.5 mmol, 0.067 g) was added to the solution of HL² and the mixture was stirred for 30 min when it turned greenish. It was then refluxed for 1 h. The color of the solution turned dark green. The mixture was cooled and filtered to remove any undissolved or precipitate materials. The filtrate was kept at ambient temperature. Black single crystals suitable for X-ray diffraction analysis were obtained within a few days.

Data for 2: yield (28%); C, H, N analysis: anal. calc. for C₂₆H₃₂Br₂Cl₄Cu₃N₄O₄: C, 32.64; H, 3.37; N, 5.86; found: C, 32.54; H, 3.22; N, 5.68%.

Synthesis of [Cu(L³)N₃]_n (3)

N-Methyl-1,3-diaminopropane (0.6 mmol, 0.0528 g) was added to a methanolic solution (10 mL) of 5-chloro-2-hydroxybenzaldehyde (0.6 mmol, 0.093 g) under stirring condition. The mixture was stirred for 30 min and then it was refluxed for 2 h. The resulting solution was orange in color. The mixture was then cooled and it was used as 'ligand (HL³)' without any characterization and purification. A methanolic solution (10 mL) of copper(II) perchlorate hexahydrate (0.6 mmol, 0.222 g) was added slowly to the ligand solution of HL³ under stirring condition. The stirring continued for 30 min. The mixture turned greenish. Sodium azide (0.6 mmol, 0.039 g) in methanol/water mixed solvent (methanol:water (v/v) ratio 1:2) (2 mL) was added dropwise with constant stirring. The color of the solution became dark. The resultant mixture was refluxed for 1 h when the mixture became dark green. The mixture was then cooled to room temperature and filtered to remove any undissolved or suspended materials. The filtrate was kept at ambient temperature. Green single crystals suitable for X-ray diffraction analysis were produced within a few days.

Data for 3: yield (55%); C, H, N analysis: anal. calc. for C₁₁H₁₄ClCuN₅O: C, 39.88; H, 4.26; N, 21.14; found: C, 39.79; H, 4.22; N, 20.97%.

X-ray data collection and structure determination

Details of the data collection and refinement parameters for complexes **1**, **2** and **3** are summarized in Table 1. The diffraction experiments were carried out on a Bruker SMART 1000 CCD diffractometer for **1** and on a Bruker APEX-II CCD diffractometer for **2** and **3** using graphite monochromated Mo K α radiation at 294(2) K. Data were processed using the Bruker APEX2 and SAINT packages.¹⁴ Absorption corrections based on multi-scans using the SADABS software¹⁴ were applied to the intensity data. The structures were solved by direct methods using SHELXT¹⁵ and refined with full-matrix least-squares on F^2 on all unique reflections using SHELXL-2014/7.¹⁶ All the non-hydrogen atoms of the complexes were refined anisotropically. The crystal selected for the X-ray diffraction experiment of **1** and **3** was refined as a merohedral twin with a fractional contribution of the minor component of 0.18(3) and 0.03(2), respectively. In **1**, the poor quality of the crystal and the presence of twinning may account for the limited overall precision of the structure, the presence of high residual peaks and the relatively high R and wR_2 values.

CCDC 1535655, 1535654, 1535653 contain the supplementary crystallographic data for **1**, **2** and **3** respectively.†

Alcohol oxidation

Primary alcohol oxidation was achieved by using *tert*-butyl hydroperoxide as an oxidant in the presence of copper(II) complexes as a catalyst. Typically, 0.5 mmol of the substrate (alcohol) in 5.0 mL of acetonitrile was taken in a two-necked round-bottomed flask connected with a condenser, followed by the addition of 0.025 mmol of the copper(II) complex. The temperature of the mixture was maintained by a thermostat. 0.5 mmol of *tert*-butyl hydroperoxide was added to the mixture to initiate the catalytic reaction under stirring condition. Aliquots from the mixture

were collected at regular time intervals. The reaction mixture was analyzed by gas chromatography. The substrate and product(s) were identified by comparison with known standards.

Blank experiments, namely oxidation of the alcohols, were performed in the absence of any catalyst under the same experimental conditions.

Results and discussion

Synthesis and characterization

L^1 , HL^2 and HL^3 have been synthesized by one-step Schiff-base condensation between an aldehyde and the respective amine in 1 : 1 molar ratio in methanol. The ligands were not characterized and used for complex formation without further purification. Complex **1** was obtained by the reaction between L^1 and $CuCl_2$ in 1 : 1 molar ratio. The reaction between HL^2 and $CuCl_2$ led to the formation of **2**. However, the reaction of copper(II) perchlorate, HL^3 and sodium azide in 1 : 1 : 1 molar ratio produced **3**. Both, HL^2 and HL^3 underwent deprotonation in the reaction medium without any external deprotonating base.

The FT-IR spectra of all of the complexes were obtained with powder sample by the ATR technique (Fig. S1–S3, ESI†). The peaks at 1651, 1633 and 1628 cm^{-1} in the spectra of complexes **1**, **2** and **3**, respectively indicate the presence of an azomethine bond in the complexes. A strong peak at 2047 cm^{-1} in **3** confirms the presence of an azido moiety.

The ESI-mass spectrometry measurements were performed with methanolic solutions of the complexes (Fig. S4–S6, ESI†). The mass spectrum of **1** shows an m/z peak at 316.96. This peak may be attributed to the $[Cu(L^1)Cl]^+$ fragment. The ESI-mass spectrum of **2** exhibits an m/z peak at 507.27 which is due to the presence of the $[Cu_2(L^2)Cl_2]^+$ fragment. Complex **3** shows an m/z

Table 1 Crystal data of complexes **1**, **2** and **3**

Complex	1	2	3
Formula	$C_{12}H_{17}Cl_2CuN_3O$	$C_{26}H_{32}Br_2Cl_4Cu_3N_4O_4$	$C_{11}H_{14}ClCuN_5O$
Formula weight	353.72	956.79	331.26
T (K)	294(2)	294(2)	294(2)
Crystal color	Dark green	Black	Green
Crystal system	Orthorhombic	Orthorhombic	Monoclinic
Space group	$Pca2_1$	$Pbca$	Cc
a (Å)	24.123(6)	9.1230(9)	13.5037(6)
b (Å)	6.7026(16)	16.1575(15)	16.8086(6)
c (Å)	17.890(4)	21.934(2)	6.7657(3)
α (°)	90.00	90.00	90.00
β (°)	90.00	90.00	119.501(4)
γ (°)	90.00	90.00	90.00
V (Å ³)	2892.6(12)	3233.2(5)	1336.56(11)
Z	8	4	4
Crystal dimensions (mm)	0.10 × 0.16 × 0.23	0.11 × 0.23 × 0.32	0.06 × 0.09 × 0.16
$F(0\ 0\ 0)$	1448	1892	676
D_c (g cm ⁻³)	1.625	1.966	1.646
λ (Mo K α) (Å)	0.71073	0.71073	0.71073
θ range (°)	1.7–25.2	1.9–25.2	2.1–25.5
Reflection collected/unique/observed	29 647, 5223, 4611	30 022, 2926, 2501	9687, 2448, 2252
Absorption correction	Multi-scan	Multi-scan	Multi-scan
R_{int}	0.067	0.045	0.034
Final R_1 index [$I > 2\sigma(I)$]	0.053	0.026	0.029
Final wR_2 index (all reflections)	0.134	0.071	0.063
Goodness-of-fit	1.05	1.04	1.04

peak at 347.97 and this peak may arise due to the presence of the $[\text{Cu}(\text{L}^3)(\text{N}_3)\text{CH}_3\text{O}]^+$ fragment.

The room temperature magnetic susceptibilities of all of the complexes were measured with powder samples using the Guoy balance method. Complexes **1**, **2** and **3** are expected to exhibit different magnetic moment values as the number of unpaired electron(s) and the geometry of the complexes are different. The magnetic moments of complexes **1**, **2** and **3** have been determined to be 1.64, 2.90 and 1.53 BM, respectively. The asymmetric units of complexes **1** and **3** contain only one copper(II) center. Complex **3** shows a slightly lower magnetic moment value than the calculated values indicating the presence of weak antiferromagnetic interaction in the complex at room temperature. The calculated magnetic moment of complex **2** at room temperature is 3.87 BM as there are three copper(II) centers.¹⁷ However, the measured magnetic moment of the complex signifies the presence of a moderately strong antiferromagnetic interaction between the metal centers.

UV-vis spectral studies

The electronic spectra of complexes **1**, **2** and **3** were recorded in methanol at room temperature (Fig. S7–S9, ESI†). UV-vis spectra of complexes **2** and **3** were also obtained in the solid state at room temperature (Fig. S10 and S11, ESI†).

For complex **2**, high intensity bands appear at 374 and 295 nm (molar extinction coefficient: $9000 \text{ M}^{-1} \text{ s}^{-1}$ and $13\,000 \text{ M}^{-1} \text{ s}^{-1}$, respectively) which may be attributed to the ligand to metal charge transfer ($\text{PhO}^- \rightarrow \text{Cu}(\text{II})$, $\text{N}(\text{amino}) \rightarrow \text{Cu}(\text{II})$) and intraligand charge transfer. The UV-vis spectrum of complex **3** exhibits high intensity bands at 382 nm and 321 nm with molar extinction coefficients of $44\,000 \text{ M}^{-1} \text{ s}^{-1}$ and $7000 \text{ M}^{-1} \text{ s}^{-1}$ respectively. These bands are probably due to $\text{PhO}^- \rightarrow \text{Cu}(\text{II})$, $\text{N}(\text{amino}) \rightarrow \text{Cu}(\text{II})$ LMCT. Another band at 291 nm with a molar extinction coefficient of $11\,000 \text{ M}^{-1} \text{ s}^{-1}$ is probably due to the intraligand charge transfer transition.

Complexes **1**, **2** and **3** show broad bands centered at 700, 640 and 680 nm respectively with low intensity in methanol.

These spectral characteristics are consistent with copper(II) complexes of distorted square pyramidal (SP) geometry. The observed bands originate from d_{xz} , $d_{yz} \rightarrow d_{x^2-y^2}$ transitions¹⁸ and they may or may not be accompanied by a low-energy shoulder ($>800 \text{ nm}$). A low energy single d–d band at $>800 \text{ nm}$ (d_{xy} , $d_{x^2-y^2} \rightarrow d_{z^2}$) with a high energy shoulder (spin forbidden, d_{xz} , $d_{yz} \rightarrow d_{z^2}$) is typically observed in the trigonal bipyramidal (TBP) geometry. Thus, the copper atoms in complexes **2** and **3** are in a distorted SP environment which is further evident from their solid state electronic spectra. Solid state spectra (Fig. S10 and S11, ESI†) show bands with maxima at 680 and 683 nm for **2** and **3** respectively along with other peaks indicating the presence of a distorted SP geometry in the solid state.

Crystal structures of complexes **1**, **2** and **3**

The ORTEP plot of the asymmetric unit of complex **1** is provided in Fig. 1. Selected bond lengths and angles for complexes **1**, **2** and **3** are given in Table 2.

The mononuclear complex **1** crystallizes from methanol in the orthogonal system, space group $Pca2_1$, with two complex molecules of similar geometry in the asymmetric unit. In each molecule the copper atom is coordinated by the N donor atoms of the neutral ligand L^1 and by two chloride anions in a distorted square pyramidal geometry as indicated by the value of the trigonal index τ . The trigonal index is calculated as the difference between the two largest donor–metal–donor angles divided by 60. Its value is 1 for an ideal trigonal bipyramid and 0 for a square pyramid.¹⁹ The values of τ are 0.028 and 0.027 for atoms Cu1 and Cu2, respectively, indicating that the coordination environments are nearly ideal square pyramidal. The Cu1 and Cu2 metals are displaced by 0.3380(9) and 0.3383(9) Å with respect to the corresponding basal plane formed by atoms N1/N2/N3/Cl1 and N4/N5/N6/Cl3, respectively. In the crystal, the $\text{C–H} \cdots \text{O}$ hydrogen bonds (Table S1, ESI†) between aromatic H atoms and the oxygen atoms of the morpholino moieties lead to the formation of molecular chains parallel to the a axis. In addition, the adjacent chains are connected into a two-dimensional double

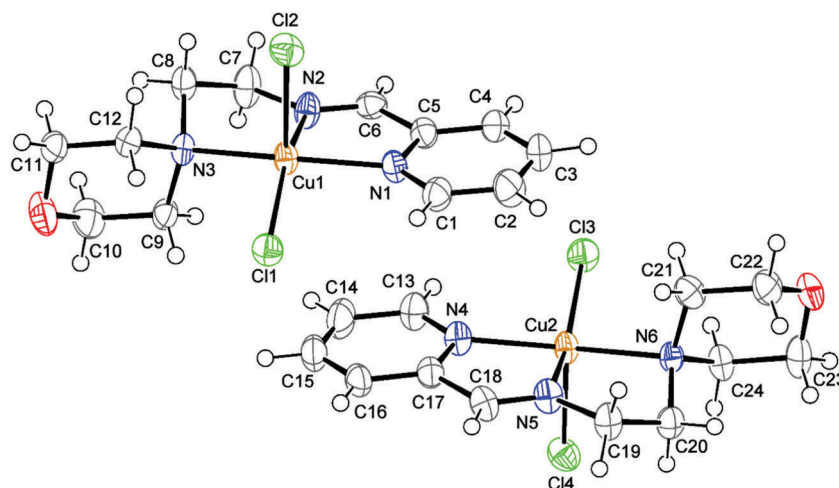


Fig. 1 A perspective view of the asymmetric unit of complex **1** with displacement ellipsoids drawn at the 50% probability level.

Table 2 Selected bond lengths (Å) and bond angles (°) of complexes **1**, **2** and **3**

Complex 1			
Cu1–N1	2.058(6)	Cu2–N4	2.052(6)
Cu1–N2	1.985(7)	Cu2–N5	1.975(7)
Cu1–N3	2.082(6)	Cu2–N6	2.099(6)
Cu1–Cl1	2.258(2)	Cu2–Cl3	2.256(2)
Cu1–Cl2	2.480(3)	Cu2–Cl4	2.475(3)
N2–Cu1–N1	79.4(3)	N5–Cu2–N4	79.5(3)
N2–Cu1–N3	81.5(3)	N5–Cu2–N6	81.7(3)
N1–Cu1–N3	158.5(2)	N4–Cu2–N6	158.7(3)
N2–Cu1–Cl1	156.8(2)	N5–Cu2–Cl3	157.1(2)
N1–Cu1–Cl1	96.1(2)	N4–Cu2–Cl3	96.2(2)
N3–Cu1–Cl1	97.79(19)	N6–Cu2–Cl3	97.25(19)
N2–Cu1–Cl2	97.1(2)	N5–Cu2–Cl4	97.2(2)
N1–Cu1–Cl2	94.0(2)	N4–Cu2–Cl4	94.7(2)
N3–Cu1–Cl2	97.85(19)	N6–Cu2–Cl4	97.5(2)
Cl1–Cu1–Cl2	105.88(9)	Cl3–Cu2–Cl4	105.64(9)
Complex 2			
Cu1–O1	1.9546(19)	Cu2–N2	2.048(2)
Cu1–Cl1	2.8787(8)	Cu2–O1	1.980(2)
Cu1–Cl2	2.3327(8)	Cu2–Cl1	2.2713(9)
Cu1···Cu2	2.9512(4)	Cu2–Cl2	2.6982(9)
Cu2–N1	1.944(2)		
O1–Cu1–O1 ⁱ	180	N1–Cu2–N2	85.53(10)
O1–Cu1–Cl2 ⁱ	85.39(6)	O1–Cu2–N2	171.69(9)
O1–Cu1–Cl2 ⁱ	94.61(6)	N1–Cu2–Cl1	157.08(8)
O1–Cu1–Cl1	74.03(6)	O1–Cu2–Cl1	89.55(6)
O1–Cu1–Cl1 ⁱ	105.97(7)	N2–Cu2–Cl1	97.05(7)
Cl1–Cu1–Cl1 ⁱ	180	N1–Cu2–Cl2 ⁱ	109.15(8)
Cl1–Cu1–Cl2	87.24(6)	O1–Cu2–Cl2 ⁱ	75.51(7)
Cl1–Cu1–Cl2 ⁱ	92.76(6)	N2–Cu2–Cl2 ⁱ	99.01(7)
Cl2–Cu1–Cl2 ⁱ	180	Cl1–Cu2–Cl2 ⁱ	93.00(3)
N1–Cu2–O1	90.35(9)		
Complex 3			
Cu1–O1	1.916(4)	Cu1–N1	1.987(5)
Cu1–N2	2.045(5)	Cu1–N3	2.028(5)
Cu1–N3 ⁱⁱ	2.427(5)		
O1–Cu1–N1	90.65(19)	O1–Cu1–N3	88.11(19)
N1–Cu1–N3	155.11(19)	O1–Cu1–N2	173.4(2)
N1–Cu1–N2	95.70(17)	N3–Cu1–N2	86.8(2)
O1–Cu1–N3 ⁱⁱ	85.35(17)	N1–Cu1–N ⁱⁱ	96.77(18)
N3–Cu1–N3 ⁱⁱ	107.9(2)	N2–Cu1–N3 ⁱⁱ	92.24(19)

Symmetry codes: (i) $-x, 1 - y, 1 - z$; (ii) $x, 1 - y, -1/2 + z$.

layer parallel to the *ab* plane by the C–H···Cl hydrogen bonds (Fig. 2).

The ORTEP plot of the asymmetric unit of complex **2** is shown in Fig. 3. The discrete molecule of complex **2** consists of three copper atoms, two 2-((2-morpholinoethylimino)methyl)-4-bromophenol Schiff-base ligands deprotonated at the O atoms (L^2), and four μ -bridging chlorine atoms. The trinuclear complex has crystallographically imposed inversion symmetry, with the Cu1 metal lying on the Wyckoff special position 4a of the space group *Pbca*. Cu1 is coordinated to four μ_2 -Cl atoms and two μ_2 -phenoxido oxygen atoms in a remarkably distorted octahedral geometry elongated along the Cu1–Cl1 bonds. Atom Cu2 coordinates to the O1 bridging phenoxido oxygen, the N1 and N2 atoms from the HL² ligand, and two μ_2 -Cl atoms in a distorted square pyramidal geometry as indicated by the τ value of 0.243.

Atoms O1, N1, N2 and Cl1 constitute the basal plane whereas Cl2 occupies the apical position. Cu2 is out of the mean basal plane towards Cl2 by 0.1751(4) Å. In the crystal, there exist both C–H···Cl and C–H···Br hydrogen bonds (Table S2, ESI[†]) linking molecules into a three-dimensional network (Fig. 4).

The asymmetric unit of complex **3** is given in Fig. 5. The asymmetric unit of complex **3** consists of one CuL³ moiety including one 2-((3-(methylamino)propylimino)methyl)-4-chlorophenol ligand deprotonated at the O atoms (L^3), and one azido anion. The Cu metal exhibits a distorted square pyramidal coordination geometry provided by the O- and N-donor atoms of the Schiff base, and by the N atoms of two μ -azido anions, with atoms O1, N1, N2 and N3 at the basal plane and atom N3ⁱⁱ occupying the apical position (ii = $x, 1 - y, -1/2 + z$). The Cu metal protrudes by 0.1500(8) Å from the mean basal plane, which shows a remarkable tetrahedral distortion (r.m.s. = 0.2501 Å; maximum displacement 0.340(7) Å for atom N3). The amplitude of the distortion from the ideal square pyramidal geometry may be inferred also from the value of 0.306 of the trigonal index τ . The azido anion acts as an end-on bridging group ($\mu_{1,1}$) linking the CuL³ moieties into polymeric chains running parallel to the *c* axis (Fig. 6). Within the chains N–H···N hydrogen bonds involving the terminal N5 azido nitrogen atoms are observed (Table S3, ESI[†]). In the crystal, the adjacent chains interact through the C–H···N hydrogen bonds to form a three-dimensional network.

Electrochemical studies

Electrochemical studies of all of the copper(II) complexes were carried out in acetonitrile using TBAP as a supporting electrolyte. A typical cyclic voltammogram (CV) was obtained by using a Pt working electrode and an Ag/AgCl reference electrode. The CV of **1** (Fig. 7) shows a quasi-reversible reduction in the negative potential region indicating conversion of Cu(II) species to Cu(I). The plot in this region shows a peak at a potential of -0.05 V with a corresponding i_{pc} value of -1.21×10^{-5} A. Cu(I) is oxidized back to Cu(II) as indicated by a peak at -0.31 V with the corresponding i_{pa} of 2.54×10^{-5} A. $E_{1/2}$ was determined as -0.18 V. The copper center's interaction with the ligand system may be the probable cause of the quasi-reversibility.

Coming to any probability of any further oxidation of the Cu(II) center, a scan was done in the positive potential region (Fig. 8). The plot shows a possible oxidation of Cu(II) \rightarrow Cu(III) with a peak at a potential of 0.22 V and I_{pa} of 5.31×10^{-6} A which completes a quasi-reversible cycle as it gets reduced back to Cu(II), yielding a peak at 0.36 V and I_{pc} of -7.48×10^{-6} A. $E_{1/2}$ was determined to be 0.29 V.

The CV of the trinuclear copper complex, **2**, shows a quasi-reversible reduction of Cu(II) to Cu(I) (Fig. 9a). The reduction from Cu(II) to Cu(I) occurs in the forward sweep as shown in the peak value of -0.88 V with an I_{pc} of -3.17×10^{-7} A. The trinuclear complex, as shown in the crystal structure, has two Cu atoms in identical positions while the other one, which links both the other Cu atoms, has a different electronic environment. It is possible that when the potential is applied in the forward sweep, the three Cu atoms end up experiencing an overall similar electronic environment due to some electronic delocalization.

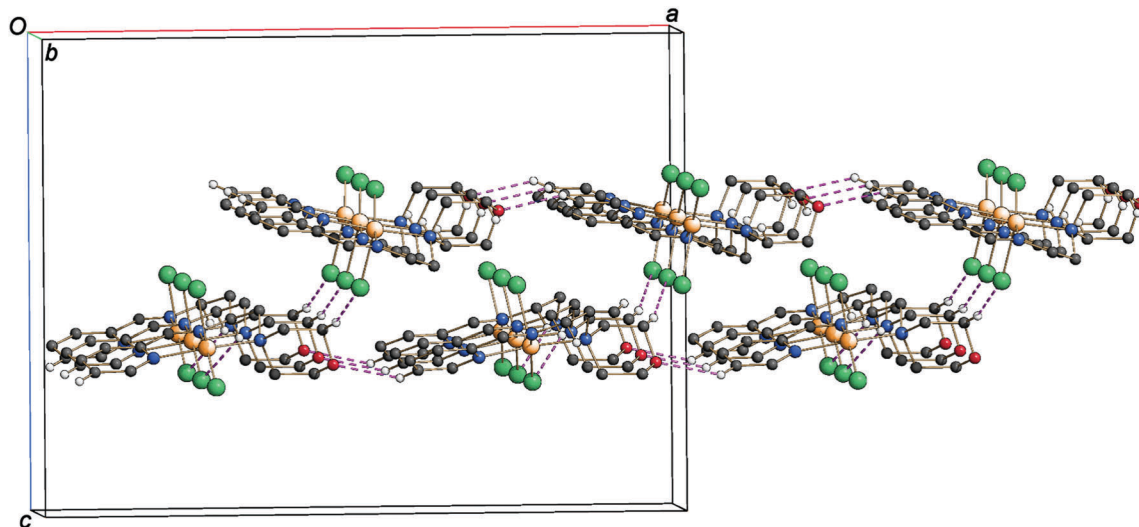


Fig. 2 Partial crystal packing of complex **1** approximately viewed down the *b* axis, showing the formation of molecular double layers parallel to the *ab* plane by the C–H...O and C–H...Cl hydrogen bonds (dashed lines). H atoms not involved in intermolecular hydrogen bonds are omitted for clarity.

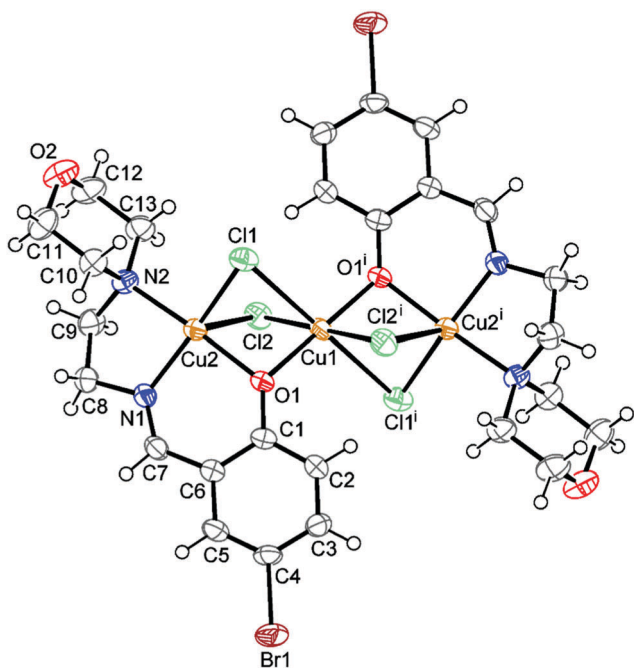


Fig. 3 The molecular structure of complex **2** with displacement ellipsoids drawn at the 50% probability level. Symmetry code: (i) $-x, 1 - y, 1 - z$.

This might have caused the three Cu centers to behave identically and give one reduction peak while getting reduced to Cu(I) species. In the reverse sweep, while getting oxidized it shows two major peaks *i.e.* at -0.77 V with an I_{pa} of $9.94 \mu\text{A}$ and another at -0.50 V with a corresponding I_{pa} of $9.41 \mu\text{A}$. The presence of two peaks here can be explained by the fact that probably after getting reduced to Cu(I) species, the electronic environment changes in such a manner that the two Cu atoms start behaving differently due to the probable lack of the electronic delocalization which had earlier caused them to behave similarly.

Hence, we get two peaks for the oxidation of two Cu centers from Cu(I) to Cu(II).

A scan in the positive potential region of the trimeric complex shows oxidation of Cu(II) species to Cu(III) species (Fig. 9b). The forward sweep is an oxidation forming Cu(III) with a peak potential of 0.308 V and a corresponding I_{pa} of $1.96 \mu\text{A}$. This tripositive species gets reduced back in the backward sweep with a potential of 0.418 V and I_{pc} of $-1.52 \mu\text{A}$.

The CV of the polynuclear complex, **3** (Fig. 9c), shows an almost reversible reduction at the Cu center as Cu(II) gets reduced to Cu(I) at -0.92 V with an I_{pc} of -7.10×10^{-7} A which again gets oxidized back to Cu(II) at -0.70 V with an I_{pa} of $7.90 \mu\text{A}$. The positive potential region shows a quasi-reversible oxidation process wherein the Cu(II) is oxidized to Cu(III). In the forward sweep, the Cu(II) gets oxidized to Cu(III) with a potential of 0.79 V and I_{pa} of $1.96 \mu\text{A}$ and gets reduced back to Cu(II) with a potential of 0.80 V and I_{pc} of $-5.31 \mu\text{A}$. One irreversible peak is observed at 1.15 V, which may be attributed to the irreversible reduction of the ligand.

Alcohol oxidation studies

The ability of complexes **1**, **2** and **3** to catalyze organic transformation reactions was checked. These complexes show galactose oxidase mimicking activity, *i.e.* they act as catalyst for the oxidation of benzyl alcohol, 4-methyl benzyl alcohol, 4-methoxy benzyl alcohol, 4-nitro benzyl alcohol and 4-bromo benzyl alcohol in the presence of *tert*-butylhydroperoxide (TBHP) as the oxidant. The corresponding aldehyde has been obtained as the sole product. The results of the oxidation reactions are given in Table 3.

It may be inferred from the table that complex **1** performs better in comparison to the other two complexes as a catalyst for the alcohol oxidation for all the substrates. Conversion of benzyl alcohol is 90% with **1** whereas with complexes **2** and **3**, the yields are 70 and 50%, respectively, indicating a much

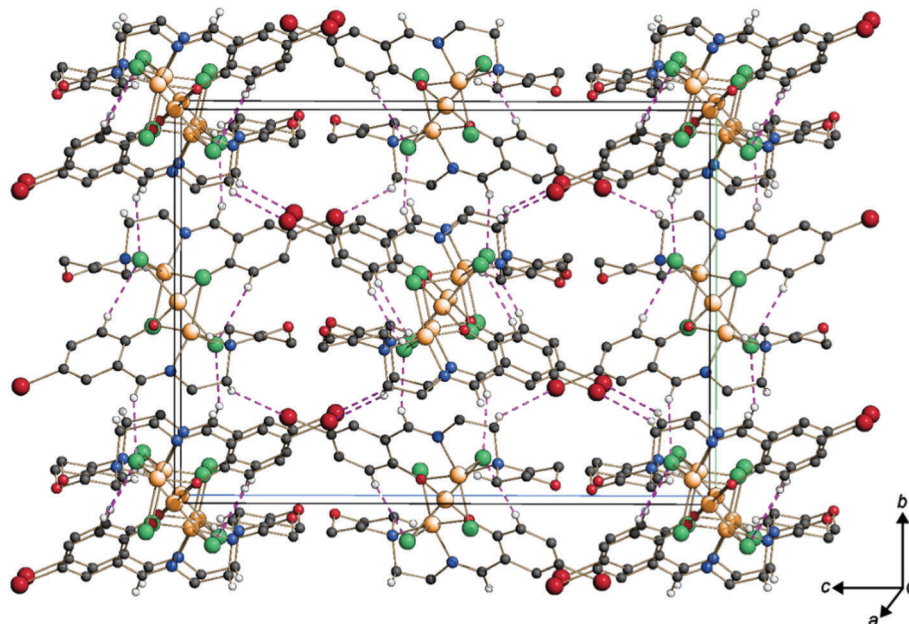


Fig. 4 Packing diagram of **2** showing the H...Cl and H...Br hydrogen bonds (dashed lines). Hydrogen atoms not involved in hydrogen bonding are omitted.

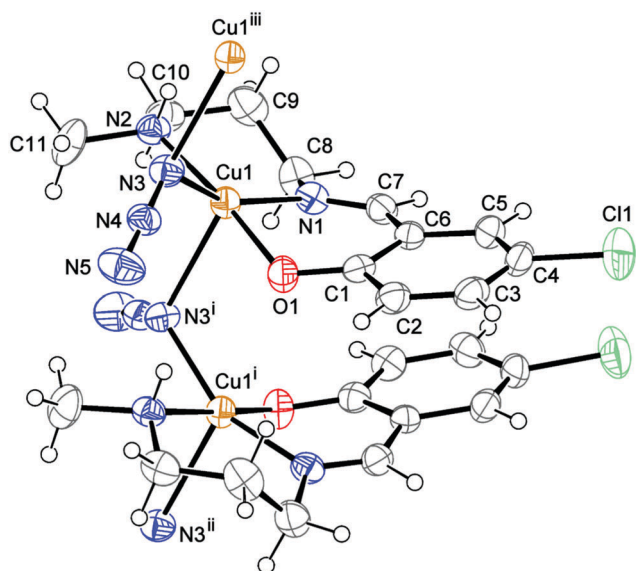


Fig. 5 The molecular structure of complex **3** with displacement ellipsoids drawn at the 40% probability level. Symmetry codes: (i) $x, 1 - y, -1/2 + z$; (ii) $x, y, -1 + z$; (iii) $x, 1 - y, 1/2 + z$.

lower activity of the latter two catalysts. When varying the substrates by introducing an electron pushing and electron withdrawing group in the aromatic ring of benzyl alcohol the trends of conversion are the same, *i.e.* the highest conversion is achieved with **1**, then with **2** and least with complex **3**. In the case of 4-methoxy benzyl alcohol, the yield is increased slightly with each of the catalysts. However, the presence of a bromo or nitro group in the aromatic ring decreases the yield to 78 and 74% respectively in the presence

of complex **1**. Only 44% yield is achieved for 4-nitro benzyl alcohol with complex **3** as a catalyst. Aliquots from the reactions mixture were collected at regular time intervals and analyzed to check the progress of the reaction. The plots of time *vs.* yield for complexes **1**, **2** and **3** are given in Fig. 10 and Fig. S12 and S13 (ESI[†]) respectively. It is evident that the yield of the reaction increases with passage of time for all of the catalysts, the maximum being observed after 14 h of reaction.

Blank reactions with all the substrates were carried out under the same experimental conditions but without any catalyst. It is to be noted that in the case of a blank reaction, the reaction proceeds very slowly and shows very poor conversion (Table 3, entry 4). It takes much longer time for the conversion of the alcohol into the aldehyde. In other words, when we compare the yield of a particular reaction in the same duration of time, *e.g.* 2 h, with and without a catalyst, there is almost no conversion of alcohol to the corresponding aldehyde in the initial time frame while the presence of a copper complex as a catalyst increases the yield of aldehyde manifold. These facts signify the importance of the copper(II) complexes as catalysts.

The effect of elevated temperature on the reaction rate and yield was also examined. At higher temperature, the reaction proceeds slowly and produces lower yield. Moreover, the solution turned a little brownish after being subjected to the reaction condition of 338 K. This probably indicates that the structure of the catalyst got altered, hence rendering it ineffective in catalytic reactions at temperatures higher than 298 K.

In order to investigate the role of the solvent and define whether the catalyst could actively participate in the oxidation

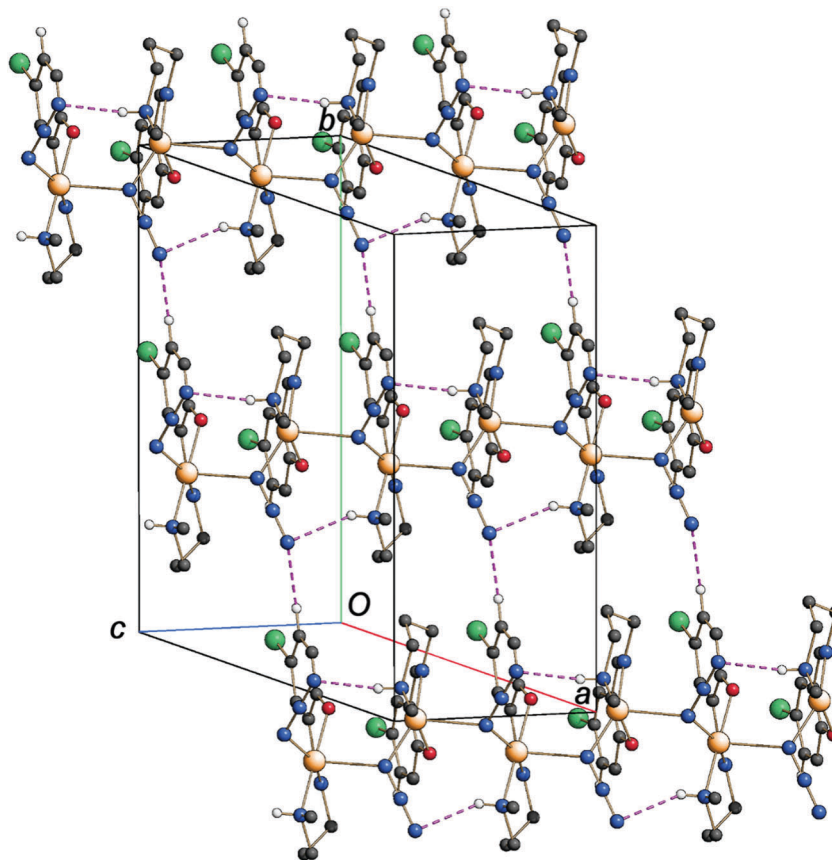


Fig. 6 Crystal packing of complex **3** displaying the formation of one-dimensional chains parallel to the *c* axis linked into layers parallel to (110) by C–H...N hydrogen bonds (dashed lines). Hydrogen atoms not involved in hydrogen bonding are omitted for clarity.

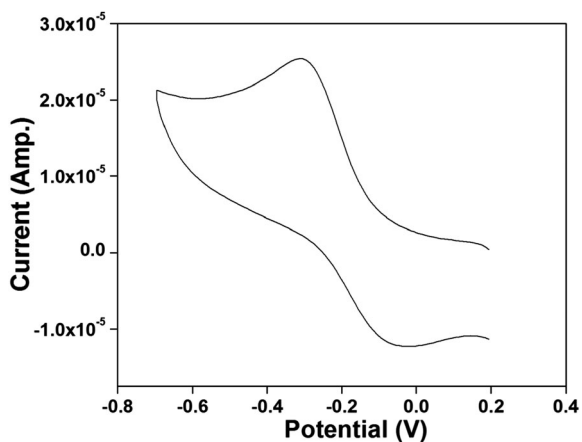


Fig. 7 Cyclic voltammogram showing reduction at the Cu center of complex **1**.

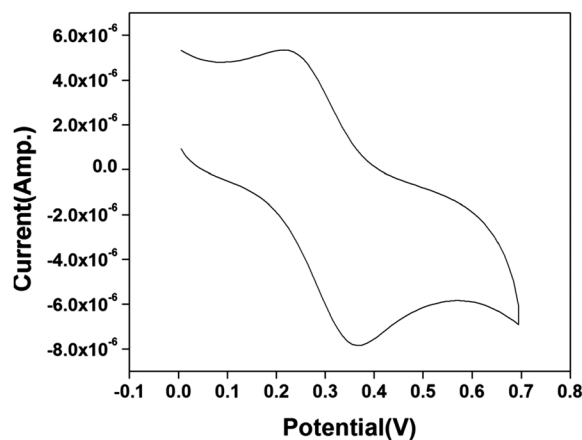


Fig. 8 Cyclic voltammogram showing oxidation at the Cu center of complex **1**.

process under homogeneous conditions, the oxidation of benzyl alcohol was performed in different solvents and the yields obtained are listed in Table 4.

The solubility of complex **1** increases in the following order: acetonitrile > dichloromethane > hexane. The reaction in hexane showed almost no conversion probably because of the low solubility of the catalysts in this solvent; hence the

conversion yields were comparable to those obtained in the blank reactions. When dichloromethane was used, the reactions produced lower yields in comparison to acetonitrile; the latter was therefore selected as the solvent of choice. Another possible explanation for the better yield achieved with acetonitrile may be found in the propensity of this solvent to stabilize Cu(I) species through coordination.

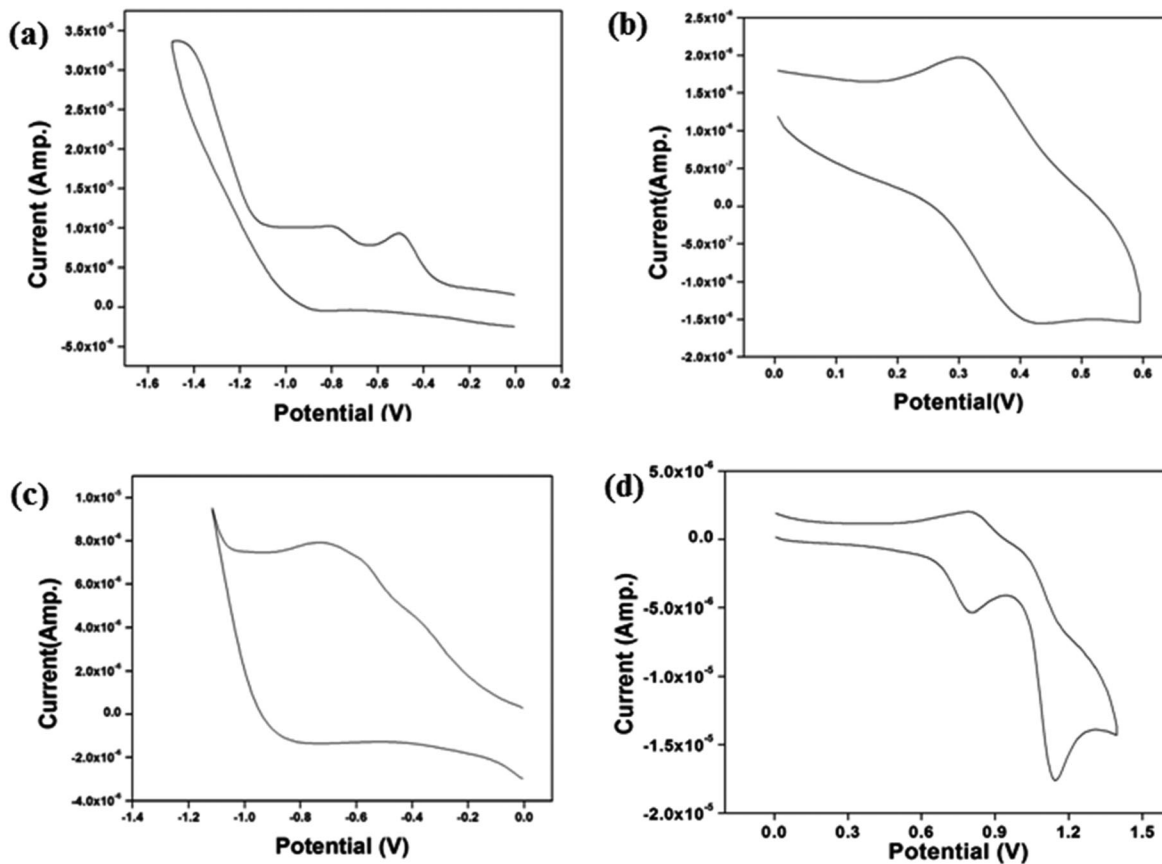


Fig. 9 Cyclic voltammogram showing reduction at the Cu center of complex **2** (a) and **3** (c); CV showing oxidation at the Cu center of complex **2** (b) and **3** (d).

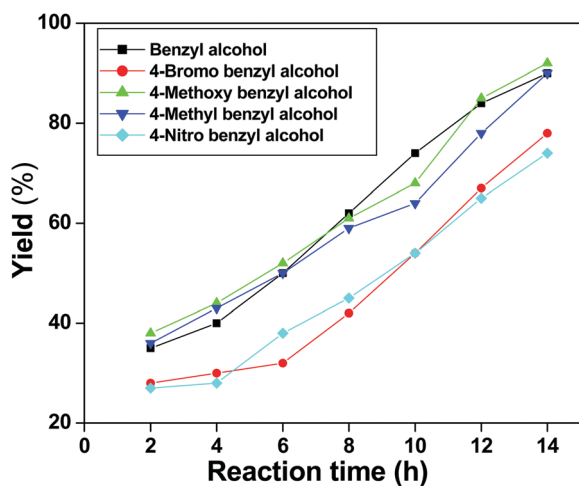


Fig. 10 Plot of yield vs. reaction time for complex **1**.

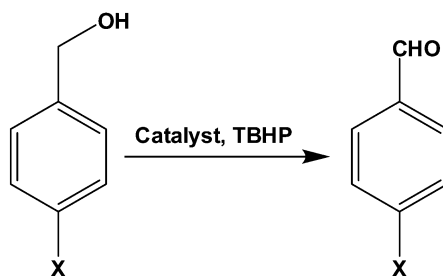
The catalytic reactions of benzyl alcohol as a representative substrate with complexes **1**, **2** and **3** were also performed in the presence of TBHP under anaerobic conditions in order to investigate the role of oxygen, if any, in the oxidation. The results of the catalytic reactions under anaerobic conditions are given in Table 5, showing that the yield of benzaldehyde with each catalyst decreases to some extent. This fact indicates

that oxidation of alcohol is mainly due to the oxidant, TBHP, not the oxygen of air which, at most, may influence the catalysis slightly.

The catalytic reactions were also carried out with varied amounts of catalyst. The results, however, indicated that the effects in terms of reaction yield were not significant, thus for all complexes a 1 : 20 catalyst/substrate ratio was used. Finally, unsuccessful attempts to recover and reuse the complexes after the reaction were carried out in anticipation of recycling the catalyst. In fact, the IR spectra of the compounds collected and dried after the catalytic reactions suggested a substantial decomposition of the complexes, thus preventing their reuse as catalysts.

A possible mechanistic pathway for the oxidation of benzyl alcohol may be proposed based on the present work and results that were obtained from earlier studies. It is known that the reactions between TBHP and Cu(II) may lead to the formation of $t\text{BuO}^\bullet$ radicals and Cu(I) species.²⁰ This radical is known to be a hydrogen atom abstractor from alcohols.²¹ Thus, the mechanism for this type of oxidation may occur *via* radical generation as proposed by Pombeiro and others.²²

It is clear from the electrochemical studies that reduction of Cu(II) to Cu(I) in complex **1** occurs at the potential of -0.05 V; for complexes **2** and **3**, the values at which reduction of Cu(II) to Cu(I) occurs are -0.88 and -0.92 V, respectively. These values

Table 3 Oxidation^a of primary alcohols with complexes **1**, **2** and **3**

Entry	Catalyst	Yield ^b % for benzyl alcohol (TON ^c)	Yield % for 4-methyl benzyl alcohol (TON ^c)	Yield % for 4-methoxy benzyl alcohol (TON ^c)	Yield % for 4-bromo benzyl alcohol (TON ^c)	Yield % for 4-nitro benzyl alcohol (TON ^c)
1	1	90 (18)	90 (18)	92 (18.4)	78 (15.6)	74 (14.8)
2	2	70 (14)	72 (14.4)	74 (14.8)	65 (13)	63 (12.6)
3	3	50 (10)	51 (10.2)	53 (10.6)	48 (9.6)	44 (8.8)
4	Blank ^d	9	10	9	7	10

^a Oxidant: TBHP; temperature: 298 K; solvent: acetonitrile. ^b Yield calculated after 14 h. ^c TON: turnover number = number of moles of product/number of moles of catalyst. ^d Catalytic reaction without any catalyst under identical conditions.

Table 4 Oxidation of benzyl alcohol in various solvents

Catalyst	Yield (%) in hexane	Yield (%) in DCM	Yield (%) in acetonitrile
Complex 1	21	77	90
Complex 2	13	47	60
Complex 3	10	33	40

Table 5 Oxidation of benzyl alcohol with complexes **1**, **2** and **3** under anaerobic conditions

Catalyst	Yield (%)
Complex 1	75
Complex 2	50
Complex 3	35

indicate that reduction of the metal center is most easy for **1**, then **2** and most difficult for **3**. Formation of Cu(I) is necessary in the catalytic reaction as discussed in the possible mechanism. The system where the formation of Cu(I) is most feasible should be most active in the oxidation reaction. Thus, the results obtained in the electrochemical and catalytic studies corroborate perfectly establishing complex **1** as the most active catalyst among them all.

Conclusions

In the present paper, the synthesis and characterization by elemental analysis, spectral analysis and single crystal X-ray diffraction of three novel mono-, tri- and polynuclear copper(II) complexes have been reported.

These complexes show galactose oxidase mimicking activity making them able to catalyze the oxidation of primary alcohols to the corresponding aldehydes. Among the three complexes, the mononuclear complex shows a far superior catalytic activity compared to the tri- and polynuclear complexes.

Acknowledgements

PR thanks DST-SERB, New Delhi (Project No. SB/EMEQ-065/2013) for financial support. AB and SH wish to thank CSIR, New Delhi for their fellowships. The authors are thankful to Dr Saurabh Das of Department of Chemistry, Jadavpur University for his helpful discussion on electrochemical studies.

References

- (a) L. Mandal, S. Mandal and S. Mohanta, *New J. Chem.*, 2017, **41**, 4689; (b) A. Panja, N. C. Jana, S. Adak, P. Brandão, L. Dlháň, J. Titiš and R. Boča, *New J. Chem.*, 2017, **41**, 3143; (c) K. Hu, F. Li, Z. Zhang and F. Liang, *New J. Chem.*, 2017, **41**, 2062; (d) S. Dey, A. Roy, G. P. Maiti, S. K. Mandal, P. Banerjee and P. Roy, *New J. Chem.*, 2016, **40**, 1365; (e) F. A. Mautner, R. C. Fischer, M. Spell, A. R. Acevedo, D. H. Tran and S. S. Massoud, *Crystals*, 2016, **6**, 91; (f) S. Adhikari, S. Lohar, B. Kumari, A. Banerjee, R. Bandopadhyay, J. S. Matalobos and D. Das, *New J. Chem.*, 2016, **40**, 10094; (g) J. L. Segura, M. J. Mancheño and F. Zamora, *Chem. Soc. Rev.*, 2016, **45**, 5635; (h) T. T. Tidwell, *Angew. Chem., Int. Ed.*, 2008, **47**, 1016.
- (a) S. Karasawa, K. Nakano, D. Yoshihara, N. Yamamoto, J.-i. Tanokashira, T. Yoshizaki, Y. Inagaki and N. Koga, *Inorg. Chem.*, 2014, **53**, 5447; (b) A. M. Abu-Dief and I. M. A. Mohamed, *Beni-Suef Univ. J. Basic Appl. Sci.*, 2015, **4**, 119; (c) R. E. P. Winpenny, *Chem. Soc. Rev.*, 1998, **27**, 447; (d) P. Roy, M. Nandi, M. Manassero, M. Riccò, M. Mazzani, A. Bhaumik and P. Banerjee, *Dalton Trans.*, 2009, 9543.
- (a) S. Halder, A. Mukherjee, K. Ghosh, S. Dey, M. Nandi and P. Roy, *J. Mol. Struct.*, 2015, **1101**, 1; (b) S. Halder, S. Dey, C. Rizzoli and P. Roy, *Polyhedron*, 2014, **60**, 85; (c) M. Nandi and P. Roy, *Indian J. Chem.*, 2013, **52A**, 1263–1268; (d) P. Roy and M. Manassero, *Dalton Trans.*, 2010, **39**, 1539; (e) P. Roy, K. Dhara, M. Manassero and P. Banerjee, *Inorg. Chem. Commun.*, 2008, **11**, 265; (f) T. Punniyamurthy and

- L. Rout, *Coord. Chem. Rev.*, 2008, **252**, 134; (g) K. C. Gupta and A. K. Sutar, *Coord. Chem. Rev.*, 2008, **252**, 1420; (h) K. C. Gupta, A. K. Sutar and C.-C. Lin, *Coord. Chem. Rev.*, 2009, **253**, 1926; (i) L. Canali and D. C. Sherrington, *Chem. Soc. Rev.*, 1999, **28**, 85.
- 4 (a) W.-J. Lian, X.-T. Wang, C.-Z. Xie, H. Tian, X.-Q. Song, H.-T. Pan, X. Qiao and J.-Y. Xu, *Dalton Trans.*, 2016, **45**, 9073; (b) R. Vafazadeh, F. Jafari, M. M. Heidari and A. C. Willis, *J. Coord. Chem.*, 2016, **69**, 1313; (c) B. K. Seth, A. Saha, S. Haldar, P. P. Chakraborty, P. Saha and S. Basu, *J. Photochem. Photobiol., B*, 2016, **162**, 463.
- 5 (a) S. Halder, A. Layek, K. Ghosh, C. Rizzoli, P. P. Ray and P. Roy, *Dalton Trans.*, 2015, **44**, 16149; (b) S. Roy, A. Dey, P. P. Ray, J. Ortega-Castro, A. Frontera and S. Chattopadhyay, *Chem. Commun.*, 2015, **51**, 12974; (c) V. Stavila, A. A. Talin and M. D. Allendorf, *Chem. Soc. Rev.*, 2014, **43**, 5994.
- 6 S. Halder, J. Mondal, J. Ortega-Castro, A. Frontera and P. Roy, *Dalton Trans.*, 2017, **46**, 1943.
- 7 P. G. Lacroix, *Eur. J. Inorg. Chem.*, 2001, 339.
- 8 T. Mallat and A. Baiker, *Chem. Rev.*, 2004, **104**, 3037.
- 9 (a) P. Chaudhuri, M. Hess, T. Weyhermüller and K. Wieghardt, *Angew. Chem., Int. Ed.*, 1999, **38**, 1095; (b) S. Itoh, M. Taki, S. Takayama, S. Nagatomo, T. Kitagawa, N. Sakurada, R. Arakawa and S. Fukuzumi, *Angew. Chem., Int. Ed.*, 1999, **38**, 2774.
- 10 (a) J. P. Klinman, *Chem. Rev.*, 1996, **96**, 2541; (b) J. Stubbe and W. A. van der Donk, *Chem. Rev.*, 1998, **98**, 705.
- 11 (a) P. A. Vigato and S. Tamburini, *Coord. Chem. Rev.*, 2004, **248**, 1717; (b) P. A. Vigato, S. Tamburini and L. Bertolo, *Coord. Chem. Rev.*, 2007, **251**, 1311; (c) P. A. Vigato and S. Tamburini, *Coord. Chem. Rev.*, 2008, **252**, 1871; (d) P. A. Vigato, V. Peruzzo and S. Tamburini, *Coord. Chem. Rev.*, 2012, **256**, 953.
- 12 (a) J. M. Hoover, B. L. Ryland and S. S. Stahl, *ACS Catal.*, 2013, **3**, 2599; (b) J. M. Hoover, B. L. Ryland and S. S. Stahl, *J. Am. Chem. Soc.*, 2013, **135**, 2357; (c) G. Zhang, L. Li, C. Yang, E. Liu, J. A. Golen and A. L. Rheingold, *Inorg. Chem. Commun.*, 2015, **51**, 13; (d) S. Hazra, L. M. D. R. S. Martins, M. F. C. G. da Silva and A. J. L. Pombeiro, *Inorg. Chim. Acta*, 2017, **455**, 549; (e) G. Zhang, Y. Z. Zhang, W.-F. Lo, J. Jiang, J. A. Golen and A. L. Rheingold, *Polyhedron*, 2016, **103**, 227; (f) E. Safaei, L. Hajikhanmirzaei, B. Karimi, A. Wojtczak, P. Cotič and Y.-I. Lee, *Polyhedron*, 2016, **106**, 153.
- 13 D. D. Perrin, W. L. F. Armarego and D. R. Perrin, *Purification of Laboratory Chemicals*, Pergamon Press, Oxford, U.K., 1980.
- 14 Bruker, APEX2, SAINT and SADABS, Bruker AXS Inc., Madison, Wisconsin, USA, 2008.
- 15 G. M. Sheldrick, *Acta Cryst.*, 2015, **A71**, 3.
- 16 G. M. Sheldrick, *Acta Cryst.*, 2015, **C71**, 3.
- 17 J. E. Huheey, E. A. Keiter and R. L. Keiter, *Inorganic Chemistry: Principles of Structure and Reactivity*, Pearson, 4th edn, 1993.
- 18 (a) *Comprehensive Coordination Chemistry*, ed. B. J. Hathaway, G. Wilkinson, R. D. Gillard and J. A. McCleverty, Pergamon Press, Oxford, England, 1987, vol. 5; (b) F. A. Mautner, C. N. Landry, A. A. Gallo and S. S. Massoud, *J. Mol. Struct.*, 2007, **837**, 72; (c) F. A. Mautner, J. H. Albering, R. Vicente, F. R. Louka, A. Gallo and S. S. Massoud, *Inorg. Chim. Acta*, 2011, **365**, 290; (d) S. S. Massoud, L. L. Quan, K. Gatterer, J. H. Albering, R. C. Fischer and F. A. Mautner, *Polyhedron*, 2012, **31**, 601.
- 19 A. W. Addison, T. N. Rao, J. Reedijk, J. Vanrijn and G. C. Verschoor, *J. Chem. Soc., Dalton Trans.*, 1984, 1349.
- 20 (a) J. K. Kochi, *Tetrahedron*, 1962, **18**, 483; (b) J. K. Kochi, *J. Am. Chem. Soc.*, 1962, **84**, 1572; (c) G. Rothenberg, L. Feldberg, H. Wiener and Y. Sasson, *J. Chem. Soc., Perkin Trans. 2*, 1998, 2429.
- 21 (a) M. S. Dronova, A. N. Bilyachenko, A. I. Yalymov, Y. N. Kozlov, L. S. Shul'pina, A. A. Korlyukov, D. E. Arkhipov, M. M. Levitsky, E. S. Shubina and G. B. Shul'pin, *Dalton Trans.*, 2014, **43**, 872; (b) V. Mahdavi and M. Mardani, *J. Chem. Sci.*, 2012, **124**, 1107; (c) R. R. Fernandes, J. Lasri, A. M. Kirillov, M. F. C. Guedes da Silva, J. A. L. da Silva, J. J. R. Fraústo da Silva and A. J. L. Pombeiro, *Eur. J. Inorg. Chem.*, 2011, 3781.
- 22 (a) I. Timokhin, C. Pettinari, F. Marchetti, R. Pettinari, F. Condello, S. Galli, E. C. B. A. Alegria, L. M. D. R. S. Martins and A. J. L. Pombeiro, *Cryst. Growth Des.*, 2015, **15**, 2303; (b) A. Sabbatini, L. M. D. R. S. Martins, K. T. Mahmudov, M. N. Kopylovich, M. G. B. Drew, C. Pettinari and A. J. L. Pombeiro, *Catal. Commun.*, 2014, **48**, 4048; (c) M. N. Kopylovich, Y. Y. Karabach, M. F. C. G. da Silva, P. J. Figiel, J. Lasri and A. J. L. Pombeiro, *Chem. – Eur. J.*, 2012, **18**, 899; (d) R. R. Fernandes, J. Lasri, M. F. C. G. da Silva, J. A. L. Silva, J. J. R. F. da Silva and A. J. L. Pombeiro, *J. Mol. Catal. A: Chem.*, 2011, **351**, 100.

Catalysis

Cu- and Ni-Grafted Functionalized Mesoporous Silica as Active Catalyst for Olefin Oxidation

Aradhita Bhattacharjee⁺,^[a] Trisha Das⁺,^[b] Hiroshi Uyama,^[c] Partha Roy,^{*[a]} and Mahasweta Nandi^{*[b]}

Mesoporous silica has been functionalized with 3-aminopropyl triethoxy silane (3-APTES), followed by Schiff-base condensation with 2-hydroxy-1-naphthaldehyde. Incorporation of copper and nickel by covalent grafting onto the Schiff-base loaded materials gives two heterogenized catalysts namely, **Cu-Cat** and **Ni-Cat**, respectively. The materials have been characterized by PXRD analyses, nitrogen sorption studies, TEM, TGA, FT-IR, UV-visible and solid state MAS-NMR spectroscopy. The metal-contents in the samples are estimated using ICP-AES studies. **Cu-Cat** and **Ni-Cat** have been used as active catalyst in the

oxidation of various olefins *e.g.* styrene, α -methyl styrene, cyclohexene, *trans* stilbene and cyclooctene in the presence of *tert*-butyl hydroperoxide as the oxidant in acetonitrile under mild conditions. Different products have been analyzed by gas chromatography and gas chromatography-mass spectrometry. The results show high conversion of the substrates, moderate to good product selectivity and high TOFs of the reactions. The catalysts are recycled without deteriorating their activities and heterogeneous nature.

Introduction

Transition metal catalyzed organic transformations are of great importance because they can not only help to achieve valuable products but also new functional groups are introduced in comparatively inert starting materials. Oxidation of olefins and alkanes is important because a large quantity of these materials is available in nature in the form of fuel and gas. Desired products/fine chemicals are obtained from these materials. Transition metal compounds play a pivotal role in their transformation.

Transition metal compounds with copper(II) and nickel(II) are widely used as catalyst in different reactions *e.g.* oxidation of alkane,^[1-5] C–S coupling,^[6] epoxidation of olefins,^[7,8] sulfoxidation,^[9,10] alcohol oxidation,^[11] C–C bond formation,^[12,13,14] hydrogenolysis,^[15,16] *etc.*^[17,18] Cu(II) or Ni(II) compounds are used because they are relatively cheap and effective as catalyst. Oxidation of alkane in the presence of copper(II) catalysts often produces corresponding alcohol and aldehyde while alkene oxidation is generally done with hydrogen peroxide, *tert*-butyl hydroperoxide, iodosyl benzene, molecular oxygen, *etc.* as

terminal oxidant in the presence of a suitable catalyst to get corresponding epoxide as the major product.^[19] Conversion of olefins into the corresponding epoxide is studied because epoxides are important building blocks for the synthesis of several organic fine chemicals and molecules with biological importance. Epoxidation of olefins is also vital as it may induce two chiral carbon centers.^[20,21] However, oxidation of alkenes may lead to the formation of several other products.

Catalytic reactions are performed either in homogeneous medium or in heterogeneous medium. Catalysis in heterogeneous medium has some advantages over that in homogeneous medium. Main problem associated with homogeneous catalysis is separation of product(s) from the catalyst because the substrate, oxidant, product and catalyst all remain in a single phase. Simple filtration in heterogeneous catalysis is employed to separate product and catalyst as catalyst in heterogeneous medium is generally insoluble in liquid phase. Heterogeneous catalyst can be reused for several times in same organic transformation without deteriorating its efficiency and character. A drawback in heterogeneous catalysis is leaching of metal ion in solution which is not at all desirable. Under catalytic condition, a small amount of metal ion that can leak in solution will disturb the heterogeneous nature of the reaction. Thus, heterogenized catalyst should be prepared in a manner so that leaching does not occur. Strong binding of metal ion in the solid matrix can prevent metal leaching.

For heterogenized catalyst, there should be a solid support to which metal atoms are bonded strongly. There are different types of solid support *e.g.* polymer,^[22,23] zeolite,^[24] alumina,^[25] silica,^[26-28] graphene,^[29] mesoporous carbon,^[30] carbon nanotube,^[31] metal-organic framework,^[32,33] metal oxide nanoparticles,^[34] *etc.*^[35,36] Use of mesoporous silica as solid support adds few advantages. Mesoporous silica has large surface area^[37] which allows greater interaction between the metal center and

[a] A. Bhattacharjee,⁺ Dr. P. Roy
Department of Chemistry, Jadavpur University, Jadavpur, Kolkata-700 032 (India)

E-mail: proy@chemistry.jdvu.ac.in

[b] T. Das,⁺ Dr. M. Nandi
Integrated Science Education and Research Centre, Siksha Bhavana, Visva-Bharati University, Santiniketan-731235 (India)

E-mail: mahasweta.nandi@visva-bharati.ac.in

[c] Prof. H. Uyama
Department of Applied Chemistry, Graduate School of Engineering, Osaka University, 2-1 Yamadaoka, Suita, Osaka 565-0871 (Japan)

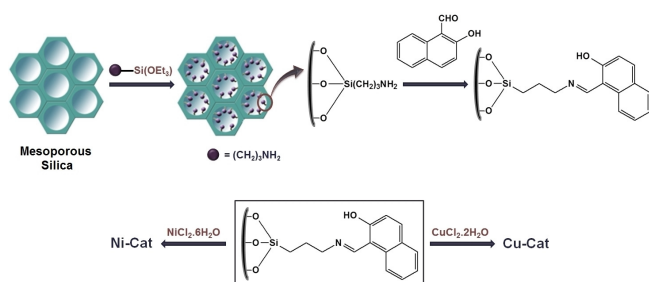
[†] The authors A. Bhattacharjee and T. Das contributed equally to this article.

Supporting information for this article is available on the WWW under <https://doi.org/10.1002/slct.201702183>

the substrate thus increasing the efficiency of the catalyst. In addition to that, the pore size of the silica support can be tuned according to requirement. Suitable selection of template, in the presence of which the mesoporous silica is synthesized, can allow achieving the desired pore size. Silica framework is thermally and chemically stable. Functionalization of silica matrix can be done to introduce appropriate number/nature of heteroatom (e.g. O, N or S) in the framework which can act as strong binding sites for metal center. Covalent bonds are formed when interaction between the functionalized material and the metal ion takes place. Heteroatoms in the silica framework are selected on the basis of possible hard-soft interactions.

Mo,^[38] Ru,^[39,40] Pd,^[41] Fe,^[42] Mn,^[43] Cu,^[44] Ni,^[45] etc.^[46] incorporated materials have been used as catalysts in C–H activation of alkenes. We have effectively used copper(II) complexes of Schiff-base ligands as catalyst in the epoxidation of olefins in homogeneous medium.^[47,48] Impregnated copper(II) or nickel(II) complexes with Schiff-base ligands on mesoporous silica can turn homogeneous catalysts into heterogeneous ones and these heterogenized catalysts have been effective in olefin epoxidation in liquid phase.^[49–51] In these cases, transition metal complexes have been synthesized and characterized by standard techniques. These complexes were then immobilized on to mesoporous silica to be used as the catalyst. However, immobilized Cu-catalyst showed metal leaching in catalytic solution. In this respect, covalently grafted metal incorporated silica can be effective to stop metal leaching in solution under catalytic conditions. 4-Methyl-2,6-diformylphenol functionalized mesoporous silica supported copper(II) and nickel(II) catalysts have been found to be active in liquid phase oxidation of olefins.^[52] But there is scope to improve catalytic efficiency in terms of conversion, reaction time, product selectivity, recyclability, etc. So, thrust is to develop new and better catalyst for important transformations.

We report here syntheses, characterization and heterogeneous catalytic properties of copper(II) (**Cu-Cat**) and nickel(II) (**Ni-Cat**) incorporated mesoporous silica materials (Scheme 1).



Scheme 1. Syntheses of Cu-Cat and Ni-Cat.

2-Hydroxy-naphthyl functionalized mesoporous silica^[53] has been used to anchor copper and nickel ions strongly by covalent bond formation. **Cu-Cat** and **Ni-Cat** have been used as catalyst in oxidation of styrene, α -methyl styrene, cyclohexene,

trans stilbene and cyclooctene in the presence of *tert*-butyl hydroperoxide (TBHP) as the terminal oxidant under mild conditions.

Results and discussion

Characterization of the framework, microstructure and porosity

Powder X-ray diffraction study of all the samples from the starting mesoporous silica to the catalysts has been carried to elucidate their microstructure. The patterns for calcined mesoporous silica, 3-APTES functionalized and 2-hydroxy-1-naphthaldehyde loaded silica are given in supporting information (Figure S1) and those for the catalysts, **Cu-Cat** and **Ni-Cat** in Figure 1. All the samples exhibit ordered 2D-hexagonal meso-

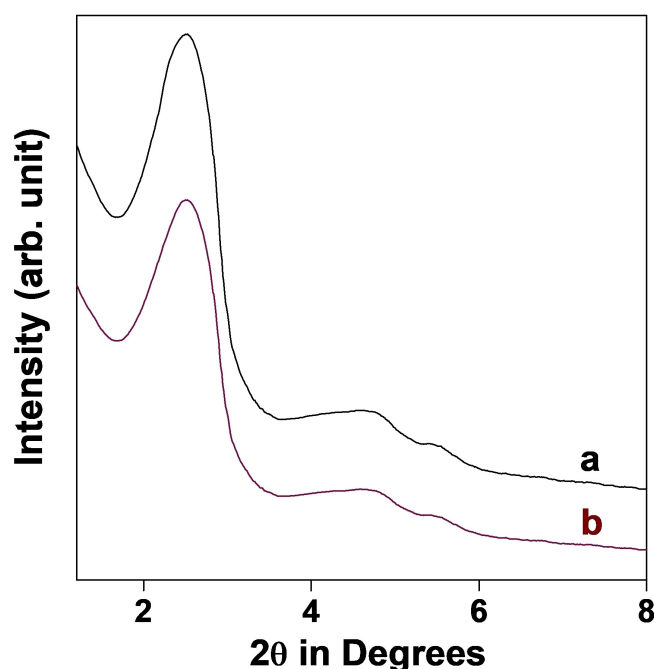


Figure 1. Powder X-ray diffraction patterns of (a) Cu-Cat and (b) Ni-Cat.

phase, evident from the three distinct diffraction peaks that can be assigned to the 100, 110 and 200 planes and a weak one for 210 plane.^[54–56] Nevertheless, the mesopore ordering in the samples decreases to some extent in each step of modification as reflected from the decrease in intensity of the peaks in the diffraction patterns.

The nitrogen adsorption/desorption isotherms of the calcined mesoporous silica and the catalysts are given in Figure 2. The BET (Brunauer-Emmett-Teller) surface area and pore volume of the calcined mesoporous silica (Figure 2a) which is taken as the starting material are $992 \text{ m}^2/\text{g}$ and 1.207 cc/g , respectively. On gradual functionalization the surface area decreases as well as the pore volume. For 3-APTES functionalized and 2-hydroxy naphthaldehyde loaded silica (supporting

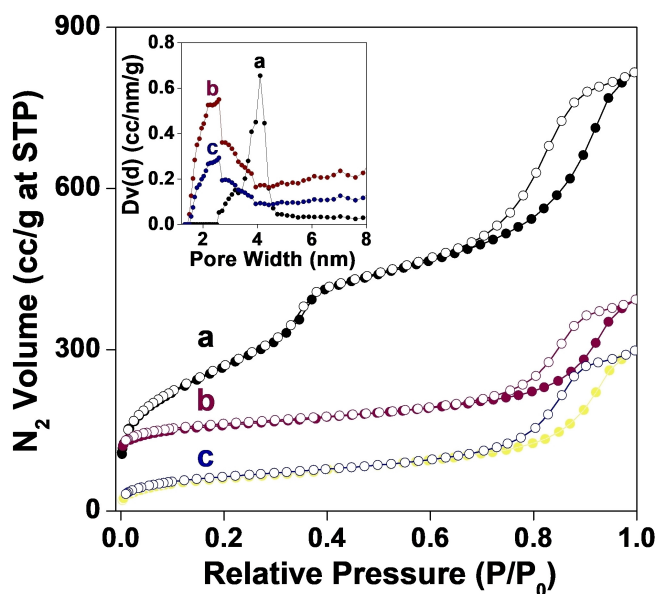


Figure 2. Nitrogen adsorption-desorption isotherms of (a) calcined mesoporous silica, (b) **Cu-Cat** and (c) **Ni-Cat** (For clarity, the Y-axis values are offset by 100 cc/g for plot b); Inset: Pore size distribution using NL-DFT model for the respective samples (For clarity, the Y-axis values are multiplied by 20 and 10 for plots b and c, respectively).

information, Figure s2) the surface areas are 462 and 305 m²/g, respectively, whereas the corresponding pore volumes are 0.72 and 0.53 cc/g. The materials show a typical type IV isotherm with steep rise due to capillary condensation at higher pressure indicating that the samples are mesoporous.^[57,58] The desorption hysteresis in the P/P_0 range of 0.6–1.0 that is observed for the samples originates due to intercrystallite adsorption.^[59] The pore volume of the Schiff base functionalized sample (0.53 cc/g) containing N and O-donor sites suggests that there is reasonable space to accommodate the metal ions inside its pores. The nitrogen adsorption-desorption isotherms for the catalysts, **Cu-Cat** and **Ni-Cat** (Figure 2b and c) also show similar type IV isotherms suggesting their mesoporous structure (Y-axis values are offset by 100 cc/g for plot b). The specific surface area and pore volume of **Cu-Cat** and **Ni-Cat** are 209 and 213 m²g⁻¹, and 0.428 and 0.436 cc/g, respectively. The pore diameter of the starting mesoporous silica as obtained from the NL-DFT (Non-local density functional theory) model is around ca. 4.0 nm and on functionalization and metal loading the size of the pores decreases to ca. 2.5 nm (Inset of Figure 2). The pore volume and pore size of the heterogeneous solid catalysts are well-suited to carry out organic transformations inside them.

The TEM images of the catalysts have been illustrated in Figure 3. In supporting information, Figure s3, the TEM images of calcined mesoporous silica, 3-APTES functionalized and 2-hydroxy naphthaldehyde loaded silica are shown. In all the materials, hexagonal arrangement of the pores with a different contrast than the pore walls can be seen. With gradual functionalization the ordering of the pores are affected, which is not unusual. The pore sizes of the samples estimated from

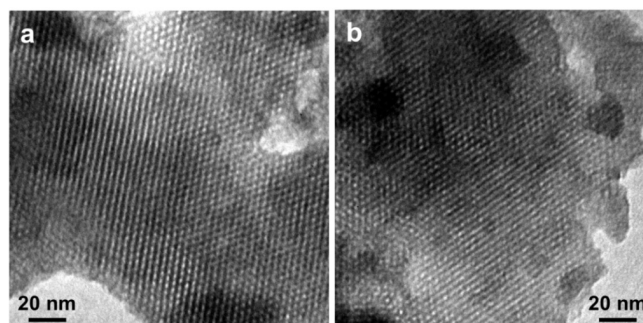


Figure 3. TEM images of (a) **Cu-Cat** and (b) **Ni-Cat**.

the TEM images are in close agreement with the pore size obtained from nitrogen adsorption isotherms. Thus, the results of small angle powder XRD patterns, gas adsorption and TEM studies confirmed the existence of mesoporosity in the samples.

The FT-IR spectra of the samples studied by ATR technique are given in Figure s4. The 3-APTES functionalized mesoporous silica shows a broad band in the region of 3625–2924 cm⁻¹ that can be ascribed to the presence of amino and methylene groups. For the Schiff-base modified sample an additional band centered around 1635 cm⁻¹ originates due to the presence of azomethine group. After the Schiff base interacts with the copper and nickel salts, these bands shift to somewhat lower wavenumber region in case of the catalysts which indicates the retention of the azomethine group as well as confirms complex formation.

Mesoporous silica, functionalized mesoporous silica and metal incorporated mesoporous silica have been further characterized by solid state MASNMR spectroscopy.¹³C CP MASNMR spectra of all but the mesoporous silica are given in Figure 4. Signals for the presence of aliphatic carbons in 3-APTES functionalized material appear at 8.3, 19.7 and 40.6 ppm (Figure 4a). After Schiff-base condensation with 2-hydroxy-1-naphthaldehyde, the material shows retention of these aliphatic peaks along with the appearance of signals for aromatic carbons at (Figure 4b) 7.8, 19.3, 40.2, 51.8, 71.7, 104.3, 124.2, 133.0, 137.0, 156.2, 176.8, 184.8, 210.8 and 229.5 ppm confirming the Schiff-base condensation between amine functionalized silica and 2-hydroxynaphthaldehyde. ¹³C CP MASNMR spectra of **Cu-Cat** and **Ni-Cat** are shown in Figure 4c and 4d. It is clear from the figures that organic moieties in these materials retain their framework and slight shifting of peak positions in **Cu-Cat** and **Ni-Cat** indicate formation of bonds between metal center and donor atoms of the functionalized silica.

²⁹Si MASNMR studies give idea about the chemical environment around Si atom in all the mesoporous silica materials. The results of the analyses are shown in Figure 5. Before any functionalization, mesoporous silica gives peak at -111.4 and -103.5 ppm (Figure 5a). These peaks may be assigned to the presence of Q⁴ and Q³ silica species of the Si(OSi)_n(OH)_{4-n} units. In 3-APTES functionalized material, peak positions slightly shift

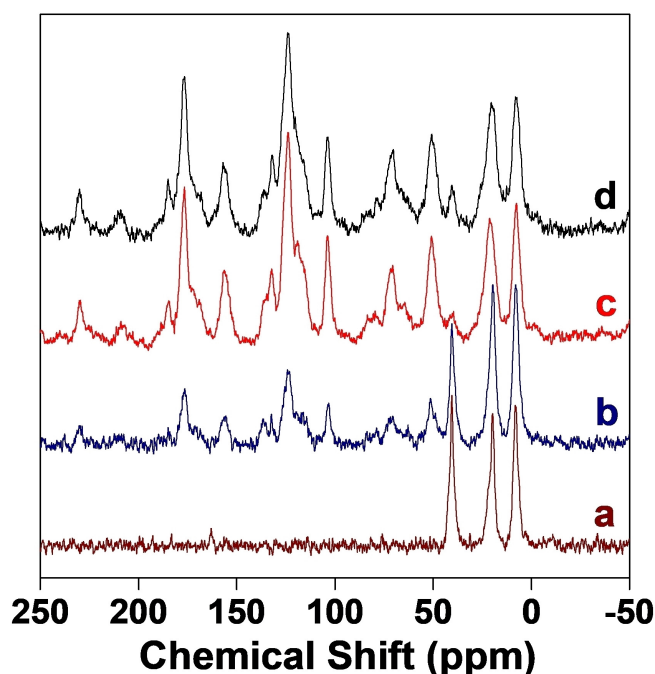


Figure 4. Solid state ^{13}C CP-MAS NMR spectra of (a) APTES-loaded mesoporous silica, (b) 2-hydroxy naphthaldehyde loaded silica, (c) **Cu-Cat** and (d) **Ni-Cat**.

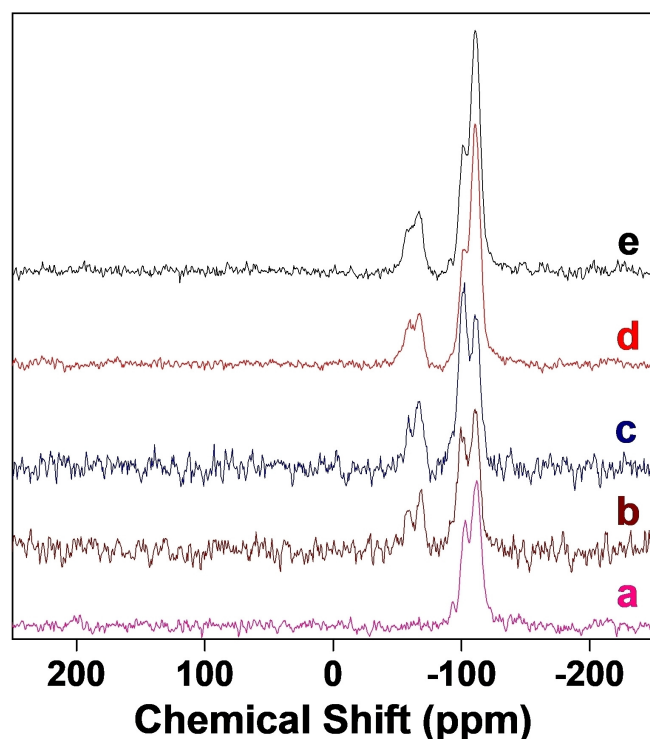


Figure 5. Solid state ^{29}Si MAS NMR spectra of (a) calcined mesoporous silica, (b) APTES-loaded mesoporous silica, (c) 2-hydroxy naphthaldehyde loaded silica, (d) **Cu-Cat** and (e) **Ni-Cat**.

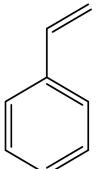
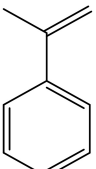
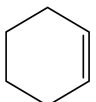
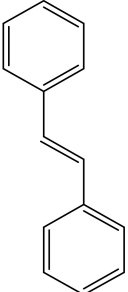
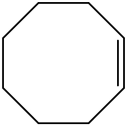
and new signals appear at -67.8 and -57.7 ppm (Figure 5b) confirming the incorporation of 3-APTES in mesoporous silica. Inagaki *et al.* previously showed that peaks at around -67 and -58 ppm appear for similar organic-inorganic mesoporous silica material. These peaks can be attributed to the presence of T^3 $(\text{SiO})_3\text{Si-R-Si}(\text{OSi})_3$ and T^2 $(\text{HO})_2(\text{OSi})\text{Si-R-Si}(\text{OSi})_2(\text{OH})$ species, respectively.^[60,61] However, materials with further functionalization with 2-hydroxy-1-naphthaldehyde followed by Cu or Ni grafting show similar peaks for silicon with different environment. These facts confirm Schiff-base condensation leading to the imine bond formation and retention of similar frameworks in **Cu-Cat** and **Ni-Cat** after complexation of the metal ions.

Thermogravimetric analyses (TGA) on various silica materials have been performed to examine thermal stability of the frameworks and also to find out the amount of organic functionalization on the mesoporous silica. TGA analyses have been carried out in the range of 30 to 1200 °C (Figure s5). The amount of Schiff-base functionalized moiety on silica framework has been determined from the figure and it has been found to be around 6.42% *i.e.* ~ 0.30 mmol of Schiff-base functionality per gram of silica framework. Presence of Cu or Ni metal in **Cu-Cat** and **Ni-Cat** has been confirmed by ICP-AES measurements. The amounts of the metal content in **Cu-Cat** and **Ni-Cat** have been determined to be 17.4 mg/g (0.274 mmol/g) and 7.8 mg/g (0.133 mmol/g), respectively. Cu(II) and Ni(II) centers in the catalysts may have tetra-coordinate environment.^[52] Here O,N donor atoms come from heterogenized Schiff-base ligand; one chloride species and another solvent molecule may provide all the coordinations. Some square planar Ni(II) complexes are known to display yellow color.^[62] Color of **Cu-Cat** and **Ni-Cat** are yellowish green. UV-vis diffuse reflectance spectra of **Cu-Cat** and **Ni-Cat** are given in Figure s6. Peaks at ~ 230 nm and 310 nm are present for both the compounds. These peaks may be attributed to the intraligand charge transfer. The most important peaks appear at 398 nm and in the range of 400 – 420 nm for **Cu-Cat** and **Ni-Cat**, respectively. These peaks are due to the presence of ligand to metal charge transfer (LMCT).

Catalytic studies

We have tried to use **Cu-Cat** and **Ni-Cat** as catalyst in oxidation of some olefins *e.g.* styrene, α -methyl styrene, cyclohexene, *trans* stilbene and cyclooctene in the presence of *tert*-butyl hydroperoxide as the terminal oxidant in acetonitrile medium under mild conditions. The results of the catalytic reactions are given in Table 1. It is clearly evident from the results that both the catalysts are quite effective in the oxidation of different substrates. Oxidation of styrene is of special attention to the researchers. **Cu-Cat** and **Ni-Cat** are active as catalyst in styrene oxidation as the yield of reaction is 90 and 70% , respectively. Benzaldehyde has been identified as the major product in both cases with 91 and 98% selectivity, respectively. In case of Cu-catalyzed oxidation, minor amount of phenylacetaldehyde and benzoic acid are produced while in case of Ni-catalyzed reaction only benzoic acid has been obtained as the minor

Table 1. Oxidation^a of different olefins in the presence of **Cu-Cat** and **Ni-Cat** as catalyst

Substrate	Catalyst	Products ^b (% Yield)		Total Yield (%)	Major Product and Selectivity (%)		TOF ^c			
	Cu-Cat	Benzaldehyde 82	Benzoic acid 3	Phenylacetaldehyde 5	Benzaldehyde	91	66			
	Ni-Cat	68	2	–				70	105	
	Blank							5		
	Cu-Cat	α -Methyl styrene oxide 51		Acetophenone 41	α -Methyl styrene oxide	55	59			
	Ni-Cat	51		25				76	67	100
	Blank							7		
	Cu-Cat	2-Cyclohexen-1-one 65	2-Cyclohexen-1-ol 5	Cyclohexene oxide 2	2-Cyclohexen-1-one	90	67			
	Ni-Cat	60	10	3				73	82	139
	Blank							4		
	Cu-Cat	<i>Trans</i> stilbene oxide 65	Benzil 9	Benzaldehyde 10	<i>Trans</i> stilbene oxide	77	35			
	Ni-Cat	41	10	35				86	48	74
	Blank							7		
	Cu-Cat	Cyclooctene oxide 81			Cyclooctene oxide	100	56			
	Ni-Cat	71						71	100	101
	Blank							6		

^aSolvent: acetonitrile; temperature: 65°C; catalyst: **Cu-Cat** and **Ni-Cat** (0.020 g each); amount of substrate: 0.5 g and oxidant: TBHP (equimolar with respect to substrate)
^bYields are measured after 12 h of the reaction,
^c TOF: turnover frequency = moles of substrate converted per mole of metal center per hour.

product. There is no production of phenylacetaldehyde with the nickel catalyst.

Oxidation of α -methyl styrene gives α -methyl styrene oxide and acetophenone as the products in the presence of both the catalysts. Yield is high but selectivity is poor for both the catalysts. Yields of 92 and 76% have been obtained with **Cu-Cat** and **Ni-Cat**, respectively, with methyl styrene oxide as the major product. Selectivity for methyl styrene oxide is only 55 and 67% in the presence **Cu-Cat** and **Ni-Cat**, respectively.

Oxidation of cyclohexene gives 72 and 73% yield for the Cu- and Ni-catalyst, respectively, and three products, namely 2-cyclohexen-1-one, 2-cyclohexen-1-ol and cyclohexene oxide are formed in the presence of both the catalysts. 2-Cyclohexen-1-one has been identified as the major product with excellent selectivity for both the catalysts.

Oxidation of *trans* stilbene has been achieved with high conversion value. Similar activity has been recorded for **Cu-Cat** and **Ni-Cat** with 84 and 86% yield, respectively. *Trans* stilbene

oxide has been identified as the major product with high selectivity (77%) for the copper catalyst. But selectivity for nickel catalyst is poor. Benzil and benzaldehyde are produced as minor product in case of the copper compound. However, selectivity for benzaldehyde with **Ni-Cat** is quite comparable with that of the *trans* stilbene oxide. For nickel catalyst, stilbene oxide and benzaldehyde are produced with 41 and 35% yield, respectively.

Both the catalysts show excellent catalytic activity towards oxidation of cyclooctene. Although yields are obtained as 81 and 71% for **Cu-Cat** and **Ni-Cat**, respectively, in both the cases cyclooctene oxide has been identified as the sole product which implies 100% selectivity.

Both the catalysts have been found to be very active in these oxidation reactions as evident from their high TOF values. However, **Ni-Cat** shows higher TOF value than that of **Cu-Cat** in each reaction. **Ni-Cat** has highest TOF value of 105 for

styrene oxidation and lowest TOF of 35 has been marked for **Cu-Cat** in *trans*-stilbene oxidation reaction.

A blank reaction has been carried out with all the substrates without any catalyst under similar reaction conditions. Very small amount of conversion has been observed in each case. Low conversion in blank reactions signifies the pivotal role played by these catalysts.

Aliquots from catalytic reaction mixtures have been collected at regular time intervals and analyzed by gas chromatography to monitor progress of the reactions. The results are given in Figure 6 and s7-s10. It has been found that

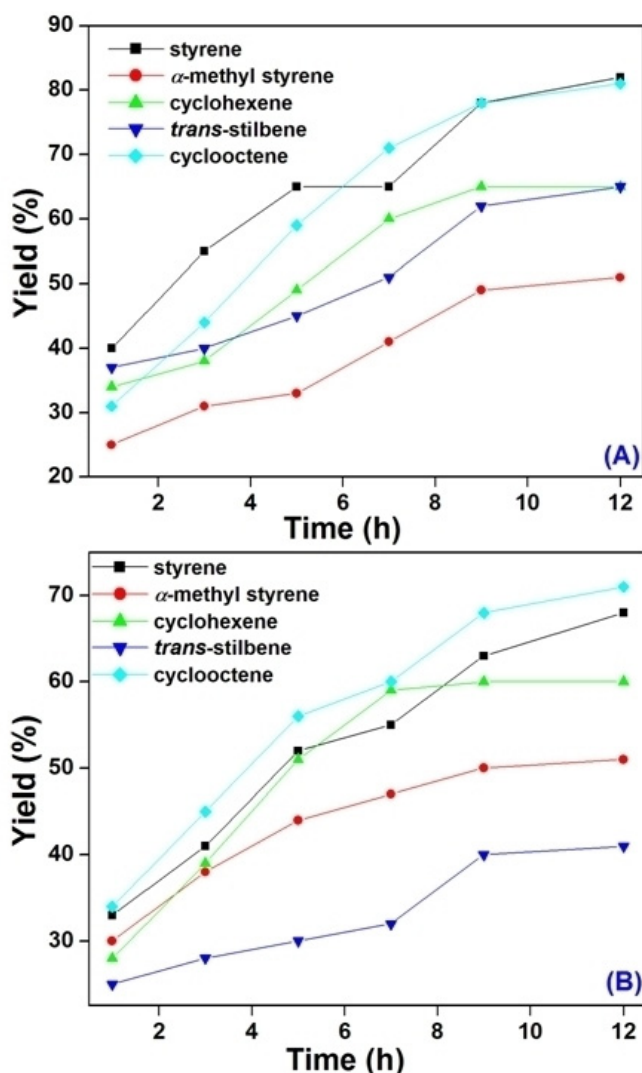


Figure 6. Oxidation of different substrates in the presence of (A) **Cu-Cat** and (B) **Ni-Cat**. Yield of major product from oxidation reaction has been plotted against time.

after 12 h of the reaction, yields do not increase noticeably for all the products. In case of styrene oxidation, benzaldehyde has been identified as the major product. With the gradual increase in reaction time, yield of benzaldehyde has also increased. After 1 h, yields of benzaldehyde are 40 and 33% (Figure s7) which

increased to 82 and 68% after 12 h in the presence of **Cu-Cat** and **Ni-Cat**, respectively. Formation of minor products after 1 h does increase significantly for both the catalysts.

In case of α -methyl styrene oxidation, corresponding oxide and acetophenone are obtained as the products. 25 and 30% of methyl styrene oxide is formed for **Cu-Cat** and **Ni-Cat**, respectively, after the first 1 h of reaction (Figure s8). However, yields reach to 51% for both the catalysts at the end of 12 h. Acetophenone is identified as another product with 15 and 12% yield after 1 h for **Cu-Cat** and **Ni-Cat**, respectively. It reaches up to 41 and 25% after 12 h.

2-Cyclohexen-1-one is the major product in cyclohexene oxidation with the formation of 34 and 28% after 1 h, and 65 and 60% after 12 h in the presence of **Cu-Cat** and **Ni-Cat**, respectively (Figure s9). The increase in the amount of minor products, namely, 2-cyclohexen-1-ol and cyclohexene oxide, is not visible on going from the first hour to twelfth hour of the reaction *i. e.* most of the amount of minor products are formed within 1 h in case of cyclohexene oxidation.

Yield of *trans* stilbene oxide increases from 40 to 65% in the presence of **Cu-Cat** within 1 h to 12 h in case of *trans* stilbene oxidation reaction (Figure s10). The increase for the corresponding **Ni-Cat** is 25 to 41% during the same time period of the reaction. The other product that is formed in the nickel catalyzed reaction is benzaldehyde. Its yield increases from 21 to 35% within the same time interval. In case of the copper catalyst benzaldehyde is formed in much less amount and the yield is 10% after 12 h.

Finally, in the case of cyclooctene oxidation, there is gradual increase in yield of cyclooctene oxide as the sole product with time and it is the sole product of the oxidation reaction for both the catalysts. The yield increases from 31 to 81% for the copper catalyst while that for the nickel catalyst it goes from 34 to 71% within 1 h to 12 h of the reaction (Figure 6).

Hot filtration test and tests for recycling ability of the catalysts have been performed to further investigate the efficiency of the catalysts. It is known that if unbound metal is present in solution in any catalytic reaction mixture, it can catalyze the olefin oxidation reaction. Thus, it becomes extremely important to detect metal leaching or metal containing any species in solution in order to comment on the heterogeneous nature of a catalyst. For this purpose, hot filtration tests have been performed on styrene oxidation reaction in the presence of **Cu-Cat** and **Ni-Cat**. The catalysts have been separated from the reaction mixtures by filtration under hot condition after completion of initial 1 h. Formation of benzaldehyde is 40 and 33% (Figure 7) for **Cu-Cat** and **Ni-Cat**, respectively, at this time. After separation, the reaction is continued in absence of catalysts and it is observed that yield of benzaldehyde increases only marginally. For the uninterrupted reactions in the presence of catalysts, catalytic process proceeds in normal course with further formation of benzaldehyde. In absence of **Cu-Cat** and **Ni-Cat**, slight increase in yield of benzaldehyde may be because of the presence of the oxidant, *tert*-butyl hydroperoxide. Blank reactions show that *tert*-butyl hydroperoxide can oxidize styrene in little yield. To further ensure about metal leaching in to the reaction mixtures,

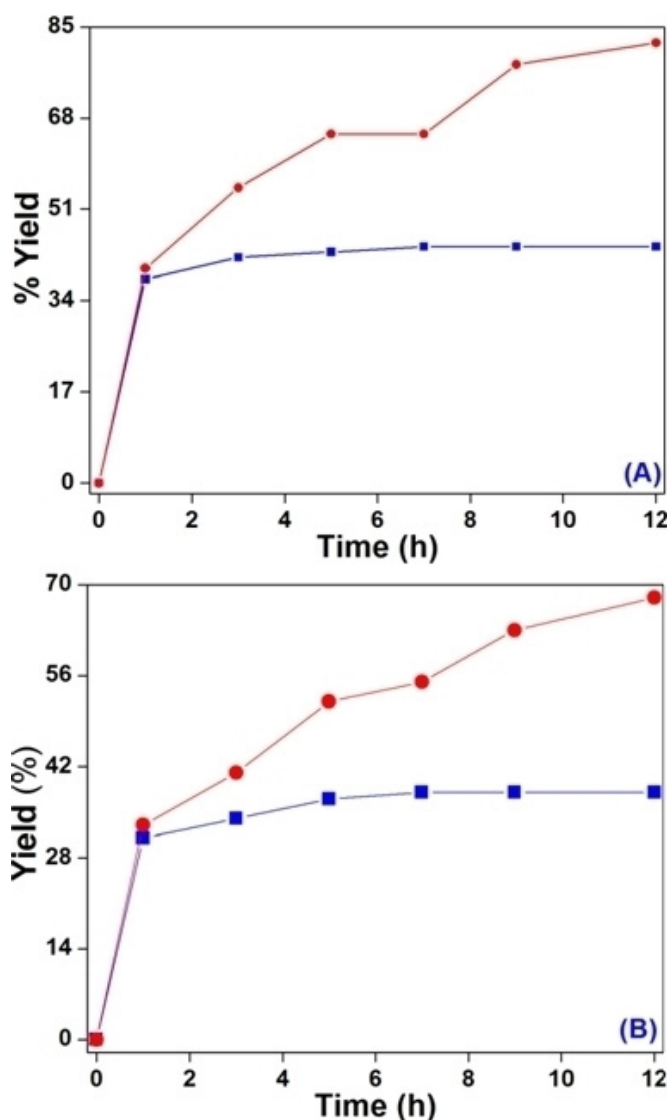


Figure 7. Hot filtration test for oxidation of styrene in the presence of (A) Cu-Cat and (B) Ni-Cat. Red line with circle indicates normal route of benzaldehyde formation whereas blue line with square box shows growth of benzaldehyde after removal of Cu-Cat and Ni-Cat after 1 h of the reaction.

ICP-AES measurement have been performed with the filtrates after catalyst separation to determine the amount of metal ion, if any. However, there is no detectable amount of copper or nickel ion in reaction mixture which confirms that no metal leaching takes place.

Recycling ability of the catalysts has been studied to check whether these catalysts can be used for several catalytic cycles without significant loss in their efficiency. For this, styrene has been chosen as the substrate. After completion of each catalytic reaction, the catalyst has been recovered and regenerated, and then used for next cycle of the same reaction. All the catalytic reactions are carried out following the original protocol. Results of styrene oxidation in three cycles in the presence of Cu-Cat and Ni-Cat are given in Figure 8 and it is evident from it that catalytic efficiency of the samples reduces

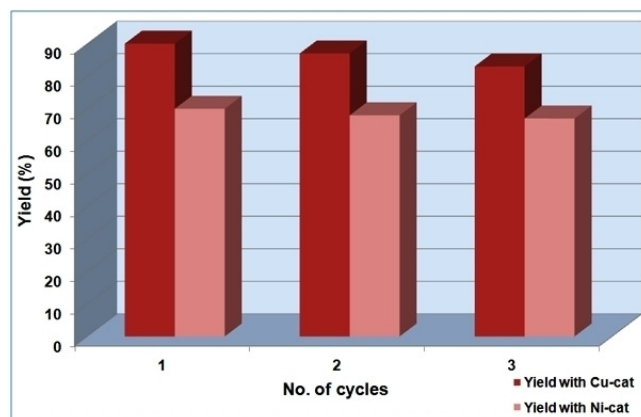


Figure 8. Oxidation of styrene in the presence of Cu-Cat and Ni-Cat in subsequent cycles.

slightly in consecutive runs. However, it is observed that selectivity for benzaldehyde always remains high. This indicates significant reusability of both the catalysts.

To study solvent dependence and select suitable medium for the catalysis with TBHP as the oxidant, styrene oxidation reaction has been carried out in different solvents, e.g. water, methanol, dichloromethane, toluene and acetonitrile. The results of the study are given in Table 2. It is clear from the

Table 2. Oxidation of styrene in the presence of Cu-Cat and Ni-Cat in different solvents under similar conditions

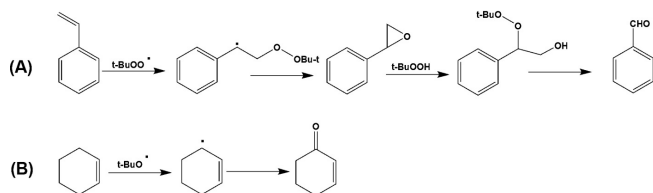
Reaction medium	Yield (%)	
	Cu-Cat	Ni-Cat
Water	20	25
Methanol	32	30
Dichloromethane	35	13
Toluene	53	40
Acetonitrile	90	70

table that highest yield is obtained in acetonitrile and that is the reason for using it as a solvent in all other catalytic reactions. In addition to that, acetonitrile is known to stabilize Cu(I) species, which is produced during catalysis, in solution by coordinating with the metal center.^[63] This can be a possible reason for higher activity of Cu-Cat in this medium.

Experiments have also been carried out to check for the efficiency of different oxidizing agents in the catalysis. Firstly, H₂O₂ has been employed for carrying out the reaction (with styrene as a representative case), which results in poor yield. The Cu-catalyst still shows about 35% conversion but the Ni-catalyst responded very poorly (only about 15% conversion). Hence, TBHP is chosen to carry out all the oxidation reactions which is found to be very efficient.

Based on previous results on catalytic oxidation of olefins by Cu(II) compounds, a plausible mechanism has been proposed to explain the formation of the products. It is well

understood that $t\text{BuOO}^\bullet$ and $t\text{BuO}^\bullet$ radicals could be formed from the reaction between TBHP and Cu(II) with the subsequent reduction of the metal center to Cu(I).^[64–67] Oxidation of styrene under similar conditions has been reported to follow radical mechanism.^[68–70] Different possible steps for styrene and cyclohexene oxidation are depicted in Scheme 2. Other olefins



Scheme 2. Possible mechanistic route for oxidation of olefins.

also follow similar steps. One of the reasons behind various product formation in such reactions is the competition between oxidation of C=C bond and the allylic position. Styrene may first give corresponding epoxide on oxidation of double bond as there is no allylic hydrogen present in it. Benzaldehyde is then obtained from the ring opening of the styrene epoxide. In case of cyclohexene, allylic oxidation may occur resulting in the formation of 2-cyclohexen-1-one as the major product. However, cyclooctene undergoes epoxidation to give cyclooctene oxide as the sole product. Cyclohexene has half chair conformation and its double bond and allylic hydrogen remains in the same plane^[71] whereas double bond of cyclooctene lies in a different plane from other carbon atoms of its chair conformation.^[72] Therefore, oxidation of allylic hydrogen is more observed in cyclohexene than in cyclooctene. Other substrates where corresponding oxide is obtained as major product either follow similar route as depicted for styrene or their catalysis proceeds through cyclohexene route. Oxidation of olefins catalyzed by **Ni-Cat** may proceed *via* formation of nickel-peroxo species^[51] similar to the titanium silicates where corresponding peroxo species are generated.^[73]

Examples of Cu or Ni anchored functionalized mesoporous silica materials are known; some of these materials have been used as catalysts in different organic transformations.^[74,75] Few of them have been used for epoxidation of olefins. Schiff-base condensation of salicylaldehyde with amine functionalized MCM-41 affords bidentate binding sites for Cu(II) to give a heterogenized catalyst for epoxidation of styrene and results show high conversion (97%) as well as high epoxide selectivity (89%).^[76] Use of unsubstituted and *tert*-butyl substituted salicylaldehyde Cu(II) compounds supported on mesoporous and amorphous silica as catalysts for the oxidation cyclohexene exhibits comparatively inferior conversion and selectivity of the products.^[77] SBA-15 material bound with salicylaldehyde has been used to prepare Cu containing heterogeneous catalyst which has been found to be highly active catalyst for the epoxidation of cyclooctene, cyclohexene and styrene (conversion over 95%) with high selectivity towards corresponding epoxide.^[78] Cu(II)-diamine complex has been incorporated into

3-APTES functionalized MCM-41 where amine N forms bond with the metal center and this material has been used as catalyst for the epoxidation of styrene (conversion 94%).^[79] 4-Methyl-2,6-diformylphenol functionalized modified mesoporous silica has been used to prepare two heterogeneous catalysts with Cu and Ni metals. These compounds show their catalytic ability for the epoxidation of cyclohexene, *trans* stilbene, styrene, α -methyl styrene and cyclooctene. Results are more or less comparable with the present studies although TOF values in the present study are significantly higher.^[52] Nickel(II) Schiff-base complex onto salicylaldehyde functionalized mesoporous silica is active catalyst for the epoxidation of several olefins with high conversion and TOF values, but time taken for the catalytic reaction is quite long (24 h).^[80] MCM-41-Ni, which has been synthesized by anchoring the metal center on 2-pyridinecarboxaldehyde functionalized MCM-41, shows excellent conversion of styrene (~95%) but selectivity towards epoxide is reasonably low (~67%).^[81] Cu(II)-Schiff complex immobilized onto three dimensional mesoporous silica KIT-6 is active on styrene epoxidation with high conversion and high selectivity towards epoxide (both ~97%).^[82] Modified SBA-15 supported Ni(II)-oxime-imine catalysts are comparable with the present study in conversion of styrene or cyclohexene, but only 26% conversion is achieved with cyclooctene.^[83] There are several factors which control conversion and selectivity of the products. Thus, in comparison to other reported heterogenized silica catalyst, our catalysts are better in few aspects whereas **Cu-Cat** and/or **Ni-Cat** are lacking in some features.

Conclusions

In summary, we have been able to synthesize and characterize Cu(II) and Ni(II) anchored functionalized mesoporous materials. These metal grafted silica materials have been found to be effective as catalysts for the oxidation of various olefins. Epoxidation and oxidation at allylic site occurs to give different products within a reasonable reaction period and at relatively low temperature. The catalysts have been recycled for a few times without seriously compromising their activities. Although the catalytic reactions show good conversion, yet similar product selectivity could not be observed i.e. the corresponding oxides are not obtained for each substrate as the major product. Thus, despite their excellent conversion and recycling ability, there is scope for improvement of product selectivity. The results obtained for cyclooctene epoxidation is significant as it yields cyclooctene oxide as the sole product.

Supporting Information Summary

Supplementary data include the experimental details of synthesis of functionalized mesoporous silica, synthesis of **Cu-Cat** and **Ni-Cat**, and olefin oxidation; PXRD patterns, nitrogen sorption isotherms, TEM images, FT-IR spectra and thermogravimetric analysis plot of (a) calcined mesoporous silica, (b) 3-APTES functionalized silica and (c) 2-hydroxy naphthaldehyde loaded silica; FT-IR spectra and UV-vis diffuse reflectance spectra of **Cu-Cat** and **Ni-Cat**; Plots of Yields (of different

products) vs. Time for the oxidation of styrene, α -methyl styrene, cyclohexene and *trans* stilbene in the presence of Cu-Cat and Ni-Cat.

Acknowledgements

MN gratefully acknowledges financial support from DST-SERB (SB/FT/CS-004/2014 dated 27/06/2014), New Delhi, India and Visva-Bharati University. PR wishes to thank DST-SERB, New Delhi for financial support (Project No.: SB/EMEQ-065/2013). AB thanks CSIR, New Delhi for her fellowship. Authors are thankful to Narayan Pradhan of Indian Association for the Cultivation of Science, Kolkata for providing TEM facilities.

Conflict of Interest

The authors declare no conflict of interest.

Keywords: Copper · Heterogeneous catalysis · Nickel · Olefin · Oxidation

- [1] A. M. Kirillov, M. N. Kopylovich, M. V. Kirillova, M. Haukka, M. F. C. G. da Silva, A. J. L. Pombeiro, *Angew. Chem., Int. Ed.* **2005**, *44*, 4345–4349.
- [2] T. Punniyamurthy, L. Rout, *Coord. Chem. Rev.* **2008**, *252*, 134–154.
- [3] M. Nandi, P. Roy, *Indian J. Chem.* **2013**, *52 A*, 1263–1268.
- [4] R. Antony, S. T. D. Manickam, S. Balakumar, *J. Inorg. Organomet. Polym.* **2017**, *27*, 418–426.
- [5] D. S. Nesterov, O. V. Nesterova, A. J. L. Pombeiro, *Coord. Chem. Rev.* **2017**, <https://doi.org/10.1016/j.ccr.2017.08.009>.
- [6] J. Mondal, A. Modak, A. Dutta, A. Bhaumik, *Dalton Trans.* **2011**, *40*, 5228–5235.
- [7] S. Banerjee, C. Adhikary, C. Rizzoli, R. Pal, *Inorg. Chim. Acta* **2014**, *409*, 202–207.
- [8] C. Adhikary, S. Banerjee, J. Chakraborty, S. Ianelli, *Polyhedron* **2013**, *65*, 48–53.
- [9] H. Mahdavi, M. Nikoorazm, A. Ghorbani-Choghamarani, S. Arshadi, *J. Porous. Mater.* **2016**, *23*, 75–82.
- [10] Z. -H. Zhang, X. -S. Yang, Q. -Q. Zhang, L. Wang, M. -Y. He, Q. Chen, X. -F. Huang, *RSC Adv.* **2016**, *6*, 104036–104040.
- [11] A. Bhattacharjee, S. Halder, K. Ghosh, C. Rizzoli, P. Roy, *New J. Chem.* **2017**, *41*, 5696–5706.
- [12] M. Tobisu, N. Chatani, *Acc. Chem. Res.* **2015**, *48*, 1717–1726.
- [13] S. L. Zultanski, G. C. Fu, *J. Am. Chem. Soc.* **2013**, *135*, 624–627.
- [14] P. Drabina, J. Svoboda, M. Sedláč, *Molecules* **2017**, *22*, 865 (1–18).
- [15] V. Molinari, C. Giordano, M. Antonietti, D. Esposito, *J. Am. Chem. Soc.* **2014**, *136*, 1758–1761.
- [16] F. Gao, J. D. Webb, J. F. Hartwig, *Angew. Chem.* **2016**, *128*, 1496–1500.
- [17] S. Z. Tasker, E. A. Standley, T. F. Jamison, *Nature* **2014**, *509*, 299–309.
- [18] K. C. Gupta, A. K. Sutar, *Coord. Chem. Rev.* **2008**, *252*, 1420–1450.
- [19] R. Noyori, M. Aoki, K. Sato, *Chem. Commun.* **2003**, 1977–1986.
- [20] K. A. Jorgensen, *Chem. Rev.* **1989**, *89*, 431–458.
- [21] T. Mukaiyama, T. Yamada, *Bull. Chem. Soc. Jpn.* **1995**, *68*, 17–35.
- [22] K. C. Gupta, A. K. Sutar, C. -C. Lin, *Coord. Chem. Rev.* **2009**, *253*, 1926–1946.
- [23] A. Maria P. Salvo, F. Giacalone, M. Gruttadauria, *Molecules* **2016**, *21*, 1288 (1–60).
- [24] D. R. Godhani, H. D. Nakum, D. K. Parmar, J. P. Mehta, N. C. Desai, *J. Mol. Catal. A* **2017**, *426*, 223–237.
- [25] A. Finiels, F. Fajula, V. Hulea, *Catal. Sci. Technol.* **2014**, *4*, 2412–2426.
- [26] H. Albuquerque, L. Carneiro, A. P. Carvalho, J. Pires, A. R. Silva, *Polyhedron* **2014**, *79*, 315–323.
- [27] L. Ma, F. Su, X. Zhang, D. Song, Y. Guo, J. Hu, *Microporous Mesoporous Mater.* **2014**, *184*, 37–46.
- [28] R. K. Sharma, S. Sharma, G. Gaba, S. Dutta, *J. Mater. Sci.* **2016**, *51*, 2121–2133.
- [29] A. Zarnegaryan, M. Moghadam, S. Tangestaninejad, V. Mirkhani, I. Mohammadpoor-Baltork, *New J. Chem.* **2016**, *40*, 2280–2286.
- [30] X. Wang, S. Wu, Z. Li, X. Yang, H. Su, J. Hu, Q. Huo, J. Guan, Q. Kan, *Microporous Mesoporous Mater.* **2016**, *221*, 58–66.
- [31] M. Bazarganipoura, M. Salavati-Niasari, *Appl. Catal. A* **2015**, *502*, 57–64.
- [32] T. Toyao, K. Miyahara, M. Fujiwaki, T. -H. Kim, S. Dohshi, Y. Horiuchi, M. Matsuoka, *J. Phys. Chem. C* **2015**, *119*, 8131–8137.
- [33] H. Noh, Y. Cui, A. W. Peters, D. R. Pahls, M. A. Ortuñ, N. A. Vermeulen, C. J. Cramer, L. Gagliardi, J. T. Hupp, O. K. Farha, *J. Am. Chem. Soc.* **2016**, *138*, 14720–14726.
- [34] D. Dehe, L. Wang, M. K. Müller, G. Dörr, Z. Zhou, R. N. Klupp-Taylor, Y. Sun, S. Ernst, M. Hartmann, M. Bauer, W. R. Thiel, *ChemCatChem* **2015**, *7*, 127–136.
- [35] C. M. A. Parlett, K. Wilson, A. F. Lee, *Chem. Soc. Rev.* **2013**, *42*, 3876–3893.
- [36] A. E. Fernandes, A. M. Jonas, O. Riant, *Tetrahedron* **2014**, *70*, 1709–1731.
- [37] C. T. Kresge, M. E. Leonowicz, W. J. Roth, J. C. Vartuli, J. S. Beck, *Nature* **1992**, *359*, 710–712.
- [38] M. Zare, Z. Moradi-Shoeili, *Appl. Organometal. Chem.* **2017**, *31*, e3611.
- [39] P. B. Arockiam, C. Bruneau, P. H. Dixneuf, *Chem. Rev.* **2012**, *112*, 5879–5918.
- [40] H. Kotzé, S. Mapolie, *Appl. Organometal. Chem.* **2016**, *31*, e3643.
- [41] W. -J. Kong, Y. -J. Liu, H. Xu, Y. -Q. Chen, H. -X. Dai, J. -Q. Yu, *J. Am. Chem. Soc.* **2016**, *138*, 2146–2149.
- [42] R. Shang, L. Ilies, E. Nakamura, *Chem. Rev.* **2017**, *117*, 9086–9139.
- [43] K. K. Krishnan, A. M. Thomas, K. S. Sindhu, G. Anilkumar, *Tetrahedron* **2016**, *72*, 1–16.
- [44] G. Yang, H. Du, J. Liu, Z. Zhou, X. Hu, Z. Zhang, *Green Chem.* **2017**, *19*, 675–681.
- [45] A. R. Jeong, J. W. Shin, J. H. Jeong, K. H. Bok, C. Kim, D. Jeong, J. Cho, S. Hayami, K. S. Min, *Chem. Eur. J.* **2017**, *23*, 3023–3033.
- [46] A. E. Kerenkan, F. Béland, T. -O. Do, *Catal. Sci. Technol.* **2016**, *6*, 971–987.
- [47] S. Halder, A. Mukherjee, K. Ghosh, S. Dey, M. Nandi, P. Roy, *J. Mol. Struct.* **2015**, *1101*, 1–7.
- [48] S. Halder, S. Dey, C. Rizzoli, P. Roy, *Polyhedron* **2014**, *78*, 85–93.
- [49] P. Roy, M. Nandi, M. Manassero, M. Riccò, M. Mazzani, A. Bhaumik, P. Banerjee, *Dalton Trans.* **2009**, 9543–9554.
- [50] P. Roy, K. Dhara, M. Manassero, P. Banerjee, *Inorg. Chem. Commun.* **2008**, *11*, 265–269.
- [51] J. Chakraborty, M. Nandi, H. Mayer-Figge, W. S. Sheldrick, L. Sorace, A. Bhaumik, P. Banerjee, *Eur. J. Inorg. Chem.* **2007**, 5033–5044.
- [52] M. Nandi, P. Roy, H. Uyama, A. Bhaumik, *Dalton Trans.* **2011**, *40*, 12510–12518.
- [53] T. Das, A. Roy, H. Uyama, P. Roy, M. Nandi, *Dalton Trans.* **2017**, *46*, 7317–7326.
- [54] A. P. Wight, M. E. Davis, *Chem. Rev.* **2002**, *102*, 3589–3614.
- [55] A. Stein, *Adv. Mater.* **2003**, *15*, 763–775.
- [56] O. Olkhoviyk, M. Jaroniec, *J. Am. Chem. Soc.* **2005**, *127*, 60–61.
- [57] S. Inagaki, Y. Fukushima, K. J. Kuroda, *J. Chem. Soc., Chem. Commun.* **1993**, 680–682.
- [58] P. T. Tanev, M. Chibwe, T. J. Pinnavaia, *Nature* **1994**, *368*, 321–323.
- [59] P. T. Tanev, T. J. Pinnavaia, *Science* **1996**, *271*, 1267–1269.
- [60] S. Inagaki, S. Guan, Y. Fukushima, T. Ohsuna, O. Terasaki, *J. Am. Chem. Soc.* **1999**, *121*, 9611–9614.
- [61] S. Inagaki, S. Guan, T. Ohsuna, O. Terasaki, *Nature* **2002**, *416*, 304–307.
- [62] N. N. Greenwood, A. Earnshaw, *Chemistry of the Elements*, 2nd Ed., Elsevier Butterworth Heinemann, Woodburn, **2005**.
- [63] C. L. Gatlin, F. Tureček, T. Valsar, *Anal. Chem.* **1994**, *66*, 3950–3958.
- [64] J. K. Kochi, *Tetrahedron* **1962**, *18*, 483–497.
- [65] J. K. Kochi, *J. Am. Chem. Soc.* **1962**, *84*, 1572–1579.
- [66] G. Rothenberg, L. Feldberg, H. Wiener, Y. Sasson, *J. Chem. Soc., Perkin Trans.* **1998**, *2*, 2429–2434.
- [67] U. Junghans, C. Suttikus, J. Lincke, D. Lässig, H. Krauyscheid, R. Gläser, *Micropor. Mesopor. Mater.* **2015**, *216*, 151–160.
- [68] L. M. Slaughter, J. P. Collman, T. A. Eberspacher, J. I. Brauman, *Inorg. Chem.* **2004**, *43*, 5198–5204.
- [69] F. Farzaneh, J. Taghavi, R. Malakooti, M. Ghandi, *J. Mol. Catal. A* **2006**, *244*, 252–257.
- [70] M. Sarkheil, M. Lashanizadegan, *Appl. Organometal. Chem.* **2017**, doi.org/10.1002/aoc.3726
- [71] E. L. Eliel, S. H. Wilen, *Stereochemistry of Organic Compounds*, John Wiley, New York, **1994**.

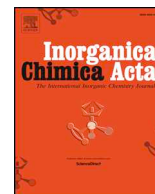
- [72] U. Neuenschwander, I. Hermans, *J. Org. Chem.* **2011**, *76*, 10236–10240.
- [73] A. Bhaumik, T. Tatsumi, *J. Catal.* **2000**, *189*, 31–39.
- [74] N. Pal, A. Bhaumik, *RSC Adv.* **2015**, *5*, 24363–24391.
- [75] M. Ozdemir, *Inorg. Chim. Acta* **2014**, *421*, 1–9.
- [76] S. Jana, B. Dutta, R. Bera, S. Koner, *Langmuir* **2007**, *23*, 2492–2496.
- [77] N. Malumbazo, S. F. Mapolie, *J. Mol. Catal. A* **2009**, *312*, 70–77.
- [78] M. Selvaraj, V. Narayanan, S. Kawi, *Microporous Mesoporous Mater.* **2010**, *132*, 494–500.
- [79] S. Jana, S. Bhunia, B. Dutta, S. Koner, *Applied Catal. A* **2011**, *392*, 225–232.
- [80] S. Bhunia, S. Koner, *Polyhedron* **2011**, *30*, 1857–1864.
- [81] Y. Gang, C. Xing, W. Xiaoli, X. Weihong, X. Nanping, *Chinese J. Catal.* **2013**, *34*, 1326–1332.
- [82] J. Sun, Q. Kan, Z. Li, G. Yu, H. Liu, X. Yang, Q. Huo, J. Guan, *RSC Adv.* **2014**, *4*, 2310–2317.
- [83] L. Paul, B. Banerjee, A. Bhaumik, M. Ali, *J. Solid State Chem.* **2016**, *237*, 105–112.

Submitted: September 18, 2017

Revised: October 12, 2017

Accepted: October 13, 2017

Please note: Minor changes have been made to this manuscript since its publication in *Chemistry Select*. The Editor.



Research paper

Synthesis, characterization and catalytic properties of dinuclear complexes of copper(II) and nickel(II): Oxidation of cyclohexane, toluene and cyclopentane

Aradhita Bhattacharjee¹, Sudipto Dey¹, Partha Roy^{*}

Department of Chemistry, Jadavpur University, Jadavpur, Kolkata 700 032, India

ARTICLE INFO

Keywords:

Homogenous catalysis
Saturated hydrocarbon
Oxidation
Copper
X-ray structure

ABSTRACT

Oxidation of saturated hydrocarbon by transition metal complexes is of great importance because this would give industrially valuable organic fine chemicals. Here, dinuclear copper(II) and dinuclear nickel(II) complexes with same N,O donor ligand have been used as catalyst for the oxidation of cyclohexane, toluene and cyclopentane using hydrogen peroxide as the oxidant to examine their catalytic activity and effect of nature of metal center on catalysis. $[\text{Cu}_2(\text{L}^1)_2(\mu_2\text{-Cl})\text{Cl}]\cdot 2.5\text{H}_2\text{O}$ (**1**) and $[\text{Ni}_2(\text{L}^1)_2(\mu_2\text{-N}_3)_2(\text{CH}_3\text{OH})_2]\cdot \text{CH}_3\text{OH}$ (**2**) have been synthesized under mild conditions where HL^1 is 1-((2-hydroxyethylimino)methyl)naphthalen-2-ol. These complexes have been characterized by elemental analysis, FT-IR, UV-Vis, mass spectroscopy, TGA-DTA and cyclic voltametric studies. Their structures have been confirmed by single crystal X-ray diffraction analysis. Some theoretical calculations have been performed to investigate spectral transitions. Copper(II) complex shows effective catalytic ability towards oxidation of the saturated hydrocarbons such as cyclohexane, toluene and cyclopentane in the presence of hydrogen peroxide when corresponding alcohols and ketones have been obtained as major products. However, complex **2** has been found to be inactive as catalyst for the oxidation. It is possible that Cu-hydroperoxo or Cu-peroxo species is formed during catalysis (as revealed from UV-vis spectral analysis) which could be the active species for the oxidation reaction.

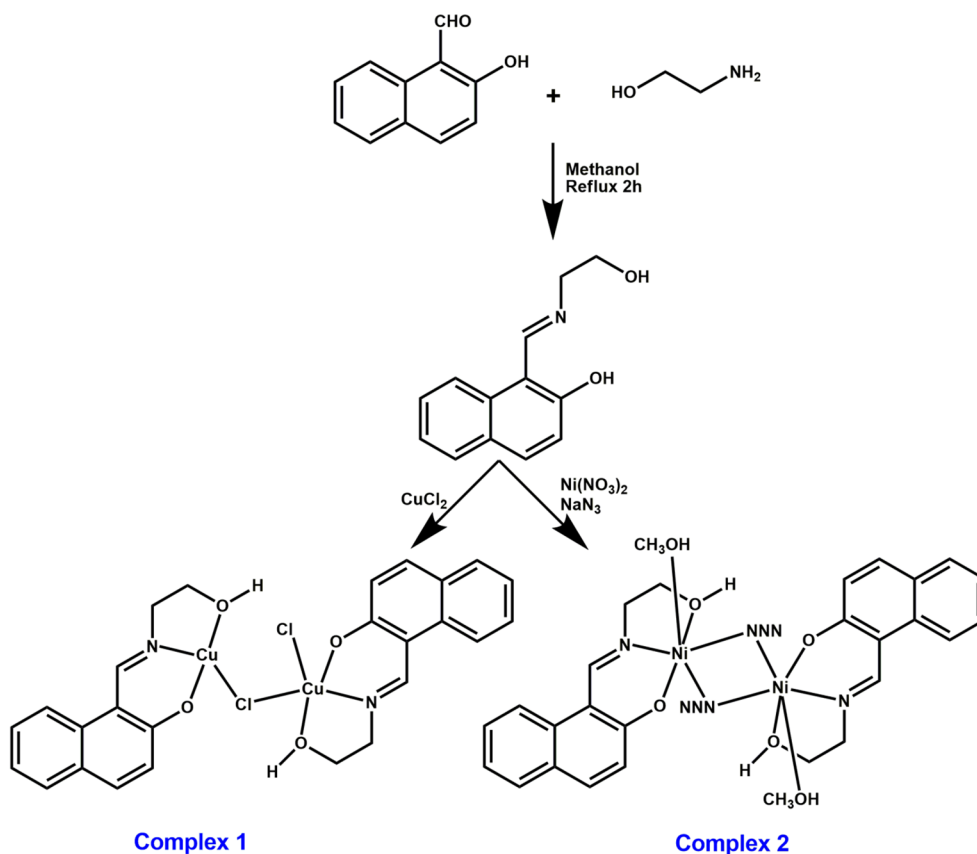
1. Introduction

Activation of $\text{C}_{\text{sp}^3}\text{-H}$ bond is one of the most difficult tasks in chemistry. Natural gas and fuel are mainly saturated hydrocarbons. This bond in methane is inert and of high energy (104 kcal/mol) at ambient temperature, thus, the oxidation requires high temperature and pressure and/or acidic reaction media in addition to the presence of metal as catalyst [1]. Transformation of these compounds may give different valuable organic fine chemicals which are of great industrial importance. For example, methane can be converted to methanol with one functional group which could be converted to other compounds easily [2]. Modeling of metalloenzymes with particular catalytic activity is of great interest for the design and development of bio-inspired catalysts. In connection with activation of $\text{C}_{\text{sp}^3}\text{-H}$ bond, we could recall an enzyme, methane monooxygenase [3]. It exists in two forms; (a) particulate methane monooxygenase (pMMO) and (b) soluble methane monooxygenase (sMMO). Both of these forms are able to convert methane to methanol. sMMO contains two iron(III) centers in the active

site. Active site of pMMO is not identified unambiguously by structural characterization of the enzyme. However, the existence of two Cu(II) centers in the active site of pMMO is of most acceptable belief [1a,3]. Therefore, there are several copper(II) complexes including dinuclear copper(II) compounds which have been used as catalyst for the activation of $\text{C}_{\text{sp}^3}\text{-H}$ bond [4]. Different hydrocarbons have been utilized as the substrates such as methane, cyclohexane, cyclopentane. Oxidation of cyclohexane is useful because its oxidized products, mainly cyclohexanol and cyclohexanone, are of great industrial importance [5]. Cyclohexanol is, mainly, used as the raw material for the manufacture of adipic acid. Adipic acid is used for the preparation of nylon-6,6', soaps and detergents, pesticides, etc. Cyclohexanone is, mainly, utilized as a solvent in industries and activator in oxidation reactions. Pombeiro *et al.* have been working for long time on the development of different copper(II) complexes as active catalyst for such oxidation reactions [6]. Few other groups have also reported C–H activation reactions by Cu(II) complexes [7]. But, conversion of substrate to product is of comparatively low percentage because of high C–H bond energy. Although

* Corresponding author.

E-mail addresses: partha.roy@jadavpuruniversity.in, proy@chemistry.jdvu.ac.in (P. Roy).¹ These authors contributed equally to this work.



Scheme 1. Synthesis of complexes 1 and 2.

there is significant importance of copper(II) complexes as catalysts in various catalytic transformations [7i–7n], the field of alkane oxidation by copper complexes is less explored. It is to be noted that in addition to the original metal present in the metalloenzyme, some functional models with other transition metals have been designed and reported. For example, phenoxazinone synthase mimicking activity has been reported by complexes with Mn(II), Co(III), etc. [8]. So other transition metal complexes can be designed for MMO activity to enable C_{sp^3} -H bond activation. Thus, search for active catalyst for high conversion and better selectivity of a particular product continues. Effort should be given to design the catalyst which can mimic activity of naturally abundant enzymes.

In this respect, we report synthesis, characterization and catalytic properties of dinuclear Cu(II) and Ni(II) complexes, $[Cu_2(L^1)_2(\mu_2-Cl)Cl] \cdot 2.5H_2O$ (1) and $[Ni_2(L^1)_2(\mu_2-N_3)_2(CH_3OH)_2] \cdot CH_3OH$ (2) where HL^1 is 1-((2-hydroxyethylimino)methyl)naphthalen-2-ol (Scheme 1). Some theoretical calculations have been performed to investigate spectral transitions of these complexes. Cu(II) complex has been prepared by the reaction between copper(II) chloride and HL^1 under mild conditions. It has been used as catalyst for oxidation of cyclohexane, toluene and cyclopentane using hydrogen peroxide as the oxidant. We wanted to check if replacement of copper by other metal, say nickel, in similar environment has any effect on catalytic activity. In other words, we wanted to use Ni for pMMO mimicking activity. Although Ni(II) complexes have been used as catalyst for different reactions including olefin epoxidation, C–C bond formation, etc. [9], attempt to use of nickel compounds in alkane oxidation is rare. Dinuclear Ni(II) complex has been synthesized with same ligand to provide similar chemical environment around the metal center.

2. Experimental

2.1. Materials and characterization

2-Hydroxy-1-naphthaldehyde, 2-aminoethanol, copper(II) chloride dihydrate, nickel(II)nitrate hexahydrate, sodium azide and tetrabutylammonium perchlorate (TBAP) were purchased from Sigma Aldrich and used without further purification. Other reagents and solvents were obtained from commercial sources and used as received. NMR spectra of the compounds were recorded on a Bruker 500 MHz spectrometer. Elemental analyses (carbon, hydrogen and nitrogen) were performed using a Perkin-Elmer 2400C elemental analyzer. FT-IR spectra were recorded on a Perkin Elmer spectrometer (Spectrum Two) with the samples by the use of attenuated total reflectance (ATR) technique. The UV-visible spectral measurements were recorded in Agilent 8453 diode array spectrophotometer. Analysis of reaction mixture of catalytic reactions was performed with a Shimadzu next generation high speed gas chromatography system (model: GC-2025 AF) equipped with a fused silica capillary column and FID detector. All electrochemical measurements were performed using a personal computer (PC)-controlled PAR model 273A electrochemistry system. A GC working electrode, a platinum wire auxiliary electrode and Ag/AgCl saturated KCl reference electrode were employed in a standard three-electrode configuration. TBAP was used as supporting electrolyte in MeCN and was done under nitrogen atmosphere. TG-DTA analysis was carried out on Perkin-Elmer Pyris Diamond TG/DTA unit. All experiments were carried out at room temperature in air unless reported otherwise.

CAUTION: Organic perchlorates are potentially explosive. Only small amount of the perchlorate salt should be handled with care.

2.2. Synthesis

2.2.1. Synthesis of 1-((2-hydroxyethylimino)methyl)naphthalen-2-ol (HL¹)

1-((2-Hydroxyethylimino)methyl)naphthalen-2-ol (HL¹) has been synthesized following a published procedure with slight modification [10]. Typically, 2-aminoethanol (0.5 mmol, 0.030 mL) was added to a methanolic solution (10.0 mL) of 2-hydroxy-1-naphthaldehyde (0.5 mmol, 0.086 g) under stirring condition. The mixture was stirred for 30 min. Then the resulting solution was refluxed for 2 h. The color of the mixture turned yellow. It was then cooled to room temperature to obtain yellow color solid product. The product was collected by filtration and dried in air. Yield: 85% (0.091 g); C, H, N analysis: anal. calc. for C₁₃H₁₃NO₂: C, 72.54; H, 6.09; N, 6.51; found: C, 72.44; H, 5.98; N, 6.56%. ¹H NMR (500 MHz, CD₃CN) δ (ppm): 14.23 (s, 1H), 8.80 (s, 1H), 7.92 (d, *J* = 8.5 Hz, 1H), 7.66 (d, *J* = 9.5 Hz, 1H), 7.58 (d, *J* = 7.5 Hz, 1H), 7.39 (1H, dd), 7.17 (dd, *J* = 6.0 Hz, 1H), 6.74 (d, *J* = 9.0 Hz, 1H), 4.11 (t, *J* = 9.0 Hz, 2H), 3.71 (t, *J* = 4.0 Hz, 2H), 3.18 (s, 1H); ¹³C NMR (500 MHz, CD₃CN) δ (ppm): 55.63, 62.08, 107.35, 119.29, 123.48, 126.10, 127.01, 129.02, 130.04, 135.45, 137.90, 160.69 and 177.62; FT-IR cm⁻¹: 3152, 2918, 1635, 1539, 1358, 1072, 838, 744, 500; ESI-MS (*m/z*): [M+H]⁺ = 215.13.

2.2.2. Synthesis of [Cu₂(L¹)₂(μ₂-Cl)Cl]·2.5H₂O (1)

A methanolic solution (10.0 mL) of copper(II) chloride dihydrate (0.5 mmol, 0.067 g) was added to 5.0 mL methanolic solution of HL¹ (0.5 mmol, 0.108 g). The mixture was stirred till it turned greenish. It was then refluxed for 1 h. Color of the solution became dark green. The mixture was finally cooled to room temperature and filtered to remove any precipitate or suspended materials. The filtrate was kept at ambient temperature. Green crystals suitable for X-ray diffraction study were produced within few days. Yield 65%, 0.218 g; C, H, N analysis: anal. calc. for C₂₆H₂₉Cl₂Cu₂N₂O_{6.5}: C, 46.50; H, 4.35; N, 4.17; found: C, 46.44; H, 4.23; N, 4.32%.

2.2.3. Synthesis of [Ni₂(L¹)₂(N₃)₂(CH₃OH)₂]-CH₃OH (2)

A methanolic solution (10.0 mL) of nickel(II) nitrate hexahydrate (0.5 mmol, 0.091 g) was added to 5.0 mL methanolic solution of HL¹ (0.5 mmol, 0.108 g) while the mixture was constantly stirred. It was stirred for 30 min. Then, sodium azide (0.5 mmol, 0.034 g) in 2.0 mL of methanol/water was added dropwise to the resulting green solution. After addition of azide, the solution turned dark green. The solution was stirred for another 30 min before it was refluxed for 1 h. The mixture was finally cooled to room temperature and filtered to remove any precipitate or suspended materials. The filtrate was kept at ambient temperature. Green crystals suitable for X-ray diffraction analysis were produced within few days. Yield 70%, 0.253 g; C, H, N analysis: anal. calc. for C₂₉H₃₆N₈Ni₂O₇: C, 47.97; H, 5.00; N, 15.43; found: C, 47.84; H, 4.92; N, 15.36%.

2.3. X-ray data collection and structure determination

Details of the data collection and refinement parameters for complexes **1** and **2** are summarized in Table 1. The diffraction experiments were carried out on a Bruker APEX-II CCD diffractometer using graphite monochromated Mo Kα radiation at 298 K for both the complexes **1** and **2**. Data were processed using the Bruker APEX2 and SAINT packages [11]. Absorption corrections based on multi-scans using the SADABS software [11] were applied to the intensity data. The structures were solved by direct methods using SHELXT [12] and refined with full-matrix least-squares on *F*² on all unique reflections using SHELXL-2014/7 [13]. All the non-hydrogen atoms of the complexes were refined anisotropically. A few hydrogen atoms, which are highly acidic, are disordered due to thermal disturbances. These have been assigned to their best possible positions by chemical speculation.

Table 1

Crystal data, data collection and structure refinement of complexes.

Complex	1	2
Formula	C ₂₆ H ₂₆ Cl ₂ Cu ₂ N ₂ O ₆	C ₂₉ H ₃₆ N ₈ Ni ₂ O ₇
Formula weight	660.47	726.08
<i>T</i> (K)	298 K	298 K
Crystal color	Dark green	Green
Crystal system	Orthorhombic	Monoclinic
Space group	P212121	P 21/n
<i>a</i> (Å)	13.5722(7)	16.7002(5)
<i>b</i> (Å)	11.8931(6)	7.4796(2)
<i>c</i> (Å)	17.3627(8)	25.7434(7)
<i>α</i> (°)	90.00	90.00
<i>β</i> (°)	90.000(3)	100.802(2)
<i>γ</i> (°)	90.00	90.00
<i>V</i> (Å ³)	2802.6(2)	3158.65(15)
<i>Z</i>	4	4
Crystal dimensions (mm)	0.5 × 0.2 × 0.15	0.4 × 0.2 × 0.1
<i>F</i> (0 0 0)	1344	1512
<i>D_c</i> (g cm ⁻³)	1.565	1.527
<i>λ</i> (Mo Kα) (Å)	0.71073	0.71073
<i>θ</i> Range (°)	1.90–24.99	1.601–27.220
Reflection collected/unique/observed	33,619, 4936, 4098	51,406, 7017, 5070
Absorption correction	Multi-scan	Multi-scan
<i>R</i> _{int}	0.0735	0.0342
Final <i>R</i> ₁ index [<i>I</i> > 2σ(<i>I</i>)]	0.0479	0.0504
Final <i>wR</i> ₂ index (all reflections)	0.1391	0.1450
Goodness-of-fit	1.150	1.033

2.4. Computational details

The singlet ground state (*S*₀) geometry of ligand, HL¹ and its copper and nickel complexes i.e. complexes **1** and **2** have been fully optimized by DFT method with B3LYP (Becke's three-parameter hybrid functional and Lee–Yang–Parr's gradient corrected correlation functional) exchange correlation functional approach using the Gaussian 09 program [14]. The B3LYP functional has been adopted along with the 6-31G basis set for H, C, N, O atoms whereas the 6-311G (d,p) basis set was utilized for Cl atoms and LANL2DZ was adopted as the basis set for Cu and Ni atoms [15]. The nature of all the stationary points was confirmed by carrying out a normal mode analysis, where all vibrational frequencies were found to be positive. On the basis of the optimized ground state (*S*₀) geometrical structures, the UV-vis absorption transition properties of the corresponding ligand and complexes **1** and **2** in methanol were computed by a time-dependent density functional theory (TDDFT) [16] approach associated with the conductor-like polarizable continuum model (CPCM) [17] using the same B3LYP level and the previous basis sets. Frontier Molecular Orbital (FMO) analysis has been done with gauss view software [18].

2.5. Catalytic studies

Oxidation of cyclohexane, toluene and cyclopentane has been performed in a similar procedure in the presence of both the metal complexes as catalysts. Typically, Metal complex (0.03 mmol) was taken in 5.0 mL of acetonitrile in a two-neck round bottom flask which was fitted with a condenser. To this, 1.5 mmol of the substrate and varying amount of HNO₃ were added. Catalytic reaction started as soon as 3–10 mmol of hydrogen peroxide (30% in H₂O) was added to it. The mixture was continuously stirred for 48 h at desired temperature under atmospheric pressure. Aliquots were collected at regular time intervals. The substrate and products from the reaction mixture were extracted with 2.0 mL diethyl ether. The product mixture was analyzed in gas chromatograph or GCMS before and after the treatment with triphenylphosphine (PPh₃). The identification was done by either the comparison with known standards or GCMS.

3. Results and discussion

3.1. Synthesis and ligand characterization

Synthesis of complexes **1** and **2** has been performed following route given in Scheme 1. First, HL¹ has been synthesized by one step Schiff-base condensation between 2-hydroxy-1-naphthaldehyde and 2-aminoethanol in 1:1 M ratio in methanol. The ligand has been characterized by elemental analysis, ¹H and ¹³C NMR spectra as well as by FT-IR and mass spectral analyses (Figs. s1–s4). ¹H NMR spectrum (Fig. s1) of the ligand shows a peak at 14.23 ppm indicating the presence of phenolic OH group. Presence of azomethine proton has been confirmed by the singlet peak at 8.80 ppm. Bands in the range of 4.19–3.66 ppm exhibit the presence of methylene protons while the peak at 3.18 ppm has been assigned to the presence of alcoholic proton. Signals for aromatic protons appear in the range of 7.92–6.72 ppm. ¹³C spectrum of the ligand corroborates well with the formation of the Schiff-base compound (Fig. s2). IR spectrum of the ligand shows most significant bands at 3152, 2918 and 1635 cm⁻¹ indicating the presence of phenolic OH, methylene and C=N moieties, respectively (Fig. s3). ESI mass spectrum of the compound shows *m/z* band at 215.13 confirming the formation of the Schiff-base ligand (Fig. s4) (calculated value 215.09). Reaction between HL¹ and copper(II) chloride dihydrate gives **1**. Complex **2** has been synthesized by the reaction between the ligand, nickel(II) nitrate hexahydrate and sodium azide where azide acts as a bridging ligand. HL¹ undergoes deprotonation in the reaction medium without any external deprotonating base.

3.2. Crystal structures of **1** and **2**

Complex **1** crystallizes from methanol in orthorhombic system with P212121 space group. A perspective view of the complex is given in Fig. 1. Selected bond lengths and bond angles are given in Table 2. Cu1 is tetracoordinated whereas Cu2 is in pentacoordination geometry. The two chloride ions from the copper(II) salt used for the complex formation, bind the Cu atoms differently as confirmed by the crystal structure. One chlorido is bridging while the other is terminal. Cu1 is in a distorted square planar environment bonded to O1, O2, N1 and Cl1. Cl1 is the bridging chlorine atom which links Cu1 and Cu2. There is deviation of donor-metal-donor bond angle from 90°. The O2-Cu1-N1 bond angle is 83°, O1-Cu1-N1 angle is 92°, Cl1-Cu1-O2 angle is 93° and Cl1-Cu1-O1 angle is 94°. The Cu1-Cl1 bond is slightly out of plane. This confirms the approximate square planar geometry around the Cu1 center. Cu2, on the other hand, is bonded to O3, O4, N2, Cl1, Cl2. It is in distorted square pyramidal geometry as indicated by the value of the trigonal index, τ . The trigonal index is calculated as the difference

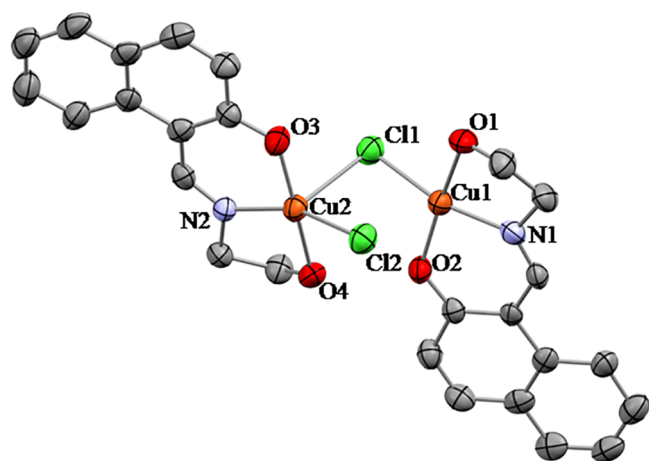


Fig. 1. A perspective view of complex **1** with partial atom numbering scheme. Hydrogen atoms and solvent molecules are omitted for the clarity.

Table 2
Selected bond lengths (Å) and bond angles (°) of complexes **1** and **2**.

Complex 1			
Cu1-O2	1.997(6)	Cu2-O3	1.885(6)
Cu1-N1	1.911(8)	Cu2-N2	1.918(7)
Cu1-O1	1.906(6)	Cu2-O4	2.022(6)
Cu1-Cl1	2.250(3)	Cu2-Cl2	2.280(3)
		Cu2-Cl1	2.724(3)
O2-Cu1-N1	83.0(3)	N2-Cu2-O4	82.5(3)
O2-Cu1-O1	170.1(3)	O3-Cu2-Cl2	96.7(2)
N1-Cu1-O1	91.7(3)	N2-Cu2-Cl2	156.8(2)
O2-Cu1-Cl1	93.0(2)	O4-Cu2-Cl2	89.9(2)
N1-Cu1-Cl1	163.0(2)	O3-Cu2-Cl1	89.9(2)
O1-Cu1-Cl1	94.45(19)	N2-Cu2-Cl1	107.1(2)
O3-Cu2-N2	92.7(3)	O4-Cu2-Cl1	85.88(19)
O3-Cu2-O4	172.4(3)	Cl2-Cu2-Cl1	94.03(9)
Complex 2			
Ni1-N8	1.969(3)	Ni2-N7	1.968(3)
Ni1-O6	1.977(2)	Ni2-O2	1.990(2)
Ni1-N1	2.035(3)	Ni2-N4	2.038(3)
Ni1-N4	2.133(3)	Ni2-N1	2.144(3)
Ni1-O4	2.155(2)	Ni2-O3	2.162(3)
Ni1-O5	2.170(3)	Ni2-O1	2.164(3)
N8-Ni1-O6	91.24(10)	N7-Ni2-O2	89.62(11)
N8-Ni1-N1	169.95(12)	N7-Ni2-N4	171.16(13)
O6-Ni1-N1	97.73(11)	O2-Ni2-N4	94.28(11)
N8-Ni1-N4	95.65(12)	N7-Ni2-N1	92.80(12)
O6-Ni1-N4	92.44(12)	O2-Ni2-N1	91.65(12)
N1-Ni1-N4	79.55(16)	N4-Ni2-N1	79.18(12)
N1-Ni1-O4	82.19(12)	N7-Ni2-O3	81.57(12)
O6-Ni1-O4	173.12(9)	O2-Ni2-O3	171.06(10)
N1-Ni1-O4	89.08(11)	N4-Ni2-O3	94.66(12)
N4-Ni1-O4	87.84(11)	N1-Ni2-O3	90.28(12)
N8-Ni1-O5	91.09(11)	N7-Ni2-O1	96.10(13)
O6-Ni1-O5	92.49(11)	O2-Ni2-O1	93.62(12)
N1-Ni1-O5	93.03(12)	N4-Ni2-O1	91.58(13)
N4-Ni1-O5	171.56(11)	N1-Ni2-O1	169.69(12)
O4-Ni1-O5	88.08(11)	O3-Ni2-O1	85.88(13)

between the two largest donor-metal-donor angles divided by 60 [19]. Its value is 1 for the ideal trigonal bipyramid and 0 for the square pyramid. Here the τ value is calculated to be 0.25 which indicates its significantly distorted square pyramidal environment. O3, O4, N2 and Cl2 atoms form the basal plane of the square pyramid and Cl1 occupies the apical position. However, Cu center is out of the mean plane by 0.150 Å towards Cl1. There are 2.5 water molecules in the crystal structure. The solvent water molecules are disordered due to molecular vibrations. The H atoms in the alcoholic moiety and the water molecule have been assigned their best possible positions in spite of being disordered. The crystal has been refined as a merohedral twin. In packing structure, there are π - π and CH- π interactions (Fig. s5). The metal-metal distance is 3.485 Å. Metal-chlorine bond distances are long compared to other metal-donor distances as expected. Although Cu-Cl bond distances are long here (Table 2), similar long copper-chlorine distances are also reported [20].

Complex **2** crystallizes from methanol into a monoclinic system with P 21/n space group. A perspective view of the complex is given in Fig. 2. Selected bond lengths and bond angles are given in Table 2. The molecule consists of two nickel atoms, two deprotonated ligands, 1-((2-hydroxyethylimino)methyl)naphthalen-2-ol (HL¹), two azido ligands and two coordinated methanol molecules. One methanol is present as solvent of crystallization. Each Ni atom is in similar coordination geometry i.e. in octahedral geometry. Ni1 is bonded with O4, N8 and O6 from the ligand, N1 and N4 from two different azido moieties and O5 from a methanol molecule. On the other hand, Ni2 is coordinated to O2, N7 and O3 atoms from the ligand, Ni and N4 from two different azido species and O1 from a methanol molecule. Two intramolecular hydrogen bonds are present in this molecule involving non-coordinated methanol (Fig. s6). Coordinated O3 atom is present in H-bonding with H-O moiety of methanol and second hydrogen bond is found involving

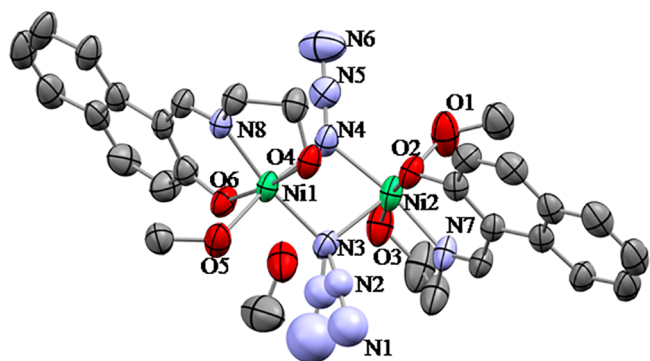


Fig. 2. A perspective view of complex 2 with partial atom numbering scheme. Hydrogen atoms are omitted for the clarity.

O atom of methanol and H-O6 moiety of alcoholic group. All of the donor–Ni bond distances are in agreement with the reported values [21].

3.3. IR spectral studies

FT-IR spectra of all of the complexes have been obtained with powder samples by ATR technique. Peaks at 1622 and 1617 cm^{-1} in the IR spectra of Cu and Ni complex respectively, confirm the presence of azomethine bond in both the complexes (Fig. s7). A sharp peak at 2054 cm^{-1} indicates the presence of azido moiety in complex 2. Both the complexes show broad band in the range of 3500–3400 cm^{-1} . Broad peak in complex 1 is due to the presence of water molecule which is present as solvent of crystallization in complex 1 and that for complex

2 is probably due to the presence of methanol molecules in the Ni complex.

3.4. UV-vis spectral studies

The electronic spectra of complexes 1 and 2 have been recorded in methanol at room temperature (Figs. s8 and s9). For complex 1, high intensity bands appear at 383 and 316 nm (molar extinction coefficient of 12,100 and 13,500 $\text{Lmol}^{-1}\text{cm}^{-1}$, respectively) which may occur due to ligand to metal charge transfer ($\text{PhO}^- \rightarrow \text{Cu(II)}$) and N(imino) \rightarrow Cu (II) and intra ligand charge transfer respectively. The Cu complex shows broad bands at 646, 673 and 720 nm with low intensity. These spectral characteristics are in consistency with copper(II) complexes of distorted square pyramidal (SP) geometry. The observed bands originate from $d_{xz}, d_{yz} \rightarrow d_{x^2-y^2}$ transitions [22]. They are accompanied by a low energy shoulder at 844 nm due to $d_{xy}, d_{x^2-y^2} \rightarrow d_{z^2}$ transitions. As the structure moves more towards TBP structure the low energy band along with high energy spin forbidden band becomes more pronounced. The characteristic bands observed here are results for distorted square pyramidal geometry.

UV spectrum of complex 2 shows high intensity bands at 312 and 395 nm with molar extinction coefficient of 9335 and 8261 $\text{Lmol}^{-1}\text{cm}^{-1}$, respectively. These bands are probably due to the intraligand charge transfer, and LMCT ($\text{PhO}^- \rightarrow \text{Ni(II)}$ and N(imino) \rightarrow Ni(II)), respectively.

Complex 2 also shows d-d transitions. The broad bands are obtained at 750 and 860 nm which probably indicate $d_{xz}, d_{yz} \rightarrow d_{z^2}$ and $d_{xy}, d_{x^2-y^2} \rightarrow d_{z^2}$ transitions [22].

Table 3

Main calculated UV-Vis transition for HL¹, complexes 1 and 2 with vertical excitation energies (E_{cal}), oscillator strengths (f_{cal}) of the lowest few excited singlets obtained from TDDFT/B3LYP/CPCM method in methanol.

Compound	Excitation (eV)	Electronic transition State	excitation (nm)	Osc. strength (f)	CI	Key transitions
HL ¹	2.904	$S_0 \rightarrow S_1$	418.14	0.0423	0.1965	(08%)HOMO-1 \rightarrow LUMO + 1
					0.6204	(77%)HOMO \rightarrow LUMO
	2.991	$S_0 \rightarrow S_2$	400.12	0.0252	0.1274	(03%)HOMO \rightarrow LUMO + 1
					0.5570	(62%)HOMO-1 \rightarrow LUMO
					0.1192	(02%)HOMO-1 \rightarrow LUMO + 1
					0.2872	(16%)HOMO \rightarrow LUMO + 1
3.983	$S_0 \rightarrow S_5$	311.24	0.6564	0.1188	(03%)HOMO-3 \rightarrow LUMO + 1	
				0.4700	(44%)HOMO-1 \rightarrow LUMO	
				0.1195	(43%)HOMO-1 \rightarrow LUMO + 2	
				0.4220	(35%)HOMO \rightarrow LUMO + 1	
Complex 1	3.070	$S_0 \rightarrow S_1$	390.05	0.0642	0.6714	(89%)HOMO \rightarrow LUMO
					0.2031	(08%)HOMO-2 \rightarrow LUMO
	3.227	$S_0 \rightarrow S_2$	384.21	0.1501	0.1180	(02%)HOMO \rightarrow LUMO + 1
					0.6418	(82%)HOMO-1 \rightarrow LUMO + 1
					0.1114	(02%)HOMO-3 \rightarrow LUMO
	3.254	$S_0 \rightarrow S_4$	380.93	0.0402	0.1834	(06%)HOMO \rightarrow LUMO
					0.2215	(10%)HOMO-2 \rightarrow LUMO
					0.1046	(02%)HOMO-9 \rightarrow LUMO
					0.5468	(60%)HOMO \rightarrow LUMO + 1
3.900	$S_0 \rightarrow S_8$	317.88	0.2581	0.1483	(04%)HOMO-2 \rightarrow LUMO + 3	
				0.6705	(90%)HOMO \rightarrow LUMO + 1	
3.956	$S_0 \rightarrow S_9$	313.40	0.0304	0.6101	(74%)HOMO-4 \rightarrow LUMO + 3	
				0.2635	(14%)HOMO-4 \rightarrow LUMO + 5	
				0.1190	(03%)HOMO-4 \rightarrow LUMO + 8	
Complex 2	3.083	$S_0 \rightarrow S_1$	400.01	0.0104	0.2156	(10%)HOMO-2 \rightarrow LUMO
					0.1169	(02%)HOMO-2 \rightarrow LUMO + 1
	3.120	$S_0 \rightarrow S_2$	396.12	0.1033	0.6153	(74%)HOMO \rightarrow LUMO
					0.1788	(06%)HOMO-2 \rightarrow LUMO
					0.3422	(23%)HOMO-3 \rightarrow LUMO
	3.961	$S_0 \rightarrow S_5$	314.40	0.0309	0.4418	(39%)HOMO-1 \rightarrow LUMO + 1
0.2967					(17%)HOMO-1 \rightarrow LUMO + 4	
3.986	$S_0 \rightarrow S_6$	311.21	0.0571	0.5512	(61%)HOMO \rightarrow LUMO + 1	
				0.2806	(15%)HOMO-3 \rightarrow LUMO + 2	
					0.1165	(02%)HOMO-3 \rightarrow LUMO + 1

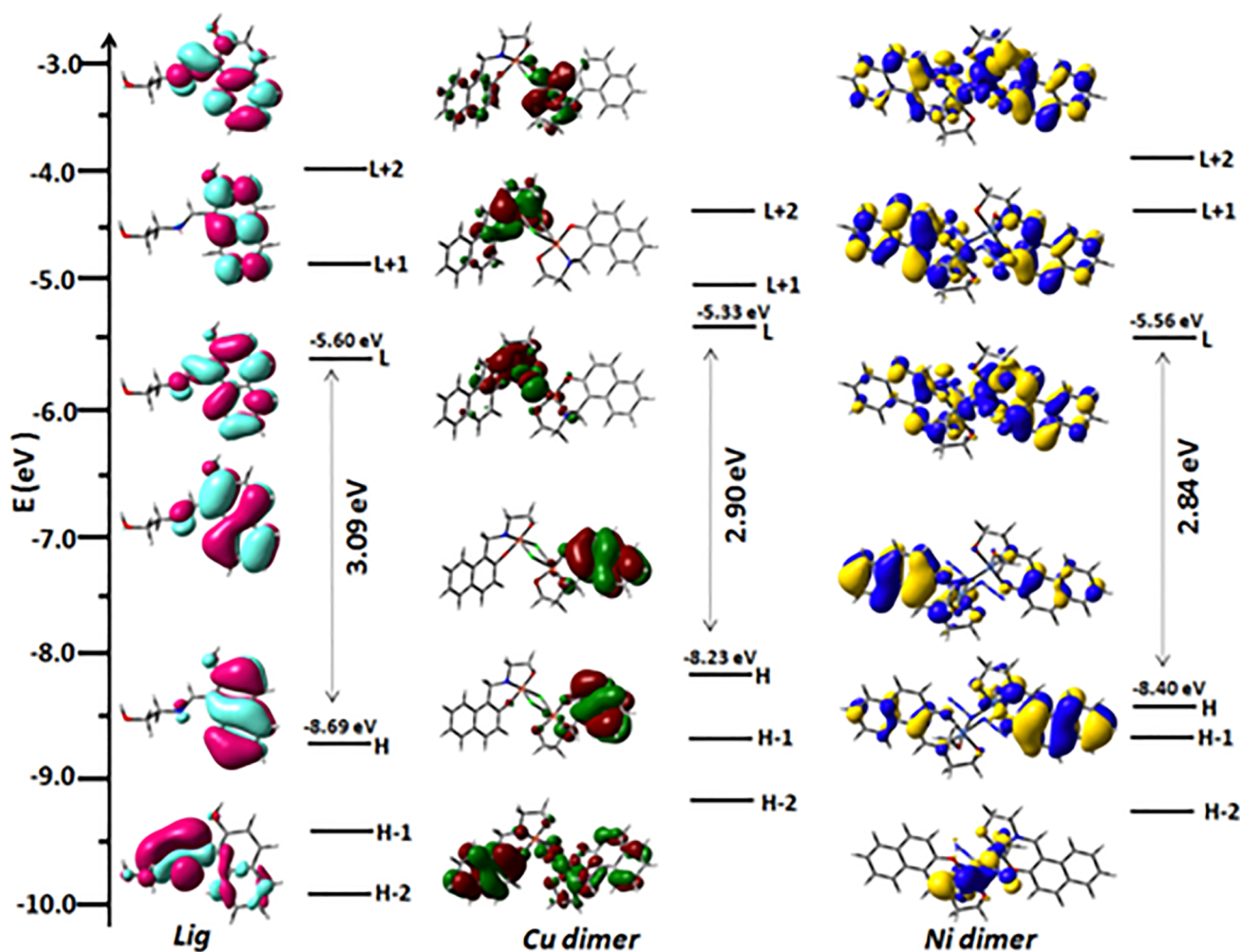


Fig. 3. Frontier MOs along with their HOMO-LUMO energy gap of HL¹, complexes 1 and 2.

3.5. Geometry optimization and computational studies

Molecular structures of HL¹ and its Cu, Ni complex have been optimized at their electronic ground state (S_0) by means of DFT at B3LYP/(6-31G) level. For better understanding of the electronic transitions involved in absorption process, TD-DFT calculations have been carried out by the B3LYP/CPCM method in methanol by utilizing the ground state optimized geometries. We have computed the lowest 40 singlet-singlet transition and results of the TD calculations are qualitatively very similar with the experimental results. The computed absorption energies along with their oscillator strengths, the main configurations, are summarized in Table 3. Fig. 3 displays the energy levels of different Frontier Molecular Orbital's of the ligand and complexes 1 and 2 associated with their HOMO-LUMO energy gap. Due to the presence of electronic correlation in the TD-DFT (B3LYP) method, it can yield more accurate electronic excitation energies. The UV spectra computed by TD-DFT calculations in methanol show the important peaks in the range 200–500 nm.

HL¹ shows lowest lying distinguishable singlet \rightarrow singlet absorption band at 418.14 nm (experimentally 415 nm, experimental absorption band in methanol are shown in Fig. s10) which is due to the contribution of HOMO-1 \rightarrow LUMO + 1, HOMO \rightarrow LUMO, HOMO \rightarrow LUMO + 1 transitions, also a moderately intense peak at 400.12 nm (experimentally 400 nm) that corresponds to HOMO-1 \rightarrow LUMO, HOMO \rightarrow LUMO, HOMO \rightarrow LUMO + 1 transitions along with a shoulder at 311.24 nm (experimentally 306 nm) corresponding to HOMO-3 \rightarrow LUMO + 1, HOMO \rightarrow LUMO + 1, HOMO-1 \rightarrow LUMO + 2

and HOMO-1 \rightarrow LUMO transitions.

Complex 1 shows an intense absorption peak at 384.21 nm (experimentally 383 nm) corresponding to HOMO-1 \rightarrow LUMO + 1, HOMO-3 \rightarrow LUMO, HOMO \rightarrow LUMO transitions along with moderately intense absorption band at 317.88 nm (experimentally 316 nm) corresponding to HOMO-2 \rightarrow LUMO + 4, HOMO \rightarrow LUMO + 6 transitions (FIGURE4A). Besides the nickel dimer shows absorption peaks at 396.12 nm (experimentally 395 nm) due to the contribution of HOMO-3 \rightarrow LUMO, HOMO-2 \rightarrow LUMO, HOMO-1 \rightarrow LUMO + 1 transitions and peak at 314.40 nm (experimentally 312 nm) corresponding to HOMO-1 \rightarrow LUMO + 4, and HOMO \rightarrow LUMO + 1 transitions (Fig. 4B).

3.6. Thermal analysis

Thermogravimetric analysis (TGA) and differential thermal analysis (DTA) have been performed on powdered samples of complexes 1 and 2 from 35 to 800 °C (for complex 1) and 35 to 750 °C (for complex 2) to examine thermal stability of the complexes and fate of solvent of crystallization molecules.

In the TGA DTA plot of complex 1, an initial loss of 2.6% is seen at temperature 50 °C which corresponds to an endothermic DTA peak. It depicts the loss of surface water probably (Fig. s11). The next visible loss at 190 °C is a weight loss of 6% which probably indicates the loss of all the water molecules (calculated loss 6.7%) also depicted by an endothermic peak. A loss of almost 32% occurs at 280 °C which probably shows loss of one ligand moiety (calculated loss 32.2%). The next decomposition at 370 °C probably indicates loss of two Cl (observed

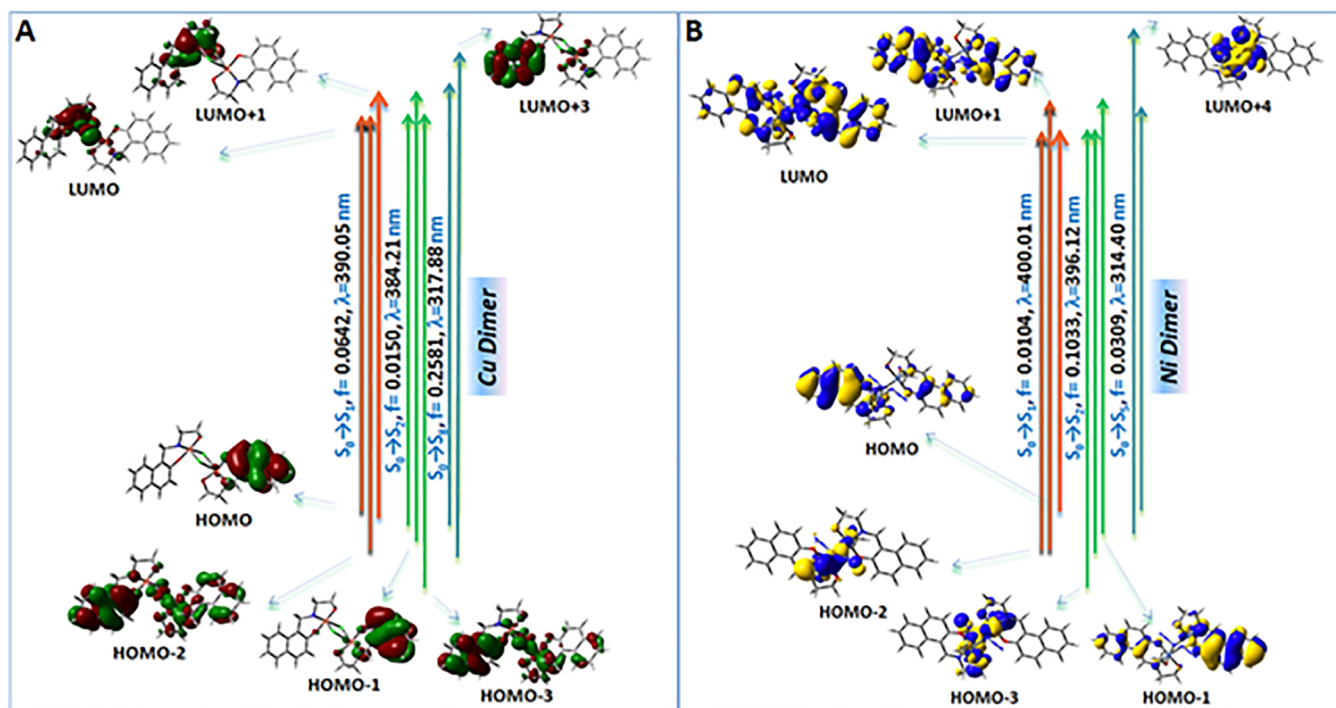


Fig. 4. Frontier molecular orbitals involved in the UV-vis absorption of complexes 1 (A) and 2 (B).

~10% vs calculated 10.6%). The final loss of 33% could be attributed to the loss of another ligand moiety after which a stable residue of CuO is obtained. All of the last three losses accompany a corresponding exothermic peak in the DTA curve.

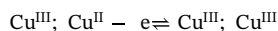
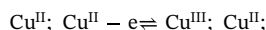
In the TGA DTA plot of complex 2, the initial loss of 13% at 86 °C can be attributed to the loss of 3 methanol molecules (bound and unbound (calculated loss 13.2%)) as confirmed by endothermic DT peak (Fig. s12). There are next two consecutive losses, each of 4%, which can be assigned to the loss of N₂ twice from the azide bridges. This loss occurs between 132 and 180 °C of temperature. The next loss of another 4% is the final decomposition of the nitrogens of the azide bridge and its evolution as another molecule of N₂ at and the process completes at 270 °C. The next loss of 40% probably confirms the loss of one part of the dinuclear complex which continues upto 400 °C. The residue as stable NiO is left behind. All show exothermic DT peaks other than the loss of solvent molecules at the starting temperatures.

3.7. Cyclic voltametric studies

Electrochemical studies of complexes 1 and 2, and the ligand have been carried out in acetonitrile using TBAP as supporting electrolyte. A typical cyclic voltammogram (CV) has been obtained by using a glassy carbon electrode and an Ag/AgCl saturated KCl reference electrode. CV plots of the complexes are shown in Fig. 5.

The CV plot of the dinuclear complex, 1 has been obtained by scanning potential -2.0 to +1.5, wherein the electrochemical behavior of the complex is elucidated properly. The scan rate has been maintained at 50 mV s⁻¹. The forward scan gives an anodic peak at 0.62 V and I_{pa} 8 × 10⁻⁶ A and the cathodic counterpart in the reverse scan at E_{pc} 0.48 V and I_{pc} of 2.2 × 10⁻⁵ A. These peaks have been attributed to the redox couple Cu(II)-Cu(III) as the peaks clearly show a quasireversible one electron transfer process [23a–d]. The similarity with literature values confirms the peaks. Of the copper centers, Cu2 is more competent to undergo oxidation to +3 state as it satisfies the 18-electron rule after the oxidation process. Comparison of the results of voltammetric peak current with those of the ferrocene-ferrocenium couple under the same experimental conditions establishes that these

responses involve one electron in each step. The electrochemical responses of the complex may be assigned as:



The anodic peak at 1.2 V indicates an irreversible ligand oxidation which is characteristic of the oxidation of the Schiff base groups [24a–c].

In the scan of range 0.0 to -2.0 V, the cathodic peak at E_{pc} -0.78 V with I_{pc} 6 × 10⁻⁶ A is seen as a broad peak which indicates two simultaneous reductions in this region. An irreversible Cu(II) to Cu(I) reduction occurs in this potential region. This is well supported by literature data [23b,25a–b]. The ligand also undergoes an irreversible reduction at this potential as confirmed by the cyclic voltammogram of the isolated ligand as well. The peak in the isolated ligand is at -1.05 V, which has shifted to the new potential (shifted gradually to slightly higher potential values) due to coordination of the ligand to the Cu(II) center [25b–c], may be assigned to the reduction of imine group [(-C=N-)/(-C=N-)] [25a]. The cathodic peak at -1.5 V indicates a further reduction of Cu(I) to Cu(0). This is a one electron process as ascertained from literature values as well [23b]. The peak in the reverse scan is the anodic dissolution wave of deposited copper, for Cu(0) → Cu(I) which is indicated by a long peak at -0.19 V [23b].

For the nickel complex, the quasireversible redox couple at E_{pc} 0.22 V and I_{pc} 7 × 10⁻⁷ A and E_{pa} 0.38 V and I_{pa} 2 × 10⁻⁶ A can be assigned to the Ni(II)/Ni(I) couple [25d–f]. The scan rate has been kept at 100 mV s⁻¹. The cathodic peak at -0.64 V indicates a ligand reduction which has also been observed in the free ligand at -1.05 V but shifted to higher potentials due to the binding to Ni(II) ion. The anodic peak at 1.05 V corresponds to a ligand oxidation as almost similarly observed in the Cu(II) complex.

The CV plot of the free ligand has been given in the Supplementary information (Fig. s16). It shows two cathodic peaks at -0.56 V and -1.05 V corresponding to the reductions on the ligand and an anodic peak at -0.57 V which corresponds to an oxidation. Scan rate has been maintained at 100 mV s⁻¹.

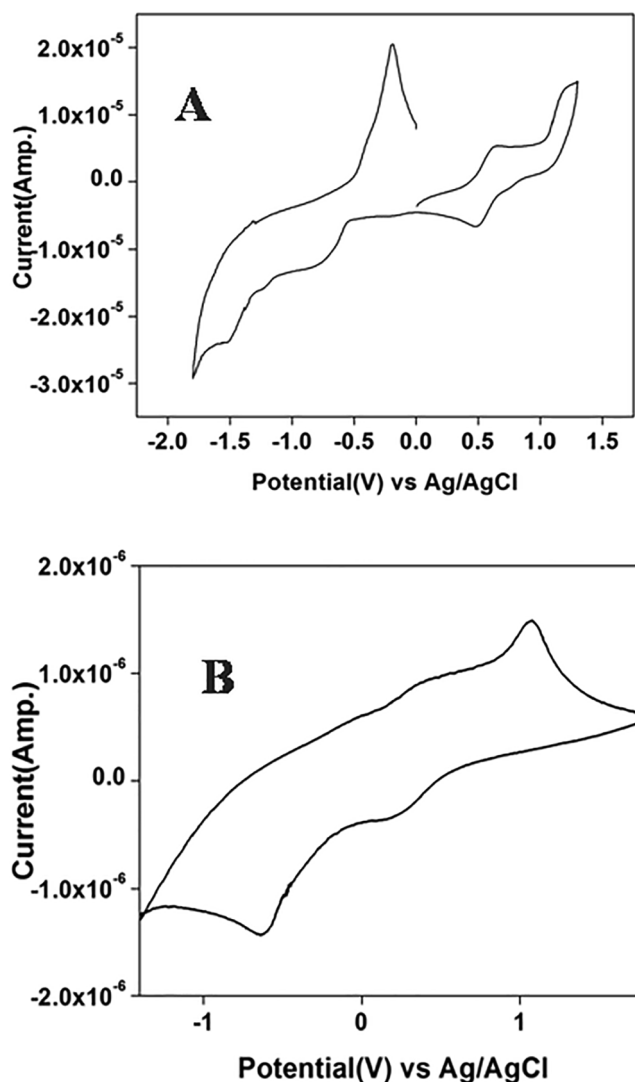


Fig. 5. Cyclic voltammograms of complexes 1 (A) and 2 (B).

3.8. Catalysis studies

We have checked catalytic activity of both the complexes for oxidation of cyclohexane, toluene and cyclopentane. The oxidation of the substrates has been performed by H_2O_2 as the oxidant in a slightly acidic medium under ambient conditions. To set optimum conditions, we have varied amount of hydrogen peroxide (30% in H_2O) as well as the acid (HNO_3) keeping fixed amount of the metal complex (0.03 mmol) in 5.0 mL of acetonitrile. The ratio $n(\text{HNO}_3)/n(\text{catalyst})$ has been varied in the range of 5–25. The $n(\text{H}_2\text{O}_2)/n(\text{catalyst})$ has been varied from 100 to 500 with the best yield obtained at 500.

Results of oxidation are summarized in Table 4. The primary products of the oxidation of cyclohexane are cyclohexanol and cyclohexanone; toluene is oxidized mainly to benzyl alcohol and benzaldehyde, whereas oxidation of cyclopentane gives cyclopentanol and cyclopentanone as the major products. Cyclohexane oxidation gives a small amount of adipic acid (~9%) in addition to the major products when the ratio $n(\text{H}_2\text{O}_2)/n(\text{catalyst})$ is 250–300. At lesser ratio $n(\text{H}_2\text{O}_2)/n(\text{catalyst})$, say 100, no adipic acid has been detected and at still higher ratio of 500 (which is the most optimized condition) the amount of adipic acid formed remains the same i.e. 9%. Benzoic acid has been obtained as a minor product from oxidation of toluene. Benzoic acid is generally obtained by aerial oxidation of benzaldehyde, hence this benzoic acid could have come from benzaldehyde which has been

formed during the oxidation of toluene. Oxidation of cyclopentane gives some high boiling combustion products along with the major cyclopentanol and cyclopentanone.

The yield has been optimized by varying the relative proportions of nitric acid and hydrogen peroxide with respect to the catalysts, temperature and varying the reaction time. It has been obvious from previous studies [6,7,26] that the presence of nitric acid has positive role in these catalytic reactions. Nitric acid has, mainly, two important roles: (i) it could increase the vacant coordination site at the metal center by the protonation of the ligand of these complexes and hence enhances oxidative properties of the catalyst; and (ii) decomposition of peroxide is retarded in the presence of nitric acid, the stability of peroxy intermediate is increased. However, it is difficult to determine the exact structure of the complex in solution. Copper center in dinuclear complex is in both tetra and penta-coordination. Thus, these metal centers would need nitric acid to increase the unsaturation at the metal center. The highest conversion has been ascertained at $n(\text{HNO}_3)/n(\text{catalyst})$ ratio 20, while the yield decreases on further increasing the ratio. Hence, this ratio is maintained throughout for all the reaction sets.

The reaction mixture has been stirred for 48 h at room temperature (35 °C) under atmospheric pressure. Different temperatures conditions have been applied to optimize the highest yield. Reaction has been carried out at 40, 50, 60 and 70 °C. The best yield was obtained at 40 °C. Upto 50 °C, the reaction proceeds showing slight decrease in yield at 50 °C which gradually declines upto 60 °C. However, after 60 °C, there is a drastic decrease in the yield of products as it has been confirmed by gas chromatographic analysis.

The catalysis has also been done at high pressure conditions which fail to yield the products. This indicates that normal pressure conditions are most desired condition for the reaction. The reaction has also been performed with TBHP as the oxidant under the similar experimental conditions but it shows lower yield, 5% in total. This can, probably, be due to its bulky structure which destabilizes the intermediate. Then, we have performed the same catalytic reaction under inert (argon) atmosphere to examine effect of the presence of oxygen. However, it has been found that this reaction shows almost equal yield when same catalytic reaction is carried out under normal experimental conditions. There is only a small decrease in amount of products formed under inert atmosphere which indicates only little participation of atmospheric oxygen in the oxidation process.

Instead of nitric acid, organic acid such as acetic acid has been employed in the reaction. The yield of product remains the same showing that organic acid is as effective in the role played by nitric acid. In order to find out the probable mechanisms, we have carried out the catalytic reaction of cyclohexane with the complex maintaining $n(\text{HNO}_3)/n(\text{catalyst})$ ratio of 20 and $n(\text{H}_2\text{O}_2)/n(\text{catalyst})$ ratio of 500 in the presence of TEMPO (2,2,6,6-tetramethylpiperidin-1-oxyl). The yield of the reaction is greatly suppressed in its presence. TEMPO is well known as a radical trap. This indirectly indicates that oxidation reactions occur mainly by mechanisms involving the formation of radicals.

Copper salts like $\text{Cu}(\text{NO}_3)_2$, under the same reaction conditions exhibit at much lower activity towards oxidation of all substrates under same experimental condition. It shows only about 6% conversion. So it is evident that the presence of N and O donor ligands is quite relevant.

To check the possibility of oxidation of all the substrates under acidic conditions, we have performed blank reactions for each of the substrates without any metal center. The amounts of nitric acid and hydrogen peroxide have been chosen at which concentration of these reagents maximum conversions of the substrates were achieved with the catalyst. Blank reactions have been carried out with substrate (1.5 mmol), hydrogen peroxide (15 mmol) and nitric acid (0.6 mmol) at 40 °C for 48 h. Conversion rate is very low (~3.7% for cyclohexane and toluene, and 4.5% for cyclopentane). This indicates that the conversion of the substrate to product is difficult reaction and accelerated by the presence of our copper complex.

The reaction is believed to proceed through the formation of alkyl

Table 4
Oxidation^a of cyclohexane, toluene and cyclopentane.

Cyclohexane						
$n(\text{H}_2\text{O}_2)/n(\text{catalyst})$	Time (h)	Yield ^b (%)		Total ^c	Selectivity ^d of cyclohexanol (%)	TON ^e
		Cyclohexanone	Cyclohexanol			
100	8	3.2	5.8	9	64.4	4.5
	48	6.4	9.1	15.5	58.7	7.75
250	8	7.6	14.1	21.7	65	10.8
	48	9.3	21.4	30.7	69.7	15.3
500	8	11.1	19.3	30.4	63.4	15.2
	48	18.4	29.8	48.2	62	24.1
	48 ^f	47	0.5	47.5	0.01	23.5
Toluene						
$n(\text{H}_2\text{O}_2)/n(\text{catalyst})$	Time (h)	Yield ^b (%)		Total ^c	Selectivity ^d of benzyl alcohol (%)	TON ^e
		Benzyl alcohol	Benzaldehyde			
100	8	7.4	4.8	12.2	60.6	6
	48	11.1	7.2	18.3	60.6	9
250	8	11.8	9.3	21.1	56	10.55
	48	19.4	14.4	33.8	57.4	16.9
500	8	19.1	13.8	32.9	58	16.45
	48	23.8	15.9	39.7	60	19.8
Cyclopentane						
$n(\text{H}_2\text{O}_2)/n(\text{catalyst})$	Time (h)	Yield ^b (%)		Total ^c	Selectivity ^d of Cyclopentanol (%)	TON ^e
		Cyclopentanone	Cyclopentanol			
100	8	5.2	5.8	11	52.7	5.5
	48	9.2	11.4	20.6	55.3	10.3
250	8	8.5	10.9	19.4	56.1	9.8
	48	13.6	14.9	28.5	52.2	14.25
500	8	14.5	17.2	31.7	54.2	15.85
	48	16.7	19.1	35.8	53.3	17.9

^a Solvent: acetonitrile.

^{b,d} Yield and selectivity calculated after treatment with PPh_3 .

^c Alcohol + ketone.

^e TON (turn over number) = moles of product/mole of catalyst.

^f before treatment with PPh_3 .

hydroperoxide (ROOH) (e.g. cyclohexyl peroxide or benzyl peroxide) along with the alcohol (e.g. cyclohexanol, benzyl alcohol and cyclopentanol) and carbonyl compounds (such as cyclohexanone, benzaldehyde and cyclopentanone). The formation and quantification of these compounds have been carried out by following a method introduced by G. B. Shul'pin [27]. According to this procedure, the reaction mixture has been analyzed by GC before and after treating with excess PPh_3 . Treatment of the reaction mixture (alkyl hydroperoxide) by PPh_3 leads to the formation of alcohol with subsequent formation of phosphane oxide (OPPh_3). We have observed that after the reduction with PPh_3 , the alcohol peak in the GC analyses rises markedly for each of the substrate while the intensity of the $> \text{C}=\text{O}$ compound's peak reduces. Alkyl hydroperoxides are, in many cases, the main primary products of alkane oxidation with hydrogen peroxide. The peroxides formed in the oxidation with H_2O_2 can, sometimes, decompose in the injector of GC during the analysis with the formation of the corresponding alcohol and ketone. If we compare the yields of reaction before and after the treatment with triphenylphosphine, we can see that yield of alcohol increases tremendously after the treatment with PPh_3 (representative case, Table 4). Before the treatment with PPh_3 , product of oxidation of cyclohexane is almost solely cyclohexanone. This indicates that the saturated hydrocarbon oxidation may follow the Shul'pin pathway.

The hydroxyl radical HO^\cdot could be formed as a result of metal-assisted decomposition of hydrogen peroxide. The hydroxyl radical abstracts H from the substrate (RH) to form R^\cdot [26a]. The formation of ROOH may be occurred by the reaction between a metal-peroxo

intermediate, e.g. bearing a Cu(II)-OOH type moiety and the organoradical R^\cdot , to form ROOH [28]. The formation of Cu-peroxo species has been determined by UV-vis spectra. The metal-assisted homolytic cleavage of alkyl hydroperoxide generates alkoxy (RO^\cdot , upon O–O bond rupture) and alkylperoxy (ROO^\cdot , upon O–H bond breakage) radicals which can form an alcohol (ROH) upon H-abstraction from the alkane (RH) by RO^\cdot or both ROH and the $> \text{C}=\text{O}$ upon decomposition of ROO^\cdot [29].

ESI-mass spectrum of complex **1** in methanol shows the presence of both mononuclear and dinuclear species (Fig. s13). Peak at 641.09 indicates the presence of dinuclear species and may be attributed to the presence of $[\text{Cu}_2(\text{L}^1)_2(\mu_2\text{-Cl})(\text{H}_2\text{O})(\text{CH}_3\text{OH})]$. It shows additional m/z peak at 277.05 which is assigned to $[\text{Cu}(\text{L}^1)]^+$. This indicates that dinuclear species also exists in solution. UV-vis spectra for the complexes have been recorded in methanol at room temperature as discussed earlier. To further observe the effect of hydrogen peroxide, we have recorded the UV-vis spectra of the complexes in the presence of hydrogen peroxide (Figs. s14 and s15). It has been observed that an intense peak at 400 nm, with a shoulder in the range of 410–420 nm, appears for complex **1**. This may be attributed to the existence of Cu-hydroperoxo or Cu-peroxo species [30]. However, there is no observable change in the UV-vis spectrum of complex **2** when it is recorded in the presence of hydrogen peroxide (Fig. s15).

Complex **2** has also been checked for its catalytic property in oxidizing the substrates. But the Ni catalyst shows very poor conversion i.e. about 7% total yield for cyclohexane, 5% for toluene and 4% for

cyclopentane. This could be attributed to the coordinatively saturated nature of the each Ni center in complex **2** with coordination number 6. The UV vis data of the complex in the presence of H₂O₂ could not confirm the presence of Ni-hydroperoxo or peroxy species like Cu-hydroperoxo or Cu-peroxo in case of complex **1**. Also electrochemical studies of the complex indicate no formation of higher oxidation state species in the said voltage range whereas Cu(III) species has been detected in the said voltage range indicating more vulnerability character of complex **1**. Thus replacement of Cu by Ni in the complex actually stops the catalytic ability of the material.

Conversion of saturated hydrocarbons is one of the most difficult reactions in organic chemistry. Results from past decade [6,7] and recent past [31] indicate that our catalyst is very good in this respect. Recent report on catalysis with copper(II) complexes of vinylphosphonic acid and 1,10-phenanthroline shows that only ~32% products are formed where main product is corresponding carboxylic acid [31a]. Formation of cyclohexanol and cyclohexanone is extremely low. Copper (II) complexes of functionalized 2,2':6',2''-terpyridines and 2,6-di(thiazol-2-yl)pyridine could be used as catalyst for cyclohexane oxidation in the presence of hydrogen peroxide and highest conversion achieved is ~23% [31b]. Three copper(II) complexes of pyromellitic acid and different aminoalcohols can catalyze cyclohexane oxidation and highest conversion is ~33% [31c]. Conversion for cyclopentane is also difficult as revealed from the small yield with Cu(II) complexes [31d].

4. Conclusions

We have been able to synthesize and characterize two dinuclear transition metal complexes with a Schiff-base ligand. One of them is copper containing complex, complex **1** and another with nickel, complex **2**. Complex **1** has been found to be active catalyst for the oxidation of cyclohexane, toluene and cyclopentane in the presence of hydrogen peroxide as the terminal oxidant. Corresponding alcohol and aldehyde have been produced as the major products. Conversion of the substrates is quite high in comparison to the results published by other groups in recent time. However, complex **2** is not able to convert these substrates under similar conditions. UV-vis spectral analysis shows that complex **1** could generate Cu-peroxo or Cu-hydroperoxo species in the presence of hydrogen peroxide whereas formation of such type of species with nickel complex is not evident from the UV-vis spectral studies. CV of complex **1** shows that two Cu(II) centers could be converted to Cu(III) center with transfer of one electron in each of two steps. Formation of higher oxidation state species of Ni is not indicated from its electrochemical studies. These analyses support that formation of Cu-peroxo as active species for the catalytic conversions. Possible mechanism indicates the involvement of Cu(III) species. Probably other metals also need higher oxidation states for this catalysis. As generation of Cu(III) center is feasible, not the higher oxidation state for nickel center evident from electrochemical studies under normal condition, the dinuclear copper complex can catalyze the oxidation of saturated hydrocarbons mimicking the activity of particulate methane monooxygenase while dinuclear nickel complex cannot.

Acknowledgements

AB wishes to thank CSIR, New Delhi for providing her senior research fellowship.

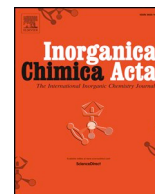
Appendix A. Supplementary data

Supplementary data to this article can be found online at <https://doi.org/10.1016/j.ica.2019.03.005>.

References

- (a) M.H. Sazinsky, S.J. Lippard, Methane Monooxygenase: Functionalizing Methane at Iron and Copper, in: P. Kroneck, Torres M. Sosa (Eds.), Sustaining Life on Planet Earth: Metalloenzymes Mastering Dioxigen and Other Chewy Gases. Metal Ions in Life Sciences, Springer, Cham, 2015; (b) A.E. Shilov, G.B. Shul'pin, Chem. Rev. 97 (1997) 2879; (c) A.A. Fokin, P.R. Schreiner, Chem. Rev. 102 (2002) 1551; (d) A. Sen, Acc. Chem. Res. 3 (1998) 550; (e) R.A. Periana, O. Mironov, D. Taube, G. Bhalla, C.J. Jones, Science 30 (2003) 814.
- (a) L. Que Jr., W.B. Tolman, Nature 455 (2008) 333; (b) J.C. Nesheim, J.D. Lipscomb, Biochemistry 35 (1996) 10240; (c) T. Punniyamurthy, S. Velusamy, J. Iqbal, Chem. Rev. 105 (2005) 2329.
- (a) A.S. Hakemian, A.C. Rosenzweig, Annu. Rev. Biochem. 76 (2007) 223; (b) M.O. Ross, A.C. Rosenzweig, J. Biol. Inorg. Chem. 22 (2017) 307; (c) S. Sirajuddin, A.C. Rosenzweig, Biochemistry 54 (2015) 2283; (d) C.E. Tinberg, S.J. Lippard, Acc. Chem. Res. 44 (2011) 280.
- (a) A.M. Kirillov, M.V. Kirillova, A.J.L. Pombeiro, Coord. Chem. Rev. 256 (2012) 2741; (b) M.M. Vinogradov, Y.N. Kozlov, A.N. Bilyachenko, D.S. Nesterov, L.S. Shul'pina, Y.V. Zubavichus, A.J.L. Pombeiro, M.M. Levitsky, A.I. Yalymov, G.B. Shul'pin, New J. Chem. 39 (2015) 187; (c) C.-C. Liu, D. Janmanchi, D.-R. Wen, J.-N. Oung, C.-Y. Mou, S.S.-F. Yu, S.I. Chan, ACS Sustain. Chem. Eng. 6 (2018) 5431.
- A.E. Shilov, G.B. Shul'pin, Activation and Catalytic Reactions of Saturated Hydrocarbons in the Presence of Metal Complexes, Kluwer Academic Publishers, Dordrecht, The Netherlands, 2000.
- (a) A.M. Kirillov, M.N. Kopylovich, M.V. Kirillova, M. Haukka, M.F.C.G. da Silva, A.J.L. Pombeiro, Angew. Chem. 117 (2005) 4419; (b) Y.Y. Karabach, A.M. Kirillov, M. Haukka, M.N. Kopylovich, A.J.L. Pombeiro, J. Inorg. Biochem. 102 (2008) 1190; (c) M.V. Kirillova, Y.N. Kozlov, L.S. Shul'pina, O.Y. Lyakin, A.M. Kirillov, E.P. Talsi, A.J.L. Pombeiro, G.B. Shul'pin, J. Catal. 268 (2009) 26; (d) K.R. Gruenwald, A.M. Kirillov, M. Haukka, J. Sanchizand, A.J.L. Pombeiro, Dalton Trans. (2009) 2109; (e) M. Sutradhar, E.C.B.A. Alegria, T.R. Barman, F. Scorzellotti, M.F.C.G. da Silva, A.J.L. Pombeiro, Mol. Catal. 439 (2017) 224; (f) E.A. Buvaylo, V.N. Kokozay, O. Yu Vassilyeva, B.W. Skelton, O.V. Nesterova, A.J.L. Pombeiro, Inorg. Chem. Commun. 78 (2017) 85.
- (a) A.A. Alshaheri, M.I.M. Tahir, M.B.A. Rahman, T.B.S.A. Ravooof, T.A. Saleh, Chem. Eng. J. 327 (2017) 423; (b) I. Garcia-Bosch, M.A. Siegler, Angew. Chem. 128 (2016) 13065; (c) A.N. Bilyachenko, A.N. Kulakova, M.M. Levitsky, A.A. Petrov, A.A. Korlyukov, L.S. Shul'pina, V.N. Khrestalev, P.V. Dorovatovskii, A.V. Vologzhanina, U.S. Tsareva, I.E. Golub, E.S. Gulyaeva, E.S. Shubina, G.B. Shul'pin, Inorg. Chem. 56 (2017) 4093; (d) A.N. Bilyachenko, V.N. Khrestalev, Y.V. Zubavichus, L.S. Shul'pina, A.N. Kulakova, X. Bantreil, F. Lamaty, M.M. Levitsky, E.I. Gutsul, E.S. Shubina, G.B. Shul'pin, Inorg. Chem. 57 (2018) 528; (e) A.N. Bilyachenko, M.M. Levitsky, A.A. Korlyukov, V.N. Khrestalev, Y.V. Zubavichus, L.S. Shul'pina, E.S. Shubina, A.V. Vologzhanina, G.B. Shul'pin, Eur. J. Inorg. Chem. (2018) 2505; (f) P. Roy, K. Dhara, M. Manassero, P. Banerjee, Eur. J. Inorg. Chem. (2008) 4404; (g) S. Thakurta, P. Roy, R.J. Butcher, M.S.E. Fallah, J. Tercero, E. Garribba, S. Mitra, Eur. J. Inorg. Chem. (2009) 4385; (h) S. Thakurta, P. Roy, G. Rosair, C.J. Gómez-García, E. Garribba, S. Mitra, Polyhedron 28 (2009) 695; (i) K.C. Gupta, A.K. Sutar, Coord. Chem. Rev. 252 (2008) 1420; (j) K.C. Gupta, A.K. Sutar, C.-C. Lin, Coord. Chem. Rev. 253 (2009) 1926; (k) A. Bhattacharjee, S. Halder, K. Ghosh, C. Rizzoli, P. Roy, New J. Chem. 41 (2017) 5696; (l) S. Halder, S. Dey, C. Rizzoli, P. Roy, Polyhedron 60 (2014) 85; (m) M. Nandi, P. Roy, H. Uyama, A. Bhaumik, Dalton Trans. 40 (2011) 12510; (n) P. Roy, M. Nandi, M. Manassero, M. Riccò, M. Mazzani, A. Bhaumik, P. Banerjee, Dalton Trans. (2009) 9543.
- (a) A. Panja, Polyhedron 79 (2014) 258; (b) A. Panja, M. Shyamal, A. Saha, T.K. Mandal, Dalton Trans. 43 (2014) 5443; (c) A. Panja, Dalton Trans. 43 (2014) 7760; (d) K. Ghosh, K. Harms, S. Chattopadhyay, Polyhedron 123 (2017) 162; (e) S.K. Dey, A. Mukherjee, Coord. Chem. Rev. 310 (2016) 80.
- (a) C. Kordulis, K. Bourikas, M. Gousi, E. Kordouli, A. Lycourghiotis, Appl. Catal. B 181 (2016) 156; (b) S. Chakraborty, P. Bhattacharya, H. Dai, H. Guan, Acc. Chem. Res. 48 (2015) 1995; (c) X. Lu, B. Xiao, Z. Zhang, T. Gong, W. Su, J. Yi, Y. Fu, L. Liu, Nat. Commun. 7 (2016) 11129; (d) J. Chakraborty, M. Nandi, H. Mayer-Figge, W.S. Sheldrick, L. Sorace, A. Bhaumik, P. Banerjee, Eur. J. Inorg. Chem. (2007) 5005.
- (a) H.-Y. Lin, P.-Y. Cheng, C.-F. Wan, A.-T. Wu, Analyst 137 (2012) 4415; (b) Yu.M. Chumakov, V.L. Tsapkov, P.A. Petrenko, L.G. Popovskii, Yu.A. Simonov, G. Bocelli, B.Ya. Antosyak, A.O. Paraschivescu, A.P. Gulea, Russian J. Coord. Chem. 35 (2009) 504; (c) K.K. Rajak, S. Mondal, S.P. Rath, Polyhedron 19 (2000) 931.
- Bruker, APEX2, SAINT and SADABS, Bruker AXS Inc., Madison, Wisconsin, USA,

- 2008.
- [12] G.M. Sheldrick, *Acta Cryst.* A71 (2015) 3.
- [13] G.M. Sheldrick, *Acta Cryst.* C71 (2015) 3.
- [14] M.J. Frisch, G.W. Trucks, H.B. Schlegel, G.E. Scuseria, M.A. Robb, J.R. Cheeseman, G. Scalmani, V. Barone, B. Mennucci, G.A. Petersson, H. Nakatsuji, M. Caricato, X. Li, H.P. Hratchian, A.F. Izmaylov, J. Bloino, G. Zheng, J.L. Sonnenberg, M. Hada, M. Ehara, K. Toyota, R. Fukuda, J. Hasegawa, M. Ishida, T. Nakajima, Y. Honda, O. Kitao, H. Nakai, T. Vreven, J.A. Montgomery Jr., J.E. Peralta, F. Ogliaro, M. Bearpark, J.J. Heyd, E. Brothers, K.N. Kudin, V.N. Staroverov, R. Kobayashi, J. Normand, K. Raghavachari, A. Rendell, J.C. Burant, S.S. Iyengar, J. Tomasi, M. Cossi, N. Rega, J.M. Millam, M. Klene, J.E. Knox, J.B. Cross, V. Bakken, C. Adamo, J. Jaramillo, R. Gomperts, R.E. Stratmann, O. Yazyev, A.J. Austin, R. Cammi, C. Pomelli, J.W. Ochterski, R.L. Martin, K. Morokuma, V.G. Zakrzewski, G.A. Voth, P. Salvador, J.J. Dannenberg, S. Dapprich, A.D. Daniels, Ö. Farkas, J.B. Foresman, J.V. Ortiz, J. Cioslowski, D.J. Fox, GAUSSIAN, 09, Revision D.01, Gaussian, Inc, Wallingford, CT, 2009.
- [15] A.D. Becke, *J. Chem. Phys.* 98 (1993) 5648.
- [16] P.J. Hay, W.R. Wadt, *J. Chem. Phys.* 82 (1985) 299.
- [17] S. Miertsch, E. Scrocco, J. Tomasi, *Chem. Phys.* 55 (1981) 117.
- [18] V. Barone, M. Cossi, J. Tomasi, *J. Comput. Chem.* 19 (1998) 404.
- [19] A.W. Addison, T.N. Rao, J. Reedijk, J. Vanrijn, G.C. Verschoor, *J. Chem. Soc. Dalton Trans.* (1984) 1349.
- [20] (a) R.L. Forman, A.J. Gale, C.P. Landee, M.M. Turnbull, J.L. Wikaira, *Polyhedron* 89 (2015) 76;
(b) A. Jaffe, Y. Lin, W.L. Mao, H.I. Karunadasa, *J. Am. Chem. Soc.* 137 (2015) 1673;
(c) M. Julve, A. Gleizes, L.M. Chamoreau, E. Ruiz, M. Verdaguier, *Eur. J. Inorg. Chem.* (2018) 509;
(d) F.F. Awwadi, M.M. Turnbull, M.I. Alwahsh, S.F. Haddad, *New J. Chem.* 42 (2018) 10642.
- [21] (a) S. Halder, J. Mondal, J. Ortega-Castro, A. Frontera, P. Roy, *Dalton Trans.* 46 (2017) 1943;
(b) P. Ghorai, A. Chakraborty, A. Panja, T.K. Mondal, A. Saha, *RSC Adv.* 6 (2016) 36020;
(c) S. Roy, A. Bhattacharyya, S. Purkait, A. Bauzá, A. Frontera, S. Chattopadhyay, *Dalton Trans.* 45 (2016) 15048.
- [22] (a) *Comprehensive Coordination Chemistry*, ed. B. J. Hathaway, G. Wilkinson, R. D. Gillard, J. A. McCleverty, Pergamon Press, Oxford, England 5 (1987).
(b) F.A. Mautner, C.N. Landry, A.A. Gallo, S.S. Massoud, *J. Mol. Struct.* 837 (2007) 72;
(c) F.A. Mautner, J.H. Albering, R. Vicente, F.R. Louka, A. Gallo, S.S. Massoud, *Inorg. Chim. Acta* 365 (2011) 290;
(d) S.S. Massoud, L.L. Quan, K. Gatterer, J.H. Albering, R.C. Fischer, F.A. Mautner, *Polyhedron* 31 (2012) 601
- [23] (a) Z. Wu, Z. Zhang, L. Liu, *Electrochim. Acta* 42 (1997) 2719;
(b) E. Chiyindiko, J. Conradie, *J. Electroanal. Chem.* 837 (2019) 76;
(c) E. Franco, E. López-Torres, M.A. Mendiola, M.T. Sevilla, *Polyhedron* 19 (2000) 441;
(d) J.P. Naskar, B. Guhathakurta, L. Lu, M. Zhu, *Polyhedron* 43 (2012) 89.
- [24] (a) J. Losada, I. del Peso, L. Beyer, *Inorg. Chim. Acta* 321 (2001) 107;
(b) F. Bedioui, E. Labbe, S. Gutierrez-Granados, J. Devynck, *J. Electroanal. Chem.* 301 (1991) 267;
(c) J. Losada, I. del Peso, L. Beyer, *J. Electroanal. Chem.* 447 (1998) 147.
- [25] (a) G. Saha, K.K. Sarkar, T.K. Mondal, C. Sinha, *Inorg. Chim. Acta* 387 (2012) 240;
(b) M. Sarigul, S.E. Kariper, P. Deveci, H. Atabey, D. Karakas, M. Kurtoglu, *J. Mol. Struct.* 1149 (2017) 520;
(c) K. Ouari, S. Bendia, J. Weiss, C. Bailly, *Spectrochim. Acta A* 135 (2015) 624;
(d) G.B. Bagihalli, P.G. Avaji, S.A. Patil, P.S. Badami, *Eur. J. Med Chem* 43 (2008) 2639;
(e) A.H. Kianfar, L. Keramat, M. Dostani, M. Shamsipur, M. Roushani, F. Nikpour, *Spectrochim. Acta Part A* 77 (2010) 424;
(f) A. Anthonysamy, S. Balasubramanian, *Inorg. Chem. Comm.* 8 (2005) 908–911.
- [26] (a) T.F.S. Silva, G.S. Mishra, M.F.G. da Silva, R. Wanke, L.M.D.R.S. Martins, A.J.L. Pombeiro, *Dalton Trans.* (2009) 9207;
(b) M. Nandi, P. Roy, *Indian J. Chem.* 52A (2013) 1263.
- [27] (a) G.B. Shul'pin, *J. Mol. Catal. A* 189 (2002) 39;
(b) G.B. Shul'pin, Y.N. Kozlov, L.S. Shul'pina, A.R. Kudinov, D. Mandell, *Inorg. Chem.* 48 (2009) 10480;
(c) G.B. Shul'pina, Y.N. Kozlov, L.S. Shul'pina, P.V. Petrovskiy, *Appl. Organometal. Chem.* 24 (2010) 464.
- [28] (a) T.F.S. Silva, E.C.B. Alegria, L.R. Martins, A.J.L. Pombeiro, *Adv. Synth. Catal.* 350 (2008) 706;
(b) M. Costas, M.P. Mehn, M.P. Jensen, L. Que Jr., *Chem. Rev.* 104 (2004) 939;
(c) M. Costas, K. Chen, L. Que Jr., *Coord. Chem. Rev.* 200–202 (2000) 517;
(d) T. Hogan, A. Sen, *J. Am. Chem. Soc.* 119 (1997) 2642.
- [29] (a) G.B. Shul'pin, *Transition Metals for Organic Synthesis*, 2nd edn, Wiley-VCH, New York, 2004, p. 215;
(b) G.B. Shul'pin, H. Stoeckli-Evans, D. Mandelli, Y.N. Kozlov, A.T. Vallina, C.B. Woitiski, R.S. Jimenez, W.A. Carvalho, *J. Mol. Catal. A* 219 (2004) 255.
- [30] (a) J. Reim, R. Werner, W. Haase, B. Krebs, *Chem. Eur. J.* 4 (1998) 289;
(b) P. Roy, K. Dhara, M. Manassero, P. Banerjee, *Inorg. Chem. Commun.* 11 (2008) 265;
(c) S. Halder, S. Dey, C. Rizzoli, P. Roy, *Polyhedron* 78 (2014) 85.
- [31] (a) E. Armakola, R.M.P. Colodrero, M. Bazaga-García, I.R. Salcedo, D. Choquesillo-Lazarte, A. Cabeza, M.V. Kirillova, A.M. Kirillov, K.D. Demadis, *Inorg. Chem.* 57 (2018) 10656;
(b) K. Czerwińska, B. Machura, S. Kula, S. Krompiec, K. Erfurt, C. Roma-Rodrigues, A.R. Fernandes, L.S. Shul'pina, N.S. Ikonnikove, G.B. Shul'pin, *Dalton Trans.* 46 (2017) 9591;
(c) T.A. Fernandes, C.I.M. Santos, V. André, J. Klak, M.V. Kirillova, A.M. Kirillov, *Inorg. Chem.* 55 (2016) 125;
(d) S.S.P. Dias, M.V. Kirillova, V. André, J. Klak, A.M. Kirillov, *Inorg. Chem.* 54 (2015) 5204.



Research paper

Intercalative DNA binding, protein binding, antibacterial activities and cytotoxicity studies of a mononuclear copper(II) complex

Aradhita Bhattacharjee^a, Subhadeep Das^b, Biswadip Das^b, Partha Roy^{a,*}

^a Department of Chemistry, Jadavpur University, Kolkata 700 032, India

^b Department of Life Science & Bio-technology, Jadavpur University, Kolkata 700 032, India



ARTICLE INFO

Keywords:

Copper complex
DNA cleavage
HSA binding
Antibacterial activity
Cell study

ABSTRACT

A mononuclear copper(II) complex, [CuL₂] (Complex 1) where HL = 4-chloro-2-((cyclohexylmethylimino)methyl)phenol), has been synthesized and characterized by standard methods including single crystal X-ray diffraction analysis. UV–vis spectral studies have been carried out to establish the intercalative binding affinity of complex 1 with DNA and the corresponding intrinsic binding constant has been determined to be $1.68 \times 10^5 \text{ M}^{-1}$. Several other studies such as competitive binding experiment, fluorescence quenching spectra, CV and CD also support intercalative binding ability of complex 1. Agarose gel electrophoresis technique has been employed to study the DNA cleavage. Interaction of complex 1 with a protein, human serum albumin (HSA) has been analyzed by UV–vis and fluorescence quenching spectra. The intrinsic binding constant (K) of complex 1 for HSA has been determined to be $1.91 \times 10^4 \text{ M}^{-1}$. HSA shows strong fluorescence at 344 nm (λ_{ex} : 295 nm). But the intensity decreases in the presence of complex 1 signifying binding of 1 with HSA. Quenching of fluorescence occurs by fluorescence energy transfer mechanism. FT-IR, 3D fluorescence spectral and CD analyses also show the considerable interaction between HSA and 1. Remarkable degradation of HSA has been observed in the presence of hydrogen peroxide when it is incubated with complex 1. On the other hand, complex 1 shows excellent antibacterial activity towards both gram positive and gram negative bacteria. To observe nuclear changes, HeLa cells have been treated with complex 1 and it shows apoptosis of the cell as predicted by the morphological changes in the cell nucleus.

1. Introduction

After the first report of antitumor activity of some platinum compounds [1] such as cisplatin by Rosenberg and coworkers, significant attention has been paid to develop and understand the role of metal-based anticancer drugs. Cisplatin and analogous platinum-based drugs suffer from severe associated toxic effects such as emetogenesis, neurotoxicity, myelotoxicity and nephrotoxicity [2]. Thus, there is a need for new compounds having antiproliferative properties and therapeutic solutions. Non-platinum complexes have then been emerged as potential anticancer agents as an alternative [3]. Different metal complexes are potential candidate as therapeutic agents in medicinal research as these compounds can efficiently interact with the proteins and DNA under physiological conditions. During last few decades, tremendous effort has been provided to grow a number of different transition metal complexes including that of copper(II) as the anticancer drugs [4]. A number of copper(II) complexes have been used as tools for mediation of strand scission of duplex DNA and as probes of DNA structure in

solution phase [5–8]. Several metal including copper complexes have shown to hydrolyze phosphate ester [9] as well as RNA with varying efficiencies [10,11]. On the other hand, Cu(II/I) complexes of synthetic and naturally occurring ligands act as nuclease mimics and a few copper(II) complexes have shown to be capable of mediating non-random double-strand cleavage of plasmid DNA [12].

Schiff base complexes of transition metal ions are one such important class of compounds in medicinal and pharmaceutical field. They show biological applications including antibacterial [13,14], antifungal [14] and antitumor activity [15]. Diamino tetradentate Schiff-bases and their complexes have been used as the model for understanding the structures of biomolecules and biological processes [16,17].

DNA binding is the critical step for DNA activity. To design effective chemotherapeutic agents and better anticancer drugs, it is needed to explore the interaction of metal complexes with DNA. Recently, there has been growing interest in studies related to the interaction of transition metal ions with nucleic acid as mentioned earlier because of their relevance in the development of tools for biotechnology and medicine

* Corresponding author.

E-mail addresses: partha.roy@jadavpuruniversity.in, proy@chemistry.jdvu.ac.in (P. Roy).

<https://doi.org/10.1016/j.ica.2020.119961>

Received 24 May 2020; Received in revised form 13 August 2020; Accepted 18 August 2020

Available online 21 August 2020

0020-1693/ © 2020 Elsevier B.V. All rights reserved.

[18]. These studies are important to understand the toxicity of drugs containing metal ions as well [19]. Moreover, molecular design of synthetic metalloproteases that cleave protein at a specific site and act as multifunctional biochemical agents is suitable for understanding the structure–activity correlations of proteins [20]. Protein degradation plays an important role in many cellular functions such as (i) removal of misfolded and damaged proteins from the cells to avoid toxicity and, (ii) to maintain the cellular concentration of regulatory proteins at optimal levels [21].

Synthetic proteases are also vital in the emerging chemistry of anti-metastasis agents to control tumor malignancy [22]. The specific delivery of a drug to target cells may be done by the use of targeting groups or by tuning the chemical and physical characteristics of the drug or drug carrier such as hydrophobicity and molecular size [23]. Among various protein carriers such as liposomes, dendrimers, protein biomolecules, poly(ethylene glycol)-polymers and nanoparticles, human serum albumin (HSA) has been regarded as the most versatile [24]. It is known to be gathered in tumor cell than in normal cell. Now it is believed that it can act as the carrier conjugate for several anticancer drugs [25]. It is an antioxidant and shows radical scavenging ability. Another key role of HSA is to sustain the blood pressure. HSA does not show toxicity and immunogenicity. Thus, it has potential to be an ideal carrier for drug delivery. It is already known that it is one of the most important multifunctional transport proteins and its crucial role in the transportation and deposition of various species in blood [26]. Different factors such as drug distribution, its concentration in unbound state, its metabolism, etc. are dependent on nature of interaction between drug and the protein. HSA controls distribution of drug as the drug reaches its target after binding with the HSA protein [27]. Thus, study on binding of the drug with proteins like HSA becomes extremely important because this can enlighten on concentration of unbound drug, its distribution and elimination.

The metal complexes often show excellent antibacterial properties, perhaps, by binding to bacterial DNA and killing them in the process. Apoptosis is a crucial process which is closely related to a variety of diseases. Apoptosis induced by copper complexes were studied extensively. Copper is redox active center and due to this property, reactive oxygen species (ROS) is formed. ROS can induce modification in the cellular components and can hinder redox processes of the cell as well. All these along with ROS related other intracellular cascade reactions can result apoptosis. A clear understanding of this can help in the designing of copper based antitumor drugs [28,29].

In this respect, we report here the synthesis, characterization, and DNA cleavage, HSA binding and antibacterial properties of a copper(II) complex, $[\text{CuL}_2]$ (Complex 1) where HL = 4-chloro-2-((cyclohexylmethylimino)methyl)phenol (Scheme 1). Complex 1 has been successfully applied in cleaving DNA as well as binding to HSA. These interactions have been studied by various biophysical experiments and biochemical assays as well.

2. Experimental

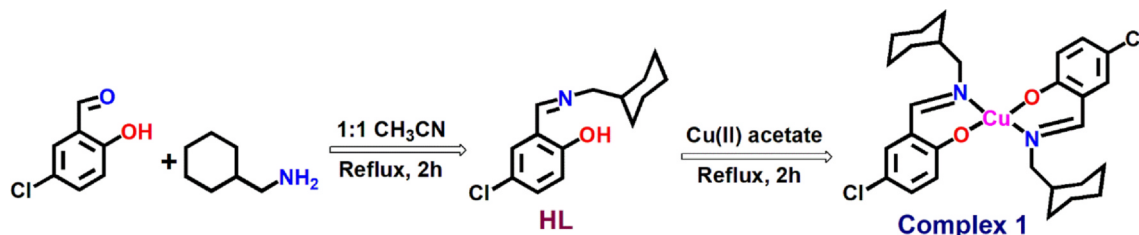
2.1. Materials and methods

5-Chloro-2-hydroxybenzaldehyde, 1-cyclohexylmethanamine and copper(II) acetate monohydrate were purchased from Sigma Aldrich and used without further purification. Other chemicals were purchased from commercial sources and used as received. 4-chloro-2-((cyclohexylmethylimino)methyl)phenol (HL) was synthesized following a published procedure [30]. Solvents were purchased from commercial sources and for synthesis purpose they were used without further purification while a purified and dried version was used for spectroscopic measurements [31]. Elemental analysis was carried out on a 2400 Series-II CHN analyzer, Perkin Elmer, USA. FT-IR spectra were recorded on a Perkin Elmer spectrometer (Spectrum Two) with the solid samples or sample solutions using the attenuated total reflectance (ATR) technique. The UV–vis spectral analysis was done in Agilent 8453 diode array spectrophotometer. The ESI-MS spectra were recorded on Qtof Micro YA263 mass spectrometer. Single crystal X ray diffraction was done on a Bruker: D8 VENTURE. Emission spectra were recorded using a Horiba Fluoromax-4C spectrofluorometer. The cyclic voltametry instrument used was METROHM AUTOLAB PGSTAT101. A glassy carbon working electrode and a platinum wire auxiliary electrode and saturated Ag/AgCl reference electrode were employed in a standard three-electrode configuration. KCl was used as supporting electrolyte in the DMSO/buffer system as the system was mostly aqueous in the form of Tris/NaCl buffer and the scan rate was 50 mV s^{-1} under argon atmosphere. CD spectra were recorded by using a quartz cuvette of 10 mm pathlength in a JASCO J-815 CD spectropolarimeter. The DNA cleavage studies were done by resolving the DNA on 1% agarose gel electrophoresis in Tris Acetyl EDTA buffer at 80 V. The HSA protein was run on 10% SDS polyacrylamide page gel. Cell lines used for the experiment were HeLa (human cervical cancer cell line). Cells were grown in 10% fetal bovine serum (FBS; Gibco, Grand Island, NY, USA)/Dulbecco's modified Eagle's medium (DMEM; Himedia, Mumbai, India) media at 37°C and 5% CO_2 .

2.2. Synthesis of $[\text{CuL}_2]$ (1)

A solution of copper(II) acetate monohydrate (0.5 mmol, 0.100 g) in acetonitrile (5 mL) was added dropwise to an acetonitrile solution (5 mL) of HL (1.0 mmol, 0.252 g) under stirring condition. The mixture turned to yellowish green in color. The mixture was stirred for another 30 min. The color of the solution changed to greenish. The resulting solution was then refluxed for 2 h and the solution became green. The mixture was finally cooled to room temperature and filtered to remove any undissolved or suspended materials. The filtrate was kept at ambient temperature for slow evaporation of the solvent. Green single crystals suitable for X-ray diffraction study were produced within few days.

Data for 1: yield (78%); C, H, N analysis: anal. calc. for $\text{C}_{28}\text{H}_{34}\text{Cl}_2\text{CuN}_2\text{O}_2$: C, 59.52; H, 6.07; N, 4.96; found: C, 59.54; H, 5.92; N, 4.78%.



Scheme 1. Synthesis of complex 1.

Table 1
Crystal data, data collection and structure refinement of complexes.

Compound	Complex 1
Formula	C ₂₈ H ₃₄ Cl ₂ CuN ₂ O ₂
Formula weight	565.01
T (K)	293
Color	clear light brown
Crystal system	triclinic
Space group	P-1
a (Å)	6.3371(2)
b (Å)	10.0817(4)
c (Å)	10.9103(4)
α (°)	85.6440(10)
β (°)	79.9620(10)
γ (°)	78.1860(10)
V (Å ³)	671.25(4)
Z	1
Crystal dimensions (mm)	0.3 × 0.21 × 0.11
Minimum and maximum transmission factors	0.769–0.892
F(0 0 0)	295
D _c (g cm ⁻³)	1.398
λ (Mo Kα) (Å)	1.040
θ Range (°)	2.79–27.39
Reflection collected/unique/observed	12185, 2945, 2775
Absorption correction	multi-scan
R _{int}	0.0538
Final R ₁ index [I > 2σ(I)]	0.0578
Final wR ₂ index (all reflections)	0.1188
Goodness-of-fit	1.261

2.3. X-ray data collection and structure determination

Details of the data collection and refinement parameters for complex 1 are summarized in Table 1. Single crystal data collections were performed with an automated Bruker D8 VENTURE diffractometer using graphite monochromatized Mo Kα radiation. The spots were measured using 10 s counting time. Unit cell parameters were determined from least-squares refinement of setting angles with θ in the range 2.79 ≤ θ ≤ 27.39°. Data were processed using the Bruker SAINT package [32]. Absorption corrections based on multi scans using the SADABS software were applied to all intensity data. The structures were solved and refined by full-matrix least-squares techniques on F² using the SHELXS-2016/6 program [33,34]. The absorption corrections were done by the multi-scan technique. All data were corrected for Lorentz and polarization effects, and the non-hydrogen atoms were refined anisotropically. Hydrogen atoms were generated using SHELXL-2016/6 and their positions calculated based on the riding mode with thermal parameters equal to 1.2 times that of the associated C atoms, and participated in the calculation of the final R-indices.

2.4. DNA binding and cleavage activities

Calf thymus (CT)-DNA was purchased from Sigma Aldrich and the supercoiled FAM134BGFP plasmid DNA was obtained from a biotechnology lab. The stock solution of CT-DNA was prepared in 5 mM Tris-HCl/50 mM NaCl buffer at pH 7.2, which gave a ratio of UV absorbance at 260 nm and 280 nm (A₂₆₀/A₂₈₀) of ca. 1.8–1.9, indicating that the DNA was sufficiently free of protein [35]. The concentration was determined by UV absorbance at 260 nm (ε = 6600 M⁻¹cm⁻¹) and the plasmid DNA was used in the wet lab cleavage studies.

2.5. HSA binding studies

Human serum albumin (HSA) was purchased from Sigma Aldrich. Human serum albumin of 1.0 × 10⁻⁴ M was prepared by dissolving protein in Tris-HCl buffer solution at pH 7.2 [36]. The protein concentration was determined spectrophotometrically using an extinction coefficient of 35,219 M⁻¹cm⁻¹ at 280 nm.

2.6. Antibacterial studies

Overnight grown cultures of *E. coli* and *S. aureus* were incubated in Luria Bertani (LB) broth. Approximately, 1 × 10⁸ cells of each bacterial strain were incubated in test tubes containing 2.0 mL of LB media and to it different concentrations of the complex was added. The tubes were incubated at 37 °C for 16–18 h. The growth observed were cells which was plated on LB media following which the plates were incubated at 37 °C again for 16–18 h and the next day colonies were counted.

2.7. Cell biological studies

Cell lines used for the experiment were HeLa (human cervical cancer cell line). Cells were grown in 10% fetal bovine serum (FBS; Gibco, Grand Island, NY, USA)/Dulbecco's modified Eagle's medium (DMEM; Himedia, Mumbai, India) media at 37 °C and 5% CO₂. The HeLa cells were seeded in 35 mm plates. The cells were treated with different concentrations of the complex and incubated for different time intervals. The cells were fixed with 4% formalin in PBS buffer. They were then blocked with 0.1% Triton X in PBS. Then, they were stained with DAPI and mounted on the slides.

3. Results and discussion

3.1. Synthesis of complex 1 and its characterization

Complex 1 has been synthesized following route given in Scheme 1. First, HL has been prepared by the condensation between cyclohexylmethylamine and 5-chlorosalicylaldehyde in 1:1 ratio in acetonitrile following a published method [30]. The reaction between HL and copper(II) acetate monohydrate yields the complex, [CuL₂]. HL has been deprotonated to bind to the Cu(II) center without adding any external agent. Probably anion of copper salt helps in the deprotonation process.

ESI-MS spectrum of complex 1 confirms the formation of the complex (Fig. s1). The m/z peak at 565.05 may be attributed to the presence of [ML₂] species. Another peak at 313.96 may assigned to [ML]⁺ species which could be fragmented from the original molecule by losing a ligand. FT-IR spectrum of complex 1 has been recorded with samples by ATR technique (Fig. s2). The strong peaks at 2848 cm⁻¹ confirms the presence of methylene moieties. The sharp peak at 1633 cm⁻¹ shows the presence of C=N bond which justifies formation of the Schiff base ligand and retention of it in the complex [37]. A band at 1170 cm⁻¹ indicates the presence of C–O bond i.e. carbon being attached to hydroxyl group. Almost strong band at 718 cm⁻¹ signifies C–Cl bond in the ligand. Medium intensity at 560–570 cm⁻¹ indicates that the ligand is coordinated to the metal center.

Magnetic properties of complex 1 have been measured and analyzed with powdered samples at 298 K. The expected value of magnetic moment for Cu(II) system is 1.73 BM. The experimental value of χ_M has been determined to be 1.58 BM. This value is almost close to the theoretical value of 1.73 BM indicating the presence of one copper atom in the complex.

3.2. Crystal structure of complex 1

The complex 1 crystallizes in the P-1 space group from acetonitrile. A perspective view of the complex is given in Fig. 1. Selected bond angles and bond lengths are listed in Table s1. Complex 1 consists of two deprotonated ligands (4-chloro-2-((cyclohexylmethylimino)methyl)phenoxide) and one copper atom. Copper atom is in a tetra-coordinated environment. Cu1 is coordinated to two phenolic oxygen atoms (O1), two nitrogen atoms (N1) from each of the ligand. It is almost a perfect square planar molecule. Both the *trans* angles O1-Cu1-O1 and N1-Cu1-N1 are 180° and the O1-Cu1-N1 angle is 88° which is very close to the ideal 90°. The Cu–O and Cu–N bond lengths are in good

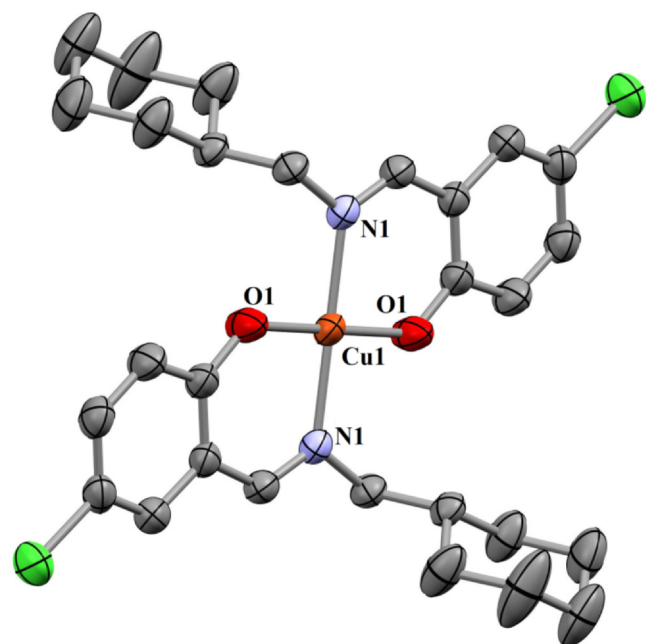


Fig. 1. A perspective view of complex 1 with partial atom numbering scheme. Hydrogen atoms are omitted for clarity.

agreement with the literature values [38,39].

3.3. UV-vis spectral studies

The electronic spectrum of complex 1 has been recorded in acetonitrile at room temperature. UV-vis spectrum of complex 1 is given in Fig. s3. It could be seen from the figure that it shows a broad band at 615 nm (ϵ : $3010 \text{ Lmol}^{-1}\text{cm}^{-1}$), which may be attributed to the $d-d$ -transition. Two strong peaks are observed at 372 and 300 nm, with molar extinction coefficients of $9800 \text{ Lmol}^{-1}\text{cm}^{-1}$ and $9500 \text{ Lmol}^{-1}\text{cm}^{-1}$, respectively. These peaks may be attributed to $\text{PhO} \rightarrow \text{Cu(II)}$, $\text{N(amino)} \rightarrow \text{Cu(II)}$ (LMCT) transfer and intraligand charge transfer [38].

3.4. Electrochemical studies

The electrochemical behavior of the complex has been investigated using cyclic voltammetry. Electrochemical studies were carried out in DMF solution by cyclic voltammetry at room temperature with TBAB (tetrabutylammonium bromide) as supporting electrolyte under argon atmosphere (Fig. 2). The negative scan shows that the Cu(II) center gets reduced to a Cu(I) species (Fig. 2a) [40]. The graph shows an I_{cathodic} peak indicating a reduction of $\text{Cu(II)} \rightarrow \text{Cu(I)}$ which is getting oxidized back $\text{Cu(I)} \leftarrow \text{Cu(II)}$ as indicated by I_{anodic} value. Thus, $I_{\text{anodic}}/I_{\text{cathodic}}$ ratio is nearly 1 which signifies a quasireversible reduction at a mononuclear copper center. ΔE_p is approximately 0.07 V indicating a one electron change i.e. $\text{Cu(II)} \rightarrow \text{Cu(I)}$ [41]. The scan in the positive potential region shows an irreversible oxidation of the ligand at high potentials (~ 1.2 V) showing that the ligand is oxidatively robust (Fig. 2b) [42].

3.5. DNA binding studies

3.5.1. UV-visible spectral studies

Absorption spectra of complex 1 have been recorded in DMSO buffer in the presence of different concentrations of DNA. It has been shown in Fig. 3. The absorption spectrum of the complex displays a highly intense interligand $\pi \rightarrow \pi^*$ absorption, that is characteristic for this complex, at 380 nm and the higher energy band at 305 nm may be

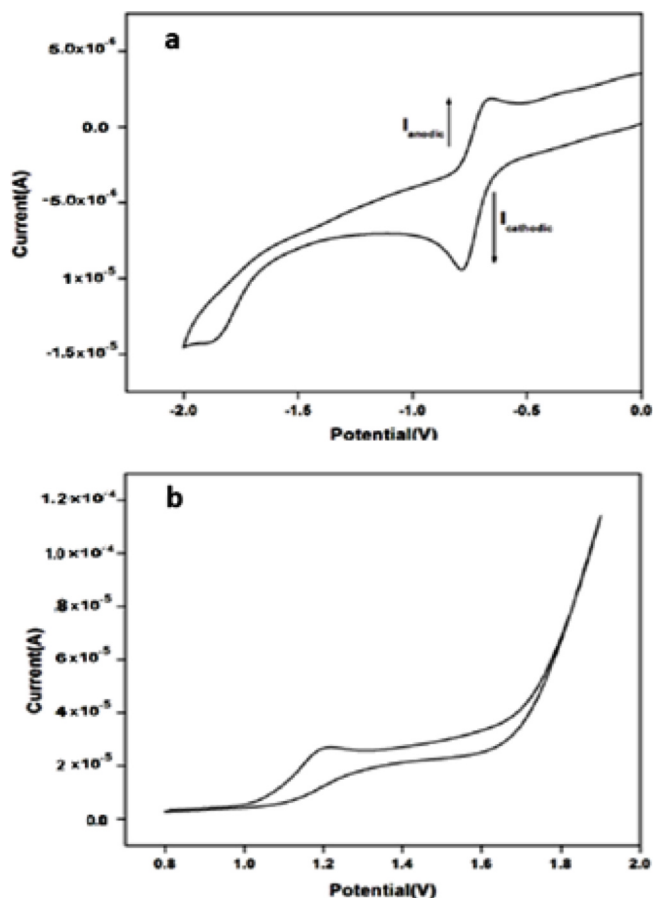


Fig. 2. Cyclic voltammetric plot of complex 1. (2a) scan in negative potential region showing reduction of Cu(II) to Cu(I) species and (2b) scan in positive potential region showing ligand oxidation.

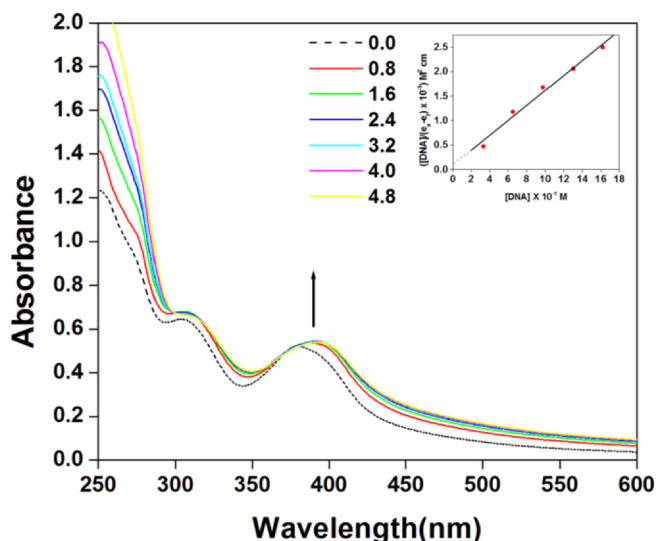


Fig. 3. Absorption spectra of complex 1 in absence (---) and in the presence (—) of increasing concentration of CT-DNA. $[\text{Complex 1}] = 4 \times 10^{-5} \text{ M}$. The upside arrow shows the absorbance changes upon increasing the DNA concentration. Inset: linear plot for the calculation of the intrinsic DNA binding constant (K_b).

due to some other charge transfer transitions. In the presence of fixed metal complex concentration and increasing concentrations of CT-DNA, ($3.3\text{--}22.5 \times 10^{-5} \text{ M}$), ratio $[\text{DNA}]/[\text{Complex 1}] = (0.0, 0.80, 1.6, 2.4,$

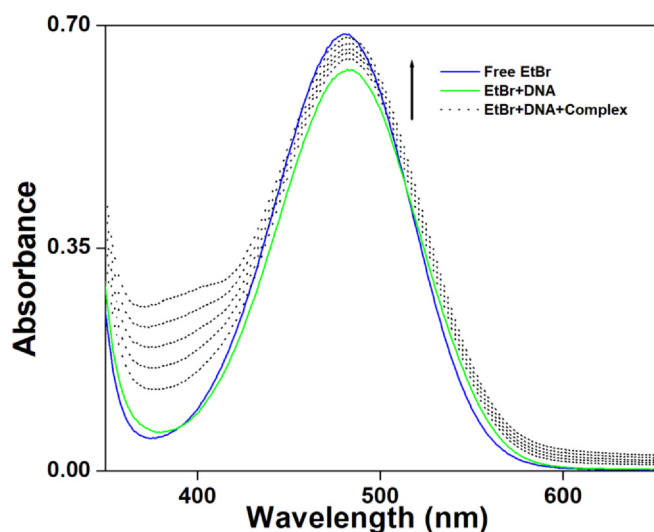


Fig. 4. Absorption spectra of free EB and EB bound to CT-DNA in the absence and presence of increasing amount of complex 1. $[EB] = [DNA] = 13.3 \times 10^{-5} \text{ M}$, $[Complex 1] = 0-10 \times 10^{-6} \text{ M}$. The upside arrow shows the absorbance changes upon increasing the complex concentration.

3.2, 4.0, 4.8), a marked hyperchromism is observed with a strong red shift of 18 nm [43] suggesting the covalent binding. The intrinsic binding constant, K_b , of complex 1 with CT DNA has been measured from Wolfe–Shimer Equation [44]. Through a plot of $[DNA]/(\epsilon_a - \epsilon_f)$ vs. $[DNA]$, where $[DNA]$ denotes the concentration of DNA, and ϵ_a , ϵ_f and ϵ_b represent the apparent extinction coefficient ($A_{obs}/[M]$), the extinction coefficient for only complex (M), and the extinction coefficient for the metal complex (M) when it is in fully bound form, respectively. In plots of $[DNA]/(\epsilon_a - \epsilon_f)$ vs. $[DNA]$, K_b is determined from the ratio of slope to intercept [44] of $[DNA]/(\epsilon_a - \epsilon_f) = [DNA]/(\epsilon_b - \epsilon_f) + 1/K_b (\epsilon_a - \epsilon_f)$.

K_b has been found to be $1.68 \times 10^5 \text{ M}^{-1}$ which suggests a moderate DNA intercalative binding constant value for complex 1.

3.5.2. Competitive binding assay

To ascertain the intercalative binding nature of complex 1 with DNA, a competitive binding experiment has been carried out to check binding ability of the complex with DNA in the presence of ethidium bromide (EB). EB is well known as an indicator of intercalation. Competitive binding assay has been measured by recording absorption intensity in UV–vis spectroscopy (Fig. 4). Initially, the absorbance of free ethidium bromide is measured and then DNA is added to it. The concentrations of both EB and DNA have been kept at $13.3 \times 10^{-5} \text{ M}$. As seen in the figure, absorbance of EB at 479 nm decreases and the peak shifts to 484 nm after addition of DNA, which indicates the characteristic of intercalation of ethidium bromide into the DNA base pairs. With the gradual addition of complex 1 ($0-10 \times 10^{-6} \text{ M}$) to the EB-DNA system, there is blue shift of the absorption peak to the original position and the absorbance is continuously decreased. This indicates that complex 1 is able to release ethidium bromide from EB-DNA system [45].

3.5.3. Fluorescence quenching spectroscopy

Ethidium bromide is well known as a classical intercalator. It produces considerable fluorescence intensity when it is allowed to intercalate in the base pairs of DNA. Small molecules can replace EB from the hydrophobic environment of the DNA double helix and then even leads to significant quenching of fluorescence of EB by the polar solvents such as water [46]. The change in fluorescence intensity of EB bound DNA in absence and in the presence of complex 1 has been given

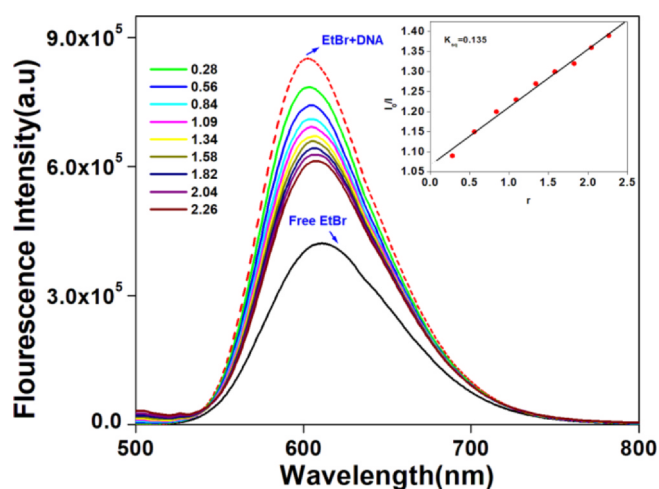


Fig. 5. Emission spectra of EB bound to CT-DNA in absence (---) and in the presence (—) of complex 1. $[Complex 1]/[DNA] = 0, 0.28, 0.56, 0.84, 1.09, 1.34, 1.58, 1.82, 2.04, 2.26$; $\lambda_{ex} = 525 \text{ nm}$. Inset: Stern–Volmer quenching curve.

in Fig. 5. The presence of complex 1 induces remarkable decrease in the fluorescence intensity of EB-DNA system. It indicates that the complex is able to replace EB molecules from EB-DNA adduct. This is characteristic observation of intercalative binding of the complex with DNA. Initially, the fluorescence intensity of free EB is remarkably increased on the addition of DNA. Concentrations of both EB and DNA have been kept equal at $6.7 \times 10^{-5} \text{ M}$ and titrated with gradually increasing concentration of complex 1 in $[complex 1]/[DNA]$ ratio of 0.28 to 2.26. The fluorescence intensity has been measured with excitation wavelength at 525 nm (λ_{ex} for EB) and the fluorescence intensity at 592 nm has been monitored. The results of fluorescence quenching phenomena are in good agreement with the observation in UV spectroscopic studies. The quenching efficiency for a species is evaluated by the Stern–Volmer constant, K_{sq} , which varies with the change in experimental conditions [47]

$$I_0/I = 1 + K_{sq}r$$

where I_0 and I are the fluorescence intensities in absence and in the presence of complex 1, respectively, and r is the ratio of total concentration of complex to that of DNA. K_{sq} is a linear Stern–Volmer quenching constant. The inset of Fig. 5 shows plot of I_0/I vs. r . It is linear in nature. Thus, fluorescence quenching of EB-DNA adduct by complex 1 is in good agreement with the linear Stern–Volmer equation. The K_{sq} value has been obtained as 0.135.

3.5.4. Cyclic voltammetry

Electrochemical studies can corroborate the results that are obtained from other relevant biophysical methods to learn about the interaction between the biomolecule and the redox active molecule. The cyclic voltammogram of the complex has been recorded in absence and in the presence of CT-DNA in aqueous solution (50 mM NaCl/5 mM Tris–HCl buffer, pH 7.2) (Fig. 6). The supporting electrolyte has been chosen to be KCl. Reduction of Copper(II) center has been observed at -0.76 V and with i_{pc} value of $-5.00 \times 10^{-7} \text{ A}$. It is oxidized back to Cu(II) from Cu(I) species at -0.58 V and with i_{pa} value of $1.72 \times 10^{-7} \text{ A}$. In the presence of DNA, there is noticeable change in the CV of the complex as seen in Fig. 6. There is a visible shift in the respective peak potentials, and the cathodic and anodic peak currents are markedly reduced which indicates some sort of interaction between the complex and the DNA. There are reductions at their respective peak potentials, cathodic and anodic peak currents. This reduction may occur due to the slow diffusion of the equilibrium mixtures of complex 1 and DNA bound complex 1 at the electrode surface. The negative shift in the

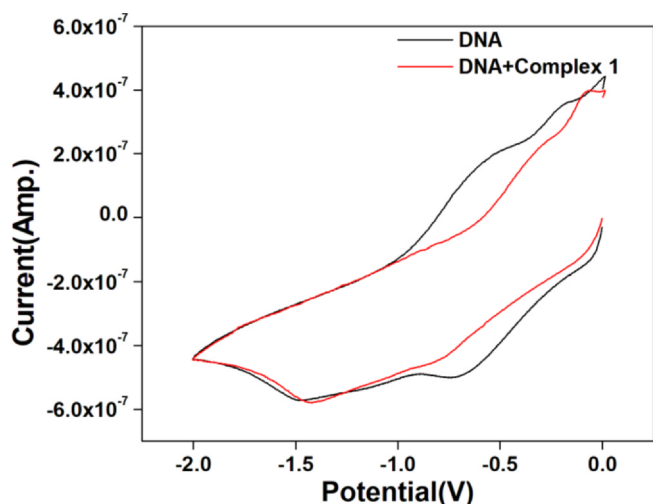


Fig. 6. Cyclic voltammogram of DNA in absence and in the presence of complex 1.

corresponding potential value indicates that complex 1 may bind with DNA through electrostatic interactions which shows up in the CV of the mixture [48].

3.5.5. Circular dichroism spectral studies on DNA binding

Circular dichroism spectroscopy is used to monitor the changes in DNA morphology when a drug molecule interacts with the DNA. The spectrum of CT-DNA shows a positive band at 274 nm characteristic of base stacking and a negative band at 272 nm which is characteristic of right handed helicity of the B-DNA form [49]. These bands are sensitive to the interaction between small molecules and CT-DNA. Interactions such as simple electrostatic or groove binding between the molecules and DNA show no or very small perturbation of positive and negative bands [50]. But the intercalation interaction increases the intensities of both the bands. The interaction of the copper complex with DNA induces an alteration in the CD spectrum of B-DNA as shown in Fig. 7. The intensities of both the bands for base stacking and helicity have been reduced significantly (shifting almost to zero level) with the gradual increase in concentration of metal complex, accompanied by a red shift (274 to 284 nm) for the positive bands. This suggests that binding of complex 1 with DNA brings on considerable changes, for example, the copper complex is able to cause the conversion of a more B-like to a

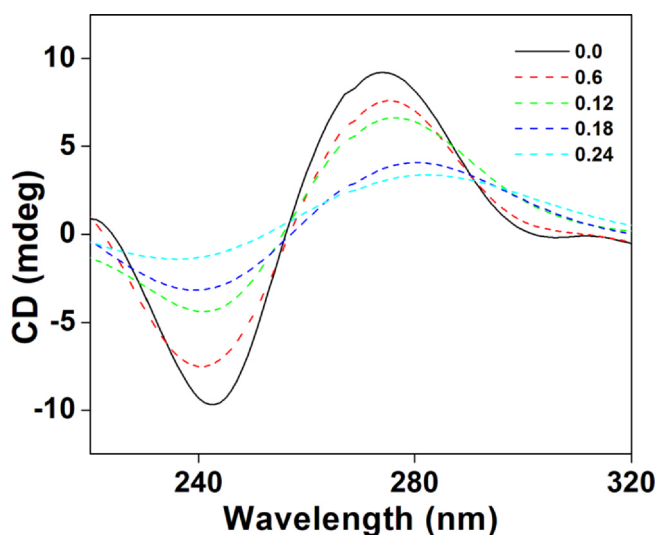


Fig. 7. CD spectra of DNA (1.2×10^{-4} M) in absence (—) and in the presence (---) of complex 1 in the $[\text{Complex 1}]/[\text{DNA}] = 0.6, 0.12, 0.18$ and 0.24 .

more C-like structure within DNA [51].

It is worthy to mention that the hydrophobic base stacking in the oligomers as well as in the polymers leads to the close contacts and Columbic interactions which in turn give intense CD bands due to each of base transitions [52]. Hence, intercalated complexes, which disturb and weaken base stacking, should induce a decrease in intensity of CD bands.

3.5.6. DNA cleavage studies

The DNA cleavage abilities of complex 1 have been studied by supercoiled FAM134BGFP plasmid DNA as a substrate in a medium of 100 mM Tris-HCl/NaCl buffer (pH = 7.5) under physiological conditions. The DNA has been seen to be chopped when treated with the complex and the intact DNA has been seen as a smear in the agarose gel electrophoresis. The supercoiled DNA has been seen as smeared on gel page which suggests that it has been cleaved appropriately by the complex. The supercoiled plasmid is subsequently cleaved into smaller forms which includes double stranded cuts as well as nicked cuts.

We have performed a concentration dependent study. The concentration of the metal complex has been increased from 20 to 40 μM gradually in 100 mM Tris-HCl/NaCl buffer (pH = 7.2) and 0.5 $\mu\text{g}/\mu\text{L}$ (6.53 nM) DNA is added to the mixture in the presence H_2O_2 (2 μM) and incubated for 30 min at 36 $^\circ\text{C}$. The results are shown in Fig. s4. The chopping off of DNA is clearly seen. We have initially standardized the time of 30 min by trying various time intervals starting from 2 min. The nuclease activity of the complex is really very high as no further breakage into other forms of the DNA has been seen but vigorous chopping off is evident from the very start. The results clearly show that as the concentration of metal complex is increased gradually, the cleavage is more pronounced and at 40 μM concentration the DNA is completely chopped off. This shows the complex is actually binding to DNA and chopping it off. The control tests have been done with all reagents except complex 1. It shows no cleavage as shown in Fig. s4. The role of H_2O_2 is very crucial in this process because without the presence of H_2O_2 the cleavage is not very effective as seen from experimental results. It can be claimed that this type of cleavage of is most likely to occur through an oxidative mechanism. In the presence of the reducing agent H_2O_2 , the Cu(II) complexes could be reduced to the Cu(I) complexes [43]. The Cu(I) complex then reacted with endogenous oxygen to form H_2O_2 , which could further react with another equivalent of Cu(I) complex to generate copper-oxido species with DNA destroying properties. The efficient DNA cleavage activity of the metal complexes in the presence of external hydrogen peroxide is probably due to the generation of a higher concentration of Cu(I) ions. Most cancer cells have an elevated intracellular concentration of hydrogen peroxide, which may help the intracellular generation of highly active copper-oxido species and ROS, causing oxidative DNA damage in cells [44]. So, H_2O_2 enhances the cleavage process started by the metal complex.

To know further about the active chemical species which is main reason for DNA damage activities by complex 1, the effect of different inhibiting agents such as hydroxyl radical scavenger (DMSO, EtOH, *tert*-butyl alcohol), reducing agent (GSH), singlet oxygen quenchers (NaN_3), hydrogen peroxide scavenger (KI), redox reagent (DTT), chelating agent (EDTA) and DNA minor groove binding agent (DAPI) has been investigated (Fig. 8). The DNA has been taken at 500 ng and the various additives at 0.4 mM concentration. The rest of the reagents like Tris/NaCl, H_2O_2 and the metal complex have been taken at the concentrations optimized in the previous set of experiments. Addition of DMSO shows no inhibition in cleavage process as we can see from lane 2 that the plasmid has been entirely chopped. But EtOH shows a marked decrease in the cleavage as seen in lane 3 of the gel electrophoresis data, and so does *tert*-butyl alcohol as seen in lane 6. It clearly shows the hydroxyl radical mainly takes part in the oxidative DNA cleavage activity which is observed from the addition of EtOH and *tert*-butyl alcohol. The addition of reducing agent GSH significantly reduces the

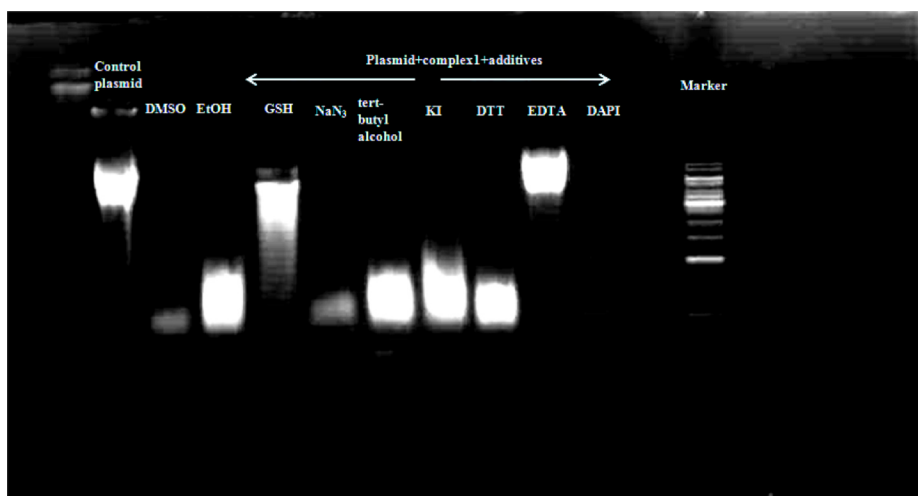


Fig. 8. DNA cleavage studies in the presence of various additives.

cleavage action of the complex as seen in lane 4. Sodium azide does not have any significant effect on the DNA cleavage (lane 5). This fact indicates that the singlet oxygen-like entities are not involved. When H_2O_2 scavenger potassium iodide (lane 7) is added to the mixture, the DNA cleavage activity by complex 1 has been inhibited to some extent. This fact indicates that the hydroxyl radical is responsible as one of the intermediates in the DNA cleavage process. Reducing agent like DTT also reduces the cleavage action of the complex (lane 8). The chelating agent EDTA totally inhibits DNA cleavage (lane 9), indicating that Cu (II) complex plays the key role in the DNA breakage. The cleavage is unaffected by the addition of minor groove binder (DAPI) which shows the non-affinity of the complex towards DNA groove (lane 10) [36,53]. Two control experiments have been performed with inorganic copper salts such as $CuCl_2$ and $Cu(OAc)_2$ which shows no effect on the plasmid DNA under the same experimental condition. From these results we can conclude that complex 1 is capable of exhibiting DNA cleavage activity through an oxidative DNA damage pathway. It can also be added that the hydroxyl radical and hydrogen peroxide are the active species involved in the scission process.

3.6. HSA binding studies

3.6.1. Absorption spectral studies

UV-vis absorption spectra have been used to observe any change in the secondary structure of protein, human serum albumin (HSA) [54] induced by complex 1 (Fig. 9). The strong absorption peak at 208 nm may be attributed to the characteristic $n \rightarrow \pi^*$ transition of peptide linkage of α helix in HSA; the comparatively weaker absorption peak at 280 nm may be due to the presence of the phenyl rings in aromatic acid residues such as Trp, Tyr and Phe [55]. Upon incremental addition of the complex ($0.76\text{--}5.8 \times 10^{-5}$ M) to HSA (4.0×10^{-6} M), a sharp decrease in the absorbance at 208 nm has been noticed. This can be attributed to the induced perturbation of α -helix of HSA by a specific interaction with the copper (II) complex. Besides, a red shift of the absorption peak from 208 to 226 nm indicates that the microenvironment of Trp-214 residue in HSA has been changed along with the destruction of tertiary structure of the HSA. Simultaneously, the intensity of absorbance at 280 nm has been enhanced in the presence of complex 1. This change suggests that the aromatic residues which are now exposed significantly to an aqueous environment. Moreover, the π - π stacking between aromatic rings of the complex and phenyl rings of DNA also makes some differences.

To evaluate the binding propensity of complex 1 with HSA, the intrinsic binding constant (K) has been determined. We assume that there exists only one type of interaction between the complex and the

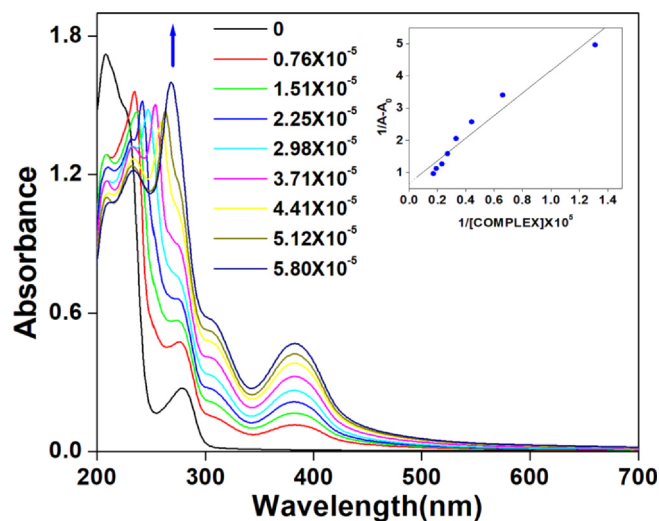
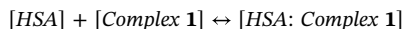


Fig. 9. UV absorption spectra of the complex 1 in the presence of HSA obtained in 5 mM Tris-HCl buffer, pH 7.2, at room temperature: $[HSA] = 4 \times 10^{-6}$ M; $[complex\ 1] = 0, 0.76, 1.51, 2.25, 2.98, 3.71, 4.41, 5.12, 5.80 \times 10^{-5}$ M, respectively. Arrow shows the intensity changes upon increasing concentration of complex 1. Inset: Plot of $1/A - A_0$ vs. $1/[Complex\ 1]$.

protein in aqueous media [55],



$$K = [HSA: Complex\ 1]/[HSA][Complex\ 1]$$

where K is the binding constant for complex 1, assuming $[HSA: Complex\ 1] = C_B$

$$K = C_B/[C_{HSA} - C_B][C_{Complex\ 1} - C_B]$$

where C_{HSA} and $C_{complex\ 1}$ are analytical concentration of HSA and complex 1 in the solution, respectively. According to the Beer-Lambert law

$$C_{HSA} = A_0/(\epsilon_{HSA} \cdot l)$$

$$C_B = (A - A_0)/(\epsilon_B \cdot l)$$

where A_0 and A are the absorbance of HSA at 280 nm, in absence and in the presence of complex 1, respectively [36]. ϵ_{HSA} and ϵ_B are the molar extinction coefficient of HSA and the HSA bound complex, respectively, and l is the light path of the cuvette (1 cm).

By substituting ϵ_{HSA} and ϵ_B in Equations.

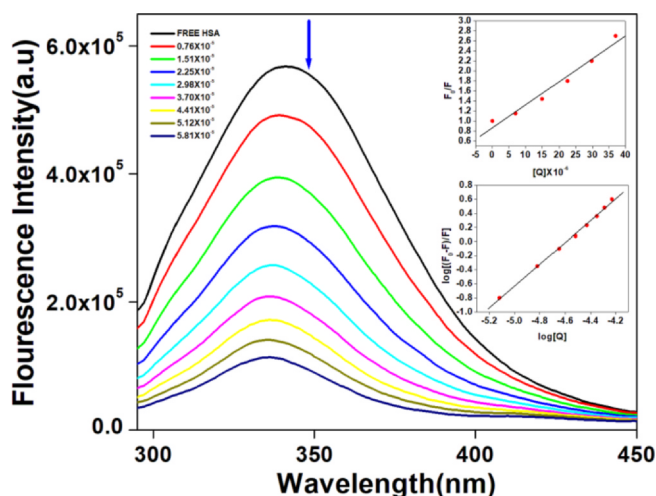


Fig. 10. The fluorescence quenching spectra of HSA by different concentrations of complex 1 with the excitation wavelength at 295 nm in 5 mM Tris-HCl buffer, pH 7.2, at room temperature: [HSA], 4.0×10^{-6} M; the concentration of complex 1 = 0, 0.76, 1.51, 2.25, 2.98, 3.70, 4.41, 5.12, 5.81 $\times 10^{-5}$ M, respectively. Arrow shows the intensity changes upon increasing concentration of the quencher.

$$A_o/(A - A_o) = \epsilon_{HSA}/\epsilon_B + ((\epsilon_{HSA} - 1)/(\epsilon_B K C_{Complex 1} \cdot 1))$$

Thus, the double reciprocal plot of $1/(A - A_o)$ vs. $1/[Complex 1]$ is linear and the binding constant is determined from the ratio of the intercept to the slope. The K_B has been found to be 1.91×10^4 M^{-1} .

3.6.2. Fluorescence quenching studies

Fluorescence spectroscopy is a powerful technique which is used to explore the interaction between small molecules and bio-macromolecules. The fluorescence spectra of HSA have been recorded in the range of 300–500 nm with excitation at 280 nm in the presence of various concentration of complex 1 (Fig. 10). HSA is one of the most abundant plasma proteins and it shows excellent drug binding ability, thereby providing a depot and carrier for several endogenous and exogenous behaviors towards the complex. The tryptophan residue is primarily responsible for the fluorescence of HSA when HSA is excited at 295 nm. Quantum yield of phenylalanine is extremely low and quenching of fluorescence of tyrosine residue is observed when it is either ionized or situated adjacent to an amino group, a carboxyl group or a tryptophan residue since both the tyrosine and phenylalanine residues do not absorb in this region. The HSA shows a strong fluorescence intensity at 344 nm, while complex 1 does not show any fluorescence under the present experiment conditions. The fluorescence spectra of HSA (4×10^{-6} M) have been obtained in the presence of different concentration (0.76×10^{-5} to 5.81×10^{-5} M) of complex 1. Fluorescence intensity of HSA at 344 nm reduces with the gradual addition of the metal complex. This suggests that the interaction of complex 1 with HSA alters the local microenvironment around the Trp 214 residue in the protein and also to the tertiary structure of HSA.

Commonly, fluorescence quenching events are described with the help of Stern–Volmer equation [47]:

$$F_o/F = (1 + K_q \tau_o [Q]) = (1 + K_{sv} [Q])$$

where F_o and F are the fluorescence intensities in absence and in the presence of quencher, respectively; K_q and K_{sv} are the quenching rate constant of the biomolecules and the Stern–Volmer quenching constant; τ_o is the average life time of the molecule without quencher ($\tau_o = 10^{-8}$ s) and $[Q]$ is the concentration of the quencher. The Stern–Volmer plot of F_o/F vs $[Q]$ for the quenching of fluorescence intensity of HSA fluorescence by complex 1 is depicted in inset of Fig. 10 and the calculated K_{sv} and K_q values have been found to be 4×10^5 M^{-1} and

4×10^{13} $M^{-1} s^{-1}$, respectively. It is clearly evident that the K_q value is significantly more than the limiting diffusion constant K_{dif} of the biomolecules ($K_{dif} = 2.0 \times 10^{10}$ $M^{-1} s^{-1}$). The fact indicates that the fluorescence quenching of HSA is happened due to the specific interaction of complex 1 with the protein which is consistent with the static quenching mechanism [56,57].

In case of static quenching, the Scatchard equation is used to determine the binding constant value and number of binding sites [58],

$$\log [F_o - F/F] = \log K + n \log [Q]$$

where, F_o and F are fluorescence intensities of HSA in absence and in the presence of quencher, respectively; K and n denote the binding constant and the number of binding sites, respectively. Thus, a plot of $\log[(F_o - F)/F]$ versus $\log[Q]$ is used to evaluate the binding constant from the intercept and the number of binding sites from the slope (Fig. 10). From the corresponding Scatchard plot, the K and n values are found to be and 1×10^7 M^{-1} and 1.54, respectively. These values are comparable with previously reported binding constant values [3h–j].

3.6.3. Energy transfer and binding distance between complex 1 and HSA

Overlapping of emission spectrum of a donor such as fluorophore with the absorption spectrum of an acceptor molecule may lead to fluorescence energy transfer. The absorption spectrum of complex 1 overlaps with the fluorescence spectrum of HSA (Fig. s5). Here the donor and acceptor are HSA and the metal complex, respectively.

Quenching of fluorescence of Trp residue is occurred by the metal complex via Forster resonance energy transfer (FRET) mechanism and the efficiency of energy transfer is given by the following equation [59]:

$$E = (1 - F/F_o) = R_o^6 / (R_o^6 + r^6)$$

where F and F_o are the fluorescence intensities of HSA in the presence and in absence of quencher, respectively, r is the distance between acceptor and donor, and R_o is the critical distance when the transfer efficiency is 50%. The value of R_o can be determined by the following equation [60]:

$$R_o^6 = 8.78 \times 10^{-25} K^2 n^{-4} \phi J$$

where K^2 is the spatial orientation factor between the emission dipole of the donor and the absorption dipole of the acceptor, n is the refractive index of the medium, ϕ is the fluorescence quantum yield of the donor, and J is the overlap integral of the fluorescence emission spectrum of the donor and the absorption spectrum of the acceptor and can be given by [53]:

$$J = \frac{\int_0^\infty F(\lambda) \epsilon(\lambda) \lambda^4 d\lambda}{\int_0^\infty F(\lambda) d\lambda}$$

where $F(\lambda)$ is the corrected fluorescence intensity of the donor at wavelength λ , and $\epsilon(\lambda)$ is the molar absorption coefficient of the acceptor at wavelength λ . Under the experimental conditions, for a solution with random orientation as in this case, $K^2 = 2/3$, $n = 1.36$, $\phi = 0.15$, J has been calculated to be 6.54×10^{-14} (from the graph), R_o has been found to be 3.44 nm, $E = 0.3$ and $r = 3.96$ nm. The distance between HSA and complex 1 is less than 7 nm, indicating that a static quenching interaction has occurred.

3.6.4. IR spectral studies

Conformational changes in the protein structures can be determined by the analysis of FT-IR spectra of proteins. IR spectra show the presence of moieties in the proteins (Fig. s6). The spectrum has been obtained in ATR mode by first taking a blank reading in the buffer solution followed by the spectrum of HSA solution in Tris buffer and then finally the spectrum of HSA treated with complex again in Tris buffer. The absorption of Tris buffer was subtracted from the spectrum of HSA solution and the HSA treated with protein solution. The amide bands of the protein can be related with its secondary structure. Amide I bands

show higher sensitivity to the alterations in the secondary structure of protein in comparison to amide II and amide III. The characteristic peak shifts of amide I and amide II are from 1649 to 1657 cm^{-1} and from 1547.03 to 1553.65 cm^{-1} , respectively. This indicates that there is interaction between complex 1 and HSA protein [53]. This shifting in the IR bands demonstrates that the secondary structure of this protein has been altered after the interaction with the copper complex which results in the amide vibrational shifts [61].

3.6.5. 3D fluorescence spectral studies

The 3D fluorescence of HSA has been studied initially and after binding with complex 1. The first peak, Peak A is a Rayleigh scattering peak ($\lambda_{\text{ex}} = \lambda_{\text{em}}$), Peak B ($\lambda_{\text{ex}} = 280\text{ nm}$, $\lambda_{\text{em}} = 350\text{ nm}$), mainly reflects the spectral properties of the Trp residue. Maximum emission wavelength or the fluorescence intensity of the residue is related with its micro-environment's polarity (Fig. s7). Peak C is the second-ordered scattering peak ($\lambda_{\text{em}} \approx 2\lambda_{\text{ex}}$) [60]. It could be seen that after interaction with complex, intensity of peak A significantly increases while that of peak B decreases remarkably. Peak C shows huge increase in the intensity [53]. All of these facts prove that the interaction of complex 1 with HSA induces some conformational as well as some micro environmental changes in HSA. These facts are well corroborated with our spectroscopic results obtained from UV-vis, fluorescence and CD measurements.

3.6.6. Circular dichroism

CD measurement has been performed with HSA protein in the presence of different concentrations of complex 1 to access the probable influence of the metal complex binding on the secondary structure of the protein. The CD spectrum of HSA (line a) exhibits two negative bands in the ultraviolet region at 206 and 220 nm (Fig. s8). The bands may be assigned to $\pi \rightarrow \pi^*$ and $n \rightarrow \pi^*$ transfers in the peptide bond and these are characteristic of α -helix structure of the protein. With the addition of complex 1, the CD signal of HSA increases. This indicates that the binding of complex 1 with the protein leads to a considerable conformational change in HSA. Moreover, the CD spectra of HSA change a lot in shape also after addition of the complex which proves that a lot of α -helical part has been destroyed on binding [60].

3.6.7. Oxidative damage of HSA by complex 1

After being incubated with complex 1, for 30 min , at $37\text{ }^\circ\text{C}$, in the presence of hydrogen peroxide, HSA exhibits remarkable degradation as indicated by a continuum of protein fragments at SDS-PAGE in 12% acrylamide gel while for the control condition, which does not include the complex, there is no degradation at all (Fig. 11). Thus, the oxidative effect of hydrogen peroxide by the generation of ROS is much more enhanced in the presence of the complex under mild conditions which otherwise would require harsher conditions. We see the clear and thick protein band at the expected molecular weight range of around 66 kDa . Different concentrations of the protein and the metal complex have been incubated with H_2O_2 [61]. The degradation process is ascertained by the thinner bands at the mentioned molecular weight of the intact protein and the subsequent smears seen on the gel indicating a degradation process. Blank sets have been also kept for comparison. The results have been indicated in Fig. 11.

3.7. Antibacterial study by complex 1

Different concentrations (400 , 350 , 250 , 100 , 25 and $10\text{ }\mu\text{g/mL}$) of complex 1 have been added to the bacterial cells in 2.0 mL LB broth and followed by incubation in a $37\text{ }^\circ\text{C}$ incubator. The next day, growth has been observed in the test tubes (Fig. 12). From the tubes, fixed amount of cell mixture has been plated on LB media again followed by incubation at $37\text{ }^\circ\text{C}$. After overnight incubation, the cell colonies have been counted on the LB plates. A stark decrease in the number of colonies has been observed for both gram positive *S. aureus* and gram

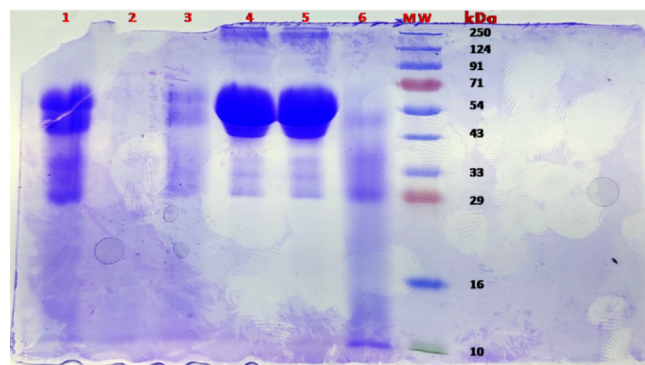


Fig. 11. SDS-PAGE electrophoresis in 12% polyacrylamide gel of HSA fragmentation, in the presence of complex 1, treated with H_2O_2 , for 30 min at $37\text{ }^\circ\text{C}$, in Tris buffer 100 mM , $\text{pH } 7.2$, MW: Molecular weight marker, Lane 1: $75\text{ }\mu\text{M}$ HSA, $75\text{ }\mu\text{M}$ complex and $750\text{ }\mu\text{M}$ H_2O_2 , Lane 2: $25\text{ }\mu\text{M}$ HSA, $50\text{ }\mu\text{M}$ complex and $750\text{ }\mu\text{M}$ H_2O_2 , Lane 3: $50\text{ }\mu\text{M}$ HSA, $100\text{ }\mu\text{M}$ complex and $750\text{ }\mu\text{M}$ H_2O_2 , Lane 4: Blank ($75\text{ }\mu\text{M}$ HSA and $750\text{ }\mu\text{M}$ H_2O_2), Lane 5: Blank ($75\text{ }\mu\text{M}$ HSA), Lane 6: $75\text{ }\mu\text{M}$ HSA, $200\text{ }\mu\text{M}$ complex and $750\text{ }\mu\text{M}$ H_2O_2 .

negative *E. coli* with increasing concentration of complex 1 which clearly indicates a strong antibacterial property of the complex.

3.8. Apoptosis evaluation by DAPI staining

To visualize nuclear changes, HeLa cells have been treated with complex 1 at different concentrations (5 , 10 and $20\text{ }\mu\text{M}$) for three time intervals (12 , 24 and 48 h). After treatment, the cells have been fixed and stained with DAPI and visualized on a fluorescence microscope. The cells have been observed to undergo a stark change with increasing concentration of the complex and time of treatment (Fig. 13). It is clear from the figure that as time of treatment and the concentration of complex 1 have been increased, the more number of nucleuses show structure deterioration. The white arrows indicate more number of bilobed nuclei. Such bilobed structure and nuclear shrinkage can be seen with increasing complex concentration and time of treatment. Moreover, as seen from the bright field images, that the HeLa cells show clear rounding and shrinkage which is a clear indication of apoptosis.

3.9. Comparison with some recently published results

Copper complexes are known to show therapeutic effects [67] including anticancer properties [68,69]. Thus, it can be said that copper complexes have immense potential as new age drugs. For this purpose, its mode of action has to be investigated which can be done only by studying its interaction behavior with cellular DNA and proteins.

Few mononuclear copper(II) complexes have been previously reported when these complexes have been used to study the interaction with DNA and proteins to evaluate their chance as drug. Different copper(II) complexes with different amine ligands show significant affinity towards BSA (bovine serum albumin). These complexes bind to CT DNA via intercalation with highest DNA-binding constant value of $4.88 (\pm 0.08) \times 10^6\text{ M}^{-1}$ [62]. A series of copper(II) complexes with ferrocenyl appended terpyridine and hydroxyquinoline ligands show cytotoxicity against the HeLa and MCF-7 cancer cells. These complexes show moderate binding to ct-DNA with binding constants in the range of $6.3 \times 10^4\text{ M}^{-1}$ – $7.4 \times 10^4\text{ M}^{-1}$ and HSA with binding constants in the range of $8.9 \times 10^4\text{ M}^{-1}$ – $3.7 \times 10^5\text{ M}^{-1}$ [63]. Two copper(II) complexes with Schiff-base ligands show binding ability with ct-DNA with binding constant value of $1.53 \times 10^5\text{ M}^{-1}$ and $3.13 \times 10^5\text{ M}^{-1}$ and also in vitro cytotoxicity against MCF7 cell line and human lung cancer A549 [64]. Three copper(II) complexes with 5-methoxyisatinthiosemicarbazone derivatives have DNA binding constants in the range of 1.8×10^4 – $8.2 \times 10^5\text{ M}^{-1}$. These complexes also show

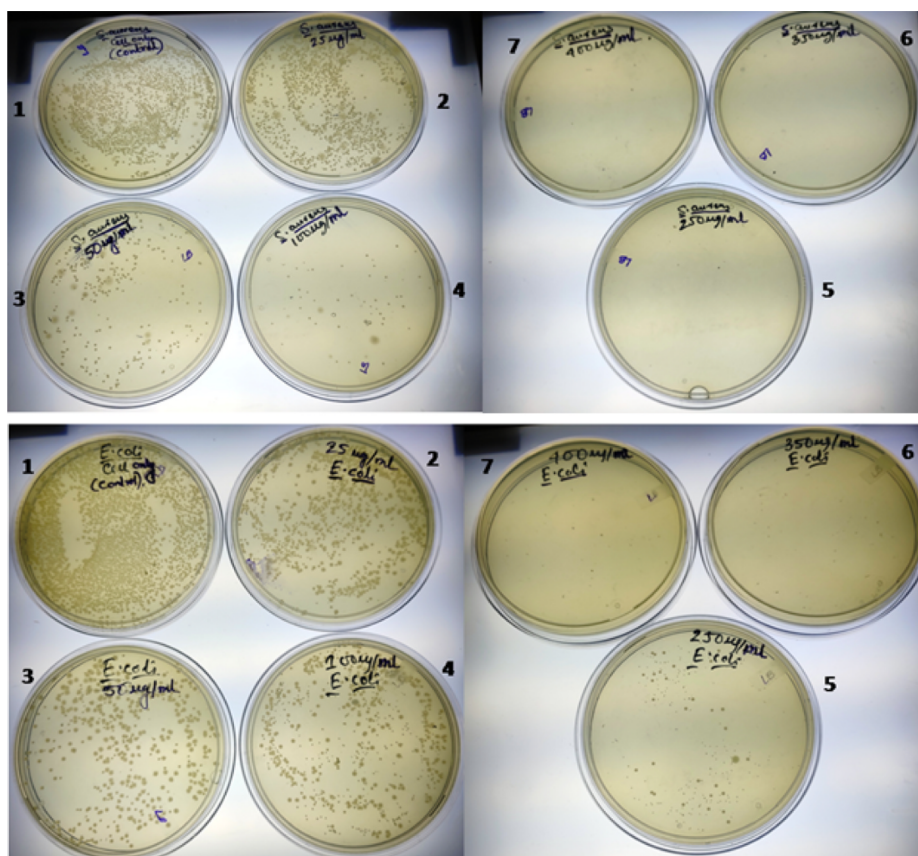


Fig. 12. *S. aureus* and *E. coli* colonies with gradually increasing concentrations of complex 1, 1: control (without complex 1), 2: 25 $\mu\text{g}/\text{mL}$ complex 1, 3: 50 $\mu\text{g}/\text{mL}$ complex 1, 4: 100 $\mu\text{g}/\text{mL}$ complex 1, 5: 250 $\mu\text{g}/\text{mL}$ complex 1, 6: 350 $\mu\text{g}/\text{mL}$ complex 1, 7: 400 $\mu\text{g}/\text{mL}$ complex 1.

protein binding, antibacterial and antifungal activities [65]. Three copper(II) complexes of azo Schiff base ligands show minor groove binding to the AT-rich sequence of DNA with the intrinsic binding constants in the range of $7.11 \times 10^5 \text{ M}^{-1}$, $8.36 \times 10^5 \text{ M}^{-1}$ and $10.81 \times 10^5 \text{ M}^{-1}$ [66]. Our complex shows DNA binding constant of $1.68 \times 10^5 \text{ M}^{-1}$ and HSA binding constant of $1.91 \times 10^4 \text{ M}^{-1}$. It also demonstrates antibacterial activity and apoptosis of HeLa cell. Different detailed studies have been performed to support its DNA and protein binding activities.

4. Conclusions

In summary, we have been able to synthesize and characterize a mononuclear copper(II) complex (Complex 1) with an N,O-donor ligand. From different studies, it has been observed that complex 1 shows the intercalative binding properties with DNA and in this process, effectively cleaves DNA into shorter fragments. This has been ascertained by agarose gel electrophoresis where the smear of DNA as compared to the compact band clearly indicates the cleavage process. Various biophysical experiments have been carried out to find out the physical parameters like binding constant etc., which clearly indicates a strong interaction between complex 1 and DNA. Moreover, it exhibits protein (here HSA) binding properties with appreciable changes in the protein structure as proved from the results of IR, 3D fluorescence spectral and circular dichroism studies. The binding constant value determined also is pretty high but lower than that of DNA complex binding constant. So, this indirectly shows that HSA can effectively interact with complex 1 and act as a carrier and deliver it to the cellular DNA through blood. The DNA complex binding being stronger, the complex will effectively be transported to the DNA. Antibacterial activity of the complex has been observed for both gram positive *S. aureus* and gram negative *E.*

coli. This point proves that complex 1 is effective in cleaving bacterial DNA and hence can act as an efficient antibacterial agent. When HeLa cells have been treated with complex 1, a clear indication of apoptosis has been noticed. Hence, we can target cellular DNA with it. Another interesting point lies in the fact that as many recent studies have shown that cancer cells have higher amounts of hydrogen peroxide than normal ones; this complex, which is showing enhanced DNA cleavage properties in the presence of the same, can be used as a drug targeted for cancer cells.

CRediT authorship contribution statement

Aradhita Bhattacharjee: Conceptualization, Data curation, Formal analysis, Investigation, Methodology, Writing - original draft. **Subhadeep Das:** Formal analysis, Investigation, Methodology. **Biswadip Das:** Supervision, Validation, Visualization. **Partha Roy:** Conceptualization, Supervision, Validation, Resources, Funding acquisition, Writing - original draft.

Declaration of Competing Interest

The authors declare that they have no known competing financial interests or personal relationships that could have appeared to influence the work reported in this paper.

Acknowledgements

PR thankfully acknowledges financial support from RUSA 2.0, Jadavpur University (Ref. No.: R-11/264/19 dated 08.03.2019). AB wishes thank CSIR-New Delhi for providing her a fellowship.

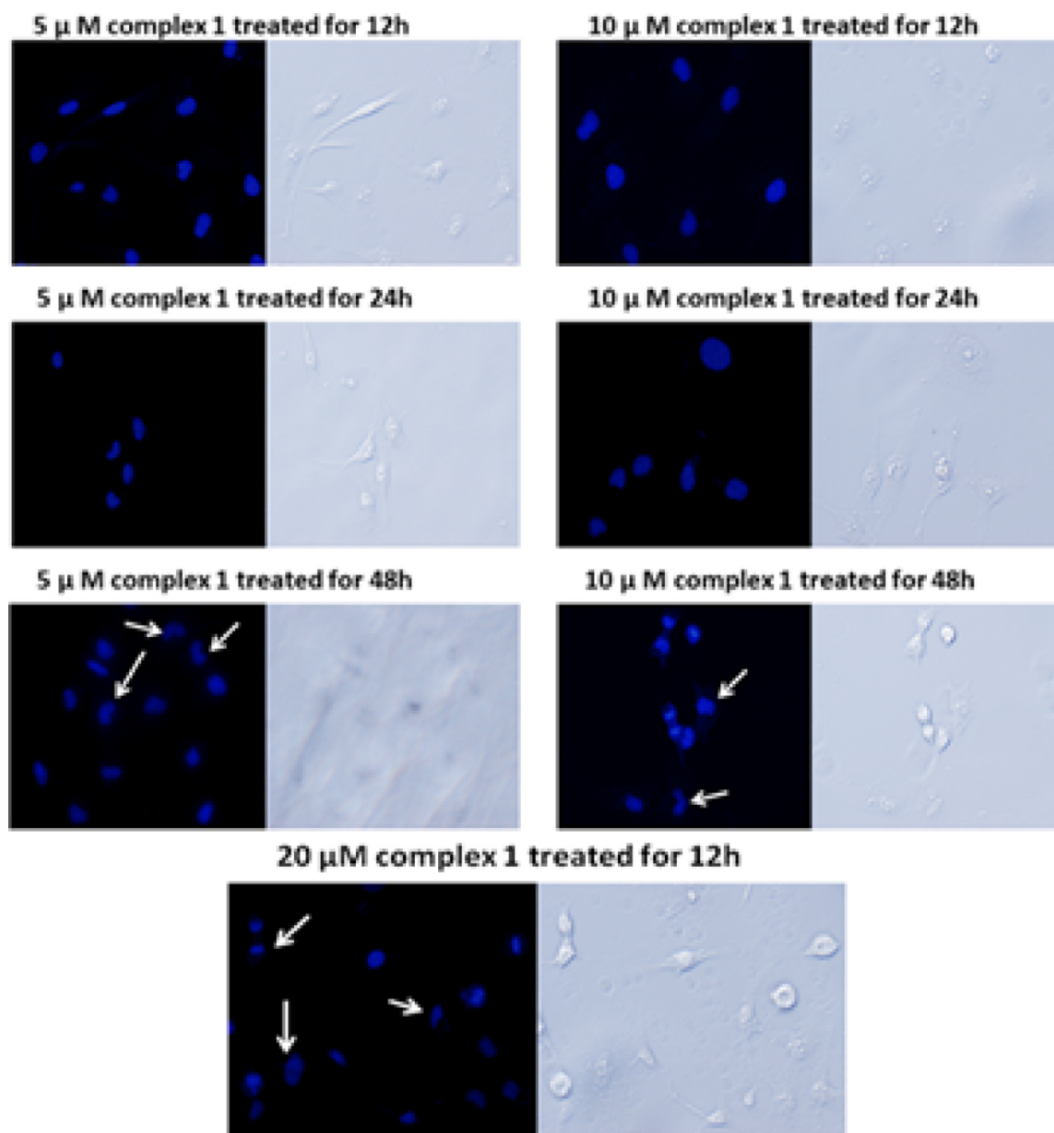


Fig. 13. Confocal microscopy images of HeLa cells treated with different concentrations of complex 1 and different durations and the morphological changes of HeLa cell nucleus that occurred indicating possible apoptosis.

Appendix A. Supplementary data

Supplementary data to this article can be found online at <https://doi.org/10.1016/j.ica.2020.119961>.

References

- [1] B. Rosenberg, L. Vancamp, J.E. Trosko, V.H. Mansour, *Nature* 222 (1969) 385.
- [2] (a) R. Oun, Y.E. Moussa, N.J. Wheate, *Dalton Trans.* 47 (2018) 6645;
(b) J. Gurruchaga-Pereda, Á. Martínez, A. Terenzi, L. Salassa, *Inorg. Chim. Acta* 495 (2019) 118981.
- [3] (a) C. Santini, M. Pellei, V. Gandin, M. Porchia, F. Tisato, C. Marzano, *Chem. Rev.* 114 (2014) 815;
(b) W. Liu, R. Gust, *Coord. Chem. Rev.* 329 (2016) 191;
(c) U. Ndagi, N. Mhlongo, M.E. Soliman, *Drug Des. Devel. Ther.* 11 (2017) 599;
(d) T.J.P. McGivern, S. Afsharpour, C.J. Marmion, *Inorg. Chim. Acta* 472 (2018) 12;
(e) C.R. Madzivire, P. Caramés-Méndez, C.M. Pask, R.M. Phillips, R.M. Lord, P.C. McGowan, *Inorg. Chim. Acta* 498 (2019) 119025;
(f) R. Tabti, N. Tounsi, C. Gaiddon, E. Bentouhami, L. Désaubry, *Med. Chem.* 7 (2017) 875;
(g) G. Gupta, S. Cherukommu, G. Srinivas, S.W. Lee, S.H. Mun, J. Jung, N. Nagesh, C.Y. Lee, *J. Inorg. Biochem.* 189 (2018) 17;
(h) S.-S. Wu, W.-B. Yuan, H.-Y. Wang, Q. Zhang, M. Liu, K.-B. Yu, *J. Inorg. Biochem.* 102 (2008) 2026;
(i) P. Živec, F. Perdih, I. Turel, G. Giester, G. Psomas, *J. Inorg. Biochem.* 117 (2012) 35;
(j) F. Dimiza, F. Perdih, V. Tangoulis, I. Turel, D.P. Kessissoglou, G. Psomas, *J. Inorg. Biochem.* 105 (2011) 476;
(k) S.D. Kettenmann, F.R. Louka, E. Marine, R.C. Fischer, F.A. Mautner, N. Kulak, S.S. Massoud, *Eur. J. Inorg. Chem.* (2018) 2322.
- [4] (a) J.A. Eremina, E.V. Lider, T.S. Sukhikh, L.S. Klyushova, M.L. Perepechaeva, D.G. Sheven, A.S. Berezin, A.Y. Grishanova, V.I. Potkin, *Inorg. Chim. Acta* 510 (2020) 119778;
(b) C.R. Munteanu, K. Suntharalingam, *Dalton Trans.* 44 (2015) 13796;
(c) C.J. Dhanaraj, I.U. Hassan, J. Johnson, J. Joseph, R.S. Joseyphus, *J. Photochem. Photobiol. B* 162 (2016) 115;
(d) M.A. Malik, O.A. Dar, P. Gull, M.Y. Wani, A.A. Hashmi, *Med. Chem. Commun.* 9 (2018) 409;
(e) T. Zou, C.-N. Lok, P.-K. Wan, Z.-F. Zhang, S.-K. Fung, C.-M. Che, *Curr. Opin. Chem. Biol.* 43 (2018) 30;
(f) L.M. Balsa, M.C. Ruiz, L.S.M. de la Parra, E.J. Baran, I.E. León, *J. Inorg. Biochem.* 204 (2020) 110975;
(g) S. Jiang, H. Ni, F. Liu, S. Gu, P. Yu, *Inorg. Chim. Acta* 499 (2020) 119186;
(h) S. Kumar, R.P. Sharma, P. Venugopalan, V. Ferretti, M. Tarpin, S. Sayen, E. Guillon, *Inorg. Chim. Acta* 488 (2019) 260.
- [5] (a) R.F. Brissos, A. Caubet, P. Gamez, *Eur. J. Inorg. Chem.* (2015) 2633;
(b) S. Khan, A.M. Malla, A. Zafar, I. Naseem, *PLoS ONE* 12 (2017) e0181783;
(c) P.B. Dervan, *Science* 232 (1986) 464;
(d) P.G. Schultz, P.B. Dervan, *J. Biomol. Struct. Dyn.* 1 (1984) 1133.
- [6] (a) J.K. Barton, *J. Biomol. Struct. Dyn.* 1 (1983) 621;
(b) J.K. Barton, *Science* 223 (1986) 727;
(c) S. Neidle, Z. Abraham, *CRC Crit. Rev. Biochem.* 17 (1984) 73;

- (d) B.P. Hudson, J.K. Barton, *J. Am. Chem. Soc.* 120 (1998) 6877;
 (e) B.S. Rajebhosale, S.N. Dongre, S.S. Deshpande, A.N. Kate, A.A. Kumbhar, *J. Inorg. Biochem.* 175 (2017) 129.
- [7] F.P. Dwyer, E. Mayhew, E.M. Roe, A. Shulman, *Br. J. Cancer* 19 (1965) 195.
 [8] A. Spassky, D.S. Sigman, *Biochemistry* 24 (1985) 8050.
 [9] (a) E.Y. Tirel, Z. Bellamy, H. Adams, V. Lebrun, F. Duarte, N.H. Williams, *Angew. Chem. Int. Ed.* 53 (2014) 8246;
 (b) A.A. Muxel, A. Neves, M.A. Camargo, A.J. Bortoluzzi, B. Szpoganicz, E.E. Castellano, N. Castilho, T. Bortolotto, H. Terenzi, *Inorg. Chem.* 53 (2014) 2943;
 (c) P. Hendry, A.M. Sargeson, *Prog. Inorg. Chem.* 38 (1990) 201.
- [10] (a) D. Bím, E. Svobodová, V. Eigner, L. Rulíšek, J. Hodačová, *Chem. Eur. J.* 22 (2016) 10426;
 (b) S.S. Massoud, C.C. Ledet, T. Junk, S. Bosch, P. Comba, R. Herchel, J. Hošek, Z. Trávníček, R.C. Fischer, F.A. Mautner, *Dalton Trans.* 45 (2016) 12933;
 (c) A.N. Modak, J.K. Gard, M.C. Merriman, K.A. Winkler, J.K. Bashkin, M.K. Stern, *J. Am. Chem. Soc.* 113 (1991) 283.
 [11] E.L. Hegg, J.N. Burstyn, *Coord. Chem. Rev.* 171 (1998) 133.
 [12] (a) C. Mari, V. Pierroz, S. Ferrari, G. Gasser, *Chem. Sci.* 6 (2015) 2660;
 (b) C. Sissi, F. Mancini, M. Gatos, M. Palumbo, P. Tecilla, U. Tonellato, *Inorg. Chem.* 44 (2005) 2310;
 (c) A. Bencini, E. Berni, A. Bianchi, C. Giorgi, B. Valtancoli, D.K. Chand, H.J. Schneider, *J. Chem. Soc., Dalton Trans.* (2003) 793;
 (d) D.K. Chand, H.J. Schneider, A. Bencini, A. Bianchi, C. Georgi, S. Ciattini, B. Valtancoli, *Chem. Eur. J.* 6 (2000) 4001;
 (e) A. Sitlani, E.C. Long, A.M. Pyle, J.K. Barton, *J. Am. Chem. Soc.* 114 (1992) 2303;
 (f) R. Herchel, Z. Dvořák, Z. Trávníček, M. Mikuriya, F.R. Louka, F.A. Mautner, S.S. Massoud, *Inorg. Chim. Acta* 451 (2016) 102;
 (g) S.S. Massoud, F.R. Louka, G.T. Ducharme, R.C. Fischer, F.A. Mautner, J. Vančo, R. Herchel, Z. Dvořák, Z. Trávníček, *J. Inorg. Biochem.* 180 (2018) 39;
 (h) S.S. Massoud, F.R. Louka, A.F. Tusa, N.E. Bordelon, R.C. Fischer, F.A. Mautner, J. Vančo, J. Hošek, Z. Dvořák, Z. Trávníček, *New J. Chem.* 43 (2019) 6186.
- [13] (a) A.A.A. Abu-Hussen, *J. Coord. Chem.* 59 (2006) 157;
 (b) M.S. Karthikeyan, D.J. Prasal, B. Poojary, K.S. Bhat, B.S. Holla, N.S. Kumari, *Bioorg. Med. Chem.* 14 (2006) 7482;
 (c) K. Singh, M.S. Barwa, P. Tyagi, *Eur. J. Med. Chem.* 41 (2006) 147;
 (d) P. Panneerselvam, R.B. Nair, G. Vijayalakshmi, E.H. Subramanian, S.K. Sridhar, *Eur. J. Med. Chem.* 40 (2005) 225.
 [14] (a) S.K. Sridhar, M. Saravanan, A. Ramesh, *Eur. J. Med. Chem.* 36 (2001) 615;
 (b) S.N. Pandeya, D. Sriram, G. Nath, E. DeClercq, *Eur. J. Pharm. Sci.* 9 (1999) 25.
 [15] (a) A.C. Hangan, G. Borodi, R.L. Stan, E. Páll, M. Cenariu, L.S. Oprean, B. Sevastre, *Inorg. Chim. Acta* 482 (2018) 884;
 (b) Z. Bao, D. Lai, P. Shen, M. Yu, R. Kumar, Y. Liu, Z. Chen, H. Liang, Z. Anorg, *Allg. Chem.* 645 (2019) 570;
 (c) R. Mladenova, M. Ignatova, N. Manolova, T. Petrova, I. Rashkov, *Eur. Polym. J.* 38 (2002) 989;
 (d) O.M. Walsh, M.J. Meegan, R.M. Prendergast, T.A. Nakib, *Eur. J. Med. Chem.* 31 (1996) 989.
 [16] (a) J.E. Kovacic, *Spectrochim. Acta* 23A (1967) 183;
 (b) R. Atkins, G. Brewer, E. Kokot, G.M. Mockler, E. Sinn, *Inorg. Chem.* 24 (1985) 127.
 [17] (a) K.E. Erkkila, D.T. Odom, J.K. Barton, *Chem. Rev.* 99 (1999) 2777;
 (b) C. Metcalfe, J.A. Thomas, *Chem. Soc. Rev.* 32 (2003) 215.
 [18] (a) B.J. Pages, D.L. Ang, E.P. Wright, J.R. Aldrich-Wright, *Dalton Trans.* 44 (2015) 3505;
 (b) V. Uma, V.G. Vaidyanathan, B.U. Nair, *Bull. Chem. Soc. Jpn.* 78 (2005) 845.
 [19] (a) Y. Yan, J. Zhang, L. Rend, C. Tang, *Chem. Soc. Rev.* 45 (2016) 5232;
 (b) C.S. Allardyce, P.J. Dyson, *Dalton Trans.* 45 (2016) 3201;
 (c) W. Szczepaniak, J. Ciesiolka, J. Wrzesinski, J. Skala, M. Jezowska-Bojczuk, *Dalton Trans.* (2003) 1488.
 [20] (a) T.M. Rana, C.F. Meares, *J. Am. Chem. Soc.* 113 (1991) 1859;
 (b) R. Miyake, J.T. Owens, D. Xu, W.M. Jackson, C.F. Meares, *J. Am. Chem. Soc.* 121 (1999) 7453.
 [21] K. Tsumura, A. Suzuki, T. Tsuzuki, S. Tanimoto, H. Kaneko, S. Mastumara, M. Imoto, K. Umezawa, D. Takahashi, K. Tushima, *Dalton Trans.* 40 (2011) 6357.
 [22] (a) A. Bergamo, G. Sava, *Dalton Trans.* (2007) 1267;
 (b) H.-K. Liu, S.J. Berners-Price, F.J. Wang, A. Parkinson, J. Xu, J. Bella, P.J. Sadler, *Angew. Chem., Int. Ed.* 45 (2006) 8153;
 (c) G. Sava, I. Capozzi, K. Clerici, R. Gagliardi, E. Alessio, G.C. Mestroni, *Clin. Exp. Metastasis* 16 (1998) 371.
 [23] M. Yokoyama, *J. Artif. Organs* 8 (2005) 77.
 [24] (a) R. Haag, F. Kratz, *Angew. Chem., Int. Ed.* 45 (2006) 1198;
 (b) J. Shi, P.W. Kantoff, R. Wooster, O.C. Farokhzad, *Nat. Rev. Cancer* 17 (2017) 20;
 (c) S. Vandghanooonia, M. Eskandania, J. Barara, Y. Omid, *Eur. J. Pharm. Sci.* 117 (2018) 301;
 (d) D. Mehta, N. Leong, V.M. McLeod, B.D. Kelly, R. Pathak, D.J. Owen, C.J.H. Porter, L.M. Kaminskis, *Mol. Pharmaceut.* 15 (2018) 4568.
- [25] (a) Z. Liu, X. Chen, *Chem. Soc. Rev.* 45 (2016) 1432;
 (b) V.T.G. Chuang, U. Kragh-Hansen, M. Otagiri, *Pharm. Res.* 19 (2002) 569;
 (c) R.K. Jain, *Cancer Res.* 50 (1990) 814s.
 [26] (a) W.H. Ang, E. Daldini, L. Juillerat-Jeanneret, P.J. Dyson, *Inorg. Chem.* 46 (2007) 9048;
 (b) T. Kosta, T. Maryama, M. Otagiri, *Pharm. Res.* 14 (1997) 1607.
 [27] N. Shahabadi, M. Maghsudi, *J. Mol. Struct.* 929 (2009) 193.
 [28] (a) C. Trejo-Solis, G. Palencia, S. Zuniga, A. Rodriguez-Ropon, L. Osorio-Rico, S.T. Luvia, I. Gracia-Mora, L. Marquez-Rosado, A. Sanchez, M.E. Moreno-Garcia, A. Cruz, M.E. Bravo-Gomez, L. Ruiz-Ramirez, S. Rodriguez-Enriquez, J. Sotelo, *Neoplasia* 7 (2005) 563;
 (b) F. Carvallo-Chaigneau, C. Trejo-Solis, C. Gomez-Ruiz, E. Rodriguez-Aguilera, L. Macias-Rosales, E. Cortes-Barberena, C. Cedillo-Pelaez, I. Gracia-Mora, L. RuizAzuara, V. Madrid-Marina, F. Constantino-Casas, *Biometals* 21 (2008) 17.
 [29] (a) A. De Vizcaya-Ruiz, A. Rivero-Muller, L. Ruiz-Ramirez, G.E. Kass, L.R. Kelland, R.M. Orr, M. Dobrota, *Toxicol. In Vitro* 14 (2000) 1;
 (b) L. Hernandez-Esquivel, A. Marin-Hernandez, N. Pavon, K. Carvajal, R. MorenoSanchez, *Toxicol. Appl. Pharmacol.* 212 (2006) 79.
 [30] L. Shi, H.-M. Ge, S.-H. Tan, H.-Q. Li, Y.-C. Song, H.-L. Zhu, R.-X. Tan, *Eur. J. Med. Chem.* 42 (2007) 558.
 [31] D.D. Perrin, W.L.F. Armarego, D.R. Perrin, *Purification of Laboratory Chemicals*, Pergamon Press, Oxford, U.K., 1980.
 [32] Bruker, APEX2, SAINT and SADABS, Bruker AXS Inc., Madison, Wisconsin, USA, 2008.
 [33] G.M. Sheldrick, *Acta Cryst. A* 71 (2015) 3.
 [34] G.M. Sheldrick, *Acta Cryst. C* 71 (2015) 3.
 [35] B. Selvakumar, V. Rajendiran, P.U. Maheswari, H. Stoeckli-Evans, M. Palaniandavar, *J. Inorg. Biochem.* 100 (2006) 316.
 [36] M. Zaki, M. Afzal, M. Ahmad, S. Tabassuma, *J. Photochem. Photobiol. B* 161 (2016) 318.
 [37] S. Dey, K. Ghosh, S. Halder, C. Rizzoli, P. Roy, *Indian J. Chem.* 54A (2015) 1451.
 [38] (a) A. Bhattacharjee, S. Halder, K. Ghosh, C. Rizzoli, P. Roy, *New J. Chem.* 41 (2017) 5696;
 (b) A. Bhattacharjee, S. Dey, P. Roy, *Inorg. Chim. Acta* 490 (2019) 93.
 [39] (a) P. Roy, K. Dhara, M. Manassero, P. Banerjee, *Eur. J. Inorg. Chem.* (2008) 4404;
 (b) S. Halder, S. Dey, C. Rizzoli, P. Roy, *Polyhedron* 78 (2014) 85.
 [40] S. Zolezzi, E. Spodine, A. Decinti, *Polyhedron* 21 (2002) 55.
 [41] K.S. Shaju, K.J. Thomas, V.P. Raphael, N. Kuriakose, *J. Appl. Chem.* 10 (2014) 2278.
 [42] D.M. Boghaei, S. Mohebi, *J. Mol. Catal. A* 179 (2002) 41.
 [43] N. Shahabadi, S. Kashanian, F. Darabi, *Eur. J. Med. Chem.* 45 (2010) 4239.
 [44] A. Wolfe, G.H. Shimer, T. Meehan, *Biochemistry* 26 (1987) 6392.
 [45] B.D. Wang, Z.Y. Yang, D.D. Qin, Z.N. Chen, *J. Photochem. Photobiol. A* 194 (2008) 49.
 [46] C.V. Kumar, J.K. Barton, N.J. Turro, *J. Am. Chem. Soc.* 107 (1985) 5518.
 [47] J.R. Lakowicz, G. Weber, *Biochemistry* 12 (1973) 4161.
 [48] L.Z. Li, C. Zhao, T. Xu, H.W. Ji, Y.H. Yu, G.Q. Guo, H. Chao, *J. Inorg. Biochem.* 99 (2005) 1076.
 [49] P. Lincoln, E. Tuite, B. Norden, *J. Am. Chem. Soc.* 119 (1997) 1454.
 [50] B. Norden, F. Tjerneld, *Nat. New Biol.* 236 (1982) 67.
 [51] S. Mahadevan, M. Palaniandavar, *Bioconjugate Chem.* 7 (1996) 138.
 [52] V.G. Vaidyanathan, B.U. Nair, *J. Inorg. Biochem.* 94 (2003) 121.
 [53] S. Tabassum, M. Zaki, M. Ahmad, M. Afzal, S. Srivastav, S. Srikrishna, F. Arjmand, *Eur. J. Med. Chem.* 83 (2014) 141.
 [54] Y.Q. Wang, X.Y. Wang, J. Wang, Y.M. Zhao, W.J. He, Z.J. Guo, *Inorg. Chem.* 50 (2011) 12661.
 [55] J.J. Stephanos, *J. Inorg. Biochem.* 62 (1996) 155.
 [56] C.-Y. Gao, X. Qiao, Z.-Y. Ma, Z.-G. Wang, J. Lu, J.-L. Tian, J.-Y. Xu, S.-P. Yan, *Dalton Trans.* 41 (2012) 12220.
 [57] G. Zhang, N. Zhao, L. Wang, *J. Lumin.* 131 (2011) 880.
 [58] S. Naveenraj, S. Anandan, *J. Photochem. Photobiol. C* 14 (2013) 53.
 [59] T. Forster, in: O. Sinanoglu (Ed.), *Modern Quantum Chemistry: Modern Quantum Chemistry*, vol. 3, Academic, New York, 1996, pp. 93–137.
 [60] X.-B. Fu, G.-T. Weng, D.-D. Liu, X.-Y. Le, *J. Photochem. Photobiol. A* 276 (2014) 83.
 [61] S. Tabassum, W.M. Al-Asbahy, M. Afzal, F. Arjmand, R.H. Khan, *Mol. Biosyst.* 8 (2012) 2424.
 [62] S. Kumar, R.P. Sharma, P. Venugopalan, V. Ferretti, S. Perontsis, G. Psomasc, J. Inorg. Biochem. 187 (2018) 97.
 [63] B. Deka, T. Sarkar, S. Banerjee, A. Kumar, S. Mukherjee, S. Deka, K.K. Saikia, A. Hussain, *Dalton Trans.* 46 (2017) 396.
 [64] M.K. Koley, S.U. Parsekar, N. Duraipandy, M.S. Kiran, B. Varghese, P.T. Manoharan, A.P. Koley, *Inorg. Chim. Acta* 478 (2018) 211.
 [65] K.N. Aneerahman, K. Ramaiah, G. Rohini, G.P. Stefy, N.S.P. Bhuvanesh, A. Sreekanth, *Inorg. Chim. Acta* 492 (2019) 131.
 [66] S. Banerjee, P. Ghorai, P. Brandão, D. Ghosh, S. Bhuiya, D. Chattopadhyay, S. Das, A. Saha, *New J. Chem.* 42 (2018) 246.
 [67] M. Wehbe, A.W.Y. Leung, M.J. Abrams, C. Orgiv, M.B. Bally, *Dalton Trans.* 46 (2017) 10758.
 [68] C. Santini, M. Pellei, V. Gandin, M. Porchia, F. Tisato, C. Marzano, *Chem. Rev.* 114 (2014) 815.
 [69] R. Tabti, T. Nasser, C. Gaidon, E. Bentouhami, L. Désaubry, *Med Chem. (Los Angeles)* 7 (2017) 875.